

UNCLASSIFIED

AD NUMBER

AD802294

LIMITATION CHANGES

TO:

Approved for public release; distribution is unlimited.

FROM:

Distribution authorized to U.S. Gov't. agencies and their contractors;  
Administrative/Operational Use; 30 JUN 1966.  
Other requests shall be referred to Army Missile Command. Redstone Arsenal, AL.

AUTHORITY

MICOM ltr 26 Feb 1968

THIS PAGE IS UNCLASSIFIED

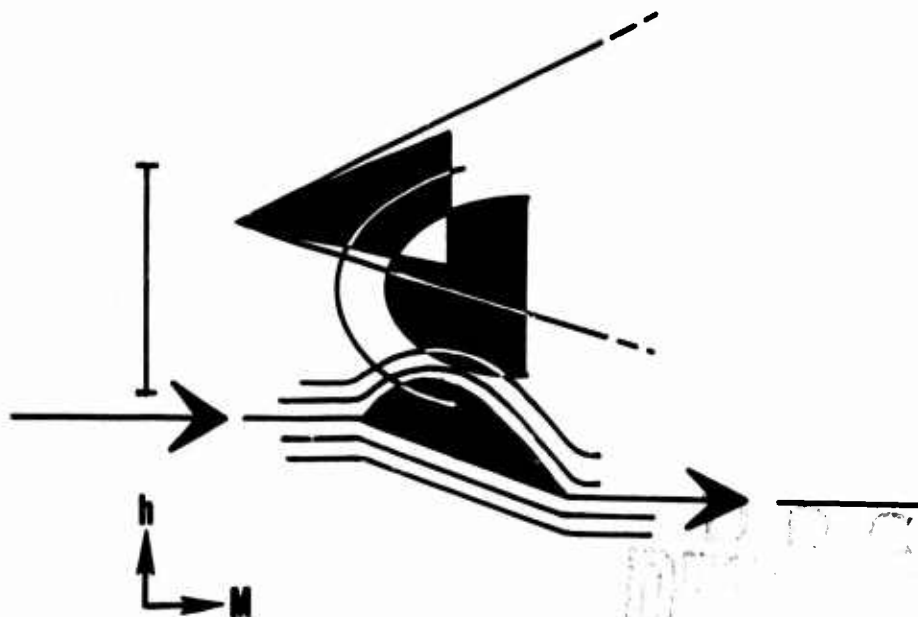
802294

VOLUME II  
**AERODYNAMIC  
FORCE ANALYSIS**

By **Branimir D. Djordjevic**

**JUNE 1966**

**DISTRIBUTION LIMITED SEE NOTICES PAGE**



**CONTRACT NO. DA-01-009-506-ORD-851 (Z)**

**AEROSPACE DEPARTMENT  
AUBURN UNIVERSITY**

For

**U.S. ARMY MISSILE COMMAND  
REDSTONE ARSENAL, ALABAMA**

**DISPOSITION INSTRUCTIONS**

Destroy this report when it is no longer needed. Do not return it to the originator.

**DISCLAIMER**

The findings in this report are not to be construed as an official Department of the Army position, unless so designated by other authorized documents.

**DISTRIBUTION LIMITATION**

This document is subject to special export controls and each transmittal to foreign governments or foreign nationals may be made only with prior approval of this Command, Attn: AMSM-RF.

30 June 1966

A E R O D Y N A M I C F O R C E  
A N A L Y S I S

by

BRANIMIR D. DJORDJEVIC

DISTRIBUTION LIMITED  
SEE NOTICES PAGE

Prepared for

FUTURE MISSILE SYSTEMS DIVISION  
RESEARCH AND DEVELOPMENT DIRECTORATE  
U. S. ARMY MISSILE COMMAND  
REDSTONE ARSENAL, ALABAMA

By

DEPARTMENT OF AEROSPACE ENGINEERING  
AUBURN UNIVERSITY

CONTRACT DA-01-009-506-ORD-851(Z)

DA Project 1S222901A206  
AMCMSC 5221. 11. 148

TABLE OF CONTENTS

Section 2.4 Skin-Friction Drag Coefficient Analysis on a Prescribed Trajectory, Including Rarefied Gas Effects

SUBSECTION	PAGE
LIST OF FIGURES	2.4-iii
LIST OF TABLES	2.4-vii
LIST OF SYMBOLS	2.4-viii
2.4.1 Free Molecule Flow Regime	2.4-2
(i) Mass, Momentum and Energy Transfer in Rarefied Free Molecule Flows	2.4-2
(1) The Thermal Accommodation Coefficient, $\alpha$	2.4-3
(2) The Parameter of a Partially Diffuse Re-emittance, $\sigma$ .	2.4-7
(3) Expression for the Number of Impinging and the Number of Re-emitted Molecules	2.4-9
(4) The Conservation of Mass Principle	2.4-10
(ii) The Momentum Transfer	2.4-10
(iii) The Internal Energy Transfer	2.4-11
2.4.2 Convective Heat Transfer Estimates for Flat Plates, Cylinders and Spheres in Free Molecular Flows	2.4-13
(i) Fundamental Assumptions	2.4-13
(ii) Modified Recovery Factor and Modified Stanton Number	2.4-13
(iii) An Approximate Evaluation of the Temperature Ratio ( $T_r / T_i$ )	2.4-14
2.4.3 Drag Force in Free Molecule Flow Definitions	2.4-18
2.4.4 Drag Force in Free Molecule Flow Regime - Simple Body Geometries	2.4-19
(i) Geometric Shapes Composed of Plane Surfaces	2.4-20
(ii) Flat Plates	2.4-24
(iii) Cylinders	2.4-28
(iv) Spheres	2.4-37
2.4.5 Slip Flow	2.4-40
(i) General Characteristics	2.4-40
(1) Two-Dimensional Laminar Boundary Layers of the Continuum Flow Regime - Kinetic Theory Approach	2.4-40
(2) Momentum Transfer in the Slip Flow Regime	2.4-46
(3) Energy Transfer in Slip Flows	2.4-50
2.4.6 Drag Coefficient and Heat Transfer in Slip Flow for Some Simple Configurations	2.4-55
(i) Flat Plate, Zero Angle of Attack, Slip Flow	2.4-55
(ii) Spheres, Slip Flow	2.4-55
(iii) Cylinders in Slip Flow Regime	2.4-61
(iv) Cones in Slip Flow Regime, Zero Angle of Attack	2.4-61
(v) Base Pressure on Cone Plus Cylinder Body Geometries	2.4-61

L

2.4.7	Heat Transfer and Skin Friction Relationships During Actual Transient Flight Conditions (Continuum, Slip, Transitional and Free Molecular Flow Regimes)	2.4-67
(i)	Basic Expressions for Heat Transfer and Skin Friction Coefficients	2.4-67
(ii)	Computations of Skin Friction Coefficients in Continuum, Slip and Free Molecule Flow Regimes Under Accelerated Flight Conditions	2.4-73
(1)	Quasi-steady Analysis on a Ascending Flight Trajectory and Preparation of the Computational Data	2.4-74
(2)	General Procedure of Determining Local and Average Skin Friction Coefficient Values For Accelerated and Quasi-steady Flight Regimes	2.4-80
2.4.8	References	2.4-144

LIST OF FIGURES

Section 2.4 Skin-Friction Drag Coefficient Analysis  
on a Prescribed Trajectory, Including  
Rarefied Gas Effects

FIGURE	TITLE	PAGE
2.4-1	Mathematical model of the diffuse molecular reflection (Ref. 2.4-12).	2.4-4
2.4-2	Flow relative to a flat surface (Ref. 2.4-12).	2.4-5
2.4-3	Reflection of free molecules (Ref. 2.4-12).	2.4-6
2.4-4	Specular reflection - a boundary condition for isentropic flow (Ref. 2.4-12).	2.4-8
2.4-5	Modified recovery factor in free molecule flow (Ref. 2.4-22).	2.4-15
2.4-6	Modified Stanton Number in free molecule flow (Ref. 2.4-22).	2.4-16
2.4-7	Local drag force per unit area, front surface, $0 \leq v \leq \infty$ , $T_w = \text{Const.}$	2.4-21
2.4-8	General double-wedge profile.	2.4-23
2.4-9	Local drag force per unit area, rear surface $-\infty \leq v \leq 0$ , $T_w = \text{Const.}$	2.4-25
2.4-10	Drag coefficient in free molecule flow, diffuse reflection on an insulated flat plate (Ref. 2.4-22).	2.4-26
2.4-11	Flat plate lift-drag ratio, diffuse reflection (Ref. 2.4-22).	2.4-27
2.4-12	Drag coefficient in free molecular flow, specular reflection from one side of an insulated flat plate (Ref. 2.4-22).	2.4-29
2.4-13	Surface temperature of an insulated plate at large and small values of the Knudsen Number (Ref. 2.4-12).	2.4-30
2.4-14	Drag coefficient of cylinders, front face, ( $0 \leq v \leq \infty$ , $T_w = \text{Const.}$ )	2.4-31
2.4-15	Drag coefficient of cylinders, rear face, ( $-\infty \leq v \leq 0$ , $T_w = \text{Const.}$ )	2.4-32
2.4-16	Drag coefficient for sphere and cylinder in free molecule flow (Ref. 2.4-22).	2.4-35
2.4-17	Drag of an insulated cylinder in helium (Ref. 2.4-12).	2.4-38
2.4-18	Heat transfer tests on a cylinder in helium (Ref. 2.4-12).	2.4-39
2.4-19	Boundary layer on a flat plate (Ref. 2.4-12).	2.4-41

2.4-20	Curves for $r(\eta)$ , $s(\eta)$ and their integrals (Ref. 2.4-42).	2.4-47
2.4-21	Velocity ratio and local skin-friction in slip flow, (Ref. 2.4-12), for flat plates, ( $\theta=0$ ).	2.4-51
2.4-22	Temperature jump and local heat transfer in slip flow, (Ref. 2.4-12), monoatomic gases.	2.4-54
2.4-23	Skin-friction drag of flat plates in slip flow (Ref. 2.4-12).	2.4-56
2.4-24	Skin-friction in slip flow for a flat plate, zero angle-of-attack (Ref. 2.4-12).	2.4-57
2.4-25	Sphere drag coefficient (Ref. 2.4-50), slip flow regime.	2.4-59
2.4-26	Convective heat transfer coefficient for spheres in supersonic flow, slip flow regime, (Ref. 2.4-54).	2.4-60
2.4-27	Thermal recovery factor for spheres in supersonic flow (Ref. 2.4-55).	2.4-62
2.4-28	Thermal recovery factor for transverse cylinders in supersonic flow (Ref. 2.4-57).	2.4-63
2.4-29	Drag coefficients for cones with $15^\circ$ semivertex angles (Ref. 2.4-60) (zero angle-of-attack).	2.4-64
2.4-30	Thermal recovery factors for cones in supersonic flow (Ref. 2.4-61).	2.4-64
2.4-31	Base pressure coefficient for cone configurations (Ref. 2.4-62, 2.4-63, 2.4-64), (zero angle-of-attack).	2.4-66
2.4-32	Variation of the mean free molecular path with altitude in the NACA Standard Atmosphere, (1947).	2.4-100
2.4-33	Mean molecular free path (Ref. 2.4-74).	2.4-101
2.4-34	The regimes of gas dynamics.	2.4-100
2.4-35	Flight regimes for ballistic vehicles.	2.4-100
2.4-36	Flight regimes for glide missile.	2.4-100
2.4-37	Flight regimes for skip and glide vehicles.	2.4-100
2.4-38	Flight regimes for ballistic vehicles.	2.4-100
2.4-39	Flight regimes for sustained flight and anti-missile missiles.	2.4-100
2.4-40	Flow regime boundaries in terms of altitude and flight speed.	2.4-100
2.4-41	Flow regime boundaries for ballistic vehicles.	2.4-100
2.4-42	Flow regime boundaries for skip and glide vehicles.	2.4-100

2.4-43	Flow regime boundaries for sustained flight and anti-missile missiles.	2.4-100
2.4-44	Illustrative example of flight altitude versus time for a hypothetical long range missile, $H = f(t)$ . (Recomputed data from Fig. 2.4-37).	2.4-102
2.4-45	Illustrative example of flight altitude versus speed for a hypothetical long range missile, $H = f(v)$ . (Replotted data from Fig. 2.4-37).	2.4-103
2.4-46	Illustrative example of flight speed versus time for a hypothetical long range missile, $V = f(t)$ . (Recomputed data from Fig. 2.4-37).	2.4-104
2.4-47	Illustrative graph of the free stream density, speed of sound, and Mach Number versus time for a hypothetical missile in a standard ARDC model atmosphere (1956).	2.4-105
2.4-48	Illustrative graph of the free stream static pressure, absolute temperature and viscosities for a hypothetical missile in a standard ARDC atmosphere (1956).	2.4-106
2.4-49	Laminar boundary layers: local adiabatic wall temperatures at perfectly insulated surfaces neglecting radiation and assuming steady aerothermal equilibrium flow conditions - allowance for variations in specific heat with temperature has been made (Ref. 2.4-68).	2.4-107
2.4-50	Turbulent boundary layers: local adiabatic wall temperatures at perfectly insulated surfaces neglecting radiation and assuming steady aerothermal equilibrium flow conditions - allowance for variations in specific heat with temperature has been made (Ref. 2.4-68).	2.4-108
2.4-51	Stagnation conditions: local adiabatic wall temperatures at perfectly insulated surfaces neglecting radiation and assuming steady aerothermal equilibrium flow conditions - allowance for variations in specific heat with temperature has been made (Ref. 2.4-68).	2.4-109
2.4-52	Stagnation-temperature rise for variable $C_p$ . (Ref. 2.4-72).	2.4-110
2.4-53	Dimensionless quantity $X$ . (after Stalder and Jukoff, Ref. 2.4-67).	2.4-111
2.4-54	Dimensionless quantity $\psi$ . (after Stalder and Jukoff, Ref. 2.4-67).	2.4-112
2.4-55	Dimensionless quantity $\chi'$ . (after Stalder and Jukoff, Ref. 2.4-67).	2.4-113
2.4-56	Dimensionless quantity $\psi'$ . (after Stalder and Jukoff, Ref. 2.4-67).	2.4-114
2.4-57	Surface emissivities (Ref. 2.4-68).	2.4-115

2.4-58	Local skin-friction coefficient for laminar boundary layer of a compressible fluid flowing along a flat plate. Prandtl Number, 0.75; $\theta = 0.505$ . (Ref. 2.4-73).	2.4-116
2.4-59	Nomograph for coefficients of friction of a turbulent boundary layer on a flat plate for air (Ref. 2.4-73).	2.4-117
2.4-60	Variation of local skin friction along flat plate (after Mirels Ref. 2.4-71).	2.4-118
2.4-61	Specific heats of some common materials:	
	(a) Plain carbon steel	2.4-119
	(b) High alloy steel	2.4-120
	(c) Alloy steel	2.4-121
	(d) Inconel-X	2.4-122
	(e) Pure molybdenum	2.4-123
	(f) Pure manganese	2.4-124
	(g) Magnesium	2.4-125
	(h) Pure beryllium	2.4-126
	(i) Pure cadmium	2.4-127
	(j) Pure vanadium	2.4-128
	(k) Pure tungsten	2.4-129
	(l) Pure chromium	2.4-130
	(m) Nickel-chromium alloys	2.4-131
	(n) Pure cobalt	2.4-132
	(o) Titanium	2.4-133
	(p) Pure tantalum	2.4-134
	(q) Pure copper	2.4-135
	(r) Pure nickel	2.4-136
	(s) Pure zinc	2.4-137
	(t) Copper-nickel alloys	2.4-138
	(u) 21.2% copper - 78.8% nickel alloy	2.4-139
	(v) 6% copper - 94% nickel alloy	2.4-140
	(w) 45.69% copper - 54.31% zinc alloy	2.4-141
	(x) 62.45% copper - 37.55% zinc alloy	2.4-142
	(y) 51.8% copper - 48.2% zinc alloy	2.4-143

LIST OF TABLES

Section 2.4 Skin-Friction Drag Coefficient Analysis on a Prescribed Trajectory, Including Rarefied Gas Effects

TABLE	TITLE	PAGE
2.4-1	Thermal accommodation coefficient $\alpha$ for air (Ref. 2.4-15).	2.4-7
2.4-2	Values of reflection coefficient $\sigma$ (Ref. 2.4-16).	2.4-7
2.4-3	Ambient standard atmosphere flight data, (related to the computational step 1, section 2.4.7).	2.4-90
2.4-4	Ambient standard atmosphere physical data, (related to the computational step 2, section 2.4.7).	2.4-91
2.4-5	Surface (wall) physical data, (related to the computational steps 3 and 4, section 2.4.7).	2.4-92
2.4-6	Local free stream data ( $\infty$ ), (related to the computational steps 3 and 4, section 2.4.7).	2.4-93
2.4-7	Initial local wall data at time $t_{K-1}$ ( $1 \leq K \leq n$ ), (related to the computational steps 5 and 6, section 2.4.7).	2.4-94
2.4-8	Prandtl Number data allowing for variation of $C_p$ with temperature, (Ref. 2.4-70).	2.4-95
2.4-9	Local skin structural and radiation data, (related to the computational steps 7 and 8, section 2.4.7).	2.4-96
2.4-10	Free molecule flow, front surfaces, local skin temperature, (related to the computational step 9, section 2.4.7).	2.4-97
2.4-11	Summary data for computations of the "f" function at initial instants $\Delta t = t_{K+1} - t_{K-1}$ , ( $t_{K-1}$ ), $1 \leq K \leq n$ , (related to the computational step 10, section 2.4.7).	2.4-98
2.4-12	Kutta-Runge numerical method of solution.	2.4-99

LIST OF SYMBOLS

Section 2.4 Skin Friction Drag Coefficient Analysis on a Prescribed Trajectory, Including Rarefied Gas Effects

I. PHYSICAL AND GEOMETRIC

- A - Surface area, sq. ft.
- b - Width, or span, ft.
- B - Stefan-Boltzmann's constant,  $B = 3.74 \times 10^{-10}$ , foot-pound per sq. ft.  $^{\circ}F^4$ .
- $C_D$  - Total average drag force coefficient due to both impinging and re-emitted molecules, dimensionless,  

$$C_D = C_{D_i} + C_{D_r} = \frac{\text{DRAG}}{(1/2) \rho_i \bar{q}_i^2 A}$$
- $C_D$  - Total average drag force coefficient, (including frictional and pressure force effects), dimensionless,  

$$C_D = \frac{D}{(1/2) \rho_i \bar{q}_i^2 A}$$
- $C_{D_i}'$  - Resultant local drag force coefficient, referred to the  $(D_i')$  force, dimensionless,  

$$C_{D_i}' = \frac{D_i'}{(1/2) \rho_i \bar{q}_i^2}$$
- $C_{D_i}$  - Resultant average drag force coefficient, (due to impinging molecules), obtained by integration of the  $(C_{D_i}')$  on a finite area (A), dimensionless.
- $C_{D_r}'$  - Resultant local drag force coefficient, referred to the  $(D_r')$  force, dimensionless,  

$$C_{D_r}' = \frac{D_r'}{(1/2) \rho_i \bar{q}_i^2}$$
- $C_{D_r}$  - Resultant average drag force coefficient due to re-emitted molecules, obtained by integration of  $(C_{D_r}')$  on a finite area (A), dimensionless.
- $C_{f'}$  - Local skin-friction coefficient due to tangential momentum component of both the impinging and the re-emitted molecules, dimensionless,  

$$C_{f'} = C_{f_i'} + C_{f_r'}$$
- $C_f$  - Average skin-friction coefficient due to tangential momentum component of both the impinging and the re-emitted molecules, dimensionless. Obtained by integration of  $(C_{f'})$  on the surface (A).

$C_f'$  - Local skin-friction coefficient referred to the free stream reference conditions,

$$C_f' = \frac{\tau_w}{(1/2)\rho_1 \bar{q}_1^2}$$

$C_{fi}'$  - Local skin-friction coefficient (at some point M), due to tangential momentum transfer component of all impinging molecules, dimensionless,

$$C_{fi}' = \frac{\tau_i}{(1/2)\rho_1 \bar{q}_1^2}$$

$C_{mi}$  - Most probable mean average molecular speed of the impinging molecules, i.e. the speed possessed by the greatest number of molecules, ft. per sec.

$C_p$  - Average pressure coefficient due to normal momentum component of both the impinging and the re-emitted molecules, dimensionless. Obtained by integration of ( $C_p'$ ) on the surface (A).

$C_p$  - Specific heat coefficient of a gas at a constant pressure, BTU per slug °F.

$C_{pi}'$  - Local pressure coefficient (at some point M), due to normal momentum transfer component of all impinging molecules, dimensionless,

$$C_{pi}' = \frac{p_i}{(1/2)\rho_1 \bar{q}_1^2}$$

$C_p'$  - Local pressure coefficient (at some point M) due to normal momentum transfer of both the impinging and the re-emitted molecules, dimensionless,

$$C_p' = C_{pi}' + C_{pr}'$$

$C_v$  - Specific heat coefficient of a gas at a constant volume, BTU per slug °F.

$d\bar{E}_i'$  - Mean average internal energy flux of the incident molecules.

$d\bar{E}_r'$  - Mean average internal energy flux of the rebounded (re-emitted) molecules.

$d\bar{E}_w'$  - Mean average internal energy flux of the re-emitted molecules, if they were re-emitted with a Maxwellian velocity distribution function so modified as to correspond to the surface temperature ( $T_w$ ).

$d\bar{E}_w'$  - Mean average internal energy flux of the molecules re-emitted in Maxwellian equilibrium ( $T_r = T_w$ ) from a surface, with no macroscopic velocity ( $\bar{q} = 0$ ).

$dA$  - Infinitesimal surface area, sq. ft.

$dF$  - Local aerodynamic force, acting on an infinitesimal surface element ( $dA$ ), lbf.

$dQ$  - Infinitesimal convective heat content, BTU.

$D$  - Alternatively, a reference body length (maximum diameter eventually), ft.

D - A characteristic dimensionless length of the body-fluid system,

$$D = \frac{\delta y(l)}{l}$$

D - Total drag force, lbf.

$$D = (D_i' + D_r') A.$$

$D_i'$  - Resultant local drag force per unit area, due to the resultant momentum exchange of all the impinging molecules at any point (M) on the surface ( $d_A$ ), lbf. per sq. ft.

$$D_i' = C_{D_i}' (1/2) \rho_i \bar{q}_i^2 = p_i \sin \theta + \tau_i \cos \theta$$

$D_f'$  - Resultant local frictional drag force per unit area, due to resultant tangential momentum exchange of both the impinging and the re-emitted molecules, lbf. per sq. ft.

$D_p'$  - Resultant local pressure drag force per unit area, due to resultant normal momentum exchange of both the impinging and the re-emitted molecules, lbf. per sq. ft.

$D_r'$  - Resultant local drag force per unit area, due to the resultant momentum exchange of all the re-emitted molecules at any point (M) on the surface ( $d_A$ ), lbf. per sq. ft.

$$D_r' = C_{D_r}' (1/2) \rho_i \bar{q}_i^2 = p_r \sin \theta$$

erf - Symbol for error function.

erfc - Symbol for complementary error function.

exp - Denotes exponential function.

E - Mean average total internal energy of an individual molecule, due to all existing individual degrees of molecular freedom of motion.

$E'_{EM}$  - Radiant emission energy from the body per unit area,

$$E'_{EM} = \epsilon B T_w^4$$

$E_i$  - Mean average total internal energy of an individual incident molecule.

$E'$  - Mean average internal molecular energy content per unit area per unit time.

$E'_i$  - Mean average internal energy content per unit area per unit time of the impinging molecules.

$E'_{IN}$  - Radiant input energy from infinitely per unit area of body surface,

$$E'_{IN} = \epsilon B T_c^4$$

$E_r$  - Mean average total internal energy of a rebounded (or re-emitted) molecule.

$E_w$  - Mean average total internal energy of a molecule that would be possessed by the re-emitted molecule, if it were re-emitted from a solid surface (wall) in accordance with a modified Maxwellian velocity distribution function changed to correspond to the surface temperature ( $T_w$ ).

- $\bar{E}_R'$  - Mean average internal energy content per unit area per unit time of the reflected (re-emitted) molecules.
- F - Total aerodynamic force, acting on a finite surface area (A), lbf.
- $H_2$  - Boltzmann's function for  $i=2$ .
- $r_w$  - Shearing stress at the wall, lbf. per sq. ft.
- $I_1$  - Modified Bessel function of the order (1).
- $I_0$  - Modified Bessel function of the order (0).
- $J'$  - The internal energy output per unit area of body surface per unit time, due to coolants.
- k - Coefficient of heat conduction for monoatomic gases, BTU per sec. ft. °R.
- $k_1$  - A constant, related to  $(x)$  and  $(X)$ , dimensionless,
- $$k_1 = \frac{x}{X}$$
- $Kn_x$  - Knudsen Number, dimensionless,
- $$Kn_x = \frac{1}{X} = \frac{\bar{\lambda}}{x}$$
- l - Total length, ft.
- $\zeta$  - Local dimensionless mean free molecular path at any point in the boundary layer,
- $$\zeta = \frac{\bar{\lambda}}{\lambda_r}$$
- $M_i$  - Mach Number of the impinging molecules, dimensionless,
- $$M_i = \frac{q_i}{a_i}$$
- $M_1$  - Mach Number, dimensionless, referred to some reference "1" station of the free stream flow,
- $$M_1 = \frac{\bar{u}_0}{a_i}$$
- $n_i$  - Total number of impinging molecules per unit volume per unit time.
- $n_i'$  - Total number of impinging molecules per unit area per unit time.
- $n_r$  - Total number of the reflected (re-emitted) molecules per unit volume per unit time.
- $n_r'$  - Total number of the reflected (re-emitted) molecules per unit area per unit time.
- Nu - Nusselt Number, dimensionless, referred to the reference (D) length,
- $$Nu = \frac{hD}{k}$$
- $N_{INT}$  - Number of internal (rotational + vibrational) degrees of molecular freedom.
- p - Normal momentum component in defining the respective

parameter of a partial diffuse re-emittance, ( $\sigma'$ ).

$p$  - Total normal stress (pressure), lbf. per sq. ft.

$$p = p_r + p_i$$

$p_i$  - Normal stress (pressure) due to impinging molecules, lbf. per sq. ft.

$$p_i = \frac{dF_i}{dA} \sin\theta$$

$p_r$  - Normal stress (pressure) due to re-emitted molecules, lbf. per sq. ft.

$$p_r = \frac{dF_r}{dA} \sin\theta$$

$Pr$  - Prandtl Number, dimensionless,

$$Pr = \frac{\mu_i C_p}{k_i}$$

$\bar{q}$  - Mean average "ordered" molecular resultant velocity of the control space-volume ( $d$ ), ft. per sec.

$$\bar{q} = (\bar{u}^2 + \bar{v}^2 + \bar{w}^2)^{\frac{1}{2}},$$
$$\bar{q} = V_\infty.$$

$Re_s$  - Reynolds Number, dimensionless, referred to free stream reference conditions (1) and the slant length of a cone ( $s$ ),

$$Re_s = \frac{\rho_i V_i s}{\mu_i}$$

$r$  - Radius, ft.

$r'$  - Modified recovery factor, accounting for the type of molecular re-emittance mechanism,

$$r' = \frac{T_r - T_i}{T_s - T_i} \frac{\gamma + 1}{\gamma}$$

$r$  - Recovery factor, dimensionless,

$$r = \frac{T_{ad} - T_i}{T_s - T_i}$$

$Re_l$  - Reynolds Number, dimensionless, referred to some reference "1" station of the free stream flow,

$$Re_l = \frac{\rho_i \lambda_i \bar{u}_i}{\mu_i}$$

$S$  - Speed ratio of the impinging molecules in a free molecule flow, dimensionless,

$$S = \frac{\bar{q}_i}{c_{m_i}} = \sqrt{\frac{\gamma}{2}} M_i$$

$s$  - Slant length of a cone, ft.

$S_r$  - Common reference area for a given missile configuration, sq. ft.

$S_v$  - Ratio of the normal-to-surface component of mean average mass velocity ( $\bar{v}_i$ ) to the most probable speed of incident molecules ( $c_{m_i}$ ).

$$S_v = S \sin\theta = \frac{\bar{v}_i}{c_{m_i}}$$

$t$  - Time, sec.

- $T_{ad}$  - Absolute adiabatic temperature, °R or °K.
- $T_w$  - Absolute temperature of the immersed surface (wall) proper, °R or °K.
- $U$  - Local dimensionless velocity component in the x-direction at any point in the boundary layer,
 
$$U = \frac{\bar{u}}{\bar{u}_1}$$
- $u', v', w'$  - Dimensionless local molecular velocity components, ft. per sec.
- $\bar{u}, \bar{v}, \bar{w}$  - Mean average velocity components within an infinitesimal time interval ( $dt$ ), ft. per sec.
 
$$\bar{u} = \bar{u}(x, y, z, t)$$

$$\bar{v} = \bar{v}(x, y, z, t)$$

$$\bar{w} = \bar{w}(x, y, z, t)$$
- $\bar{u}', \bar{v}', \bar{w}'$  - Time-average of the ( $u', v', w'$ ) fluctuating molecular velocity components, with the time interval ( $T$ ) long enough to allow
 
$$\bar{u}' = \frac{1}{T} \int_0^T u' dt = 0 \quad \text{etc.}$$
- $x', y', z'$  - Dimensionless coordinates of a local point, ft.
 
$$x' = \frac{x}{L}, \quad \text{etc.}$$
- $X$  - Dimensionless longitudinal position coordinate of a point,
- $Y$  - Dimensionless lateral position coordinate of a point,
 
$$Y = \frac{y}{\lambda_1},$$
- $Z_1$  - A molecular speed ratio function,
 
$$Z_1 = \pi e^{-\frac{1}{2} S_v^2} I_0\left(\frac{1}{2} S^2\right)$$
- $Z_2$  - A molecular speed ratio function,
 
$$Z_2 = \pi S^2 e^{-\frac{1}{2} S_v^2} \left[ I_0\left(\frac{1}{2} S^2\right) + I_1\left(\frac{1}{2} S^2\right) \right]$$
- $\delta_u(x)$  - Local "momentum" boundary layer thickness, or local boundary layer thickness at a station ( $x$ ), defined in terms of the ordered mass velocity deficiency, ft.
- $\Delta$  - A characteristic dimensionless length of the body-fluid system,
 
$$\Delta = \bar{\lambda} / \delta_u(l)$$
- $\epsilon$  - Emissivity for "gray" bodies, dimensionless.
- $\theta$  - Alternatively semi-vertex angle of a cone.
- $\theta$  - Angle of incidence of the impinging molecular stream (possessing the mean average resultant velocity  $q_i$ ), radius.
- $\Theta$  - Dimensionless absolute temperature,

- $\sigma$  - Parameter of a partial diffuse re-emittance, i.e. the fraction of incident molecules which is reflected diffusely from a surface. Alternatively, ( $\sigma$ ) denotes the parameter of a partial diffuse re-emittance due to partial tangential momentum transfer only if a more elaborate interpretation is accepted, i.e.:
- $$\sigma = \frac{\dot{q} - \dot{q}_r}{\dot{q}_i - \dot{q}_w} \quad , \quad \dot{q}_w = 0$$
- $\sigma$  - Geometric diameter of a molecule, ft.
- $\sigma'$  - Parameter of a partial diffuse molecular re-emittance due to a partial normal momentum transfer at the surface (wall),
- $$\sigma' = \frac{\dot{q}_n - \dot{q}_{nr}}{\dot{q}_n - \dot{q}_{nw}}$$
- $\tau$  - Generally, shearing stress, or the tangential force per unit area, lbf. per sq. ft.
- $a$  - Speed of sound,  $\left[ \frac{\text{ft}}{\text{sec}} \right]$
- $$a = \sqrt{\gamma \frac{p}{\rho}} = f(t)$$
- $[a_\infty]_x$  - Local speed of sound, referred to free stream conditions outside the boundary layer,  $[\text{ft}/\text{sec}]$
- $$[a_\infty]_x = f(T_\infty)_x$$
- $[a_w]_x$  - Local speed of sound, referred to conditions at the body surface,  $[\text{ft}/\text{sec}]$
- $$[a_w]_x = f(T_w)_x$$
- $C_{f_\infty}$  - Average skin friction coefficient referred to the free stream conditions, dimensionless; for a flat plate, zero angle of attack, laminar boundary layer
- $$C_{f_\infty} = \frac{1}{b_{FP} l_{FP}} \int_0^{l_{FP}} [C_{fx}]_\infty dx \quad b_{FP} = 2 [C_{fx}]_\infty$$
- with
- $$[V_\infty]_x = V_A = V$$
- $[C_{fx}]_\infty$  - Local skin friction coefficient at a station  $[x]$  from leading edge, referred to the local free stream flow conditions just outside the boundary layer, dimensionless; by a general definition:
- $$[C_{fx}]_\infty = \frac{\tau_w}{1/2 [\rho_\infty]_x [V_\infty]_x^2}$$
- $[C_{fx}]_w$  - Local skin friction coefficient at a station  $[x]$  from leading edge, referred to the local conditions at the body surface, dimensionless; by a general definition:
- $$[C_{fx}]_w = \frac{\tau_w}{1/2 [\rho_w]_x [V_\infty]_x^2}$$
- $[C_{p_\infty}]_x$  - Local specific heat coefficient at constant pressure, evaluated at the outer edge of the boundary layer,
- $$\left[ \frac{\text{ft}^2}{\text{R sec}} \right] \quad \text{or} \quad [C_{p_\infty}]_x = f(T_\infty)_x \quad , \quad \text{for a given set of gas and flow conditions.}$$

- $[C_{pw}]_x$  - Local specific heat coefficient at constant pressure evaluated at the body surface,  

$$\left[ \frac{ft^2}{sec^2 R} \right] \quad , \quad [C_{pw}]_x = f(T_w)_x$$
for a given set of gas and flow conditions.
- $[C_{px}]_\infty$  - Local pressure coefficient, referred to the local free stream conditions, dimensionless,  

$$[C_{px}]_\infty = \left[ \frac{P_\infty - P_A}{\rho_\infty V_\infty^2 / 2} \right]_x$$
- $[C_{px}]_A$  - Local pressure coefficient, referred to the ambient flight conditions, dimensionless,  

$$[C_{px}]_A = \frac{[P_\infty]_x - P_A}{\rho_A V_A^2 / 2}$$
- $[C_w]_x$  - Local conductive specific heat coefficient of a given skin material,  

$$\left[ \frac{Btu}{slug^2 R} \right] \quad \text{or} \quad \left[ \frac{Btu}{lb ft^2 R} \right]$$
- $[e_i]_x$  - Local energy flux into surface due to impinging (incident) molecules,  

$$\left[ \frac{lb ft}{ft^2 sec} \right]$$
- $[e_r]_x$  - Local energy flux out of surface due to re-emitted molecular stream  

$$\left[ \frac{lb ft}{ft^2 sec} \right]$$
- $[e_s]_x$  - Local energy flux into surface due to ambient (Solar) radiation,  

$$\left[ \frac{lb ft}{ft^2 sec} \right]$$
- $[e_w]_x$  - Local energy flux out of surface due to re-emitted radiation,  

$$\left[ \frac{lb ft}{ft^2 sec} \right]$$
- $[G_w]_x$  - Local heat absorption capacity for a given skin geometry and skin material,  

$$[G_w]_x = [c_w \delta_w w_w]_x \quad \left[ \frac{Btu}{ft^2 R} \right]$$
- H - Flight altitude, [ft],
- $h_x$  - Local film coefficient of heat transfer in the flowing medium (air),  

$$\left[ \frac{Btu}{sec ft^2 R} \right]$$
- $Kn_L$  - Knudsen Number in terms of the characteristic body length, dimensionless,  

$$Kn_L = \frac{\bar{\lambda}}{L}$$

- $[Kn_x]_\infty$  - Local Knudsen Number, at a station (X), referred to the local point distance from leading edge and the local conditions outside the boundary layer, dimensionless,

$$[Kn_x]_\infty = \frac{[\lambda_\infty]_x}{X} \sim \frac{[M_x]_\infty}{[Re_x]_\infty}$$

- $[Kn_x]_w$  - Local Knudsen Number at a station (X), referred to the local point distance from the leading edge and the conditions at the body surface, dimensionless,

$$[Kn_x]_w = \frac{[\lambda_w]_x}{X} \sim \frac{[M_x]_w}{[Re_x]_w}$$

- $Kn_\delta$  - Knudsen Number in terms of a laminar boundary layer thickness, dimensionless

$$Kn_\delta = \frac{\lambda}{\delta}$$

- $[Kn_{\delta_x}]_\infty$  - Local Knudsen Number at a station (X) from leading edge, referred to the local laminar boundary layer thickness and the local conditions outside the boundary layer, dimensionless

$$[Kn_{\delta_x}]_\infty = \frac{[\lambda_\infty]_x}{\delta_x} \sim \frac{[M_x]_\infty}{[Re_x]_\infty^{1/2}}$$

- $[Kn_{\delta_x}]_w$  - Local Knudsen Number at a station (x), referred to the laminar boundary layer local thickness and the conditions at the body surface, dimensionless

$$[Kn_{\delta_x}]_w = \frac{[\lambda_w]_x}{\delta_x} \sim \frac{[M_x]_w}{[Re_x]_w^{1/2}}$$

- L - Aerodynamic lift force, [lbf]

- L - Characteristic length of a particular body geometry, or of the whole vehicle in general, [ft] .

- l - Length, [ft] .

- M - Flight Mach Number, dimensionless.

$$M = \frac{V}{a}$$

- $[M_x]_w$  - Local Mach Number at a station (x) from leading edge, referred to the conditions at the body surface,

$$[M_x]_w = \frac{[V_\infty]_x}{[a_w]_x}$$

- $m_A$  - Mass on one molecule of air

$$m_A = \frac{p_A}{N_A} \quad \left[ \frac{\text{slugs}}{\text{molecule}} \right]$$

- $N_A$  - Number of molecules contained per cubic foot of the ambient atmospheric gas at some altitude (A),

$$N_A = N_0 \left( \frac{p_A}{p_0} \right) \left( \frac{T_0}{T_A} \right) \quad \left[ \frac{\text{molecules}}{\text{ft}^3} \right]$$

- $N_0$  - Number of molecules contained per cubic foot of the atmospheric gas at sea level,

$$N_0 = 7.63 \times 10^{23} \quad \left[ \frac{\text{molecules}}{\text{ft}^3} \right]$$

- P - Static pressure,

$$\left[ \frac{\text{lbf}}{\text{ft}^2} \right]$$

- $p_{\infty}$  - Local free stream static pressure, outside the boundary layer,  $\left[ \frac{\text{lb} \cdot \text{f}}{\text{ft}^2} \right]$
- $p_A$  - Ambient atmospheric static pressure  $\left[ \frac{\text{lb} \cdot \text{f}}{\text{ft}^2} \right]$
- $p_0$  - Static pressure at sea level,  
 $p_0 = 2117 \left[ \frac{\text{lb} \cdot \text{f}}{\text{ft}^2} \right]$
- $[Pr_x]_{\infty}$  - Local Prandtl Number, dimensionless; in the present case:  
 $[Pr_x]^{1/2} = \left( \frac{T_{aw} - T_{\infty}}{T_{s\infty} - T_{\infty}} \right)_x$  laminar flows  
 $[Pr_x]^{1/3} = \left( \frac{T_{aw} - T_{\infty}}{T_{s\infty} - T_{\infty}} \right)_x$  turbulent flows
- $[\Delta Q]_x$  - Local heat transfer rate into (or out of) a surface element ( $\Delta s$ ),  $\left[ \frac{\text{Btu}}{\text{sec}} \right]$   
 $[\Delta Q]_x = \Delta q_x \Delta S$
- $[\Delta q_a]_x$  - Local aerodynamic heat flux,  $\left[ \frac{\text{Btu}}{\text{ft}^2 \text{ sec}} \right]$   
 $[\Delta q_a]_x = h_x [T_{aw} - T_w]_x$
- $[\Delta q_i]_x$  - Local heat flux to or from the skin due to internal (artificial) heating or cooling effects,  $\left[ \frac{\text{Btu}}{\text{ft}^2 \text{ sec}} \right]$
- $[\Delta q_r]_x$  - Local radiation flux out of skin into the ambient atmosphere,  $\left[ \frac{\text{Btu}}{\text{sec ft}^2} \right]$   
 $[\Delta q_r]_x = [\epsilon_w T_w^4]_x B$
- $[\Delta q_s]$  - Ambient (Solar) radiative heat flux into the skin,  $\left[ \frac{\text{Btu}}{\text{sec ft}^2} \right]$   
 $\Delta q_s = \epsilon_s (B T_s^4)$
- $\Delta q_x$  - Local instantaneous heat flux into (or out of) surface  $\left[ \frac{\text{Btu}}{\text{sec ft}^2} \right]$   
 $\Delta q_x = \left[ G_w \frac{dT_w}{dt} \right]_x$
- $R$  - Universal gas constant (air)  $\left[ \frac{\text{lb} \cdot \text{f} \cdot \text{ft}}{\text{lb} \cdot \text{mole} \cdot \text{°R}} \right]$   
 $R = 1544$
- $Re_L$  - Reynolds Number in terms of the characteristic body length, dimensionless  
 $Re_L = \frac{VL}{\nu}$
- $[Re_x]_{\infty}$  - Local Reynolds Number at a station (x) from leading edge, referred to the local free stream conditions outside the boundary layer, dimensionless  
 $[Re_x]_{\infty} = \frac{[V_{\infty}]_x X}{[\nu_{\infty}]_x} = \frac{[\rho_{\infty}]_x [V_{\infty}]_x X}{[\mu_{\infty}]_x}$

- $[R_{\theta x}]_w$  - Local Reynolds Number at a station (X) from leading edge, referred to conditions at the body surface, dimensionless
- $$[R_{\theta x}]_w = \frac{[V_{\infty}]_x X}{[\nu_w]_x} = \frac{[\rho_w]_x [V_{\infty}]_x X}{[\mu_w]_x}$$
- $r_x$  - Local recovery factor, dimensionless; in the present case:
- $$r_x = [Pr_x]^{1/2} \quad \text{laminar flows}$$
- $$r_x = [Pr_x]^{1/3} \quad \text{turbulent flows}$$
- $[St_x]_{\infty}$  - Local Stanton Number, referred to the local free stream conditions outside the boundary layer, dimensionless,
- $$[St_x]_{\infty} = \frac{h_x}{[C_{p_{\infty}}]_x [\rho_{\infty}]_x [V_{\infty}]_x}$$
- $[St_x]_{\infty}$  - Local Stanton Number, dimensionless; in the present case:
- $$[St_x]_{\infty} = [Pr_x]_{\infty}^{-2/3} \frac{[Cf_x]_{\infty}}{2} = f [M_x]_{\infty}$$
- for laminar flows
- $$[St_x]_{\infty} = .6 [Cf_x]_{\infty} = r [M_x]_{\infty}$$
- for turbulent flows (i.e. a modified Reynolds Analogy law)
- $T$  - Absolute temperature,  $[^{\circ}R]$ .
- $[T_{\infty}]_x$  - Local absolute free stream temperature at the outer edge of the boundary layer,  $[^{\circ}R]$
- $[T_{0w}]_x$  - Local adiabatic wall temperature,  $[^{\circ}R]$
- $T_{0w}$  - Maximum (usually related to the stagnation point conditions) permissible equilibrium skin temperature in a sustained flight for a presumed skin material, in absence of artificial cooling of any kind (ablative, internal, ejected externally etc.),  $[^{\circ}R]$
- $T_i$  - Temperature of the impinging molecular stream,  $[^{\circ}R]$ , conditionally,
- $$T_i = T_A$$
- $T_0$  - Absolute temperature at sea level,
- $$T_0 = 492 [^{\circ}R]$$
- $T_r$  - Temperature of the re-emitted molecular stream,  $[^{\circ}R]$  conditionally  $T_r = T_w$
- $T_s$  - Absolute temperature of the outer (Solar) ambient,  $[^{\circ}R]$
- $u, v, w$  - Local speed components in the  $x, y, z$  directions respectively
- $v$  - Flight speed  $\left[ \frac{ft}{sec} \right]$

- W - Dynamic lift on a trajectory, [lb]  

$$W = L + CF$$
- w - Molecular weight of gas (air), Standard Atmosphere conditions,  

$$W = 28.97 \left[ \frac{\text{lb}}{\text{mole}} \right]$$
- x, y, z - Right-hand local coordinates of a point, generally taken in the local tangent and the local normal and the local binormal directions at the surface, [ft].
- a - Accommodation coefficient, dimensionless  

$$a = \frac{\theta_i - \theta_r}{\theta_i - \theta_w}$$
- $\gamma$  - Specific heat ratio, dimensionless
- $\delta$  - Boundary layer thickness, [ft]
- $\delta_L$  - Boundary layer thickness at the station "L" (ft) from the leading edge, [ft].
- $\delta_x$  - Local boundary layer thickness at a station (x) from leading edge, [ft].
- $\epsilon_s$  - Ambient (Solar) emissivity, dimensionless, conditionally equal to the skin absorptivity, i.e. to the skin emissivity, using an approximation of the gray body law:  

$$\epsilon_s = \epsilon_w$$
- $[\epsilon_w]_x$  - Local emissivity of the skin surface, (assumed equal to the surface absorptivity), dimensionless,
- $\bar{\lambda}$  - Mean free molecular path, [ft].
- $[\bar{\lambda}_w]_x$  - Local mean free molecular path, referred to the conditions at the body surface, [ft].  

$$[\bar{\lambda}_w]_x = f [T_w]_x$$
- $[\bar{\lambda}_\infty]_x$  - Local mean free molecular path, referred to the conditions at the outer edge of the boundary layer,  

$$[\bar{\lambda}_\infty]_x = f [T_\infty]_x \quad [\text{ft}]$$
- $\mu$  - Coefficient of viscosity,  

$$\left[ \frac{\text{slug}}{\text{ft sec}} \right] \text{ or } \left[ \frac{\text{lb sec}}{\text{ft}^2} \right]$$
- $[\mu_\infty]_x$  - Local coefficient of viscosity referred to the local free stream temperature conditions at the outer edge of boundary layer,  

$$\left[ \frac{\text{slug}}{\text{ft sec}} \right] \text{ or } \left[ \frac{\text{lb sec}}{\text{ft}^2} \right], \quad [\mu_\infty]_x = f [T_\infty]_x$$
- $[\mu_w]_x$  - Local coefficient of viscosity referred to the local temperature conditions at the body surface,  

$$\left[ \frac{\text{slug}}{\text{ft sec}} \right] \text{ or } \left[ \frac{\text{lb sec}}{\text{ft}^2} \right], \quad [\mu_w]_x = f (T_w)_x$$
- $\nu$  - Kinematic coefficient of viscosity,  $\left[ \frac{\text{ft}^2}{\text{sec}} \right]$ .

- $[\nu_\infty]_x$  - Local kinematic coefficient of viscosity, referred to the local free stream conditions, at the outer edge of boundary layer,  

$$\left[ \frac{ft^2}{sec} \right], \quad [\nu_\infty]_x = \left[ \frac{\mu_\infty}{\rho_\infty} \right]_x$$
- $[\nu_w]_x$  - Local Kinematic coefficient of viscosity, referred to the conditions at the body surface,  

$$\left[ \frac{ft^2}{sec} \right], \quad [\nu_w]_x = \left[ \frac{\mu_w}{\rho_w} \right]_x$$
- $\rho$  - Fluid density,  

$$\left[ \frac{slug}{ft^3} \right]$$
- $[\rho_\infty]_x$  - Local air density at the outer edge of the boundary layer,  

$$\left[ \frac{slug}{ft^3} \right] \text{ or } \left[ \frac{lb\ sec^2}{ft^4} \right]$$
- $[\rho_w]_x$  - Local air density at the body surface,  

$$\left[ \frac{slug}{ft^3} \right] \text{ or } \left[ \frac{lb\ sec^2}{ft^4} \right]$$
- $\tau_w$  - Local shear stress at the body surface,  

$$\left[ \frac{lb}{ft^2} \right], \quad \tau_w = \mu_w \left| \frac{\partial u}{\partial y} \right|_{y=0}$$
for two-dimensional laminar conditions at the surface,
- $\psi$  - A dimensionless quantity, functionally presented in Fig. ( 22 ) in terms of  

$$\left( \frac{VA}{V_m} \right) \sin \theta$$
- $\phi$  - A function of the molecular speed ratio (S) and the angle of incidence of the impinging stream ( $\theta$ ),  

$$\phi(S, \theta) = \frac{e^{-S^2}}{\sqrt{\pi} S_V (1 + \text{erf } S_V)}$$

## II. SUBSCRIPTS

- A - Refers to the ambient standard atmosphere conditions.
- a - Refers to aerodynamic aspects.
- i - Refers to impinging molecular stream.
- i - Refers to internal conditions.
- L - Refers to the characteristic length of the body geometry in question.
- o - Refers to standard atmosphere conditions at sea level.
- r - Refers to radiation into ambient.
- r - Refers to re-emitted molecular stream.
- s - Refers to the stagnation point conditions.
- s - Refers to radiation from ambient (Solar).
- w - Refers to the conditions at the body surface.
- x - Refers to the local conditions at a given section along the body surface.

- $\infty$  - Refers to the local free stream conditions just outside the boundary layer.
- $\delta$  - Refers to the boundary layer thickness.
- 1,2,3,4 - Refers to various surfaces on a general diamond-shape two-dimensional airfoil section.
- 1 - Denotes some free stream (reference station 1) value of a physical quantity.
- ad - Denotes adiabatic flow conditions.
- b - Denotes rear face of a surface (not directly incident to the oncoming stream).
- CYL - Refers to a circular cylinder.
- DIFF - Denotes completely diffuse molecular reflection.
- EM - Refers to radiation emission from the body.
- f - Denotes front incident face of a surface.
- FP - Refers to a flat plate.
- i - Denotes conditions at the impinging (on-coming) molecular stream.
- IN - Refers to radiation input to the body (from outer boundary).
- INT - Denotes internal (rotational + vibrational) degrees of molecular freedom in a flowing gas.
- r - Denotes conditions at the reflected or re-emitted molecular stream.
- s - Denotes conditions at the fluid layer directly in contact with the washed surface (or wall).
- SPEC - Denotes completely specular molecular reflection.
- TR - Denotes translational degrees of molecular freedom in a flowing gas, only.
- w - Denotes conditions of the solid wall proper.
- x,y - Denotes dimensional partial derivative operations, respectively.
- x',y' - Denotes dimensionless partial derivative operations, respectively.

### III. SUPERSCRIPTS

- ' - Denotes a dimensionless form of a physical variable.
- ' - Alternatively denotes the individual fluctuating velocity components of a molecule, in excess of the respective mean average velocity component values.
- ' - Alternatively denotes energy flux, to distinguish from energy content.

- ' - Denotes a nondimensionalized physical quantity.
- ' - Alternatively denotes number of molecules per unit area per unit time, in order to distinguish it from the respective number of molecules per unit volume per unit time (no superscript).
- ' - Alternatively denotes local value of the aerodynamic coefficients.
- ' - Alternatively denotes modified values of the local recovery factor ( $r'$ ) and the local Stanton Number ( $S_1'$ ).
- " - Denotes a physical quantity referred to an infinitesimal surface area ( $dA$ ).
- - Denotes mean average value of a physical quantity.

## 2.4 SKIN-FRICTION DRAG COEFFICIENT ANALYSIS ON A PRESCRIBED TRAJECTORY, INCLUDING RAREFIED GAS EFFECTS

A high-speed, high-altitude missile flight history, including the launch, the atmospheric reentry and the target-approach phases, generally can be subdivided into four basic flow regimes, see Section 1.7:

1. Continuum flow regime,

$$\frac{\bar{\lambda}}{\delta} = Kn_{\delta} \sim \frac{M}{(Re_L)^{1/2}} < 10^{-2}, Re_L \gg 1, \quad (2.4-1)$$

2. Slip flow regime,

$$10^{-2} < \frac{\bar{\lambda}}{\delta} = Kn_{\delta} \sim \frac{M}{(Re_L)^{1/2}} < 10^{-1}, Re_L > 1, \quad (2.4-2)$$

3. Transitional flow regime,

$$10^{-1} < \frac{M}{(Re_L)^{1/2}} \text{ UP TO } \frac{M}{Re_L} < 3, \quad (2.4-3)$$

4. Free-molecule flow regime,

$$\frac{Kn_L}{Re_L} > 3. \quad (2.4-4)$$

The momentum, mass and energy transfer mechanisms in each of the four

characteristic regimes are intrinsically different, and the resulting analytical expressions for skin-friction drag and pressure drag coefficients are consequently obtained by respectively varied analytic methods.

The fundamental physical aspects of the continuum flow regime and the respective skin-friction drag force analysis methods are presented in Section 2.3 for steady or quasi-steady flow conditions restrictively. In this Section, the skin friction phenomena are considered in a broader sense, as they actually occur on a prescribed trajectory, i.e., in terms of the transient characteristics due to a generally accelerated flight time history and including the high altitude atmospheric rarefaction effects. Therefore, the basic features of the rarefied gas flows are briefly stated first, in as much as they are needed for the aerodynamic drag force estimates, including the normal pressure coefficient expressions, which shall be needed later for the pressure drag force analysis in Sections 2.5 and 2.6. The material should be treated as an extension and modification of the fundamental concepts from Sections 1.7, 2.2 and 2.3.

## 2.4.1 FREE MOLECULE FLOW REGIME

### Basic Reference Works:

Knudsen	(Ref. 2.4-1 and 2.4-2)	}	for low speed flows
Smoluchowski	(Ref. 2.4-3)		
Sanger	(Ref. 2.4-4)	}	for high speed flows
Tsien	(Ref. 2.4-5)		
Ashley	(Ref. 2.4-6)		
Stalder	(Ref. 2.4-7 and 2.4-8)		
Oppenheim	(Ref. 2.4-9)		
Shaaf	(Ref. 2.4-10)		
Epstein	(Ref. 2.4-11)		
Maxwell	(Ref. 2.4-13)		

Under the extremely rarefied conditions ( $Kn > 3$ ), the internal mechanism of the simplified monoatomic molecular model (see Section 2.2.5), is changed as follows:

Due to appreciably increased free molecular distances (or low densities), the frequency of molecular collisions within the control space volume,  $d\tau$ , becomes negligibly small, although the number of molecules contained in  $d\tau$  is still retained to be sufficiently large, allowing for a subsequent statistical mean-averaging procedure, which leads to determination of the bulk matter physical properties ( $\rho, \rho, T$ ). As a consequence, when the mean free molecular path,  $\lambda$ , is greater than the characteristic solid surface dimension,  $L$ , the stream of incident molecules is reflected from the solid surface without experiencing any appreciable effect due to very few (or none) intermolecular collisions. This automatically leads to disappearance of the boundary layer and the bow shock wave concepts, and the interaction between the free molecular stream and the solid surface can be investigated on the basis of the Maxwellian velocity distribution laws, see Section 2.2.5.

#### (i) Mass, Momentum and Energy Transfer in Rarefied Free Molecule Flows.

##### General Assumptions:

A monoatomic molecular model is assumed, having translational degrees of freedom only, with partial conceptual modifications as pointed out above.

Immersed surfaces are at a uniform, constant temperature,  $T_w$ , moving steadily relative to a macroscopically uniform gas at rest, extending to infinity, or vice versa.

The gas is in a condition of extreme rarefaction, the mean free molecular path being several times the characteristic body length.

The interaction between the impinging stream of molecules and the immersed surface is completely independent of the intermolecular collisions ( $\bar{\lambda} > L$ ), i.e., the body presence is not felt by the oncoming stream of molecules: the molecular random motion proceeds unaffected by body presence. The molecules that individually collide with the solid surface are temporarily trapped, and then re-emitted, i.e., the time histories of motion of the incident and the rebounded molecules are mutually independent.

##### Consequences:

Since ( $\bar{\lambda} > L$ ) it is valid to neglect the effect of the re-emitted particles on the incident stream, or vice versa,

in the vicinity of body.

No shock waves are formed, nor is there any aerodynamic interference effects between various sections of the body geometry.

The boundary layer concept from the classical continuum flow theory is absent.

The impinging molecules shall follow the Maxwellian velocity distribution law for gases at rest, or for isentropic gas flows (if an observer is at the body). The Maxwellian velocity distribution function corresponds to a temperature,  $T_i$ , of the isentropic impinging stream (ambient atmospheric temperature).

In the time interval in which the impinging molecules are trapped in the microscopic crevices at the surface, a thermal accommodation process is effected, since ( $T_i \neq T_w$ ) in general. The accommodation can be partial, i.e., some temperature difference ( $T_w - T_i$ ) results, or total ( $T_i = T_w$ ), depending upon the time interval during which the molecule is trapped, and the general surface conditions.

The re-emitted molecules are then consequently treated as being either partially ( $T_r \neq T_w$ ) or totally ( $T_r = T_w$ ) diffusely reflected, where  $T_r$  is the temperature of the reflected stream of molecules. Thus, the diffusely re-emitted molecules shall have random motions represented by a changed velocity distribution function, corresponding to the temperature ( $T_r$ ), i.e., as if they were issuing from a gas at rest apparently on the other side of the surface having the temperature ( $T_r$ ), see Figs. (2.4-1), (2.4-2) and (2.4-3).

The independence of motion of the impinging and of the reflected molecules means that the respective mass, momentum and energy transfer processes can be treated separately for the two molecular motions.

#### Assumptions regarding the momentum and the energy transport mechanisms.

The determination of the momentum and the energy transfer in the free molecule flow of rarefied gases requires a specification of the interaction mechanism between the impinging particles and the body surface, i.e., a specification of the type or the degree of diffusive re-emittance of the temporarily trapped molecules at the body surface.

This thermal interaction phenomena can be suitably defined by the following two average parameters, introduced by Smoluchowski(3), Knudsen(2), Maxwell(13), and further experimentally elaborated by Herzfeld(14), Wiedemann(15) and others:

(1) The thermal accommodation coefficient,  $\alpha$ .

$$\alpha = \frac{d\bar{E}_i' - d\bar{E}_r'}{d\bar{E}_i' - d\bar{E}_w'} \quad (2.4-5)$$

characterizing the thermal interaction mechanism for the energy transfer investigations, i.e., the degree in which the internal molecular energy of the re-emitted molecules (subscript  $r$ ) is "accommodated" to what it could be if the reflected molecules would possess the energy amount  $d\bar{E}_w'$  (total diffusion), where:

$d\bar{E}_i'$  AND  $d\bar{E}_r'$  - are the mean average internal energy fluxes of the incident ( $i$ ) and the re-emitted ( $r$ ) molecules from a differential surface element,  $dA$ , per unit time.

$d\bar{E}_w'$  - is the mean internal energy flux that would be possessed by the re-emitted molecules if all the impinging molecules were re-emitted (no absorption case) with a modified Maxwellian velocity distribution function, (see Ref. 2.4-12), corresponding to the surface temperature  $T_w$ .

$\alpha=1$  means a perfect accommodation ( $d\bar{E}_r' = d\bar{E}_w'$ ), or a complete diffusive re-emittance of molecules.

$\alpha=0$  represents a completely isentropic (specular) reflection ( $d\bar{E}_r' = d\bar{E}_i'$ ), see Section 1.7.

For polyatomic and diatomic molecular models, the average molecular energy comprises contributions of all active degrees of freedom (translational and rotational, see Section 1.7), and it is assumed that all the energetic degrees of the random molecular motion are accommodating in the same degree of thermal intensity. This is approximately correct for translational and rotational degrees, while the vibrational energetic modes participate but little in the energy exchange during the molecule-surface collisions. Some experimental values of the thermal accommodation coefficient are presented in Table 2.4-1. Other data

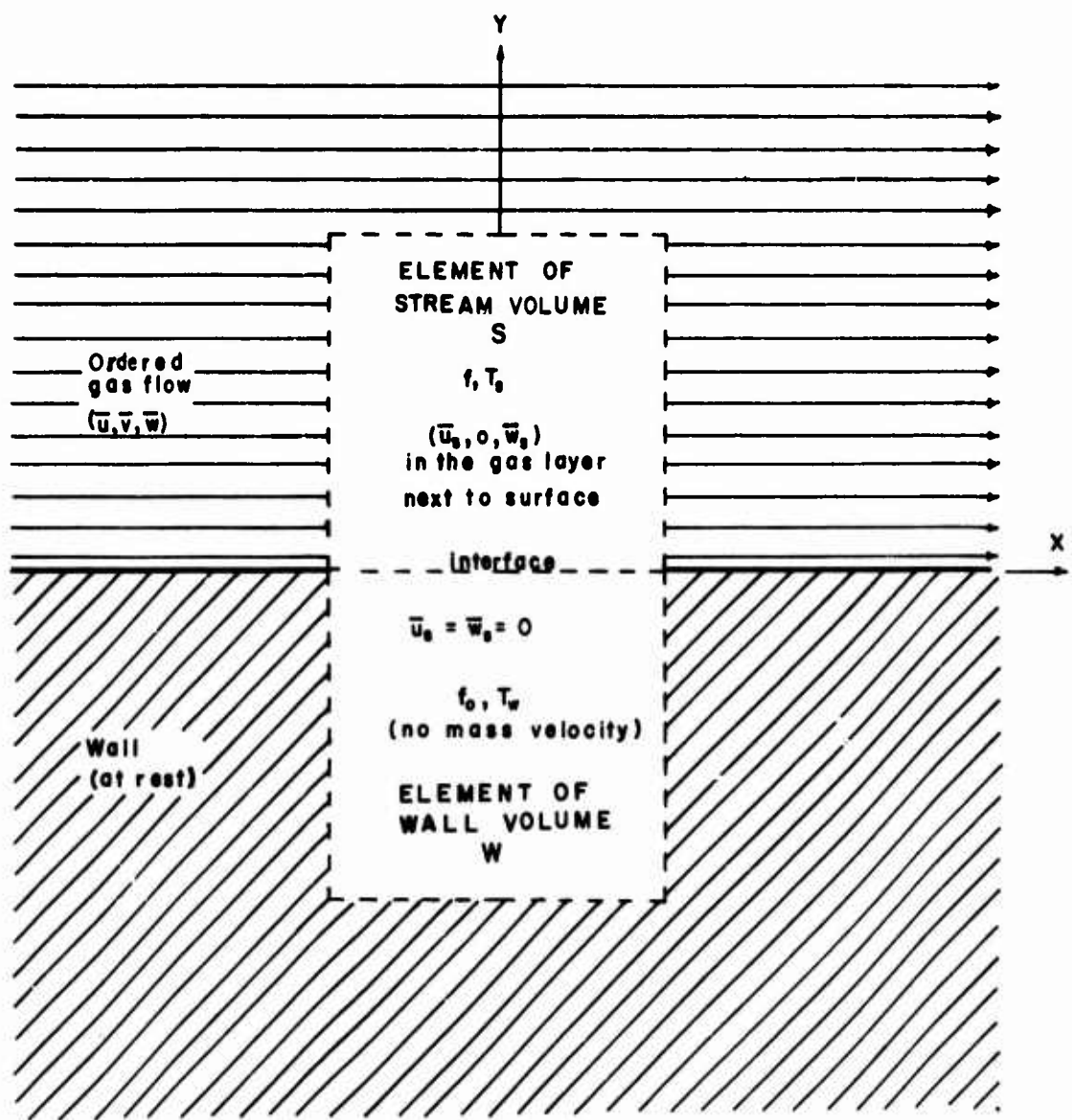


FIG. (2.4-1) MATHEMATICAL MODEL OF THE DIFFUSE MOLECULAR REFLECTION. (REF. 2.4-12)



FREE MOLECULE FLOW  
(RAREFIED GASES)

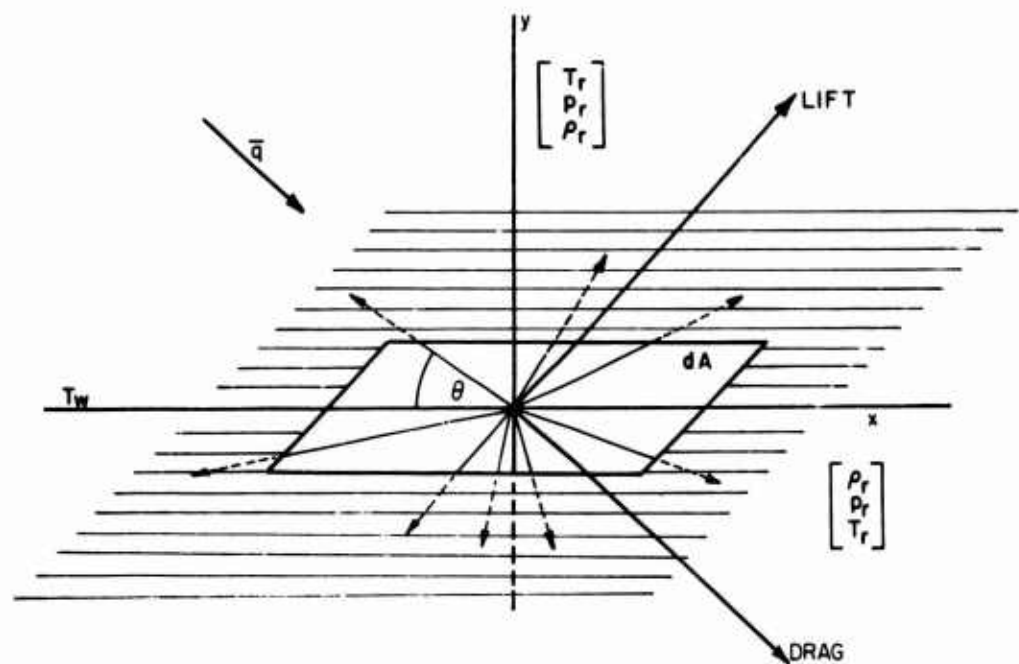


FIG.(2.4-3) REFLECTION OF FREE MOLECULES (REF. 2.4-12)  
(NON-ISENTROPIC)

Table (2.4-1) Thermal accommodation coefficient  $\alpha$  for air (Ref. 2.4-15)

Surface	$\alpha$
Flat lacquer on bronze	0.88-0.89
Polished bronze	0.91-0.94
Machined bronze	0.89-0.93
Etched bronze	0.93-0.95
Polished cast iron	0.87-0.93
Machined cast iron	0.87-0.88
Etched cast iron	0.89-0.96
Polished aluminum	0.87-0.95
Machined aluminum	0.95-0.97
Etched aluminum	0.89-0.97

Table (2.4-2) Values of reflection coefficient  $\sigma$  (Ref. 2.4-16)

Gas and surface combination	$\sigma$
Air or CO <sub>2</sub> on machined brass or old shellac	1.00
Air on oil	0.895
CO <sub>2</sub> on oil	0.92
H <sub>2</sub> on oil	0.93
Air on glass	0.89
He on oil	0.87
Air on fresh shellac	0.79

can be found in Ref. (2.4-17) to (2.4-20).

(2) The parameter of a partially diffuse re-emittance;  $\sigma$ .

For the momentum transfer analysis of the re-emitted molecules, it is assumed that only a fraction,  $\sigma$ , of the incident molecules is reflected diffusely, (i.e., after being trapped temporarily at the surface), while the rest  $(1-\sigma)$  of the incident molecules are reflected specularly (see Section 1.7 and Fig (2.4-4).

A pure diffuse reflection means that the impinging molecules are first temporarily trapped at the surface, losing their total incident momentum, and then re-emitted with a modified Maxwellian velocity distribution at a temperature  $T_r$  different from both  $T_i$  and  $T_w$  in general, see Figs (2.4-1) and (2.4-3).

According to Hurlbert<sup>(21)</sup>, the re-

flection pattern of air molecules from engineering surfaces is more complex and cannot be adequately represented in the above idealized ways. Instead, to discriminate the normal and the tangential momentum transfer effects, it seems necessary to assume a mathematical reflection model in which two fractional coefficients,  $\sigma'$  and  $\sigma$ , should be introduced, analogous to the above definition:

$$\sigma = \frac{T_i - T_r}{T_i - T_w} \quad , \quad (\tau_w = 0) \quad , \quad (2.4-6)$$

$$\sigma' = \frac{p_i - p_r}{p_i - p_w} \quad , \quad (2.4-7)$$

where:

$r$  - is the tangential momentum component,

$p$  - is the normal momentum component,

A specular reflection means that the tangential velocity component remains unchanged, while the normal velocity

component is reversed, effecting a normal momentum transfer, see Fig. (2.4-4).

Fig (2.4-4) see Fig. (2.2-7) (Ref. 2.4-12)

- the subscripts (i) and (r) refer to the incident and the reflected molecular fluxes,

- the subscript (w) refers to the molecules re-emitted from the surface with a Maxwellian velocity distribution, corresponding to the surface temperature  $T_w$ .

On the basis of the  $\alpha$ ,  $\sigma$ , and  $\sigma'$  definitions, the following limiting cases are theoretically possible:

$\alpha=1$  - results in  $T_r = T_w$ , indicating a perfect thermal accommodation of those re-emitted molecules, which have been necessarily trapped at the surface crevices for a sufficiently long time interval. Such molecules are then re-emitted diffusely, having  $\sigma=1$  and  $\sigma'=1$ . Nevertheless, notice that  $T_i \neq T_r = T_w$  in general.

$\alpha=0$  - results in  $T_i = T_r$ , indicating no thermal accommodation, i.e., such molecules are re-emitted specularly, having  $\sigma=0$  and  $\sigma'=0$ , i.e., the surface is considered perfectly smooth and insulated. The special case of a generally noninsulated perfectly smooth surface can be conceived under the circumstances also, provided the collision time interval is taken (in a limit) to approach zero. The specular reflection results in a reversal of the normal momentum component and a preservation of the tangential momentum component of the impinging molecular stream. No skin-friction is possibly present.

$\sigma=1$  - represents a completely diffuse reflection of the reemitted molecular stream, with a temperature  $T_r \neq T_w \neq T_i$  in general ( $0 < \alpha < 1$ ). If  $\alpha=1$ , indicating a perfect thermal accommodation,  $T_r = T_w \neq T_i$ . If  $\alpha=0$ , indicating no thermal accommodation,  $T_r = T_i \neq T_w$ , which would represent an insulated rough surface, reemitting the trapped molecules completely diffusely without a thermal accommodation whatsoever. By the definition (2.4-6), the  $\sigma=1$  condition implies  $r_r = 0$ , i.e., no resultant frictional force of the reemitted molecular stream, which, emerging completely diffusely, has no resultant velocity of ordered motion.

$\sigma'=1$  - denotes similarly a completely diffuse reemittance of the trapped molecules, having  $p_r = p_w \neq p_i$ , see Eq (2.4-7). The additional thermal conditions of  $\alpha=1$  and  $\alpha=0$  indicate  $T_r = T_w \neq T_i$  for a non-insulated surface,

and  $T_r = T_w = T_i$  for an insulated surface respectively.

$\sigma=0$  - represents a completely specular reflection, indicating  $r_r = r_i$ , i.e., the preservation of the tangential momentum components of the ordered motion of the impinging and the reflected molecular streams. The thermal accommodation coefficient is  $\alpha=0$  necessarily, specifying  $T_r = T_i$  for a smooth, insulated surface, and  $T_i = T_r \neq T_w$  for a smooth, non-insulated surface.

$\sigma'=0$  - denotes a completely specular reflection with a completely elastic reversal of the normal momentum component of the impinging molecular stream,  $p_i = p_r$ . The accommodation coefficient is  $\alpha=0$  necessarily, indicating  $T_i = T_r$  for an insulated, smooth surface, and  $T_i = T_r \neq T_w$  for a non-insulated smooth surface.

Obviously, a number of intermediate combinations of ( $0 < \alpha < 1$ ), ( $0 < \sigma < 1$ ) and ( $0 < \sigma' < 1$ ) can appear, denoting partially specular, partially diffuse reflections with  $T_i \neq T_w \neq T_r$  in general. In the proceeding analytical expressions for the drag force coefficient values, only four distinct cases are considered:

(a) A completely specular reflection from a smooth, insulated surface:

$$\alpha = \sigma = \sigma' = 0, \quad T_i = T_r, \quad (2.4-8)$$

(b) A completely diffuse reflection from a microscopically rough insulated surface:

$$\sigma = \sigma' = 1, \quad \alpha = 0, \quad T_i = T_r, \quad (2.4-9)$$

(c) A completely diffuse reflection from a microscopically rough, non-insulated surface:

$$\sigma = \sigma' = 1, \quad \alpha = 1, \quad T_r = T_w \neq T_i \quad (2.4-8a)$$

(d) A partially diffuse, partially specular reflection from a real non-insulated surface with a complete thermal accommodation:

$$0 < \sigma < 1, \quad 0 < \sigma' < 1, \quad \alpha = 1 \quad (2.4-9a)$$

$$T_r = T_w \neq T_i.$$

(3) Expressions for the number of impinging and the number of re-emitted molecules (12)

Fixing the reference coordinate system to the body surface, the total number of impinging molecules per unit volume is (see Fig 2.4-2):

$$n'_i = n_i \left( \frac{RT_i}{2\pi} \right)^{\frac{1}{2}} \left[ e^{-S_v^2} + S_v \sqrt{\pi} (1 + \text{erf } S_v) \right], \quad (2.4-10)$$

where:

$n'_i$  - is the total number of impinging molecules per unit area per unit time,

$n_i$  - is the number of impinging molecules per unit volume per unit time,

$S \sin \theta = S_v = \bar{v} \sqrt{\beta} = \frac{\bar{v}}{C_{m_i}}$  - is the ratio of the component of mass velocity normal to the surface to the most probable speed of the incident molecules,

$S = \frac{\bar{q}}{C_{m_i}} = \sqrt{\frac{Y}{2}} M_i$  - is the speed ratio in free molecule flow,

$\bar{v}$  - is the mean average normal velocity component of the ordered motion, or the normal (to the surface) velocity component of the surface moving relatively with respect to a gas at rest,

$\bar{q}$  - is the mean average speed of the ordered mass motion, or the speed of the surface moving relatively with respect to a gas at rest,  $\bar{q} = (\bar{u}^2 + \bar{v}^2 + \bar{w}^2)^{1/2}$ ,

$C_{m_i}$  - is the most probable speed of the random motion of the impinging molecules, see Section 1.7,

$M_i$  - is the random motion type of Mach Number,

$\theta$  - see Fig (2.4-2).

The total number of diffusely reflected molecules per unit area per unit time is found independently on the basis of the introduced assumptions, i.e., as if the "apparent gas" at the reverse side of the surface were at rest with a different temperature,  $T_r$ , and as if it were escaping through an equivalent aperture freely, (see Fig 2.4-3):

$$n'_r = n_r \sqrt{\frac{RT_r}{2\pi}}, \quad (2.4-11)$$

where the subscript ( , ) stands for the "reflected", and the ( $n'_r$ ) and ( $n_r$ ) symbols have the same respective meanings

as specified for the impinging molecules.

(4) The conservation of mass principle requires that:

$n'_i = n'_r$ , per unit area per unit time, i.e.,

$$n_r = n_i \sqrt{\frac{T_i}{T_r}} \left[ e^{-S_v^2} + S_v \sqrt{\pi} (1 + \text{erf } S_v) \right], \quad (2.4-12)$$

per unit volume per unit time.

(ii) The Momentum Transfer

(a) The local (superscript ' ) normal pressure coefficient,  $C_p'$ , on the surface is found as the sum of the momenta of the impinging molecules just prior to their impact, and the sum of normal momenta of the diffusely escaping molecules, supposedly emerging from the reverse side of the surface:

$$C_p' = \frac{p}{\frac{1}{2} \rho_i \bar{q}^2}, \quad (2.4-13)$$

$$C_p' = C_{p_i}' + C_{p_r}' = \sin^2 \theta \left[ \frac{1}{S_v} \left( \frac{1}{\sqrt{\pi}} + \frac{1}{2S_v} \sqrt{\frac{T_r}{T_i}} \right) e^{-S_v^2} + \left( 1 + \frac{1}{2S_v^2} + \frac{\sqrt{\pi}}{2S_v} \left( \frac{T_r}{T_i} \right) (1 + \text{erf } S_v) \right) \right] = f \left( \frac{T_r}{T_i}, \theta \right), \quad (2.4-14)$$

Specifically, for bodies at rest, ( $\bar{q}=0$ ) and ( $T_r=T_i$ ),

$$p = p_i + p_r = \rho_i R T_i, \quad \text{if } T_r = T_i. \quad (2.4-15)$$

In general, the local normal pressure coefficient depends on the temperature ratio,  $T_r/T_i$ , and the inclination,  $\theta$ , of the surface relative to the velocity vector of the ordered motion,  $\bar{q}$ , and is independent of the Knudsen Number, provided  $Kn > 3$ .

(b) The local shearing stress,  $\tau_w$ , and the local coefficient of skin friction,  $C_f'$ , in free molecule flows are found on the supposition that the impinging molecules are temporarily trapped by the surface (a supposition permitting for a successive diffusive reflection concept), which means that the impinging molecules lose all their tangential momentum on contact with the

surface, yielding:

$$\frac{T_w}{\frac{1}{2} \rho_i \bar{q}_i^2} = C_f = \quad (2.4-16)$$

$$= \sin \theta \cos \theta \left[ \frac{1}{\sqrt{\pi} S_v} e^{-S_v^2} + 1 + \operatorname{erf} S_v \right]$$

$$\text{For } \theta = 0, C_f = \frac{1}{S_v \sqrt{\pi}} \quad (2.4-17)$$

The diffusely reflected molecules do not contribute anything to the skin friction, since they have no preference regarding individual direction of emergence (complete diffusion).

### (iii) The Internal Energy Transfer

The presumed monoatomic molecules convey the total internal energy per unit time per unit area to and from the surface, the total energy content corresponding to their translational degrees of freedom only(12):

$$\bar{E}' = \bar{E}_i' - \bar{E}_r' \quad (2.4-18)$$

$$\bar{E}_i' = \frac{1}{2} m n_i' \left[ \bar{q}_i'^2 + RT_i \left( 4 + \frac{1}{\phi + 1} \right) \right] \quad (2.4-19)$$

where

$$\phi(S, \theta) = \frac{e^{-S_v^2}}{\sqrt{\pi} S_v (1 + \operatorname{erf} S_v)} \quad (2.4-20)$$

and

$$\bar{E}_r' = \sqrt{\frac{2}{\pi}} \rho_r (RT_r)^{3/2} = 2 m n_r' RT_r \quad (2.4-21)$$

or, with  $n_i' = n_r'$ ,

$$\bar{E}_r' = \sqrt{\frac{2}{\pi}} \rho_i RT_r (RT_i)^{1/2} \left[ e^{-S_v^2} + \sqrt{\pi} S_v (1 + \operatorname{erf} S_v) \right] \quad (2.4-22)$$

For a completely diffuse reflection ( $T_r = T_w$ ):

$$\bar{E}_r' = \bar{E}_w' = 2 m n_i' RT_w =$$

$$= \sqrt{\frac{2}{\pi}} \rho_i RT_w (RT_i)^{1/2} \left[ e^{-S_v^2} + \sqrt{\pi} S_v (1 + \operatorname{erf} S_v) \right] \quad (2.4-23)$$

In general(22) for polyatomic molecular structures, the energy flux,  $d\bar{E}_i'$ , of the impinging molecules and the energy flux,  $d\bar{E}_w'$  or  $d\bar{E}_r'$  of the re-emitted molecules (both fluxes referred to a surface element,  $dA$ , inclined at an angle,  $\theta$ , with respect to the oncoming stream,  $\bar{q}_i$ , can

be broken into two components:

$[d\bar{E}_i']_{TR}$  or  $[d\bar{E}_r']_{TR}$  - due to the translational degrees of molecular motion,

$[d\bar{E}_i']_{INT}$  or  $[d\bar{E}_r']_{INT}$  - due to the internal (rotation and vibration) degrees of molecular motion.

Then, according to Stalder and Jukoff(7), the convective heat,  $dQ$ , removed from the surface element,  $dA$ , per unit time is:

$$dQ = d(d\bar{E}_i' - d\bar{E}_w') \quad (2.4-24)$$

where

$$\alpha = \frac{d\bar{E}_i' - d\bar{E}_r'}{d\bar{E}_i' - d\bar{E}_w'} \sim 1.0 \quad (2.4-25)$$

$$d\bar{E}_i' = [d\bar{E}_i']_{TR} + [d\bar{E}_i']_{INT} \quad \text{etc.} \quad (2.4-26)$$

Then, on the basis of previous results, the Eq (2.4-19) can be alternatively expressed as(22):

$$[d\bar{E}_i']_{TR} = \rho RT_i \left( \frac{RT_i}{2\pi} \right)^{1/2} \left[ (S^2 + 2) e^{-S_v^2} + \sqrt{\pi} (S^2 + \frac{3}{2}) S_v (1 + \operatorname{erf} S_v) \right] dA$$

and

$$[d\bar{E}_i']_{INT} = N_{INT} \frac{mRT}{2} n_i'' \quad (2.4-28)$$

where:

$N_{INT} \approx \frac{5-\gamma}{\gamma-1}$  - is the approximate number of internal degrees of freedom,

$n_i''$  - is the number of molecules impinging on the surface element,  $dA$ , per unit time,

$$n_i'' = \frac{\rho}{m} \left( \frac{RT_i}{2\pi} \right)^{1/2} \left[ e^{-S_v^2} + \sqrt{\pi} S_v (1 + \operatorname{erf} S_v) \right] dA \quad (2.4-29)$$

$m$  - is the molecular mass, (2.4-29)

$R$  - is the individual gas constant.

Similarly, assuming that the trapped molecules are reemitted from

the surface element,  $dA$ , in a Maxwellian equilibrium, corresponding to the wall temperature,  $T_w$ , with no macroscopic (ordered) velocity:

$$d\bar{E}'_w = (4 + N_{INT}) \frac{mRT_w}{2} n_w \approx \frac{\gamma+1}{2(\gamma-1)} mRT_w n_w, \quad (2.4-30)$$

where ( $n_w = n_f$ ) for steady states.

With the Eqs. (2.4-27), (2.4-28) and (2.4-30), the expression (2.4-24) becomes:

$$dQ = \alpha \rho RT_i \left( \frac{RT_i}{2\pi} \right)^{\frac{1}{2}} \left\{ \left( S^2 + \frac{\gamma}{\gamma-1} - \frac{\gamma+1}{2(\gamma-1)} \frac{T_w}{T_i} \right) \left[ e^{-S_v^2} + \sqrt{\pi} S_v (1 + \operatorname{erf} S_v) \right] - \frac{1}{2} e^{-S_v^2} \right\} dA \quad (2.4-31)$$

2.4.2 CONVECTIVE HEAT TRANSFER ESTIMATES FOR FLAT PLATES, CYLINDERS, AND SPHERES IN FREE MOLECULAR FLOWS

Basic References:

Oppenheim,	Ref. (2.4-23)
Stalder and others	Ref. (2.4-7), (2.4-8), (2.4-19)
Sauer,	Ref. (2.4-24)

(i) Fundamental assumption:

A monoatomic molecular model is assumed, possessing the translational degrees of freedom only. Consequently, the heat transfer is accomplished by convection exclusively (i.e., no radiation, conduction or internal vibrational and rotational modes are present).

Steady state equilibrium  $Q=0$ , and the convective heat transfer characteristics  $Q \neq 0$  to and from the body, are investigated, assuming constant temperature surface conditions. Surfaces are everywhere convex to gas stream, i.e., the possibility of molecular interaction is excluded.

Approximate constancy of the surface temperature can be realized only if the thermal conductivity of body materials is sufficiently large, and the heat flux to and from the body surface small enough.

(ii) Modified recovery factor and modified Stanton Number:

$$r' = \frac{T_r - T_i}{T_s - T_i} \frac{\gamma + 1}{\gamma}, \quad (2.4-32)$$

$$S_f' = \frac{Q}{A \bar{q}_i C_p (T_r - T_w)} \frac{\gamma}{\alpha(\gamma + 1)}, \quad (2.4-33)$$

where:

$T_r$  - is the temperature of the re-emitted molecular stream,

$T_i$  - is the temperature of the incident stream,

$T_s$  - is the stagnation temperature of the flow,  $T_s = T_i (1 + \frac{\gamma-1}{\gamma} S^2)$ , (2.4-34)

$S = \sqrt{\gamma/2} M_i$  - is the speed ratio in free molecule flow,

$A$  - is the total wetted surface area,

$\bar{q}_i = V_M$  - is the macroscopic (ordered motion) relative speed,

$T_w$  - is the temperature of the solid surface,

$\alpha$  - is the thermal accommodation coefficient.

(1) A flat plate, at an angle of incidence,  $\theta$ , both surfaces exposed to the gas flow and both surfaces in a perfect thermal contact with each other(12).

$$r' = \frac{1}{S^2} \left[ 2S^2 + 1 - \frac{1}{1 + \sqrt{\pi} S_v \operatorname{erf} S_v e^{S_v^2}} \right],$$

$$S_f' = \frac{1}{4\sqrt{\pi} S} \left[ e^{-S_v^2} + \sqrt{\pi} S_v \operatorname{erf} S_v \right], \quad (2.4-35)$$

$$S_v = S \sin \theta, \quad (2.4-37)$$

$A$  - is the total area of both sides.

(2) A flat plate at an angle of incidence,  $\theta$ , the upper and the lower surfaces completely insulated from each other, while both surfaces are exposed to the gas flow:

(a) For the surface directly exposed to the stream:

$$r' = \frac{1}{S^2} \left[ 2S^2 + 1 - \frac{1}{1 + \sqrt{\pi} S_v (1 + \operatorname{erf} S_v) e^{S_v^2}} \right], \quad (2.4-38)$$

$$S_f' = \frac{1}{4\sqrt{\pi} S} \left[ e^{-S_v^2} + \sqrt{\pi} S_v (1 + \operatorname{erf} S_v) \right], \quad (2.4-39)$$

$A$  - is the area of one side of plate.

(b) For the "shaded" surface of the flat plate: substitute,  $\theta$ , by  $(-\theta)$  in the Eqs. (2.4-38) and (2.4-39):

$$r' = \frac{1}{S^2} \left[ 2S^2 + 1 - \frac{1}{1 - \sqrt{\pi} S_v (1 - \operatorname{erf} S_v) e^{S_v^2}} \right], \quad (2.4-40)$$

$$S_i = \frac{1}{4\sqrt{\pi}S} \left[ e^{-S^2} - \sqrt{\pi} S_v (1 - \text{erf } S_v) \right] \quad (2.4-41)$$

(3) A right circular cylinder, with its axis normal to the flow ( $\bar{q}_i$ ):

$$r' = \frac{(2S^2+3) I_0(S^2/2) + (2S^2+1) I_1(S^2/2)}{(S^2+1)(I_0(S^2/2) + (S^2 I_1)(S^2/2))} \quad (2.4-42)$$

$$S'_i = \frac{e^{-S^2/2}}{4\pi} \left[ \frac{S^2+1}{S} I_0 \frac{S^2}{2} + S I_1 \frac{S^2}{2} \right] \quad (2.4-43)$$

where,

A - is the area of the cylinder side surface, the base areas not included,

$I_0$  and  $I_1$  - are the modified Bessel functions of the order (0) and (1) respectively:

$$I_0 = \frac{1}{\pi} \int_{-1}^1 \frac{e^{(1/2)S^2 x}}{\sqrt{1-x^2}} dx \quad (2.4-44)$$

$$I_1 = \frac{S^2}{2\pi} \int_{-1}^1 e^{1/2 S^2 x} \sqrt{1-x^2} dx \quad (2.4-45)$$

(4) A sphere:

$$r' = \frac{(2S^2+1) \left[ 1 + \frac{1}{S} \text{ierfc}(S) \right] + \frac{2S^2-1}{2S^2} \text{erf}(S)}{S^2 \left[ 1 + \frac{1}{S} \text{ierfc}(S) \right] + \frac{1}{2S^2} \text{erf}(S)} \quad (2.4-46)$$

$$S'_i = \frac{1}{8S^2} \left[ S^2 + S \text{ierfc}(S) + \frac{1}{2} \text{erf } S \right] \quad (2.4-47)$$

where,

$\text{ierfc}(S)$  - is the integrated complementary error function (see Ref. 2.4-25).

(iv) A graphical presentation of the results is given in Figs (2.4-5) and (2.4-6). For the free molecule flow conditions the recovery factor,  $r'$ , is always greater than unity, which means that, contrary to the continuum flow concept ( $r < 1$ ), the equilibrium temperature,  $T_r$ , in the free molecule flow is greater than the stagnation temperature,  $T_s$ , of the incident molecular stream. Further, the modified recovery factor,  $r'$ , and the equilibrium temperature,  $T_r$ , are independent of the thermal accommodation coefficient,  $\alpha$ , see Eq (2.4-32), which is true if

the heat transfer mechanism is accomplished by convection only. In the presence of convective, radiative and internal (rotational and vibrational) conductive heat transfer modes, the equilibrium temperature,  $T_r$ , and the modified recovery factor,  $r'$ , become functions of the thermal accommodation coefficient,  $\alpha$ , since in this case there is an inter-balance involved between the various modes of energy transfer in general.

For  $\alpha = \sigma = \sigma' = 0$  (specular reflection), the energy exchange by convection is non-existent.

(iii) An approximate evaluation of the temperature ratio ( $T_r/T_i$ ).

Assuming a constant surface temperature,  $T_w$ , and no radiation or internal conduction, the drag force coefficient in a free molecule flow depends upon the molecular speed ratio,

$$S = \sqrt{\frac{Y}{2}} M_i \quad (2.4-48)$$

and the temperature ratio,

$$\left( \frac{T_r}{T_i} \right) \quad (2.4-49)$$

provided the re-emittance of molecules is interpreted as completely diffuse (no average speed of ordered motion) and the molecular model is treated as monoatomic. These assumptions can serve as an acceptable engineering approach, since in most practical cases the thermal accommodation coefficient is near unity (see Table 2.4-1),

$$.9 < \alpha < 1.0 \quad (2.4-50)$$

allowing for the supposition of a completely diffuse  $\sigma = \sigma' = 1, \tau_r = 0$  molecular reflection. Neglecting radiation, the vibrational, dissociative and ionizing degrees of freedom for not-too-excessive temperatures are insignificant, and the contribution of internal rotational modes for polyatomic molecular structures can be eventually introduced into the picture through a corresponding choice of the ( $\gamma$ ) value in the equations (2.4-32) and (2.4-33). Then, using the graphical data for  $r'$ , from Fig (2.4-5), the important temperature ratio ( $T_r/T_i$ ) can be approximately acquired from the equations (2.4-32) and (2.4-34) as a function of the molecular speed ratio (S):

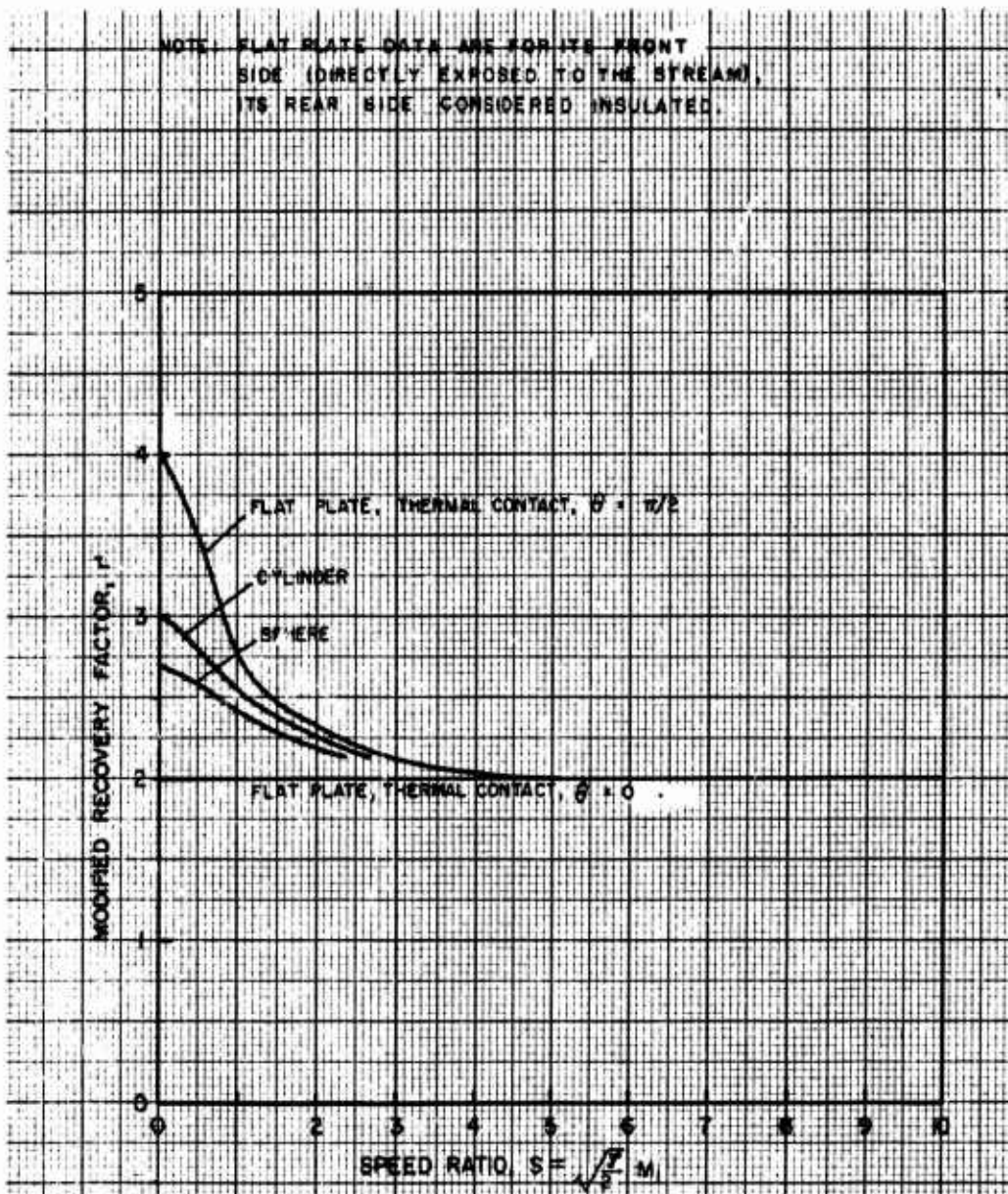


Fig. (2.4-5) Modified recovery factor in free molecule flow. (Ref.2.4-22)  
(Convective heat transfer)

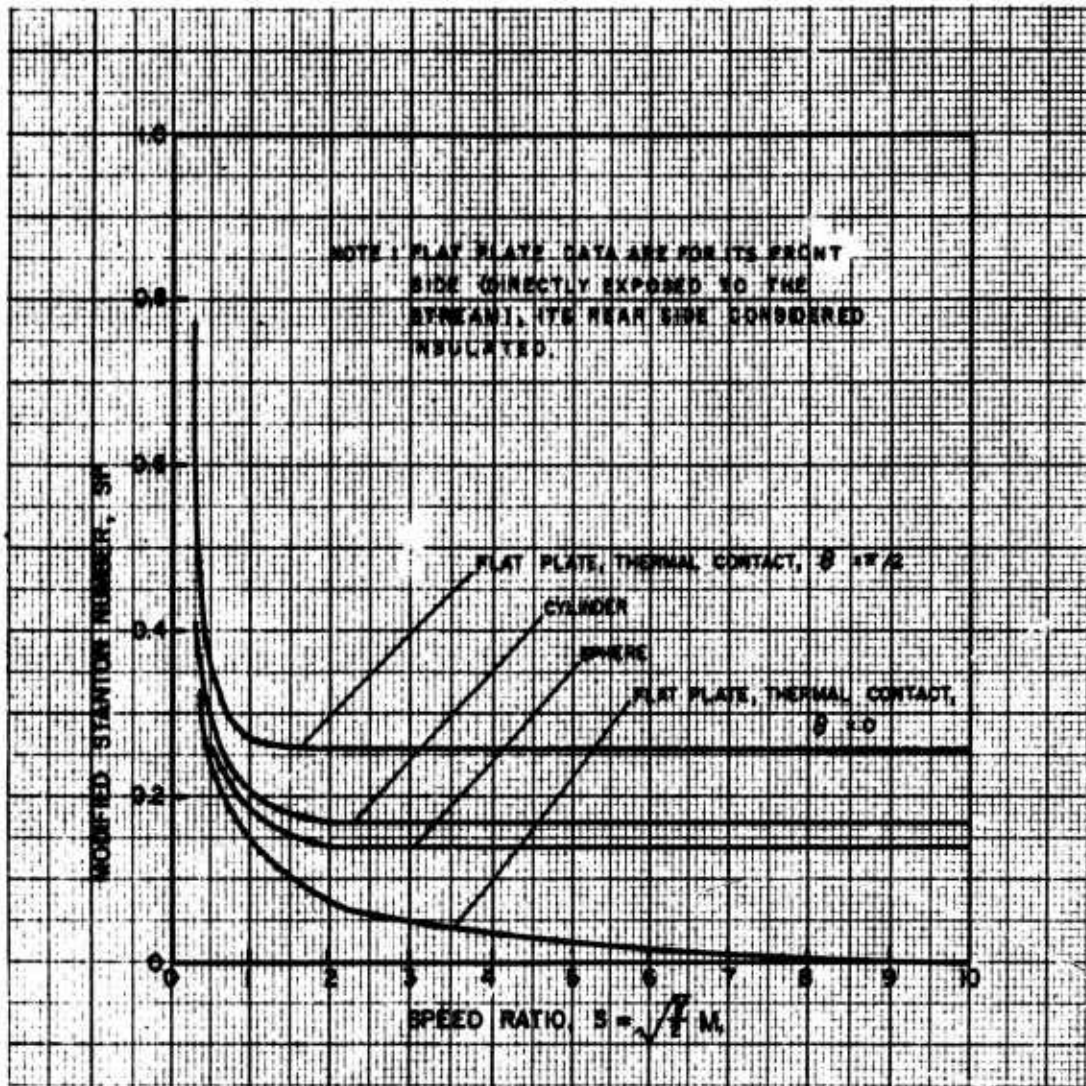


Fig. (2.4-6) Modified Stanton Number in free molecule flow. (Ref. 2.4-22)  
(Convective heat transfer)

$$\frac{T_r}{T_i} = 1 + r' \frac{\gamma-1}{\gamma+1} S^2 \quad (2.4-33)$$

A more general method of evaluating the  $(T_r/T_i)$  temperature ratio shall require use of the Eq (2.4-31).

### 2.4.3 DRAG FORCE IN FREE MOLECULE FLOW-DEFINITIONS

#### (i) General aerodynamic force expressions.

The local aerodynamic force,  $dF$ , acting on a surface element,  $dA$ , in a free molecule flow, is

$$dF = dF_i + dF_r, \quad (2.4-51)$$

where,

$dF_i$  - is the force component due to incident molecules,

$dF_r$  - is the force component due to re-emitted molecules.

In terms of stresses:

$$\frac{dF}{dA} = p_i + \tau_i + p_r + \tau_r, \quad (2.4-52)$$

where,

$p_i$  - is the normal stress (pressure) due to impinging molecules,

$p_r$  - is the normal stress (pressure) due to re-emitted molecules,

$\tau_i$  and  $\tau_r$  - are the tangential stresses (shears) due to impinging and re-emitted molecules respectively.

Explicitly(12), for the case of ( $0 < \sigma < 1$ ,  $0 < \sigma' < 1$ ,  $\alpha = 1$ ):

$$p_i = \frac{\rho_i \bar{q}_i^2}{2\sqrt{\pi} S} \left[ S_v e^{-S_v^2} + \sqrt{\pi} \left( \frac{1}{2} + S_v^2 \right) (1 + \text{erf } S_v) \right], \quad (2.4-53)$$

$$\tau_i = - \frac{\rho_i \bar{q}_i^2 \cos \theta}{2\sqrt{\pi} S} \left[ e^{-S_v^2} + \sqrt{\pi} S_v (1 + \text{erf } S_v) \right], \quad (2.4-54)$$

$$p_r = (1 - \sigma') p_i + \sigma' p_w, \quad (2.4-55)$$

$$\tau_r = (1 - \sigma) \tau_i, \quad (2.4-56)$$

i.e., the total local pressure,  $p$ , and the total local shearing stress,  $\tau$ , are:

$$p = p_i + p_r = (2 - \sigma') p_i + \sigma' p_w, \quad (2.4-57)$$

$$\tau = \tau_i - \tau_r = \sigma \tau_i, \quad (2.4-58)$$

where,

$p_w$  - is the pressure exerted by molecules leaving the surface with no macroscopic velocity (fraction  $\sigma'$  of molecules completely diffusely re-emitted), i.e., in a Maxwellian equilibrium ( $\alpha = 1$ ) at a temperature,  $T_w = T_r \neq T_i$ :

$$p_w = \frac{1}{2} m \sqrt{2\pi R T_w} n_i'', \quad (2.4-59)$$

$n_i''$  - see Eq.(A-541).

Thus, the general forms for total local pressure and local shear forces are:

$$p = \frac{\rho_i \bar{q}_i^2}{2 S^2} \left\{ \left[ \frac{2 - \sigma'}{\sqrt{\pi}} S_v + \frac{\sigma'}{2} \left( \frac{T_w}{T_i} \right)^{1/2} \right] e^{-S_v^2} + \left[ (2 - \sigma') \left( S_v^2 + \frac{1}{2} \right) + \frac{\sigma'}{2} \left( \frac{\pi T_w}{T_i} \right)^{1/2} S_v \right] (1 + \text{erf } S_v) \right\}, \quad (2.4-60)$$

$$\tau = - \frac{\sigma \rho_i \bar{q}_i^2 \cos \theta}{2\sqrt{\pi}} \left[ e^{-S_v^2} + \sqrt{\pi} S_v (1 + \text{erf } S_v) \right]. \quad (2.4-61)$$

The total aerodynamic force is obtained by integrating the above expressions. In general,

$$F = F(T_w, \sigma, \sigma').$$

## 2.4.4 DRAG FORCE IN FREE MOLECULAR FLOW REGIME--SIMPLE BODY GEOMETRIES

### Simplifying Assumptions

(1) A uniform surface temperature,  $T_w$ , equal to the free stream temperature,  $T_i = T_\infty = T_w$ , is assumed.

(2) Molecular reflections are treated either as completely diffuse ( $\sigma = \sigma' = \alpha = 1$ ), or as completely specular ( $\sigma = \sigma' = \alpha = 0$ ).

(3) The internal heat conduction and the external skin-radiation are neglected.

(4) Instead of the two coefficients,  $\sigma$  and  $\sigma'$ , only one coefficient,  $\sigma$ , is assumed as a governing factor (Maxwell's original supposition), i.e., the fraction,  $\sigma$ , of the incoming molecules is re-emitted completely diffusely, and the rest of  $(1-\sigma)$  molecules are reflected

completely specularly in treating both  $(p)$  and  $(r)$ . Then Eqs (2.4-57) and (2.4-58) take forms:

$$p = (2-\sigma)p_i + \sigma p_r, \quad \sigma = \sigma' = 1, \\ 0 < \alpha < 1, \quad (2.4-63)$$

$$\tau = \sigma \tau_i, \quad \tau_r = 0, \quad \sigma = \sigma' = 1, \\ 0 < \alpha < 1, \quad (2.4-64)$$

where the temperature,  $T_r$ , at which the molecules are diffusely leaving the surface is not equal to  $T_w$ , and can be found as stated in Section 2.4.2 in terms of  $r'$  and  $T_i$ .

### References for the Drag Force Estimate for Simple Body Geometries

Flat Plate:	Ref. (2.4-5) (2.4-4) (2.4-26) (2.4-27) (2.4-28) (2.4-29)
Cylinder:	Ref. (2.4-26) (2.4-28) (2.4-29) (2.4-30)
Sphere:	Ref. (2.4-26) (2.4-27) (2.4-28) (2.4-29) (2.4-8) (2.4-19)
Cone:	Ref. (2.4-26) (2.4-27) (2.4-28) (2.4-29) (2.4-30)
Ogive:	Ref. (2.4-27) (2.4-28) (2.4-30)
Ellipsoid:	Ref. (2.4-26) (2.4-30)
Composite bodies:	Ref. (2.4-27) (2.4-28) (2.4-30)

### The general drag force coefficient expression

The total drag force coefficient is defined:

$$C_D = \frac{D}{(1/2)\rho_i V_i^2 S_{REF}} = \frac{(D/A)}{(1/2)\rho_i V_i^2} \frac{A}{S_{REF}} = C_{Df} + C_{Dp} \quad (2.4-65)$$

comprising the pressure force component,  $p$ , and the tangential force component,  $\tau$ , in the direction of the ordered motion. The surface reference area,  $A$ , shall be explicitly specified in each case. The general expressions for  $p$  and  $\tau$  are given by Eqs (2.4-60) and (2.4-61), or alternatively by Eqs (2.4-63) and (2.4-64).

Alternatively, in terms of the adopted total drag force breakdown scheme for general or compound shapes, see Section 1.7.4:

$$C_D = \sum_i [C_{Df} + C_{Dp} + C_{Db}] \quad (2.4-66)$$

or

$$C_D = \sum_i [C_{Dof} + C_{Dop} + C_{Dob}]_{\theta=0}^{\theta} \\ + \sum [C_{Df} + C_{Dp} + C_{Db}]_{\theta}, \quad (2.4-67)$$

where  $(\theta)$  is the angle of incidence,

corresponding to the geometric angle of attack, (i) stands for the "i-th" body part, and all the coefficients are referred to the same common reference area,  $S_{REF} \neq A$ .

Note that in the free molecular flow regime there are no viscous pressure terms (no boundary layers), no interference effects either between the various body geometries "in situ" or due to boundary layer-shock wave interaction patterns (no shock waves).

In the following explicit expressions for various body geometries, the following main assumptions are introduced:

- Steady flow states,  $\bar{q}_i = V_H = \text{const}$ ,
- Constant, uniform surface temperatures,  $T_w = \text{const}$ ,
- Monoatomic molecular model (only translational degrees of freedom),
- Molecular reflection is treated as completely diffuse ( $\sigma' = \sigma = 1$ ), with no ordered motion velocity of the re-emitted molecular stream and with the random molecular motion velocity distribution function being of the modified Maxwellian form, corresponding to a temperature,  $(T_r)$ , different from both  $(T_i)$  and  $(T_w)$ , i.e.,  $0 < \alpha < 1$ ,
- No skin radiation or internal heat conduction effects through the body skin are considered.

#### (i) Geometric Shapes Composed of Plane Surfaces

The momentum transfer analysis for an inclined flat surface (with one face exposed to free stream only) can serve as a starting basis for developing the  $C_D$  expressions for other geometries: the assumed wetted surface area,  $A$ , in Figs (2.4-2) and (2.4-3) is replaced by locally tangential infinitesimal plane areas,  $dA$ , and the analysis of the impinging and the reflected molecules is then applied along the lines described in the previous paragraph, with a subsequent integration across the actual body geometry in any special body geometry case. Obviously, in a final form, all the coefficients are reduced to a common reference area  $S_{REF} \neq A$ . The resulting expressions can be summarized for a few simple geometries as follows:

- (1) Front plane surfaces ( $0 \leq \nu \leq \infty$  ,

$T_w = \text{const}$ ) of total wetted area,  $A$ , (one side), inclined by with respect to  $\theta$  the resultant vector,  $\bar{q}_i$ , of the ordered motion, see Fig (2.4-7).

The time rates of change of normal and tangential momentum components per unit area (superscript') of  $A$ , due to the impinging molecular stream at any local point,  $M$ , which is characterized by the respective infinitesimal area  $dA$ , is (22)

$$D'_i = C'_{D_i} (1/2) \rho_i \bar{q}_i^2 = p_i \sin \theta + \tau_i \cos \theta, \quad (2.4-68)$$

$$\therefore C'_{D_i} = C_{p_i} \sin \theta + C_{\tau_i} \cos \theta, \quad (2.4-69)$$

where:

$D'_i$  - is the resultant local drag force per unit area due to the total momentum exchange of the impinging molecules at any point  $M$ ,

$$C_{p_i} = \frac{p_i}{(1/2) \rho_i \bar{q}_i^2}, \quad (2.4-70)$$

$$C_{\tau_i} = \frac{\tau_i}{(1/2) \rho_i \bar{q}_i^2}, \quad (2.4-71)$$

$$p_i \sin \theta = \frac{\sin^3 \theta}{(1/2) \rho_i \bar{q}_i^2} \left[ \frac{1}{\sqrt{\pi}} S_v e^{-S_v^2} + \left(1 + \frac{1}{2S_v^2}\right) (1 + \text{erf } S_v) \right], \quad (2.4-72)$$

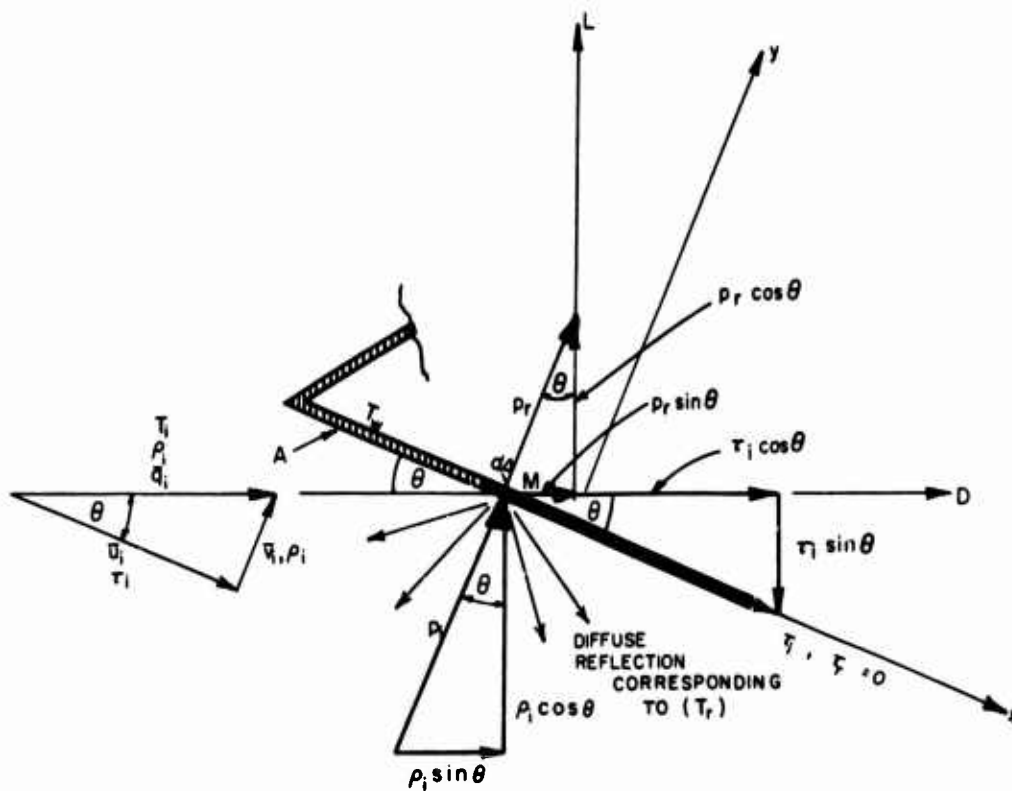
$$\tau_i \cos \theta = \frac{\sin \theta}{(1/2) \rho_i \bar{q}_i^2} \left[ \frac{1}{\sqrt{\pi}} S_v e^{-S_v^2} + (1 + \text{erf } S_v) \right] - \sin^3 \theta \left[ \frac{1}{\sqrt{\pi}} S_v e^{-S_v^2} + (1 + \text{erf } S_v) \right], \quad (2.4-73)$$

i.e.,

$$C'_{D_i} = \left[ \frac{1}{\sqrt{\pi}} S_v e^{-S_v^2} + \left(1 + \frac{\sin^2 \theta}{2S_v^2}\right) (1 + \text{erf } S_v) \right] \sin \theta = C_{D_{iWET}}, \quad (2.4-74)$$

$$C'_{D_i} = \frac{D'_i}{1/2 \rho_i \bar{q}_i^2} = \frac{A D'_i}{1/2 \rho_i \bar{q}_i^2 A} = \frac{D_i}{1/2 \rho_i \bar{q}_i^2 A} = C_{D_{iWET}}, \quad (2.4-75)$$

$$C_{D_i} = \frac{D_i}{1/2 \rho_H V_H^2 S_{REF}} = \frac{D_i}{1/2 \rho_i \bar{q}_i^2 A} \frac{A}{S_{REF}} = C_{D_{iWET}} \frac{A}{S_{REF}}, \quad (2.4-76)$$



LOCAL DRAG FORCE PER UNIT AREA

$$D' = D_i' + D_r' = (p_i \sin \theta + \tau_i \cos \theta) + (p_r \sin \theta)$$

NOTE: SIGN OF  $p$  AND  $\tau$  RELATED TO  $x$  AND  $y$ ,  
WHILE DRAG IS POSITIVE AS INDICATED.

FIG (2.4-7) FRONT SURFACE,  $0 \leq \nu \leq \infty$ ,  $T_w = \text{CONST.}$   
(FREE MOLECULE FLOW)

where the drag coefficient  $C_{DiWET}$  is for the whole plane surface  $A$ , due to all impinging molecules, since ( $\theta = \text{const.}$ ). Note that the subscript (i) here refers to the "impinging" molecular stream, and not to the "i-th" configurational part, while the subscript (WET) denotes the wetted area,  $A$ .

The tangential component of the momentum transfer for the completely diffusely re-emitted free molecules ( $\sigma = \sigma' = 1, 0 < \alpha < 1$ ) does not contribute to the shearing stress ( $\tau_r = 0$ ) since ( $\bar{q}_i = 0$ ). The rate of change of the normal momentum component per unit area due to a completely diffuse molecular re-emittance yields a local drag force per unit area  $D'_r$  at any point  $M$  ( $T_i \neq T_r \neq T_w$ ):

$$D'_r = C'_{D_r} \left(\frac{1}{2}\right) \rho_i \bar{q}_i^2 = p_r \sin \theta, \quad (2.4-77)$$

$$\therefore C'_{D_r} = C'_{D_p} \sin \theta, \quad (2.4-78)$$

$$C'_{D_r} = \frac{\sin^3 \theta}{2 S_V^2} \left(\frac{T_r}{T_i}\right)^{1/2} \left[ e^{-S_V^2} + \sqrt{\pi} S_V (1 + \text{erf} S_V) \right] = C_{D_{rWET}}, \quad (2.4-79)$$

$$\therefore C_{D_r} = C_{D_{rWET}} \frac{A}{S_{REF}} \quad (2.4-80)$$

where the drag coefficient  $C_{D_{rWET}}$  is for the whole wetted surface  $A$  due to all diffusely re-emitted molecules, since ( $\theta = \text{const.}$ ).

Finally, the total drag force coefficient of the wetted area  $A$  and the reference dynamic pressure ( $\frac{1}{2} \rho_i \bar{q}_i^2 = \frac{1}{2} \rho_H V_H^2$ ) is:

$$C_D = \frac{D'A}{\frac{1}{2} \rho_H V_H^2 S_{REF}} = \frac{D}{\frac{1}{2} \rho_i \bar{q}_i^2 A} \frac{A}{S_{REF}} = (C_{DiWET} + C_{D_{rWET}}) \frac{A}{S_{REF}}, \quad (2.4-81)$$

$$\therefore C_D = \frac{\sin \theta}{\sqrt{\pi} S_V} \left\{ (1 + \text{erf} S_V) \sqrt{\pi} S_V \left[ \frac{\sqrt{\pi} \sin^2 \theta}{2 S_V} \left(\frac{T_r}{T_i}\right)^{1/2} + \left(1 + \frac{\sin^2 \theta}{2 S_V^2}\right) \right] + e^{-S_V^2} \left[ 1 + \frac{\sqrt{\pi} \sin^2 \theta}{2 S_V} \left(\frac{T_r}{T_i}\right)^{1/2} \right] \right\} \times \frac{A}{S_{REF}} \quad (2.4-82)$$

Alternatively, by a direct grouping of the pressure drag components of the impinging and of the diffusely re-emitted molecules and by taking the skin-friction drag component separately, the same final expression (2.4-82) can be obtained:

$$D = D'_p + D'_f = D/A, \quad (2.4-83)$$

$$C_D = C_{D_{WET}} = C_p \sin \theta + C_f \cos \theta, \quad (2.4-84)$$

$$C_p = \frac{(p_i + p_r)}{\frac{1}{2} \rho_i \bar{q}_i^2} = C_{p_i} + C_{p_r}, \quad C_f = \frac{\tau_i}{\frac{1}{2} \rho_i \bar{q}_i^2} = C_{f_i}, \quad (2.4-85)$$

$$C_p = \sin^2 \theta \left\{ \frac{1}{S_V} \left[ \frac{1}{\sqrt{\pi}} + \frac{1}{2 S_V} \left(\frac{T_r}{T_i}\right)^{1/2} \right] e^{-S_V^2} + \left[ 1 + \frac{1}{2 S_V^2} + \frac{\sqrt{\pi}}{2 S_V} \left(\frac{T_r}{T_i}\right)^{1/2} \right] (1 + \text{erf} S_V) \right\}, \quad (2.4-86)$$

$$C_f = \sin \theta \cos \theta \left[ \frac{1}{\sqrt{\pi} S_V} e^{-S_V^2} + (1 + \text{erf} S_V) \right], \quad (2.4-87)$$

$$\therefore C_D = \frac{\sin \theta}{\sqrt{\pi} S_V} \left\{ (1 + \text{erf} S_V) \sqrt{\pi} S_V \left[ \frac{\sqrt{\pi} \sin^2 \theta}{2 S_V} \times \left(\frac{T_r}{T_i}\right)^{1/2} + \left(1 + \frac{\sin^2 \theta}{2 S_V^2}\right) \right] + e^{-S_V^2} \left[ 1 + \frac{\sqrt{\pi} \sin^2 \theta}{2 S_V} \left(\frac{T_r}{T_i}\right)^{1/2} \right] \right\} \frac{A}{S_{REF}} \quad (2.4-82)$$

For a general shape double wedge on Fig. (2.4-8), the expression (2.4-82) is valid for each of the directly wetted surfaces (1), (2) and (4), provided the specified angular conditions are satisfied. The surface (3) is "shaded", and shall require a separate analysis to determine its  $C_{D_3}$  value. For the whole wedge the total drag force coefficient, referred to any reference area  $S_{REF}$  is then:

$$C_D = C_{D_1}(A_1/S_r) + C_{D_2}(A_2/S_r) + C_{D_3}(A_3/S_r) + C_{D_4}(A_4/S_r). \quad (2.4-88)$$

(2) Rear plane ("shaded") surfaces ( $-\infty \leq v \leq 0, T_w = \text{const.}$ ) of a shaded area  $A$  (one side), inclined at an incidence angle  $\theta$  with respect to the free stream, see Fig (2.4-9):

At any point  $M$ , characterized by an infinitesimal area  $dA$ , the local drag force coefficient (per unit area) is:

(a) Due to impinging molecules:

$$D'_i = \frac{1}{2} C'_{D_i} \rho_i \bar{q}_i^2 = (p_i \sin \theta) + (\tau_i \cos \theta), \quad (2.4-89)$$

$$\therefore C'_{D_i} = (C_{p_i} \sin \theta) + (C_{f_i} \cos \theta), \quad (2.4-90)$$

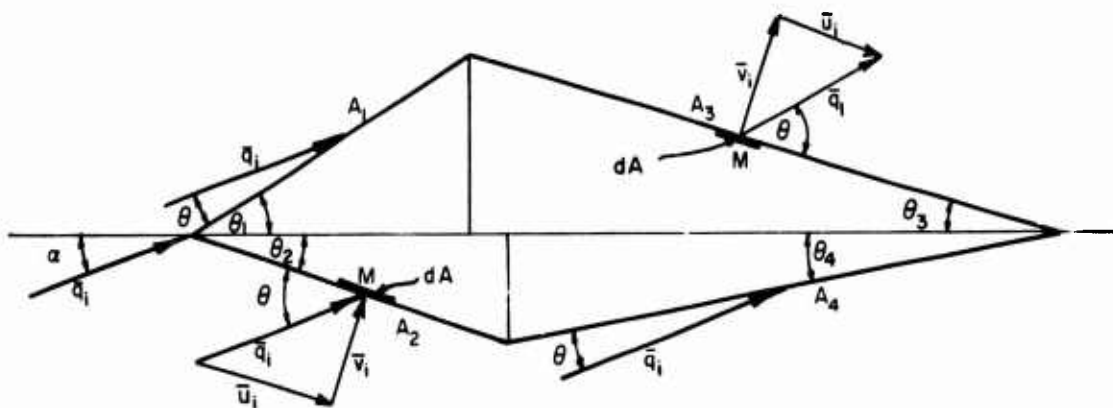
where ( $C_{p_i}$ ) and ( $C_{f_i}$ ) are given by Eqs (2.4-72) and (2.4-73) respectively, with ( $-\theta$ ) substituted for  $\theta$ :

$$C'_{D_i} = \left[ \frac{1}{S_V \sqrt{\pi}} e^{-S_V^2} - \left(1 + \frac{\sin^2 \theta}{2 S_V^2}\right) (1 - \text{erf} S_V) \right] \sin \theta =$$

NOTE :  $u = \bar{u} + H_1 / (2\beta_1)^{1/2}$   
 $v = \bar{v} + H_2 / (2\beta_1)^{1/2}$   
 $w = \bar{w} + H_3 / (2\beta_1)^{1/2}$  } FOR EACH CLASS OF MOLECULES

SURFACES  $A_1, A_2, A_4$  :  $0 \leq v \leq \infty$

SURFACE  $A_3$  :  $-\infty \leq v \leq 0$



SURFACE  $A_1$  :  
 $\alpha \leq \theta_1 \leq (\pi/2 + \alpha)$   
 $0 \leq \theta = (\theta_1 - \alpha) \leq \pi/2$

SURFACE  $A_3$  :  
 $0 \leq \theta_3 \leq (\pi/2 + \alpha)$   
 $0 \leq \theta = (\theta_3 + \alpha) \leq \pi/2$

SURFACE  $A_2$  :  
 $0 \leq \theta_2 \leq (\pi/2 - \alpha)$   
 $0 \leq \theta = (\theta_2 + \alpha) \leq \pi/2$

SURFACE  $A_4$  :  
 $0 \leq \theta_4 \leq \alpha$   
 $0 \leq \theta = \alpha - \theta_4 \leq \pi/2$

$\bar{q}_i = \bar{u}_i + \bar{v}_i + \bar{w}_i$  , VELOCITY VECTORS OF THE RELATIVE ORDERED MOTION OF GAS WITH RESPECT TO THE WEDGE AT REST. ( $\bar{q}_i = V$ ,  $\bar{w}_i = 0$  FOR THE TWO DIMENSIONAL FLOW CASE.)

FIG(2.4-8) GENERAL DOUBLE-WEDGE PROFILE (FREE MOLECULE FLOW)

$$= C_{D1WET} = [C_{D1}]_3 \quad (2.4-91)$$

or directly, by writing the Eq (2.4-74) in the alternate form (with  $S_v = S \sin \theta$ ) and ( $\theta = \text{const.}$ ):

$$C_{D1WET} = C_{D1} = \left[ \frac{1}{S\sqrt{\pi}} e^{-S_v^2} + \left(1 + \frac{1}{2S^2}\right) (1 + \text{erf } S_v) \sin \theta \right] \quad (2.4-92)$$

and by substituting  $(-\theta)$  for  $(\theta)$ , the drag coefficient component for a "shaded" surface A due to all impinging molecules is obtained as:

$$C_{D1WET} = \left[ \frac{1}{S\sqrt{\pi}} e^{-S_v^2} - \sin \theta \left(1 + \frac{1}{2S^2}\right) (1 - \text{erf } S_v) \right] \quad (2.4-93)$$

$$\therefore -C_{D1} = \left[ \frac{-1}{S\sqrt{\pi}} e^{-S_v^2} + \left(1 + \frac{\sin^2 \theta}{2S^2}\right) (1 - \text{erf } S_v) \right] \sin \theta = [C_{D1}]_3 \quad (2.4-91)$$

(b) Due to diffusely reflected molecules:

$$D_r' = \frac{1}{2} C_{D_r}' \rho_1 \bar{q}_1^2 = \rho_1 \sin \theta = \frac{1}{2} C_{D_r}' \rho_1 \bar{q}_1^2 \sin \theta \quad (2.4-92)$$

or, by substituting into the expression (2.4-79)  $(-\theta)$  for  $(\theta)$ :

$$C_{D_r}' C_{D1} = -\frac{\sin \theta}{2S^2} \left(\frac{T_r}{T_i}\right)^{1/2} \left[ e^{-S_v^2} - \sqrt{\pi} S_v (1 - \text{erf } S_v) \right] = [C_{D_r}]_3 \quad (2.4-93)$$

(c) Finally, the total drag coefficient of the shaded reference area A is:

$$C_{D3} = \frac{\text{TOTAL DRAG}}{\frac{1}{2} \rho_1 \bar{q}_1^2 A_3} = [C_{D1}]_3 + [C_{D_r}]_3 \quad (2.4-94)$$

$$C_{D3} = \frac{\sin \theta}{\sqrt{\pi} S_v} \left\{ (1 - \text{erf } S_v) \sqrt{\pi} S_v \left[ \frac{\sqrt{\pi} \sin^2 \theta}{2S_v} \left(\frac{T_r}{T_i}\right)^{1/2} + \left(1 + \frac{\sin^2 \theta}{2S^2}\right) \right] + e^{-S_v^2} \left[ 1 - \frac{\sqrt{\pi} \sin^2 \theta}{2S_v} \left(\frac{T_r}{T_i}\right)^{1/2} \right] \right\} \quad (2.4-95)$$

For the general double wedge on Fig (2.4-8) the term  $C_{D3}$  can be now included in the Eq (2.4-88). It is numerically negative, i.e., a push force coefficient.

(ii) Flat Plates

Using the general expressions (2.4-60) and (2.4-61) the drag coefficient of a flat plate, referred to the reference area of one side A, is (22):

(1) Assuming completely diffuse re-emittance of molecules ( $\sigma = \sigma' = 1$ ) and a uniform surface temperature ( $T_w \neq T_i$ ) and ( $T_w = T_r, \alpha = 1$ ):

$$[C_{D_{DIFF}}]_{WET} = \frac{2}{\sqrt{\pi} S} \left[ e^{-S_v^2} + \sqrt{\pi} S_v \left(1 + \frac{1}{2S^2}\right) \text{erf } S_v + \frac{\pi S}{S_w} \sin^2 \theta \right] \quad (2.4-96)$$

$$[C_{D_{DIFF}}]_{WET} = \frac{2}{\sqrt{\pi} S} \left[ e^{-S_v^2} + \sqrt{\pi} S_v \left(1 + \frac{1}{2S^2}\right) \text{erf } S_v + \frac{\pi S}{S_w} \sin^2 \theta \right] \quad (2.4-97)$$

for one side of the non-insulated flat plate, where:

$$S_v = S \sin \theta = \sqrt{\frac{\gamma}{2}} M_1 \sin \theta \quad (2.4-98)$$

$$S_w = \frac{\bar{q}_1}{\sqrt{2RT_w}} \quad T_w \neq T_i \quad (2.4-99)$$

i.e., a knowledge of the actual surface temperature,  $T_w$ , is required in general.

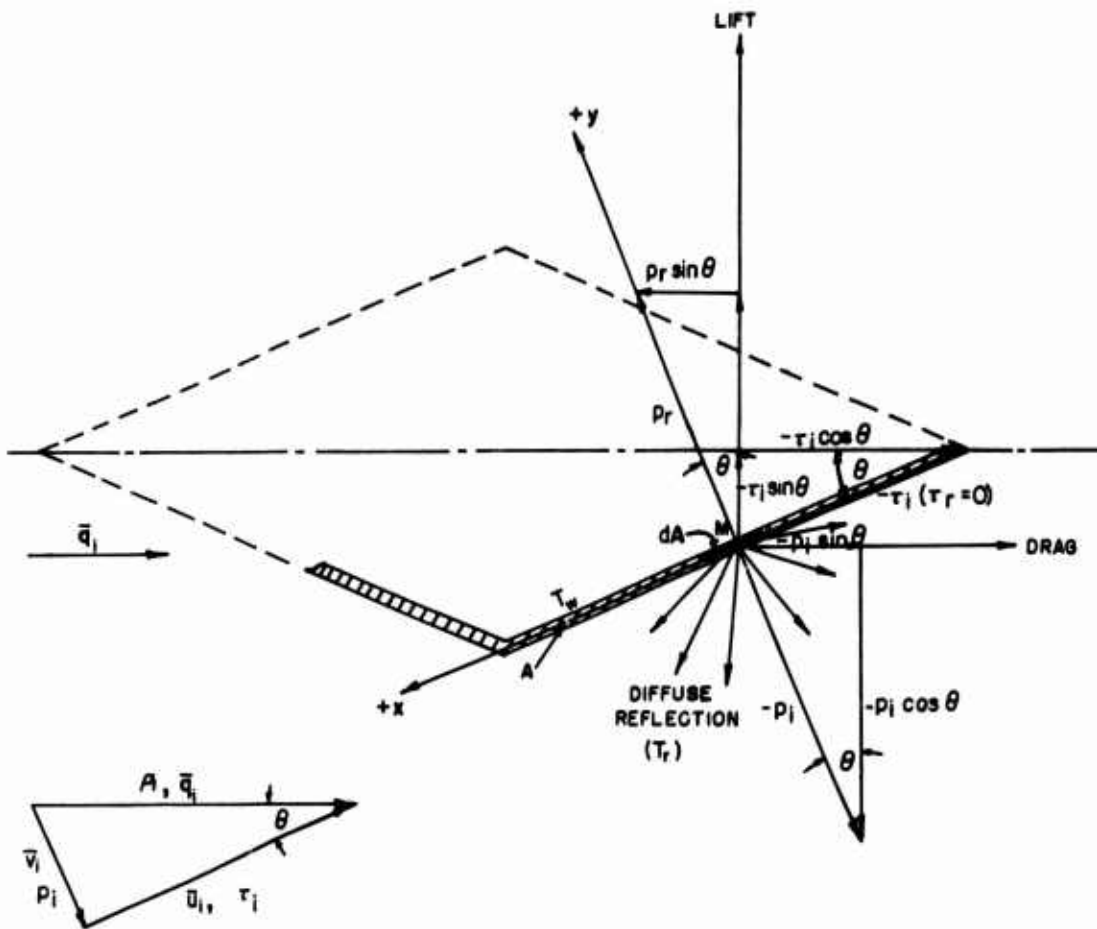
If it is assumed that ( $T_i = T_w$ ) i.e., an insulated plate with ( $\alpha = 0$ ), the above expression (2.4-97) is simplified, since then ( $S = S_w$ ). In Fig (2.4-10), the relationship  $C_{D_{DIFF}} = f(S, \theta)$  is presented graphically for the case.

In the absence of radiation and internal heat conduction effects, a more realistic approach would be to equate the uniform surface temperature,  $T_w$ , with the equilibrium temperature,  $T_r$ , instead of ( $T_w = T_i$ ), where the ratio ( $T_r/T_i$ ) can be found through the corresponding recovery factor ( $r'$ ), see Eq (2.4-33). Since the recovery factor is larger than unity, the drag coefficient value shall be somewhat greater than in Fig (2.4-10) which represents the case of ( $T_w = T_i$ ).

(2) Assuming completely specular reflection of molecules ( $\sigma = \sigma' = 0, \alpha = 0$ ) from one side of an insulated flat plate:

$$[C_{D_{SPEC}}]_{WET} = \frac{4 \sin \theta}{\sqrt{\pi} S^2} \left[ S_v e^{-S_v^2} + \sqrt{\pi} \left(\frac{1}{2} + S_v^2\right) \text{erf } S_v \right] \quad (2.4-100)$$

The  $C_{D_{SPEC}} = f(S, \theta)$  relationship is pre-



LOCAL DRAG FORCE PER UNIT AREA

$$D' = D'_i + D'_r = (-p_i \sin \theta) + (-\tau_i \cos \theta) - (p_r \sin \theta)$$

NOTE: SIGN OF  $p$  AND  $\tau$  RELATED TO  $x$  AND  $y$  WHILE DRAG IS POSITIVE AS INDICATED.

FIG (2.4-9) REAR SURFACE,  $-\infty \leq v \leq 0$ ,  $T_w = \text{CONST.}$   
(FREE MOLECULE FLOW)

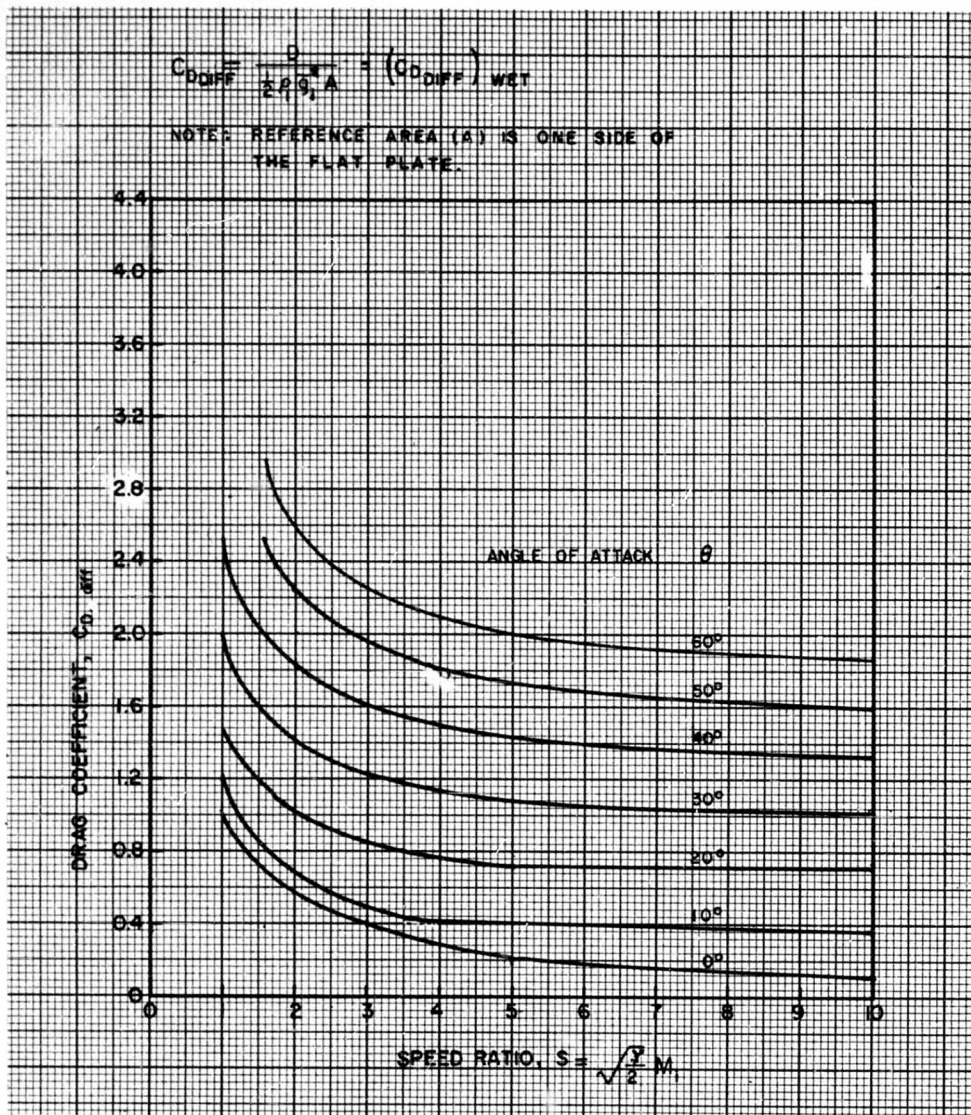


Fig (2.4-10) Drag coefficient in free molecule flow, diffuse reflection on an insulated flat plate. (Ref 22)

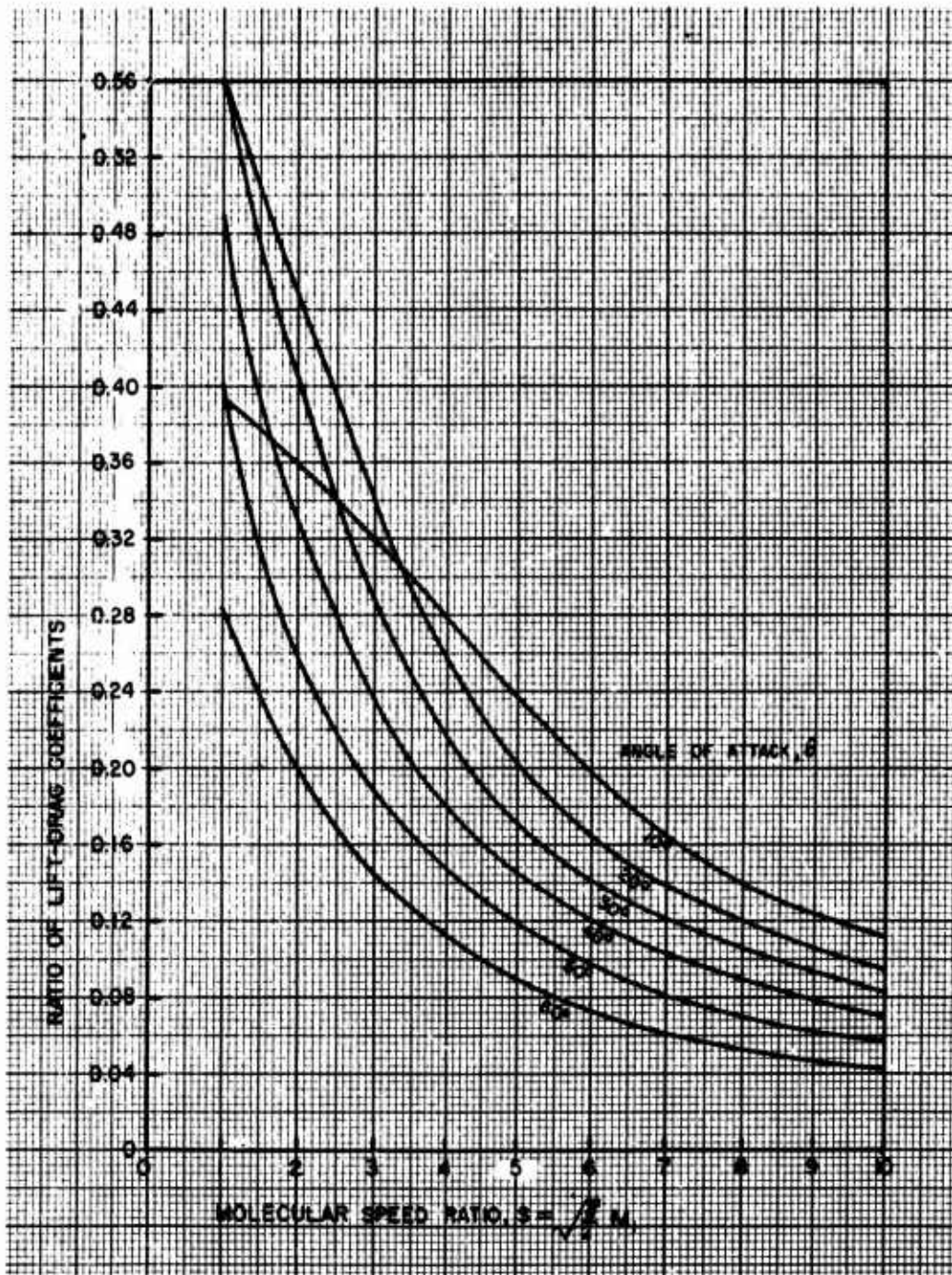


Fig (2.4-II) Flat plate lift-drag ratio, diffuse reflection (Ref 22)

sented graphically in Fig. (2.4-12)

(3) The Knudsen Number Effect on heat transfer on a flat plate

The influence of Knudsen Number (i.e., of the flow type) on the surface-to-free stream temperature ratio ( $T_w/T_i$ ) can be investigated in its simplest form in the case of a flat plate by assuming adiabatic conditions in a monoatomic gas (12):

(a) Free molecule flow,  $Kn > 3$

For the front surface of a flat plate exposed to the free stream at an arbitrary angle  $\theta$ , the energy balance for the adiabatic conditions takes form(22):

$$\frac{1}{2} \bar{q}_i^2 + 2RT_i \left[ 1 + \frac{1}{4(\phi + 1)} \right] = 2RT_w, \quad (2.4-101)$$

where ( $T_w = T_{ow}$ ), i.e.:

$$\therefore \frac{T_w}{T_i} = 1 + \frac{1}{4(\phi + 1)} + \frac{1}{2} S^2,$$

$$S = \sqrt{\frac{\gamma}{2}} M_i, \quad M_i = \frac{\bar{q}_i}{a}, \quad \gamma = \frac{5}{3} \quad (2.4-102)$$

(monoatomic gas),

$$\phi(S, \theta) = \frac{e^{-S_v^2}}{\sqrt{\pi} S_v (1 + \text{erf } S_v)}, \quad (2.4-103)$$

For ( $\theta = 0$ ), the Eq (2.4-103) takes the simplest form:

$$\frac{T_w}{T_i} = 1 + \frac{1}{2} S^2, \quad (2.4-104)$$

since then,

$$\phi(S, \theta) = \frac{e^{-S_v^2}}{\sqrt{\pi} S_v (1 + \text{erf } S_v)} \rightarrow \infty, \quad (2.4-105)$$

$$S_v = S \sin \theta = 0. \quad (2.4-106)$$

(b) Continuum flow,  $Kn \ll 1$ , laminar boundary layer, ( $\theta = 0$ ):

$$\frac{T_w}{T_i} = 1 + \frac{\gamma - 1}{2} r(0) M_i^2 = 1 + .326 S^2, \quad (2.4-107)$$

$r(0) = .815$  (recovery factor, monoatomic gases),

$\gamma = \frac{5}{3}$  (monoatomic gas),

and at the stagnation point, with  $r(0)$  and ( $T_w = T_s$ ):

$$\frac{T_w}{T_i} = 1 + \frac{2}{\gamma} S^2. \quad (2.4-108)$$

The above comparative expressions are represented graphically in Fig (2.4-13), showing that a higher adiabatic equilibrium wall temperature exists in a free molecule flow ( $Kn > 3$ ) than in a continuum (laminar) flow ( $Kn \ll 1$ ), and that the free molecule flow equilibrium temperature is even greater than the stagnation temperature in laminar boundary layers of continuum flow concept.

(iii) Cylinders (with longitudinal axis perpendicular to the free stream)

For cylindrical bodies of circular cross-section with their axis perpendicular to the velocity vector of the ordered motion,  $\bar{q}_i$ , the drag force coefficient is obtainable by applying the plane surface analysis from preceding paragraphs to an infinitesimal area(12):

$$dA = r l d\theta, \quad (2.4-109)$$

inclined at a local angle,  $\theta$ , with respect to  $\bar{q}_i$  and by a subsequent integration from 0 to  $\pi/2$  for the front (washed) and the rear (shaded) cylindrical halves respectively, see Figs (2.4-14) and (2.4-15).

(1) Front face ( $0 \leq \nu \leq \infty, T_w = \text{const.}$ ), see Fig (2.4-14).

(a) Molecules impinging on an area-element,  $dA$ , yield a local drag force coefficient per unit area,

$$C'_{D1} = \frac{(\rho_i \sin \theta + \tau_i \cos \theta)}{\frac{1}{2} \rho_i \bar{q}_i^2}, \quad (2.4-110)$$

$$\therefore C'_{D1} = \sin \theta \left[ \frac{1}{S_v \sqrt{\pi}} e^{-S_v^2} + \left( 1 + \frac{\sin^2 \theta}{2 S_v^2} \right) \times (1 + \text{erf } S_v) \right], \quad (2.4-111)$$

or the respective total drag force coefficient for the whole front face,

$$[C_{D1}]_f = \int_0^{\pi/2} \left[ \frac{1}{S_v \sqrt{\pi}} e^{-S_v^2} + \left( 1 + \frac{\sin^2 \theta}{2 S_v^2} \right) \times (1 + \text{erf } S_v) \right] \sin \theta d\theta,$$

with the reference cross-section area of ( $2r l$ ).

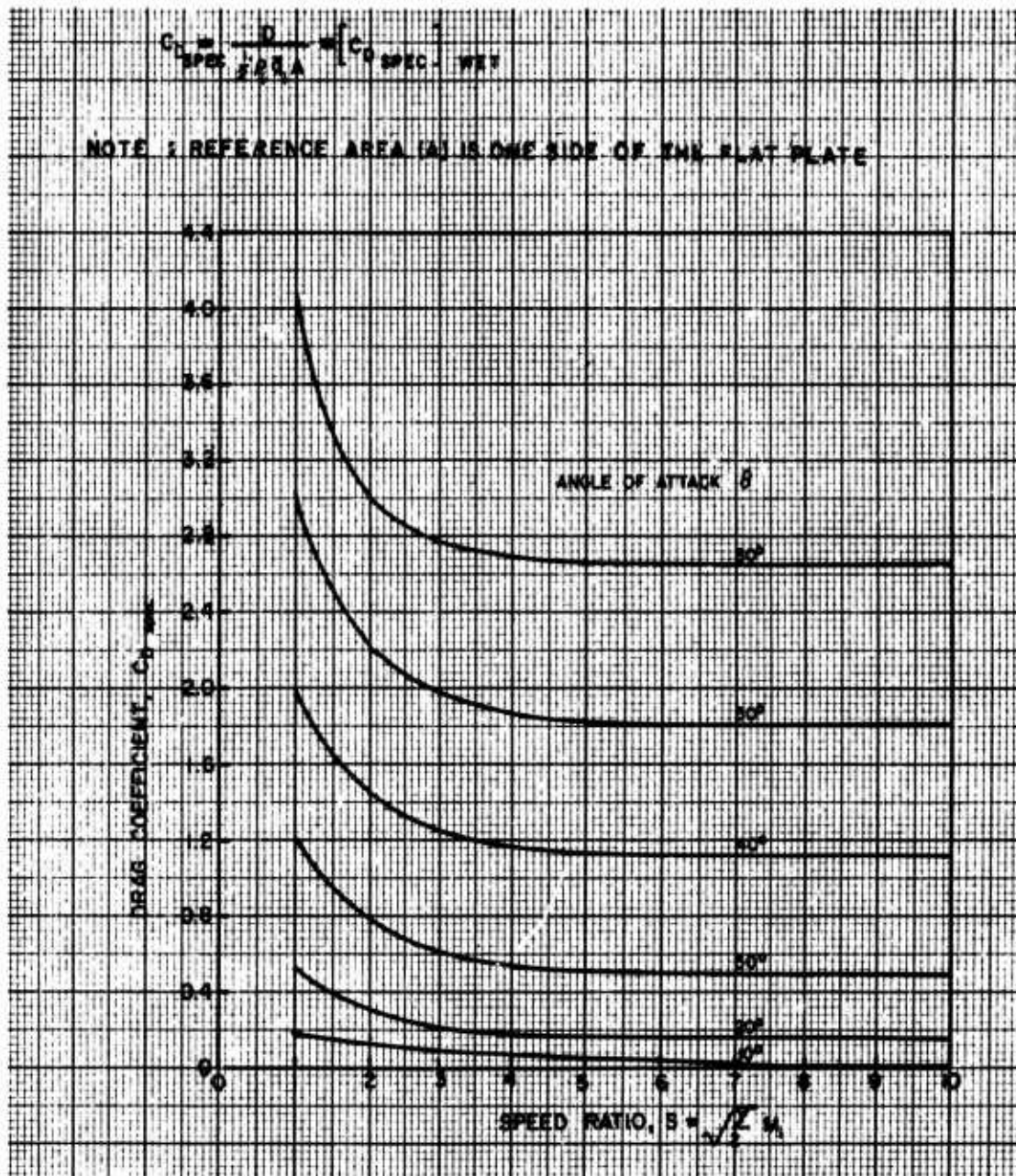
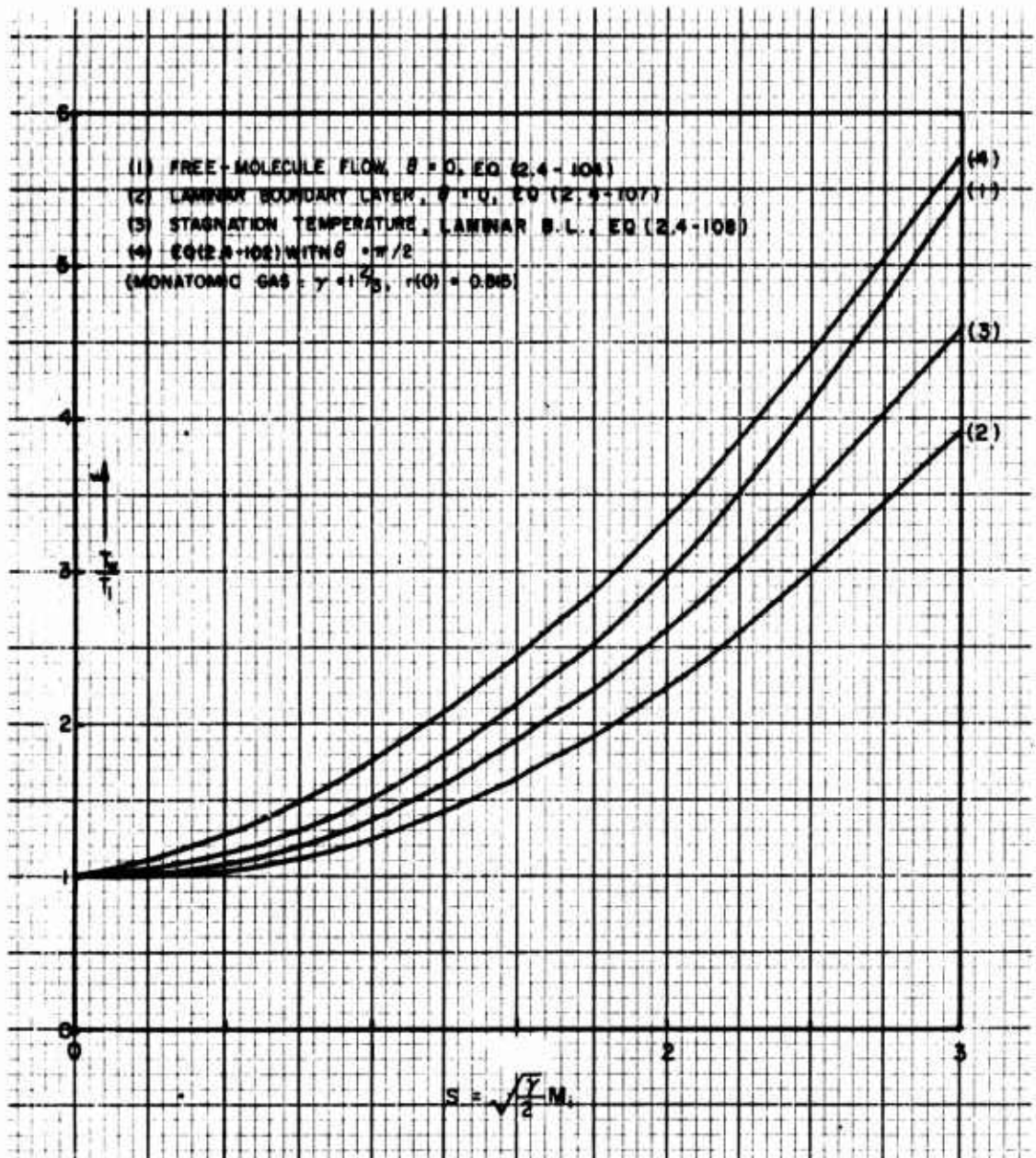
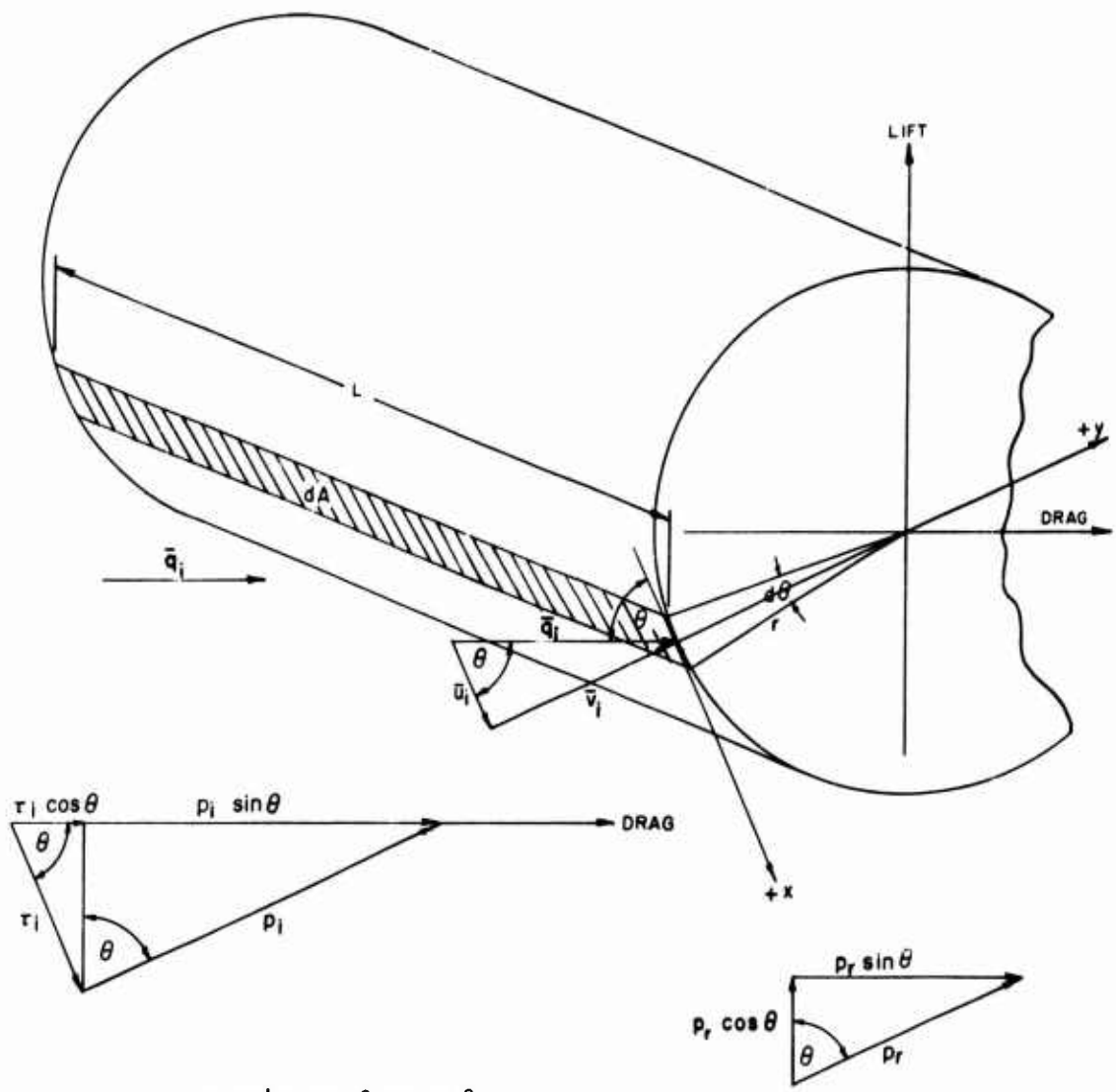


Fig (2.4-12) Drag coefficient in free molecular flow, specular reflection from one side of an insulated flat plate, (Ref 22)



Fig(2.4-13) Surface temperature of an insulated plate at large and small values of the Knudsen number, (Ref. 12)



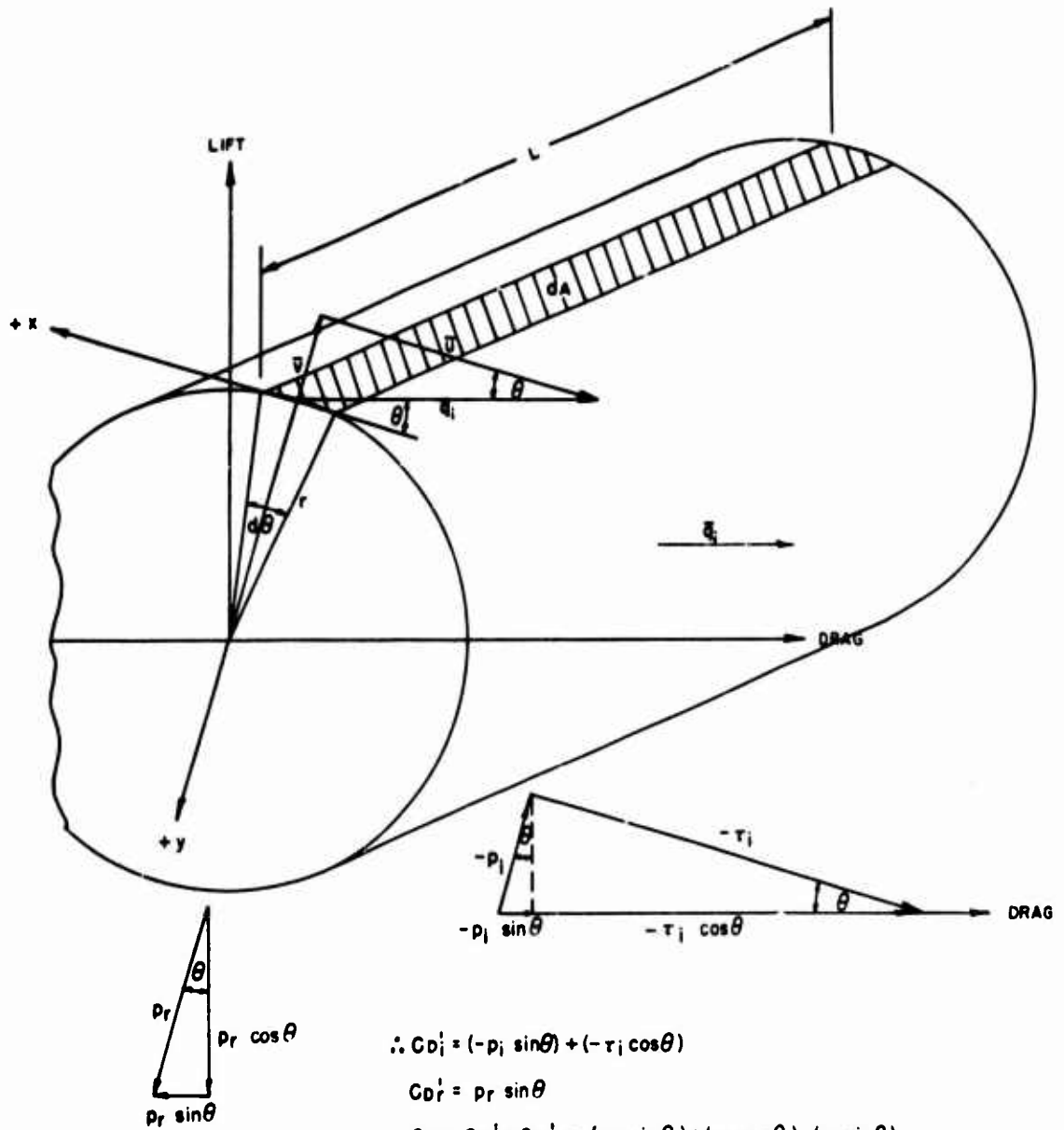
$$\therefore CD_i' = p_i \sin \theta + \tau_i \cos \theta$$

$$CD_r' = p_r \sin \theta$$

$$CD = CD_i' + CD_r' = (p_i \sin \theta + \tau_i \cos \theta) + p_r \sin \theta$$

NOTE: SIGN OF p AND tau RELATED TO x AND y WHILE CD IS POSITIVE AS INDICATED.

Fig.(2.4-14) FRONT FACE, ( $0 \leq v \leq \infty, T_w = \text{CONST.}$ )  
DRAG COEFFICIENT OF CYLINDERS



$$\therefore C_{D_i} = (-p_i \sin \theta) + (-\tau_i \cos \theta)$$

$$C_{D_r} = p_r \sin \theta$$

$$C_D = C_{D_i} + C_{D_r} = (-p_i \sin \theta) + (-\tau_i \cos \theta) - (p_r \sin \theta)$$

NOTE: SIGN OF  $p$  AND  $\tau$  RELATED TO  $x$  AND  $y$  WHILE  $C_D$  IS POSITIVE AS INDICATED.

FIG(2.4-15) REAR FACE,  $(-\infty \leq v \leq 0, T_w = \text{CONST.})$   
DRAG COEFFICIENT OF CYLINDERS

(b) Molecules emerging diffusely from an area element,  $dA$ , yield a local drag coefficient per unit area,

$$C_{D_r}' = \frac{p_r \sin \theta}{1/2 \rho_i \bar{q}_i^2}, \quad (2.4-112)$$

or the respective total drag force coefficient for the whole front face,

$$|C_{D_r}|_f = \frac{1}{2 S v^2} \left( \frac{T_r}{T_i} \right)^{1/2} \left[ e^{-Sv^2} + \sqrt{\pi} S v (1 + \operatorname{erf} S v) \right] \int_0^{\pi/2} \sin^3 \theta d\theta, \quad (2.4-113)$$

with the reference cross-section area of ( $2r_l = A$ ).

(c) The total drag force coefficient for the front face is then:

$$[C_D]_f = [C_{D_i}]_f + [C_{D_r}]_f = [C_{D_f}]_{\text{CROSS-SECTION}} \quad (2.4-114)$$

(2) Rear Face ( $-\infty \leq v \leq 0, T_w = \text{const}$ ), see Fig (2.4-15)

(a) Molecules impinging on an element,  $dA$ , yield a local drag force coefficient per unit area, with  $(-\theta)$  instead of  $\theta$ :

$$[C_{D_i}]_b = \left[ -p_i \sin \theta - r_i \cos \theta \right] / 1/2 \rho_i \bar{q}_i^2 = (-C_{D_i}')_b + (-C_{D_r}')_b,$$

$$\therefore [C_{D_i}]_b = \left[ \frac{1}{\sqrt{\pi} S v} e^{-Sv^2} - \left( 1 + \frac{\sin^2 \theta}{2 S v^2} \right) \times (1 - \operatorname{erf} S v) \right] \sin \theta, \quad (2.4-116)$$

or the respective average drag force coefficient for the whole rear face, with ( $A = 2r_l$ ):

$$[C_{D_i}]_b = \int_0^{\pi/2} \left[ \frac{1}{\sqrt{\pi} S v} e^{-Sv^2} - \left( 1 + \frac{\sin^2 \theta}{2 S v^2} \right) \times (1 - \operatorname{erf} S v) \right] \sin \theta d\theta. \quad (2.4-117)$$

(b) Molecules reflected diffusely from an area element,  $dA$ , yield a local drag coefficient per unit area,

$$|C_{D_r}'|_b = \frac{-\sin^3 \theta}{2 S v^2} \left( \frac{T_r}{T_i} \right)^{1/2} \left[ e^{-Sv^2} - \sqrt{\pi} S v (1 - \operatorname{erf} S v) \right], \quad (2.4-118)$$

or the respective average drag force coefficient for the whole rear face with

reference area ( $A = 2r_l$ ):

$$[C_{D_r}]_b = - \frac{1}{2 S v^2} \left( \frac{T_r}{T_i} \right)^{1/2} \left[ e^{-Sv^2} - \sqrt{\pi} S v (1 - \operatorname{erf} S v) \right] \int_0^{\pi/2} \sin^3 \theta d\theta. \quad (2.4-119)$$

(c) The total drag force coefficient for the rear face is:

$$[C_D]_b = [C_{D_i}]_b + [C_{D_r}]_b = [C_{D_b}]_{\text{CROSS-SECTION}} \quad (2.4-120)$$

(3) Total cylinder, assuming the reference area ( $A = 2r_l$ ):

$$C_D = [C_D]_f + [C_D]_b = [C_{D_{CYL}}]_{\text{CROSS-SECTION}}, \quad (2.4-121)$$

or, after regrouping (12):

$$C_D = [ |C_{D_i}|_f + |C_{D_i}|_b ] + [ |C_{D_r}|_f + |C_{D_r}|_b ], \quad (2.4-122)$$

$$C_D = \left\{ \frac{\sqrt{\pi} e^{-1/2 S v^2}}{S} [ I_0 + (S^2 + 1/2)(I_0 + I_1) ] \right\} + \left\{ \frac{\pi^{3/2}}{4 S} \left( \frac{T_r}{T_i} \right)^{1/2} \right\}, \quad (2.4-123)$$

$$[C_{D_{CYL}}]_{\text{CROSS-SECTION}} = C_D = \frac{\sqrt{\pi}}{S} \left\{ e^{-1/2 S^2} \times [ I_0 + (S^2 + 1/2)(I_0 + I_1) ] + \frac{\pi}{4} \left( \frac{T_r}{T_i} \right)^{1/2} \right\}, \quad (2.4-124)$$

where:

$$S = \frac{\bar{q}_i}{C_i} = \sqrt{\frac{\gamma}{2}} M_i \text{ is the molecular speed ratio,}$$

$C_i$  - is the most probable incident speed of molecules,  $C_i = (2RT_i)^{1/2} = C_{m_i}$ .

$\bar{q}_i$  = the velocity of the ordered motion,  $|\bar{q}_i| = |V_H|$ ,

$T_r$  - is the temperature of diffusely reflected molecules,

$T_i$  - is the temperature of incident molecules,

$$I_0 = \frac{1}{\pi} \int_{-1}^1 \frac{e^{1/2 S^2 x}}{(1-x^2)^{1/2}} dx, \text{ a modified Bessel function of the order of 0,}$$

$$I_1 = \frac{S^2}{2\pi} \int_{-1}^1 e^{1/2 S^2 x} (1-x^2)^{1/2} dx, \text{ a modified Bessel function of the order of 1,}$$

$$x = \frac{H_2}{\sqrt{2}},$$

H<sub>2</sub> - Boltzmann's function.

Note that in case of any other (common) reference area, S<sub>r</sub>, for a given missile configuration, the expression (2.4-124) for the drag coefficient shall read:

$$C_{D_{CYL}} = \frac{A}{S_r} [C_{D_{CYL}}]_{\text{CROSS-SECTION}}, \quad (2.4-125)$$

where

C<sub>D<sub>CYL</sub></sub> - is referred to the common reference area, S<sub>r</sub>, for the whole missile,

[C<sub>D<sub>CYL</sub></sub>]<sub>CROSS SECTION</sub> is referred by derivation to the area (A = 2r<sub>l</sub>),

$$S_r = \frac{\pi D^2}{4} \quad (\text{usually}).$$

Alternatively, from Ref. 22, for a right circular cylinder with its axis normal to the flow and (A = 2r<sub>l</sub>), for a completely diffuse reflection (σ = σ' = 1), the average drag coefficient expression can be written in the form:

$$[C_{D_{DIFF}}]_{CYL} = [C_D]_{DIFF} = \frac{\sqrt{\pi} e^{-1/2 S^2}}{S} \left\{ [(S^2 + 3/2) I_0 \times (S^2/2) + (S^2 + 1/2) I_1(S^2/2)] + \frac{\pi^{3/2}}{4 S_w} \right\}, \quad (2.4-126)$$

and for purely specular reflection, (σ = σ' = 0):

$$[C_{D_{SPEC}}]_{CYL} = [C_D]_{SPEC} = \frac{4}{3} \left[ [C_D]_{DIFF} - \frac{\pi^{3/2}}{4 S_w} \right], \quad (2.4-127)$$

where

$$S_w = \frac{\bar{q}_i}{\sqrt{2RT_w}} = f(T_w),$$

$$S = \frac{\bar{q}_i}{\sqrt{2RT_i}} = \sqrt{\frac{\gamma}{2}} M_i. \quad (2.4-128)$$

Using the expression (2.4-126) and (2.4-127) and assuming (S<sub>w</sub> = S), i.e., (T<sub>w</sub> = T<sub>w</sub>), the influence of (γ) is eliminated, and the results are applicable both to monoatomic and diatomic gases. Graphical presentations of C<sub>D</sub> = f(S) for the case are given in Fig (2.4-16).

Eq (2.4-124) indicates that the drag force coefficient of a cylinder

in a free molecule flow depends upon the molecular speed ratio, S, and the temperature ratio T<sub>r</sub> / T<sub>i</sub>. The effective temperature, T<sub>r</sub>, of emergent molecules can be found from the energy balance between the body and the gaseous medium by defining first the wall temperature, T<sub>w</sub>. Assuming a constant surface temperature T<sub>w</sub> of a "gray" body, the energy balance for any infinitesimal body area, dA, shall consist of (for monoatomic gases, no dissociation or ionization, Ref. 12):

(a) The translational energy per unit area per unit time conveyed by the incident molecules:

On the Front Surfaces (0 ≤ ν ≤ ∞):

$$[\bar{E}'_i]_f = \frac{1}{2} m [n'_i]_f \left[ \bar{q}_i^2 + RT_i \left( 4 + \frac{1}{\phi_{f+1}} \right) \right], \quad (2.4-129)$$

$$\text{where } \phi_f(S, \theta) = \frac{e^{-S^2}}{\sqrt{\pi} S_v (1 + \text{erf } S_v)} \quad (2.4-130)$$

[n'<sub>i</sub>]<sub>f</sub> = total number of impinging molecules per unit time per unit area,

$$[n'_i]_f = [n_i]_f \sqrt{\frac{RT_i}{2\pi}} \left[ e^{-S_v^2} + S_v \sqrt{\pi} (1 + \text{erf } S_v) \right], \quad (2.4-131)$$

[n<sub>i</sub>]<sub>f</sub> - total number of impinging molecules per unit volume per unit time.

On the Rear Surfaces (-∞ ≤ ν ≤ 0):

$$[\bar{E}'_i]_b = \frac{1}{2} m [n'_i]_b \left[ \bar{q}_i^2 + RT_i \left( 4 - \frac{1}{\phi_{b-1}} \right) \right], \quad (2.4-132)$$

where

$$\phi_b(S, \theta) = \frac{e^{-S^2}}{S_v \sqrt{\pi} (1 - \text{erf } S_v)}, \quad (2.4-133)$$

$$[n'_i]_b = [n_i]_b \sqrt{\frac{RT_i}{2\pi}} \left[ e^{-S_v^2} - S_v \sqrt{\pi} (1 - \text{erf } S_v) \right]. \quad (2.4-134)$$

(b) The translational energy per unit area per unit time, possessed by the emerging molecules. It can be determined through a choice of the accommodation coefficient, α.

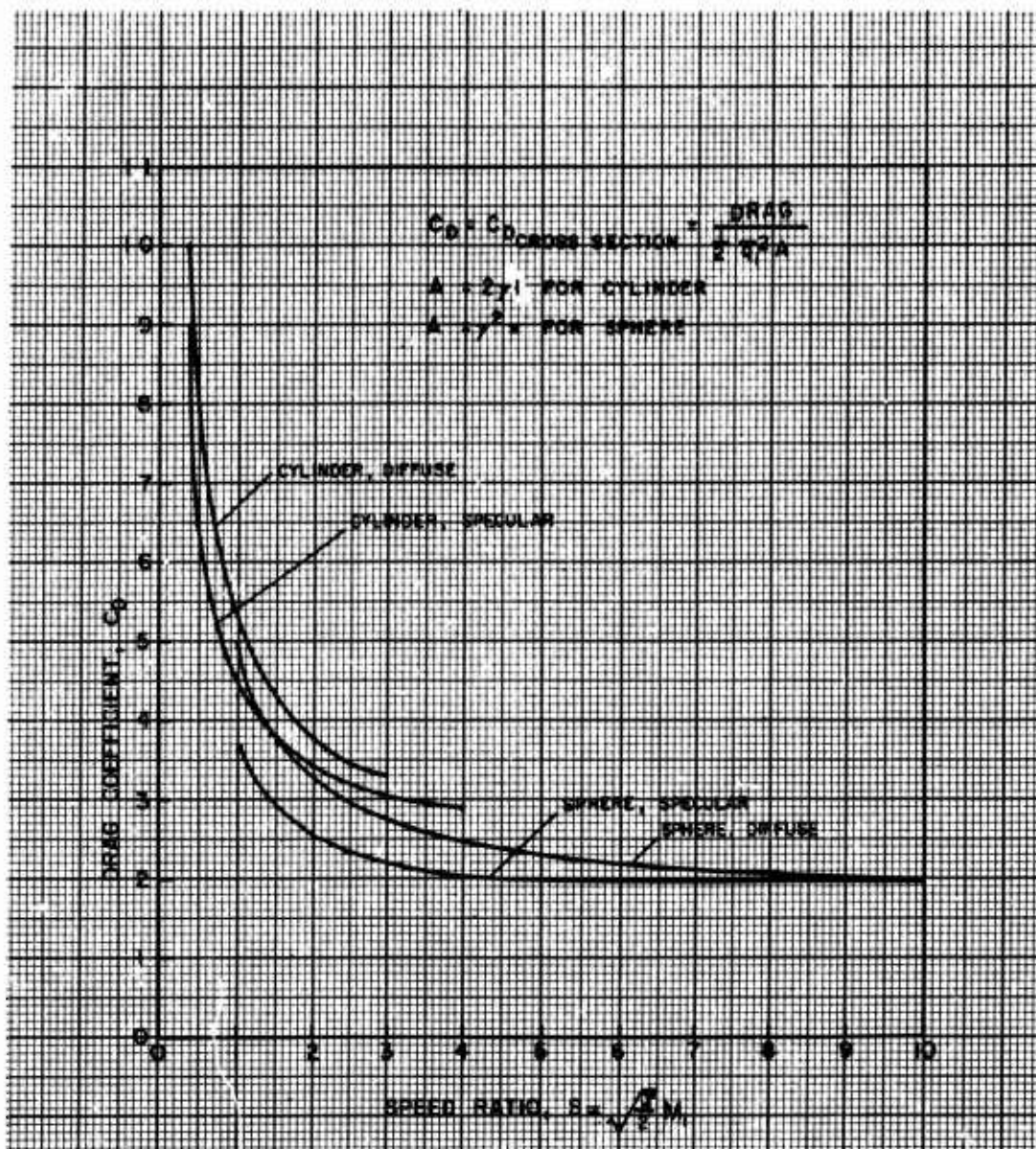


Fig (2.4-16) Drag coefficient for sphere and cylinder in free molecule flow.  
(Ref 22)

$$T_w = T_1, \text{ is. } S_w = S$$

On Front Surfaces ( $0 \leq \nu \leq \infty$ ):

$$[\bar{E}'_r]_f = (1 - \alpha) [\bar{E}'_i]_f + 2 \alpha m R [n'_i]_f T_w . \quad (2.4-135)$$

On Rear Surfaces ( $-\infty \leq \nu \leq 0$ ):

$$[\bar{E}'_r]_b = (1 - \alpha) [\bar{E}'_i]_b + 2 \alpha m R [n'_i]_b T_w . \quad (2.4-136)$$

(c) The radiation energy, evaluated for a supposedly "gray" body, i.e., a body emitting and receiving radiant energy with the emissivity,  $\epsilon$ , independent of both wave length and gas density:

Radiant Input From the Ambient Gas to Unit Area of the Body Surface:

$$[\bar{E}'_{in}] = \epsilon B T_c^4 , \quad (2.4-137)$$

where

$\epsilon$  - is the emissivity for "gray" bodies, dimensionless,

B - is the Stefan - Boltzmann's constant,  $B = 3.74 \times 10^9$  (foot-pound per square foot,  $^{\circ}F^4$ ),

$T_c$  - is the temperature of the outer boundary, containing both the gas and the body;  $^{\circ}F$ , assumed constant.

Radiant Emission From Body Surface:

$$[\bar{E}'_{EM}] = \epsilon B T_w^4 , \quad T_w = \text{const.} \quad (2.4-138)$$

(d) The internal energy output ( $J'$ ) from unit area of the body surface per unit time due to coolants (or any other concepts).

Then, the conservation of energy principle, expressed through the energy balance, yields that for the total body surface:

$$\begin{aligned} \int [\bar{E}'_i]_f dA + \int [\bar{E}'_i]_b dA + \epsilon B T_c^4 A &= \\ = \int [\bar{E}'_r]_f dA + \int [\bar{E}'_r]_b dA + A \epsilon B T_w^4 + J' A . \end{aligned} \quad (2.4-139)$$

In case of the cylinder ( $dA = r_i d\theta$ ) with its axis perpendicular to the free stream, the Eq (2.4-139) takes form (after substitution for  $\bar{E}'_r$ ):

$$\begin{aligned} \alpha \int_0^{\pi/2} [|\bar{E}'_i|_f + |\bar{E}'_i|_b] d\theta - \\ - 2 \alpha m R T_w \int_0^{\pi/2} [|\bar{n}'_i|_f + |\bar{n}'_i|_b] d\theta + \\ + 2 \pi [\epsilon B (T_c^4 - T_w^4) - J'] = 0 . \end{aligned} \quad (2.4-140)$$

or after substitution for  $|\bar{E}'_i|_f$ ,  $|\bar{E}'_i|_b$ ,  $|\bar{n}'_i|_f$  and  $|\bar{n}'_i|_b$  and after reduction of the integrals, the temperature,  $T_w$ , can be obtained in terms of molecular speed ratio,  $S$ , gas temperature,  $T_i$ , gas density,  $\rho_i$ , and temperature  $T_c$ :

$$\begin{aligned} 2 \frac{T_w}{T_i} (Z_1 + Z_2) - \left[ (S^2 + 2) Z_1 + (S^2 + \frac{5}{2}) Z_2 \right] + \\ + \frac{\sqrt{2}}{\alpha \rho_i} \left( \frac{\pi}{R T_i} \right) [\epsilon B (T_w^4 - T_c^4) - J'] = 0 , \end{aligned} \quad (2.4-141)$$

where  $Z_1 = \pi \sigma^{-1/2} S^2 I_0(\frac{1}{2} S^2)$ ,  $(2.4-142)$

$$Z_2 = \pi S^2 \sigma^{-1/2} S^2 \left[ I_0(\frac{1}{2} S^2) + I_1(\frac{1}{2} S^2) \right] . \quad (2.4-143)$$

$I_0$  and  $I_1$  are modified Bessel functions.

From the expression (2.4-141) for  $T_w$  the effective temperature  $T_r$  of the emergent molecules can be determined by specifying the proper value of the factor,  $\sigma$ , which determines the degree in which  $T_r$  approaches  $T_w$ . For adiabatic flow conditions (insulated cylinder) with ( $\sigma = \sigma' = 1$ ) and no exchange of either radiant or internal (coolant) energy, the reflected molecules shall emerge with a temperature equal to the surface temperature, ( $T_r = T_w$ ). Then, the expression (2.4-142) reduces to

$$\frac{T_r}{T_i} = \frac{T_w}{T_i} = \frac{(S^2 + 2) Z_1 + (S^2 + \frac{5}{2}) Z_2}{2(Z_1 + Z_2)} = F(S) , \quad (2.4-144)$$

and the drag force coefficient (for insulated cylinders in monoatomic gases), becomes:

$$\begin{aligned} C_{D \text{ CYLWET}} = \\ = C_D = \frac{\sqrt{\pi}}{S} \left\{ \sigma^{-1/2} S^2 \left[ I_0 + (S^2 + \frac{1}{2}) (I_0 + I_1) \right] + \right. \end{aligned} \quad (2.4-145)$$

$$+ \frac{1}{4} \left[ \frac{(S^2 + 2) Z_1 + (S^2 + \frac{1}{2}) Z_2}{2(Z_1 + Z_2)} \right]^{1/2} \} . \quad (2.4-145)$$

Eqs (2.4-144) and (2.4-145) are graphically presented in Figs (2.4-17) and (2.4-18) respectively. Note that the drag coefficient and  $(T_w / T_i)$  are functions only of the molecular speed ratio,  $S$ , and that the drag coefficient is independent of the Knudsen Number,  $Kn$ , provided  $Kn > 3$  which assures the free molecule flow conditions.

(iv) Spheres

The drag coefficient of a sphere in a free molecule flow can be found along the same lines as shown for flat plates and cylinders. For a sphere with a reference cross-section area ( $A = r^2 \pi$ ), where  $r$  is the sphere radius (22):

$$C_{D_{DIFF}} = \frac{e^{-S^2/2}}{\sqrt{\pi} S^3} (1 + 2S^2) + \frac{4S^4 + 4S^2 - 1}{2S^4} \times \\ \times \exp(S) + \frac{2\sqrt{\pi}}{3S_w}, \quad (2.4-146)$$

and

$$C_{D_{SPEC}} = C_{D_{DIFF}} - \frac{2\sqrt{\pi}}{3S_w}, \quad (2.4-147)$$

where

$$S_w = \frac{\bar{q}_1}{\sqrt{2RT_w}}, \quad (2.4-148)$$

$$S = \frac{\bar{q}_1}{\sqrt{2RT_i}} = \sqrt{\frac{\gamma}{2}} M_1. \quad (2.4-149)$$

Assuming  $(T_w = T_i)$ , i.e.,  $(S_w = S)$ , the above expressions become valid for both monoatomic and diatomic gases (i.e., independent of  $\gamma$ ). A graphical presentation of the  $C_{D_{SPHERE}} = f(S)$  case is presented in Fig (2.4-16).

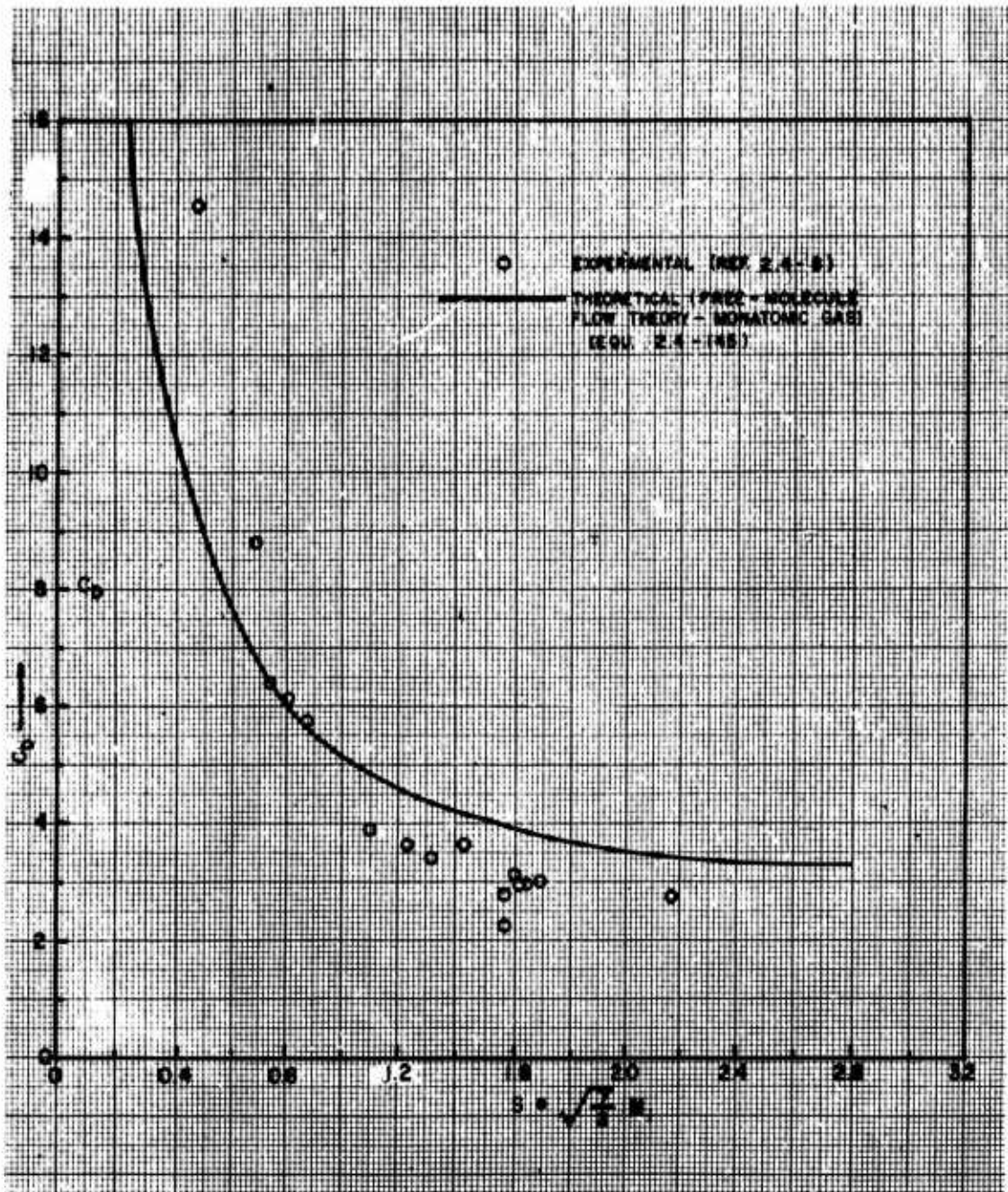


Fig (2.4-17) Drag of an insulated cylinder in helium. (Ref 12)

Assumption:  $T_r = T_w$ ,  $\sigma = \sigma' = 1$ ,

Adiabatic flow conditions,  
no radiant or internal  
coolant energy exchange.

Reference area,  $A = 2rL$ ,  $C_D = (C_{D,CYL})_{CROSS-SECTION} = \frac{DRAG}{\frac{1}{2} \rho_1 \bar{u}_1^2 A}$

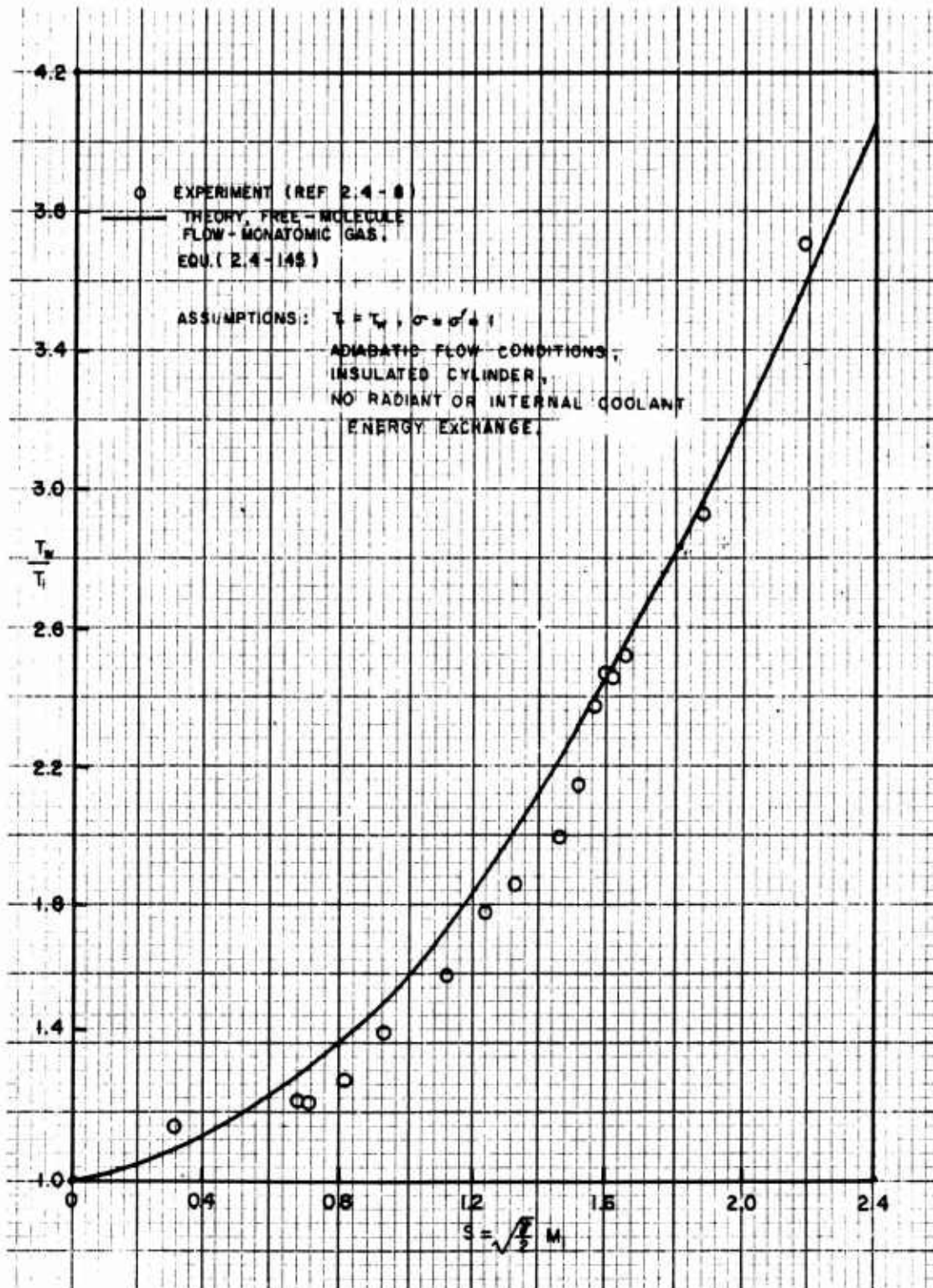


Fig (2.4-18) HEAT TRANSFER TESTS ON A CYLINDER IN HELIUM.  
(REF 12)

## 2.4.5 SLIP FLOW

### (i) General characteristics

In the slip flow regime the gas density is slightly less than for a continuum flow regime. The slip flow domain is defined by the Knudsen Number values,

$$.01 < \frac{M}{Re_L^{1/2}} \sim Kn_0 < .1, Re_L > 1. \quad (2.4-150)$$

Actually, in the slip flow regime the three governing parameters,  $Kn$ ,  $M$ ,  $Re$ , which represent the rarefaction, the compressibility and the viscosity effects respectively, are mutually so interrelated that the Eq (2.4-150) is satisfied either for large values of  $M$ , for small values of  $Re$ , or both.

In the equilibrium kinetic theory of gases, the slip flow is characterized by a non-Maxwellian velocity distribution law, the degree of rarefaction being less than in the free molecule flow case. The relatively simple theoretical approach, which has been adopted in the free molecule flow analysis, is not applicable to the slip flow regime: the motion is nonisentropic, requiring a more general velocity distribution function and more generalized boundary conditions. A modified boundary layer concept is introduced: it is expected that the boundary layer will be laminar and of an appreciable thickness. The interaction between such thick boundary layers and the inviscid outer flow becomes significant<sup>(31, 32, 33)</sup>. Due to this pronounced and complex interrelationship between the viscous, the compressible and the rarefied gas effects, there are no generalized theoretical approaches handling all the factors simultaneously. It can be only anticipated that, other factors being similar, the over-all effect of the rarefied slip flow and the associated velocity and temperature jumps at the inner boundary will result in a reduction of the skin friction coefficient value.

The formulation of the slip flow problem in form of differential equations can be done along several approximate theoretical or semi-empirical lines. Two basic well-known approaches are:

- A modification of the classical Navier-Stokes equations, resulting in the Burnett equations for the slip-flow

changed boundary conditions, including the associated temperature jump<sup>(5)</sup>.

- The use of the Thirteen Moment principle<sup>(34)</sup>. Neither the Burnett nor the Thirteen Moment equations have shown any real advantages in handling the problem<sup>(22)</sup>. Instead, some recent experimental evidence indicates that a more straightforward handling of the Navier-Stokes equations with the changed slip-velocity and temperature-jump boundary conditions may yield better results than the two mentioned theoretical approaches.

A brief outline of the main features of the slip flow regime can be illustrated by investigating it on the basis of the classical kinetic theory of gases. The slip-flow regime is treated as a non-Maxwellian motion of a rarefied gas with the specified boundary conditions different from those in the continuum flow case.

### (1) Two-dimensional laminar boundary layers of the continuum flow regime - kinetic theory approach.

The non-Maxwellian molecular velocity distribution function<sup>(12)</sup> for slightly non-isentropic conditions is confined to a thin layer adjacent to the flat plate surface, the gas flow within the laminar layer being regarded as steady, laminar, and compressible. Everywhere outside the thin boundary layer, i. e., beyond the predominant influence of the solid surfaces, the gas flow is considered completely isentropic with the molecular velocity distribution function conforming to the isentropic form of the Maxwell's law. The concept is compatible to the Prandtl's postulate from the continuum flow theory.

The boundary layer thickness can be defined in terms of either the ordered mass velocity,  $\delta_u(x)$ , or temperature,  $\delta_T(x)$ , see Fig (2.4-19), reflecting the twofold nature of a nonisentropic flow random molecular transport mechanism, the momentum and the heat transfer effects respectively. The two boundary layer thicknesses are different in general, but it is assumed that they are of the same order of magnitude, expressed through some modified form of the Reynolds Analogy Concept.

$\delta_u(x) - \delta_T(x)$  of the same order of magnitude  
 $T_g$  = Maximum temperature in boundary layer

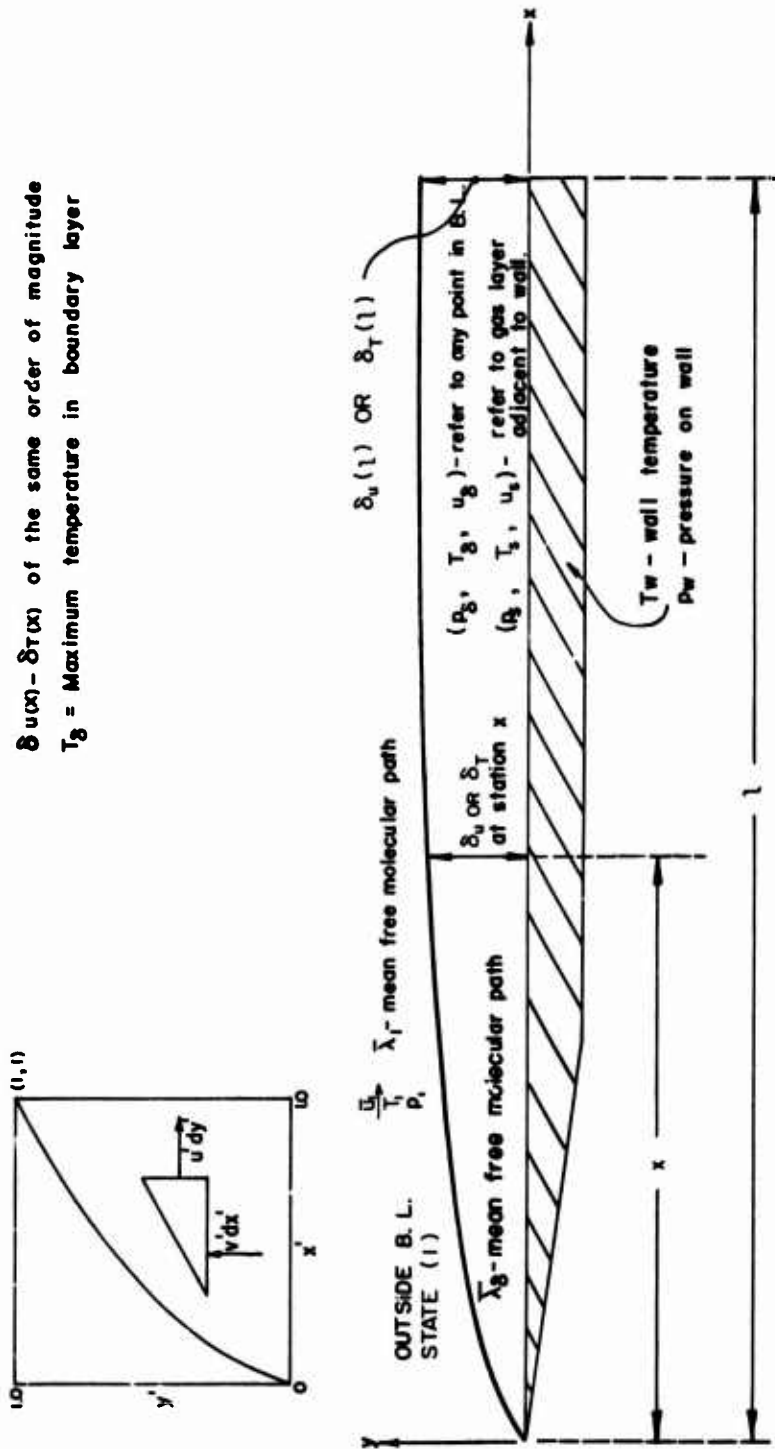


FIG (2.4-19) BOUNDARY LAYER ON A FLAT PLATE (REF 12)

The general equations of motion for steady, two-dimensional, non-isentropic, compressible flows can be written in the form(12):

$$\frac{\partial}{\partial x} (\rho \bar{u}) + \frac{\partial}{\partial y} (\rho \bar{v}) = 0, \quad (2.4-151)$$

$$\rho \frac{d\bar{u}}{dt} = -\frac{\partial}{\partial x} \left[ p - \mu \left( \frac{4}{3} \frac{\partial \bar{u}}{\partial x} - \frac{2}{3} \frac{\partial \bar{v}}{\partial y} \right) \right] + \frac{\partial}{\partial y} \left[ \mu \left( \frac{\partial \bar{v}}{\partial y} + \frac{\partial \bar{v}}{\partial x} \right) \right],$$

$$\rho \frac{d\bar{v}}{dt} = +\frac{\partial}{\partial x} \left[ \mu \left( \frac{\partial \bar{u}}{\partial y} + \frac{\partial \bar{v}}{\partial x} \right) \right] - \frac{\partial}{\partial y} \left[ p + \mu \left( \frac{2}{3} \frac{\partial \bar{u}}{\partial x} - \frac{4}{3} \frac{\partial \bar{v}}{\partial y} \right) \right], \quad (2.4-152)$$

$$\rho c_v \frac{dT}{dt} = - \left[ p - \mu \left( \frac{4}{3} \frac{\partial \bar{u}}{\partial x} - \frac{2}{3} \frac{\partial \bar{v}}{\partial y} \right) \right] \frac{\partial \bar{u}}{\partial x} - \left[ p + \mu \left( \frac{2}{3} \frac{\partial \bar{u}}{\partial x} - \frac{4}{3} \frac{\partial \bar{v}}{\partial y} \right) \right] \frac{\partial \bar{v}}{\partial y} + \mu \left( \frac{\partial \bar{u}}{\partial y} + \frac{\partial \bar{v}}{\partial x} \right)^2 + \frac{\partial}{\partial x} \left( k \frac{\partial T}{\partial x} \right) + \frac{\partial}{\partial y} \left( k \frac{\partial T}{\partial y} \right). \quad (2.4-153)$$

This general form of the two-dimensional, slightly nonisentropic flow equations shall be applied to laminar viscous flows across a flat noninsulated plate at a zero angle of attack. The molecular motion in the layer directly adjacent to the surface needs to be first defined, i.e., the boundary conditions at the surface specified. The actual mechanism of interaction between the real gas molecules and a real surface is as yet not completely understood. The related experimental observations depend upon the method and the apparatus used, surface material, surface absorption rates of the molecules, condensation effects, etc. Most theories distinguish between the following two basic premises:

(a) A specular (isentropic) reflection of molecules

Only if a surface is insulated and assumed ideally smooth, and a monoatomic gas flow considered as ideally isentropic, can a specular molecular reflection occur; the tangential velocity component remains unchanged, while the normal velocity component reverses its sign. The boundary conditions are then specified as being for a "perfect slip

flow", and the simplest isentropic form of the Maxwell's velocity distribution function(12) holds both for the impinging and the perfectly elastically rebound molecules on the surface. The molecular motion in the layer adjacent to the surface is purely Maxwellian, i.e., isentropic.

Obviously, under these premises, the viscous effects in a laminar boundary layer cannot be investigated.

(b) A diffuse (nonisentropic) molecular reflection

Real solid surfaces are microscopically of an irregular grain pattern, promoting a diffuse reflection of molecules to a greater or lesser extent, see Section 2.4.1.

A diffuse molecular reflection is characterized by a complete loss of the tangential ordered velocity component of the impinging molecules at the surface ( $\bar{v}_s = 0$ ). The molecules are temporarily trapped at the surface and re-emitted with random molecular speeds ( $\bar{u}', \bar{v}'$ ) after attaining either partially or completely the thermal equilibrium with the surface. The re-emitted molecules have no velocity of ordered motion ( $\bar{u} = \bar{v} = 0$ ). The random molecular speed distribution function of the diffusely reflected molecules is supposed to follow the Maxwell's law, but modified to correspond to a temperature which is different both from the temperature of the impinging stream and the temperature of the surface. Due to the discontinuity of molecular motion during the transient period of time in which the molecules are trapped at the surface irregularities, there is no directional preference for the reflected molecules: all directions of random molecular motion away from the surface are equally probable.

The mathematical model for the diffuse reflection (three-dimensional) is illustrated in Fig (2.4-1), with the reference axes fixed to the wall at rest. The molecules in the element of volume (S) of the oncoming stream, adjacent to the solid wall ( $\bar{v}_s = 0$ ), have a relative ordered velocity components ( $u_s, v_s = 0, w_s$ ) with respect to the wall at rest and the random motion velocity components ( $u', v', w'$ ), which are governed by the Maxwellian velocity distribution function (f) of slightly nonisentropic flows. The diffusely reflected molecules are treated as if

they were re-emitted from an element of the wall volume, (W), on the other side of the interface, where the molecules are supposedly trapped ( $\bar{u}_s, \bar{v}_s, \bar{w}_s$ ). Consequently, the rejected molecules have no velocity components of the ordered motion, and their random molecular velocity components ( $u', v', w'$ ) distribution law ( $f_0$ ) is assumed to follow the free-molecule Maxwell's velocity distribution function of isentropic gases, where the ( $f_0$ ) function is evaluated for a temperature ( $T_r \neq T_w, T_r \neq T_s$ ), in general.

The boundary conditions for the diffuse molecular reflection pattern are characterized by small discontinuities of normal pressure ( $p$ ), tangential mass velocity of ordered motion ( $\bar{u}$ ,  $\bar{v}$ ) and temperature ( $T$ ) at the interface between the gas layer adjacent to the wall and the wall proper. These discontinuities arise from the fact that (1) the molecular random motion of the impinging molecules of the oncoming stream is non-Maxwellian (nonisentropic) near the wall, and (2) the molecular random motion of the diffusely reflected molecules is Maxwellian but evaluated for a temperature ( $T_w$ ) different from ( $T_s$ ). Using the subscript ( $s$ ) to denote conditions in the stream layer adjacent to the wall, and the subscript ( $w$ ) to denote conditions of the solid surface, the stated small discontinuities in pressures, temperatures and ordered motion velocities are analytically given for the assumed slightly nonisentropic conditions by (12):

$$\frac{p_s}{p_w} = 1 - \frac{5}{6} \left[ \frac{\bar{\lambda}}{\bar{c}} \left( \frac{\partial \bar{u}}{\partial x} + \frac{\partial \bar{w}}{\partial z} - 2 \frac{\partial \bar{v}}{\partial y} \right) \right]_s + \frac{15}{16} \left[ \frac{\bar{\lambda}}{T} \frac{\partial T}{\partial y} \right]_s, \quad (2.4-154)$$

$$\frac{T_s}{T_w} = 1 - \frac{5}{54} \left[ \frac{\bar{\lambda}}{\bar{c}} \left( \frac{\partial \bar{u}}{\partial x} + \frac{\partial \bar{w}}{\partial z} - 2 \frac{\partial \bar{v}}{\partial y} \right) \right]_s + \frac{15\pi}{128} \left[ \frac{\bar{\lambda}}{T} \frac{\partial T}{\partial y} \right]_s, \quad (2.4-155)$$

$$\bar{u}_s = \bar{\lambda}_s \left[ \frac{5\pi}{16} \left( \frac{\partial \bar{u}}{\partial y} + \frac{\partial \bar{v}}{\partial x} \right) + \frac{15\pi}{128} \frac{\bar{c}}{T} \frac{\partial T}{\partial x} \right]_s, \quad (2.4-156)$$

$$\bar{w}_s = \bar{\lambda}_s \left[ \frac{5\pi}{16} \left( \frac{\partial \bar{w}}{\partial y} + \frac{\partial \bar{v}}{\partial z} \right) + \frac{15\pi}{128} \frac{\bar{c}}{T} \frac{\partial T}{\partial x} \right]_s,$$

$$\bar{v}_s = 0. \quad (2.4-157)$$

These discontinuities can be treated either as negligibly small or significant, depending upon the state of gas and the conditions of the real surface. For gases at ordinary temperatures and only slightly rarefied, i.e., for continuum flow conditions, it is customary

to assume in the boundary layer theory that the viscous and the slightly non-isentropic effects are well represented if both the diffusely re-emitted molecules and the impinging molecules of the stream next to a smooth wall have a Maxwellian random motion. Then the discontinuities can be regarded as negligibly small, and

$$p_s = p_w, \quad \bar{u}_s = \bar{w}_s = 0, \quad T_s = T_w. \quad (2.4-158)$$

For rarefied gases under "slip flow" boundary conditions and with accompanying "temperature jumps" between the wall and the gas, the discontinuities represented by Eqs (2.4-154) to (2.4-157) cannot be treated as negligible.

Within the continuum flow concepts, the boundary conditions (2.4-158) are taken as valid. They shall be applied to the general form of the two-dimensional equations (2.4-151) (2.4-152) and (2.4-153), after they have been reduced to a simpler first-order laminar boundary layer form by a proper nondimensionalization and an order-of-magnitude analysis, as follows:

Assuming relatively thin boundary layers, see Fig (2.4-19), it follows that:

$$0 \leq x \leq l,$$

$$0 \leq y \leq \delta_u(l), \text{ or } \delta_T(l),$$

$$\delta_u(l) \sim \delta_T(l) \ll l, \quad (2.4-159)$$

i.e., ( $x$ ) and ( $y$ ) coordinates are of different orders of magnitude. This assumption permits introduction of the respective nondimensional quantities (primed) of length:

$$x' = \frac{x}{l}, \quad y' = \frac{y}{\delta_u(l)} \sim \frac{y}{\delta_T(l)}, \quad \delta' = \frac{\delta_u(l)}{\delta_T(l)}, \quad (2.4-161)$$

which are all of the order one.

Assuming further that the free stream temperature ( $T_1$ ) the maximum temperature in the boundary layer ( $T_0$ ) and the temperature of the gas layer adjacent to the wall ( $T_s$ ), are of the same order of magnitude, i.e., that for any point in the boundary layer,

$$T_1 \leq T \leq T_0, \quad (2.4-162)$$

it follows that:

$$T' = \frac{T}{T_s} \sim \text{ORDER OF ONE} \quad (2.4-163)$$

By similar considerations, the inequality

$$\bar{u}_s \leq u \leq \bar{u}_1 \quad (2.4-164)$$

leads to

$$u' = \frac{u}{\bar{u}_1} \sim \text{ORDER OF ONE} \quad (2.4-165)$$

and also

$$\rho' = \frac{\rho}{\rho_1} \sim \text{ORDER OF ONE} \quad (2.4-166)$$

$$p = \frac{p}{p_1} \sim \text{ORDER OF ONE} \quad (2.4-167)$$

The assumption of a relatively thin boundary layer can be expressed also as

$$D = \frac{\delta_u(l)}{l} \ll 1 \quad (2.4-168)$$

i.e., by a nondimensional length (D) which is a small number of a lesser order of magnitude than one.

Introducing further the assumption that for laminar boundary layers formed by not-too-rarefied gases (near standard gas conditions), another nondimensional length,

$$\Delta = \frac{\bar{\lambda}_1}{\delta_u(l)} \ll 1 \quad (2.4-169)$$

is also a small number of about the same order of magnitude (less than one) as (D), it follows that the velocity component perpendicular to the wall,

$$v \ll u \quad (2.4-170)$$

since both

$$y \ll x,$$

$$\delta_u(l) \ll l,$$

$$\text{and } \bar{\lambda}_1 \ll \delta_u(l).$$

Under the premises, in order to define a nondimensional velocity com-

ponent normal to the wall ( $v'$ ) of the order of one (i.e., of the same order as  $u'$ ), the following line of argumentation may be used:

Mass flux across an element of any line within the boundary layer is

$$\psi' = \rho (\bar{u} dy - \bar{v} dx) \quad (2.4-171)$$

and if the line is a streamline,

$$\bar{u} dy = \bar{v} dx \quad (2.4-172)$$

$$\therefore \frac{\bar{v}}{\bar{u}} = \frac{dy}{dx} = \frac{\bar{v}}{\bar{u}} \quad (2.4-173)$$

Eq (2.4-173) together with Eqs (2.4-168) and (2.4-161) yields:

$$dy = dy' \delta_u(l),$$

$$dx = dx' l,$$

$$dy' \sim dx' \quad (\text{AS INDEPENDENT VARIABLES}),$$

$$v' = \frac{\bar{v}}{\bar{v}_1} = \frac{\bar{v}}{\bar{u}} \frac{dx}{dy} = \frac{\bar{v}}{\bar{u}} \frac{l}{\delta_u(l)},$$

$$\therefore v' = \frac{\bar{v}}{\bar{u}} \frac{1}{D} \quad (2.4-174)$$

The corresponding nondimensional forms of the boundary conditions, Eqs (2.4-154) to (2.4-157), are then:

$$\frac{p'_s}{p'_w} = 1 - L'_s \Delta \left[ \frac{a_1 M_1 D}{(T')^{1/2}} \left( \frac{\partial u'}{\partial x'} - 2 \frac{\partial v'}{\partial y'} \right) - \frac{a_2 \delta'}{T'} \frac{\partial T'}{\partial y'} \right]_s \quad (2.4-175)$$

$$u'_s = L'_s \Delta \left[ a_3 \left( \frac{\partial u'}{\partial y'} + \frac{\partial v'}{\partial x'} \right) + \frac{a_4 D}{M_1 (T')^{1/2}} \frac{\partial T'}{\partial x'} \right]_s \quad (2.4-176)$$

$$\frac{T'_s}{T'_w} = 1 - L'_s \Delta \left[ \frac{a_5 M_1 D}{(T')^{1/2}} \left( \frac{\partial u'}{\partial x'} - 2 \frac{\partial v'}{\partial y'} \right) - \frac{a_6 \delta'}{T'} \frac{\partial T'}{\partial y'} \right]_s \quad (2.4-177)$$

where

$$L'_s = \frac{l}{\rho'_s} \quad , \quad M_1 = \frac{\bar{u}_1}{\sigma_1} \sim \text{ORDER ONE} \quad ,$$

$a_1, a_2, a_3, a_4, a_5,$  and  $a_6$  are constants.

All primed quantities are of the

order of one. Since  $\Delta$  is negligibly small, the bracketed terms in the Eqs (2.4-175) to (2.4-177) become negligibly small also, and the boundary conditions are as stated earlier:

$$\bar{u}_s = 0, \quad p_s = p_w, \quad T_s = T_w. \quad (2.4-178)$$

Finally, for two-dimensional compressible, steady laminar boundary layers along smooth, flat plates at a zero-angle-of-attack, it can be assumed that there is no pressure gradient in the x-direction,

$$\frac{\partial p}{\partial x} = 0, \quad (2.4-179)$$

leading to only a negligible pressure gradient in the y-direction also:

$$\frac{\partial p}{\partial y} = 0, \quad (2.4-180)$$

The general forms of the governing Eqs (2.4-151) to (2.4-153) are then reduced to:

$$\frac{\partial}{\partial x}(\rho \bar{u}) + \frac{\partial}{\partial y}(\rho \bar{v}) = 0, \quad (2.4-181)$$

$$\rho(\bar{u} \frac{\partial \bar{u}}{\partial x} + \bar{v} \frac{\partial \bar{u}}{\partial y}) = \frac{\partial}{\partial y}(\mu \frac{\partial \bar{u}}{\partial y}), \quad (2.4-182)$$

$$\rho c_v(\bar{u} \frac{\partial T}{\partial x} + \bar{v} \frac{\partial T}{\partial y}) = -\rho(\frac{\partial \bar{u}}{\partial x} + \frac{\partial \bar{v}}{\partial y}) + \mu(\frac{\partial \bar{u}}{\partial y})^2 + \frac{\partial}{\partial y}(k \frac{\partial T}{\partial y}), \quad (2.4-183)$$

$$p = \rho R T, \quad (2.4-184)$$

$$\frac{\mu}{\mu_i} = \frac{k}{k_i} = f\left(\frac{T}{T_i}\right). \quad (2.4-185)$$

where the second of the momentum equations (2.4-152) becomes of a negligible order of magnitude in all terms.

The momentum transfer equation, assuming a constant temperature of the flat plate surface, yields for the local skin friction coefficient ( $C_f'$ ) the following expression in terms of the isentropic mean free molecular path ( $\bar{\lambda}$ ) taken as a reference length<sup>(42)</sup>:

$$C_f' = \tau_w = .664 \left( \frac{\sigma}{X Re_i} \right)^{1/2}, \quad (2.4-186)$$

where

$X = \left( \frac{x}{\lambda_i} \right)$  - is the dimensionless position coordinate,

$\bar{\lambda}_i$  - is the mean free molecular path outside the boundary layer (isentropic flow),

$Re_i$  - is the Reynolds Number at the station ( $X = x/\lambda_i$ ), referred to the molecular path ( $\bar{\lambda}_i$ ),

$$Re_i = \frac{\rho_i \bar{\lambda}_i u_i}{\mu_i},$$

$\sigma = \frac{\mu}{\mu_i} = (\Theta_w)^{1/2} \left( \frac{1 + \alpha/T_i}{\Theta_w + \alpha/T_i} \right)^{-1}$  is the best suitable constant for the ( $\mu$ ) estimates, over the relevant temperature-viscosity ratio (assuming the constant surface dimensionless temperature, ( $\Theta_w$ ), obtained by matching expressions,

$$\frac{\mu}{\mu_i} = \left( \frac{T}{T_i} \right)^{3/2} \left( \frac{T_i + \kappa}{T + \kappa} \right),$$

and

$$\frac{\mu}{\mu_i} = \sigma \left( \frac{T}{T_i} \right),$$

according to Chapman and Rubesin (42),

$\Theta = \frac{T}{T_i}$  - is the dimensionless temperature ratio at any point within the boundary layer,

$\Theta_w = \frac{T_w}{T_i}$  - is the dimensionless temperature ratio at the surface, assumed constant.

$$\alpha = 1.09924.$$

The average skin-friction coefficient per unit width on one side of the plate of length  $l$ , based on the free stream dynamic pressure ( $1/2 \rho_i \bar{u}_i^2$ ), with the mean free molecular path ( $\bar{\lambda}_i$ ) as the basic reference length is then:

$$C_f = \frac{\bar{\lambda}_i}{l} \int_0^{l/\bar{\lambda}_i} \tau_w dx = 1.328 \left( \frac{\sigma K_n}{Re_i} \right)^{1/2}. \quad (2.4-187)$$

where  $K_n = \bar{\lambda}_i/l = \Theta \Delta$  is the Knudsen Number.

The Knudsen Number must be very small,

$$K_n \ll 1,$$

if the continuum flow boundary layer equations (2.4-181) to (2.4-185) and

the assumed boundary conditions (2.4-158) are to be valid, i.e., the continuum flow conditions of not-too-rarefied gaseous states must be satisfied. For higher rarefactions, violating the condition (2.4-188) the above analysis and solutions are invalidated, since the momentum and the heat transport mechanisms are radically different: collisions between gas molecules become then increasingly less significant regarding the molecular transport processes, which are instead accomplished more through a direct exchange mechanism between the freely moving molecules and the solid surface.

Similarly, from the energy transfer equation analysis, a particular solution assuming constant surface temperature conditions for steady, continuum flow laminar boundary layers is obtained(42):

$$\Theta = \left[ 1 + r(\eta) \frac{\gamma-1}{2} M_1^2 + (\Theta_w - \Theta_{ow}) \frac{s(\eta)}{s(0)} \right] ,$$

where: (2.4-189)

$\eta$  - is a nondimensional parameter of transformation used in solution of the laminar boundary layer equations, related to the perpendicular ( $y$ ) distance from the flat plate at a given position ( $x$ ) by the expression,

$$f(\eta) = \frac{(Re_1/\sigma)^{1/2} \Psi}{(x/\lambda_1)^{1/2}} , \quad (2.4-190)$$

$\Psi$  - is the dimensionless stream function,

$$\left[ (\bar{u}/\bar{u}_1)(\rho/\rho_1) \right] = \frac{\partial \Psi}{\partial y} ,$$

$$\left[ (\bar{v}/\bar{v}_1)(\rho/\rho_1) \right] = - \frac{\partial \Psi}{\partial x} , \quad (2.4-191)$$

$r(0)$  - is the recovery factor, obtainable from

$$\Theta_{ow} = 1 + r(0) \frac{\gamma-1}{2} M_1^2 ,$$

$r(0) = 1$  for  $Pr = 1$ ,

$r(0) = .85$  for  $Pr = .74$  (air),

$M_1 = \bar{u}/\bar{a}_1$  - is the free stream Mach Number,

$\gamma = C_p/C_v$  - is the specific heat ratio,

$\Theta_{ow} = (T_{ow}/T_1)$  - dimensionless equilibrium temperature, corresponding to no heat transfer condition at the surface, i.e., the adiabatic wall temperature,

$\Theta_w = (T_w/T_1)$  - is the actual wall temperature ( $\Theta_w < \Theta_{ow}$ ),

$r(\eta)$  and  $s(\eta)$  are functions of the Prandtl

Number and  $\eta$ , see Fig (2.4-20)

$Pr = \frac{\mu_1 C_p}{k_1} = \frac{4\gamma}{9\gamma-5}$  is the Prandtl Number, free stream reference value,

$\Theta = (T/T_1)$  is the dimensionless temperature at any point in the boundary layer.

Analogous to  $(C_f)$ , the local dimensionless heat transfer coefficient through unit area in unit time at the surface is

$$S_f = q'_w = .296 \left( \frac{\Theta_w - \Theta_{ow}}{Pr} \right) \left( \frac{\sigma}{Re_1 X} \right)^{1/2} ,$$

(2.4-193)

and the ratio of the local coefficients of heat transfer and friction on the surface is

$$(S_f/C_f) = (.445/Pr) (\Theta_w - \Theta_{ow}) .$$

(2.4-194)

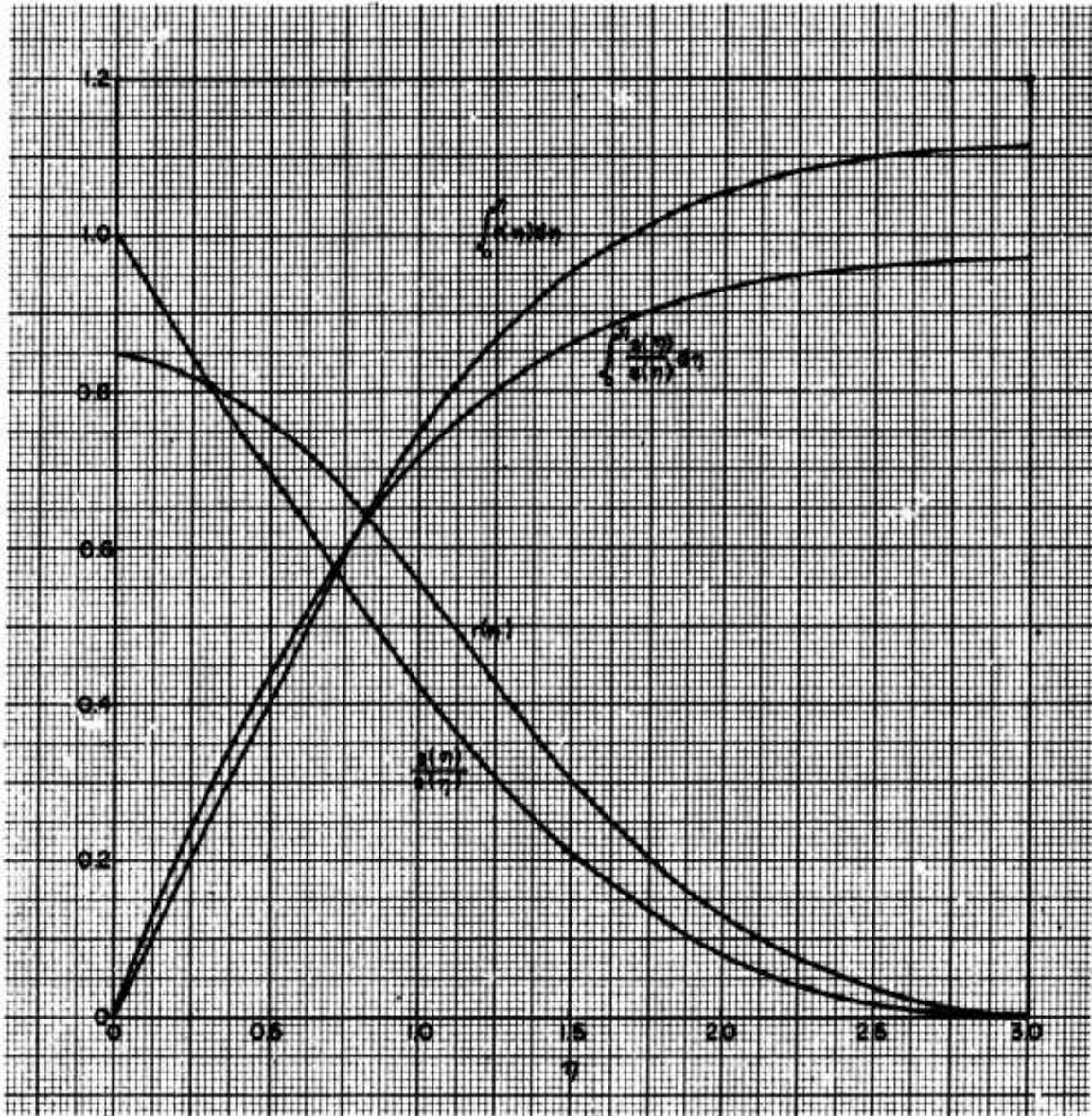
The average heat transfer coefficient on one side of a flat plate of length ( $l$ ), called the average Stanton Number, is:

$$S_f = \frac{\lambda_1}{l} \int_0^{l/\lambda_1} q'_w dx = .5915 \left( \frac{\Theta_w - \Theta_{ow}}{Pr} \right) \left( \frac{\sigma K_n}{Re_1} \right)^{1/2} .$$

(2) Momentum transfer in the slip flow regime

The basic expressions for the local and the average skin-friction coefficients under the slip flow conditions are obtained by modifying the flat plate laminar boundary layer equations and the associated continuum flow boundary conditions accordingly. A treatment of the problem is presented by Nonweiler(35), Shaaf(10,36,38) Mirels(37), Lin and Shaaf(39), representing approximate solutions based on a suitable extension and modification of the Rayleigh's(40) analysis of nonstationary flows which are created by an instantaneous (impulsive) acceleration of an infinite flat plate from a rest state to a constant speed regime. The main fundamentals that lead to the extension and modification of the continuum flow (laminar) boundary layer theory to the concepts of the laminar boundary layers in the slip flow regime is the following:

In treating the classical continuum laminar boundary layers equations (2.4-151) to (2.4-153) for steady gas flows at ordinary densities, it



Fig(2.4-20) Curves for  $r(\eta)$ ,  $s(\eta)$  and their integrals (Ref 2.4-42)

has been assumed that due to ( $K_n \ll 1$ ), both the ratio ( $D$ ) of the thickness of the velocity layer ( $\delta_v$ ) at a station ( $l$ ), and the ratio ( $\Delta$ ) of the reference mean free molecular path ( $\bar{\lambda}$ ) to the thickness of the boundary layer ( $\delta_v$ ) at ( $x=l$ ), are quantities of the same negligibly small order of magnitude:

$$\Delta = \frac{\bar{\lambda}_l}{\delta_v(l)} \approx \left(\frac{Re_l}{\sigma X}\right)^{1/2} \ll 1, \quad (2.4-196)$$

$$D = \frac{\delta_v(l)}{l} \approx \left(\frac{l}{\sigma Re_l X}\right)^{1/2} \ll 1. \quad (2.4-197)$$

The negligible smallness of the above dimensionless parameters, ( $\Delta$ ) and ( $D$ ), allows for a reduction of the boundary conditions in the continuum flow domain to the well-known "no-slip" velocity condition at the surface and to the equality of pressures and temperatures of the gas layer next to the surface (subscript  $s$ ) and the body surface itself (subscript  $w$ ), provided the surface is insulated, i.e.:

$$\bar{u}_s = 0, \quad p_s = p_w, \quad T_s = T_w, \quad (2.4-198)$$

$$\frac{\partial p}{\partial x} = 0, \quad \frac{\partial p}{\partial y} = 0, \quad \frac{\partial v}{\partial x} = 0. \quad (2.4-199)$$

Obviously, the classical laminar boundary layer equations do not hold in the region near the leading edge of the flat plate: there, the local coordinate ( $x$ ) can be of the same order of magnitude as the mean free molecular path ( $\lambda_l$ ), violating the basic assumption that

$$x \gg \lambda_l, \quad (2.4-200)$$

i.e., both ( $\Delta$ ) and ( $D$ ) become significant quantities (of the order of  $<1$ ), with ( $\Delta$ ) being more prominent in importance at supersonic Mach Numbers.

This leading edge "anomaly" of the classical continuum flow boundary layer theory spreads more and more along the flat plate as the rarefaction of the undisturbed (ambient) free stream is increased. When the ambient gas density is decreased to such a level that the mean free path becomes comparable to the total plate length,

$$\bar{\lambda}_l \approx l, \quad (2.4-201)$$

both ( $\Delta$ ) and ( $D$ ) must be taken into account for the whole laminar boundary layer, changing the boundary conditions from the classical "no-slip" to a new "slip-flow" form (subscript  $s$ ),

$$\bar{u}_s = \left(\zeta \frac{\partial u}{\partial y}\right)_s \bar{u}_l < 1, \quad (2.4-202)$$

i.e., the velocity of the gas layer next to the surface,  $\bar{u}_s$ , is small but finite, where

$U = \frac{u}{\bar{u}_l}$  - is the dimensionless velocity at any point ( $y$ ) in the boundary layer,

$Y = \frac{y}{\lambda_l}$  - is the dimensionless vertical position coordinate,

$\left(\zeta \frac{\partial u}{\partial x}\right)_s$  - is evaluated at the wall,

$\bar{u}_l$  - is the free stream velocity ( $\bar{u}_l = V_M$ ), for a two-dimensional flat plate at a zero angle-of-attack,

$\zeta = \frac{\bar{\lambda}}{\lambda_l}$  - is the dimensionless ratio of the mean free molecular paths at any point ( $y$ ) within the boundary layer,

$\bar{\lambda}_l$  - is the mean free molecular path at free stream (undisturbed) conditions.

The change in the order-of-magnitude of the characteristic flow parameters and the changed boundary conditions shall subsequently alter the form of the classical boundary layer equations, which have been obtained from the general slightly nonisentropic flow expressions for mass, momentum and energy conservation by an application of the order of magnitude analysis, i.e., by retaining only the terms that proved to be of the order of 1 (see Sections 2.2 and 2.3), and by neglecting all the terms of the negligibly small orders of magnitude ( $\Delta$ ), ( $D$ ), ( $\Delta D$ ), and ( $D^2 \Delta$ ). Under the changed slip flow conditions, the terms of the order ( $\Delta$ ) and ( $D$ ) shall be retained in addition to the terms of the order 1, and only the quantities of the order ( $D \Delta$ ) and ( $D^2 \Delta$ ) neglected. (Note that the important "orders" now are 1 and  $\Delta \approx D < 1$ ). As a consequence, the momentum equation in the  $y$ -direction for two-dimensional boundary

layers cannot be neglected, and all the terms of the order of  $(\Delta)$  and  $(D)$  should be retained.

Instead of handling directly the very complex system of the modified differential equations for the slip-flow conditions, an alternative approach of extending the Rayleigh's problem<sup>(40)</sup> can be used, leading to an approximate solution<sup>(12)</sup> for the slip flow conditions.

The Rayleigh's equations<sup>(10,40)</sup>, which express the stationary conditions achieved after an infinite flat plate has been instantaneously accelerated from rest to a constant speed, can be reversed to the equivalent conditions occurring when a viscous compressible gas is impulsively accelerated to a constant free stream mass velocity  $(\bar{u}_1 = \bar{v}_1 = v_{H1})$  along a fixed flat plate, yielding the following equations of mass, momentum and energy conservation (two-dimensionally):

$$\frac{\partial \rho}{\partial t} + \frac{\partial}{\partial y}(\rho v) = 0, \quad (2.4-203)$$

$$\rho \frac{d\bar{u}}{dt} = \frac{\partial}{\partial y}(\mu \frac{\partial \bar{u}}{\partial y}), \quad \rho \frac{d\bar{v}}{dt} = \frac{4}{3} \frac{\partial}{\partial y}(\mu \frac{\partial \bar{v}}{\partial y}),$$

$$\rho C_v \frac{dT}{dt} = -\rho \frac{\partial \bar{v}}{\partial y} + \frac{4}{3} \mu \left(\frac{\partial \bar{v}}{\partial y}\right)^2 +$$

$$\mu \left(\frac{\partial \bar{u}}{\partial y}\right)^2 + \frac{\partial}{\partial y}(\kappa \frac{\partial T}{\partial y}), \quad (2.4-205)$$

with  $\rho = \text{const}$  throughout the fluid field.

Properly nondimensionalized for the changed slip-flow conditions, the system of equations (2.4-203), (2.4-204) and (2.4-205) yields to the following method of solution<sup>(12)</sup>:

The conservation of mass equation (2.4-203), is identically satisfied in steady two-dimensional flows by introduction of the stream-function concept. Then, applying the von Mises transformation<sup>(41)</sup> to the nondimensional form of the momentum equation (2.4-204), solutions for the shearing stress and the skin-friction coefficients are obtained independently of the energy transfer equation (2.4-205) for the following specific cases:

(a) For a "no slip" boundary condition  $(\bar{u}_0 = 0)$ , corresponding to a time

interval in which a build-up of the classical continuum theory compressible laminar boundary layer on a flat, insulated plate under nonstationary flow conditions occurs, (i.e., prior to achieving a steady flow state), the local skin-friction coefficient is<sup>(12)</sup>:

$$C_f' = 2 \left( \frac{\sigma}{\pi R_{01} \chi} \right)^{1/2} \quad \text{and} \quad \delta_u(x) \sim \left( \frac{\sigma x}{R_{01}} \right),$$

where

$$(2.4-206)$$

$\delta_u(x)$  - is the boundary layer thickness,

$\sigma$  - is the best suitable constant for the  $(\mu)$  estimates, see Eq (2.4-186),

$\chi = \frac{\bar{u}_1 t_1}{\lambda_1}$  - is the dimensionless time ratio,

$C_f'$  - is the local skin-friction coefficient,

$R_{01} = \frac{\rho_1 \bar{\lambda}_1 \bar{u}_1}{\mu}$  - is the Reynolds Number at a free stream reference point (1), related to the free stream mean free molecular path  $(\bar{\lambda}_1)$ , see Fig (2.4-19).

This nonsteady solution for  $(C_f')$  and  $(\delta_u)$ , compared to the respective classical steady continuum flow expressions, see Eq (2.4-186):

$$C_f' = .664 \left( \frac{\sigma}{R_{01} \chi} \right)^{1/2}, \quad \delta_u \sim \left( \frac{\sigma x}{R_{01}} \right)^{1/2}, \quad (2.4-186)$$

shows that the transitional skin-friction coefficient and the boundary layer thickness build-up in time, on a flat plate (from a rarefied flow impulsive onset until a steady state is achieved) is similar in form with local skin friction and boundary layer thickness variations along a flat plate in a steady continuum flow (Eq 2.4-186). Then, by matching the expressions (2.4-206) and (2.4-186) it follows that formally

$$x = k_1 X \quad (2.4-207)$$

where

$$k_1 = 2.888 \cdot (2.4-208)$$

(b) For relatively mild "slip flow" conditions (i.e., for large values of

X), with

$$\bar{u}_0 = \left( 1 - \frac{\partial U}{\partial Y} \right) \bar{u}_1 < 1 \quad (2.4-209)$$

Solution of the momentum equation (2.4-204) results in the following expression for the skin friction coefficient build-up in time from the accelerated flow onset until the steady flow state is achieved(12):

$$C_f = \frac{2\sigma}{Re_1} \exp\left(\frac{\sigma X}{Re_1}\right) \operatorname{erfc}\left(\frac{\sigma X}{Re_1}\right)^{1/2} \quad (2.4-210)$$

where

$$\operatorname{erfc}\left(\frac{\sigma X}{Re_1}\right)^{1/2} = 1 - \operatorname{erf}\left(\frac{\sigma X}{Re_1}\right)^{1/2} \quad (2.4-211)$$

is the complementary error function, i.e., in general:

$$\operatorname{erf} x = \frac{2}{\sqrt{\pi}} \int_0^x e^{-y^2} dy \quad (2.4-212)$$

$$\operatorname{erf} cx = 1 - \operatorname{erf} x = \frac{2}{\sqrt{\pi}} \int_0^\infty e^{-y^2} dy \quad (2.4-213)$$

Assuming that the matching relationship (2.4-207) for the continuum flow "no slip" condition can be also extended to the "small slip" conditions, the equation (2.4-210) can be used to find the corresponding expression for the local laminar skin-friction coefficient in steady slip flows along insulated flat plates:

$$C_f' = \frac{2\sigma}{Re_1} \exp\left(\frac{\sigma k_1 X}{Re_1}\right) \operatorname{erfc}\left(\frac{\sigma k_1 X}{Re_1}\right)^{1/2} \quad (2.4-214)$$

For monoatomic gases:

$$Re_1 = 1.648 M_1 \quad (2.4-215)$$

and thus,

$$M_1 C_f' = 1.214 \sigma \exp\left(\frac{7}{4} \frac{\sigma X}{M_1}\right) \operatorname{erfc}\left(\frac{7}{4} \frac{\sigma X}{M_1}\right)^{1/2} \quad (2.4-216)$$

where

$$\frac{X}{M_1} = \frac{x}{M_1 l} \frac{1}{Kn_1} \quad , \quad Kn_1 = \frac{\lambda_1}{l} \quad , \quad Kn_x = \frac{\lambda_1}{x} = \frac{1}{X} \quad (2.4-217)$$

Notice that in the free molecule flow ( $\bar{u}_0 = \bar{u}$ ) for ( $\Theta = 0$ ) it was earlier found that (see Section 2.4.2):

$$M_1 C_f' = \left(\frac{2}{\pi \gamma}\right)^{1/2} \quad (2.4-218)$$

With the assumed large values of (X), corresponding to the "small slip" conditions, the complementary error function takes an asymptotic form(37), and the expression (2.4-216) reduces to:

$$C_f' = .664 \left(\frac{\sigma}{Re_1 X}\right)^{1/2} \left(1 - \frac{Re_1}{2\sigma k_1 X} + \dots\right) \quad (2.4-219)$$

in a first approximation, i.e.,

$$C_f'_{SMALLSLIP} = C_f'_{NO SLIP} \left(1 - \frac{Re_1}{2\sigma k_1 X} + \dots\right) \quad (2.4-220)$$

meaning that the local skin friction coefficient is only slightly less in slip flow compared with its value in the classical continuum flow regime.

The equations (2.4-206) and (2.4-216) are graphically presented in Fig (2.4-21) in terms of the characteristic ratio (X/M) for monoatomic gases assuming ( $\sigma=1$ ). The greatest effect of the "slip flow" on the boundary layer thickness and the local skin friction coefficient reduction are encountered near the leading edge, where the local values of (X) are the smallest.

### (3) Energy Transfer in Slip Flows

Slip flows are characterized by pressure and temperature jumps. Retaining all the terms of the orders (1) and (D) or ( $\Delta$ ) in the boundary conditions, the energy equation (2.4-205) is used for additional investigation of the temperature jump effects under equilibrium slip-flow condi-

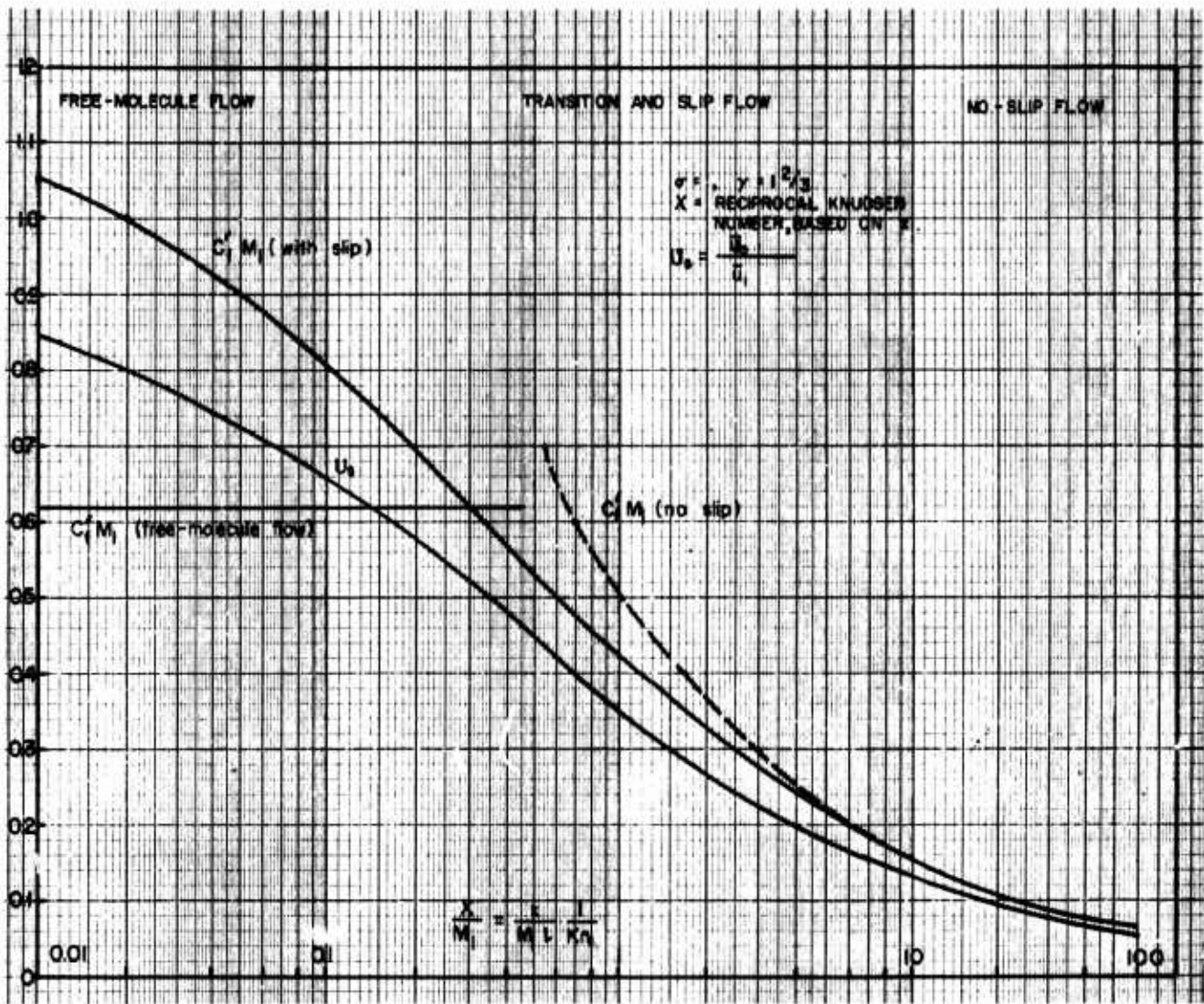


Fig (2.4-21) Velocity ratio and local skin-friction in slip flow,  
 (Ref 1-2), for flat plates, ( $\theta = 0$ )

tions(12):

$$\frac{T'_s}{T'_w} = 1 - \bar{\lambda}'_0 \Delta \left[ \frac{a_1 M_1 D}{(T'_w)^2} (u'_w - 2v'_w) - \frac{a_2 \delta'}{T'_w} T'_w \right], \quad (2.4-221)$$

or by neglecting terms of the order (Δ) and (D) one gets alternatively:

$$\frac{T'_s}{T'_w} = 1 + \left( \frac{2\kappa \Delta \delta'}{T'_w} \right) \bar{\lambda}'_0 \left( \frac{\partial T'}{\partial y} \right)_s, \quad (2.4-222)$$

with

$$\theta_s - \theta_w = \chi \left( l \frac{\partial \theta}{\partial y} \right)_s, \quad (2.4-223)$$

where

$l$  - is the flat plate length,

$\theta = \frac{T'}{T'_i}$  - is the dimensionless temperature ratio,

$\bar{\lambda} = \frac{\bar{\lambda}_1}{\lambda_1}$  - is the dimensionless ratio of mean free molecular paths,

$\kappa = a_2 = \frac{75\pi}{128}$ , a constant,

$\gamma = \frac{y}{\lambda_1}$  - is the dimensionless position coordinate,

$$\chi = \frac{x}{\lambda_1}, \quad \delta' = \frac{\delta'_u(l)}{\delta'_t(l)},$$

$\delta_u(l)$  - is the boundary layer velocity thickness at the station (l) of the flat plate,

$\delta_t(l)$  - is the boundary layer thermal thickness at the station (l) of the flat plate,

$$T'_s = \frac{T'_w}{T'_i}, \quad u'_s = \frac{u'_w}{u'_i}, \quad v'_s = \frac{v'_w}{u'_i} \frac{l}{D},$$

$$x' = \frac{x}{l}, \quad y' = \frac{y}{\delta_u(l)}, \quad y'' = \frac{y}{\delta_t(l)}$$

$$T'_w = \frac{T'_i}{T'_i}, \quad u'_w = \frac{\partial u'}{\partial x'}, \quad v'_w = \frac{\partial v'}{\partial y'}, \quad T'_y = \frac{\partial T'}{\partial y'}$$

$a_1, a_2, \dots, a_6$  are constants,

$$\bar{\lambda}'_0 = \frac{1}{\rho'_0}, \quad \Delta = \frac{\bar{\lambda}_1}{\delta_u(l)}, \quad D = \frac{\delta_u(l)}{l},$$

Prime (') is used to denote a non-dimensional quantity,

Subscript (l) denotes conditions "at infinity",

Subscript (s) denotes state of gas at wall,

Subscript (w) denotes state of the wall.

The problem of the energy transfer with a temperature jump cannot be solved independently from the momentum transfer equation (2.4-204), since the momentum transfer processes strongly contribute to the mechanism of the energy exchange. As a consequence, solution of the energy equation is, in general, a more complicated task. Specifically, for small values of ( $M_1$ ) a corresponding simplification of the energy equation is obtained in Ref. 12, resulting in the following expressions for the nondimensional temperature at the surface of a flat plate ( $\theta_s$ ) and the coefficient of the heat transfer on the surface of a flat plate ( $q_w$ ):

$$\theta_s = \theta_w - (\theta_w - 1) \exp\left(\frac{\gamma \sigma \chi}{\kappa^2 P_r R_{e1}}\right) \times \operatorname{erfc}\left(\frac{1}{\kappa} \sqrt{\frac{\gamma \sigma \chi}{P_r R_{e1}}}\right), \quad (2.4-224)$$

$$q_w = \frac{\sigma}{P_r R_{e1}} \left( \frac{\theta_w - 1}{\kappa} \right) \exp\left(\frac{-\gamma \sigma \chi}{\kappa^2 P_r R_{e1}}\right) \times \operatorname{erfc}\left(\frac{1}{\kappa} \sqrt{\frac{\gamma \sigma \chi}{P_r R_{e1}}}\right), \quad (2.4-225)$$

where most of the symbols are as already defined in this section, and additionally:

$$\gamma = \frac{C_p}{C_v}$$

$$P_r = \frac{\mu C_p}{k_1} = \frac{4\gamma}{9\gamma - 5} \quad \text{is the Prandtl Number at a reference free stream point (1),}$$

$$\kappa = a_2 = \frac{75\pi}{128}, \quad \text{a constant.}$$

Introducing a further assumption of small temperature discontinuities at the surface, and allowing for the asymptotic form of the complementary error function for large values of

(X) the expressions (2.4-224) and (2.4-225) take the simpler forms:

$$\Theta_s = \Theta_w - \kappa (\Theta_w - 1) \left( \frac{P_r R_{\Theta_s}}{\pi \gamma k_2 \sigma X} \right)^{1/2}, \quad (2.4-226)$$

$$q_w = \frac{(\Theta_w - 1)}{(\pi \gamma k_2 P_r)^{1/2}} \left( \frac{\sigma}{R_{\Theta_s} X} \right)^{1/2} \left[ 1 - \frac{1}{2} \frac{\kappa^2 P_r}{k_2 \gamma} \times \right. \\ \left. \times \left( \frac{R_{\Theta_s}}{\sigma X} + \dots \right) \right]. \quad (2.4-227)$$

For a monoatomic gas in particular:

$Re_1 = 1.648 M$ ,  $\Theta_s = 1$  (dimensionless equilibrium temperature, insulated wall),

$$P_r = \frac{2}{3}, \quad \gamma = \frac{5}{3}, \quad k_2 = \frac{X}{X}.$$

i.e.,

$$\frac{\Theta_w - \Theta_s}{\Theta_w - 1} = \exp\left(\zeta \frac{X}{M_1}\right) \operatorname{erfc}\left(\zeta \frac{X}{M_1}\right)^{1/2}, \quad (2.4-228)$$

$$\frac{M_1 q_w}{\Theta_w - 1} = \frac{\sigma}{1.648 \kappa P_r} \exp\left(\zeta \frac{X}{M_1}\right) \operatorname{erfc}\left(\zeta \frac{X}{M_1}\right)^{1/2}, \quad (2.4-229)$$

where

$$\zeta = \frac{\gamma k_2 \sigma}{1.648 \kappa^2 P_r}. \quad (2.4-330)$$

For free molecule flow ( $\Theta_s = 1$ ) for low values of ( $M_1$ ):

$$\frac{M_1 q_w}{\Theta_w - 1} = \frac{\gamma - 1}{\gamma} \sqrt{\frac{2}{\pi \gamma}}. \quad (2.4-231)$$

Relations (2.4-228), (2.4-229) and (2.4-231) are plotted in Fig (2.4-22).

Conclusion: for low values of ( $M_1$ ), the effect of a small temperature jump at the surface ( $\Theta_w - \Theta_s$ ), is to reduce the rate of heat transfer in both free molecule and slip flow regimes.

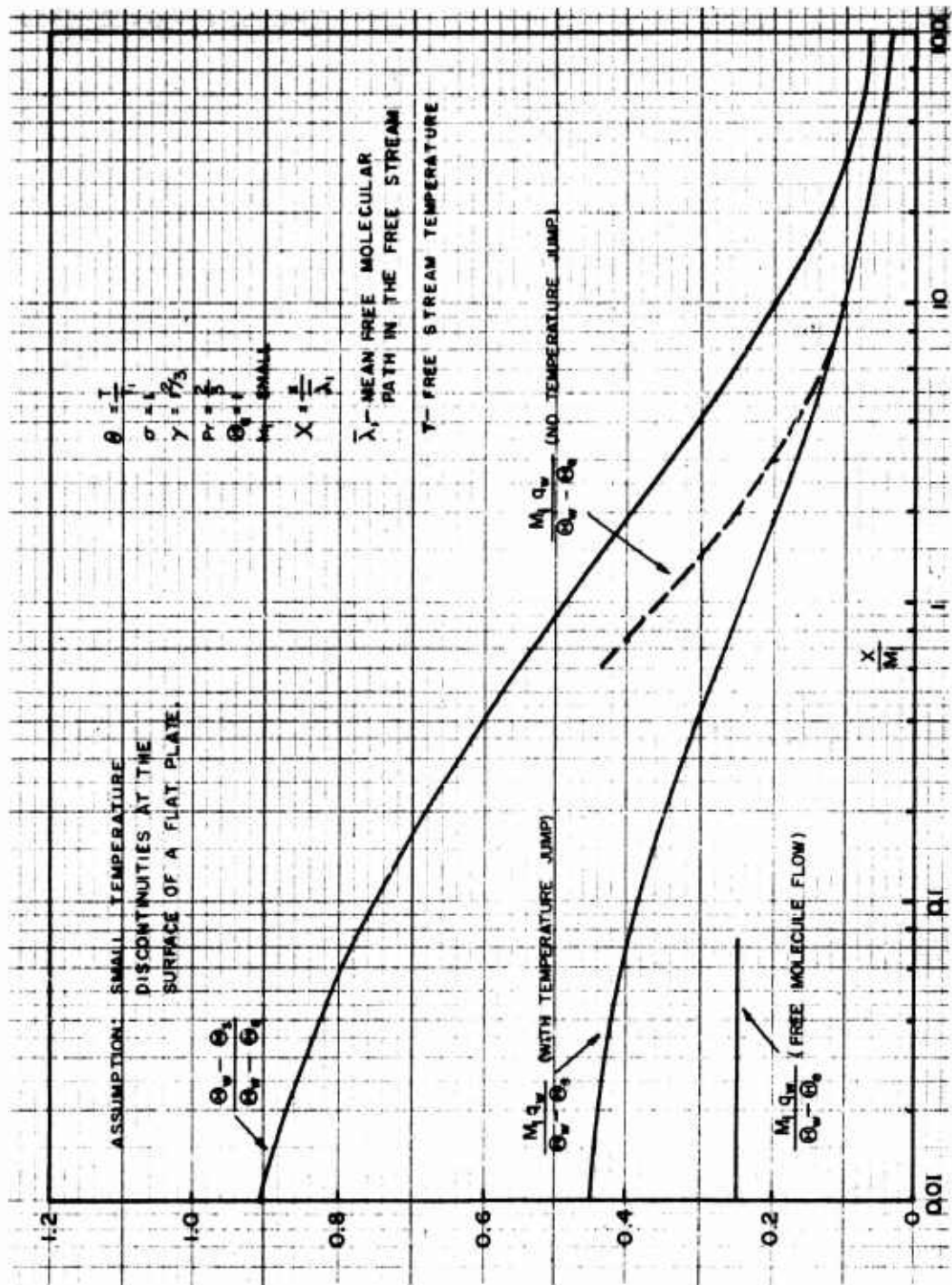


Fig (2.4-22) Temperature jump and local heat transfer in slip flow, (Ref 12), monatomic gases.

2.4.6 DRAG COEFFICIENT AND HEAT TRANSFER IN SLIP FLOW FOR SOME SIMPLE CONFIGURATIONS

(i) Flat Plates, Zero Angle-of-Attack, Slip Flow

References:

- (2.4-12), (2.4-22), (2.4-36), (2.4-37)  
 (2.4-38), (2.4-43), (2.4-44), (2.4-35)  
 (2.4-31), (2.4-32), (2.4-33), (2.4-2)  
 (2.4-3), (2.4-45), (2.4-46), (2.4-47)

Based upon the material presented in the preceding Section 2.4.3, the average skin-friction drag coefficient for one side of an insulated flat plate at a zero angle of attack ( $\alpha_1 = \alpha_2 = \theta = 0$ ) in a steady, two-dimensional slip flow is:

$$C_D = \frac{D}{\frac{1}{2} \rho_1 u_1^2 b l} = \frac{\bar{\lambda}_1}{l} \int_0^{\sqrt{\lambda}_1} C_f' dx, \quad (2.4-232)$$

By substituting the respective  $C_f'$  value, (see Eq (2.4-214)), and after integrating, the following explicit expression for the average skin friction coefficient is obtained (38):

$$C_D = \frac{1}{2} \frac{\Lambda}{Z^2} \left[ e^{Z^2} \operatorname{erfc} Z - 1 + \frac{2Z}{\sqrt{\pi}} \right] \quad (2.4-233)$$

where

$$Z^2 = \frac{\sigma k_1}{Re_1 Kn} = \frac{25 \pi \sigma k_1 Re_1}{1207 M_1^2},$$

$$Z^2 = \frac{Re_1}{2.25 M_1^2} \quad \text{for air,}$$

$$Kn = \Delta D = \frac{\bar{\lambda}_1}{l} = \frac{Re_1}{Re_l}$$

$$Kn \approx \frac{15 M_1}{Re_l} \quad \text{for diatomic gases, or air,}$$

$$\Lambda = \frac{4 \sigma}{Re_1} = \frac{5}{2} \left( \frac{\pi}{2 \gamma} \right)^{\frac{1}{2}} \frac{\sigma}{M_1},$$

$$\Lambda \approx 2.67 \quad \text{for air,}$$

$$Re_l = \frac{\rho_1 \bar{\lambda}_1 u_1}{\mu_1} = \frac{16}{5} \left( \frac{\gamma}{2 \pi} \right)^{\frac{1}{2}} M_1, \quad Re_1 = \frac{\rho_1 l u_1}{\mu_1},$$

$$Re_l \approx 1.5 \quad \text{for diatomic gases, or air,}$$

in a first approximation the equation (2.4-233) reduces to:

(a) For Slip Flows ( $Z$  large,  $Kn$  small):

$$C_D = \frac{1}{2} \frac{\Lambda}{Z^2 \sqrt{\pi}} \left[ 2Z - \sqrt{\pi} + \frac{1}{Z} \right] \quad (2.4-234)$$

(b) For No-Slip Flows ( $Z$  very large,  $Kn$  very small):

$$C_D = \frac{\Lambda}{Z^2 \sqrt{\pi}} = 1.328 \left( \frac{\sigma Kn}{Re_1} \right)^{1/2} \quad (2.4-235)$$

Equations (2.4-234) and (2.4-235) are represented graphically in the Fig (2.4-23) for two alternative values of ( $Z^2$ ) as indicated.

In Fig (2.4-24) the experimental data from Ref (2.4-38) are compared with the Blasius' solution of the continuum flow for incompressible laminar boundary layers and with the corresponding theoretical solution for rarefied gases ( $M \approx 0$ ) by Janour, Ref (2.4-46).

(ii) Spheres, Slip Flow

References: (2.4-48), (2.4-49)  
 (2.4-50), (2.4-51)

(1) Low Subsonic Mach Numbers

(a) For very low Reynolds and Mach Number values, the total (friction + pressure) drag coefficient value is (48):

$$C_D = \frac{12}{Re_{D/2}} \left( \frac{1 + 2 \frac{2-\sigma}{\sigma} \frac{\bar{\lambda}_1}{D/2}}{1 + 3 \frac{2-\sigma}{\sigma} \frac{\bar{\lambda}_1}{D/2}} \right), \quad (2.4-236)$$

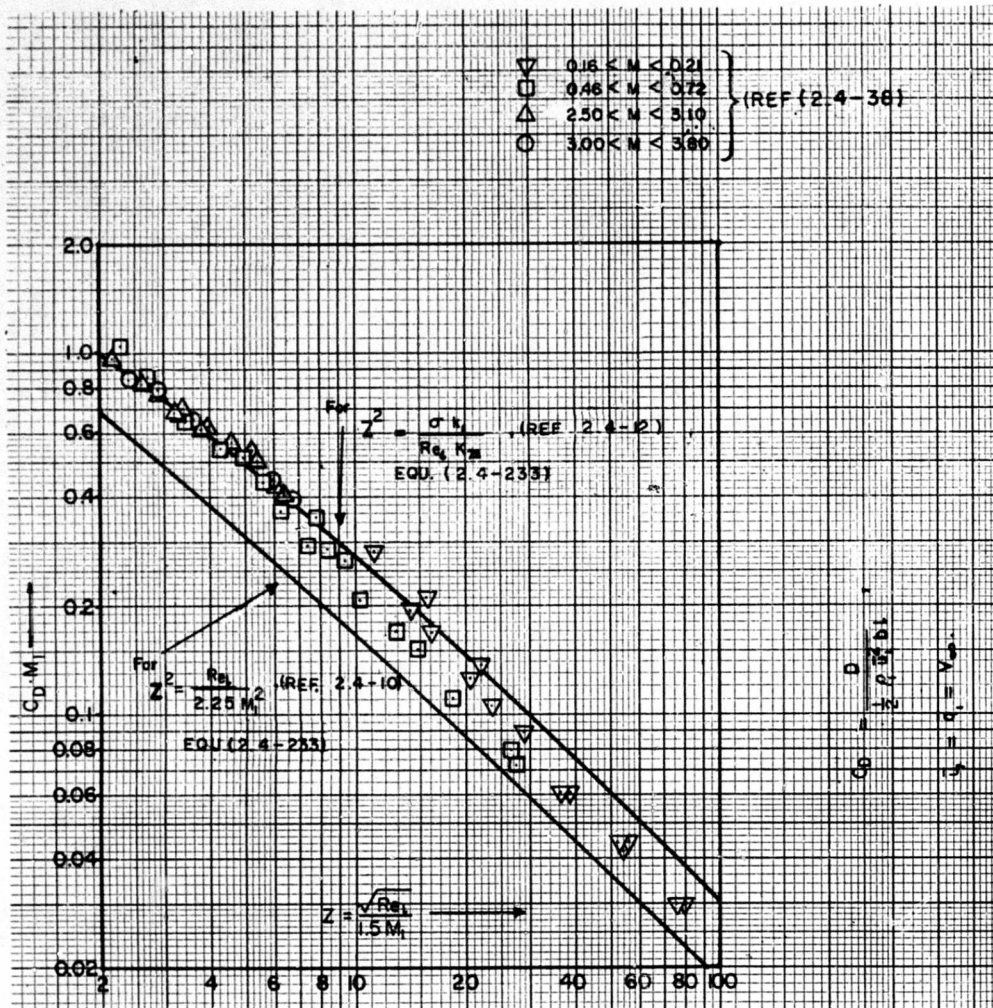
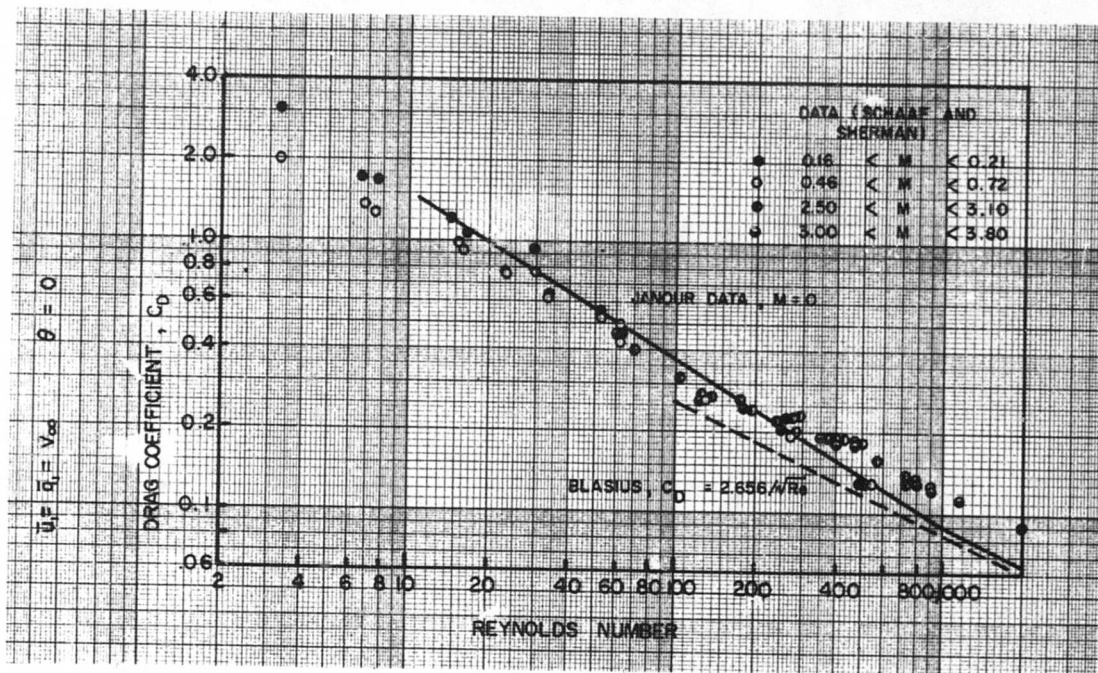


Fig (2.4-23) Skin-friction drag of flat plates in slip flow (Ref 2.4-12)



Fig(2.4-24) Skin friction in slip flow for a flat plate,  
 zero angle-of-attack. Ref(2.4-12)

where:

$\sigma$  - is the fraction of molecules diffusely reflected from the surface,

$D$  - is the spheres diameter,

$\bar{\lambda}_1$  - is the mean free molecular path, free stream conditions

$$Re_{D/2} = \frac{\bar{q}_1 \rho_1 D/2}{\mu_1}, \quad \bar{q}_1 = V_H.$$

(b) When the effects of compressibility for ( $M < 1$ ) and of heat transfer are taken into account, (49):

$$C_D = \frac{12}{Re_{D/2}} \left[ \frac{\left(1 + \frac{15}{2} \frac{2-\sigma}{a} \frac{\bar{\lambda}_1}{D/2}\right) \left(1 + 2 \frac{2-\sigma}{\sigma} \frac{\bar{\lambda}_1}{D/2}\right) + \frac{6}{\pi} \frac{\bar{\lambda}_1^2}{D^2}}{\left(1 + \frac{15}{2} \frac{2-\sigma}{a} \frac{\bar{\lambda}_1}{D/2}\right) \left(1 + 3 \frac{2-\sigma}{\sigma} \frac{\bar{\lambda}_1}{D/2}\right) + \frac{9}{5\pi} \left(4 + 9 \frac{2-\sigma}{\sigma} \frac{\bar{\lambda}_1}{D/2}\right) \frac{\bar{\lambda}_1^2}{D^2}} \right], \quad (2.4-237)$$

where

$a$  - is the accommodation coefficient.

(c) An approximation to the Basset's (48) result has been developed by Millikan (50), valid for small values of ( $M/Re$ ) ratio:

$$C_D = \frac{12}{Re_D} \frac{1}{1 + \text{const.} \frac{M}{Re_D}}, \quad (2.4-238)$$

and alternatively, by using the Epstein's (11) results, an empirical equation for the drag coefficient valid over the entire range of the ( $M/Re$ ) values is proposed again by Millikan (50):

$$C_D = \frac{12}{Re_D \left\{ 1 + \frac{\bar{\lambda}_1}{D/2} \left[ A + B e^{-C \bar{\lambda}_1 / D/2} \right] \right\}}, \quad (2.4-239)$$

provided both ( $Re$ ) and ( $M$ ) are small, and the parameters  $A$ ,  $B$  and  $C$  are to be determined empirically. For oil drops in air Millikan obtained:

$$A = 1.22, \quad B = 0.41, \quad C = 8.75.$$

The Eq (2.4-239) is graphically presented in Fig (2.4-25).

## (2) Higher (Supersonic) Mach Num-

bers ( $M < 5$ )

The pronounced compressibility effects and the bow shock wave have a strong interfering effect on the total friction and pressure drag coefficient values in the slip flow regime.

Kane's (51) empirical formula is:

$$C_D = \left( 0.97 + \frac{1.32}{(Re_D)^{1/2}} \right) \left[ 1 + \frac{1.0}{(Re_D)^{1/2}} \right]^4, \quad (2.4-240)$$

where

$$Re_D = \frac{\rho_2 V_2 D}{\mu_2},$$

$\rho_2, V_2, \mu_2$  - evaluated behind the normal shock. Eq (2.4-240) is graphically presented in Fig (2.4-25).

## (3) The Heat Transfer to Spheres in Slip Flow Regime (Temperature Jump)

References: (2.4-52), (2.4-53) (2.4-54)

The heat transfer with a temperature jump for a sphere is expressed through the Nusselt Number concept by Kavanau (54) as:

$$Nu = \frac{Nu^{(0)}}{1 + 3.42 \frac{M}{Re_D Pr} Nu^{(0)}}, \quad (2.4-241)$$

where:

- the constant (3.42) is empirical,

$Re_D = \frac{\rho_2 V_2 D}{\mu_2}$  - evaluated behind the shock (subscript 2),

$Nu^{(0)}$  - the value of Nusselt Number assuming no temperature jump, defined by Drake and Backer (52) (solid curve in Fig (2.4-26)).

The Eq (2.4-241) and some supporting experimental data are plotted in Fig (2.4-26).

As already pointed out in the Section on heat transfer in the slip flow region, the viscous layer on convex bodies is so thick that the heat generation by dissipation of the molecular momentum is done at a greater rate than it can be conducted away. The direct

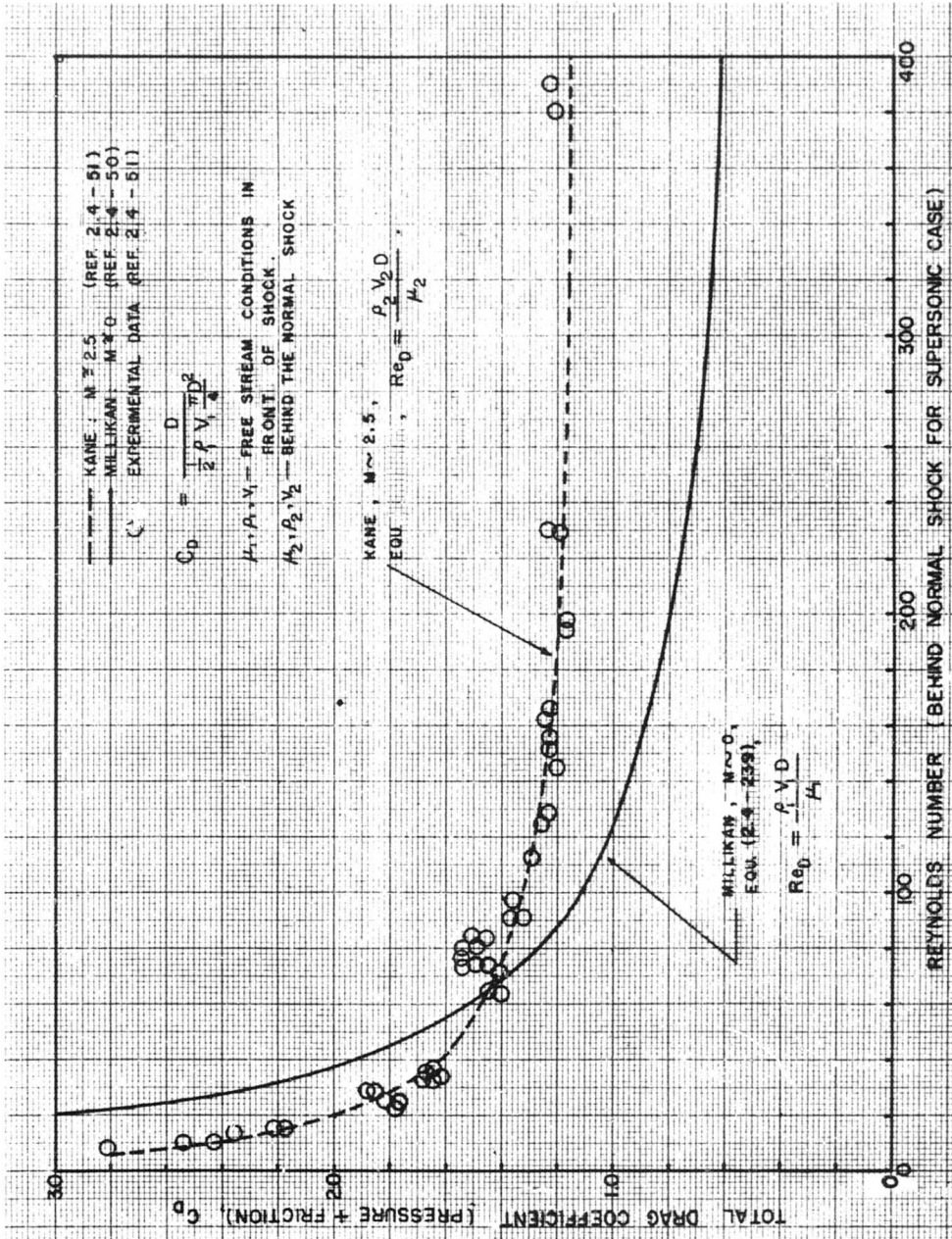


Fig (2.4-25) Sphere drag coefficient (Ref 2.4-50), slip flow regime.

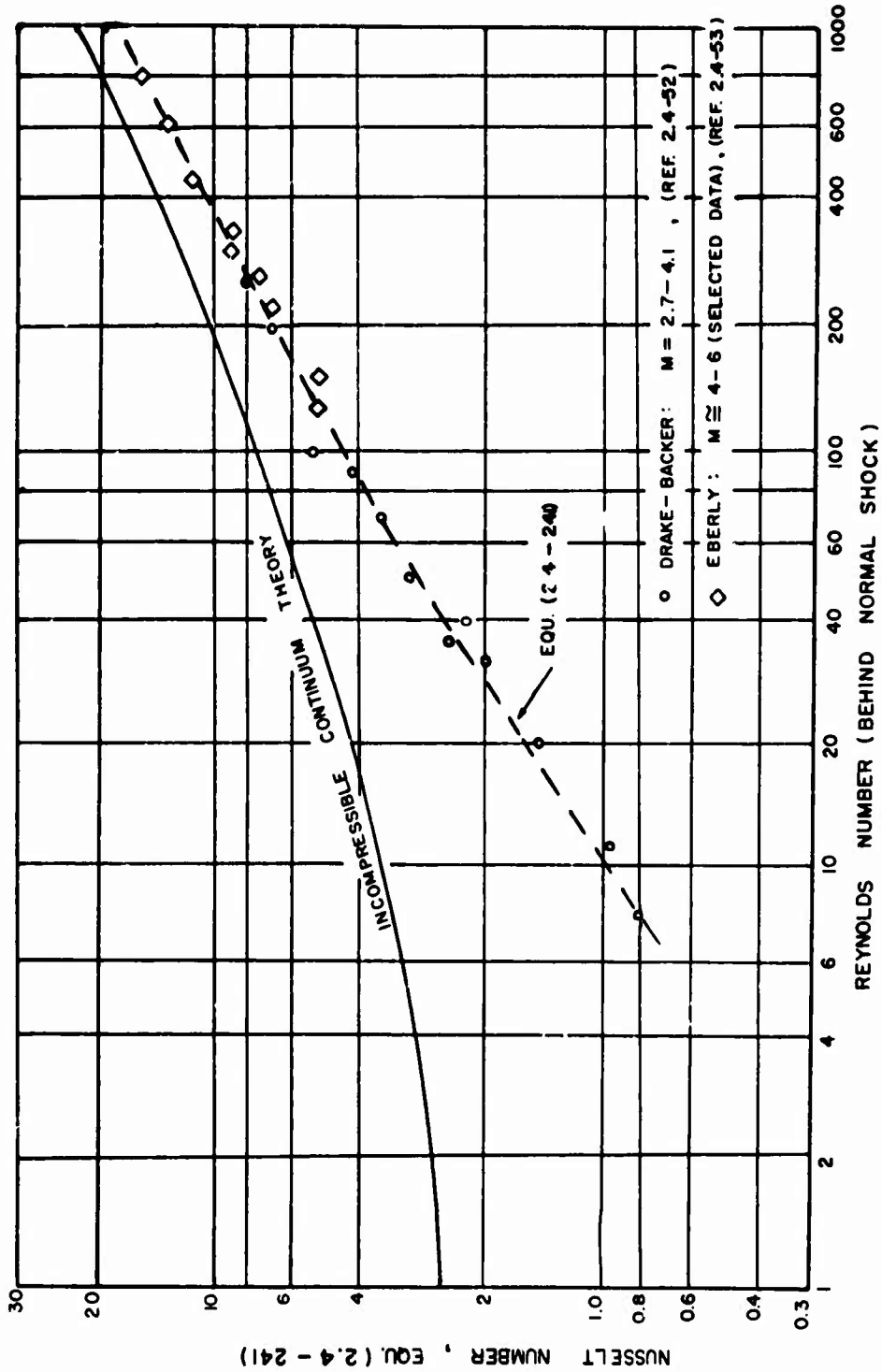


FIG (2.4-26) CONVECTIVE HEAT TRANSFER COEFFICIENT FOR SPHERES IN SUPERSONIC FLOW, SLIP FLOW REGIME, (REF. 2.4-54)

consequence is that the recovery factor has a value greater than unity.

In Ref. (2.4-55) the recovery factor,  $r$ , has been investigated by Mack and Shaaf and specifically for the stagnation point region of an adiabatic sphere it has been found that:

$$r = \frac{T_{aw} - T_1}{T_s - T_1} = 1 + \frac{f(Re_D)}{Re_D}, \quad (2.4-242)$$

where

$$Re_D = \frac{\rho_1 V_1 D}{\mu_1}$$

$f(Re)$  is a slowly varying function,

$T_{ad}$  - is the adiabatic sphere temperature,

$T_1$  - is the local free stream temperature,

$T_s$  - is the local stagnation temperature,

The Eq (2.4-242) is presented graphically in Fig (2.4-27).

#### (iii) Cylinders in Slip Flow Regime

(Right, circular cylinders with their axis perpendicular to the free stream velocity)

For incompressible flows Tsien(5) gives:

$$C'_D = \frac{4\pi}{Re_{D/2} \left[ \ln \frac{4}{Re_{D/2}} - 1.28 + 1.26\sqrt{\gamma} \frac{2-\sigma}{\sigma} \frac{M}{Re_{D/2}} \right]}$$

(2.4-243)

where subscript (1) refers to the free stream conditions at infinity, and:

$\sigma$  - is the fraction of molecules reflected diffusely.

$$C'_D = \frac{\text{DRAG PER UNIT LENGTH}}{(D/2)\rho_1 V_1^2}, \quad Re_{D/2} = \frac{\rho_1 V_1 \frac{D}{2}}{\mu}$$

No results pertinent to the cylinders in compressible slip flow regime have been found.

The heat transfer and the recovery factor have been experimentally investigated by Stalder, Goodwin, and Creager (19), Kovaszny and Tormarck(56), Laufer and McClennan(57). The results are presented in Fig (2.4-28) with:

$$K_n = \frac{\lambda_1}{D}, \quad Re_D = \frac{\rho_1 V_1 D}{\mu_1}$$

#### (iv) Cones in Slip Flow Regime, Zero Angle of Attack

The relatively thick (laminar) boundary layer in the slip (and transitional) flow regimes displaces the inviscid free stream flow outwards, creating a pressure distribution which rises towards the cone vertex, i.e., the constant pressure distribution from the inviscid perfect fluid theory (zero angle-of-attack, supersonic Mach Numbers, attached oblique shock waves) is appreciably distorted. The rising pressure gradient interference with the relatively thick laminar boundary layer in the slip flow regime results in an increase of the skin friction coefficient.

The related partial theoretical and experimental data from Talbot(58) Probst and Elliott(59) Ipsen(60), Drake and Maslach(61) are presented in Figs (2.4-29) and (2.4-30), with:

$Re_s = \frac{\rho_1 V_1 S}{\mu_1}$  the Reynolds Number, based upon the free stream conditions at infinity (1), and the slant length of cone (S),

$C'_D = \frac{\text{TOTAL DRAG}}{\frac{1}{2} \rho_1 V_1^2 \frac{D}{2} \pi S}$  - is the total drag = pressure drag + viscous drag

$$S = \frac{l}{\cos \theta}$$

$l$  - cone length

$\theta$  - semivertex angle

$C_{D,IDEAL}$  - is the corresponding inviscid (pressure only) drag coefficient at the same Mach Number, referred to the same nondimensionalizing reference parameter as  $C_D$ .

$M = \frac{V_1}{M_1}$  - is the inviscid flow reference value of Mach Number.

#### (v) Base Pressure on Cone + Cylinder

In Fig (2.4-31) the ratio of the free stream static pressure to the base pressure,  $(p/p_b)$ , is plotted against Reynolds Number ( $Re_b$ ) and  $(2.1 < M < 4.0)$  from Ref. (2.4-62) and Ref (2.4-63) by

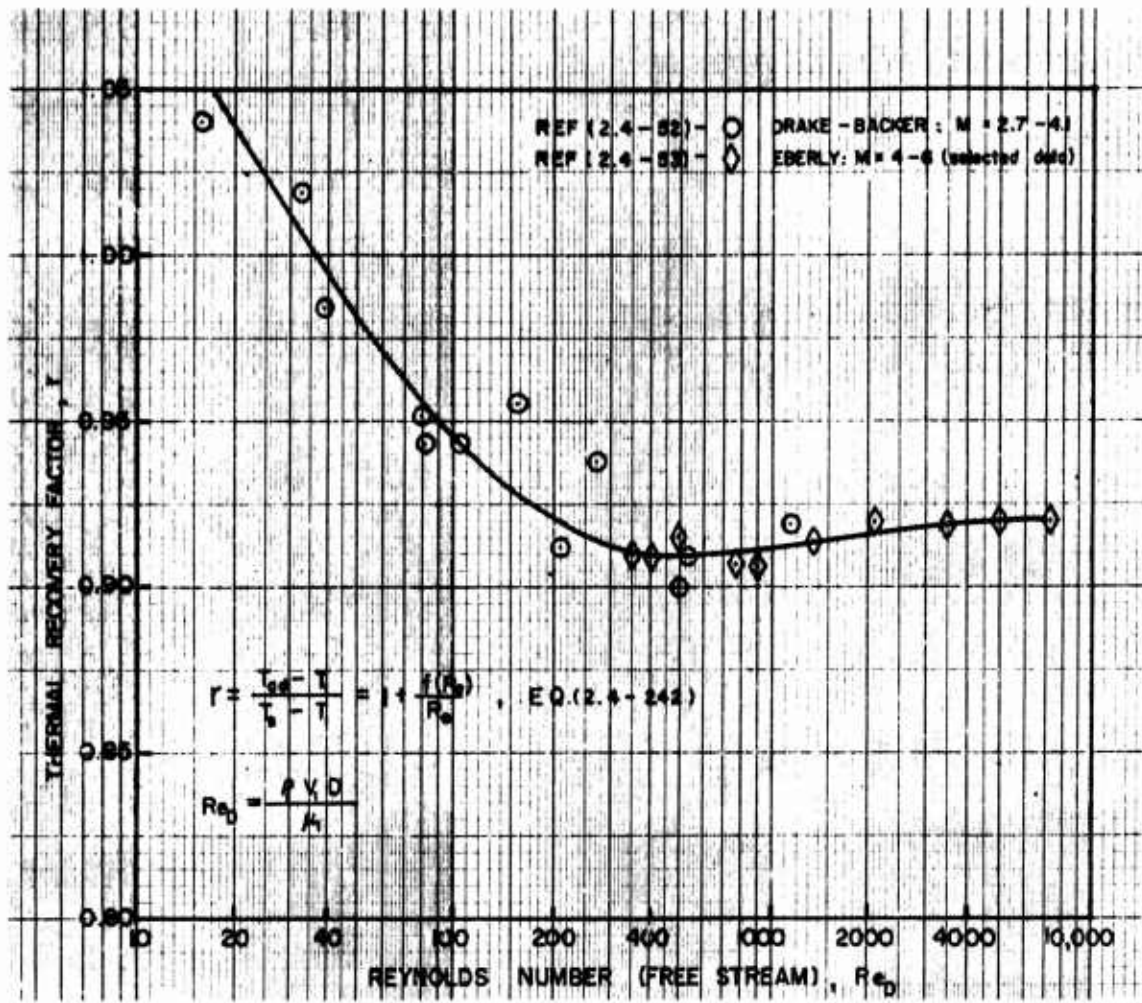


Fig (2.4-27) Thermal recovery factor for spheres in supersonic flow. (Ref 2.4-55)

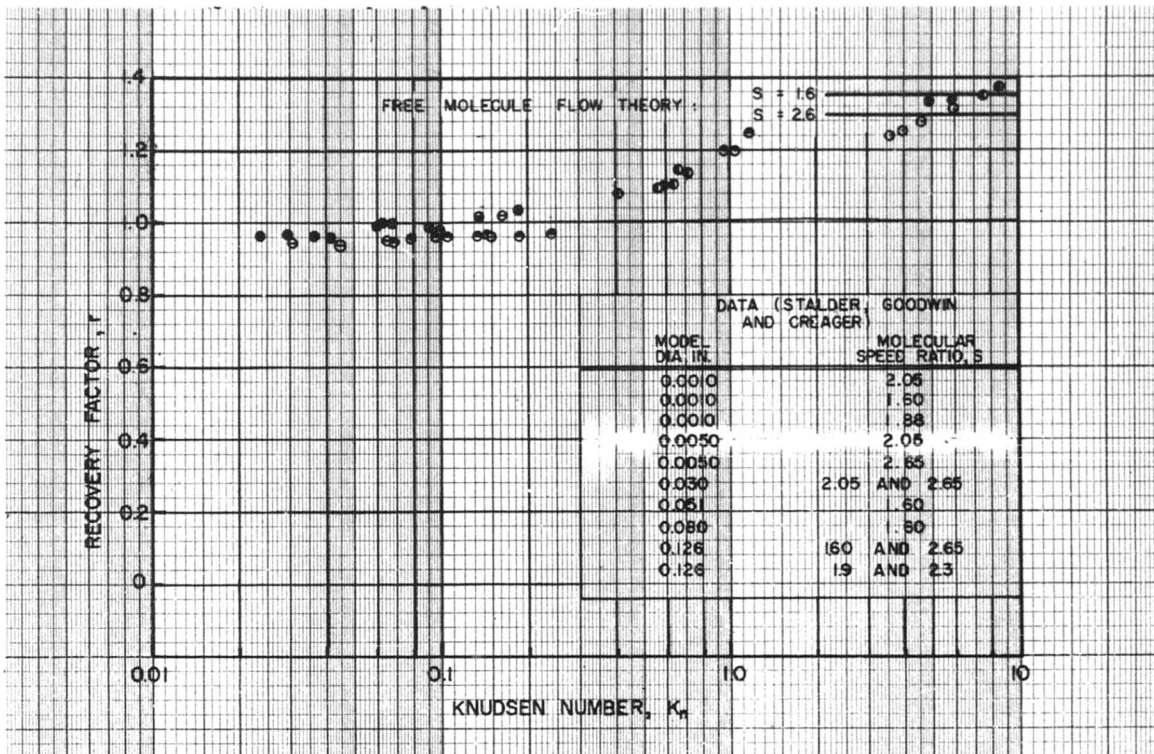
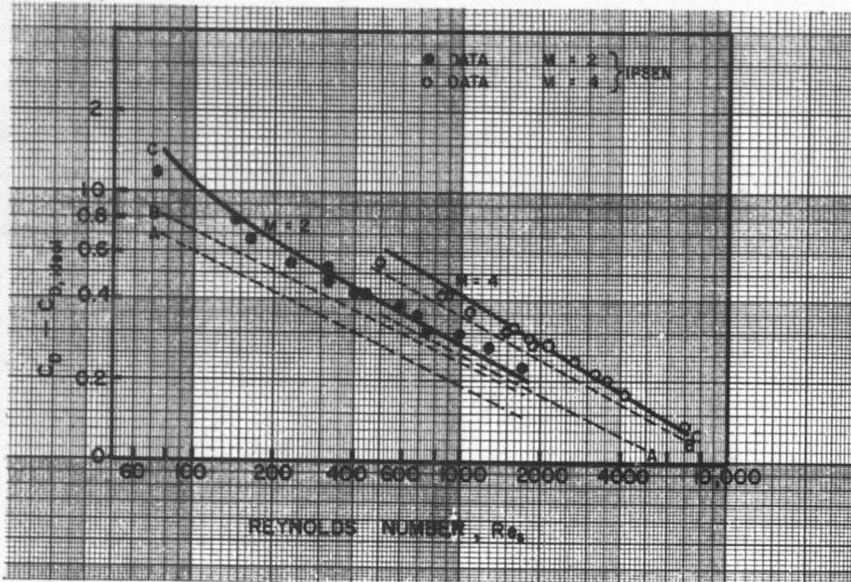
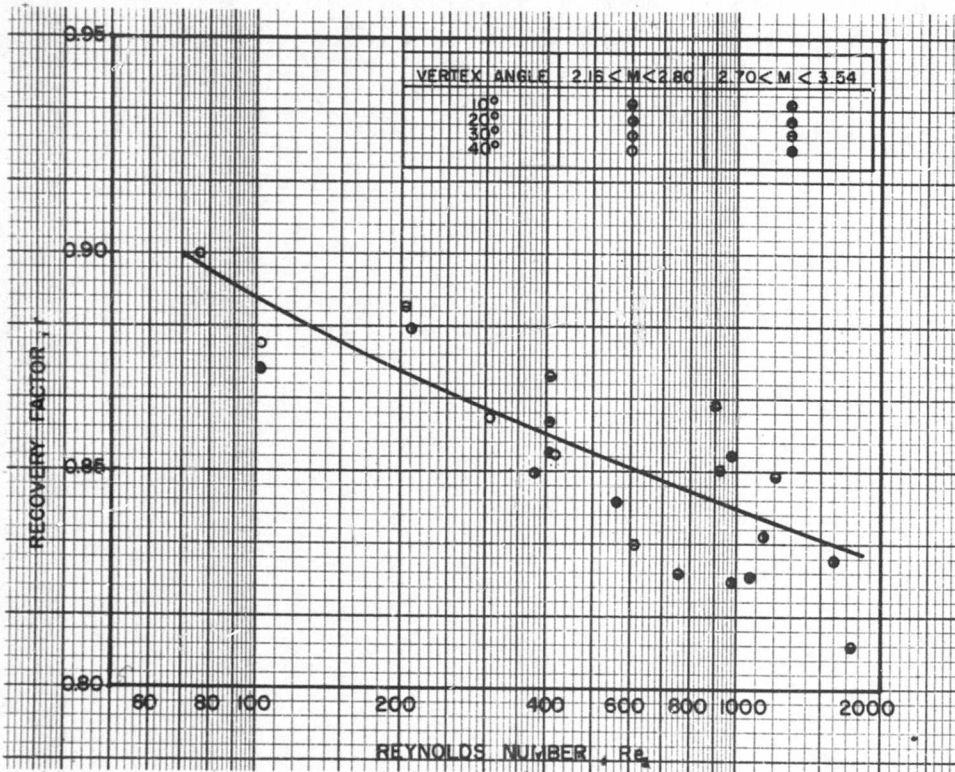


Fig (2.4-28) Thermal recovery factor for transverse cylinders in supersonic flow. ( Ref 2.4-57 )

$$\left( K_n = \frac{\bar{\lambda}_1}{D} \right)$$



Fig(2.3-29) Drag coefficients for cones with 15° semivertex angles. (Ref 2.4-60) (Zero angle of attack)



Fig(2.4-30) Thermal recovery factors for cones in supersonic flow (Ref. 2.4-61).

Kavanau for the slip flow regime and from Ref. (2.4-64) by Bogdonoff for the continuum flow regime, with

$R_q = \frac{\rho V L}{\mu}$  referred to the free stream conditions (subscript 1).

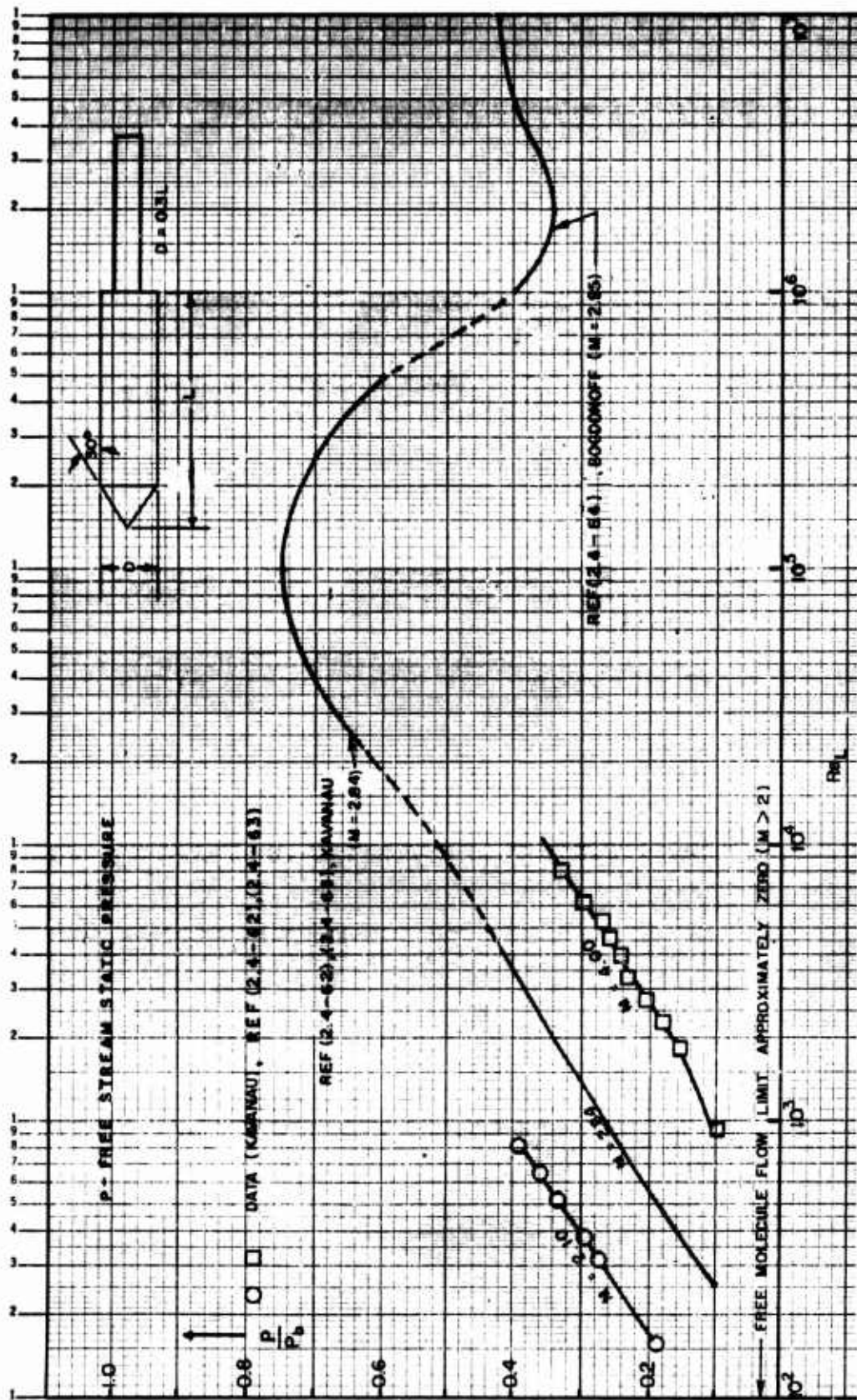


Fig (2.4-31) Base pressure coefficient for cone configurations. Ref (2.4-62), (2.4-63), (2.4-64) (Zero angle-of-attack)

2.4.7 HEAT TRANSFER AND SKIN FRICTION RELATIONSHIPS DURING ACTUAL TRANSIENT FLIGHT CONDITIONS (CONTINUUM, SLIP, TRANSITIONAL AND FREE MOLECULAR FLOW REGIMES)

Note: All the related Figures are given at the end of this Section, 2.4.7.

Basic Assumptions

- A Standard Atmosphere is assumed.  
 - The heat transfer effects during steady and accelerated (transient) flight regimes are considered only in as much as the actual skin-temperature affects the skin-friction coefficient values. The additional aerodynamic "apparent mass" effects upon the aerodynamic coefficient values during the pronouncedly accelerated or unsteady flight regimes are not taken into account. These effects stem from the restricted reciprocity of the relatively accelerated motions for the solid body-fluid closed systems, see Ref. (2.4-66).

-The zero-lift coefficient evaluation procedures are based on very simplified theoretical assumptions regarding the real gas effects, i.e., only slightly nonisentropic steady flow conditions for supposedly monoatomic or diatomic mathematical molecular models of the kinetic theory of gases are assumed. Effects of the vibrational, dissociative and ionizing molecular degrees of freedom are considered only partially in a few simplified cases.

-No mass-injection or ablative processes are treated.

(i) Basic Expressions for Heat Transfer and Skin Friction Coefficients

The skin friction - heat transfer functional relationships in the four characteristic flow regimes (continuum, slip, transitional and free molecular) shall differ according to the changing physical aspects of the fluid-body interaction patterns in a generally unsteady relative motion. Neglecting the apparent mass effects and the actual aerodynamic time-lag phenomena in highly accelerated flight regimes, the instantaneous local skin friction coefficient values can be computed from the following simplified aerothermodynamic analysis, using the engineering lbf-ft-sec-°R system of units:

The local instantaneous heat transfer rate,  $(\Delta Q_x)$ , into (or out of) a surface element,  $(\Delta S)$ , is in general given by,

$$\Delta Q_x = \Delta S \Delta q_x = \Delta S \left\{ [\Delta q_o]_x - [\Delta q_r]_x \pm [\Delta q_i]_x + [\Delta q_s]_x \right\}, \left[ \frac{\text{Btu}}{\text{sec}} \right] \quad (2.4-244)$$

where

$\Delta q_x = \left[ G_w \frac{dT_w}{dt} \right]_x, \left[ \frac{\text{Btu}}{\text{sec ft}^2} \right]$  - is the local heat transfer flux into (or out of) the surface element  $dS$ ,

$$[\Delta q_o]_x = h_x [T_{ow} - T_w]_x, \left[ \frac{\text{Btu}}{\text{sec ft}^2} \right]$$

- is the local aerodynamic heat flux,  
 $[\Delta q_r]_x = [\epsilon_w T_w^4]_B, \left[ \frac{\text{Btu}}{\text{sec ft}^2} \right]$  - is the local radiative heat flux out of the surface element  $dS$ ,

$[\Delta q_i]_x, \left[ \frac{\text{Btu}}{\text{sec ft}^2} \right]$  - is the local heat flux to (plus) or from (minus) the skin element  $dS$  due to any internally conducted (heating or cooling) or internally radiated heat transfer process,

$[\Delta q_s] = \epsilon_s [B T_s^4], \left[ \frac{\text{Btu}}{\text{sec ft}^2} \right]$  - is the local heat flux into the surface element  $dS$  due to solar or ambient atmosphere radiation,

$[G_w]_x = [C_w \delta_w W_w]_x, \left[ \frac{\text{Btu}}{\text{ft}^2 \text{ } ^\circ\text{R}} \right]$  - is the local heat absorption capacity of the skin element  $dS$ ,

$\Delta S [\text{ft}^2]$  - is the area of the local skin element,

$C_w \left[ \frac{\text{Btu}}{\text{slug } ^\circ\text{R}} \right]$  or  $\left[ \frac{\text{Btu}}{\text{lbf } ^\circ\text{R}} \right]$  - is the local conductive specific heat coefficient of the skin material,

$\delta_w [\text{ft}]$  - is the local skin thickness,

$W_w \left[ \frac{\text{slug}}{\text{ft}^3} \right]$  or  $\left[ \frac{\text{lbf}}{\text{ft}^3} \right]$  - is the specific mass or weight of the skin material,

$T_w [^\circ\text{R}]$  - is the local wall temperature at the exposed face of the skin,

$t [\text{sec}]$  - is the time,

$h_x \left[ \frac{\text{Btu}}{\text{sec ft}^2 \text{ } ^\circ\text{R}} \right]$  - is the dimensional heat transfer or film coefficient of the flowing fluid (air),

$T_{ow} [^\circ\text{R}]$  - is the local adiabatic wall temperature,

$\epsilon_w$  [dimensionless] - is the emissivity of the skin surface material,

$\epsilon_s$  [dimensionless] - is the solar or the ambient atmospheric gas emissivity,

$T_s$  [°R] - is the ambient (solar) temperature of the radiating medium,

$$B = \frac{173 \times 10^{-10}}{3600} = 4.8 \times 10^{-13} \cdot \left[ \frac{\text{Btu}}{\text{sec ft}^2 \cdot \text{R}^4} \right]$$

- is the Stephan-Boltzman's radiation constant.

Neglecting the radiation effects between the inner surface of the skin and the inner ambient of the vehicle, as well as the heat flux between the skin and the structural elements inside the vehicle,  $[\Delta q]_x = 0$  the instantaneous local heat flux is:

$$\therefore \left[ G_w \frac{dT_w}{dt} \right]_x = h_x [T_{\infty} - T_w]_x - [\epsilon_w T_w^4]_x B + \epsilon_s B [T_s]^4 \cdot x \left[ \frac{\text{Btu}}{\text{ft}^2 \text{ sec}} \right]$$

(2.4-245)

Alternatively, introducing the local Stanton Number and the local Mach Number definition,

$$[St_{\infty}]_x = \frac{J h_x}{[C_p \rho_{\infty} V_{\infty}]_x} \cdot [\text{dimensionless}] \quad (2.4-246)$$

$$[M_{\infty}]_x = \left[ \frac{V_{\infty}}{a_{\infty}} \right]_x \cdot [\text{dimensionless}] \quad (2.4-247)$$

$$\therefore [St_{\infty}]_x = \frac{J h_x}{[C_p \rho_{\infty} M_{\infty} a_{\infty}]_x} \cdot [\text{dimensionless}] \quad (2.4-248)$$

the Eq (2.4-245) takes the form:

$$\left[ \frac{dT_w}{dt} \right]_x = \frac{1}{J [G_w]_x} [St_{\infty}]_x [C_p \rho_{\infty} M_{\infty} a_{\infty}]_x [T_{\infty} - T_w]_x - \frac{1}{[G_w]_x} \{ [\epsilon_w T_w^4]_x B - \epsilon_s B T_s^4 \} \cdot \left[ \frac{\text{R}}{\text{sec}} \right]; \quad (2.4-249)$$

where:

$$J = 778 \left[ \frac{\text{ft lbf}}{\text{Btu}} \right] - \text{is the mechanical equivalent of heat,}$$

$$[C_p]_x = \left[ \frac{\text{ft lbf}}{\text{slug} \cdot \text{R}} \right] - \text{is the local (x) specific heat at}$$

constant pressure of the flowing fluid (air),

$[\rho_{\infty}]_x \left[ \frac{\text{slug}}{\text{ft}^3} \right]$  - is the air density outside the boundary layer ( $\infty$ ), at a local station (x),

$[v_{\infty}]_x \left[ \frac{\text{ft}}{\text{sec}} \right]$  - is the inviscid stream ( $\infty$ ) flow speed at a local station (x),

$[a_{\infty}]_x \left[ \frac{\text{ft}}{\text{sec}} \right]$  - is the inviscid stream ( $\infty$ ) speed of sound at a local station (x),

$[M_{\infty}]_x$  - is the inviscid stream Mach Number at a local station (x),

$[St_{\infty}]_x$  - is the local (x) Stanton Number, referred to the local (x) inviscid stream conditions.

Note that in the expressions (2.4-246), (2.4-248) and (2.4-249) the mechanical equivalent of heat (J) is introduced because of the specific heat units  $[(\text{ft-lbf})/\text{slug} \cdot \text{R}]$ . If the  $[C_p]_x$  were expressed in  $[\text{BTU}/\text{slug} \cdot \text{R}]$ , there would be no need for (J). Also notice that the units of  $(C_p)$  and  $(W_w)$  must be matched correspondingly.

The local Stanton Number,  $[St_{\infty}]_x$ , can be related to the local skin-friction coefficient,  $[Cf_{\infty}]_x$ , through some kind of a modified Reynolds Analogy concept, depending upon the degree of approximations involved and the type of boundary layer flow.

(1) For laminar continuum flow conditions, the following expressions are assumed valid:

$$[St_{\infty}]_x = \frac{[Cf_{\infty}]_x}{2} [Pr_{\infty}]_x^{-1/3} \quad (2.4-250)$$

- is the adopted dimensionless modified Reynolds Analogy, Eq (2.4-250),

$$[r]_x = [Pr_{\infty}]_x^{1/2} = \left[ \frac{T_{aw} - T_{\infty}}{T_{\infty} - T_{\infty}} \right]_x = \left[ \frac{T_{aw} - T_{\infty}}{V_{\infty}^2 / 2 C_p} \right]_x \quad (2.4-251)$$

- is the dimensionless laminar boundary layer recovery factor, Eq (2.4-251),

$$[T_{aw}]_x = [T_{\infty}]_x \left[ 1 + r \frac{\gamma - 1}{2} M_{\infty}^2 \right]_x \quad (2.4-252)$$

- is the local (x) adiabatic wall tem-

perature, [°R], Eq (2.4-252),

$$\left[ \frac{V_{\infty}^2}{2} + C_p T_{\infty} \right]_x = C_p T_{s_{\infty}}$$

- is the energy equation for adiabatic inviscid flow conditions ( $\infty$ ), taken locally ( $x$ ), Eq.(2.4-253),

$T_{s_{\infty}}$  [°R] - is the local ( $x$ ) inviscid stream ( $\infty$ ) stagnation temperature,

$$[C_{f_{\infty}}]_x = \frac{\tau_w}{[1/2 \rho_{\infty} V_{\infty}^2]_x} - \text{is the local (x) skin-friction coefficient, referred}$$

to the local inviscid fluid conditions outside the boundary layer, Eq (2.4-254)

$$[\alpha_{\infty}^2]_x = \gamma R [T_{\infty}]_x = \left[ \frac{V_{\infty}^2}{M_{\infty}^2} \right]_x \cdot \left[ \frac{ft^2}{sec^2} \right]_x$$

$$\left[ \frac{2 V_{\infty}^2}{2 V_{\infty}^2} \frac{T_{aw} - T_{\infty}}{T_{aw} - T_{\infty}} \right]_x \equiv 1, \quad (2.4-255)$$

$$(2.4-256)$$

$\tau_w \left[ \frac{lbf}{ft^2} \right]$  - is the local shear stress at the wall.

Then, after multiplying the Eq (2.4-249) with the unit identity Eq (2.4-256), and assuming that the simple form of the energy equation (2.4-253) and the local laminar recovery factor,  $[r_x]$ , expressions (2.4-251) and (2.4-252) are valid, the Eq (2.4-249) takes a specific governing form for the laminar continuum flow regime:

$$\left[ \frac{dT_w}{dt} \right]_x = \frac{.25}{J[G_w]_x} \left[ C_{f_{\infty}} Pr_{\infty}^{-2/3} \rho_{\infty} M_{\infty}^3 \alpha_{\infty}^3 \left( \frac{T_{aw} - T_w}{T_{s_{\infty}} - T_{\infty}} \right) \right]_x - \frac{1}{[G_w]_x} \left\{ [\epsilon_w T_w^4]_x B - \epsilon_s B T_s^4 \right\} \left[ \frac{^{\circ}R}{sec} \right]_x \quad (2.4-257)$$

(2) For turbulent continuum flow conditions, the general aerothermodynamic Eq (2.4-249), can be likewise brought to the corresponding specific governing form:

$$\left[ \frac{dT_w}{dt} \right]_x = \frac{.3}{J[G_w]_x} \left[ C_{f_{\infty}} \rho_{\infty} M_{\infty}^3 \alpha_{\infty}^3 \left( \frac{T_{aw} - T_w}{T_{s_{\infty}} - T_{\infty}} \right) \right]_x - \frac{1}{[G_w]_x} \left\{ [\epsilon_w T_w^4]_x B - \epsilon_s B T_s^4 \right\} \left[ \frac{^{\circ}R}{sec} \right]_x \quad (2.4-258)$$

assuming that the modified Reynolds analogy and the local recovery factor

concepts for a turbulent boundary layer are:

$$[St_{\infty}]_x = .6 [C_{f_{\infty}}]_x, \quad [\text{dimensionless}] \quad (2.4-259)$$

$$[r_x] = [Pr_{\infty}^{1/3}]_x = \left[ \frac{T_{aw} - T_{\infty}}{T_{s_{\infty}} - T_{\infty}} \right]_x = \left[ \frac{T_{aw} - T_{\infty}}{V_{\infty}^2 / 2 C_p \rho_{\infty}} \right]_x \quad (2.4-260)$$

and:

$$[T_{aw}]_x = [T_{\infty}]_x \left[ 1 + r_x \frac{\gamma-1}{2} M_{\infty}^2 \right]_x, \quad [^{\circ}R], \quad (2.4-261)$$

$$\left[ \frac{V_{\infty}^2}{2} \right]_x + [C_p T_{\infty}]_x = C_p T_{s_{\infty}} \quad (2.4-262)$$

$$[\alpha_{\infty}^2]_x = \gamma R [T_{\infty}]_x = \left[ \frac{V_{\infty}^2}{M_{\infty}^2} \right]_x \cdot \left[ \frac{ft^2}{sec^2} \right]_x \quad (2.4-263)$$

$$\left[ \frac{2 V_{\infty}^2}{2 V_{\infty}^2} \frac{T_{aw} - T_{\infty}}{T_{aw} - T_{\infty}} \right]_x \equiv 1 \quad (2.4-264)$$

(3) For slip flow regimes a conceptually modified laminar boundary layer may be assumed to exist: the boundary surface conditions are changed and a temperature jump at the body surface exists, see Sections 2.4.5 and 2.4.6. Nevertheless, for practical engineering purposes, the actually modified recovery factor,  $[r_x]$ , due to the temperature jump may be neglected, since both the theoretical analysis and the empirical evidence regarding the slip flow regime are rather uncertain. Therefore, with a first approximation, the laminar continuum flow governing aerothermal Eq (2.4-257) is assumed to be valid for the slip flow regime as well.

(4) The transitional flow remains until present times analytically almost completely unwieldy for practical purposes. It can be treated for engineering purposes conditionally either by extending the free molecule regime below its lower boundary, or by extending tentatively the slip flow regime analysis beyond its upper boundary. In the latter case it should be born in mind that the local skin friction coefficient values of this arbitrarily extended slip flow regime shall be somewhat exaggerated (conservative).

When using the governing Eqs (2.4-257) and (2.4-258), the following should be realized:

(a) The functional relationships

represented by Eqs (2.4-257) and (2.4-258) form ordinary differential equations of the first degree and the first order, the independent variable being time, (t). They can be solved by suitable numerical analysis methods, provided the intrinsic variations of the constituent physical parameters ( $\rho_\infty, M_\infty, T_{0w}, T_{s\infty}, \mu_\infty, \epsilon, C_{x\infty}, Pr_\infty, G_w$ ) with time (t) and the wall temperature ( $T_w$ ) are explicitly known. Then, the governing Eqs- (2.4-257) and (2.4-258) reduce to the form,

$$\frac{dT_w}{dt} = f(T_w, t) \quad (2.4-258a)$$

the solution of which is later tentatively handled by the Runge-Kutta step-by-step numerical integration procedure for a chosen time interval, ( $\Delta t$ ), and a given set of initial ( $T_w$ ) boundary conditions in each step.

Thus obtained instantaneous solutions yield the local instantaneous skin-temperature conditions  $[T_w]_x = f(t)$  for a given body configuration and a known flight trajectory, represented by  $H=H(t)$  and  $V=V(t)$  variations.

(b) The local skin friction coefficient,  $[C_{f\infty}]_x$ , is in general a function of many physical conditions existing within the body-fluid system in a relative motion, such as body geometry, body attitude, type of flow (continuum, slip, transitional, free molecule), boundary layer structure (laminar, turbulent) and the associated specific heat and momentum transfer mechanisms across the boundary layers, relative speed of motion, type of motion (steady, accelerated), body surface conditions (roughness, temperature), etc. The practical estimates of the local skin friction coefficient values under different conditions has been elaborated in the preceding Section, 2.3. Using the respective skin friction expressions from there, the corresponding local  $[C_{f\infty}]_x$  values are introduced in each step (i.e. time interval) when iteratively computing the Eq (2.4-258), the solution of which then gives,

$$[C_{f\infty}]_x = \phi([T_w]_x, t) \quad (2.4-259a)$$

i.e., the instantaneous values of the local skin friction coefficient in terms of the actual instantaneous local wall temperature conditions for generally transient flight regimes, all other flow and body surface conditions functionally already related and known in

terms of (t) and  $[T_w]_x$ .

(c) Once the local values of the skin friction coefficient,  $[C_{f\infty}]_x$ , are thus determined along a given body shape and a given transient (accelerated) flight regime, the average two-dimensional skin friction coefficient  $[C_{fA}]$  is then obtained by integration,

$$C_{fA} (S_{WET}) \frac{\rho_A V_A^2}{2} = \left\{ \frac{1}{l} \int_0^l [C_{f\infty}]_x \right.$$

$$\left. \frac{\rho_\infty V_\infty^2}{2} dx \right\} (S_{WET}) = \phi(t) \quad (2.4-260a)$$

where the subscript "A" denotes that the particular quantity is referred to the ambient (flight) conditions, and the subscript ( $\infty$ ) refers to the free stream conditions outside the boundary layer locally (x).

The local dynamic pressure values,

$$\left[ \frac{\rho_\infty V_\infty^2}{2} \right]_x,$$

can be in general functionally related to the ambient dynamic pressure (which is usually taken as the basic reference),

$$\left[ \frac{\rho_A V_A^2}{2} \right],$$

by using the corresponding perfect fluid potential flow theory analysis. If a flat plate at a zero angle-of-attack is used as the basic representative body geometry, the Eq (2.4-260) takes immediately the simple form,

$$C_{fA} = \frac{1}{l} \int_0^l [C_{f\infty}]_x dx = \phi(t) \quad (2.4-261a)$$

in view of

$$\frac{\partial p}{\partial x} = 0 \quad (2.4-262a)$$

$$[C_{p\infty}]_x = \frac{p_A - p_\infty}{\left[ \frac{\rho_\infty V_\infty^2}{2} \right]_x} = \frac{p_A - p_\infty}{\frac{\rho_A V_A^2}{2}} = [C_{pA}]_x = 0 \quad (2.4-263a)$$

$$\frac{\rho_\infty V_\infty^2}{2} = \frac{\rho_A V_A^2}{2} \quad (2.4-264a)$$

Conversion of the flat plate results to the conical body shapes is performed directly by use of the axisymmetric flow rules for laminar and turbulent boundary layers, see Section 2.3. Also, in case of laminar boundary layers on flat plates,

$$C_{fA} = 2 [C_{f\infty}]_{x=0} \quad (2.4-265)$$

regardless of Mach Number, Reynolds Number or the wall-to-free stream temperature ratio.

(d) The governing Eqs (2.4-257) and (2.4-258) necessarily incorporate many approximations, that may be traced back through the supporting theoretical presentations in the previous Sections. Thus, for instance, these equations do not account for mass transfer phenomena, apparent mass effects, aerodynamic time-lag phenomena, and thermal relaxation times necessary for realization of an equilibrium state in vibrational, ionization and dissociation energetic levels. The radiative effects are treated also approximately only, and the inner skin surface is assumed insulated from the interior ambient and structural temperature conditions. The outer skin surface is assumed completely smooth.

(e) In view of the relatively lengthy iterative computational procedure, required in solving the governing Eqs. (2.4-257) and (2.4-258), in practical applications their use should be restricted to more elaborate investigations of the transient flight regimes when so ultimately necessary. For a preliminary design order-of-magnitude drag force evaluation needs, simpler and relatively less accurate quasi-steady predictions can be performed by approximate treatments as described in Section 2.3, even for transient flight phases.

(5) The skin friction coefficient evaluation in the free molecular flow regime (transient or steady) requires a completely separate analytic approach. Details of the related theoretical analysis are given in Sections 2.4.2 and 2.4.3. Here it is stressed that the momentum and the energy equations are closely interconnected and a number of explicit analytic or graphical expressions for the skin-friction coefficient values in terms of the thermal ambient and surface conditions can be taken from the Section 2.4.3 directly for several simple body shapes. The degree of accuracy of the expressions

depends upon the assumptions and approximations involved (pure specular reflection, pure diffuse reflection, actual value of the accommodation coefficient, etc). Such explicitly elaborated free molecule flow skin friction data necessitate a separate determination of the skin-temperature conditions. Furthermore, there are some flight cases when a preliminary knowledge of the skin temperature,  $[T_w]_x$ , from the free molecule flow regime is required in order to compute subsequently the skin friction data in the slip flow regime under the general transient flight conditions. Thus, for instance, for a re-entry flight history, when using the Kutta-Runge numerical integration method in the slip flow domain, the initial boundary conditions in the first step of the computations are the final free molecule flow conditions, since then the free molecule flow regime precedes historically the succeeding slip flow phase. For the purpose, the instantaneous local skin temperature from the end point of the free molecule flow regime,  $[T_w]_{x \text{ free final}}$  becomes the initial instantaneous local skin temperature,  $[T_w]_{x \text{ slip initial}}$ , in the first iterative computational step of the slip flow regime.

Therefore, a relatively computational method of predicting the free molecule (and extended tentatively through transitional) flow instantaneous skin temperature conditions is presented, including the solar radiation effects. Thus, for a representative flat plate at an angle ( $\theta$ ) with respect to the oncoming molecular stream, the energy balance for the exposed front surface is(67):

$$[e_i + e_s]_x = [e_r + e_w \pm \Delta q_i]_x \left[ \frac{\text{lb} \cdot \text{ft}}{\text{ft}^2 \cdot \text{sec}} \right], \quad (2.4-266)$$

where:

$[e_i]_x \left[ \frac{\text{lb} \cdot \text{ft}}{\text{ft}^2 \cdot \text{sec}} \right]$  - is the local energy flux into surface due to impinging (incident) molecules,

$[e_s]_x \left[ \frac{\text{lb} \cdot \text{ft}}{\text{ft}^2 \cdot \text{sec}} \right]$  - is the local energy flux into surface due to ambient (Solar) radiation,

$[e_r]_x \left[ \frac{\text{lb} \cdot \text{ft}}{\text{ft}^2 \cdot \text{sec}} \right]$  - is the local energy flux out of surface

due to re-emitted molecular stream,

$[e_w]_x \left[ \frac{\text{lb} \cdot \text{ft}}{\text{ft}^2 \cdot \text{sec}} \right]$  is the local energy flux out of surface due to re-emitted radiation,

$[\Delta q_1]_x \left[ \frac{\text{lb} \cdot \text{ft}}{\text{ft}^2 \cdot \text{sec}} \right]$  - is the local heat flux removed from or added to skin due to any artificial or structural cooling or heating effects.

Using the common kinetic theory of gases monoatomic molecular model, corrected for diatomic molecular properties of air, but neglecting the vibrational degrees of freedom, the constituent terms in the governing Eq (2.4-266) become for a non-dissociating, non-ionized flow at a local point (x) on the exposed flat plate surface:

$$\alpha \left\{ n_A \left[ \frac{m_A V_A}{2} + (\psi + 1) B_1 T_A - \frac{5}{2} B_1 T_w \right] \right\}_x + \epsilon_s B_2 T_s^4 - \epsilon_w B_2 [T_w^4]_x \pm [\Delta q_1]_x = 0, \quad \left[ \frac{\text{lb} \cdot \text{ft}}{\text{ft}^2 \cdot \text{sec}} \right], \quad (2.4-267)$$

where:

$\alpha = \frac{\epsilon_1 - \epsilon_r}{\epsilon_1 - \epsilon_w} \leq 1$  - is the thermal accommodation coefficient, see Section 2.4.2,

$n_A = \frac{N_A V_m}{2\sqrt{\pi}} \{X\} \left[ \frac{\text{molecules}}{\text{ft}^2 \cdot \text{sec}} \right]$  - is the flux number of molecules impinging upon the flat plate exposed surface,

$N_A = N_0 \left( \frac{P_A}{P_0} \right) \left( \frac{T_0}{T_A} \right) \left[ \frac{\text{molecules}}{\text{ft}^3} \right]$  - is the number of molecules contained per cubic foot of the ambient atmospheric gas at some altitude (A), expressed in terms of the standard atmospheric conditions at sea-level (subscript 0),

$$N_0 = 7.63 \times 10^{23} \left[ \frac{\text{molecules}}{\text{ft}^3} \right],$$

$$T_0 = 492 \text{ }^\circ\text{R},$$

$$P_0 = 2117 \left[ \frac{\text{lb} \cdot \text{ft}}{\text{ft}^2} \right],$$

$V_m = \frac{1}{\beta} = \left( \frac{2gRT_A}{W} \right)^{1/2} \left[ \frac{\text{ft}}{\text{sec}} \right]$  - is the most probable molecular speed,

$g = 32.17 \left[ \frac{\text{ft}}{\text{sec}^2} \right]$  - is the gravitational constant,

$R = 1544 \left[ \frac{\text{ft} \cdot \text{lb} \cdot \text{ft}}{\text{lb} \cdot \text{mole} \cdot \text{ }^\circ\text{R}} \right]$  - is the universal gas constant (air)

$W = 28.97 \left[ \frac{\text{lb} \cdot \text{ft}}{\text{lb} \cdot \text{mole}} \right]$  - is the molecular weight of air (standard composition),

$\chi$  = a dimensionless quantity, functionally presented in Fig (2.4-53) by the straight line law (for air):

$$\chi = \frac{7}{2} \left( \frac{V}{V_m} \sin \theta \right) + 1, \quad (2.4-268)$$

$m_A = \frac{P_A}{N_A} \left[ \frac{\text{slugs}}{\text{molecule}} \right]$  - is the mass of one molecule of air in a Standard Atmosphere,

$\psi$  = a dimensionless quantity, functionally presented in Fig (2.4-54) in terms of  $(V_A / V_m) \sin \theta$ ,

$B_1 = 5.66 \times 10^{-24} \left[ \frac{\text{ft} \cdot \text{lb} \cdot \text{ft}}{\text{ }^\circ\text{R} \cdot \text{molecule}} \right]$  - is the Stephan-Boltzmann's constant,

$B_2 T_s^4 = 93.4 \left[ \frac{\text{ft} \cdot \text{lb} \cdot \text{ft}}{\text{sec} \cdot \text{ft}^2} \right]$  is the mean value of solar radiation at the edge of atmosphere impinging perpendicularly to a flat surface; radiation from the ambient gases is neglected.

$\epsilon_s$  - is the skin emissivity, assumed constant and equal to skin absorptivity for all wave lengths and temperatures (a gray-body absorption), i.e.,  $\epsilon_s \approx \epsilon_w$  [dimensionless], see Fig (2.4-57),

$B_2 = 3.74 \times 10^{-10} \left[ \frac{\text{ft} \cdot \text{lb} \cdot \text{ft}}{\text{ft}^2 \cdot \text{sec} \cdot \text{ }^\circ\text{R}^4} \right]$  - is the Stephan-Boltzmann's constant.

Notice that the governing Eq (2.4-267), although derived for a flat plate exposed surface, can be readily applied to any curved surface locally, the investigated point being treated as a small tangential flat surface inclined at a local angle ( $\theta$ ) with respect to the impinging orderly molecular stream ( $V_A$ ). Also, in the Eq (2.4-267), it has been implicitly assumed that the impinging molecules temperature ( $T_i$ ) is equal to the ambient atmospheric temperature ( $T_A$ ), and that the re-emitted molecules' temperature ( $T_r$ ) is equal to the surface temperature ( $T_w$ ), i.e.,  $\alpha = 1$ .

In case of a "shaded" surface (i.e., not directly exposed to the oncoming molecular stream,  $90^\circ \leq \theta \leq 180^\circ$ ), the governing Eq (2.4-267) retains the same form, but ( $n_A$ ) becomes ( $n'_A$ ), ( $\psi$ ) becomes ( $\psi'$ ), and ( $\chi$ ) becomes ( $\chi'$ ), where, according to Ref (2.4-67):

$$n_A' = \frac{N_A V_m}{2\sqrt{\pi}} [X'] \left[ \frac{\text{molecules}}{ft^2 \text{ sec}} \right],$$

$[X']$  - see Fig. (2.4-55),

$[\psi']$  - see Fig. (2.4-56).

The same ( $n_A', X', \psi'$ ) values should be used for ( $\theta = 0$ ).

(ii) Computations of Skin-Friction Coefficients in Continuum Slip, and Free Molecule Flow Regimes Under Accelerated Flight Conditions.

Within the assumptions and restrictions stated in the preceding paragraph (i), the determination of the skin-friction drag coefficient values for a given body geometry and the body skin structural characteristics under the actual transient high speed - variable altitude flight conditions involves a rather lengthy step-by-step computational procedure. When investigating the interdependence of the main physical quantities for practical engineering purposes, the attention can be focused on the following few most important preparatory computational aspects:

(a) In accordance with the accepted approximate procedure in Section 2.3, the skin friction coefficients for the simple body geometries of a vehicle (nose cones or ogives, cylindrical afterbodies, slender bodies of revolution, wedges, thin airfoil shapes) can be evaluated either (1) by treating their "equivalent flat plate" counterparts, and then correcting the flat plate skin-friction data for the respective actual body shape, or (2) by directly reading their skin-friction data from the corresponding graphs, when available. The first approach is advantageous in view of the fact that the flat plate skin-friction results are relatively more accurate and available for wide ranges of Mach Number, Reynolds Number and Knudsen Number variations. The accuracy of a subsequent correction of the equivalent flat plate results is quite satisfactory. The corrective factors are given in Section 2.3, based on Mangler's transformation (68).

(b) The skin-friction results on flat plates are computed for the zero-angle of attack condition. Nevertheless, in accordance with the basic approximations for the skin friction drag force definition in Section 1.7.4, the results are applicable to small angle-of-attack

conditions as well as for practical engineering purposes.

(c) For the generally transient accelerated flight conditions on a prescribed trajectory, any instantaneous local value of the skin friction estimate is made by accounting for:

- Dependence of the local skin-friction coefficient,  $[C_{f\infty}]_x$  or  $[C_{f_w}]_x$ , upon the actual transient local skin temperature,  $[T_w]_x = f(t)$ , and vice versa,

- Dependence of the local Knudsen Number,  $[Re_x]_\infty$ , or  $[Re_x]_w$ , upon the actual instantaneous local skin temperature,  $[T_w]_x = f(t)$ , and vice versa,

- Dependence of the local Knudsen Number,  $[Kn_x]_w$ ,  $[Kn_{\delta_x}]_w$ , or  $[Kn_x]_\infty$ ,  $[Kn_{\delta_x}]_\infty$ , upon the actual instantaneous local skin temperature,  $[T_w]_x = f(t)$ , and vice versa,

- Dependence of the local coefficient of viscosity,  $[\mu_w]_x$  or  $[\mu_\infty]_x$ , upon the actual instantaneous local skin temperature,  $[T_w]_x = f(t)$ ,

- Dependence of the gaseous local specific heat coefficient,  $[C_p]_x$  and the body-skin local heat conductivity coefficient,  $[C_w]_x$ , upon the actual instantaneous local skin temperature,  $[T_w]_x = f(t)$  and vice versa,

- Dependence of the local speed of sound,  $[a_w]_x$  or  $[a_\infty]_x$ , upon the actual instantaneous local skin temperature,  $[T_w]_x = f(t)$ ,

- Dependence of the local Mach Number,  $[M_x]_w$  or  $[M_x]_\infty$ , upon the actual instantaneous local skin temperature,  $[T_w]_x = f(t)$ , and vice versa,

- Dependence of the local Prandtl Number,  $[Pr_x]_w$ , upon the actual instantaneous local skin temperature,  $[T_w]_x = f(t)$ ; or the local recovery factor,  $[r_x]$ , the local adiabatic wall temperature,  $[T_{aw}]_x$  and the stagnation temperature,  $[T_{0\infty}]_x$ , respective combinations.

(d) The functional analytical relationships between the physical parameters shall take different forms in the continuum slip and free molecule characteristic flow regimes, see the respective governing equations and auxiliary relationships.

(e) As a consequence, an analytical

evaluation of the local skin friction coefficient,  $[C_{fx}]_w$  or  $[C_{fx}]_\infty$ , and a subsequent determination of its average value for a given body geometry by an appropriate integration procedure at any given time instant,  $(t)$ , during a generally transient flight history of a given vehicle, shall inevitably require:

An iterative process in determining locally the existence of the one of the four possible characteristic flow regimes: continuum, slip, transitional and free molecule, as affected by the local Knudsen Number,  $[Kn_x]_w$ , dependence on the actual local skin-temperature conditions,  $[T_w]_x = f(t)$ ,

An iterative process in determining locally the boundary layer type (laminar or turbulent within the continuum flow concept, and laminar for the slip flow regime), in terms of the local Mach Number,  $[M_x]_w$  and the local Reynolds Number  $[Re_x]_w$  criteria, which are in their turn, functions of the actual local non-equilibrium skin-temperature conditions,  $[T_w]_x = f(t)$ .

A suitable functional representation of all other local physical or dimensionless parameters ( $r, \sigma, k, \mu, M, \rho, p, Pr, St$ , etc.) in terms of the local transient skin temperature value,  $[T_w]_x = f(t)$ , in as much as these functional relationships appear in the final analytical expressions for both the local skin-friction coefficient  $[C_{fx}]_\infty$  and the inevitably associated local heat transfer coefficient  $[St_x]_\infty$  in different flow regimes.

The complexity of such numerical computations and the associated analytical investigations for a compound body geometry of any given vehicle is clearly evident when it is realized:

-That the iterative stepwise computational process has to be repeated for a sufficient number of local points in order to yield a mean average integrated skin friction coefficient value,  $[C_{fA}]$ , representative instantaneously for the whole vehicle at a given point on its trajectory,

-That such a trajectory-point computation of the instantaneously representative skin-friction coefficients has to be in the wholeness repeated for enough of the points on a vehicle trajectory in order to yield the required average values of  $C_{fA} = f(t)$  corresponding to the respective time intervals  $(\Delta t)$  on a trajectory  $V = V(t)$  and

-That at any successive time-instant both the average skin friction  $[C_{fA}]$  and the heat transfer,  $[St]_A$ , coefficient values

are functions of all the previous time-history of their variations (including the initial conditions) up to the investigated moment, since such is the case with the actual skin temperature  $[T_w]_x$  time history.

In view of the facts, it is therefore proposed that the evaluation of the average skin-friction coefficient values,  $[C_{fA}]$ , be conducted by somewhat simplified engineering methods, as outlined next.

(1) Quasi-steady analysis on an ascending flight trajectory and preparation of the computational data.

The compound vehicle configuration is broken into its main constituent parts (nose section, body, wings, fins, etc.), according to the general breakdown scheme from Section 1.7.4. The skin friction drag force coefficient for each of the simple body geometries is to be evaluated separately, and the partial skin-friction drag force data then summed up as specified in Section 2.3. The individual skin-friction coefficients are estimated either by using the corresponding data for the specific simple body shape, or by using the "equivalent flat plate" method. For reasons discussed already, the latter approach is given the preference here. The equivalent flat plate is at a zero (or near zero) angle-of-attack.

A completely insulated (nonconducting) skin and a quasi-steady flow conditions are assumed at any point on the flight trajectory, permitting for realization of a local thermal adiabatic equilibrium at the plate surface and throughout the boundary layer. The local lengthwise pressure gradient,  $(\partial p / \partial x)$  is then zero, and so is the dimensional pressure coefficient value, i.e.,

$$[C_{px}]_\infty = \left[ \frac{p_\infty - p_A}{(\rho_\infty V_\infty^2 / 2)} \right]_x = \frac{[p_\infty]_x - p_A}{(\rho_A V_A^2 / 2)} = [C_{px}]_A = 0, \quad (2.4-270)$$

which shall prove additionally helpful in shortening the computational efforts involved.

The above approximate treatment amounts to an implicit assumption that at each point on the vehicle's trajectory the flow conditions are "allowed" to become fictitiously quasi-steady, and that the thermal adiabatic conditions at the insulated flat plate and in the boundary layer are in equilibrium,  $[T_w]_x \rightarrow [T_{ow}]_x$ , so that actually at each point on the vehicle trajectory the skin friction coefficients (local and average) can be evaluated

independently of the preceding flight time history. Evidently such an approach may prove far from being satisfactory or acceptable for highly accelerated flight phases and shall be then consequently used as a first, rough estimate only. The method is more appropriate for prolonged steady flight conditions.

The computational procedure is as follows:

#### STEP I

For a given vehicle, the basic plots of the requested flight characteristics shall be graphically plotted or analytically known as follows:

- The flight altitude (H) versus time (t) history, see the illustrative Fig (2.4-44) for a hypothetical case,

- The flight altitude (H) versus flight speed (V) history, see the illustrative Fig (2.4-45) for a hypothetical case, or the illustrative Figs (2.4-35), (2.4-36), (2.4-37), (2.4-38) and (2.4-39) for some characteristic missile categories in general,

- The flight speed (V) versus time (t) history, see Fig (2.4-46) for a hypothetical case.

Any one of the graphs, for instance  $H=f(t)$ , can serve as a conversion aid for the remaining two. Then the second graph,  $H=f(V)$ , can be subsequently used for determination of the ambient atmospheric boundaries between the four characteristic fluid flow regimes, see the illustrative Fig (2.4-40), while the third graph,  $V=f(t)$ , shall correspondingly serve as a practically very convenient plot for later heat transfer-skin friction dependence estimates (by means of respectively simplified analytic expressions) as pertinent to the four characteristic fluid flow regimes and the flight dynamics conditions (steady or quasi-steady and transient or accelerated flight cases respectively).

It should be noted that the characteristic flow boundaries, established by taking the particular characteristic length of the equivalent flat plate (or the body part itself, see Fig 2.4-40), serve as a first approximation only. In a more accurate analysis, the characteristic flow types (continuum, slip, transitional and free molecule) should

be determined in terms of the local flow conditions at the body surface, i.e., by taking the distance  $x$  of the investigated local point.

A general note: Within the existing theoretical and practical limitations of handling the drag force problem in general, it is immediately evident that the accuracy of the drag coefficient predictions at any instant of time shall be, in accelerated flight cases, a direct function of the accuracy with which the corresponding time histories of the trajectory characteristics  $V=f_1(t)$  and  $H=f_2(t)$  are known, and vice versa. Since the flight dynamics trajectory computations presupposes knowledge of the aerodynamic drag force data, an iterative process of the trajectory-drag computations suggests itself in a lesser or greater extent, the degree of accuracy depending upon the particular importance of the drag force and trajectory predictions. But in no case, the suggested iterative computational accuracy should exceed the limits of the drag-force predictability per se, which even for idealized steady flight conditions in a presumably Standard Atmosphere and for presumably perfect engineering hardware realizations, may be assumed to be of the order of  $\pm 10\%$  when relatively simple body geometries (flat plate, cone, cylinder, hemisphere) are considered.

Consequently, depending upon the overall level of accuracy required, the respective margins of accuracy with which the suggested three basic data trajectory graphs (Figs (2.4-44), (2.4-45), (2.4-46) should be plotted or analytically known shall vary an accelerated flight phase, and the time interval choice for the stepwise computations of the skin friction-temperature dependence shall be likewise accordingly adjusted. Due to a wide range of possible flight conditions, missile configurations and final objectives that may be considered, no generalized recommendation regarding the computational accuracies can be suggested. As a specific illustration, in Ref. (2.4-70) it is, for example, suggested that for engineeringly acceptable heat transfer estimates during transient (accelerated) missile flight phases, the one-second time intervals are required in which the local skin temperatures and the related local skin-friction coefficients should be computed and known. This would evidently impose a one-second time interval

accuracy in presentation of the basic graphs in Figs (2.4-44) and (2.4-46) or the respective tabular plotting (see Table 2.4-3) of the corresponding functional relationships  $H = f_1(t)$  and  $V = f_2(t)$  with the one-second interval basis.

### STEP 2

Using a Standard Model Atmosphere and the basic trajectory data  $H = f_1(t)$  and  $V = f_2(t)$  from Figs (2.4-44) and (2.4-46) (or the respective tabulated numerical data alternatively, see Table (2.4-3), the following ambient atmospheric flight parameters are plotted (or numerically tabulated, see Table (2.4-4), using the engineering lbf-ft-sec-OR system of units:

(a) The ambient static temperature, ( $T_A$ ), versus flight time involved, ( $t$ ), i.e.:

$$T_A = T_A(H) = T_A(t), \quad [^{\circ}R], \quad (2.4-271)$$

(b) The ambient speed of sound, ( $a_A$ ), versus flight time involved, ( $a_A$ ), i.e.:

$$a_A = a_A(T_A) = a_A(H) = a_A(t), \quad (2.4-272)$$

$$\therefore a_A = 49.02 (T_A)^{1/2}, \quad [ft/sec], \quad (2.4-273)$$

(c) The flight Mach Number, ( $M_A$ ), referred to the ambient Standard Atmosphere value of the speed of sound, ( $a_A$ ), versus time, ( $t$ ), i.e.:

$$M_A = \frac{V}{a_A} = M_A(V, T_A), \quad (2.4-274)$$

$$= M_A(V, H) = M_A(t),$$

(d) The ambient atmospheric density variation, ( $\rho_A$ ), with flight time ( $t$ ), i.e.:

$$\rho_A = \rho_A(H) = \rho_A(t), \quad [lbf \text{ sec}^2 / ft^4],$$

$$\therefore \rho_A = \frac{p_A}{g R_A T_A} = \frac{p_A}{(32.17)(53.35) T_A}, \quad (2.4-275)$$

$$[lbf \text{ sec}^2 / ft^4]; \quad (2.4-276)$$

where:

$$g = 32.17 \left[ \frac{ft}{\text{sec}^2} \right] \text{ -average gravitational}$$

acceleration, assumed constant; alternatively  $g = g(H)$  and latitude,

$$R_A = 53.35 \left[ \frac{lbf \text{ ft}}{lbf \text{ }^{\circ}R} \right] \text{ -absolute atmospheric gas constant for dry air, standard composition; alternatively } R_A = R_A(H) \text{ and humidity,}$$

(e) The ambient atmospheric pressure, ( $p_A$ ), variation with time, ( $t$ ):

$$p_A = p_A(H) = p_A(t), \quad [lbf/ft^2], \quad (2.4-277)$$

$$p_A = g R_A \rho_A T_A = (32.17)(53.35) \rho_A T_A, \quad [lbf/ft^2], \quad (2.4-278)$$

(f) The coefficient of ambient atmospheric viscosity, ( $\mu_A$ ), as a function of time, ( $t$ ):

$$\mu_A = \mu_A(T_A) = \mu_A(H) = \mu_A(t), \quad [lbf \text{ sec} / ft^2], \quad (2.4-279)$$

(g) The ambient coefficient of the kinematic viscosity, ( $\nu_A$ ), versus the flight time, ( $t$ ):

$$\nu_A = \frac{\mu_A}{\rho_A} = \nu_A(T_A, \rho_A) = \nu_A(H) = \nu_A(t), \quad [ft^2/sec], \quad (2.4-280)$$

The ambient atmospheric flight parameters ( $a$  to  $g$ ) are presented illustratively in Figs (2.4-47) and (2.4-48) for the chosen hypothetical missile. In each particular design case, the time scale should be chosen to correspond to the desired degree of accuracy of the drag force estimates, as stated earlier.

### STEP 3

For the representative flat plate at a zero angle-of-attack and for the presumed aerothermal steady equilibrium flow conditions, the main characteristic flow regimes (continuum, slip, transitional, free molecule), as encountered at various points on a given flight trajectory, can be discriminated on the premises of convertibility of the local ambient (subscript A) physi-

cal parameters to their corresponding local free stream (subscript  $\infty$ ) values outside the boundary layer: at any point along the flat plate the specific condition of no pressure gradient ( $\partial p / \partial x = 0$ ) and the zero value of the local pressure coefficient,  $[C_{px}]_{\infty}$  or  $[C_{px}]_A$  (see Eq (2.4-220)), make the local free stream values (subscript  $\infty$ ) of all involved physical parameters simply equal to their instantaneous steady ambient (subscript A) values. This feature is invalidated for geometries different from a flat plate and angles of attack different from zero: then the pressure coefficient is no more equal to zero, and the functional relationships between the local free-stream ( $\infty$ ) and the instantaneous ambient (A) values of the steady flow parameters have to be established by use of the corresponding inviscid flow theories and across-the-shock conditions, as appropriate for the particularly investigated body geometry and the flow regime. As an illustration, for a conical body geometry in the continuum flow regime, the second-order inviscid perfect fluid theory may be used for ( $M_A < 5$ ) and the conical shock expansion theory for ( $M_A > 5$ ), yielding the influential parametric ratios ( $T_{\infty}/T_A, V_{\infty}/V_A, \rho_{\infty}/\rho_A, M_{\infty}/M_A, Re_{\infty}/Re_A$ , etc.) locally. The fundamental approximate premises of an either completely non-conducting (insulated) body skin, or of a steady, aerothermally in equilibrium flow, remain still in force.

For the particular flat plate case at a zero angle-of-attack, the ambient Standard Atmosphere physical parameters from the Step 2 (see Figs 2.4-47 and 2.4-48 and Table 2.4-4) are at the same time the local free-stream (subscript  $\infty$ ) values.

#### STEP 4

The local free stream (just outside the boundary layer) and the local equilibrium wall temperature ratios can be now established in two ways for the assumed quasi-steady, prolonged duration flight regimes:

(a) The flat plate is assumed completely insulated, i.e., the idealized adiabatic flow conditions are supposed to exist. Then, the necessary conversion of the adiabatic wall (subscript  $\infty w$ ) values of the involved physical parameters to their respective Standard Atmosphere ambient values (subscript A) is performed, in a first approximation, as follows:

For the representative insulated flat plate at a zero angle-of-attack under the assumed quasi-steady aerothermal flow equilibrium (neglecting radiation), the insulated skin temperature becomes equal to the "adiabatic wall" temperature at any local point,

$$T_w = T_{\infty w} \quad (2.4-281)$$

The local temperature ratio,

$$\begin{aligned} \left[ \frac{T_{\infty w}}{T_{\infty}} \right]_x &= \left[ \frac{T_{\infty w}}{T_A} \frac{T_A}{T_{\infty}} \right]_x = \left[ \frac{T_{\infty w}}{T_A} \right]_x \cdot 1 = \\ &= \frac{T_{\infty w}}{T_A} = \frac{T_w}{T_A} \quad (2.4-282) \end{aligned}$$

becomes constant along the flat plate length, since

$$[T_{\infty}]_x = T_A \quad (2.4-283)$$

The ratio,

$$\frac{T_w}{T_A} = \frac{T_{\infty w}}{T_A} = f(M_A, H) \quad (2.4-284)$$

is obtainable for continuum flow laminar and turbulent boundary layers from Figs (2.4-49) and (2.4-50) respectively. The stagnation point temperature is obtainable from Fig (2.4-51) in particular, if required for other reasons. Variation of the specific heats with temperature is accounted for in these figures<sup>(68)</sup>.

It should be noted that for the always laminar boundary layer in the slip flow regime, it has been here assumed that the values of ( $T_{\infty w}$ ) from the continuum theory are applicable in a good approximation, especially so when investigating the lower boundary (i.e., the beginning) of the slip flow regime<sup>(71)</sup>. This means that the "temperature jump" effect at wall has been neglected, or that the continuum laminar flow recovery factor is retained unchanged.

In the free molecule flow regime there is no equivalent of a boundary layer concept.

Once the value of

$$T_w = T_{\infty w} = f(M_A, H) = \phi(t) \quad (2.4-285)$$

is determined at each point of a given

flight trajectory, i.e., suitably tabulated for a properly chosen time scale (see Table 2.4-5), the Mach Number, the Reynolds Number and the Knudsen Number values referred to the wall conditions can be computed in terms of the assumed steady adiabatic isothermal conditions on the flat, insulated plate at a zero angle-of-attack, taking into account that in this case:

$$\frac{\partial p}{\partial x} = 0, \quad [C_{p\infty}]_x = C_{pA} = 0,$$

$$\frac{T_A}{[T_\infty]_x} = 1, \quad \frac{p_A}{[p_\infty]_x} = 1,$$

$$\frac{\rho_A}{[\rho_\infty]_x} = 1, \quad \frac{\mu}{[\mu_\infty]_x} = 1, \quad \frac{\nu_A}{[\nu_\infty]_x} = 1,$$

$$\frac{\alpha_A}{[\alpha_\infty]_x} = 1,$$

$$\frac{\partial p}{\partial y} = 0, \quad p_w = p_{aw} = [p_\infty]_x = p_A,$$

and

$$\alpha_w = \alpha_{Aw} = \alpha_A \left( \frac{T_{Aw}}{T_A} \right)^{1/2}, \quad (2.4-286)$$

$$\rho_w = \rho_{aw} = \rho_A \left( \frac{T_A}{T_{Aw}} \right),$$

$$\mu_w = \mu_{aw} = \mu_A \left( \frac{T_{Aw}}{T_A} \right)^\omega, \quad \omega \approx .76,$$

$$\nu_w = \nu_{aw} = \nu_A \left( \frac{\mu_{aw}}{\mu_A} \right) \left( \frac{\rho_A}{\rho_{aw}} \right),$$

$$(2.4-287)$$

both locally at any point and for the flat plate as a whole.

The ambient flight parameters (subscript A) are presented in Figs (2.4-47) and (2.4-48) for a hypothetical case, and should be determined from Standard Atmosphere Data in general.

Then, the local (subscript x) values of the dimensionless characteristic flow parameters,  $[M_x]_w$ ,  $[Re_x]_w$ ,  $[Kn_x]_w$ ,  $[Kn_{\delta x}]_w$ , as referred to the local physical flow conditions ( $\alpha_w$ ) at the flat, insulated plate surface are:

$$[M_x]_w = M_w = M_A \left( \frac{T_A}{T_w} \right)^{1/2} = M_A \left( \frac{T_A}{T_{Aw}} \right)^{1/2}, \quad (2.4-288)$$

$$[Re_x]_w = [Re_x]_A \left( \frac{T_A}{T_w} \right)^{1.76} = [Re_x]_A \left( \frac{T_A}{T_{Aw}} \right)^{1.76} \sim [Re_x]_A \left( \frac{T_A}{T_{Aw}} \right)^{7/4}, \quad (2.4-289)$$

$$[Kn_x]_w \sim \frac{M_w}{[Re_x]_w}, \quad [Kn_{\delta x}]_w \sim \frac{M_w}{[Re_x]_w^{1/2}}, \quad (2.4-290)$$

where:

$$M_w = \frac{V_A}{\alpha_w}, \quad M_A = \frac{V_A}{\alpha_A}, \quad V_A = V \left[ \frac{ft}{sec} \right],$$

$$[Re_x]_w = \frac{V_A X}{\nu_w}, \quad [Kn_x]_w = \frac{[\bar{\lambda}_x]_w}{x},$$

$$[Re_x]_A = \frac{V_A X}{\nu_A}, \quad [Kn_{\delta x}]_w = \frac{[\bar{\lambda}_x]_w}{\delta_x}, \quad (2.4-291)$$

$[\bar{\lambda}_x]_w$  - local mean free molecular path, corresponding to  $[T_w]_x$ ,

$\delta_x$  - local boundary layer thickness, [ft].

The following isentropic criteria in determining the local instantaneous characteristic flow regimes can be used, see Section 1.7.1.

Instantaneous local continuum flow regime prevails up to

$$[Kn_{\delta x}]_w \sim \frac{M_w}{[Re_x]_w^{1/2}} = \frac{M_A}{[Re_x]_A^{1/2}} \left( \frac{T_{Aw}}{T_A} \right)^{3/8} < 10^{-2},$$

$$[Re_x]_w = [Re_x]_A \left( \frac{T_A}{T_{Aw}} \right)^{7/4} \gg 1. \quad (2.4-292)$$

Instantaneous local slip flow regime boundaries are

$$10^{-2} < [Kn_{\delta x}]_w \sim \frac{M_w}{[Re_x]_w^{1/2}} = \frac{M_A}{[Re_x]_A^{1/2}} \left( \frac{T_{Aw}}{T_A} \right)^{3/8} < 10^{-1},$$

$$[Re_x]_w = [Re_x]_A \left( \frac{T_A}{T_{Aw}} \right)^{7/4} \sim 0(1). \quad (2.4-293)$$

Local instantaneous transitional flow regime boundaries are

$$10^{-1} < [Kn_{\delta x}]_w \sim \frac{M_w}{[Re_x]_w^{1/2}} = \frac{M_A}{[Re_x]_A^{1/2}} \left( \frac{T_{Aw}}{T_A} \right)^{3/8}, \text{ lower,} \quad (2.4-294)$$

$$3 > [Kn_x]_w \sim \frac{M_w}{[Re_x]_w} = \frac{M_A}{[Re_x]_A} \left( \frac{T_w}{T_A} \right)^{5/4} = \frac{M_A}{[Re_x]_A}, \text{ upper.} \quad (2.4-295)$$

Instantaneous local free molecule flow regime starts from

$$[Kn_x]_w \sim \frac{M_w}{[Re_x]_w} = \frac{M_A}{[Re_x]_A} \left( \frac{T_w}{T_A} \right)^{5/4} = \quad (2.4-296)$$

$$= \frac{MA}{[Re_x]_A} > 3 \text{ up. (2.4-296)}$$

It should be noted that the above boundaries are not an exceptionally strict criteria, and that other numerical critical values are used in some instances(70).

The physical and the respective dimensionless quantities from the STEPS 3 and 4 are computed for a given time instant on the vehicle trajectory, see Table (2.4-5).

In the continuum flow regime, discrimination between the laminar and the turbulent boundary layers is established by using an order of magnitude criteria, for instance,

$$[Re_x]_w = \frac{V_x}{\nu_w} \leq 10^6, \quad (2.4-297)$$

at the investigated local (x) point along the surface.

(b) The flat plate is alternatively assumed non-insulated, but an equilibrium temperature ( $T_{we}$ ) during prolonged steady flight regimes is achieved, assuming that the convective heat transfer from the boundary layer to the surface is equal to the heat lost by the surface by overall (inwardly and outwardly directed) radiation. In addition, the isothermal conditions along the flat surface are presumed, as stated earlier.

The procedure of determining the equilibrium temperature ( $T_{we}$ ) for the laminar and the turbulent boundary layers in the continuum flow regime, as well as for a laminar boundary layer in the slip flow regime, is explicitly described in Section 2.3 and the results graphically presented in the respective figures there. Here, under the same premises as in case of an insulated flat plate, the ( $T_{ew} = T_w$ ) values are substituted in the expressions (2.4-285) to (2.4-296) instead of the adiabatic wall temperature ( $T_{ow}$ ), and the local flow type criteria similarly computed for the non-insulated flat plate case, see Table (2.4-5).

#### STEP 5

Once the characteristic flow regime at a local point is known, the corres-

ponding local and average skin-friction coefficient value [ $C_{f,x}$ ]<sub>A</sub> and [ $C_{f,A}$ ] can be computed in terms of the skin temperature ( $T_w = T_{ow}$ ) or ( $T_w = T_{ew}$ ), the flight Mach Number, ( $MA$ ), the Reynolds Number, [ $Re_x$ ]<sub>A</sub> or [ $Re_A$ ]<sub>A</sub> and the Knudsen Number, [ $Kn_x$ ]<sub>A</sub> or [ $Kn_A$ ]<sub>A</sub>, at any time instant. The representative flat plate data can be then converted directly to conical bodies, the cone-cylinder body configurations, and the wedged airfoil sections as described at a length in Section 2.3. The flat plate explicit analytical expressions or equivalent graphical data for the skin-friction coefficient computations in the four characteristic flow regimes are presented in the next subparagraph (2) of this Section.

Since under the presumed steady, equilibrium flow conditions, ( $T_w = T_{we}$ ), for a non-insulated flat plate, the local heat fluxes in and out of the skin are equal at any instant of time (or at any point on a given trajectory):

$$\frac{dT_w}{dt} = 0,$$

and the governing equations for the local skin-friction computations reduce to:

For continuum turbulent boundary layers:

$$.3 \left[ C_{f \infty} M_{\infty}^3 \sigma_{\infty}^3 \rho_{\infty} \left( \frac{T_{ow} - T_{ew}}{T_{s \infty} - T_{\infty}} \right) \right]_x \\ = J \left\{ \left[ \epsilon_w T_{ew}^4 \right]_x B - \epsilon_s B T_s^4 \right\} \left[ \frac{\text{lb ft}}{\text{sec ft}^2} \right] \quad (2.4-298)$$

For continuum laminar boundary layers:

$$.25 \left[ C_{f \infty} Pr_{\infty}^{-2/3} M_{\infty}^3 \sigma_{\infty}^3 \rho_{\infty} \left( \frac{T_{ow} - T_{ew}}{T_{s \infty} - T_{\infty}} \right) \right]_x \\ = J \left\{ \left[ \epsilon_w T_{ew}^4 \right]_x B - \epsilon_s B T_s^4 \right\} \left[ \frac{\text{lb ft}}{\text{sec ft}^2} \right] \quad (2.4-299)$$

For slip flow (laminar) regime - governing Eq (2.4-299)

Notice that here the heat absorption capacity, [ $G_w$ ]<sub>x</sub>, of the skin does not influence the equilibrium wall temperature, [ $T_{ew}$ ]<sub>x</sub>.

For free molecule flow regime,  
 $\theta \sim \text{small}$ )

$$\alpha \left\{ n_A \left[ \frac{m_A V_A^2}{2} + (\psi + 1) B_1 T_A \right] \right\}_x - \frac{5}{2} \alpha n_A B_1 [T_{w0}]_x + \epsilon_s B_2 T_s^4 - \epsilon_w B_2 [T_{w0}^4]_x = 0 \quad \left[ \frac{\text{lb ft}}{\text{ft}^2 \text{ sec}} \right]$$

$$T_{w0} = T_w = T_r, \quad \alpha \approx 1,$$

$$C_f = f\left(\frac{T_r}{T_A}\right) \quad (2.4-300)$$

see Section 2.4.6.

Note that for laminar boundary layers on flat plates the average skin friction coefficient is

$$C_{fA} = 2 [C_{f0}]_{x=1},$$

regardless of Mach Number, Reynolds Number or wall-to-free stream ratio, provided isothermal wall conditions are assumed.

(2) General Procedure of Determining the Local and the Average Skin Friction Coefficient Values for Accelerated (Transient) or Quasi-steady Flight Regimes

Excluding the "apparent mass" effects and the time lag of an aerodynamic pressure distribution build-up, the following local and average skin-friction coefficient computational procedure is proposed: (a) for generally accelerated flight regimes characterized by a time-dependent wall temperature,

$$[T_w]_x = f(t), \quad T_w < T_{0w} < T_{0\infty}, \quad (2.4-301)$$

where  $(T_w)_x$  is the actually acquired transient (nonequilibrium) local skin temperature at a given instant of time, and (b) for quasi-steady, equilibrium thermal conditions,

$$[T_{w0}]_x = f(t) \quad T_w = T_{0w} \neq T_{0\infty}, \quad (2.4-301a)$$

on a generally non-insulated flat plate, see data preparation in the preceding subparagraph (1).

The general types of the local

transient (accelerated) flow regimes are characterized by a strong dependence of the actual (non-equilibrium) skin temperature,  $(T_w)_x$ , on the involved flight time interval,  $(\Delta t)$ , the given set of flight parameters (Mach Number, altitude, body attitude) and the related flow variables (pressure, density, speed of sound, coefficient of viscosity, etc.). Such an infinitesimally small time-interval analysis leads, in general, to a first order linear ordinary non-homogeneous differential equation of the type, see subparagraph (i) of this section:

$$\frac{dT_w}{dt}_x = f(\text{body geometry, skin surface conditions, } G_w, Pr, T_{0w}, T_{s\infty}, C_{f\infty}, T_{\infty}, C_{f\infty}, \rho_{\infty}, p_{\infty}, a_{\infty}, M_{\infty}, \epsilon, B, \Delta Q, T_w, t, x, \alpha)_x, \quad (2.4-301)$$

$$\therefore \left[ \frac{dT_w}{dt} \right]_x = f(T_w, C_{f\infty}, t)_x \quad (2.4-302)$$

for a given set of initial conditions and for a known auxiliary functional law,

$$(C_{f0})_x = f(T_w)_x. \quad (2.4-303)$$

The solution of the Eq (2.3-302) within a specified small time interval  $(\Delta t = t_K - t_{K-1})$ , and for a given set of the initial flight dynamics and fluid flow parameters at the time instant  $(t_{K-1})$ , is obtained by some numerical analysis iterative process. During the iteration, the auxiliary functional relationship (2.4-303), is used at first as determined for the initial wall temperature value  $(T_w)_{K-1}$  at the initial time instant  $(t_{K-1})$ . The completed first iteration of Eq (2.4-302) shall then yield the wall temperature value  $(T_w)_K \neq (T_w)_{K-1}$ . A second iteration for the same time interval,  $(\Delta t = t_K - t_{K-1})$ , is then required, this time using the  $(C_{f0})_x$  value from the auxiliary relationship (2.4-303) corresponding to the computed wall temperature  $(T_w)_K$ . When the second iteration is done, a new value of  $(T_w)_K \neq (T_w)_{K-1}$  is obtained. The successive iterative process for the same time interval  $(\Delta t = t_K - t_{K-1})$  may be thus theoretically continued until a satisfactory set of values both in  $(T_w)_K$  and  $(C_{f0})_x$  is obtained. Instead, for practical purposes of the aerodynamic skin-friction drag force analysis, it is considered acceptable to perform just one iteration for a

given time interval ( $\Delta t = t_k - t_{k-1}$ ), by using the Kutta-Runge method. The Kutta-Runge iterative method comprises itself intermediate corrective steps within any given time interval ( $\Delta t = t_k - t_{k-1}$ ), which should suffice for achieving a practically acceptable order-of-accuracy of the  $(C_{f\infty})_x$  predictions in one full step of iteration, provided the time interval is small enough, ( $\Delta t \sim dt$ ).

Then the final conditions at a preceding time instant ( $t = t_{k-1}$ ) are taken as initial conditions for computation of the above functional relationship at the immediately following time instant ( $t = t_{k+1}$ ),  $1 \leq k \leq n$ , etc. The computations are illustrated in a tabular form in Table (2.4-12), each computational step being fully elaborated in the following text. Once the transient instantaneous local skin temperature values,  $(T_w)_x$ , are thus computed, the corresponding instantaneous local skin friction coefficient,  $(C_{f\infty})_x$ , is also known in terms of the skin temperature  $(T_w)_x$ , as already stated.

Application of the method is restricted to the laminar continuum, the turbulent continuum and the laminar slip flow regimes. The free-molecule flow type is handled separately.

A gravitational (lbf-ft-sec-°R) system of functional physical dimensions is used,

- [F] = Force,
- [L] = Length,
- [t] = Time,
- [T] = Absolute Temperature,

with the corresponding American gravitational system of units

- [lbf] = pound-force,
- [ft] = foot,
- [sec] = ephemeris second,
- [°R] = degree Rankine.

CASE I - TRANSIENT FLIGHT PHASE (VARIABLE ALTITUDE-CONSTANT SPEED, OR CONSTANT ALTITUDE-VARIABLE SPEED, OR VARIABLE ALTITUDE-VARIABLE SPEED):

(a) Continuum Flow, Turbulent Boundary Layer, Governing Equation:

$$\left[ \frac{dT_w}{dt} \right]_x = \frac{.3}{J[G_w]_x} \left[ C_{f\infty} \rho_\infty M_\infty^3 a_\infty^3 x \right. \\ \left. \times \left( \frac{T_{aw} - T_w}{T_{s\infty} - T_\infty} \right)_x - \right. \\ \left. - \frac{1}{[G_w]_x} \left\{ [\epsilon_w T_w^4]_x B - \epsilon_s B T_s^4 \pm [\Delta q_i]_x \right\}, \left[ \frac{^\circ R}{\text{sec}} \right], \right.$$

$$[Re_x]_w = \frac{XV}{[\nu_w]_x} \geq 10^6, \quad (2.4-304)$$

(b) Continuum Flow, Laminar Boundary-Layer - Governing Equation:

$$\left[ \frac{dT_w}{dt} \right]_x = \frac{.25}{J[G_w]_x} \left[ C_{f\infty} Pr_\infty^{-2/3} \rho_\infty M_\infty^3 a_\infty^3 x \right. \\ \left. \times \left( \frac{T_{aw} - T_w}{T_{s\infty} - T_\infty} \right)_x - \right. \\ \left. - \frac{1}{[G_w]_x} \left\{ [\epsilon_w T_w^4]_x B - \epsilon_s B T_s^4 \pm [\Delta q_i]_x \right\}, \left[ \frac{^\circ R}{\text{sec}} \right], \right.$$

$$[Re_x]_w = \frac{XV}{[\nu_w]_x} \leq 10^6 \quad (2.4-305)$$

(c) Slip Flow, Laminar Boundary Layer-Governing Equation (2.4-305)

(d) Free Molecule Flow (Including Transitional Flow Regime) - Governing Equation:

$$\alpha \left\{ n_A \left[ \frac{m_A v_A^2}{2} + (\psi + 1) B_i T_A \right]_x - \frac{5}{2} \alpha n_A B_i [T_w]_x + \right. \\ \left. + \epsilon_s B_2 T_s^4 - \epsilon_w B_2 [T_w^4]_x \pm [\Delta q_i]_x \right\} = 0, \left[ \frac{\text{lbf ft}}{\text{ft}^2 \text{sec}} \right]. \quad (2.4-306)$$

CASE II - QUASI-STEADY FLIGHT, I.E., AN EQUILIBRIUM SKIN TEMPERATURE IS REACHED:

$$T_w = T_{ew} \geq T_{ow}, \\ \frac{dT_w}{dt} = 0, \quad (2.4-307)$$

(a) Continuum Flow, Turbulent Boundary Layer, Governing Equation:

$$.3 \left[ C_{f\infty} M_\infty^3 a_\infty^3 \rho_\infty \left( \frac{T_{aw} - T_w}{T_{s\infty} - T_\infty} \right)_x \right. \\ \left. = J \left\{ [\epsilon_w T_w^4]_x B - \epsilon_s B T_s^4 \pm \right. \right. \\ \left. \left. \pm [\Delta q_i]_x \right\}, \left[ \frac{\text{lbf}}{\text{sec ft}} \right], \quad (2.4-308)$$

(b) Continuum Flow, Laminar Boundary Layer, Governing Equation:

$$.25 \left[ C_{f\infty} Pr_\infty^{-2/3} M_\infty^3 a_\infty^3 \rho_\infty \left( \frac{T_{aw} - T_w}{T_{s\infty} - T_\infty} \right)_x \right. \\ \left. = J \left\{ [\epsilon_w T_w^4]_x B - \epsilon_s B T_s^4 \pm \right. \right. \\ \left. \left. \pm [\Delta q_i]_x \right\}, \left[ \frac{\text{lbf}}{\text{sec ft}} \right], \quad (2.4-309)$$

(c) Slip Flow, Laminar Boundary Layer, Governing Equation (2.4-309):

(d) Free Molecule Flow (Including Transitional Flow Regime), Governing

Equation (2.4-306)

Interpretation of individual terms in the above governing equations is given earlier.

In order to find the local skin-friction coefficient value dependence upon the local equilibrium wall temperature,

$$[C_{f,x}]_{\infty} = f([T_{ew}]_x), \quad (2.4-310)$$

for a steady, constant altitude, flight condition (CASE II), any simple trial and error iteration process can be used.

For the transient flight conditions (CASE I), the Kutta-Runge numerical method is suggested, and the step-wise computations are described below.

In both cases, the local skin-friction values,  $[C_{f,x}]_x$ , should be evaluated from the corresponding graphs in Sections 2.3 and 2.4.

$$[C_{f,x}]_x = f[M, Re, Kn, T_w, t]_x \quad (2.4-311)$$

COMPUTATIONAL PROCEDURE:

STEP 1. As illustrated in subparagraph (I)

STEP 2. As illustrated in subparagraph (I)

STEP 3. Using the basic ambient data, the corresponding local free stream (i.e., outside the boundary layer), values of the Mach Number,  $[M_{\infty}]_x$ , the static pressure,  $[p_{\infty}]_x$ , the density,  $[\rho_{\infty}]_x$ , and the temperature,  $[T_{\infty}]_x$ , should be determined from the perfect fluid theory related to the body geometry in question and the ambient Mach Number,  $(M_A)$ , flow type: subsonic, transonic, supersonic, or hypersonic. There is an abundance of available data and theories of various degrees of accuracy and refinement for most of the simple body geometries in practical use.

The required number of the local points to be thus investigated is dictated by the level of accuracy desired and by the body geometry and the flow type proper. It should be sufficient to enable a definition of the equivalent flat plate, following the conditions specified by Mangler's transfor-

mation<sup>(69)</sup>, as well as for a later integration procedure along the body or the equivalent flat plate surface for an acceptable determination of the skin-friction coefficient mean average values at each instant or flight time interval. As already stated, in case of laminar boundary layers on flat plates, the equivalence of conditions need be established locally at the end point  $x=L$  only, see STEP 5 of the previous paragraph (1).

Using the same time basis as for the ambient Standard Atmosphere flight data, the local point free stream flow data are then either tabulated or plotted in a manner similar to the illustrated in Figs (2.4-47) and (2.4-48) and in Table (2.4-6). For instance, when the local free stream ambient standard atmosphere ratios are determined on the basis of the corresponding potential or perfect fluid theory, the following plots are required:

$$(T_{\infty})_x = \frac{[T_{\infty}]_x}{T_A} \left(\frac{\sigma_A}{49.02}\right)^2 = \frac{[T_{\infty}]_x}{T_A} T_A = \psi_1(t), \quad (2.4-312)$$

$$[\sigma_{\infty}]_x = \frac{[\sigma_{\infty}]_x}{\sigma_A} \sigma_A = \left(\gamma_{\infty} \frac{p_{\infty}}{\rho_{\infty}}\right)_x^{1/2} = 49.02 (T_{\infty})_x^{1/2} = \psi_2(t), \quad (2.4-313)$$

$$[M_{\infty}]_x = \frac{[V_{\infty}]_x}{[\sigma_{\infty}]_x} = \frac{[M_{\infty}]_x}{M_A} M_A = \psi_3(t), \quad (2.4-314)$$

$$[\rho_{\infty}]_x = \frac{[\rho_{\infty}]_x}{\rho_A} \rho_A = \frac{[\rho_{\infty}]_x}{(32.17)(53.35)[T_{\infty}]_x} = \psi_4(t), \quad (2.4-315)$$

$$[p_{\infty}]_x = \frac{[p_{\infty}]_x}{p_A} p_A = (32.17)(53.35)[\rho_{\infty}]_x [T_{\infty}]_x = \psi_5(t), \quad (2.4-316)$$

$$[\mu_{\infty}]_x = \frac{[\mu_{\infty}]_x}{\mu_A} \mu_A = \mu_A \left(\frac{[T_{\infty}]_x}{T_A}\right)^{\omega} = \psi_6(t), \quad (2.4-317)$$

$\omega = .76$ ,

$$[\nu_{\infty}]_x = \frac{[\nu_{\infty}]_x}{\nu_A} \nu_A = \left[\frac{\mu_{\infty}}{\rho_{\infty}}\right]_x = \psi_7(t), \quad (2.4-318)$$

$$[V_{\infty}]_x = \frac{[V_{\infty}]_x}{V_A} V_A = \frac{[V_{\infty}]_x}{V} M_A \sigma_A = [M_{\infty} \sigma_{\infty}]_x = \psi_8(t), \quad (2.4-319)$$

$$[Re_x]_{\infty} = \left[\frac{\rho_{\infty} V_{\infty} X}{\mu_{\infty}}\right]_x = \left[\frac{V_{\infty} X}{\nu_{\infty}}\right]_x = \psi_9(t); \quad (2.4-320)$$

where  $x$  - is the distance of the investigated local point from the leading edge, measured along the surface.

**Note:** The above relationships can be used for continuum and slip flow regimes. (The transitional flow regime is included for engineering purposes under the heading of the free molecule flow.) In the free-molecule flow domain, the ambient Standard Atmosphere data (A) are equated with the physical properties (i) of the impinging molecular stream.

**STEP 4**

The governing analytic expressions (2.4-304) and (2.4-305), which shall be used for the local skin-friction computational purposes in the continuum and the slip flow regimes, require knowledge of the stagnation point-local free stream temperature difference  $(T_{s\infty} - T_{\infty})_x$  at any time instant. From Ref. 72, it has been found that a graph of  $(T_{s\infty} - T_{\infty})$  versus  $(V_{\infty})$  with  $(T_{\infty})$  as a parameter yields a family of curves which can be acceptably approximated by a single curve for engineering purposes up to 370,000 ft. of altitude. The curve,

$$(T_{s\infty} - T_{\infty}) = f(V_{\infty}), \quad (2.4-321)$$

is replotted in Fig (2.4-52), including the temperature variation effects on the specific heat coefficient at constant pressure,  $(C_p)_x$ .

Alternatively, the stagnation point absolute temperature can be taken directly from the Fig (2.4-51) in terms of the static ambient temperature  $(T_A)$  and the ambient Mach Number  $(M_A)$ . The plots have been taken from Ref (2.4-68), allowing again for the constant pressure specific heat  $(C_p)_x$  variations in a non-dissociating air.

Using the trajectory graph  $V = V(t)$ , or  $T_A = T_A(t)$  and  $M_A = M_A(t)$  respectively, the time history of the temperature difference,

$$(T_{s\infty} - T_{\infty}) = f(t), \quad (2.4-322)$$

can be tabulated or plotted graphically within the accuracy of the already chosen time basis, see Table (2.4-6).

**STEP 5**

In order to discriminate the type of

viscous flow regime (continuum, slip, free molecule) existing locally ( $x$ ) at any instant of time ( $t$ ), the local value of the dimensionless parameters  $[Re_x]_w$  and  $(M_w)$ , referred to the conditions at the local point on the body surface (subscript  $w$ ), should be known:

$$[Re_x]_w = \left[ \frac{\rho_w V_{\infty} X}{\mu_w} \right]_x = [Re_x]_{\infty} \left( \frac{\rho_w}{\rho_{\infty}} \frac{\mu_{\infty}}{\mu_w} \right)_x,$$

$$[M_w]_x = \left[ \frac{V_{\infty}}{a_w} \right]_x = [M_{\infty}]_x \left( \frac{T_{\infty}}{T_w} \right)_x^{1/2}. \quad (2.4-323)$$

Then the local characteristic flow regime at any point ( $x$ ) (excluding the immediate neighborhood of the leading edge) at the body surface at a given time instant ( $t$ ) is found using the Tsine's criteria:

(1) Continuum flow regime, laminar boundary layer:

$$\left[ \frac{M_x}{(Re_x)^{1/2}} \right]_w < 10^{-2}, \quad 1 \ll [Re_x]_w \leq 10^6, \quad (2.4-325)$$

(2) Continuum flow regime, turbulent boundary layer:

$$\left[ \frac{M_x}{(Re_x)^{1/2}} \right]_w < 10^{-2}, \quad [Re_x]_w \geq 10^6, \quad (2.4-326)$$

where  $[Re_x]_w \sim 10^6$  represents a critical value for transition from laminar to turbulent boundary layer pattern,

(3) Slip flow regime, the boundary layer laminar always,

$$10^{-2} < \left[ \frac{M_x}{(Re_x)^{1/2}} \right]_w < 10^{-1}, \quad [Re_x]_w > 1, \quad (2.4-327)$$

(4) Transitional flow regime, characterized by a mixture of the slip and the free molecule flow patterns,

Lower Boundary:

$$\left[ \frac{M_x}{(Re_x)^{1/2}} \right]_w > 10^{-1}, \quad [Re_x]_w > 1, \quad (2.4-328)$$

Upper Boundary:

$$\left[ \frac{M_x}{Re_x} \right]_w < 3, \quad [Re_x]_w \sim 1.$$

(5) Free molecule flow regime starts from:

$$\left[ \frac{M_x}{Re_x} \right]_w > 3 \text{ on, } [Re_x]_w \sim 1. \quad (2.4-329)$$

In engineering applications, the transitional flow regime cannot be treated separately, due to an almost complete lack of available practical data. Instead, it is incorporated tentatively either in the slip or in the free molecule flow regimes.

Computations of the local instantaneous values of the Reynolds and the Mach Numbers in terms of the "wall" conditions (Eqs (2.4-323) and (2.4-324)) are performed by assuming the following relationships:

$$\rho = \rho RT \text{ (classical form of the equation of state),} \quad (2.4-330)$$

$$\frac{\partial p}{\partial y} \sim 0 \text{ (common boundary layer theory assumption, Eq (2.4-331),}$$

$$[R_w]_x = [\rho_\infty]_x \quad (\rho_\infty \text{ computed locally from the respective perfect fluid theory, or defined by Eq (2.4-316),}$$

$$[\rho_w]_x = \left[ \rho_\infty \frac{T_\infty}{T_w} \right]_x, \quad (2.4-332)$$

$$[a_w]_x = \left[ a_\infty \left( \frac{T_\infty}{T_w} \right)^{1/2} \right]_x, \quad (2.4-333)$$

$$[\mu_w]_x = \left[ \mu_\infty \left( \frac{T_w}{T_\infty} \right)^\omega \right]_x, \quad \omega \sim .76, \quad (2.4-334)$$

$$[Re_x]_w = \left[ \frac{\rho_w V_w X}{\mu_w} \right]_x = [Re_x]_\infty \left( \frac{\rho_w \mu_\infty}{\rho_\infty \mu_w} \right)_x \\ = [Re_x]_\infty \left( \frac{T_\infty}{T_w} \right)^{1+\omega} \sim [Re_x]_\infty \left( \frac{T_\infty}{T_w} \right)^{7/4}, \quad (2.4-335)$$

$$[M_x]_w = \left[ \frac{V_w}{a_w} \right]_x = [M_x]_\infty \left( \frac{T_\infty}{T_w} \right)^{1/2}, \quad (2.4-336)$$

$$[Kn_x]_w \sim \left[ \frac{M_x}{Re_x} \right]_w = \left[ \frac{M_x}{Re_x} \right]_\infty \left( \frac{T_w}{T_\infty} \right)^{5/4}, \quad (2.4-337)$$

$$[Kn_x]_w \sim \left[ \frac{M_x}{(Re_x)^{1/2}} \right]_w = \left[ \frac{M_x}{(Re_x)^{1/2}} \right]_\infty \left( \frac{T_w}{T_\infty} \right)_x^{3/8}, \quad (2.4-338)$$

where the subscript ( $\infty$ ) values and the subscript (w) values should be substituted from the complete computations already carried out for the immediately preceding time instant ( $t = t_{k-1}$ ) (see Kutta-Runge method).

The computational procedure is outlined in the Table (2.4-7).

#### STEP 6

In the governing Eq (2.4-304) and (2.4-305), the local adiabatic wall temperature,  $(T_{aw})_x$ , appears, and it has to be either directly determined by use of Figs (2.4-49) and (2.4-50) for continuum laminar and continuum turbulent boundary layer conditions, or alternatively the expression,

$$(T_{aw} - T_w)_x,$$

should be computed from:

$$(T_{aw} - T_w)_x = (Pr)_x^{1/3} (T_{s\infty} - T_\infty)_x + (T_\infty)_x - (T_w)_x, \quad (2.4-339)$$

for local turbulent boundary layer conditions in the continuum flow domain, and from

$$(T_{aw} - T_w)_x = (Pr)_x^{1/2} (T_{s\infty} - T_\infty)_x + (T_\infty)_x - (T_w)_x \quad (2.4-340)$$

for local laminar boundary layer conditions in the continuum or slip flow regime, the slip flow treatment involving the approximation of no-temperature jump assumption (or of no change in the recovery factor value).

In the above expressions, the Prandtl Number values can be taken from Table (2.4-8)b, in which the allowance is made for variation of the specific heat of air at constant pressure ( $C_p$ ) with the wall temperature  $(T_w)_x$  as known for the immediately preceding time interval ( $t = t_{k-1}$ ). Note that the Prandtl Number is a weak function of temperature, i.e., its variations are small in the correspondingly small time intervals.

The directly computed values of  $(T_{aw})_x$  or of the difference  $(T_{aw} - T_w)_x$ , should be tabulated for the chosen time scale for each local point (x) as illustrated in Table (2.4-7).

## STEP 7

The local skin-material physical and structural characteristics are ascertained as characterized by the so-called skin heat-absorption capacity coefficient  $(G_w)_x$ . In case of no ablative phenomena, the coefficient  $(G_w)_x$  can be defined as:

$$[G_w] = [C_w \delta_w W_w]_x = f(T_w)_x, \left[ \frac{Btu}{ft^2 \circ R} \right], \quad (2.4-341)$$

where:

- subscript (W) refers to the skin, and  $C_w = C_w(T_w) [Btu/lb \circ R]$  is the local specific heat value for a given skin material. It should be chosen from specially prepared tables in terms of the local skin temperature  $(T_w)_x$  and the skin material in use, see Figs (2.4-61)a to (2.4-61)y. The local skin-temperature condition  $(T_w)_x$  at any initial time instant  $(t = t_{k-1})$  is known from the already effected overall (i.e., including all the STEPS) computations up to the immediately preceding time instant  $(t = t_{k-1})$ , as obtained from the Kutta-Runge computational method,

$[\delta_w]_x [ft]$  is the local skin thickness,

$[W_w]_x [lb/ft^3]$  is the specific weight of the skin material,

$[T_w] [^\circ R]$  is the actual local temperature at the outer face of skin at the initial time instant  $(t = t_{k-1})$ .

In order to obtain the heat-absorption capacity in the engineering system of units (lb-ft-sec- $^\circ R$ ), the expression (2.4-341) is multiplied by the mechanical equivalent of heat,

$$J = 778 \left[ \frac{lb \cdot ft}{Btu} \right], \quad (2.4-342)$$

$$J[G_w]_x = J[C_w \delta_w W_w]_x \left[ \frac{lb \cdot ft}{ft^2 \circ R} \right]. \quad (2.4-343)$$

(see Table 2.4-9)

## STEP 8

The radiation heat term in the governing expressions (2.4-304), (2.4-305) and (2.4-306) is evaluated in the first approximation in terms of the following premises:

- The surface emissivity,  $(\epsilon_w)$ , is assumed to be equal to the surface absorptivity under all surface conditions and for all wave lengths,

- An allowance is made for the surface emissivity,  $(\epsilon_w)$ , variation with temperature, which is a weak functional dependence for most materials,

- The surface emissivity,  $(\epsilon_w)$ , is a strong function of the skin surface conditions. Some data for the surface emissivity functional relationship in terms of the skin material, skin surface condition and the skin surface temperature are presented in Fig (2.4-57). When choosing the proper values of  $(\epsilon_w)$  from the Fig (2.4-57), the initial skin temperature values,  $(T_w)_x$ , corresponding to the preceding time interval  $(t = t_{k-1})$  should be used, see Kutta-Runge numerical method of computation, Step 9.

The Stephan-Boltzmann's constant in the expressions

$$(B \epsilon_w T_w^4)_x,$$

has the value  $B = 4.8 \times 10^{-13} \left[ \frac{Btu}{sec \cdot ft^2 \circ R^4} \right], \quad (2.4-344)$

- The surface heat absorption of the radiation from the ambient Standard Atmosphere gaseous envelope is not taken into account, since the radiation of the gaseous medium is negligible for engineering purposes of the drag force analysis. The radiation to and from the vehicles interior is neglected also,

- The solar radiation is taken into account approximately by assuming that in the upper atmosphere the mean intensity of the radiation relative to a normally orientated surface is a constant

$$B T_s^4 = .12 \left[ \frac{Btu}{ft^2 \cdot sec} \right]; \quad (2.3-345)$$

where

$B = 4.8 \times 10^{-13} \left[ \frac{Btu}{ft^2 \cdot sec \circ R^4} \right]$  is the Stephan-Boltzmann's constant,

and  $\epsilon_s \approx \epsilon_w$ .

Note: Any other more accurate method should be used instead, if required. Solar radiation effects are most

prominent in the free molecule and the transitional flow regimes, which normally occur at higher altitudes.

- The artificial internal cooling, or heating (if any), is represented by the term,

$$\pm \Delta q_i, \quad (2.4-347)$$

where  $(\Delta q_i)$  is the known coolant heat absorption capacity per unit time,

$$\left[ \frac{\text{Btu}}{ft^2 \text{ sec}} \right]$$

The computational outline for the STEPS 7 and 8 is given in the Table (2.4-9).

#### STEP 9

With all the necessary data prepared in STEPS 1 through 8, the governing equations (2.4-304) and (2.4-305) take form,

$$\left[ \frac{dT_w}{dt} \right]_x = f([T_w]_{k-1}, t_{k-1}), \quad \left[ \frac{^{\circ}R}{\text{sec}} \right], \quad (2.4-348)$$

where the time  $(t_{k-1})$  denotes the initial instant of the time interval,

$$dt \sim \Delta t = (t_{k+1} - t_{k-1}), \quad [\text{sec}], \quad (2.4-349)$$

for which the Kutta-Runge numerical method will be applied. This means that for any value of  $k$ ,

$$1 \leq k \leq n,$$

the whole preceding time history of the skin temperature,  $[T_w]_x$ , must be already known. The computational process is thus necessarily of an unbroken step-wise nature. The very initial value of the skin-temperature to start with is

$$[T_w]_0, \quad K=1, \quad (2.4-350)$$

and depends obviously upon the history and type of the vehicles motion. Thus, for example,

$$[T_w]_0 = T_A, \quad [^{\circ}R], \quad (2.4-351)$$

for investigations of skin temperatures starting from launch, and

$$[T_w]_0 = [T_w]_{\text{FREE}}, \quad [^{\circ}R] \quad (2.4-352)$$

for investigations of re-entry cases, where  $[T_w]_{\text{FREE}}$  denotes the final skin temperature at the end of the free molecule flow phase (including the transitional flow regime tentatively, as suggested earlier).

The skin-friction and the skin-temperature computations in the free molecule flow regime do not require the Kutta-Runge numerical method, but rather follow the computational procedure as defined by the respective free molecule governing Eq (2.4-306). Therefore, in order to cover such re-entry cases, in the Table (2.4-10) a computational outline for determination of the local skin temperatures,  $[T_w]_x$ , in the free molecule flow regime (including optionally the transitional flow regime also) is presented.

#### Note:

The governing Eq (2.4-306) includes transitional and rotational degrees of molecular freedom for diatomic molecular models; no vibrational, dissociation or ionization effects are taken into account. It is valid for not-too-dense gaseous states and applicable to flat surfaces. In case of curved exposed surfaces it is valid locally. Other important limitations and assumptions, pertinent to the approximation treatment of radiation phenomena and the assumed molecular model are briefly stated in the preceding section, and more fully elaborated in Refs. (2.4-67) and (2.4-12).

#### STEP 10

A computational procedure for the governing Eqs (2.4-304) and (2.4-305) for continuum and slip flow regimes by the Kutta-Runge numerical method is illustrated in the Table (2.4-12). Due to the iterative nature of the Kutta-Runge numerical method within each time interval,

$$\Delta t = t_{k+1} - t_{k-1}, \quad (\text{sec}),$$

$$1 \leq K \leq n, \quad (2.4-353)$$

the computations of the "f" function in the preceding Table (2.4-11) should be performed in dependence of the necessary data in the Kutta-Runge Table (2.4-12) as follows:

(a) The initial local wall temperature  $[T_w]_x$  at the time instant  $t = t_{k-1}$ ,  $1 \leq K \leq n$ , is taken as the reference bound-

ary condition, and all the physical quantities, comprising the "f" function,

$$\left(\frac{\Delta T_w}{\Delta t}\right)_x = f([T_w]_x, t_{k-1}), \quad (2.4-354)$$

on the right hand sides of the governing Eqs (2.4-304) or (2.4-305) are computed, as indicated in Tables (2.4-3) to (2.4-10).

When performing the computations of the "f" function, the flow type at the particular initial instant ( $t_{k-1}$ ) must be known in advance from the auxiliary Table (2.4-7). Then the "f" function in the first row of the Table (2.4-11) is:

If the local flow is of the continuum turbulent type,

$$"f"_{(k-1)} = \textcircled{69} = \frac{.3}{\textcircled{43}} \left[ \textcircled{63} \times \textcircled{24} \times \textcircled{60} \times \textcircled{61} \times \frac{\textcircled{39}}{\textcircled{30}} \right] - \textcircled{65} + \textcircled{66} \pm \textcircled{67} \left[ \frac{^{\circ}R}{\text{sec}} \right]; \quad (2.4-355)$$

where:

$$\textcircled{65} = \left[ \frac{\epsilon_w T_w^4 B}{G_w} \right]_x = \frac{\textcircled{44}}{\textcircled{42}} \times \textcircled{31}^4 \times 4.8 \times 10^{-13}, \quad (2.4-356)$$

$$\textcircled{66} = \left[ \frac{\epsilon_s T_s^4 B}{G_w} \right]_x = \frac{\textcircled{44}}{\textcircled{42}} \times .12, \quad (2.4-357)$$

and the turbulent continuum flow local skin-friction coefficient value,

$$\textcircled{63} = [C_{f\infty}]_x = f(T_w)_{k-1}, \quad (2.4-358)$$

is obtained from the corresponding graphs or equations, as indicated in Section 2.3. Note that the above value of  $(C_{f\infty})_x$  is the final value of it at the initial time instant ( $t_{k-1}$ ), as already discussed at the beginning of this paragraph.

If the local flow is of the continuum laminar type,

$$"f"_{k-1} = \textcircled{70} = \frac{.25}{\textcircled{43}} \left[ \textcircled{64} \times \textcircled{59} \times \textcircled{24} \times \textcircled{60} \times \textcircled{61} \times \frac{\textcircled{39}}{\textcircled{30}} \right] - \textcircled{65} + \textcircled{66} \pm \textcircled{67} \left[ \frac{^{\circ}R}{\text{sec}} \right], \quad (2.4-359)$$

where the laminar continuum flow local skin-friction coefficient value,

$$\textcircled{64} = [C_{f\infty}]_x = f(T_w)_{k-1}, \quad (2.4-360)$$

is obtained from the corresponding graphs or equations, as indicated in Section 2.3. Note that the above value of  $(C_{f\infty})_x$  is the final value of it at the initial time instant ( $t_{k-1}$ ).

If the local flow is of the laminar slip flow type,

$$"f"_{k-1} = \textcircled{68} = \frac{.25}{\textcircled{43}} \left[ \textcircled{62} \times \textcircled{59} \times \textcircled{24} \times \textcircled{60} \times \textcircled{61} \times \frac{\textcircled{39}}{\textcircled{30}} \right] - \textcircled{65} + \textcircled{66} \pm \textcircled{67} \left[ \frac{^{\circ}R}{\text{sec}} \right], \quad (2.4-361)$$

where the laminar slip flow local skin-friction coefficient value,

$$\textcircled{62} = [C_{f\infty}]_x = f(T_w)_{k-1}, \quad (2.4-362)$$

is obtained from the corresponding graphs or equations, as indicated in Section 2.4.4. Note that the above value of  $[C_{f\infty}]_x$  is the final value of it at the initial time instant ( $t_{k-1}$ );

(b) The respectively computed value of the " $f$ "<sub>(k-1)</sub> function is entered in the first row, fifth column of the Kutta-Runge Table (2.4-12), and the sixth column value computed:

$$f_{(k-1)} \times \Delta t = q_{(k-1)}, \quad (^{\circ}R), \quad (2.4-363)$$

$$\Delta t = t_{k+1} - t_{k-1}, \quad (\text{sec}),$$

$$1 \leq k \leq n; \quad (2.4-364)$$

(c) A new intermediate reference temperature,

$$(T_w)'_{(k)} = (T_w)_{(k-1)} + \frac{1}{2} q_{(k-1)}, \quad [^{\circ}R], \quad (2.4-365)$$

corresponding to a half time interval,

$$\frac{\Delta t}{2} = t_k - t_{k-1}, \quad (\text{sec}), \quad (2.4-366)$$

is computed and entered both in the fourth column, second row of the Kutta-Runge Table (2.4-12) and in the second row of the Table (2.4-11) (time in-

instant  $t_k$ );

(d) The corresponding intermediate value of the  $f'_{(k)}$  function is then computed in the Table (2.4-11), following the same instructions as indicated in the paragraph (a);

(e) The  $f'_{(k)}$  value, corresponding to the intermediate time instant,

$$t_k = t_{k-1} + \frac{\Delta t}{2}, \text{ (sec)}, \quad (2.4-367)$$

is then entered in the second row, fifth column of the Kutta-Runge Table (2.4-12), and the sixth column value computed:

$$\begin{aligned} f'_{(k)} \times \Delta t &= q'_{(k)}, \text{ (}^\circ\text{R)}, \\ \Delta t &= t_{k+1} - t_{k-1}, \text{ (sec)}, \\ 1 \leq k \leq n; \end{aligned} \quad (2.4-368)$$

(f) Another intermediate reference temperature,

$$(T_w)_{(k)} = (T_w)_{(k-1)} + \frac{1}{2} q'_{(k)}, \text{ (}^\circ\text{R)}, \quad (2.4-369)$$

corresponding again to the half-time interval,

$$\frac{\Delta t}{2} = t_k - t_{k-1}, \text{ (sec)}, \quad (2.4-370)$$

is computed and entered both in the fourth column, third row of the Kutta-Runge Table (2.4-12), and in the third row of the Table (2.4-11) (time instant  $t_k$ ). This computation is similar to the one performed in the paragraph (c), representing a second intermediate approximation;

(g) The corresponding second intermediate value of the  $f''_{(k)}$  function is then computed in the Table (2.4-11) following the same instructions as indicated in the paragraph (a);

(h) The  $f''_{(k)}$  value, corresponding to the intermediate time instant,

$$t_k = t_{k-1} + \frac{\Delta t}{2}, \text{ (sec)}, \quad (2.4-371)$$

is subsequently entered in the third row, fifth column of the Kutta-Runge Table, and the sixth column value computed:

$$\begin{aligned} f''_{(k)} \times \Delta t &= q''_{(k)}, \text{ (}^\circ\text{R)}, \\ \Delta t &= t_{k+1} - t_{k-1}, \text{ (sec)}, \end{aligned}$$

$$1 \leq k \leq n; \quad (2.4-372)$$

(i) A third approximation intermediate temperature,

$$(T_w)_{(k+1)}''' = (T_w)_{k-1} + q''_{(k)}, \text{ (}^\circ\text{R)}, \quad (2.4-373)$$

corresponding now to the whole time interval,

$$\Delta t = t_{k+1} - t_{k-1}, \text{ (sec)}, \quad (2.4-374)$$

is computed and entered in both the fourth column, fourth row of the Kutta-Runge Table (2.4-12) and in the fourth row of the Table (2.4-11) (time instant  $t_{k+1}$ );

(j) A corresponding third approximation value of the  $f'''_{(k+1)}$  function is then computed in the Table (2.4-11), following the same instructions as indicated in the paragraph (a);

(k) The  $f'''_{(k+1)}$  value, corresponding to the time instant,

$$t_{k+1} = t_{k-1} + \Delta t, \text{ (sec)}, \quad (2.4-375)$$

is then entered in the fourth row, fifth column of the Kutta-Runge Table (2.4-12), and the sixth column value computed:

$$\begin{aligned} f'''_{(k+1)} \times \Delta t &= q'''_{(k+1)}, \text{ (}^\circ\text{R)}, \\ \Delta t &= t_{k+1} - t_{k-1}, \end{aligned} \quad (2.4-376)$$

$$1 \leq k \leq n;$$

(l) The final local skin-temperature is then obtained from

$$\begin{aligned} (T_w)_{k+1} &= (T_w)_{k-1} + \frac{1}{3} \left[ \frac{1}{2} (q_{(k-1)} + q'''_{(k+1)}) + \right. \\ &\quad \left. + q'_{(k)} + q''_{(k)} \right], \text{ (}^\circ\text{R)}, \end{aligned} \quad (2.4-377)$$

and entered in both the fifth row of the Kutta-Runge Table (2.4-12) and in the fifth row of the Table (2.4-11).

This final local value,

$$(T_w)_{k+1}, \text{ (}^\circ\text{R)}, \quad (2.4-378)$$

is now used to find the corresponding final local skin-friction coefficient,

$$[C_{f\infty}]_x = f(T_w)_{K+1}, \quad (2.4-379)$$

directly, at the time instant,

$$t_{K+1} = t_{K-1} + \Delta t, (\text{sec}); \quad (2.4-380)$$

(m) At the same time, this local value of the skin temperature,

$$(T_w)_{K+1}, \quad (OR), \quad (2.4-381)$$

serves as the initial temperature in a repetition of the computations for the next time instant,

$$t_{K+3} = t_{K+1} + \Delta t = t_{K-1} + 2\Delta t, (\text{sec}), \quad (2.4-382)$$

repeating all the steps from (a) to (l);

(n) Once the local skin-friction coefficient values are thus computed for the whole trajectory, the results can be plotted either in terms of the ambient Mach Number,  $(M_A)$ , or in terms of the time (t):

$$(C_{f\infty})_x = f(M_A) = \phi(t); \quad (2.4-383)$$

(o) To find the corresponding average value of the skin-friction coefficient,

$$C_{f\infty} = \frac{1}{l} \int_0^l [C_{f\infty}]_x dx, \quad (2.4-384)$$

the total computational procedure, as described in the STEPS 1 to 10 (n) should be repeated for a sufficient number of the local points,

$$0 < x \leq l, \quad (2.4-385)$$

the number depending upon the body geometry.

For a flat plate at a zero angle-of-attack, regardless of the Mach Number, Reynolds Number, or wall-to-free

stream temperature ratio,

$$C_{f_A} = 2(C_{f\infty})_{x=l}, \quad (2.4-386)$$

i.e., the average skin-friction coefficient for the total flat plate length can be found by finding its local value at the Station  $x=l$  only, provided the boundary layer is laminar (continuum or slip flow);

(p) For cones, the Manguler's (69) conversion factors for the computed average skin-friction coefficient of an equivalent flat plate are (see Section 2.3):

$$(C_{f_A})_{\text{CONE}} = \frac{2}{\sqrt{3}} (C_{f_A})_{\text{FLAT PLATE}} = 1.15 (C_{f_A})_{\text{FLAT PLATE}} \quad (2.4-387)$$

for laminar boundary layers, and

$$(C_{f_A})_{\text{CONE}} = 1.022 (C_{f_A})_{\text{FLAT PLATE}} \quad (2.4-388)$$

for turbulent boundary layers.

Note: In Section 1.7.4, the skin friction drag coefficient break-down has been elaborated in detail. The expressions defined there remain basically unchanged in the extended domain of flight Mach Numbers and flight altitudes, covered in this Section, 2.4.

There is no need in repeating here the already effected drag force coefficient breakdown scheme. The changed numerical values of the skin-friction coefficients in the free molecule, transitional, slip and continuum flow regimes in terms of the skin-temperature, body shape and boundary layer type, which are needed for computations in this Section, 2.4.7, should be taken from the respective tables and graphs of the Section 2.3 for laminar and turbulent boundary layers up to  $M_A=20$ , from the Sections 2.4.4 and 2.4.6 for the laminar slip flow and the free molecule flow regimes respectively. The detailed graphs and equations are not repeated here. Instead, as an illustration only, three graphs for a flat, non-insulated plate are reproduced in Figs (2.4-58), (2.4-59), and (2.4-60) for the sake of an example.

TABLE (2.4-3)

(RELATED TO THE COMPUTATIONAL STEP 1, SECTION 2.4-7)

AMBIENT STANDARD ATMOSPHERE FLIGHT DATA

PHYSICAL QUANTITY	TIME	AMBIENT FLIGHT SPEED	STANDARD FLIGHT ALTITUDE
SYMBOL	$t$	$V \equiv V_A$	$H \equiv H_A$
UNITS	SEC	$\frac{\text{FT.}}{\text{SEC}}$	FT.
TEXT EQUATION	—	—	—
OPERATION NUMBER	①	②	③
	$t_0$	$V_0$	$H_0$
	$t_1$	$V_1$	$H_1$
	$t_2$	$V_2$	$H_2$
	$t_3$	$V_3$	$H_3$
	etc.	etc.	etc.

TABLE (2.4-4)  
 (RELATED TO THE COMPUTATIONAL STEP 2, SECTION 2.4-7)  
 AMBIENT STANDARD ATMOSPHERE PHYSICAL DATA

PHYSICAL QUANTITY	TIME	AIR TEMPERATURE	SPEED OF SOUND	FLIGHT MACH NUMBER	AIR DENSITY	STATIC PRESSURE	COEFFICIENT OF VISCOSITY	KINEMATIC VISCOSITY
SYMBOL	$t$	$T_A$	$a_A$	$M_A$	$\rho_A$	$P_A$	$\mu_A$	$\nu_A$
UNITS	sec	$^{\circ}R$	$\frac{ft}{sec}$	—	$\frac{lb\ sec^2}{ft^4}$	$\frac{lb}{ft^2}$	$\frac{lb\ sec}{ft^2}$	$\frac{ft^2}{sec}$
FIGURE	—	FIG (2.4-48)	FIG (2.4-47)	FIG (2.4-47)	FIG (2.4-47)	FIG (2.4-48)	FIG (2.4-48)	FIG (2.4-48)
OPERATION NUMBER	①	④	⑤	⑥	⑦	⑧	⑨	⑩
	$t_0$							
	$t_1$							
	$t_2$							
	$t_3$							
	etc.							

TABLE ( 2.4 - 5 )  
 ( RELATED TO THE COMPUTATIONAL STEP 3 AND 4, SECTION, 2.4-7 )

SURFACE ( WALL ) PHYSICAL DATA

PHYSICAL QUANTITY	TIME	SPEED OF SOUND	AIR DENSITY	AIR VISCOSITY	KINEMATIC VISCOSITY	TEMP. RATIO	MACH NUMBER	REYNOLDS NUMBER	MACH NUMBER	REYNOLDS NUMBER	KNUDSEN NUMBER	KNUDSEN NUMBER
SYMBOL	t	$a_w$	$\rho_w$	$\mu_w$	$\nu_w$	$\left(\frac{T_w}{T_A}\right)$ OR $\left(\frac{T_w}{T_A}\right)$	$M_A$	$[R_{e_s}]_A$	$M_w$	$[R_{e_s}]_w$	$[Kn_s]_w$	$[Kn_s]_w$
UNITS	sec	$\frac{ft}{sec}$	$\frac{lb \cdot sec^2}{ft^4}$	$\frac{lb \cdot sec}{ft^2}$	$\frac{ft^2}{sec}$	°R	—	—	—	—	—	—
TEXT EQUATION	—	EQ (2.4-287)	EQ (2.4-287)	EQ (2.4-287)	EQ (2.4-287)	EQ (2.4-284)	TABLE (2.4-4)	EQ (2.4-290)	EQ (2.4-288)	EQ (2.4-289)	EQ (2.4-292)	EQ (2.4-292)
OPERATION NUMBER	①	⑪	⑫	⑬	⑭	⑮	⑯	⑰	⑱	⑲	⑳	㉑
	t <sub>0</sub>											
	t <sub>1</sub>											
	t <sub>2</sub>											
	t <sub>3</sub>											
	etc											

TABLE ( 2.4-6 )

(RELATED TO THE COMPUTATIONAL STEPS 3 AND 4, SECTION, 2.4-7)

LOCAL FREE STREAM DATA (  $\infty$  ).

PHYSICAL QUANTITY	TIME	LOCAL TEMPERATURE	LOCAL SPEED OF SOUND	LOCAL MACH NUMBER	LOCAL AIR DENSITY	LOCAL STATIC PRESSURE	LOCAL VISCOSITY	LOCAL KINEMATIC VISCOSITY	LOCAL SPEED	LOCAL REYNOLDS NUMBER	LOCAL TEMPERATURE DIFFERENCE
SYMBOL	t	$[T_{\infty}]_x$	$[a_{\infty}]_x$	$[M_{\infty}]_x$	$[\rho_{\infty}]_x$	$[p_{\infty}]_x$	$[\mu_{\infty}]_x$	$[\nu_{\infty}]_x$	$[V_{\infty}]_x$	$[Re_x]_{\infty}$	$[T_{s_{\infty}} - T_{\infty}]_x$
UNITS	sec	°R	$\frac{ft}{sec}$	—	$\frac{lbm \cdot sec^2}{ft^4}$	$\frac{lbm}{ft^2}$	$\frac{lbm \cdot sec}{ft^2}$	$\frac{ft^2}{sec}$	$\frac{ft}{sec}$	—	°R
TEXT EQUATION	—		EQ (2.4-312)	EQ (2.4-314)	EQ (2.4-315)	EQ (2.4-316)	EQ (2.4-317)	EQ (2.4-318)	EQ (2.4-319)	EQ (2.4-320)	EQ (2.4-321)
OPERATION NUMBER	(1)	(21)	(22)	(23)	(24)	(25)	(26)	(27)	(28)	(29)	(30)
	t <sub>0</sub>										
	t <sub>1</sub>										
	t <sub>2</sub>										
	t <sub>3</sub>										
	etc										

TABLE (2.4-7)  
 (RELATED TO THE COMPUTATIONAL STEPS 5 & 6, SECTION 2.4.7 )  
 INITIAL LOCAL WALL DATA AT TIME  $t_{k-1}$  (ISKSn)

Physical Quantity	Time	Initial Wall Temperature	Initial Temperature Ratio $(\frac{T_w}{T_{\infty}})^{5/4}$	Initial Temperature Ratio $(\frac{T_w}{T_{\infty}})^{3/6}$	Knudsen Number $[Kn]_w$	Knudsen Number $[Kn]_w$	Knudsen Number $[Kn]_w$	Initial Temperature Ratio $(\frac{T_w}{T_{\infty}})^{7/4}$	Reynolds Number Criteria $[Re]_w$	Adiabatic Wall Temperature $[T_{aw}]_x$	Temperature Difference $(T_{aw} - T_w)_x$	Prandtl Number $[Pr]_x$
Symbol	$t$	$[T_w]_x$	$(\frac{T_w}{T_{\infty}})^{5/4}$	$(\frac{T_w}{T_{\infty}})^{3/6}$	$[Kn]_w$	$[Kn]_w$	$[Kn]_w$	$(\frac{T_w}{T_{\infty}})^{7/4}$	$[Re]_w$	$[T_{aw}]_x$	$(T_{aw} - T_w)_x$	$[Pr]_x$
Units	sec	$^{\circ}R$	—	—	—	—	—	—	—	$^{\circ}R$	$^{\circ}R$	—
Text Equation	—	Previous Step Kutta-Runge	$[\frac{(31)}{(21)}]^{5/4}$	$[\frac{(31)}{(21)}]^{3/6}$	$\frac{(23)}{(29)} \times \frac{(32)}{(29)}$	$\frac{(23)}{(29)} \times \frac{(32)}{(29)}$	$\frac{(23)}{(29)} \times \frac{(33)}{(29)^{1/2}}$	$[\frac{(21)}{(31)}]^{7/4}$	$(29) \times (36)$	FIG (2.4-49) or FIG (2.4-50)	EO (2.4-339) or EO (2.4-340)	Table (2.4-8)
Operation Number	①	③①	③②	③③	③④	③⑤	③⑥	③⑦	③⑧	③⑨ or ③⑩	④①	④②
	$t_{k-1}$ $t_k$ $t_{k+1}$ etc.	$[T_w]_{k-1}$										

TABLE (2.4-8)

$[T_w]_{K-1}$	Pr	$Pr^{1/2}$	$Pr^{1/3}$	$Pr^{2/3}$
400	0.73	0.855	0.9005	0.809
450	0.72	0.849	0.896	0.802
500	0.71	0.8425	0.8925	0.795
550	0.70	0.836	0.888	0.788
600	0.70	0.836	0.888	0.788
650	0.69	0.83	0.885	0.780
700	0.68	0.825	0.880	0.771
750	0.68	0.825	0.880	0.771
800	0.68	0.825	0.880	0.771
900	0.67	0.82	0.875	0.766
1000	0.66	0.813	0.871	0.757
1100	0.66	0.813	0.871	0.757
1200	0.66	0.813	0.871	0.757
1300	0.66	0.813	0.871	0.757
1400	0.65	0.806	0.867	0.750
1500				
1600				
1700				
1800				
1900				
2000				
2100				
2200				
2300				
2400				

Prandtl Number data allowing for variation of Cp with temperature, ( Ref 2.4-70)

$[T_w]_{K-1}$  in degrees Rankine

TABLE ( 2.4-9 )  
 (Related To The Computational Steps 7 And 8, Section 2.4.7)  
 Local Skin Structural And Radiation Data

PHYSICAL QUANTITY	SYMBOL	TIME	INITIAL WALL TEMP.	SKIN SPECIFIC HEAT COEFF.	SKIN HEAT CAPACITY	SKIN HEAT CAPACITY	SKIN HEAT CAPACITY	SKIN EMISSIVITY	RADIATION FROM SKIN	RADIATION INTO SKIN	ARTIFICIAL COOLING
		t	$[T_w]_k$	$[C_w]_k$	$[G_w]_k$	$J[G_w]_k$	$\epsilon_w$	$[\epsilon_w T_w^4]_k$	$[\epsilon_w B T_s^4]_k$	$\Delta q_i$	
UNITS		'sec	°R	$\frac{Btu}{lb f^2 \circ R}$	$\frac{Btu}{ft^2 \circ R}$	$\frac{lb f ft}{ft^2 \circ R}$	—	$\frac{Btu}{ft^2 sec}$	$\frac{Btu}{ft^2 sec}$	$\frac{Btu}{ft^2 sec}$	
TEXT EQUATION		—	PREVIOUS STEP (KUTTA-RUNGE)	MATERIAL DATA (2.4-61)	EQ (2.4-341)	EQ (2.4-343)	FIG. (2.4-57)	$(44) \times (31) \times B$	EQ $\times (44)$ (2.4-345)	DESIGN DATA	
OPERATION NUMBER		(1)	(31)	(41)	(42)	(43)	(44)	(45)	(46)	(47)	
		$t_{k-1}$	$[T_w]_{k-1}$								
		$t_k$									
		$t_{k+1}$									
		etc.									

$$B = 4.8 \times 10^{-13} \left[ \frac{Btu}{sec ft^2 \circ R^4} \right], \quad [BT_s^4] = .12 \left[ \frac{Btu}{ft^2 sec} \right],$$

$$\epsilon_w = \epsilon_s, \quad J = 778 \left[ \frac{lb f ft}{Btu} \right],$$

TABLE  
(RELATED TO THE COMPUTATIONAL STEP B  
FREE MOLECULE FLOW, FRONT SURFACES,

Physical Quantity	Time	Molecular Flux	Molecular Mass	Flight Speed	Most Probable M.M. Speed	Speed Ratio	Dimensionless Quantity	Dimensionless Quantity
Symbol	t	$n_A$	$m_A$	$\frac{V_A}{\lambda}$	$V_M$	$\frac{V_A}{V_M}$ or $\frac{V_A}{V_A}$	X	$\phi$
Units	sec	$\frac{\text{molecules}}{\text{ft}^2 \text{ sec}}$	$\frac{\text{slug}}{\text{molecule}}$	$\frac{\text{ft}}{\text{sec}}$	$\frac{\text{ft}}{\text{sec}}$	—	—	—
Test Equation	—	EO (2 4 - 306)	EO (2 4 - 306)	EO (2 4 - 306)	EO (2 4 - 306)	EO (2 4 - 306)	FIG (2 4 - 53)	FIG (2 4 - 54)
Operation	(1)	(20)	(21)	(22)	(23)	(24)	(25)	(26)
	$t_0$ $t_1$ $t_2$ $t_3$ etc							

a - accommodation coefficient

$$B_1 = 5.08 \times 10^{-24} \left[ \frac{\text{ft} \cdot \text{lb}}{\text{molecule}} \right]$$

$$B_2 = 3.74 \times 10^{-10} \left[ \frac{\text{ft} \cdot \text{lb}}{\text{ft}^2 \text{ sec}^2} \right]$$

9 5 0 5 1

(2 4 - 10)  
SECTION 2 4 7)  
LOCAL SKIN TEMPERATURE

Ambient Temperature	Surface Emissivity	Cooling Heat Flux
$T_a$	$\epsilon_w \cdot \epsilon_s$	$\Delta q_c$
"R	—	$\frac{\text{BTU}}{\text{ft}^2 \text{ sec}}$
TABLE (2 4 - 4)	EO (2 4 - 57)	Constant Data
(27)	(28)	(29)

RESULTANT EQUATION, VALID LOCALLY AT ANY POINT OF AN EXPOSED SURFACE ( $\theta$  LOCAL  $590^\circ$ )

$$\epsilon_w \left[ \epsilon_s \cdot (B_1 \cdot T_a^4) + (B_2 \cdot T_a^4) + (B_3 \cdot T_a^4 - \frac{1}{2} B_4 T_a) \right] \cdot \epsilon_w \cdot B_5 T_s^4 - \epsilon_w \cdot B_6 [T_s^4] + \Delta q_c = 0 \quad \text{EO(2 4 - 306)}$$

SHOULD BE SOLVED FOR  $[T_s]_s$

a - Stephan Boltzmann's constant

$$B_5 T_s^4 = 93.4 \left[ \frac{\text{BTU}}{\text{ft}^2 \text{ sec}} \right] - \text{mean Solar radiation}$$

b - Stephan Boltzmann's constant

$$T_s = T_a$$

TABLE  
(Related To The Computational Step  
Summary Data For Computations Of The  $\tau$  Function

Physical Quantity	Time	Local Surface Temperature	Skin Heat Capacity	Skin Heat Capacity	Prandtl Number (Laminar)	Local Air Density	Mach Number	Speed of Sound	Temperature Difference (Laminar)
Symbol	$t$	$[T_w]_t$	$[C_w]_t$	$d[C_w]_t$	$[Pr_w]_t^{1/3}$	$[r_w]_t$	$[M]_t$	$[a]_t$	$(T_w - T_a)_t$
Units	sec	°R	$\frac{Btu}{ft^2 \cdot ^\circ R}$	$\frac{Btu}{ft^2 \cdot ^\circ R}$	—	$\frac{lbm}{ft^3}$	—	$\frac{ft}{sec}$	°R
Ref. Equation Or Table	—	(2.4.9)	(2.4.9)	(2.4.9)	(2.4.8)	(2.4.4)	(2.4.6)	(2.4.6)	(2.4.7)
Operation	(1)	(3)	(42)	(43)	(58)	(24)	(60)	(61)	(59)
Intermediate Steps	Final	$T_{a-1}$	$[T_w]_{a-1}$						
		$T_a$	$[T_w]_a$						
		$T_a$	$[T_w]_a$						
		$T_{a+1}$	$[T_w]_{a+1}$						
	Final	$T_{a+1}$	$[T_w]_{a+1}$						

NOTE  $[T_w]_{a-1} = [T_w]_a$  for  $R=1$ ,  $T_{a-1} = T_a$ , Launch Phase, or  $[T_w]_{a-1} = [T_w]_{a+1}$  at  $T_a = R=1$ .

(2.4-11)  
O, Section 2.4-7.1  
At initial instants  $\Delta t = t_{a+1} - t_a$   
 $(t_a)_{a+1} = t_a$

Temperature Difference (Turbulent)	Temperature Difference (Laminar)	Local Skin Friction Coeff (Laminar Slip)	Local Skin Friction Coeff (Turbulent Cont)	Local Skin Friction Coeff (Laminar Cont)	Skin Emissivity	Radiation Term	Radiation Term	Cooling Term
$(T_w - T_a)_t$	$(T_w - T_a)_t$	$(C_{f_w})_t$	$(C_{f_w})_t$	$(C_{f_w})_t$	$\epsilon_w(t)_t$	$\left[\frac{C_{f_w}^2 B}{G_w^2}\right]_t$	$\left[\frac{C_{f_w}^2 B}{G_w^2}\right]_t$	$\left[\frac{\Delta q_w}{G_w}\right]_t$
°R	°R	—	—	—	—	$\frac{Btu}{ft^2 \cdot sec}$	$\frac{Btu}{ft^2 \cdot sec}$	$\frac{Btu}{ft^2 \cdot sec}$
1	1	SECTION	SECTION	SECTION	1	EQ	EQ	1 (2.4-9)
(2.4-7)	(2.4-6)	2.7.4	2.3	2.3	(2.4-9)	(2.4-356)	(2.4-357)	(63)/(42)
(59)	(30)	(62)	(63)	(64)	(44)	(65)	(66)	(67)
Intermediate Steps	Final	$(C_{f_w})_{a-1}$	$(C_{f_w})_{a-1}$	$(C_{f_w})_{a-1}$				
		$(C_{f_w})_a$	$(C_{f_w})_a$	$(C_{f_w})_a$				
		$(C_{f_w})_a$	$(C_{f_w})_a$	$(C_{f_w})_a$				
		$(C_{f_w})_{a+1}$	$(C_{f_w})_{a+1}$	$(C_{f_w})_{a+1}$				
	Final	$(C_{f_w})_{a+1}$	$(C_{f_w})_{a+1}$	$(C_{f_w})_{a+1}$				

Re-entry Phase, where  $[T_w]_{a+1}$  is the end temperature of the free molecule regime

$\tau$ Function Laminar Slip	$\tau$ Function Turbulent Cont	$\tau$ Function Laminar Cont	
$\frac{Btu}{ft^2 \cdot sec}$	$\frac{Btu}{ft^2 \cdot sec}$	$\frac{Btu}{ft^2 \cdot sec}$	
EQ (2.4-361)	EQ (2.4-355)	EQ (2.4-359)	
(68)	(69)	(70)	
$T_{a-1}$	$T_{a-1}$	$T_{a-1}$	Final
$T_a$	$T_a$	$T_a$	Intermediate Steps
$T_a$	$T_a$	$T_a$	
$T_{a+1}$	$T_{a+1}$	$T_{a+1}$	Final

TABLE (2.4-12)  
KUTTA — RUNGE NUMERICAL METHOD OF SOLUTION

STEP	TIME INSTANT	TIME INTERVAL	LOCAL SURFACE TEMPERATURE	f-FUNCTION (T-9)	$f \times \Delta t = q$
1 INITIAL	$t_{k-1}$	—	INITIAL $[T_w]_{k-1}$	$f_{(k-1)}$	$q_{(k-1)}$
2	$t_k$	$\frac{\Delta t}{2}$	$[T_w]'_k$	$f'_{(k)}$	$q'_{(k)}$
3	$t_k$	$\frac{\Delta t}{2}$	$[T_w]''_k$	$f''_{(k)}$	$q''_{(k)}$
4	$t_{(k+1)}$	$\Delta t$	$[T_w]'''_{(k+1)}$	$f'''_{(k+1)}$	$q'''_{(k+1)}$
5 FINAL	$t_{(k+1)}$	$\Delta t$	FINAL $[T_w]_{(k+1)}$		
1 INITIAL	$t_{k+1}$	—	INITIAL $[T_w]_{k+1}$	$f_{(k+1)}$	$q_{(k+1)}$
etc	etc	etc	etc	etc	etc

$$\Delta t = t_{k+1} - t_{k+1}, \quad (\text{sec})$$

$$1 \leq k \leq n$$

$$q_{(k-1)} = f_{(k-1)} \times \Delta t$$

$$[T_w]'_k = [T_w]_{k-1} + \frac{1}{2} q_{(k-1)}$$

$$q'_{(k)} = f'_{(k)} \times \Delta t,$$

$$[T_w]''_k = [T_w]_{(k-1)} + \frac{1}{2} q'_{(k)}$$

$$q''_{(k)} = f''_{(k)} \times \Delta t$$

$$[T_w]'''_{(k+1)} = [T_w]_{(k-1)} + q''_{(k)}$$

$$q'''_{(k+1)} = f'''_{(k+1)} \times \Delta t,$$

$$[T_w]_{(k+1)} = [T_w]_{(k-1)} + q,$$

$$q = \frac{1}{3} [ \frac{1}{2} (q_{(k-1)} + q'''_{(k+1)}) + q'_{(k)} + q''_{(k)} ]$$

TIME INTERVAL  $t_{k+1} - t_{k+1} = \Delta t$

The following Figures, related to the text in this Section 2.4.7, are not reproduced here, since they already appeared in the previous Section 1.7.

FIGURE NO.	SEE FIGURE NO.	SECTION	PAGE
(2.4-32)	1.18	1.7.1	1.7-6
(2.4-34)	1.17	1.7.1	1.7-5
(2.4-35)	1.21	1.7.1	1.7-11
(2.4-36)	1.22	1.7.1	1.7-12
(2.4-37)	1.23	1.7.1	1.7-13
(2.4-38)	1.24	1.7.1	1.7-14
(2.4-39)	1.25	1.7.1	1.7-15
(2.4-40)	1.19	1.7.1	1.7-7
(2.4-41)	1.26	1.7.1	1.7-16
(2.4-42)	1.27	1.7.1	1.7-17
(2.4-43)	1.28	1.7.1	1.7-18

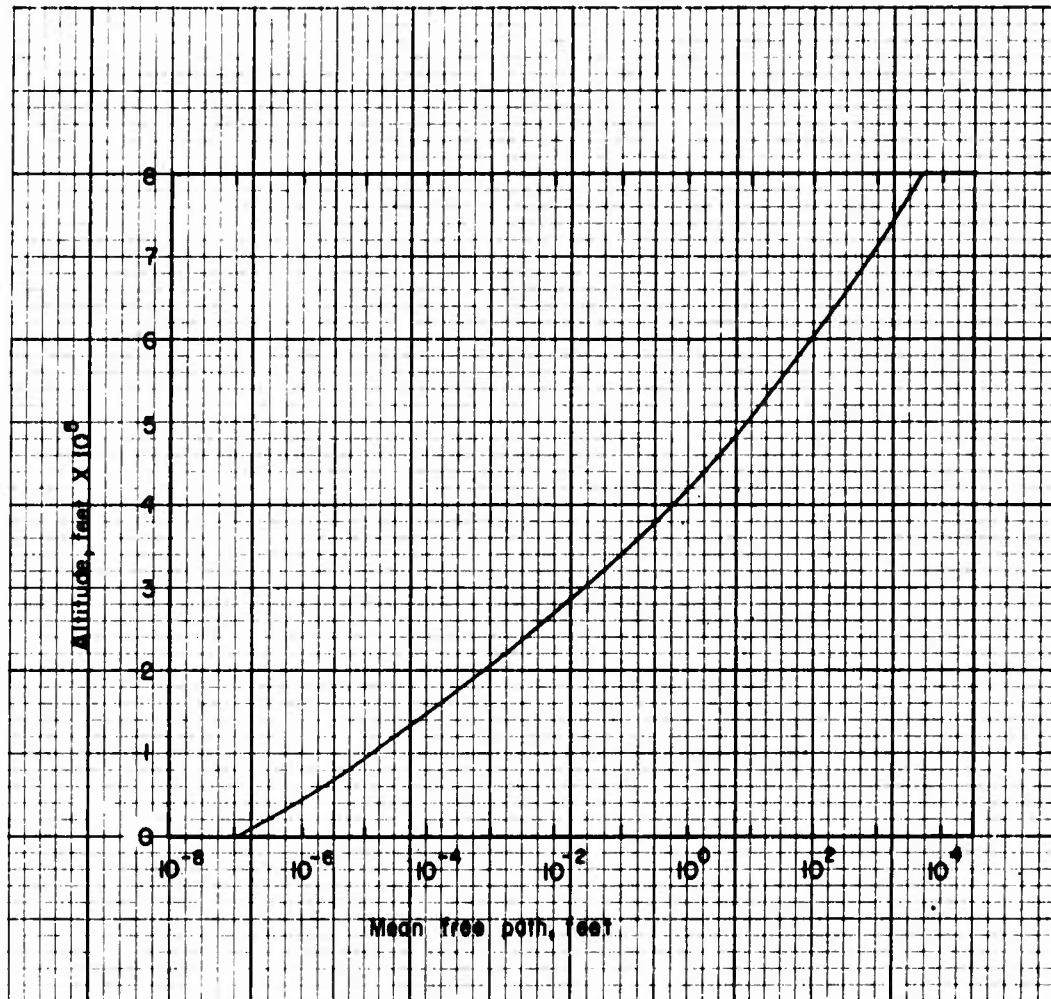


Fig. (2.4-33) Mean molecular free path. (Ref. 2.4-74)

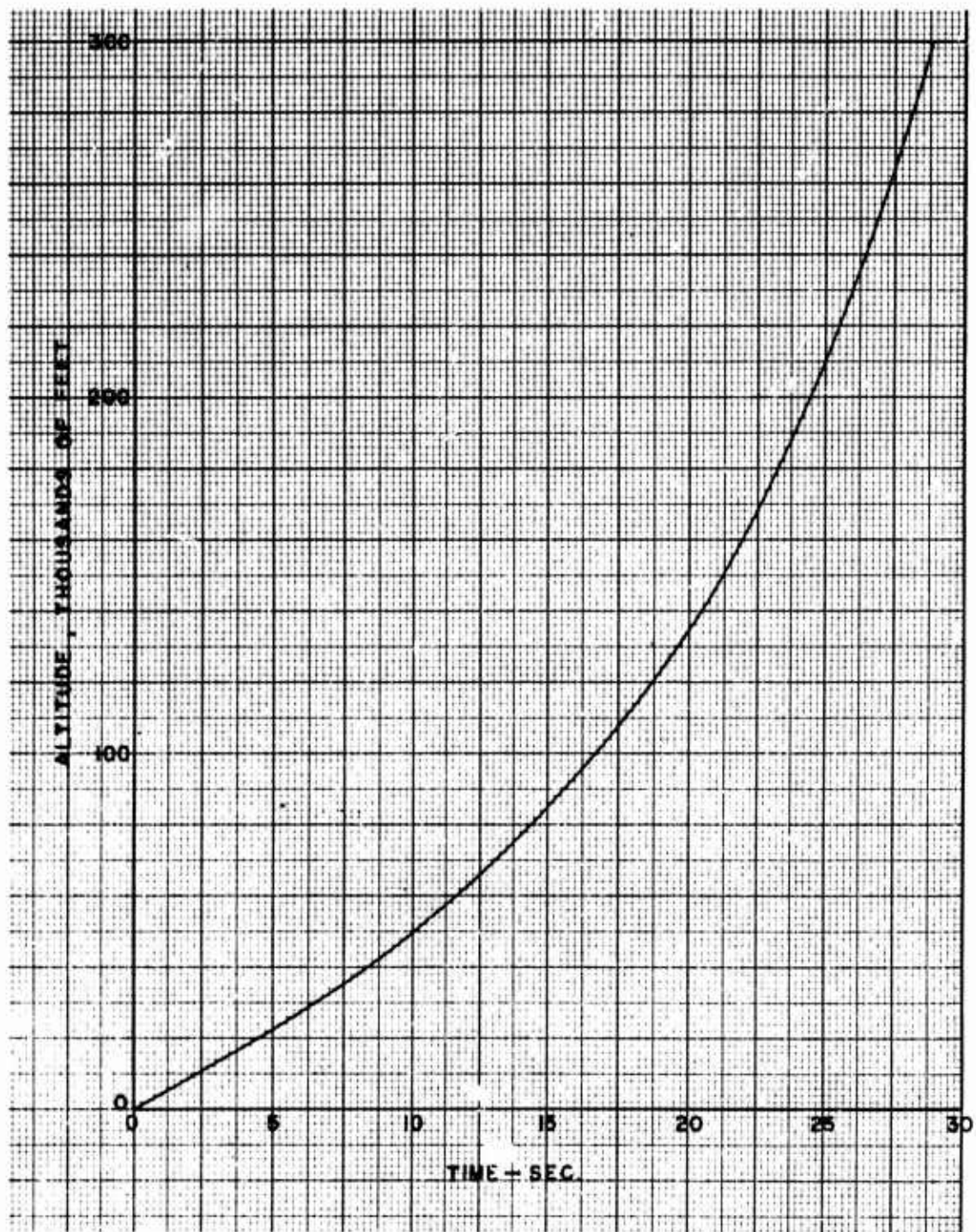


Fig. (2.4-44) Illustrative example of flight altitude versus time for a hypothetical long range missile,  $H=f(t)$ . (Recomputed data from Fig. 2.4-37)

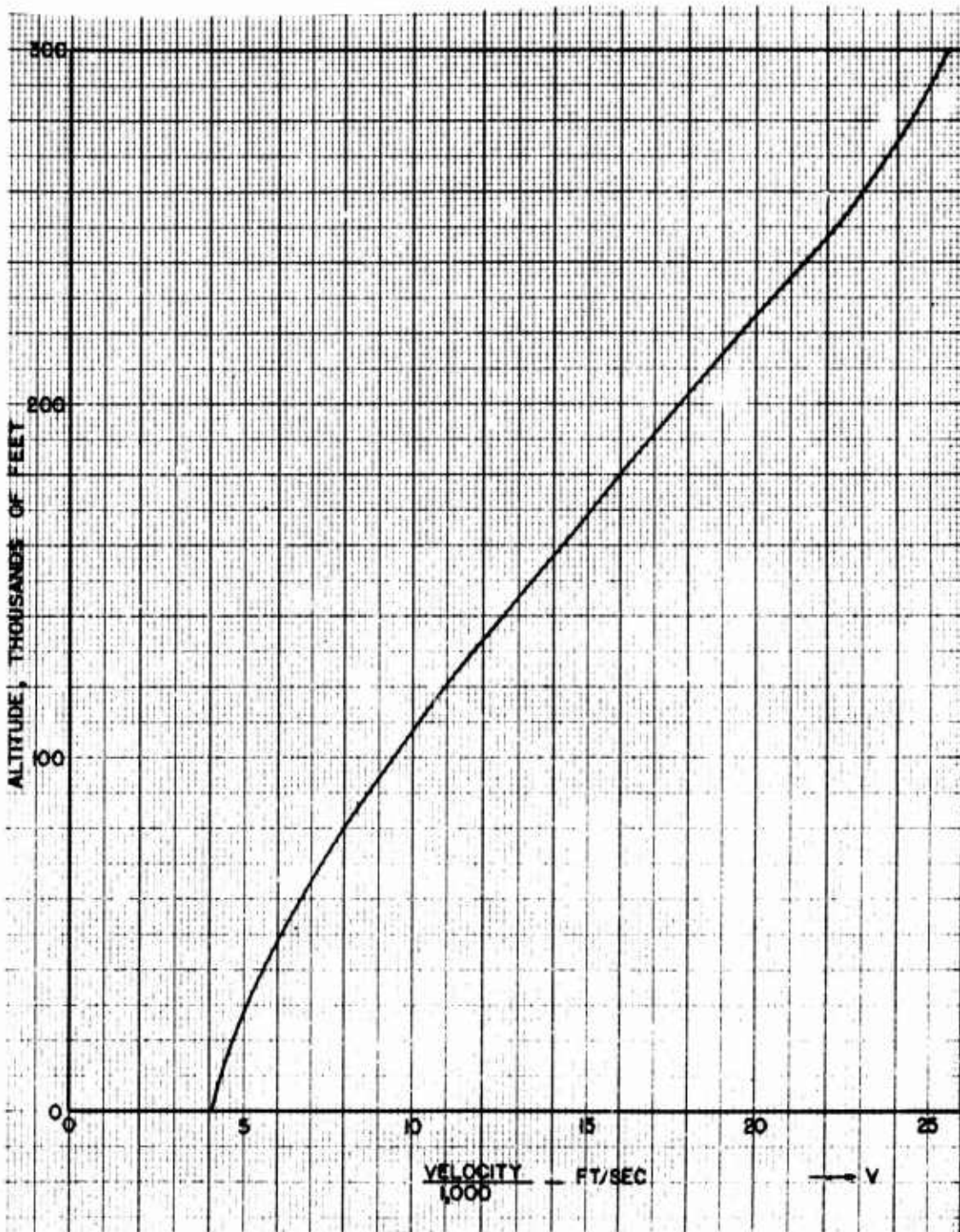


Fig. (2.4-45) Illustrative example of flight altitude versus speed for a hypothetical long range missile,  $H = f(V)$ . Replotted data from Fig. 2.4-37)

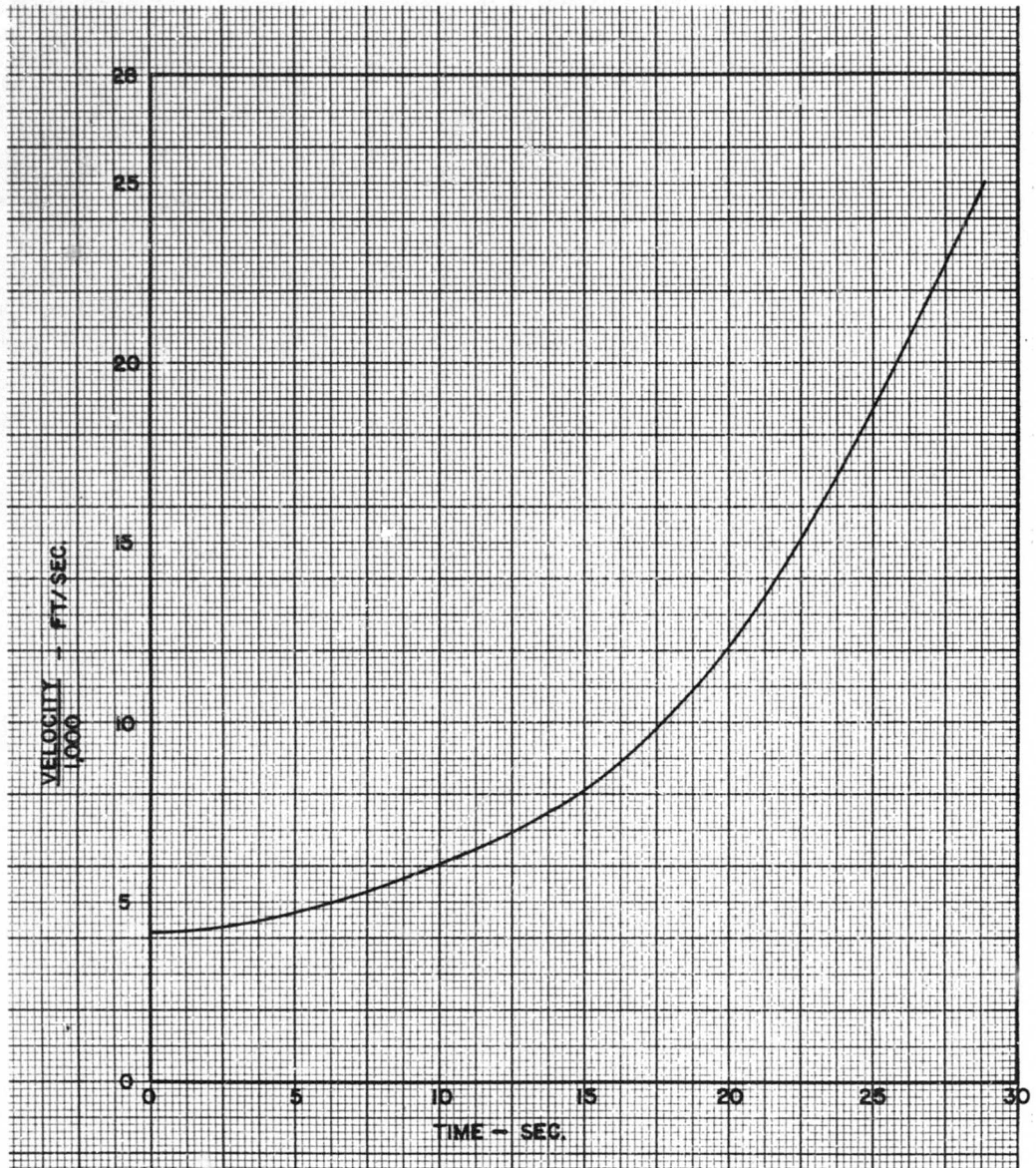


Fig. (2.4-46) Illustrative example of flight speed versus time for a hypothetical long range missile,  $V = f(t)$ . (Recomputed data from Fig. 2.4-37)

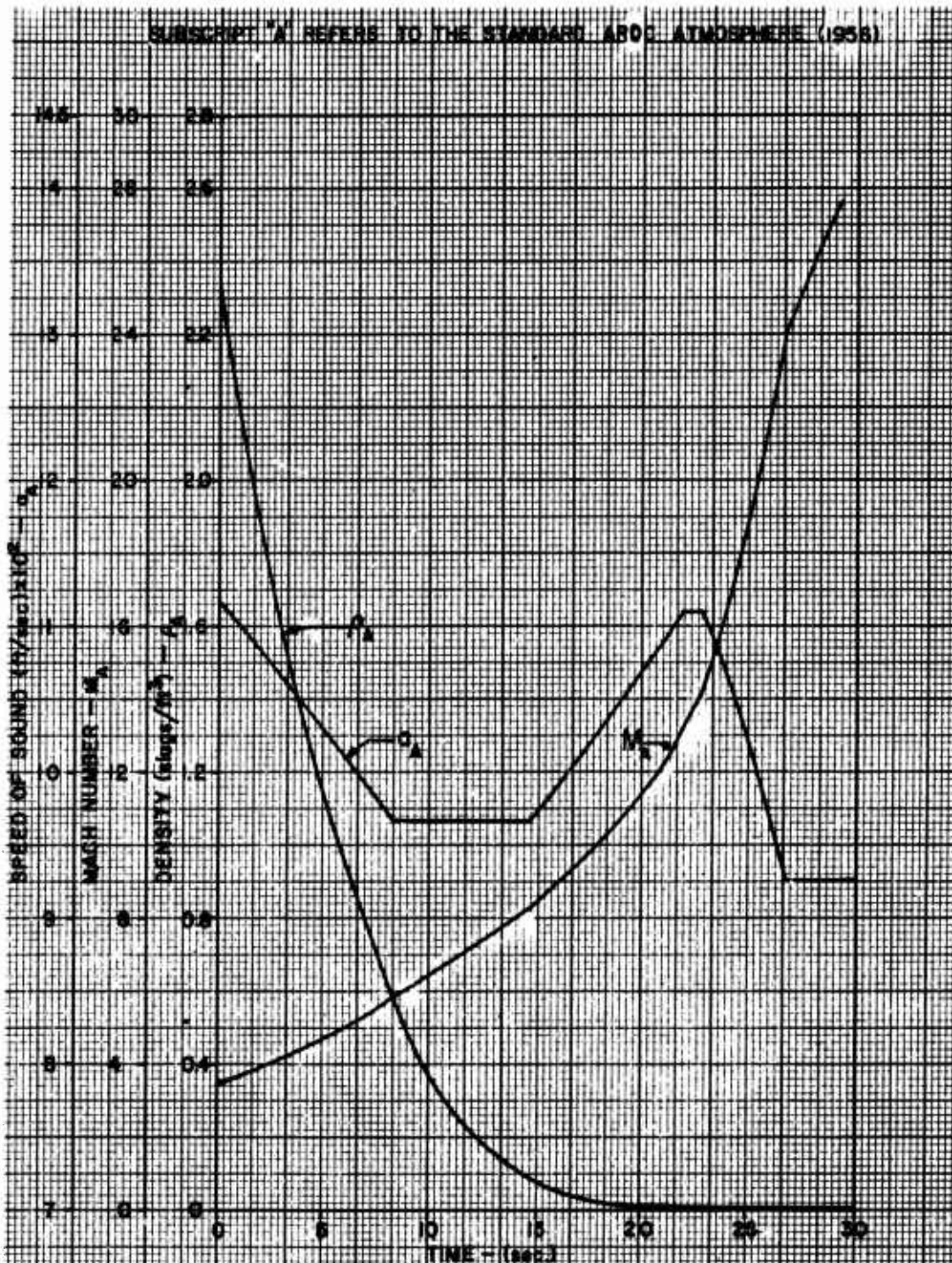


Fig. (2.4-47) Illustrative graph of the free stream density ( $\rho_A$ ), speed of sound ( $a_A$ ) and Mach Number ( $M_A$ ) versus time ( $t$ ) for a hypothetical missile in a standard ARDC model atmosphere (1956):  $\rho_A = f(t)$ ,  $a_A = f(t)$ ,  $M_A = f(t)$  Data related to Figs.(2.4-44), (2.4-45), (2.4-46).

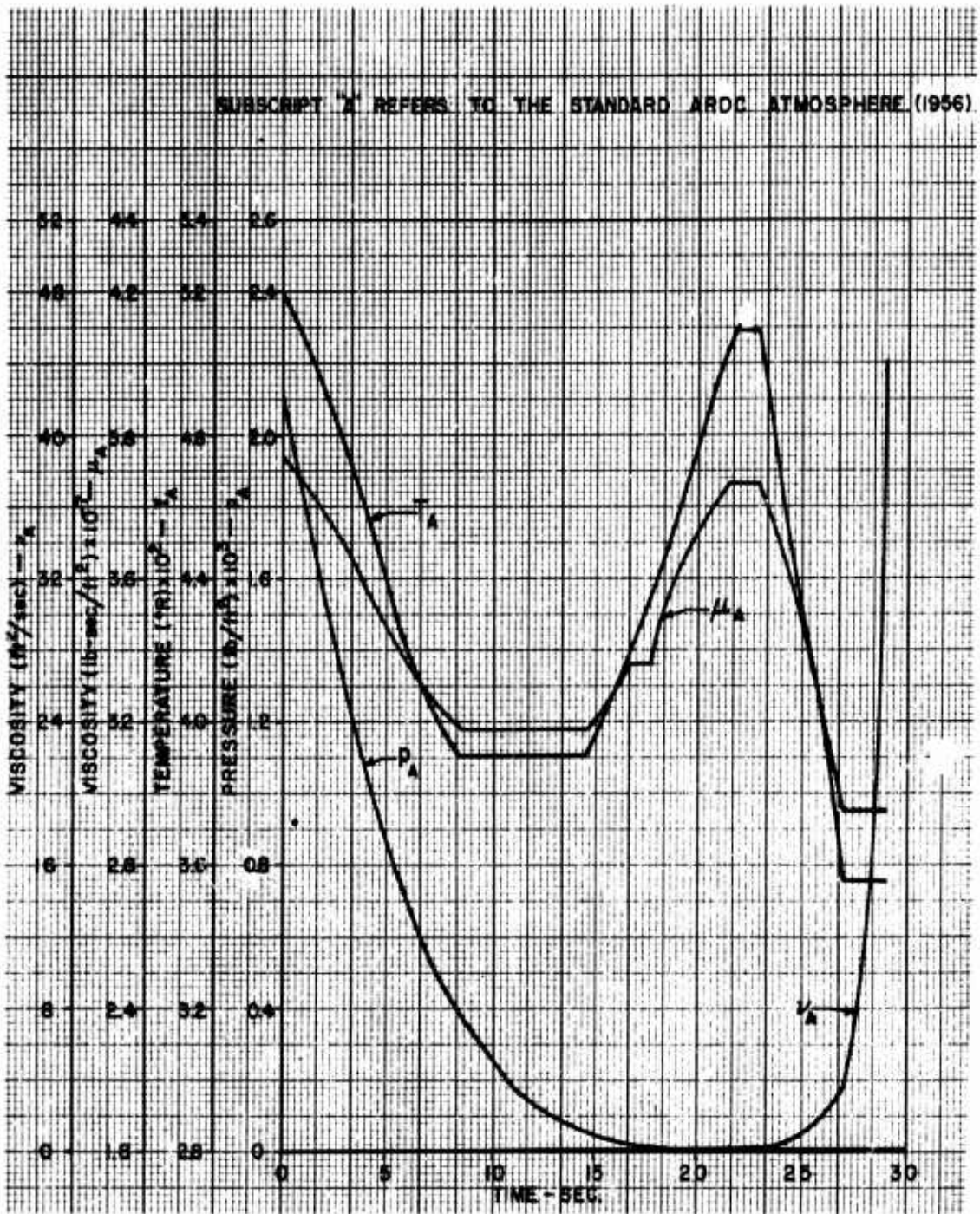


Fig. (2.4-48) Illustrative graph of the free stream static pressure ( $p_A$ ), absolute temperature ( $T_A$ ) and viscosities ( $\mu_A$  and  $\nu_A$ ) for a hypothetical missile in a standard ARDC atmosphere (1956),  $p_A = f(t)$ ,  $T_A = f(t)$ ,  $\mu_A = f(t)$ ,  $\nu_A = f(t)$ . Data related to Figs. (2.4-44), (2.4-45), (2.4-46).

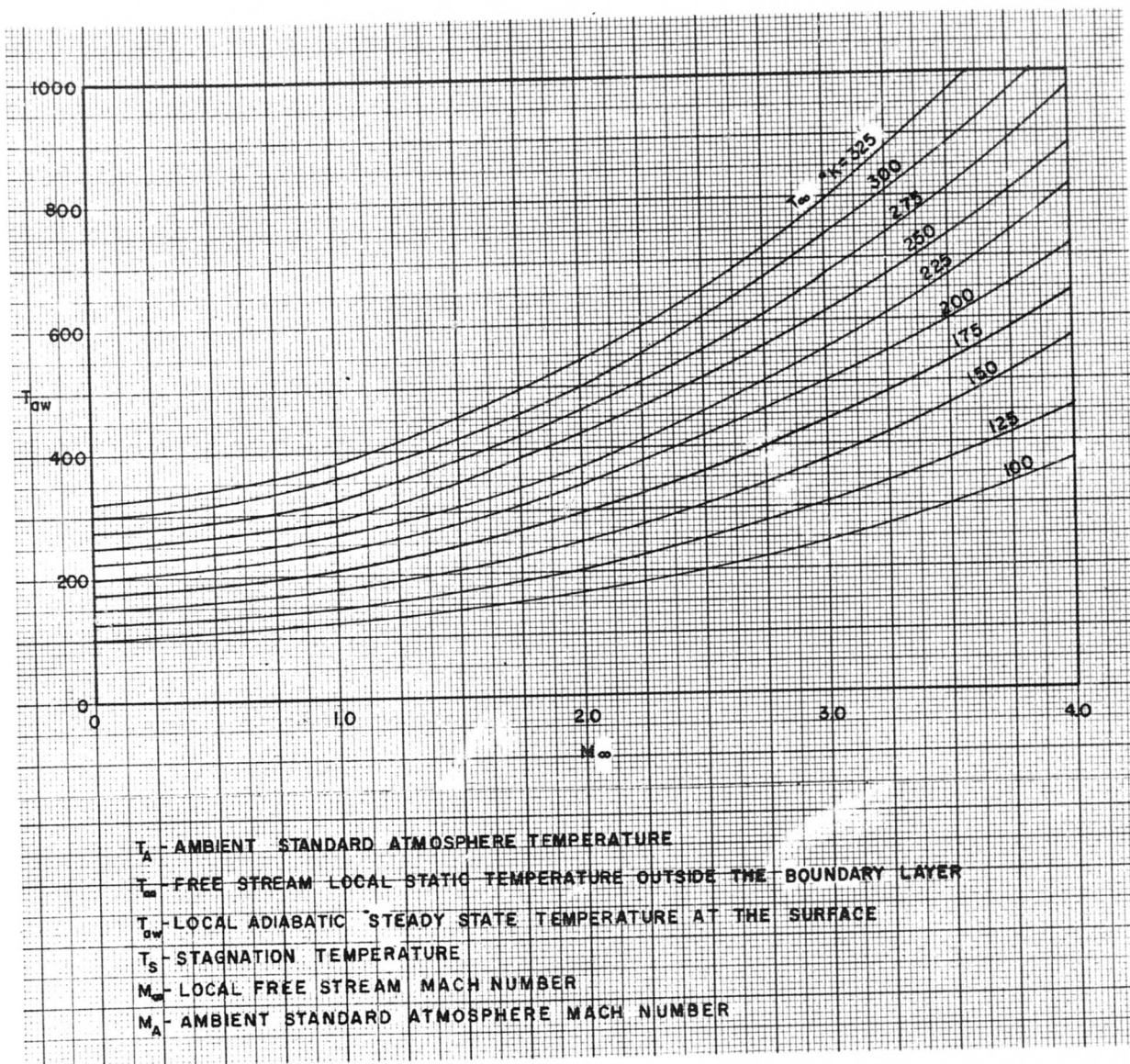


Fig. (2.4-49) Laminar boundary layers: local adiabatic wall temperatures,  $T_{aw}$ , at perfectly insulated surfaces neglecting radiation and assuming steady aerothermal equilibrium flow conditions—allowance for variations in specific heat with temperature has been made. (Ref. 2.4-68)

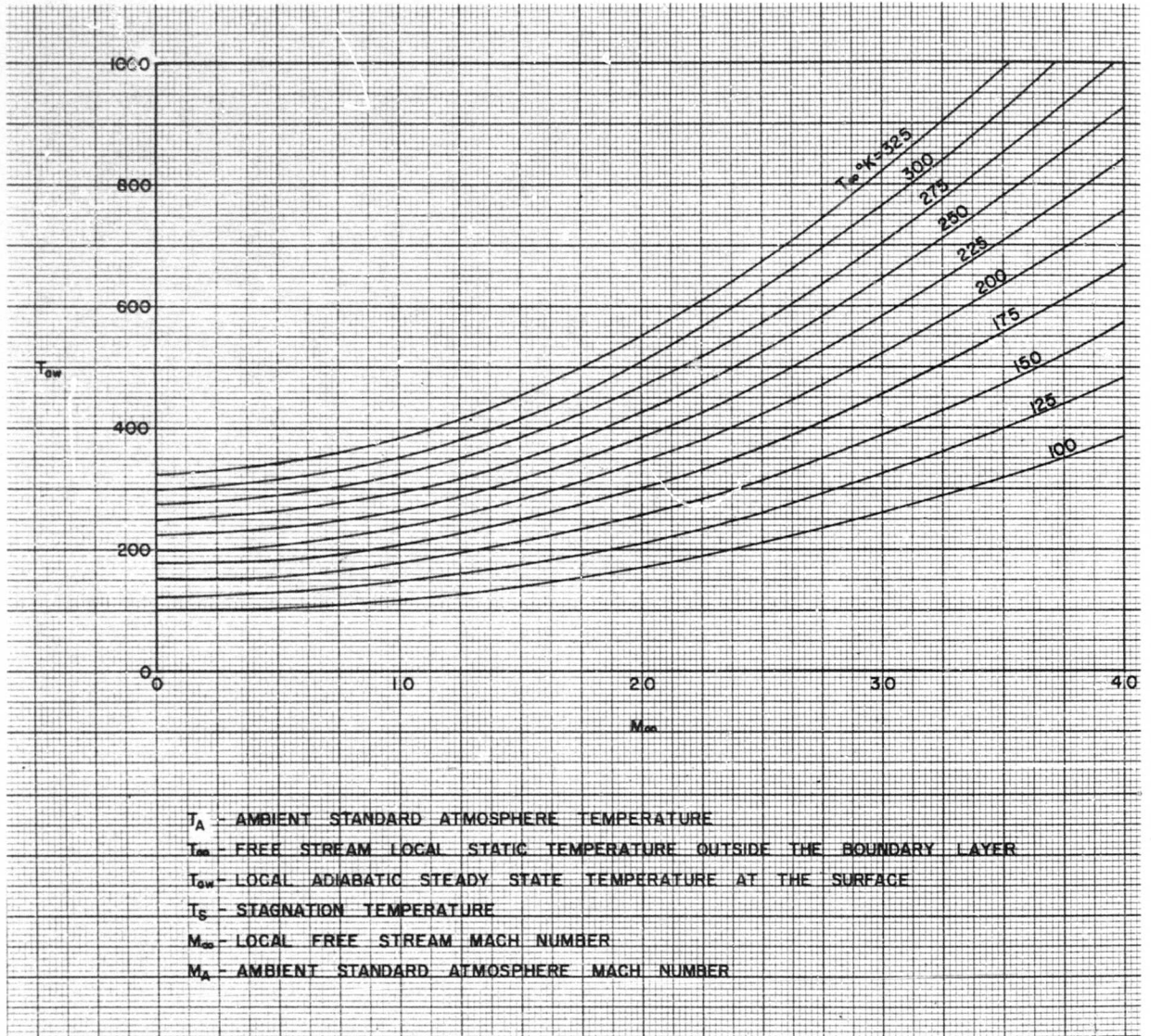


Fig. (2.4-50) Turbulent boundary layers: local adiabatic wall temperatures,  $T_{ow}$ , at perfectly insulated surfaces neglecting radiation and assuming steady aerothermal equilibrium flow conditions—allowance for variations in specific heat with temperature has been made. (Ref. 2.4-68)

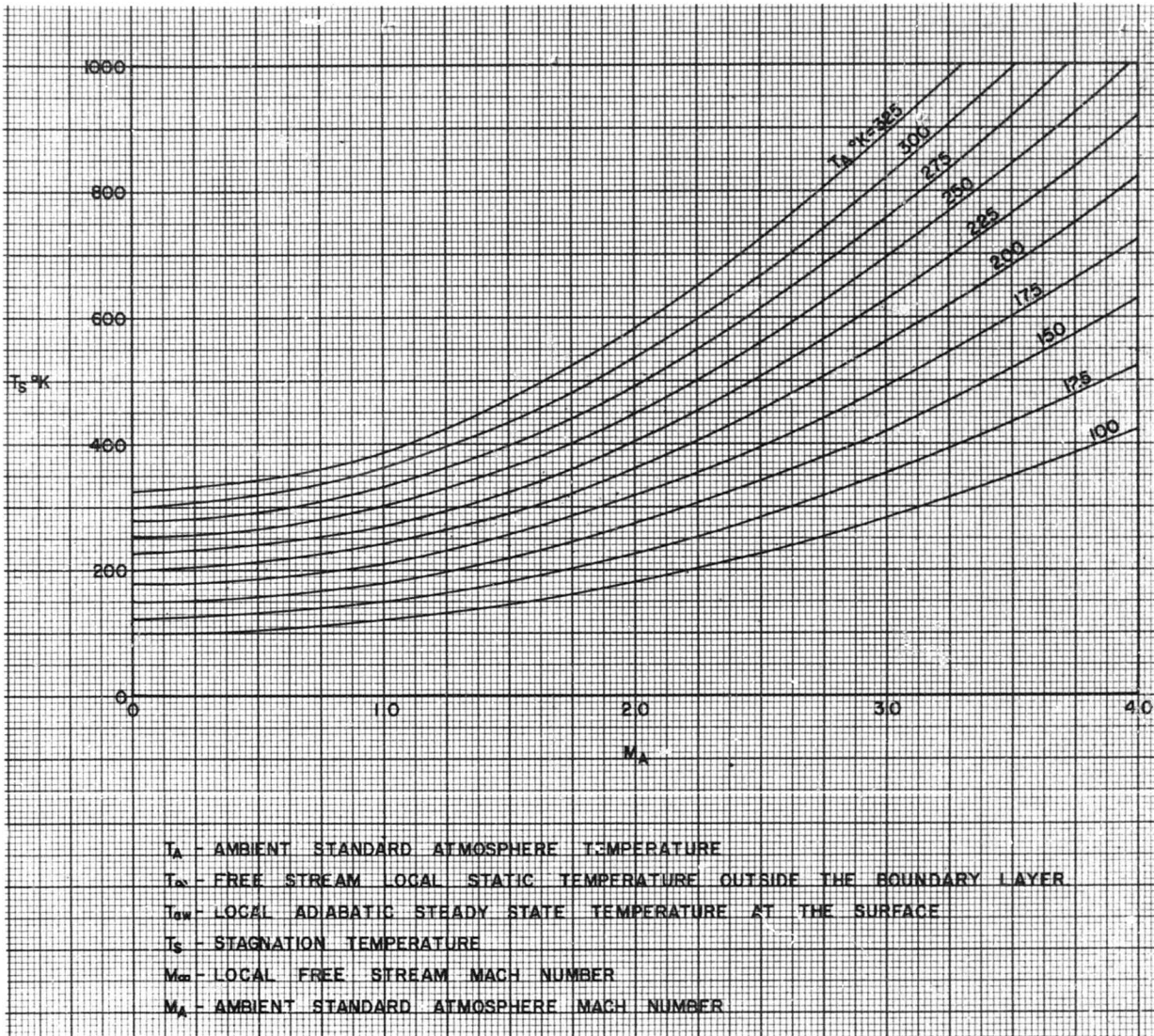


Fig. (2.4-51) Stagnation conditions: local adiabatic wall temperatures,  $T_{ow}$ , at perfectly insulated surfaces neglecting radiatio and assuming steady aerothermal equilibrium flow conditions- allowance for variations in specific heat with temperature has been made. (Ref. 2.4-68)

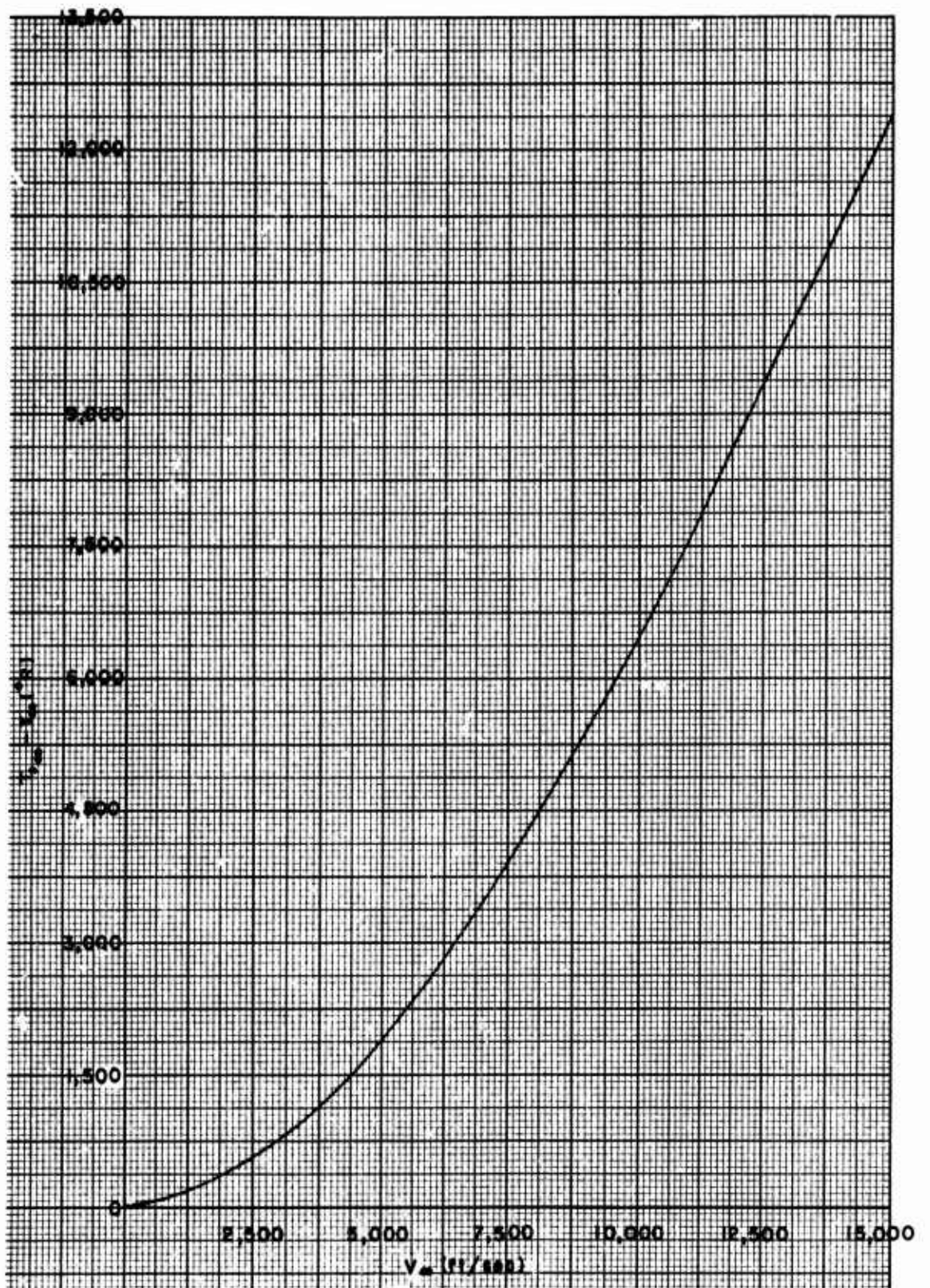


Fig. (2.4-52) Stagnation-temperature rise for variable  $C_p$ . (Ref. 2.4-72)

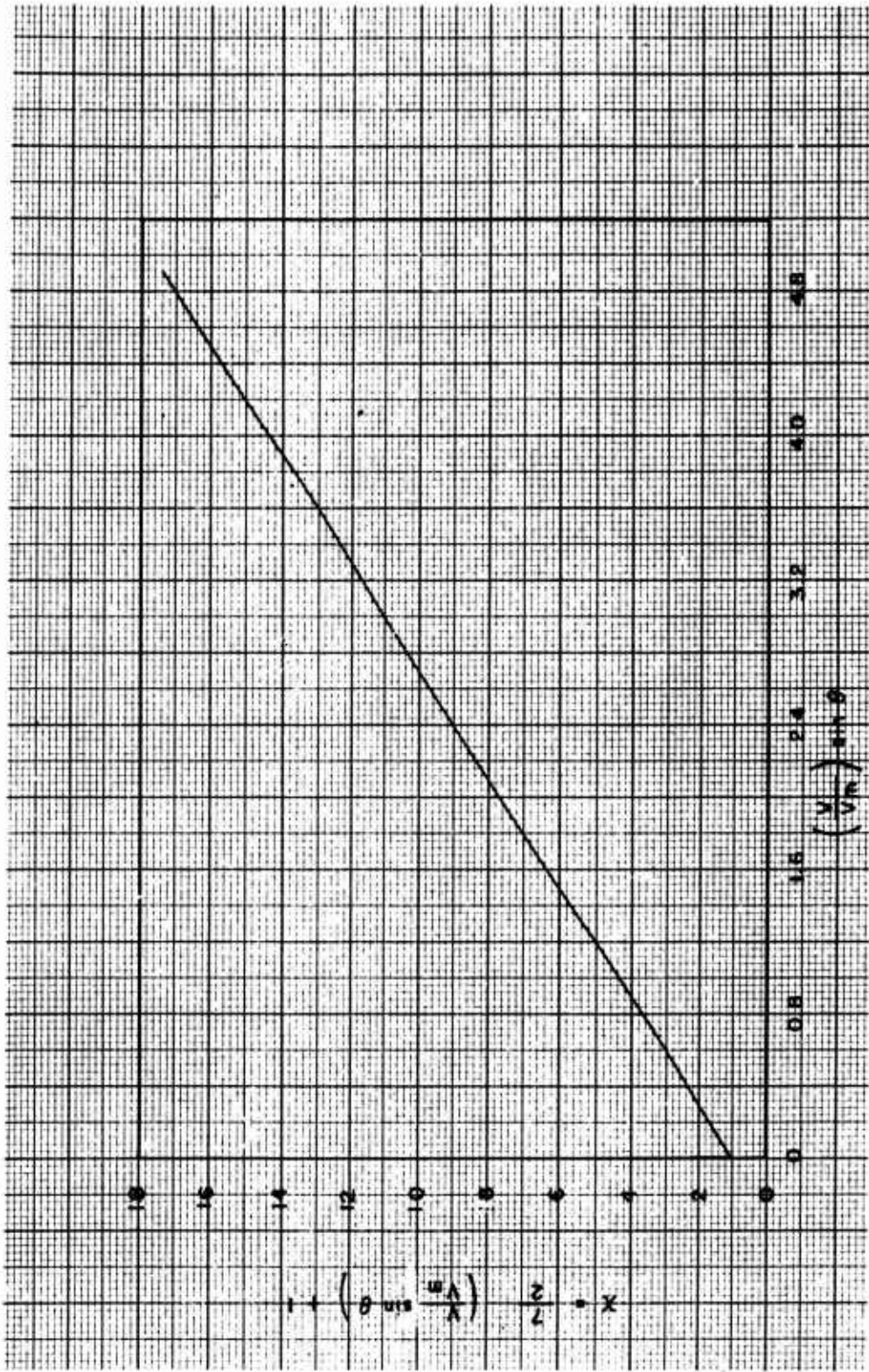


Fig. (2.4-53) Dimensionless quantity  $X$  . (After Stalder and Jukoff, Ref. 2.4-67)

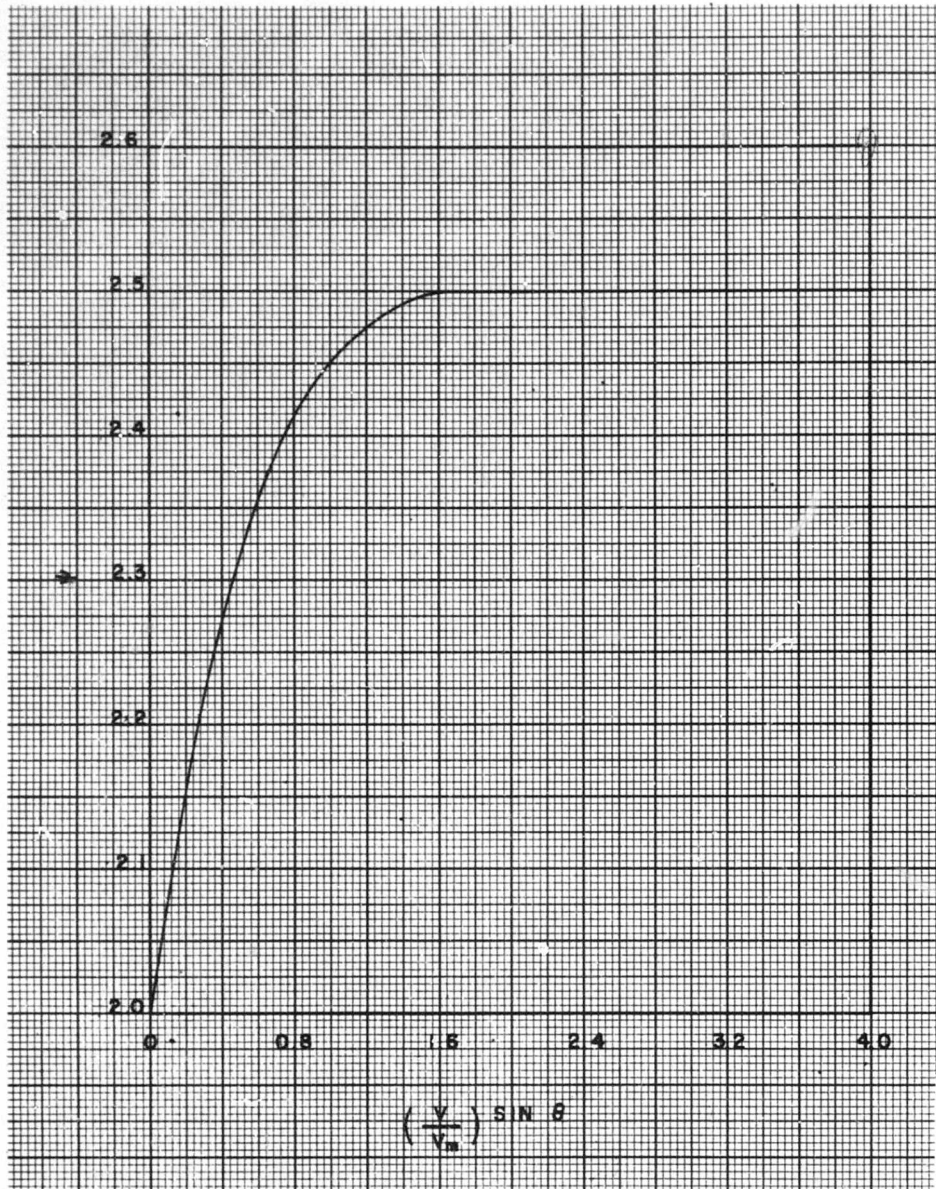


Fig. (2.4-54) Dimensionless quantity  $\psi$ . (After Stalder and Jukoff, Ref. 2.4-67)

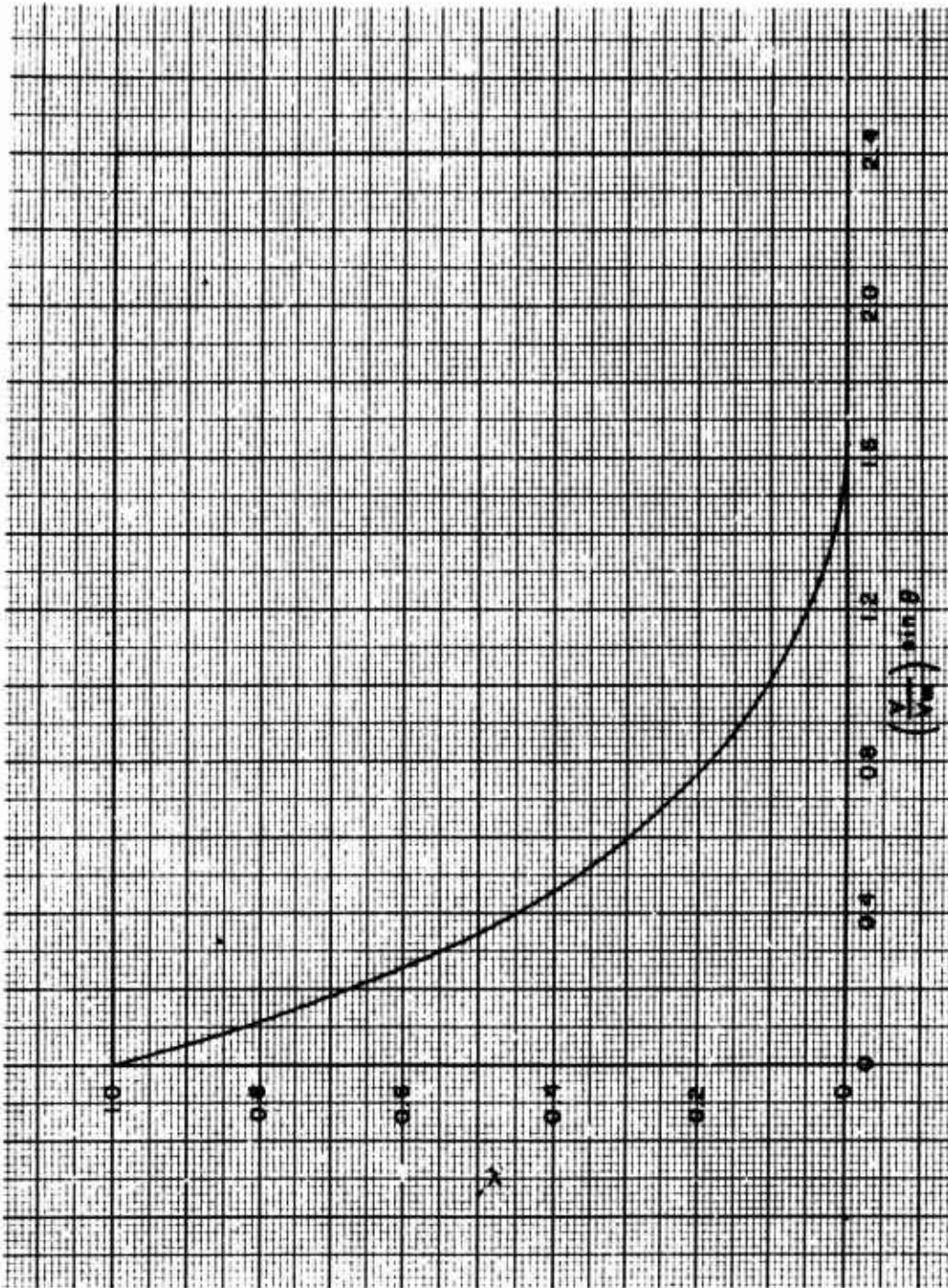


Fig (2.4-55) Dimensionless quantity  $x'$ . (After Stalder and Juhoff, Ref 2.4-67)

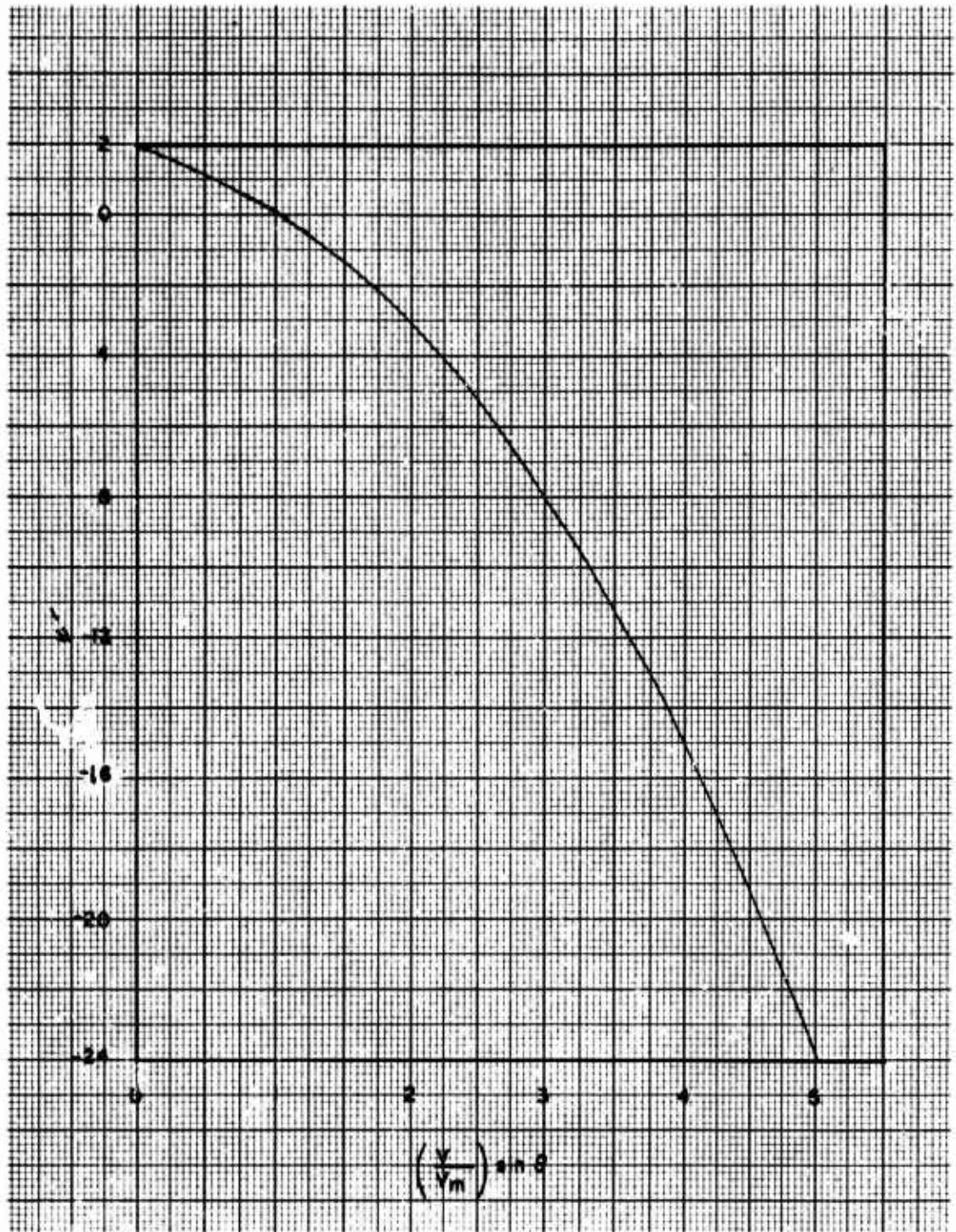


Fig (2.4-56) Dimensionless quantity  $\psi'$ . (After Stalder and Jukoff, Ref 2.4-67)

EMISSIVITIES  $\epsilon$

MATERIAL	50°C	250°C	550°C
ALUMINIUM —			
POLISHED	0.04	0.05	0.08
OXIDISED	0.11	0.12	0.18
CHROMIUM	0.08	0.17	0.26
GLASS	0.9	—	—
GRAPHITE	0.41	0.49	0.54
IRON —			
PURE, POLISHED	0.06	0.08	0.13
WROUGHT, POLISHED	0.28	0.27	—
SMOOTH	0.35	—	—
CAST	0.21	—	—
CAST, OXIDISED	0.63	0.66	0.76
NICKEL —			
ELECTROLYTIC	0.04	0.06	0.10
OXIDISED	0.39	0.49	0.67
STEEL —			
POLISHED	0.07	0.10	0.14
CARBONISED	0.52	0.53	0.56
OXIDISED	0.79	0.79	0.79
ZINC —			
PURE, POLISHED	0.02	0.03	0.04
ON SHEET IRON	0.23	—	—

PIGMENTS	50° C	400° C
LAMPBLACK PAINT	0.96	0.97
BLUE ( $\text{CO}_2\text{O}_3$ )	0.87	0.86
RED ( $\text{Fe}_2\text{O}_3$ )	0.96	0.70
GREEN ( $\text{Cu}_2\text{O}_3$ )	0.95	0.67
YELLOW ( $\text{PbO}$ )	0.74	0.49
YELLOW ( $\text{PbCrO}_4$ )	0.95	0.59
WHITE ( $\text{ZnO}$ )	0.97	0.91
WHITE ( $\text{ThO}_2$ )	0.93	0.53

FIG.(2.4-57) EMISSIVITIES,  $\epsilon$ , (REF. 2.4-68)

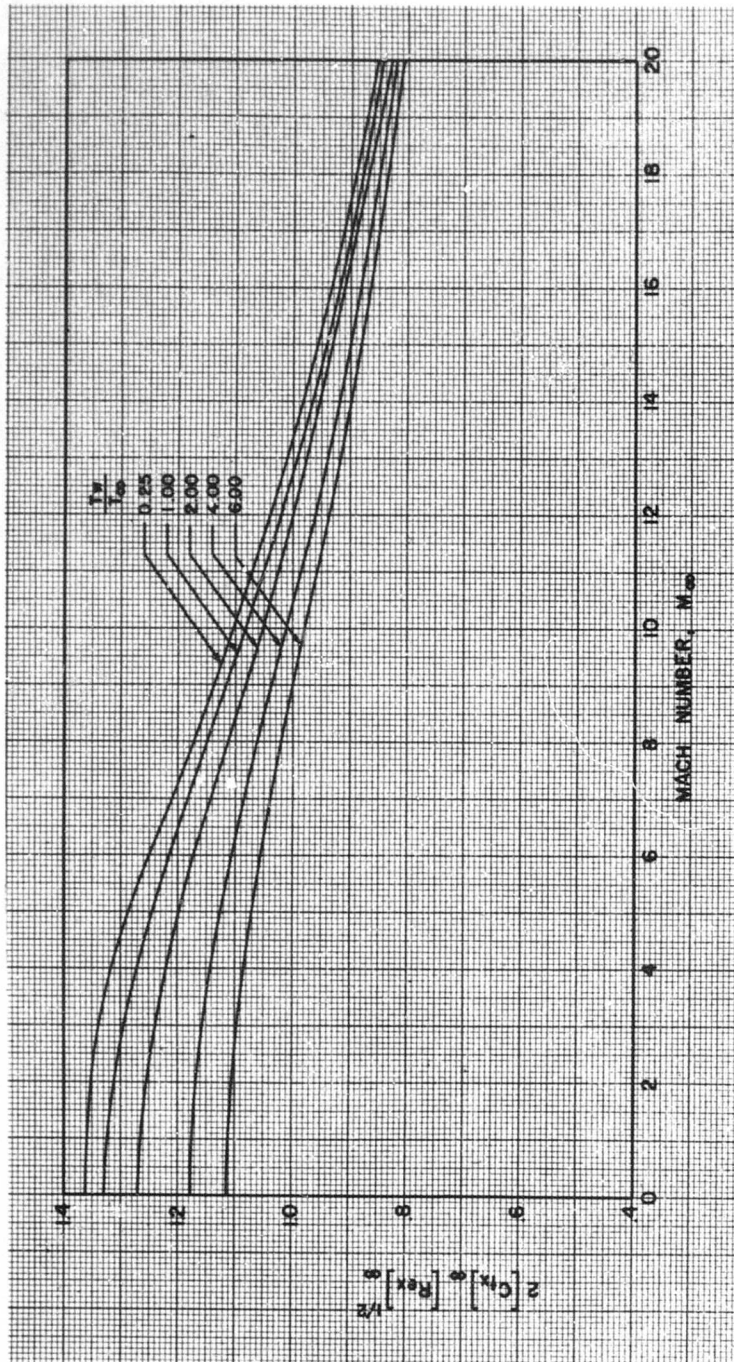


Fig (2.4-58) Local skin-friction coefficient for laminar boundary layer of a compressible fluid flowing along a flat plate. Prandtl Number, 0.75;  $\theta = 0.505$ . (Ref 2.4-73)



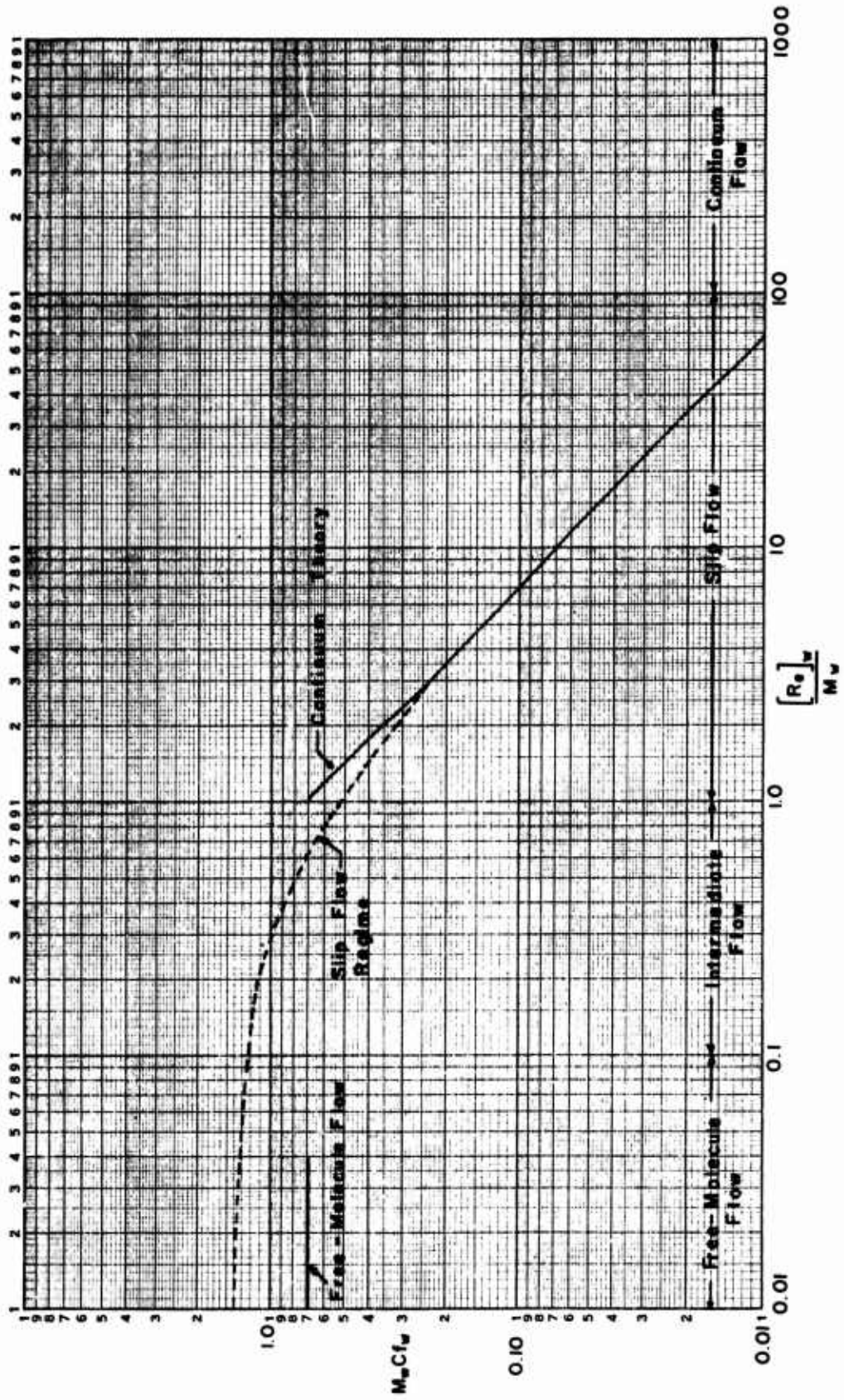
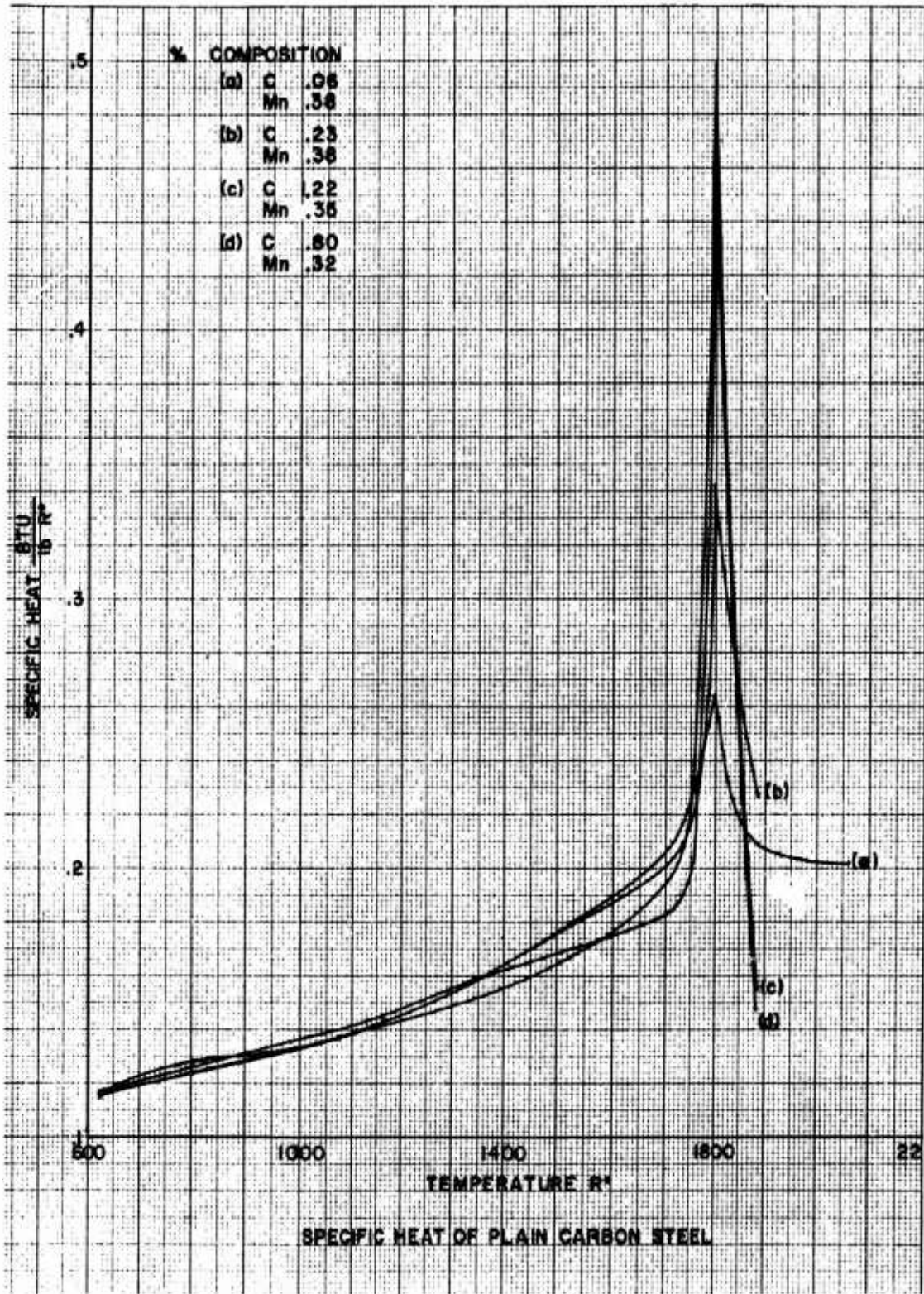
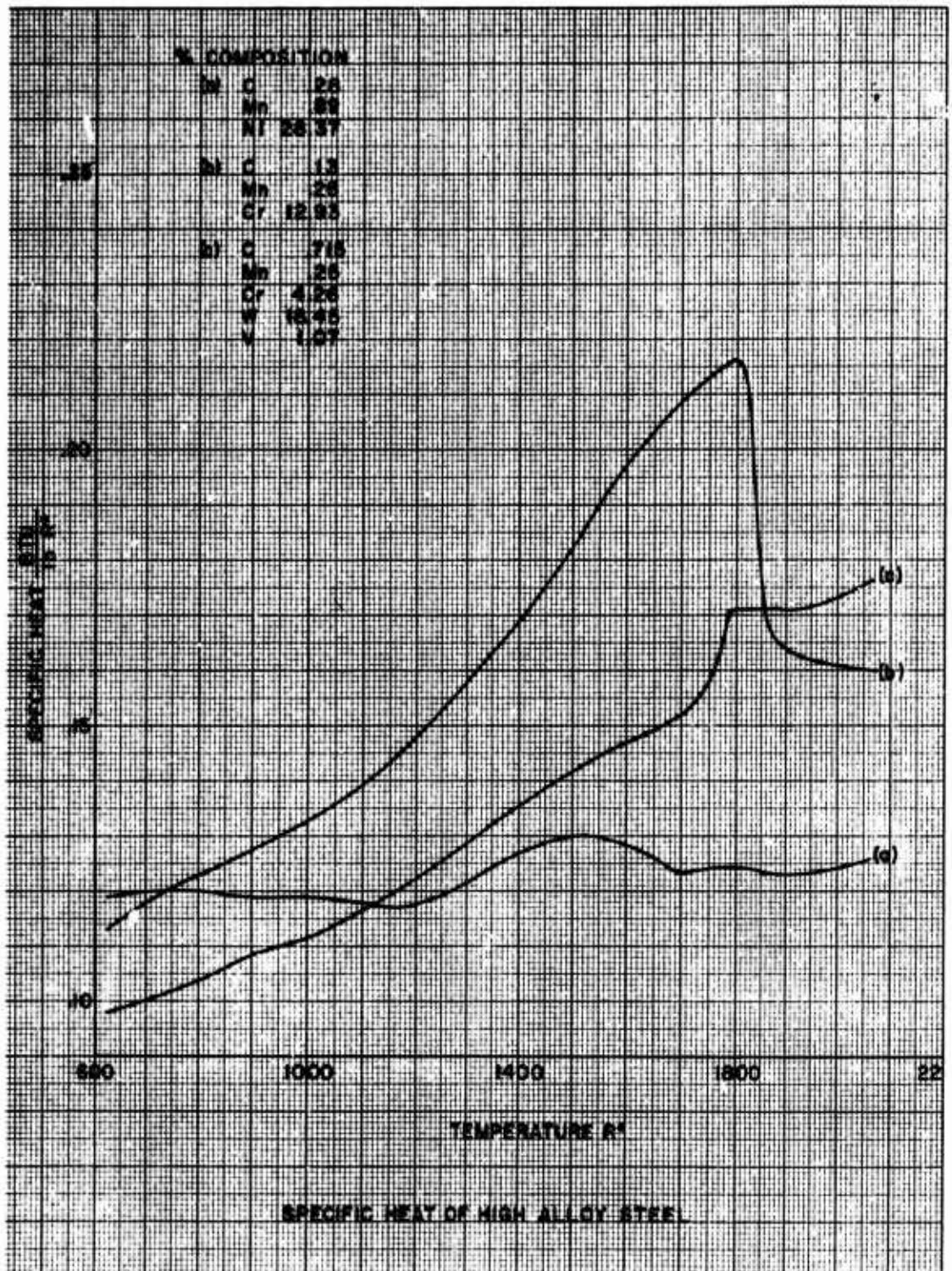


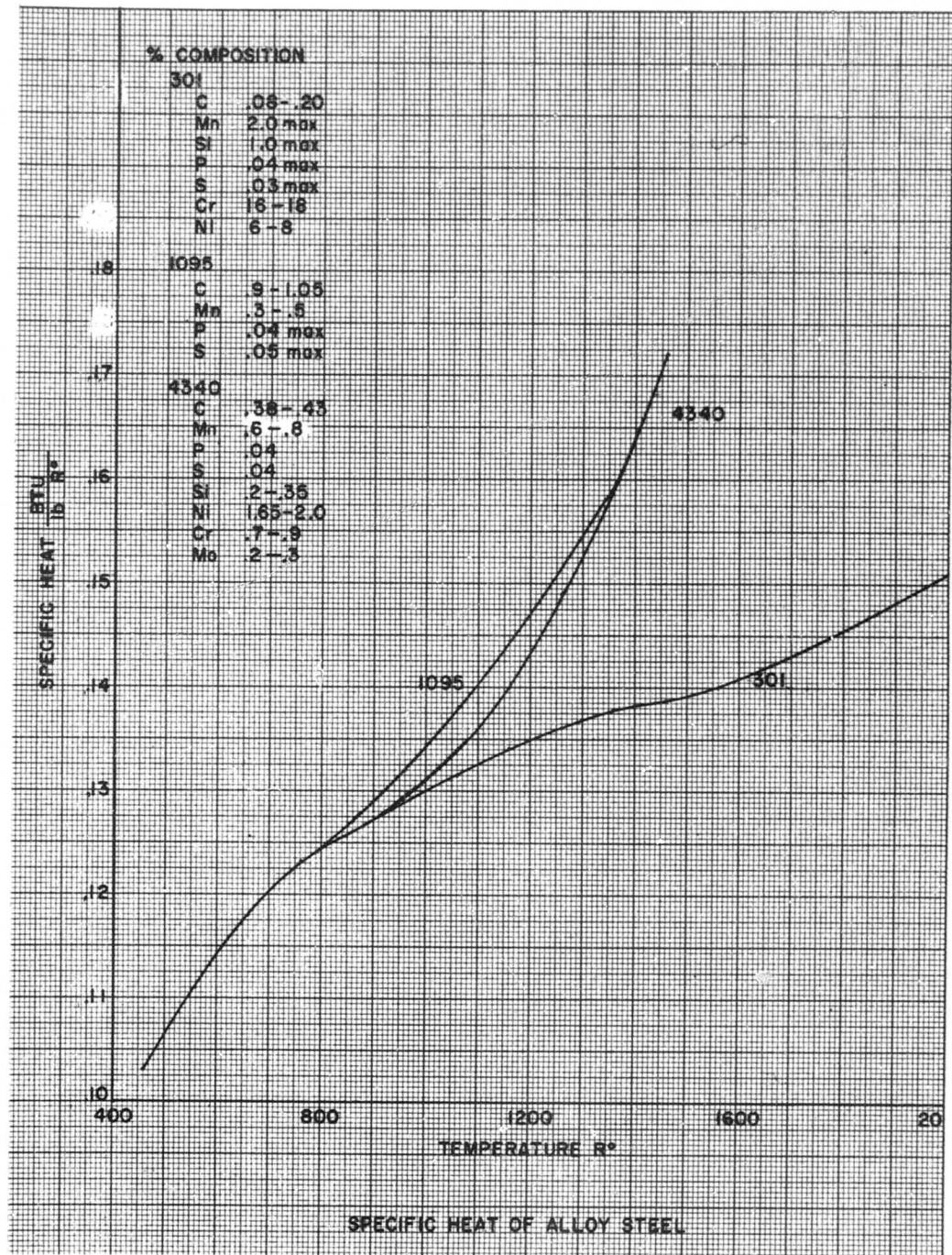
Fig (2.4-60) Variation of local skin friction along flat plate. (After Miralis Ref 2.4-71)



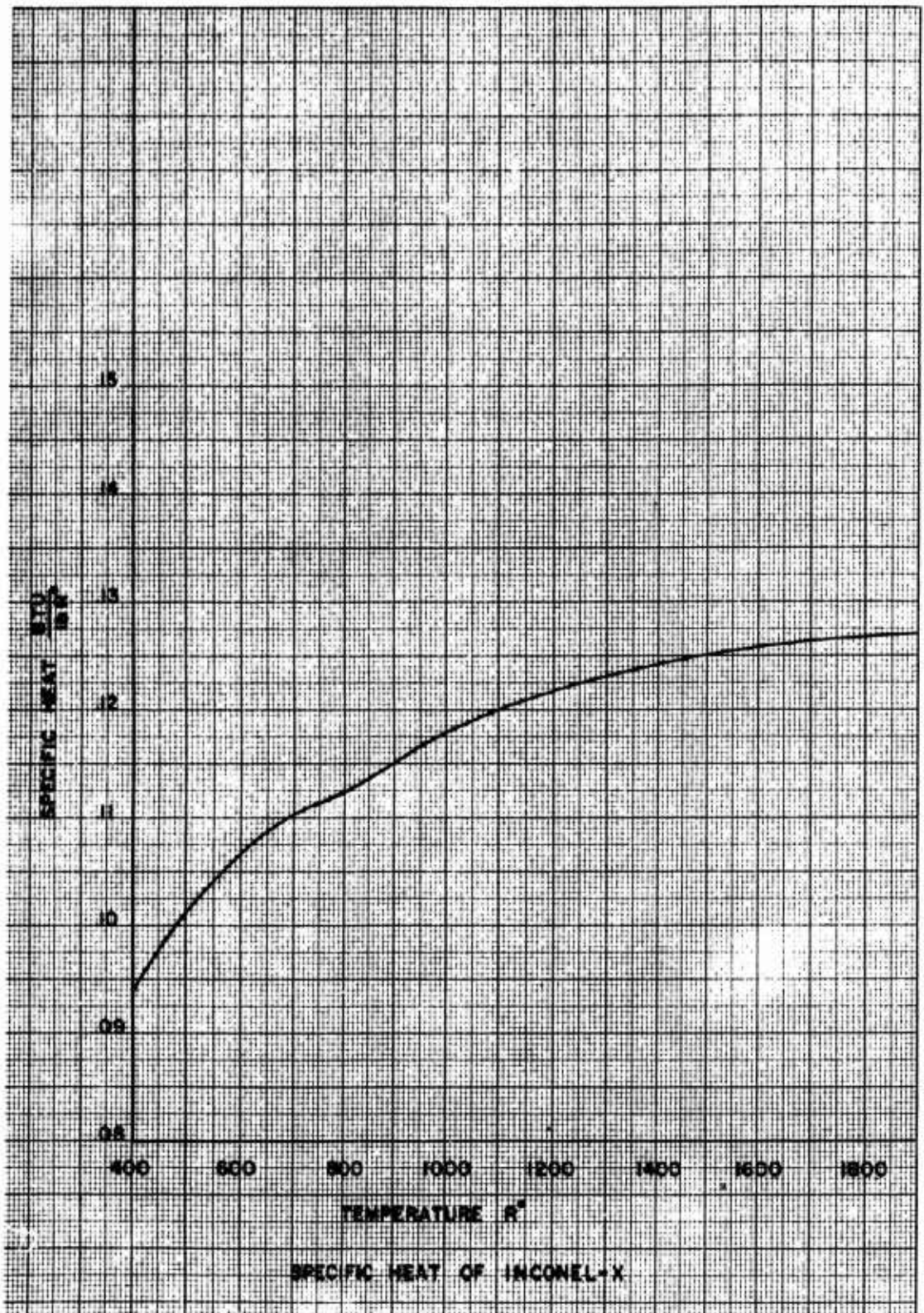
(2.4 - 61) a



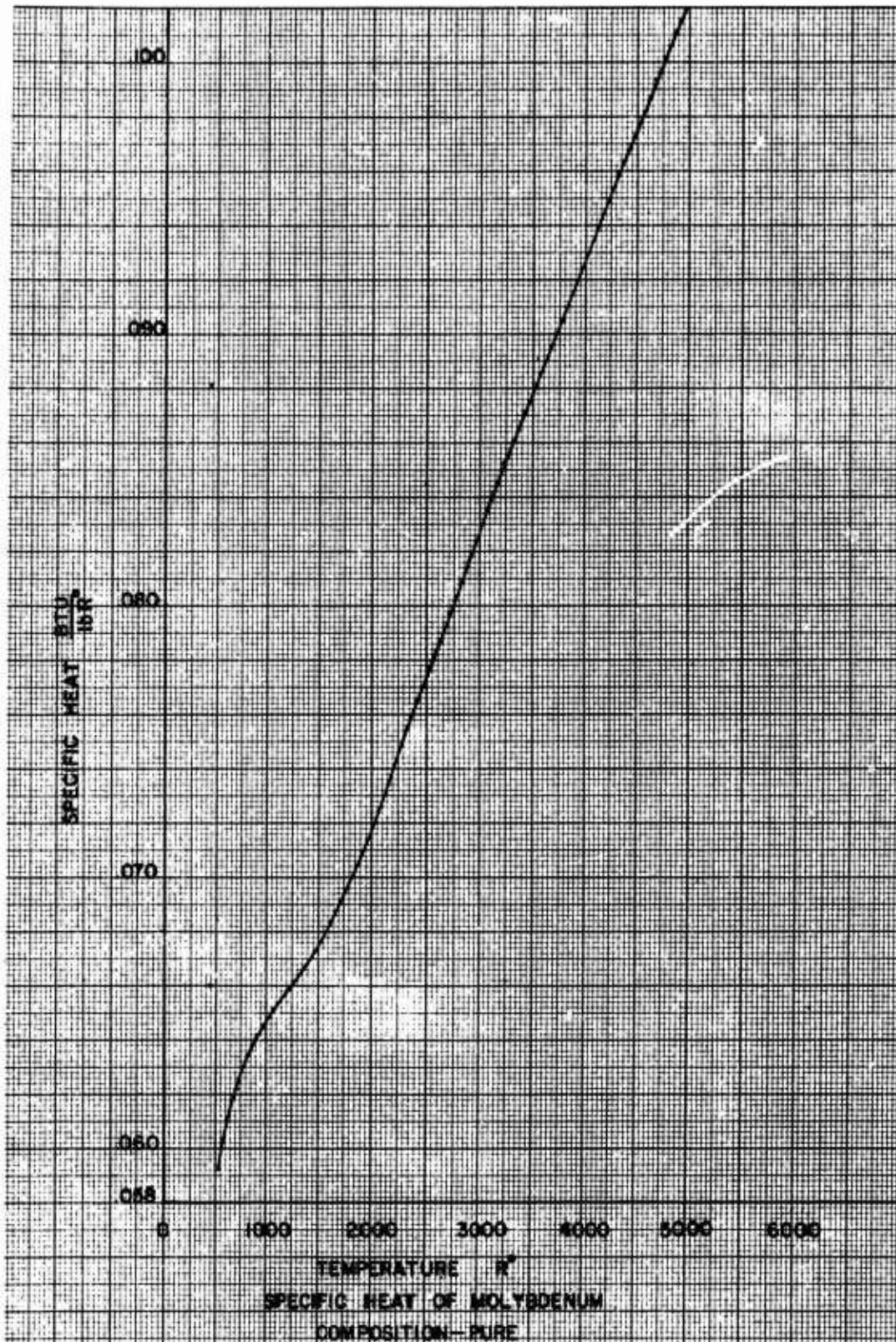
(2.4-61)b



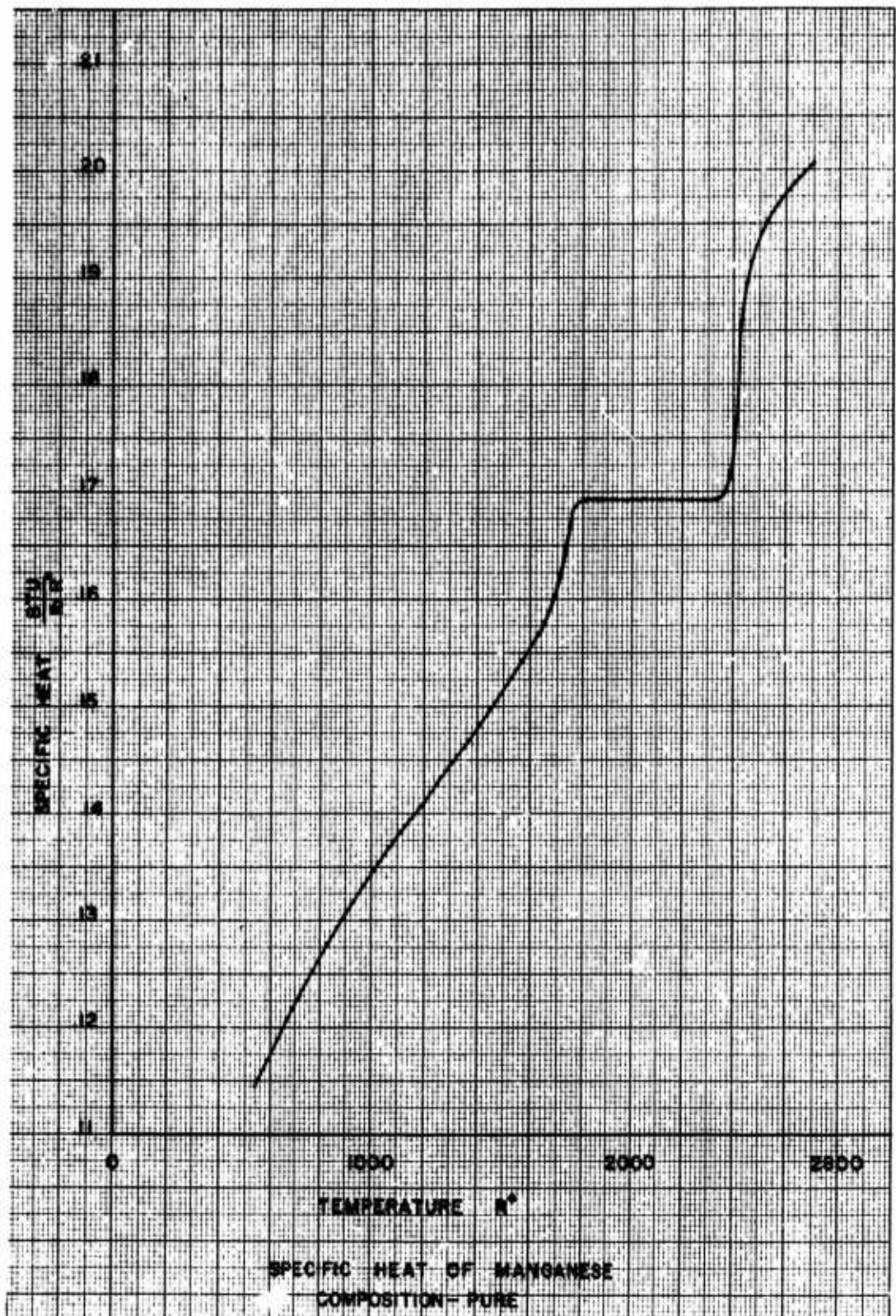
(2.4-61)c



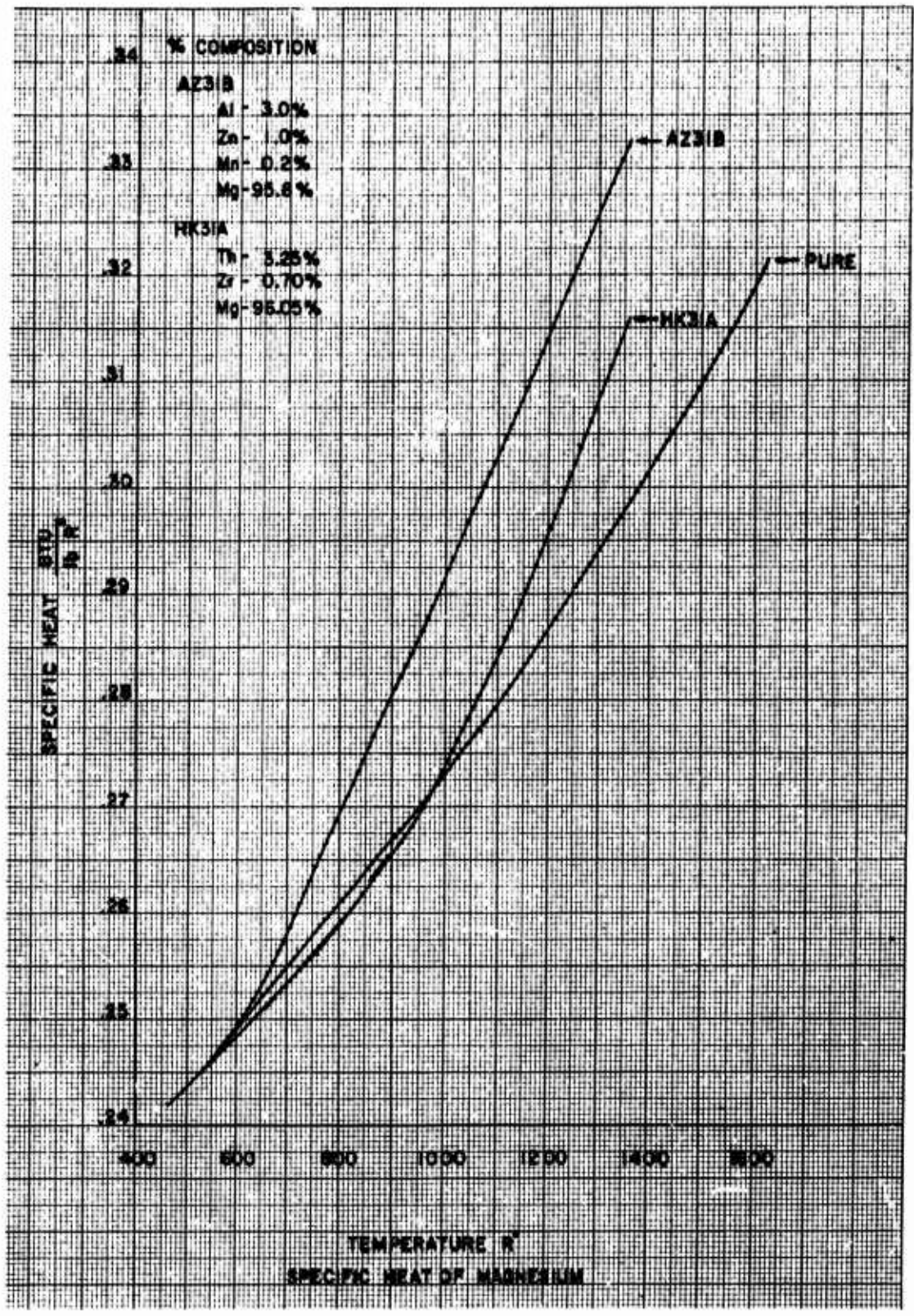
(2.4-61) d



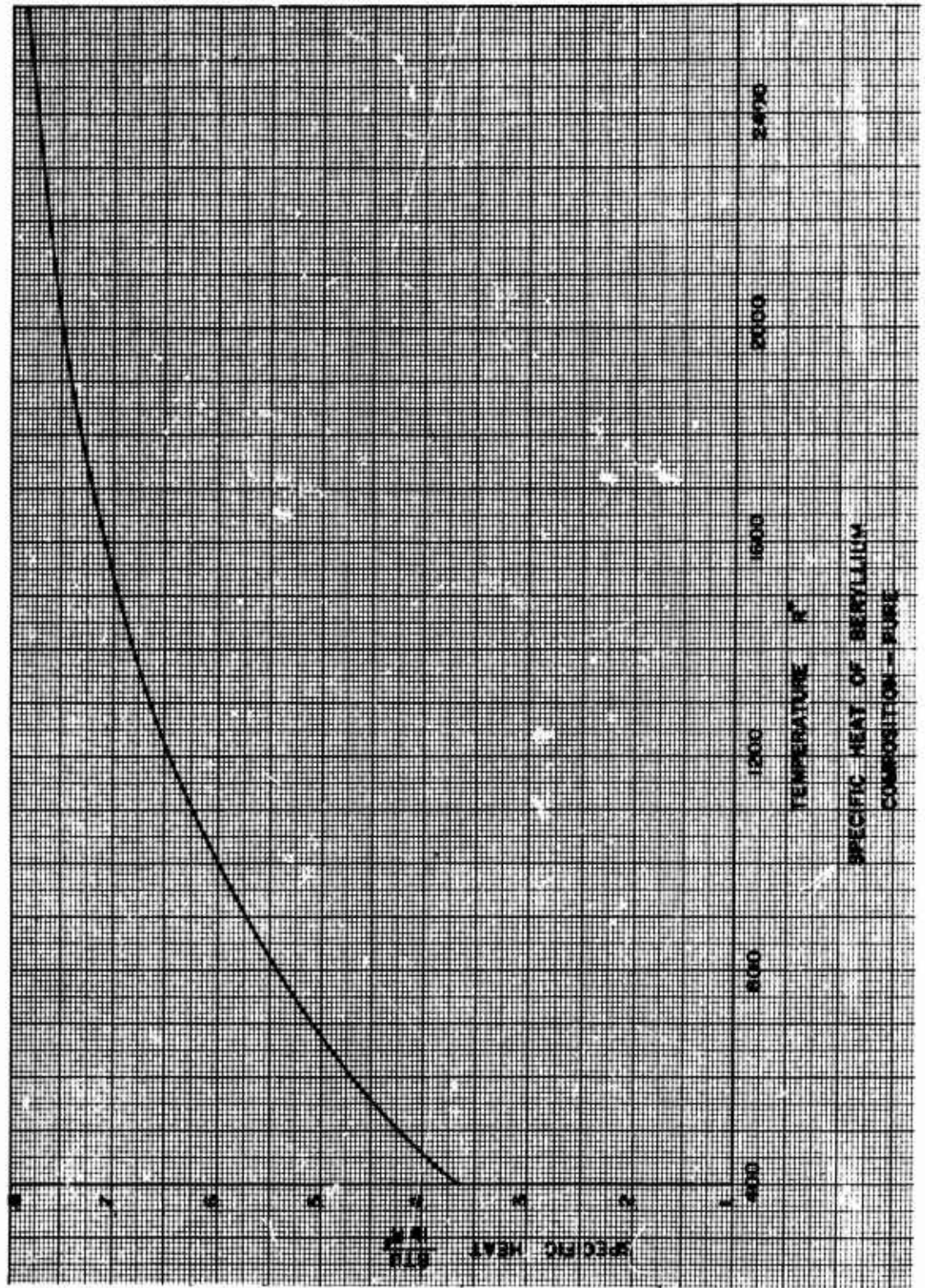
(2.4-61)•



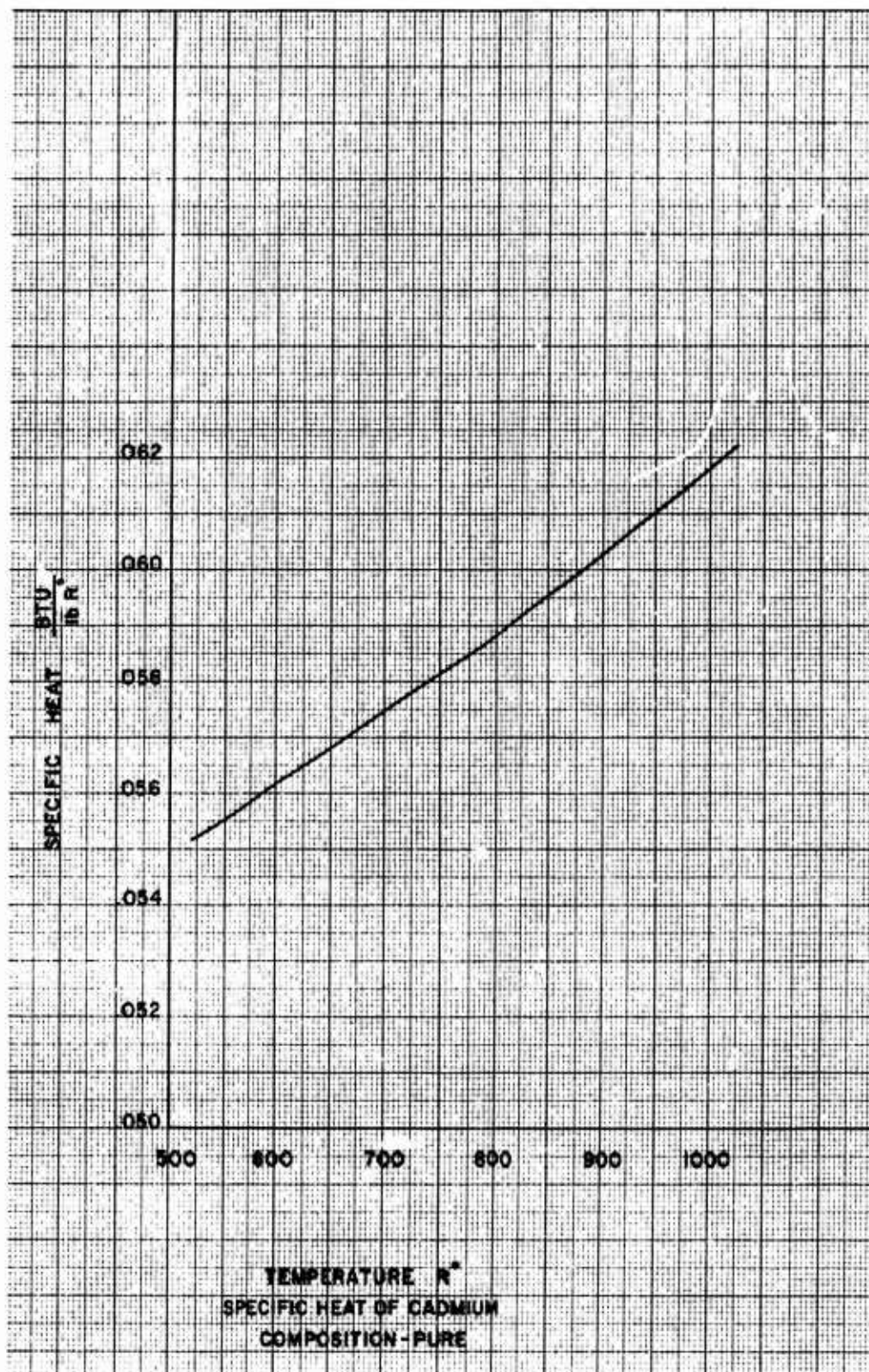
(2.4-61) f



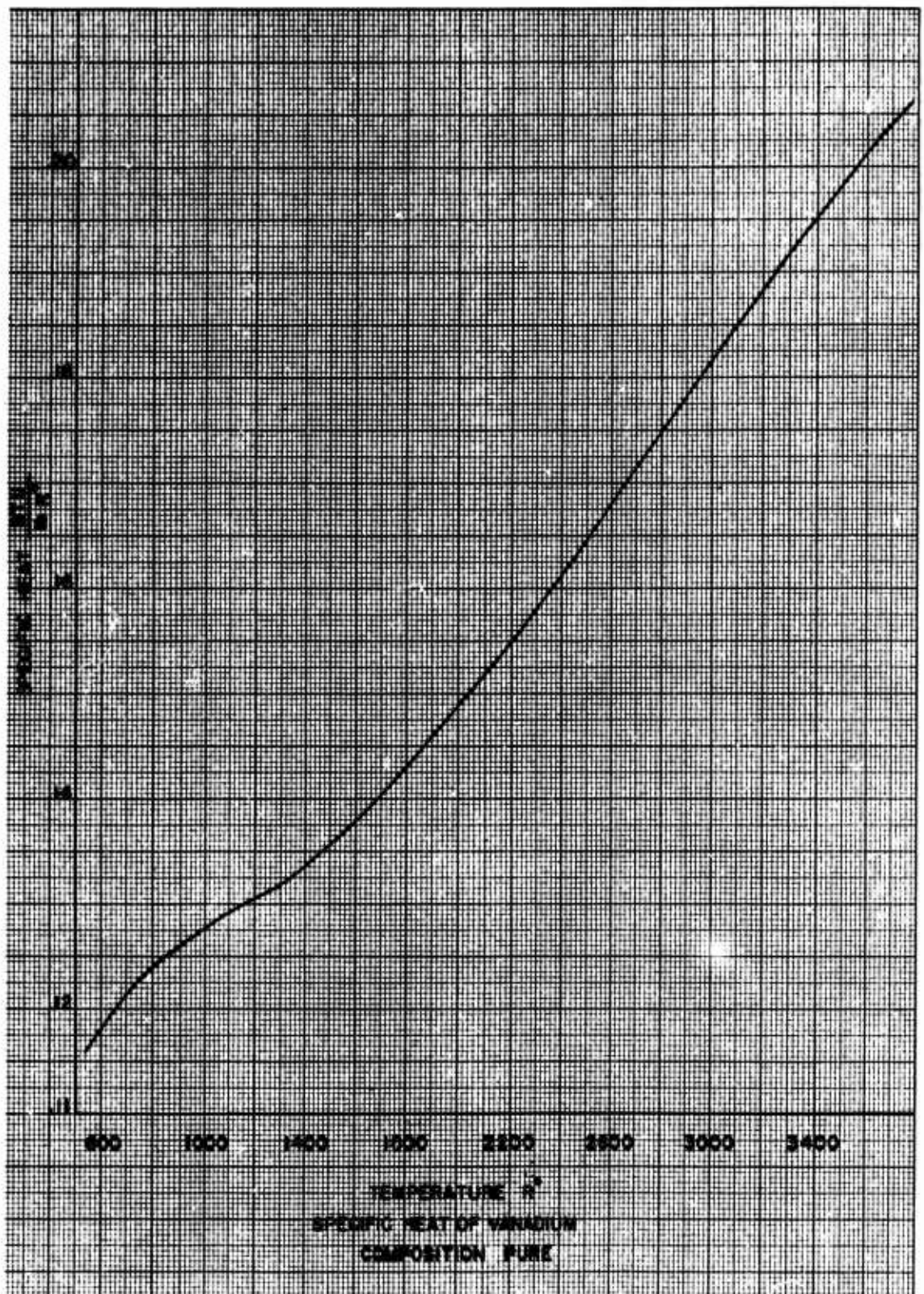
(2.4-61) g



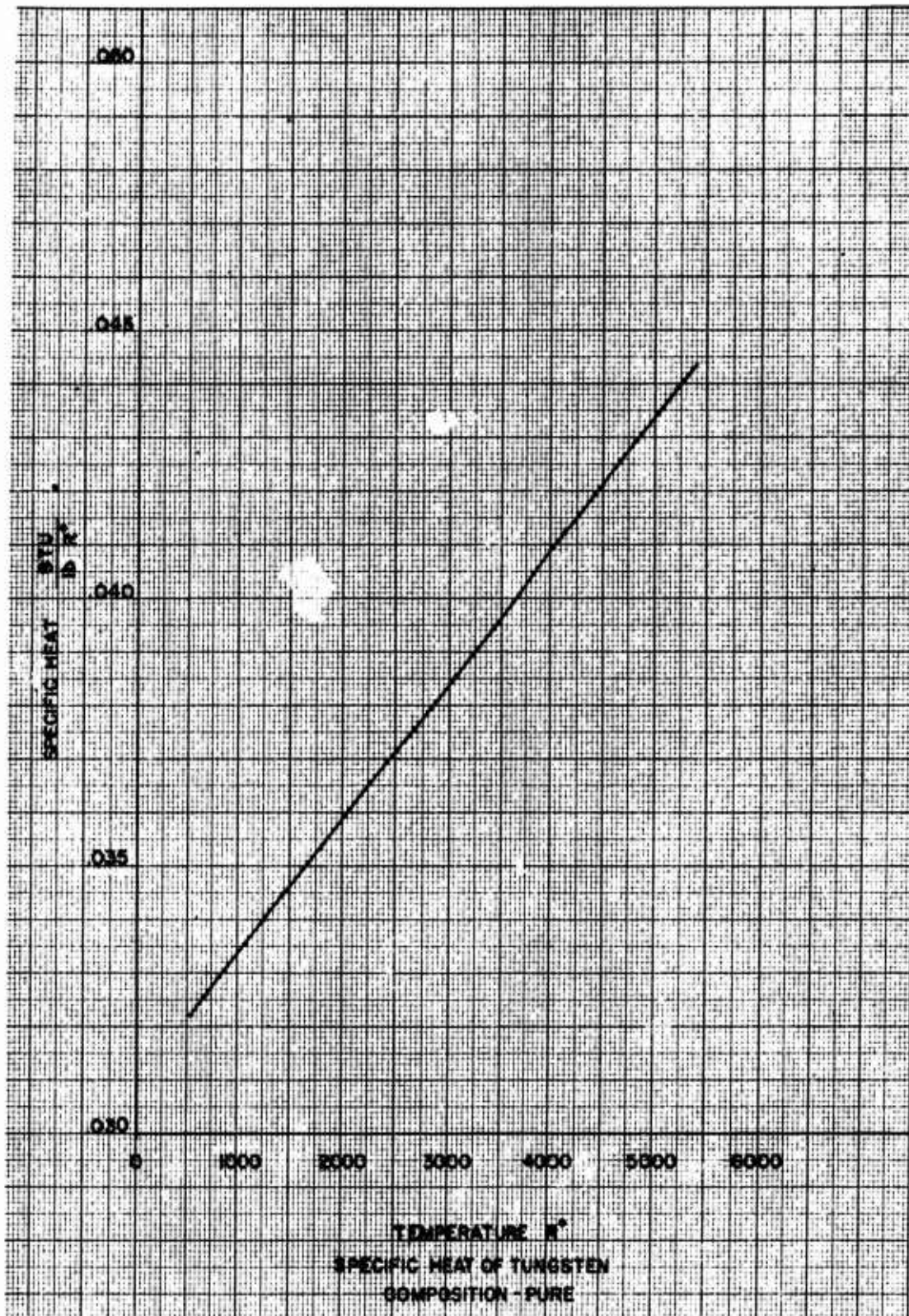
(2.4-61)h



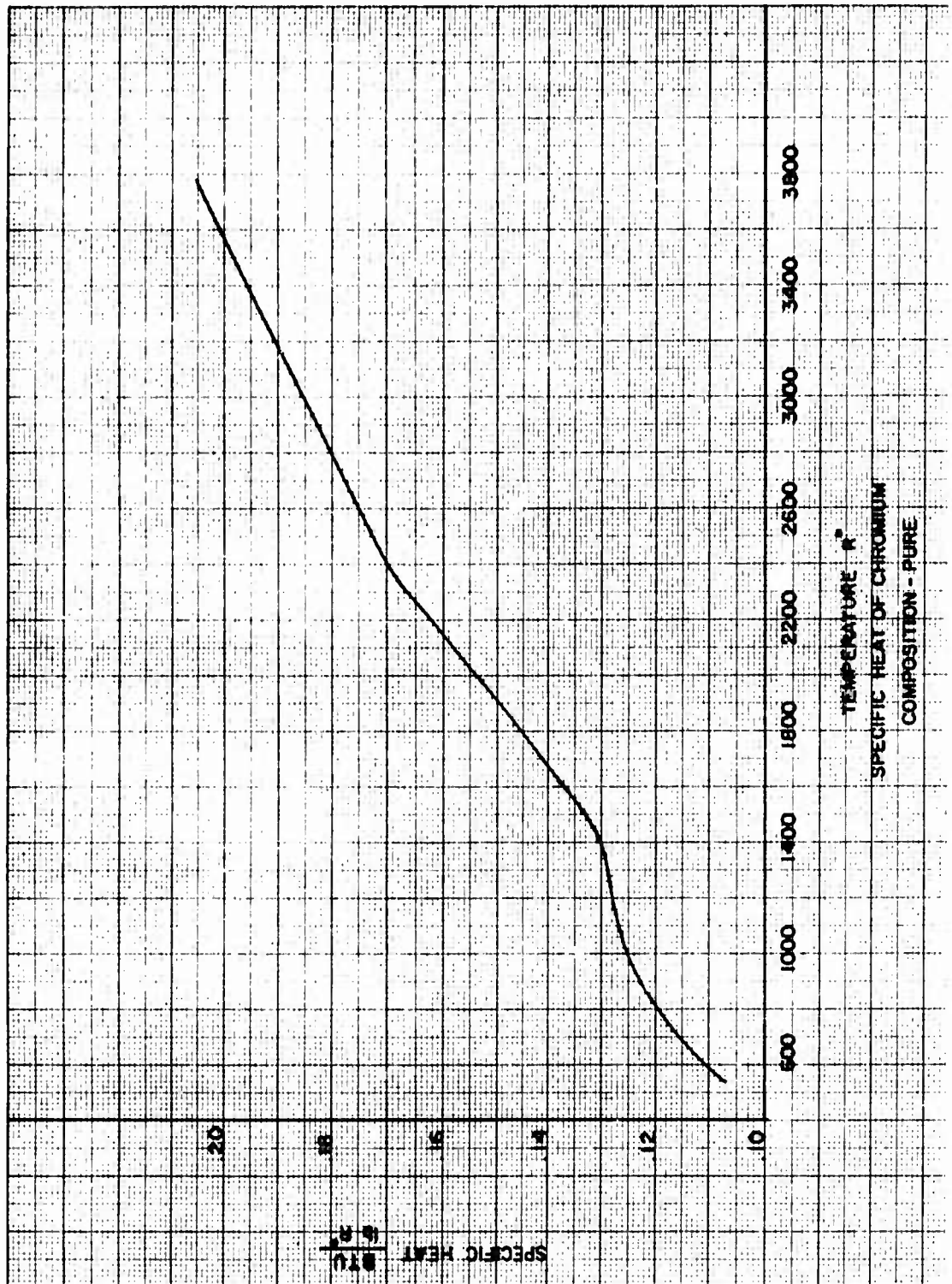
(2.4-61) i



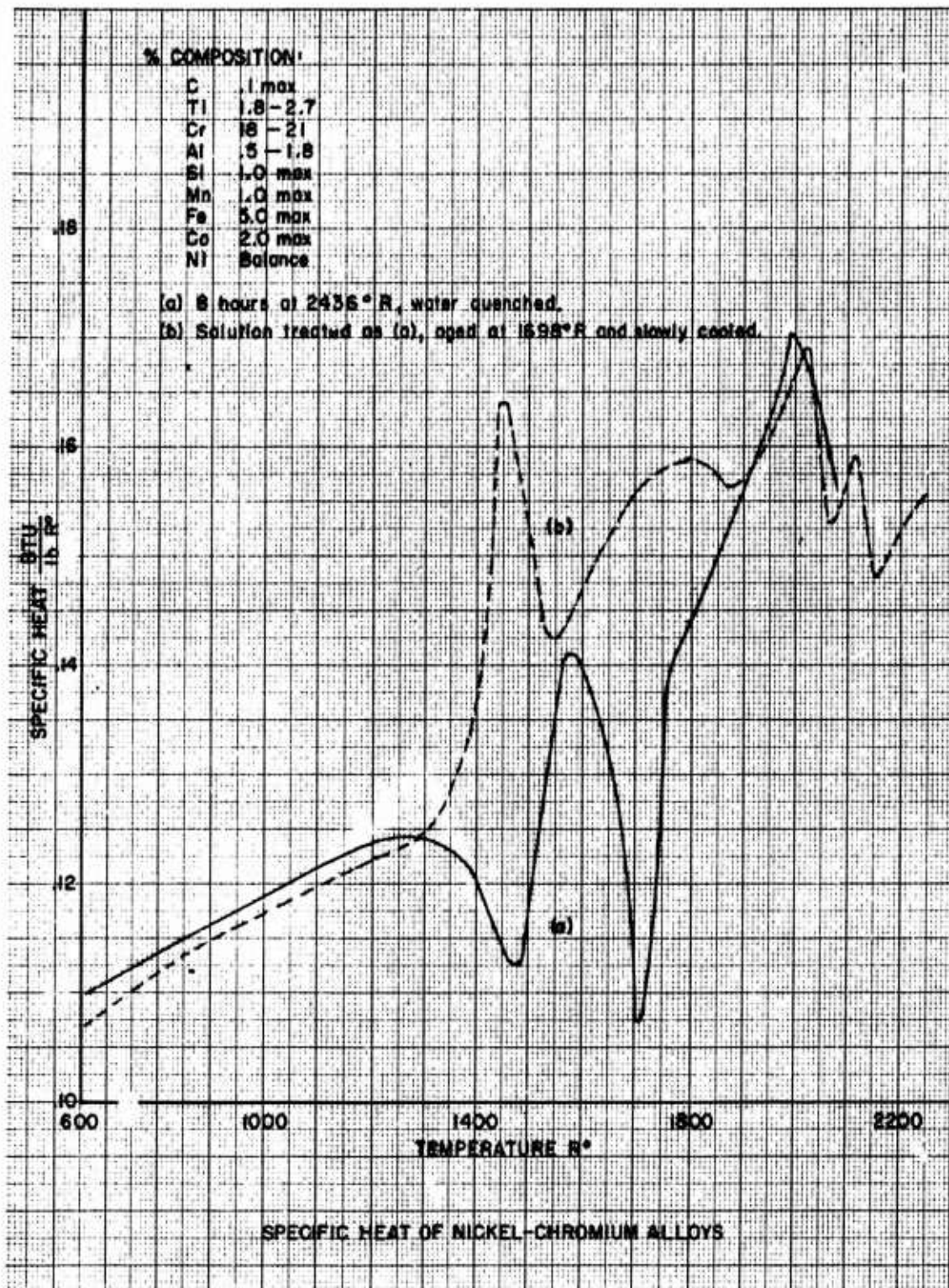
(2.4-61) j



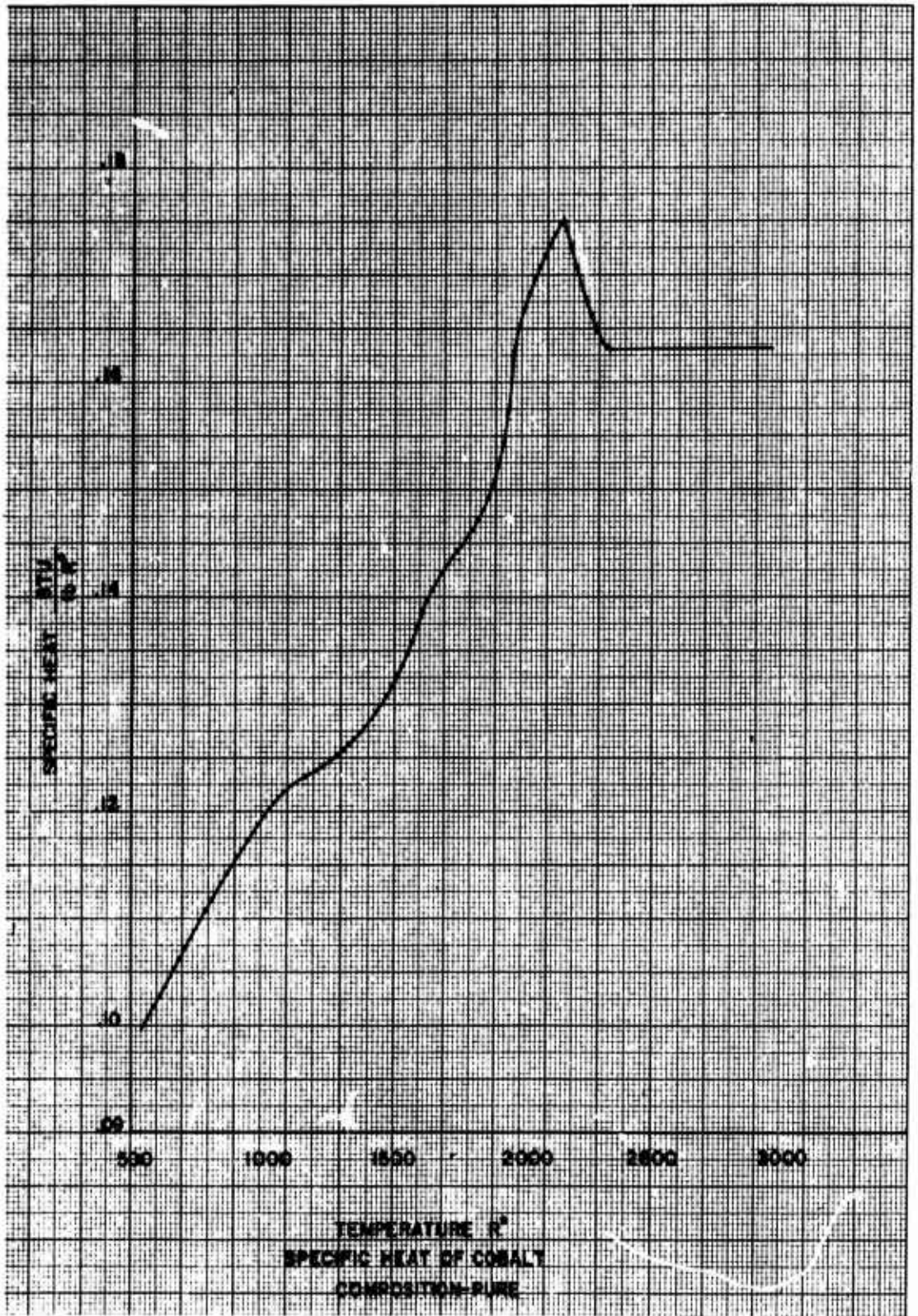
(2.4 - 61) k



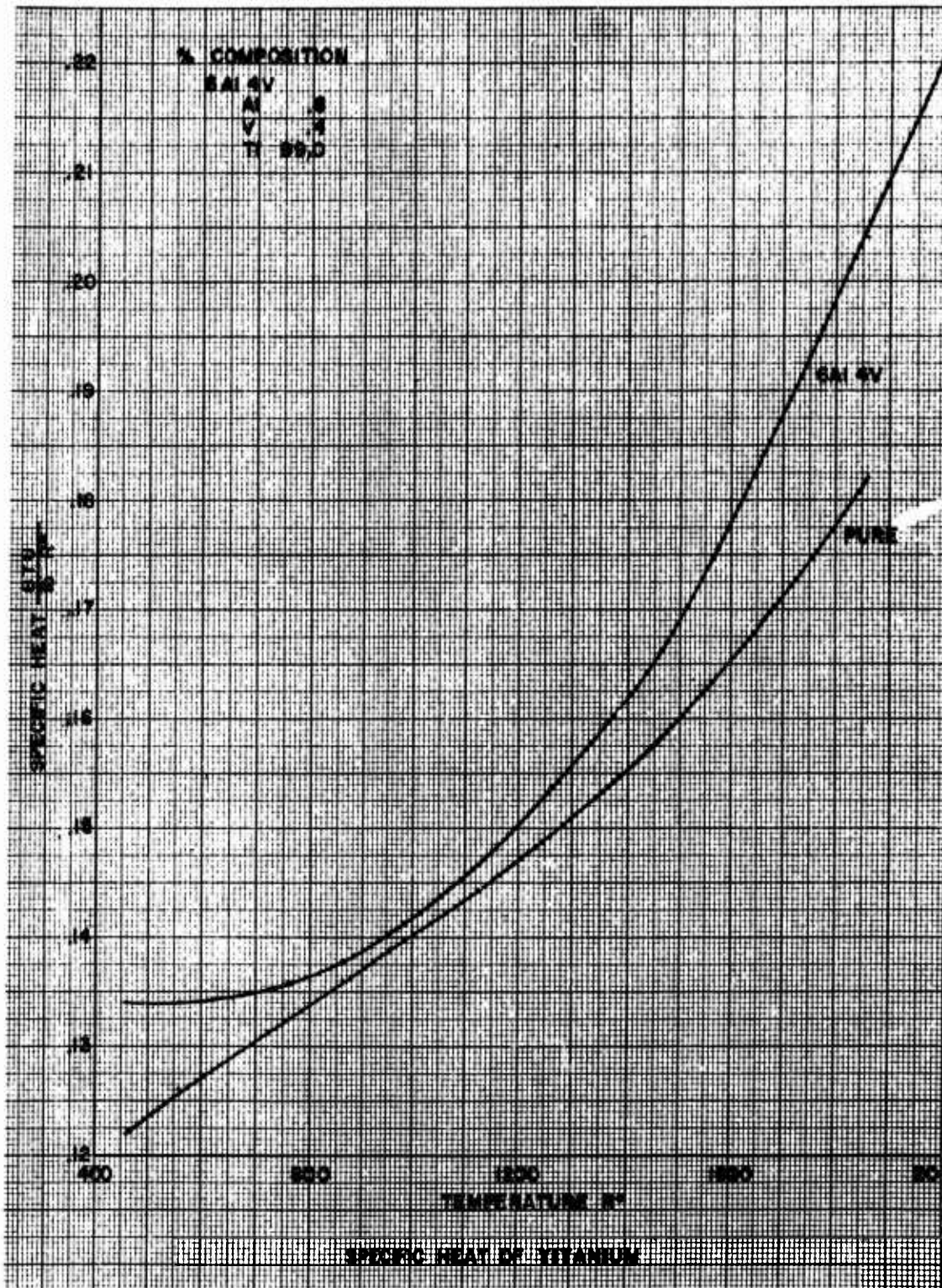
(2.4 - 61) I



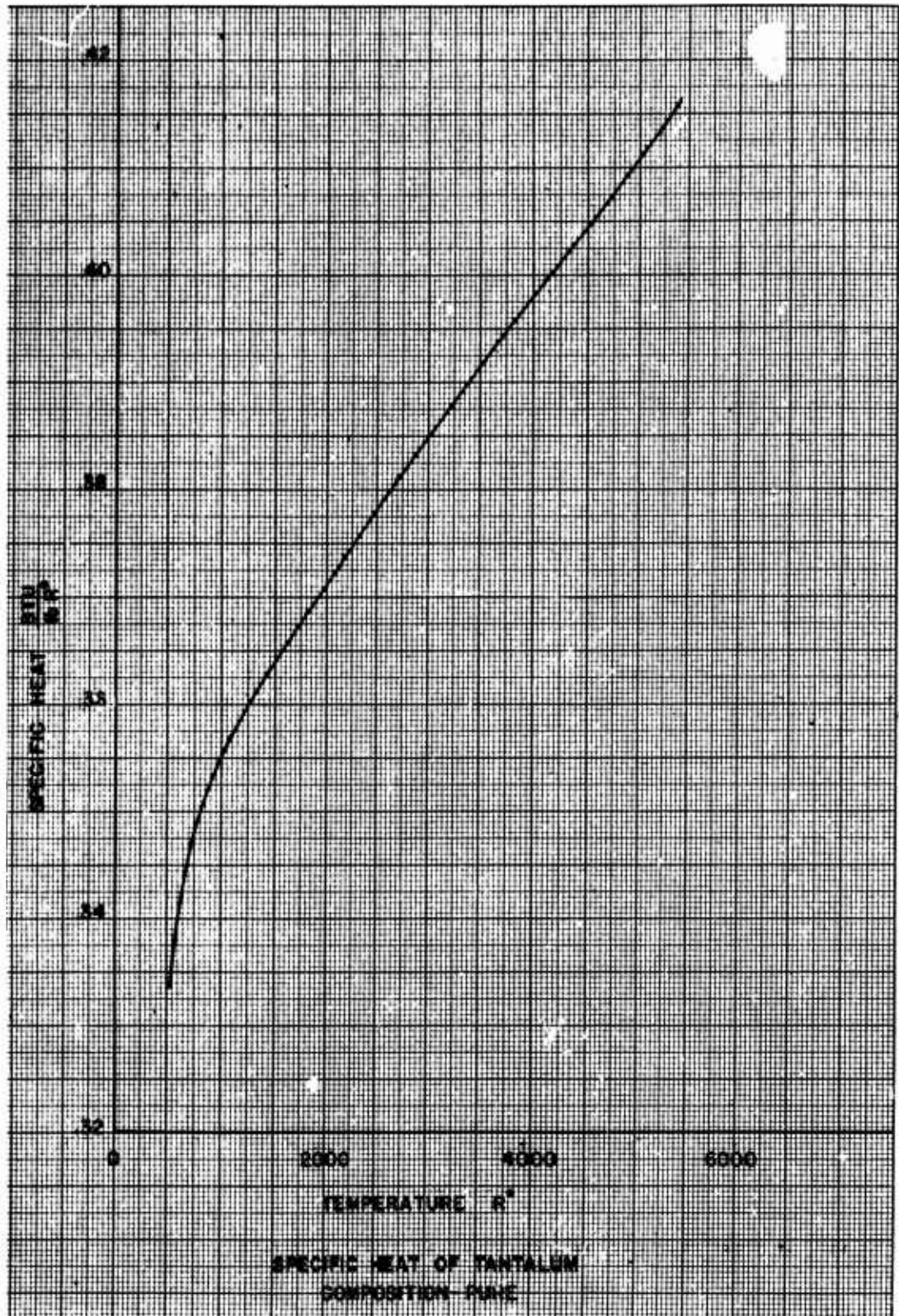
(2.4-61)m



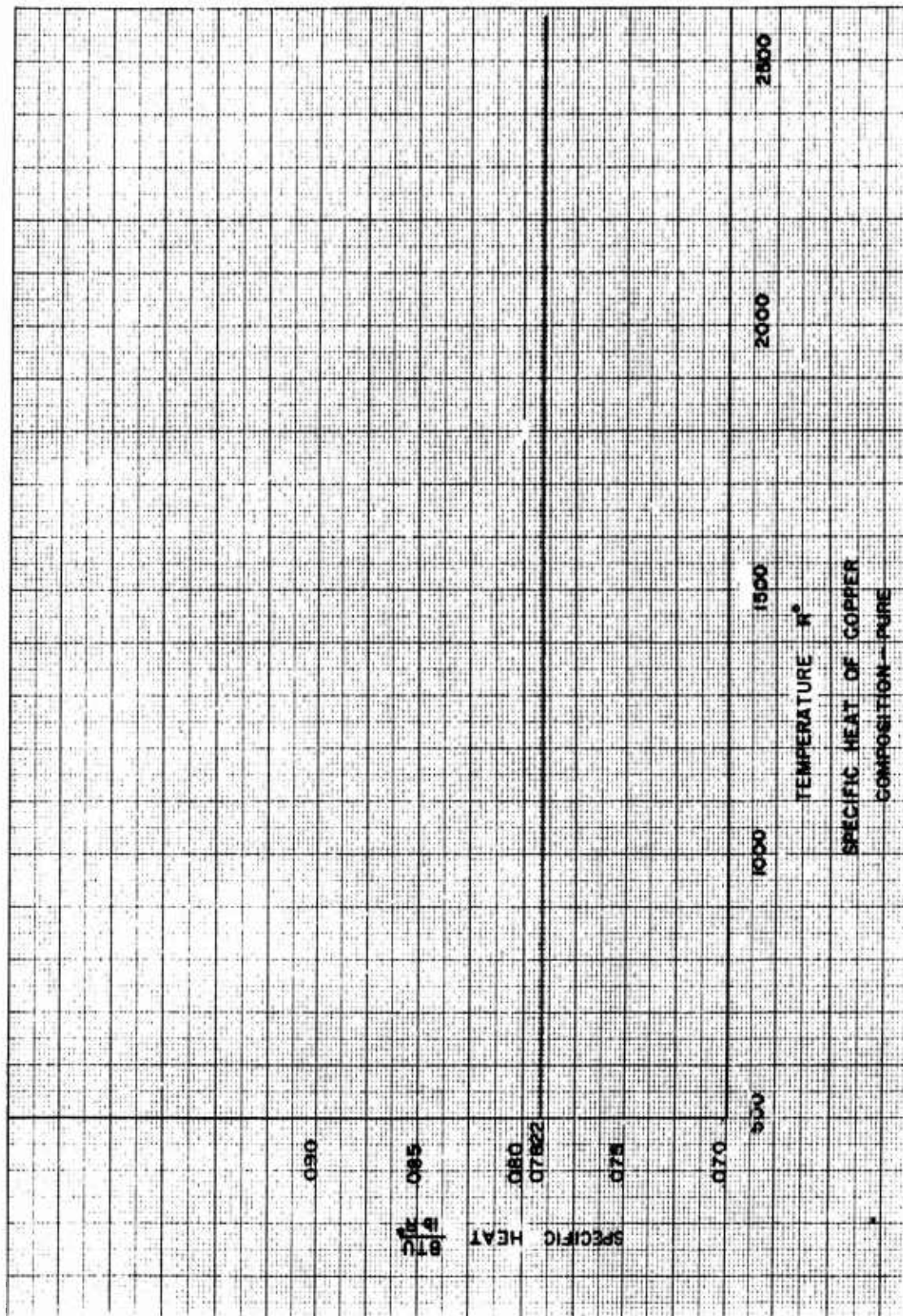
(2.4-61)n



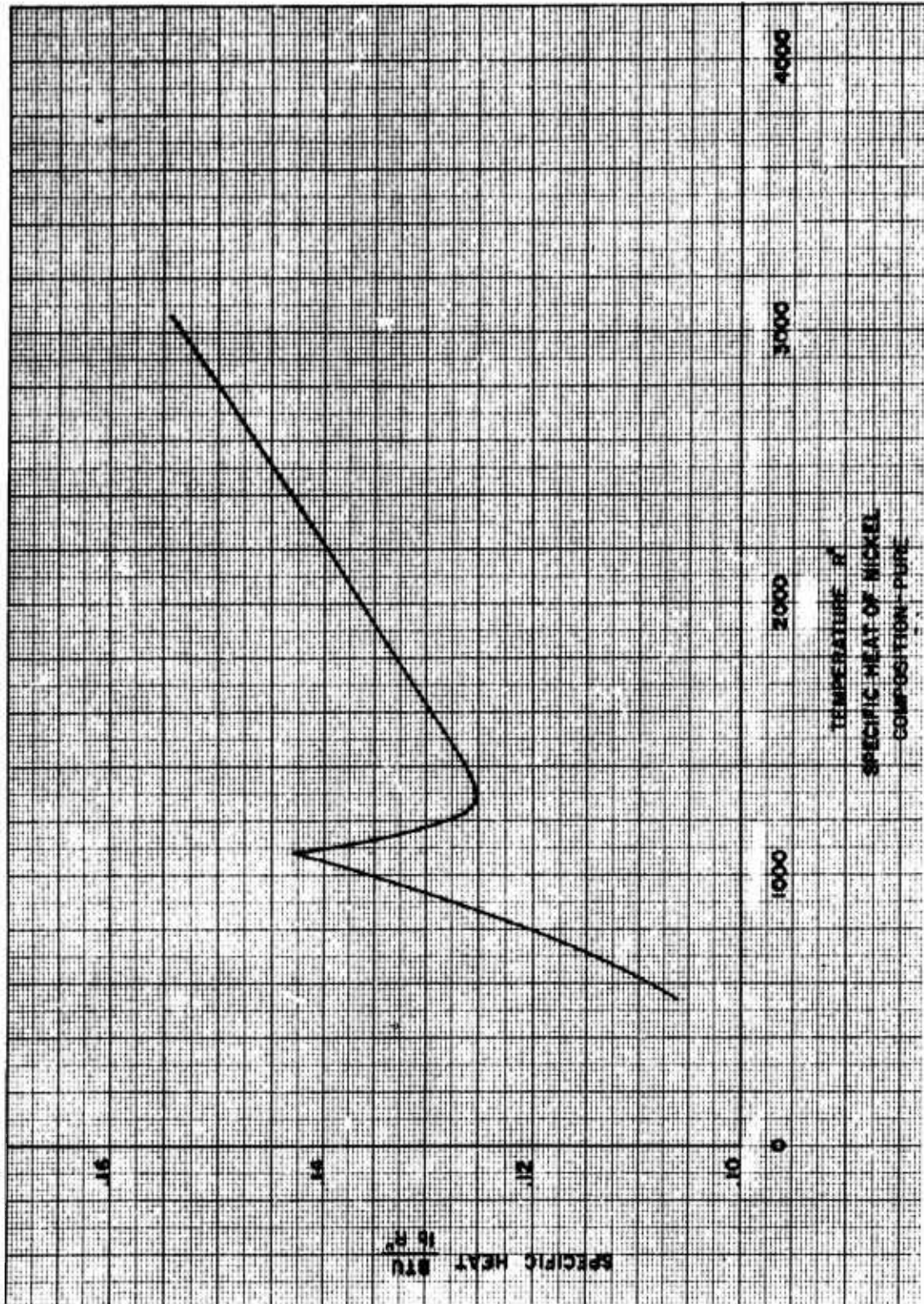
(2.4-61)°



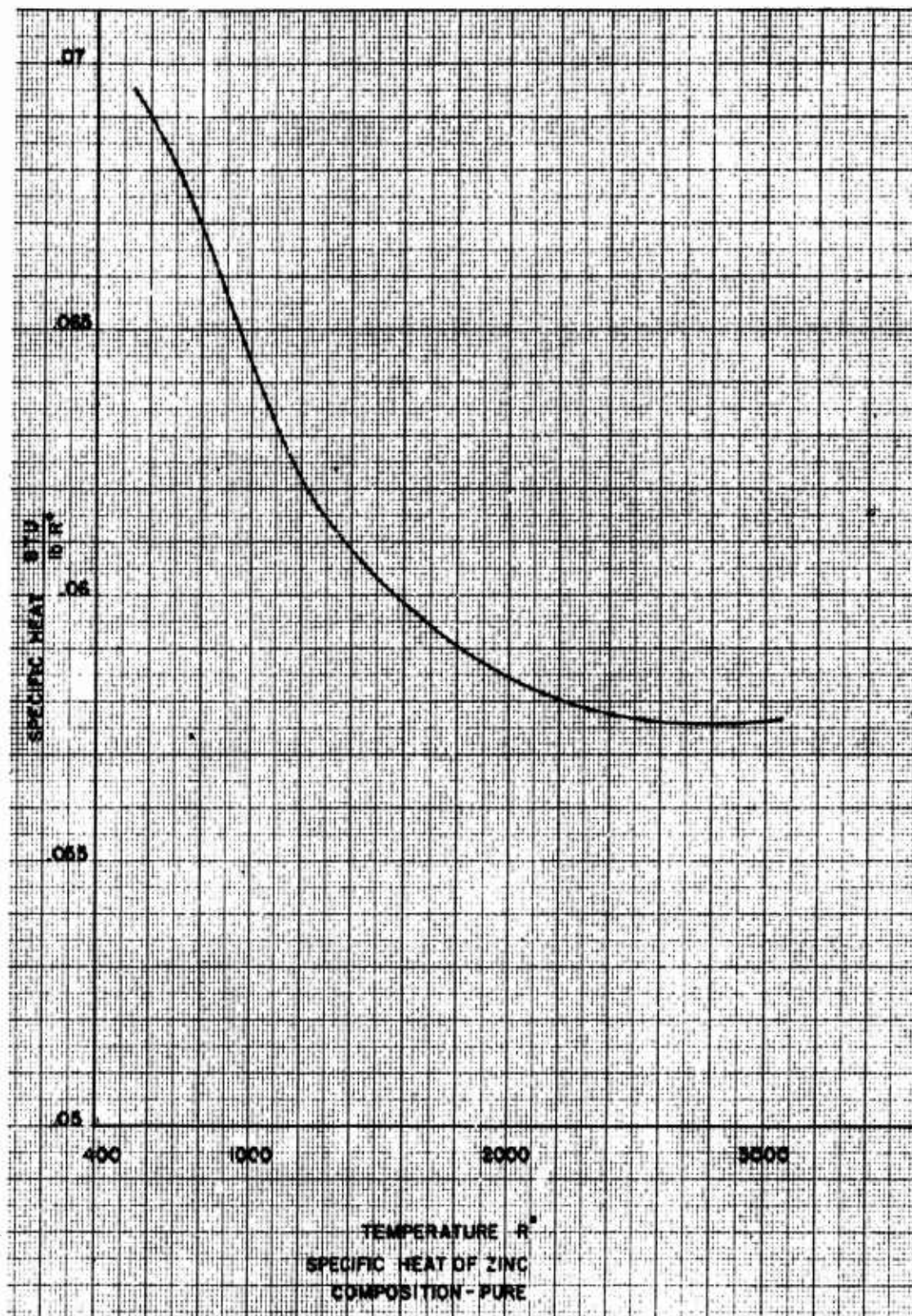
(2.4-61)p



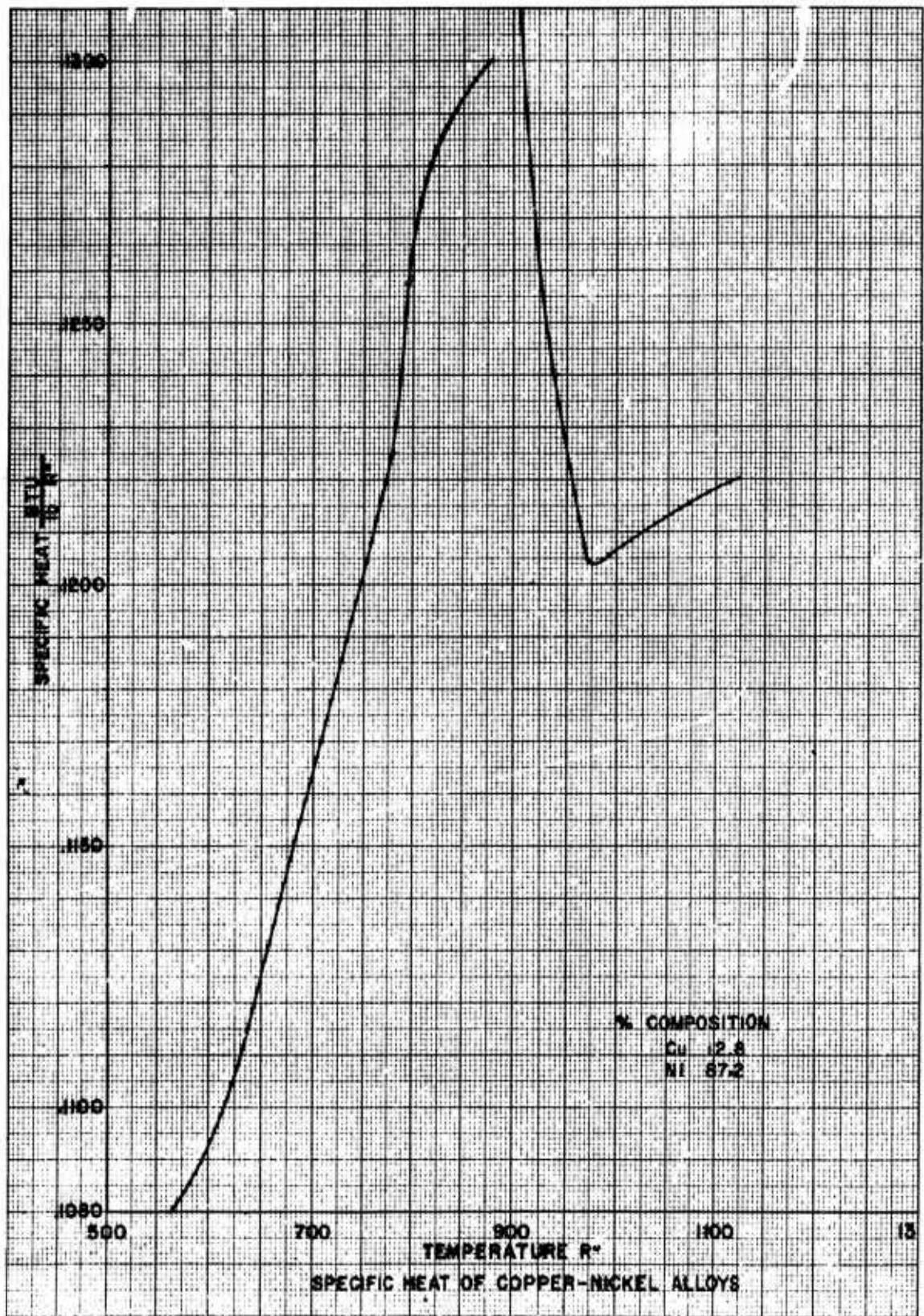
(2.4 - 61) q



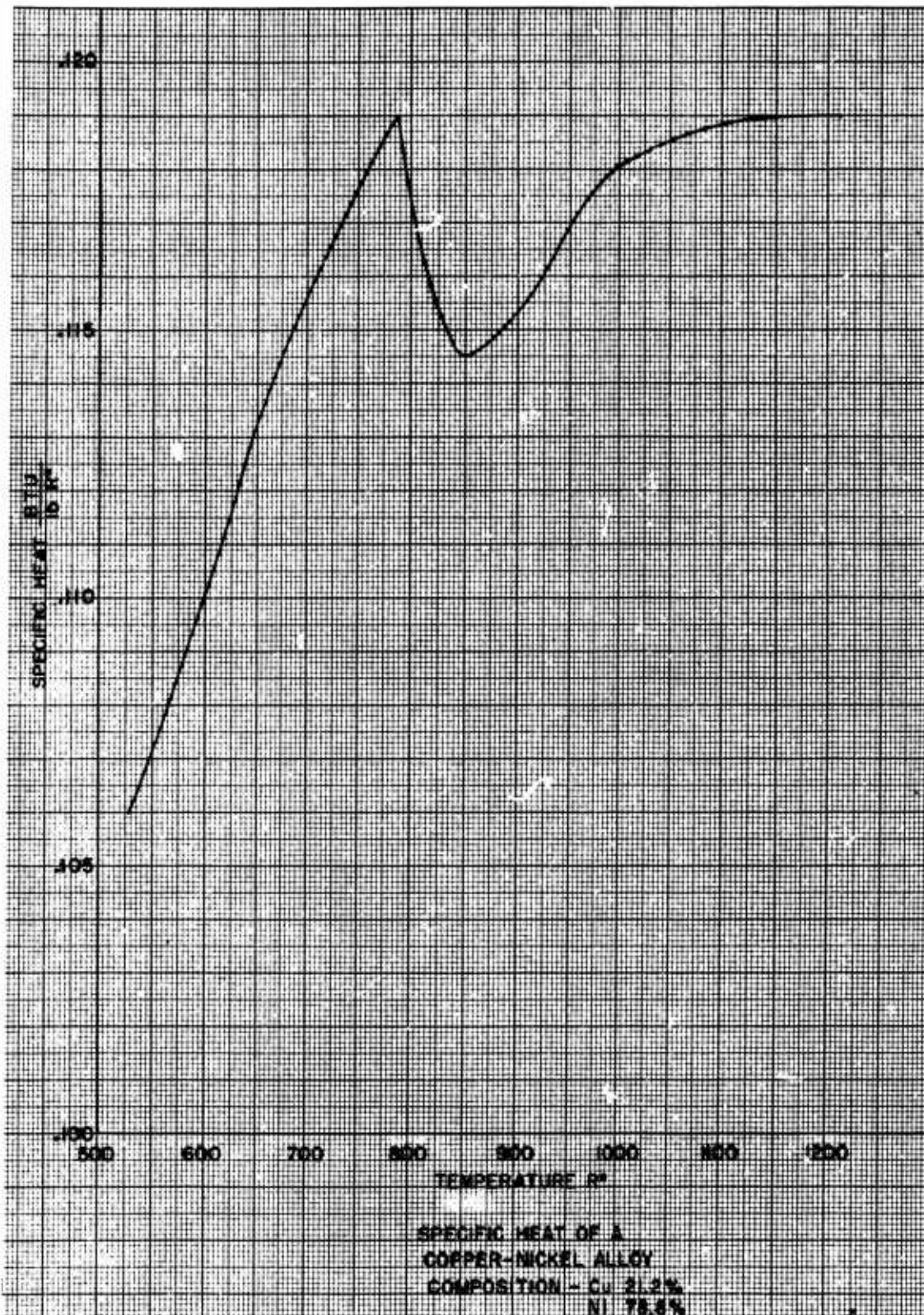
(2.4-61)r



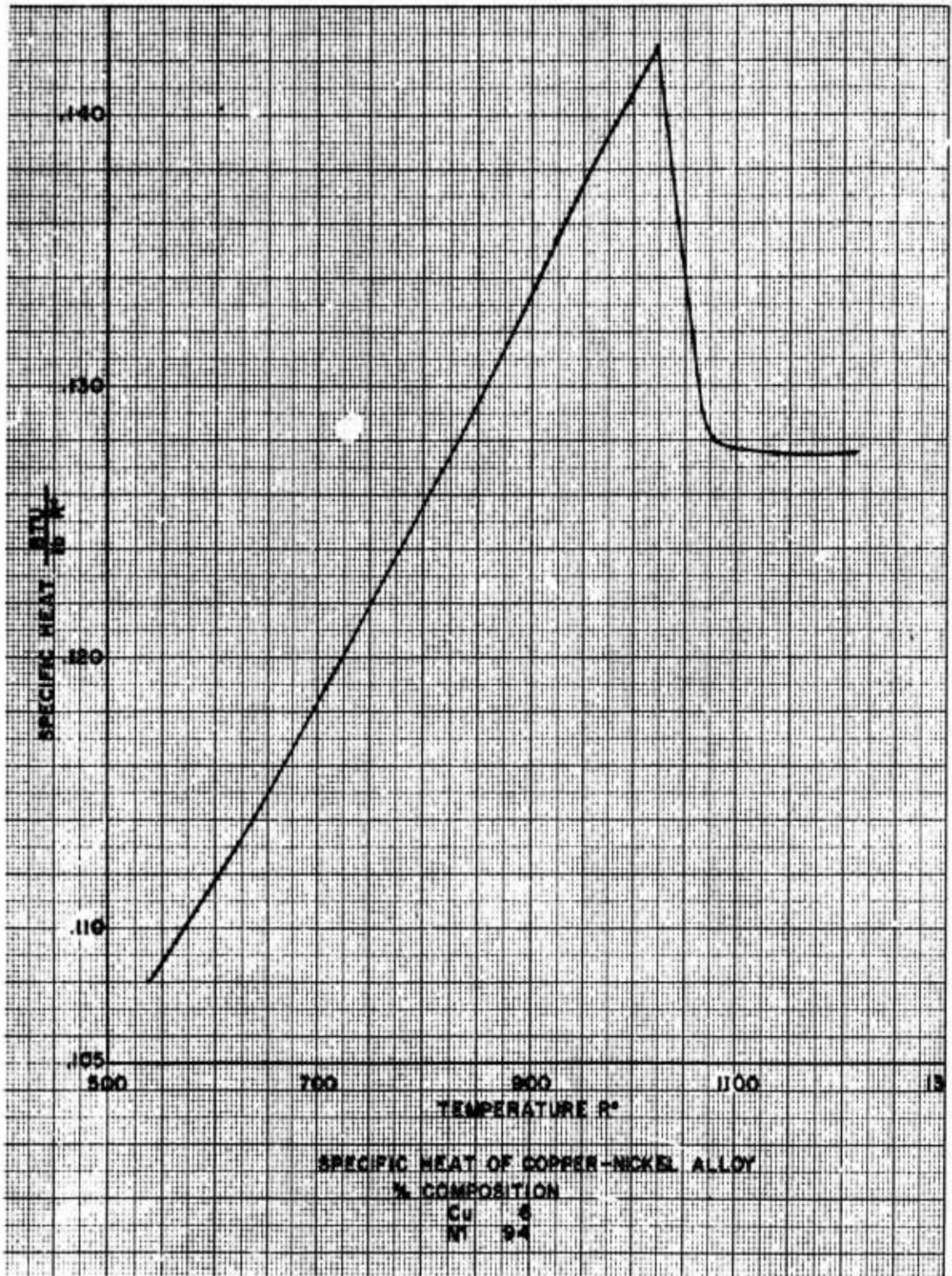
(2.4-61) s



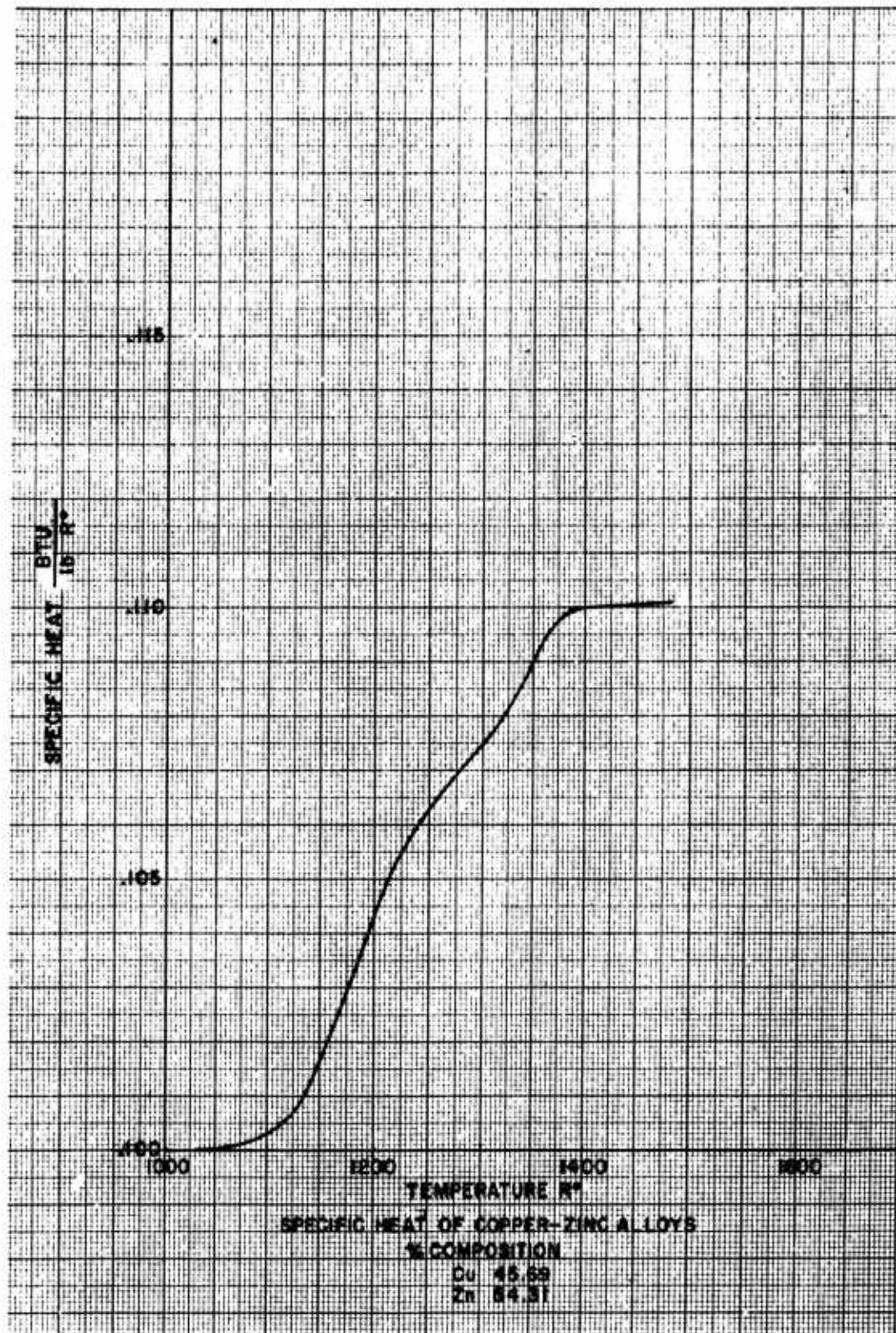
(2.4-61) †



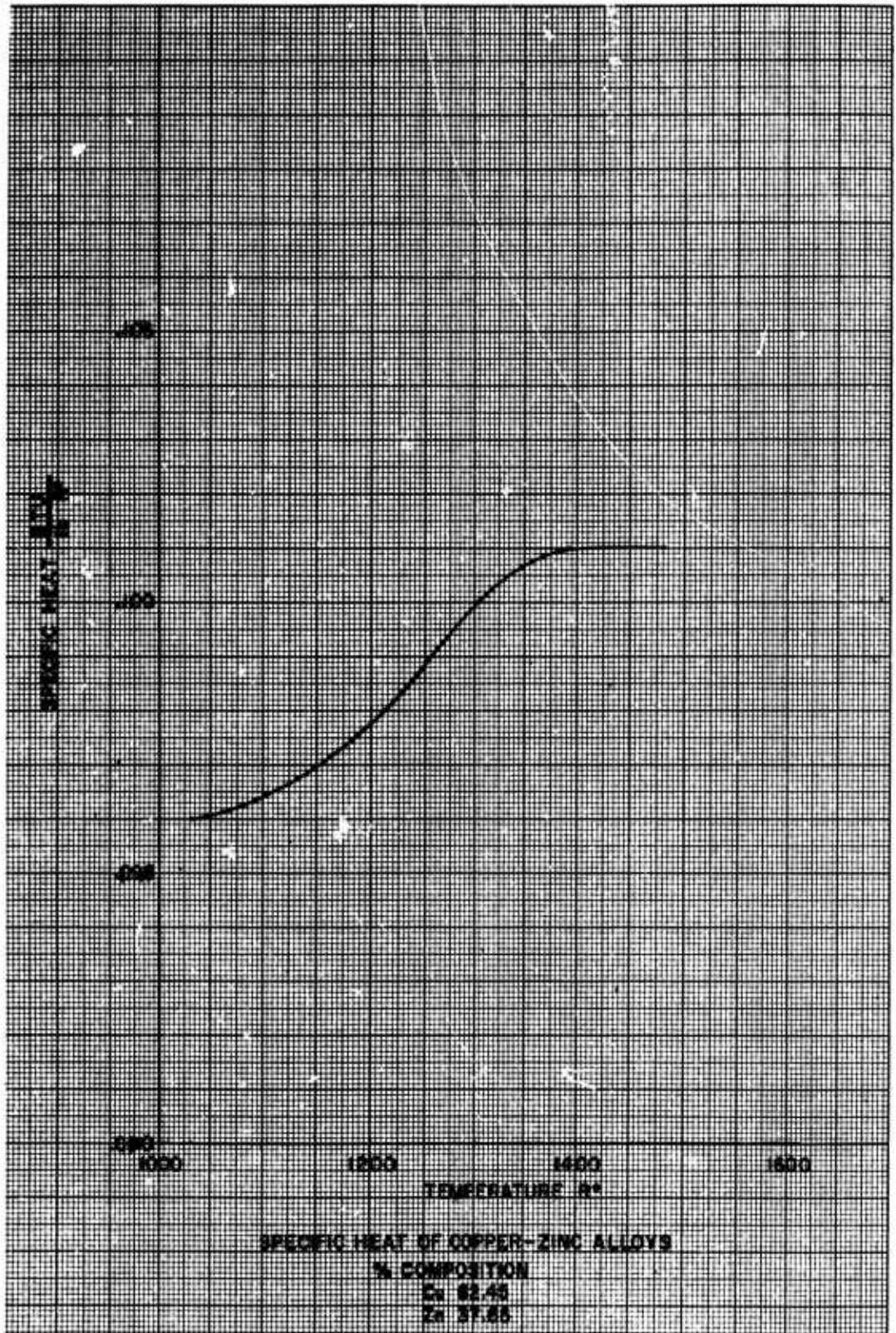
(2.4-61)u



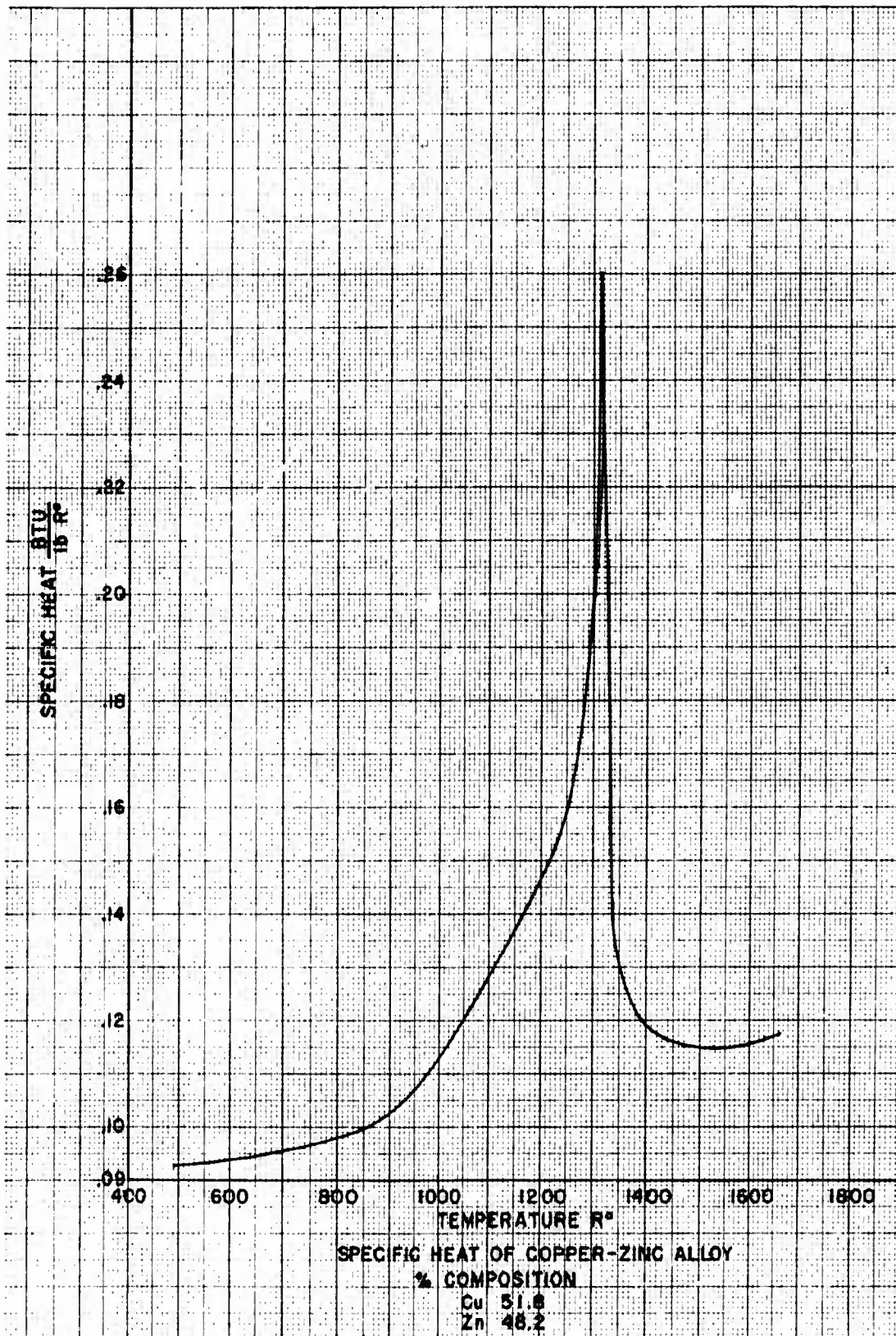
(2.4-61)v



(2.4-61)w



(2.4-61)r



(2.4-61)y

## 2.4.8 REFERENCES

- 2.4-1 Knudsen, M. The Kinetic Theory of Gases. Methuen and Co., Ltd., London, 1934.
- 2.4-2 Knudsen, M. "Die molekulare Wärmeleitung der Gase und der Akkomodations-koeffizient", Ann. Physik, Vol. 34, p. 593, (1911).
- 2.4-3 Smoluchowski, M. von, "Zur kinetischen Theorie der Transportation und Diffusion verdünnter Gase," Ann. Physik, Vol. 33, p. 1559, (1910)
- 2.4-4 Sanger, E. "The Gas Kinetics of Very High Flight Speeds," NACA Technical Memorandum, No. 1270, (1950)
- 2.4-5 Tsien, H. S. "Superaerodynamics, Mechanics of Rarefied Gases," J. Aero. Sci., Vol. 13, p. 653, (1946).
- 2.4-6 Ashley, H. "Applications of the Theory of Free Molecule Flow to Aeronautics," J. Aero. Sci., Vol. 16, p. 95, (1949).
- 2.4-7 Stalder, J. R. and Tukoff, D. "Heat Transfer to Bodies Travelling at High Speed in the Upper Atmosphere," NACA Tech. Report 944, (1949).
- 2.4-8 Stalder, J. R., Goodwin, G., and Creager, M. O. "A Comparison of Theory and Experiment for High Speed Free Molecule Flow," NACA Tech. Report 1032, (1951).
- 2.4-9 Oppenheim, A. K. "Generalized Theory of Convective Heat Transfer in a Free Molecule Flow," University of California, Institute of Engineering Research, HE-150-93, (1952).
- 2.4-10 Shaaf, S. A. "Theoretical Considerations in Rarefied Gas Dynamics," University of Michigan, Engineering Research Institute, Heat Transfer Symposium, (1953).
- 2.4-11 Epstein, P. S. Physics Rev., Vol. 23, p. 710.
- 2.4-12 Patterson, G. N. Molecular Flow of Gases John Wiley and Sons, 1956.
- 2.4-13 Maxwell, T. C. Collected Works, Cambridge University Press, (1890).
- 2.4-14 Herzfeld. "Hand und Jahrbuch der Chemischen Physics," Vol. 3, Pt. II, Section IV, Akad. Verlagsgesellschaft, Leipzig, 1949.
- 2.4-15 Wiedmann, M. L. "Trans. Am. Soc. Mech. Engrs., Vol. 68, p. 57, (1946).
- 2.4-16 Millikan, R. A. Phys. Rev., Vol. 21, p. 217, (1923).
- 2.4-17 Knudt, A. and Warburg, E. "On Friction and Thermal Conductivity in Rarefied Gases," Phil. Mag., Vol. 50, p. 53, (1875).
- 2.4-18 Berry, A. J., and Soddy, F. "Conduction of Heat Through Rarefied Gases," Proc. Roy. Soc., Vol. A83, p. 254, (1910).
- 2.4-19 Stalder, J. R., Goodwin, G., and Creager, M. O. "Heat Transfer to Bodies in a High Speed Rarefied Gas Stream," NACA Report 1093, (1952).
- 2.4-20 Wiedmann, M. L., and Trumpler, R. R. "Thermal Accommodation Coefficient," Trans. of A.S.M.E., Vol. 68, p. 57, (1946).
- 2.4-21 Hurlbut, F. C. "An Experimental Molecular Beam Investigation of the Scattering of Molecules from Surfaces," Ph.D. Thesis, Univ. of California, (1954).

- 2.4-22 Howard, W. E. (Ed), (Shaaf and Chambre, Section H.). "Fundamentals of Gas Dynamics," High Speed Aerodynamics and Jet Propulsion Series, Vol. III, Section H. Princeton University Press, 1958.
- 2.4-23 Oppenheim, A. K. J. Aero. Sci., Vol. 18, p. 49, (1953).
- 2.4-24 Sauer, F. M. J. Aero. Sci., Vol. 18, p. 353 (1951).
- 2.4-25 Hartee, D. R. Memo. and Proc. Manchester Lit. and Phil Soc., Vol. 80, p. 85 (1935).
- 2.4-26 Heineman, M. Commun. on Pure and Appl. Math., Vol. 1, p. 259, (1948).
- 2.4-27 Snow, R. M. "Aerodynamics in a Highly Attenuated Atmosphere," Appl. Phys. Lab., Johns Hopkins University, Rep. CM 336, (1946).
- 2.4-28 Ashley, H. J. Aero. Sci., Vol. 16, p. 95, (1949).
- 2.4-29 Stalder, J. R. and Zurick, V. T. "Theoretical Aerodynamic Characteristics of Bodies in a Free Molecule Flow Field," NACA TN 2423, (1951).
- 2.4-30 Garfunkel, I. M. "Generalizations of Applications of Free Molecule Flow," University of Michigan, Rep. EMB58.
- 2.4-31 Lees, L. and Probst, R. F. "Hypersonic Viscous Flow Over a Flat Plate," Princeton University, Aero. Engineering Dept., Rep. 195, (1952).
- 2.4-32 Lees, L. J. Aero. Sci., Vol. 20, p. 143, (1953).
- 2.4-33 Li, T. Y., and Nagamatsu, H. T. J. Aero. Sci., Vol. 20, p. 345, (1954).
- 2.4-34 Grad, H. Commun. on Pure and Appl. Math., Vol. 2, p. 331, (1949).
- 2.4-35 Nonweiler, T. "The Laminar Boundary Layer in Slip Flow," College of Aeronautics, Rep. 62, (1952).
- 2.4-36 Shaaf, S. A. "A Note on the Flat Plate Drag Coefficient," University of California, Institute of Engineering Research, HE-150-66 (1950).
- 2.4-37 Mirels, H. "Estimate of Slip Effect on Compressible Laminar Boundary Layer Skin Friction," NACA TN 2609, (1952).
- 2.4-38 Shaaf, S. A. and Shermann, F. S. "Skin Friction in Slip Flow," J. Aero. Sci., Vol. 21, p. 85, (1954).
- 2.4-39 Lin, T. C., and Shaaf, S.A. "Effect of Slip on Flow Near a Stagnation Point and in a Boundary Layer," NACA TN 2568, (1951).
- 2.4-40 Rayleigh, Lord, "On the Motion of Solid Bodies Through a Viscous Liquid," Phil. Mag., Vol. 21, p. 697, (1911).
- 2.4-41 Goldstein, S., (ed) Modern Developments in Fluid Dynamics, (p. 126). Oxford University Press, London, (1938).
- 2.4-42 Chapman, D. R. and Rubesin, M. W. "Temperature and Velocity Profiles in the Compressible Laminar Boundary Layer with Arbitrary Distribution of Surface Temperature," J. Aero. Sci., Vol. 16, p. 547, (1949)
- 2.4-43 Donaldson, C. du P. "An Approximate Method for Estimating the Incompressible Laminar Boundary Layer Characteristics on a Flat Plate in Slipping Flow," NACA R.M. L9C02, (1949).

- 2.4-44 Maslen, S. A. "Second Approximation to Laminar Boundary Layer Flow on Flat Plates in Slip Flow," NACA TN 2818, (1952).
- 2.4-45 Martino, R. L. "Heat Transfer in Slip Flow," Univ. of Toronto, Inst. Aerophys., Rept. 35, (1955).
- 2.4-46 Janour, Z. "Resistance of a Plate in Parallel Flow at Low Reynolds Numbers," NACA TM 1316, (1951).
- 2.4-47 Laurmann, T. A. "Experimental Investigation of the Flow About the Leading Edge of a Flat Plate," Univ. of Calif. Inst. Engrg. Research, Rept. HE-150-126, (1954).
- 2.4-48 Basset, A. B. "Hydrodynamics" Deighton, Bell and Co., Cambridge, (1888).
- 2.4-49 Goldbert, R. "The Flow of a Rarefied Perfect Gas Past a Fixed Spherical Obstacle" Ph.D. Thesis, New York Un., (1954).
- 2.4-50 Millikan, R. A. Phys. Rev., Vol. 22, No. 1, (1923).
- 2.4-51 Kane, E. D. J. Aero. Sci., Vol. 18, p. 259, (1951).
- 2.4-52 Drake, R. M. and Backer, G. H. Trans. Am. Soc. Mech. Engrs., Vol. 74, p. 1241, (1952).
- 2.4-53 Eberley, D. K. "Forced Convection Heat Transfer From Spheres to a Rarefied Gas," Univ. of California Inst. Engrg. Research, Rept. HE-150-140, (1956).
- 2.4-54 Kavanau, L. L. Trans. Am. Soc. Mech. Engrs., Vol. 77, p. 617, (1955).
- 2.4-55 Mack, S. F., and Shaaf, S. A. "Viscous Effects on Stagnation Point Temperatures," Univ. of Calif, Inst. Engrg. Research, Rept. HE-150-96, (1951).
- 2.4-56 Kovasznay, L. S. G., and Tormarck, S. I. A. "Heat Loss of Hot Wires in Supersonic Flow," Johns Hopkins Univ. Aeronaut. Dept., Bumblebee Rept. 127, (1950).
- 2.4-57 Laufer, I. and McClellan, R. "Equilibrium Temperature and Heat Transfer Characteristics of Hot Wires in Supersonic Flow", Guggenheim Aeronaut. Lab., Calif. Inst. of Technology. External Rept. 315, (1956).
- 2.4-58 Talbot, L. "Viscosity Corrections to Cone Probes in Rarefied Supersonic Flow at a Nominal Mach Number of 4," NACA TN 3219, (1954).
- 2.4-59 Probstein, R. F. and Elliott, D., "The Transverse Curvature Effects in Compressible Axially-Symmetric Laminar Boundary Layer Flow," J. Aero. Sci., Vol. 28, p. 208, (1956).
- 2.4-60 Ipsen, D. C. "Cone Drag in a Rarefied Gas Flow," Ph.D. Thesis, Un. of Calif., (1953).
- 2.4-61 Drake, R. M. and Maslach, G. T. "Heat Transfer From Right Circular Cones to a Rarefied Gas in Supersonic Flow," Univ. of Calif. Inst. Engrg. Research, Rept. HE-150-91, (1952).
- 2.4-62 Kavanau, L. L. J. Aero. Sci., Vol. 21, p. 257, (1954).
- 2.4-63 Kavanau, L. L. "Base Pressure Studies in Rarefied Supersonic Flow," J. Aero. Sci., Vol. 23, p. 193, (1956).

- 2.4-64 Bogdonoff, S. M. J. Aero. Sci., Vol. 19, p. 201, (1952).
- 2.4-65 Ipsen, D. C. Units, Dimensions and Dimensionless Numbers, McGraw-Hill Book Company, Inc. New York, 1960.
- 2.4-66 Prandtl, L. "Essentials of Fluid Dynamics," Blackie and Sons, Ltd., 1960, London, England.
- 2.4-67 Stalder, J. R. and Jukoff, D. "Heat Transfer to Bodies Traveling at High Speed in the Upper Atmosphere," NACA Rep. 944, 1949.
- 2.4-68 Aerodynamic Data Sheets, Royal Aeronautical Society, London, England, Vol. I, Vol. II and Vol. III.
- 2.4-69 Mangler, W. "Zusammenhang Zwischen ebener und rotations symmetrischen Grenzschichten in tompressiblen Flussigkeiten, Zamm, Vol. 28 (1948)p.7.
- 2.4-70 Truitt, R. W. Fundamentals of Aerodynamic Heating, The Ronald Press Company, 1960, New York 10, N.Y.
- 2.4-71 Mirels, H. "Flat Plate Laminar Skin Friction and Heat Transfer in the Free Molecule to Continuum Flow Regimes." Jet Propulsion, October, 1958.
- 2.4-72 Keenan, J. H. and Kaye, J. Thermodynamic Properties of Air. John Wiley and Sons, Inc., New York (1945).
- 2.4-73 Van Driest, E. R. "Investigation of Laminar Boundary Layer in Compressible Fluids Using the Crocco Method," NACA TN 2597, January, 1952.
- 2.4-74 Kuethe, A. M. and Scnetzer, T. D. Foundations of Aerodynamics. John Wiley and Sons, Second Edition, New York, New York, 1959.

**BLANK PAGE**

TABLE OF CONTENTS

Section 2.5 Inviscid and Viscous Pressure Drag,  
Exclusive of Base Drag

SUBSECTION	PAGE
LIST OF FIGURES	2.5-iii
LIST OF TABLES	2.5-vi
LIST OF SYMBOLS	2.5-vii
2.5.1 Introduction	2.5-1
(i) Inviscid Pressure Drag on Bodies at Supersonic and Hypersonic Speeds - Theoretical References	2.5-1
(ii) Inviscid Pressure Drag on Bodies - Practical Considerations For Use of Various Data	2.5-2
(1) High Fineness Ratio Slender Bodies of Circular Cross-Section With Boattails, at a Zero Angle of Attack	2.5-2
(2) Cones at a Zero Angle of Attack	2.5-3
(3) Cone-Cylinder Combinations at $M=1$	2.5-3
(4) Ogives at a Zero Angle of Attack	2.5-7
(5) Bodies of Revolution For Least Pressure Drag at a Zero Angle of Attack	2.5-7
(iii) Inviscid Pressure Drag on Wings and Fins	2.5-12
(1) Two Dimensional Theories	2.5-12
(2) Three Dimensional Supersonic Wing Theories	2.5-12
(iv) Wing-Body Interference Drag	2.5-17
(v) Viscous Form Drag	2.5-18
(vi) Boundary Layer - Shock Wave Interaction	2.5-18
(vii) Leading Edge Bluntness Effects	2.5-18
2.5.2 The Basic Expression for the Total Zero Lift Pressure Drag Coefficient (Exclusive of Base Drag)	2.5-21
2.5.3 The Expressions and the Data for the Body Pressure Drag Coefficient Estimates	2.5-22
(i) Inviscid Forebody Pressure Drag	
(1) Cones at Supersonic Speeds, Zero Angle of Attack	2.5-22
(2) Ogives at Supersonic Speeds, Zero Angle of Attack	2.5-22
(3) Minimum Drag Forebodies at Supersonic Speeds, Zero Angle of Attack	2.5-22
(4) Cone-Cylinder and Parabolic Tangent Ogive Pressure Drag at $M=1$	2.5-22
(5) Forebody Bluntness Effects	2.5-23
(ii) Inviscid Afterbody Pressure Drag	2.5-23
(1) Truncated Conical Afterbodies of Circular Cross-Section	2.5-23
(2) Truncated Parabolic Afterbodies of Circular Cross-Section	2.5-23
(3) A Semiempirical Method for Inviscid Afterbody Pressure Drag Estimates	2.5-23
(4) Fin Interference Effects on Afterbody Pressure Drag $M=1$	2.5-24
(5) Forebody-Afterbody Inviscid Interference Drag	2.5-24
(iii) Viscous Form Drag	2.5-24
(iv) The Final Expression for the Body Zero-Lift Pressure Drag Coefficient at Supersonic Speeds	2.5-24
2.5.4 The Expressions and the Data for the Pressure Drag Coefficient Estimates on Wings and Fins	2.5-26
(i) Inviscid Pressure Drag	2.5-27

(ii)	Two-Dimensional Inviscid Plus Viscous Pressure Drag of Double Wedge, Double Symmetry Airfoil Sections	2.5-27
(iii)	Three-Dimensional Inviscid Plus Viscous Pressure Drag on Wings and Fins	2.5-28
	I. Straight Rectangular Planform Wings	2.5-28
	(I.1) Straight Rectangular Planform Wings With Double Wedge, Double Symmetry Airfoil, No Taper, Zero Angle of Attack	2.5-28
	(I.2) Straight Rectangular Planform Wings With Arbitrary Airfoil Section, No Taper, Zero Angle of Attack	2.5-29
	II. Delta Wing Planforms	2.5-30
	(II.1) Supersonic Delta Wing With Double Wedge Symmetric Airfoil	2.5-30
	(II.2) Supersonic Delta Wing With Arbitrary Airfoil Section	2.5-31
	III. Straight Tapered Wing Planforms	2.5-32
	(III.1) Straight Tapered Wings With Double Wedge, Double Symmetry Airfoil Section	2.5-32
	(III.2) Straight Tapered Wings With Arbitrary Airfoil Sections	2.5-32
	IV. Clipped Delta Wing Planforms	2.5-32
	(IV.1) Clipped Delta Wing With Double Wedge, Double Symmetry Airfoil Section	2.5-32
	(IV.2) Clipped Delta Wing With Arbitrary Airfoil Sections	2.5-32
	V. Straight Swept-Back No Taper Wings	2.5-32
(iv)	Wing-Body Interference Drag	2.5-33
(v)	Viscous Form Drag	2.5-33
(vi)	Leading Edge Bluntness Effects	2.5-33
(vii)	The Final Expression for the Wing and Fin Zero-Lift Pressure Drag at Supersonic Speeds	2.5-34
2.5.5	Instructions for Use of the Proposed Methods for the Total Zero Lift Pressure Drag Coefficient Estimates (Exclusive of Base Drag)	2.5-77
	(i) Basic Data Preparation	2.5-77
	(1) List of Working Graphs for Body Pressure Drag	2.5-77
	(a) Supersonic Speeds	2.5-77
	(b) Mach Number $M=1$	2.5-77
	(2) List of Working Graphs for Wing (or Fin) Pressure Drag	2.5-77
	(a) Inviscid Pressure Drag	2.5-77
	(b) Viscous Pressure Drag	2.5-77
	(c) Leading Edge Bluntness Drag	2.5-77
	(3) The Proposed Method for the Total Zero Lift Pressure Drag Estimates (Exclusive of Base Drag)	2.5-78
2.5.6	References	2.5-92

## LIST OF FIGURES

Section 2.5 Inviscid and Viscous Pressure  
Drag Exclusive of Base Drag

FIGURE	TITLE	PAGE
2.5-1	Drag coefficients of cones at supersonic speeds, Ref. (2.5-18)	2.5-4
2.5-2	Correlation of drag coefficients of cones at supersonic speeds by hypersonic similarity parameter, Ref. (2.5-18).	2.5-5
2.5-3	Accuracy of various methods for estimating pressure drag of nonslender missile noses at zero angle of attack, Ref. (2.5-20)	2.5-6
2.5-4	Variation of pressure drag coefficient with thickness ratio for a cone-cylinder at Mach Number 1, Ref. (2.5-19)	2.5-8
2.5-5	Variation of pressure drag coefficient with thickness ratio for the front half of a parabolic-arc body at Mach Number 1, Ref. (2.5-20)	2.5-9
2.5-6	Correlation curves for drag of cones and tangent ogives on basis of hypersonic similarity parameter, Ref. (2.5-31)	2.5-10
2.5-7	Pressure distribution on ogival forebodies at zero angle of attack (Ref. 2.5-1), R.A.S. Data Sheets, Aerodynamics, Vol. 1, Bodies, S.05.03.01	2.5-11
2.5-8	Comparison of shape of von Karman ogive with that of a Newtonian body of least pressure drag, Ref. (2.5-18)	2.5-13
2.5-9	Comparison of profiles of minimum drag noses for given length and base diameter	2.5-14
2.5-10	Leading edge bluntness effect, a scheme for approximate estimates of $C_{DOPWLE}$ or $C_{DOPFLE}$	2.5-20
2.5-11	Supersonic flow past circular cones at zero angle-of-attack, Ref. (2.5-1) , R.A.S. Data Sheets, Aerodynamics, Vol. 1, S.00.03.13	2.5-35
2.5-12	Conditions for shock wave detachment and for subsonic flow behind nose shock waves on cones at zero angle-of-attack and on wedges, Ref. (2.5-1), R.A.S. Data Sheets, Aerodynamics, Vol. 1, S.00.03.06	2.5-36
2.5-13	Drag increase of ogives, as a function of similarity parameter, $K$ , Ref. (2.5-31)	2.5-37
2.5-14	Variation of wave drag parameter, $C_{DOPN}(q/p)$ , with the similarity parameter for the minimum drag nose shapes of specified length and diameter	2.5-38
2.5-15	Pressure drag increase due to forebody tip-bluntness effects, zero angle-of-attack, Ref. (2.5-1), R.A.S. Data Sheets, Vol. 1, Bodies S.02.03.06	2.5-39

2.5-16	Inviscid pressure drag on truncated conical afterbodies of circular section at zero angle-of-attack, Ref. (2.5-1), R.A.S. Data Sheets, Aerodynamics, Vol. 1, Bodies S.02.03.04	2.5-40
2.5-17	Inviscid pressure drag on truncated parabolic (or circular arc) afterbodies of circular section at zero angle-of-attack, Ref. (2.5-1) R.A.S. Data Sheets, Aerodynamics, Vol. 1, Bodies S.02.03.05	2.5-41
2.5-18	Determination of the functional relationship $\frac{D_B}{D} = f\left(\frac{L_{BT}}{D}\right)$ for given value $\Theta_p$	2.5-42
2.5-19	Pressure drag coefficient for boattails as a function of boattail base angle, $\Theta_p$ , $D_B / D$ , and Mach Number. See Tables (2.5-3) and (2.5-4), Ref. (2.5-60)	2.5-43
2.5-20	Forebody-afterbody inviscid interference pressure drag for pointed conical forebodies and afterbodies with midbodies, zero angle-of-attack, Ref. (2.5-1), R.A.S. Data Sheets, Aerodynamics, Vol. 1, S.02.03.08	2.5-50
2.5-21	Forebody-afterbody inviscid interference pressure drag for pointed parabolic forebodies and afterbodies with midbodies, zero angle-of-attack, Ref. (2.5-1), R.A.S. Data Sheets, Aerodynamics, Vol. 1, Bodies, S.02.03.10	2.5-53
2.5-22	Graphs and tables of limiting value of inclination of an element of surface to the wind, at various Mach Numbers. The front shock wave will be attached to the leading edge only if no part of the wing surface facing forward exceeds this limiting value, Ref. (2.5-3)	2.5-54
2.5-22a	Variation of Busemann coefficients with Mach Number, Ref. (2.5-3)	2.5-55
2.5-23	Corrective factor for viscous form drag effects, turbulent b.l.	2.5-56
2.5-24	Van Driest's Law for turbulent boundary layer thickness ratio $\delta / \delta_l$ versus Mach Number, $M_\infty$ , Ref. (2.5-63)	2.5-57
2.5-25	$\beta = (M_\infty^2 - 1)^{1/2}$ versus	2.5-58
2.5-26	Effect on drag of chordwise shift of position of maximum thickness of double-wedge wing, Ref. (2.5-3)	2.5-59
2.5-27	Chart for determining pressure drag coefficient at zero lift, diamond airfoil section, Ref. (2.5-45)	2.5-60
2.5-28	Ratio of wing drag coefficients to thickness ratio squared for several aspect ratios as a function of Mach Number. Rectangular planform, Ref. (2.5-45)	2.5-61
2.5-29	Ratio of wing drag coefficients to thickness ratio squared for several aspect ratios as a function of Mach Number. Diamond planform, Ref. (2.5-45)	2.5-62
2.5-30	Drag of delta wings with supersonic leading edge parameter "n" measures the shape of the wing and the Mach Number; parameter "r" measures the position of maximum thickness, Ref. (2.5-43).	2.5-63

2.5-31	Drag of delta wings at zero lift, showing useful working range, Ref. (2.5-69)	2.5-64
2.5-32	Ratio of three-dimensional pressure drag coefficient to its two-dimensional value for straight tapered wings, Ref. (2.5-69)	2.5-65
2.5-33	Ratio of three-dimensional pressure drag coefficient to its two-dimensional value for clipped delta wings; linearized theory, Ref. (2.5-69)	2.5-66
2.5-34	Inviscid pressure drag of wings with constant chord, constant spanwise thickness-chord ratio, double-wedge sections, no taper, maximum thickness at $0.5 \bar{c}$ , Ref. (2.5-1) R.A.S. Data Sheets, Aerodynamics, Vol. 2, Wings, S.02.03.01	2.5-67
2.5-35	Inviscid pressure drag of wings with constant chord, constant spanwise thickness-chord ratio, parabolic arc sections, no taper, Ref. (2.5-1), R.A.S. Data Sheets, Aerodynamics, Vol. 2, Wings, S.02.03.01	2.5-68
2.5-36	Inviscid pressure drag of wings with constant chord, constant spanwise thickness-chord ratio, double-wedge sections, no taper, maximum thickness at $0.3 \bar{c}$ , Ref. (2.5-1), R.A.S. Data Sheets, Aerodynamics, Vol. 2, Wings, S.02.03.01.	2.5-69
2.5-37	Leading edge pressure drag due to leading edge bluntness, two-dimensional sections at zero angle-of-attack, Ref. (2.5-1), R.A.S. Data Sheets, Aerodynamics, Vol. 2, Wings, S.02.03.05	2.5-70

## LIST OF TABLES

Section 2.5 Inviscid and Viscous Pressure Drag, Exclusive of Base Drag

TABLE	TITLE	PAGE
2.5-1	Coordinates of bodies of least wave drag. See Figs. (2.5-8) and (2.5-9)	2.5-15
2.5-2	Illustration of respective accuracies of various theoretical methods of calculating inviscid pressure drag on two-dimensional airfoils, Ref. (2.5-1).	2.5-16
2.5-3	Relations between boattail base angle, $D_B/D$ , and $L_{AFTERBODY} / D$ . See Fig. (2.5-19)	2.5-71
2.5-4	Higher order Busemann coefficients. See Fig. (2.5-19) and (2.5-22)	2.5-72
2.5-5	Analytical expressions and related graphs for pressure drag-coefficient estimates on wings (fins) at supersonic speeds, including viscous form drag	2.5-79
2.5-6	Total pressure drag coefficient, evaluation of two-dimensional corrective factor for various profile shapes.	2.5-82
2.5-7	Total pressure drag coefficient, straight rectangular wing planforms	2.5-83
2.5-8	Alternative method of computing factor $A \times B = 70$ from direct readings of Figs. (2.5-27).	2.5-84
2.5-9	Total pressure drag coefficient, delta wing planforms	2.5-85
2.5-10	Total pressure drag coefficient, straight tapered wing planforms.	2.5-85
2.5-11	Total pressure drag coefficient, straight, swept-back, no taper wing planforms	2.5-86
2.5-12	Pressure drag coefficient due to leading-edge bluntness	2.5-87
2.5-13	Summary of wing (or fin) total pressure drag results as computed in tables (2.5-7) to (2.5-12)	2.5-88
2.5-14	Total pressure drag coefficient on bodies of revolution, circular cross-section, estimates using figure set "A"	2.5-89
2.5-15	Total pressure drag coefficient on bodies of revolution, circular cross-section, estimates using figure set "B"	2.5-90
2.5-16	Total pressure drag force of a missile configuration	2.5-91

LIST OF SYMBOLS

Section 2.5 Inviscid and Pressure Drag,  
Exclusive of Base Drag,

I. GEOMETRY

- AR - Aspect ratio,  

$$AR = \frac{b^2}{S}$$
- b - Span, ft.
- c - Local chord, ft.
- $\bar{c}$  - Mean geometric or aerodynamic chord, ft.
- $c_r$  - "Root" chord of the exposed wing or fin (i.e., at the wing-body juncture, or the fin-body juncture), ft.
- $c_t$  - Tip chord, ft.
- D - Reference body diameter; maximum diameter of missile body, ft.
- d - Local diameter, ft.
- $L_{BT}$  - Length of the boattail body section, ft.
- $L_{CYL}$  - Length of the cylindrical body section, ft.
- $L_N$  - Nose section length, ft.
- $n = \frac{\tan \Delta_0}{\beta}$  - Factor, delta planform.
- $R_{BL}$  - Leading edge bluntness radius, ft.
- $r = \frac{(x)t/c}{\bar{c}}$  - Position of airfoil maximum thickness in fractions of its mean geometric chord.
- $r = \frac{\tan \Delta_1}{\tan \Delta_0}$  - Geometric factor of delta wings.
- $S_{WET}$  - Wetted area of missile part, sq. ft.
- $S_{WEXP}$  - Total exposed wing planform area, ft.<sup>2</sup>  
 $S_{WEXP} = b_{WEXP} \bar{c}_{WEXP}$
- t - Airfoil thickness, ft.
- (t/c) - Airfoil thickness ratio, nondimensional.
- x - Longitudinal distance, ft.
- $\alpha$  - Angle of attack, degrees.
- $\theta_B$  - Boattail angle, degrees.
- $\theta_B^\circ$  - Conical afterbody semi-apex, degrees. For parabolic frustrum afterbodies, semi-apex angle of an inscribed cone.
- $\theta_N$  - Cone vertex angle; inscribed cone vertex angle for ogives; degrees.
- $\theta_p^\circ$  - Angle between the tangent and the center line at the base of a parabolic afterbody frustrum, degrees.  $\theta_p = 2\theta_B$

A - Angle of sweep-back, degrees.

$\lambda$  - Taper ratio, nondimensional.

$$\lambda = \frac{C_f}{C_r}$$

$\mu$  - Angle, defined by  $\tan \mu = \cot m = \beta = (M_\infty^2 - 1)^{1/2}$  for delta planforms.

## II. PHYSICAL

$C_p$  - Average pressure coefficient due to normal momentum component of both the impinging and the re-emitted molecules, dimensionless. Obtained by integration of  $(C_p')$  on the surface (A).

$C_p$  - Specific heat coefficient of a gas at a constant pressure, BTU per slug °F.

$\kappa$  - Maximum diameter location coefficient.

M - Mach Number, nondimensional; a similarity parameter,

$$M = \frac{V}{a}$$

$p$  - Static pressure; local static pressure, lb./sq.ft.

$p_H$  - Static pressure "at infinity" at a given altitude H ft., Standard Atmosphere, lb./sq.ft.

$p_\infty$  - Same as  $p_H$ .

$q_H$  - Reference dynamic pressure, referred to conditions "at infinity" at a given altitude H ft., Standard Atmosphere,

$$q_H = \left( \frac{\rho V^2}{2} \right)_H = \frac{1}{2} (\gamma \rho M^2)_H \text{ lb./sq. ft.}$$

$q_\infty$  - Same as  $q_H$ .

Re - Reynolds Number, nondimensional; a similarity parameter,

$$Re = \frac{VL}{\nu}$$

T - Local static temperature at any point, °R.

$\beta$  - Glauert's (similarity) parameter,  $\beta = (M_\infty^2 - 1)^{1/2}$  for supersonic speeds,  $\beta = (1 - M_\infty^2)^{1/2}$  for subsonic speeds.

$\gamma$  - Specific heat ratio, nondimensional,  $\gamma = \frac{C_p}{C_v} = 1.40$  for air, Standard Sea-Level conditions.

$\delta$  - Local boundary layer thickness, ft.

$\rho$  - Air density, slug/ft.<sup>3</sup>

a - Speed of sound, ft./sec.

$C_D$  - Drag force coefficient, nondimensional, referred to the common reference area,  $S_r$ , and the flow conditions at "infinity", Standard Atmosphere at each flight altitude, H:

$$C_D = \frac{\text{Drag Force}}{q_H S_r}$$

$C_{D0}$  - Zero-lift drag force coefficient, nondimensional, referred to the common reference area,  $S_r$ , and the flow conditions at "infinity", Standard Atmosphere at each flight altitude, H:

$$C_{D0} = \frac{\text{Zero-Lift Drag Force}}{q_H S_r}$$

$C_{D0b}$  - Zero-lift base pressure drag force coefficient, nondimensional, referred to the common reference area,  $S_r$ , and the flow conditions at "infinity", Standard Atmosphere at each flight altitude, H:

$$C_{D0b} = (-C_{pb}) \left( \frac{S_{BASE}}{S_r} \right)$$

$C_{D0p}$  - Zero-lift pressure drag force coefficient, (exclusive of base drag), nondimensional, referred to the common reference area,  $S_r$ , and the flow conditions at "infinity", Standard Atmosphere at each flight altitude, H:

$$C_{D0p} = (C_p) \left( \frac{S_{EXP}}{S_r} \right) \cos(V_H, n) \approx \frac{\iint_{S_{EXP}} p \cos(V_H, n) dS}{q_H S_{EXP}} \left( \frac{S_{EXP}}{S_r} \right)$$

### III. SUBSCRIPTS

- B - Refers to the body in general.
- BL - Refers to bluntness effect.
- BT - Refers to the boattail section of body.
- BT(F) - Refers to the boattail in presence of fins.
- BT(FORE) - Refers to the boattail in presence of forebody.
- BT(W) - Refers to the boattail in presence of wings.
- CYL - Refers to the cylindrical section of body.
- EXP - Refers to the respective exposed area of a missile part.
- F - Refers to fins.
- FORE - Refers to the forebody, i.e. to the body section ahead of the wings.
- F(W+B) - Refers to fins in presence of the body and the wings.
- LE - Refers to wing or fin leading edge.
- NTIP - Refers to the nose section tip.
- M(W) - Refers to the body mid-section in presence of wing.
- p - Refers to the pressure force effects.
- VIS - Refers to viscous effects on pressure drag.
- TE - Refers to wing or fin trailing edge.
- W - Refers to wing.
- (W+B) - Refers to wing + body conditions.
- W(B) - Refers to the wing in presence of body.
- WET - Refers to the wetted area of a missile part.

- b - Refers to the base pressure effects.
- cr - Refers to the critical Reynolds Number value.
- JET - Refers to effects due to jet presence.
- $\infty$  - Refers to the local free stream conditions just outside the boundary layer.

#### IV. SUPERSSCRIPTS

- ' - Mean value of quantity.

## 2.5 INVISCID AND VISCOUS PRESSURE DRAG, EXCLUSIVE OF BASE DRAG, $C_{D0p} + C_{D0pvis}$

### 2.5.1 INTRODUCTION

The pressure drag force represents the component of the normal pressure distribution in the "wind direction", and is treated within the perfect fluid theory without flow separation, but including correctively the viscous form drag contributions at the rear portions of bodies (or wings and fins). A summation of the local pressure-force (normal to the body surface) components in the general drag direction has to be performed for all aircraft parts. The proposed pressure drag force breakdown scheme and the corresponding definition of the pressure drag force components are given in Sections 1.7.3 and 1.7.4.

Since an analytical interpretation of the inviscid pressure drag both for slender bodies of revolution and for thin airfoils can be fairly accurately done by existing potential theories, it is felt that the engineering predictions of  $C_{D0p}$  for the zero-lift case could be accomplished with a good accuracy by using the respective theoretical results at subsonic, supersonic and hypersonic speeds, and by taking into account the existing empirical data at transonic speed, when the theoretical results may prove to be inadequate. Semi-empirical corrections for viscous effects on pressure drag estimates are then added to the potential drag theory results.

In accordance with the potential theory of perfect fluids, there is no inviscid pressure drag at incompressible subsonic speeds, excluding the base and the viscous pressure drag contributions. A comprehensive compilation of the profile drag data for classical aerodynamic shapes at subsonic speeds can be found in Refs. (2.5-1), (2.5-2) and (2.5-3). As already stated in Sections 1.7 and 1.8, the profile drag consists of form drag and skin friction drag, the former being the drag components of the overall normal pressure at no-lift condition. When such data are used, both the leading edge "bluntness" effects and the wake flow effects are included in the form drag term for aerodynamically smooth and slender shapes.

At supersonic and hypersonic speeds,

the pressure drag due to entropy losses through presumably weak oblique shocks is neglected.

The viscous form drag is caused by the increased "effective" cross-sectional body (or wing) area when the boundary layer thickness is added to the solid body (or wing) geometry. The effectively changed body configuration causes a corresponding pressure redistribution within the perfect fluid concept. With a good approximation, it can be assumed that the effects of the boundary layer growth along forebody and midbody parts are small (negligible). Thus, the contribution of the viscous form drag is confined to the afterbody where the boundary layer thickens more rapidly. The same trend of analysis applied to wings (fins) confines the viscous form drag effects to the regions near the trailing edges. The respective computational procedures and data may be found for some body geometries in Ref. (2.5-4) by Fraenkel and in Ref. (2.5-6) by Young for wings (fins). In Ref. (2.5-5) by Young, the profile drag of wings with bi-convex airfoil sections are presented for a range of Reynolds and Mach Numbers, boundary layer transition locations and wing thicknesses.

#### (i) Inviscid Pressure Drag on Bodies at Supersonic and Hypersonic Speeds - Theoretical References

The principal perfect fluid theories used for estimation of the inviscid pressure drag component on bodies of revolution are listed in the order of increasing accuracy and accompanying computational complexity:

##### (1) Linearized theories:

(a) "Exact linearized", with solutions obtained through a numerical integration of the corresponding basic differential linearized equation of the perfect fluid potential function. The solution satisfies boundary conditions of the body surface, See Refs. (2.5-7) by Karman and Moore, (2.5-8) by Brown and Parker, (2.5-9) by Lighthill, and (2.5-10) by Ward.

(b) "Slender-body" theory, Ref.

2.5-1 (RAS DATA SHEETS), representing permissible simplifications of the "exact" solutions in case of very slender bodies of revolution.

(c) "Quasi-cylinder" theory, Ref. (2.5-10) by Ward, applicable to bodies of nearly constant radius, with the boundary conditions of the "exact" equations satisfied only at a mean radius.

(2) The second-order theory of van Dyke, Ref. (2.5-11) and (2.5-12), represents further improvement of the "exact-linearized" solution, which is re-substituted back into the original exact differential equation. A second approximation is thus computed by a step-by-step method along the body length.

(3) The Method of Characteristics, Ref. (2.5-13) by Isenberg, allows for solutions of any degree of accuracy by performing respective step-by-step computations not only along the body length, but also through any associated disturbed flow field regions that might affect the pressure distribution on the body surface.

The validity range of the principal theories (1), (2) and (3) may be conveniently ascertained through the parameter,

$$\kappa = (M_\infty^2 - 1) (dy/dx)_{\text{MAX}} \quad (2.5-1)$$

where the  $(dy/dx)_{\text{MAX}}$  term represents the maximum slope of the body profile and  $(M_\infty)$  is the free stream value of Mach Number ahead of the bow shock. Thus, with a permissible error of  $\pm 5\%$ , the respective ranges of applicability are:

- (1) "linearized theories":  $\kappa < .10$ ,
- (2) "second order theory":  $\kappa < .50$ ,
- (3) "method of characteristics":  $\kappa < .90$ , if the entropy-gradient and vorticity effects behind a curved shock are neglected.

The inviscid pressure drag component at hypersonic speeds for bodies of revolution, as well as for general slender body shapes, can be obtained from Ref. (2.5-14) by Truitt. The compiled data cover the whole range of hypersonic Mach Numbers ( $3 < M_\infty < \infty$ ), with the indicated order of accuracy of various theories in different Mach Number ranges.

## (ii) Inviscid Pressure Drag on Bodies - Practical Considerations for Use of Various Data

### (1) High Fineness Ratio Slender Bodies of Circular Cross-Section With Boat-Tails, At a Zero Angle of Attack

Analytical treatments by the slender body theory lead to the following qualitative conclusions:

(a) Slender cylindrical bodies with sharp pointed nose sections and an assumed atmospheric base pressure at a blunted base would theoretically have only the pure wave drag of the head wave, i.e., only the foredrag pressure component, because with the base pressure equal to the atmospheric and the body pressure close to the base also nearly equal to the atmospheric pressure, there is no trailing wave within the inviscid fluid theory.

It can be also noted that the drag force for such a slender, pointed body at some angle of attack is theoretically equal to one-half that of a flat plate at the same angle-of-attack.

(b) If a boattail is included in the above case, the flow toward the base shall have an inward radial velocity. This converging flow pattern has subsequently to be straightened out into the free-stream direction by a conical shock-wave, provided the base pressure is again assumed equal to atmospheric, i.e., an additional drag component due to boattailing will appear; its theoretical value shall be different from that obtainable under real fluid flow conditions.

(c) All conditions existing as in the above paragraph (b), except for the base pressure taken different (less) from atmospheric, the flow behind the base shall no longer have a tendency to straighten out in the free-stream direction, but shall converge toward a point in the base wake through a rather complicated mixing process between the outer flow, the dead-air low pressure region behind the base, and the extended boundary layer overflow in real, viscous fluids. An additional drag correction due to these effects represents a first approximation to the actual state of affairs and should be separately investigated.

## (2) Cones at a Zero Angle-of-Attack

The problem of low-fineness ratio missile noses of conical shapes at supersonic speeds can be handled by simple non-linear theories of Taylor and Maccoll<sup>(15)</sup>, or by using the respective tables for cones<sup>(16)</sup>. In general, the pressure field on a cone is a function of two independent variables: the free stream Mach Number,  $M_\infty$ , and the cone semi-apex angle,  $\Theta_N/2$ .

The  $M_\infty$  and  $\Theta_N/2$  can be combined to form a unique parameter, called the "hypersonic similarity parameter",  $K$ ,

$$K = \frac{M_\infty}{(L_N/D)} \quad (2.5-2)$$

This concept was introduced by Tsien<sup>(17)</sup> and originally applied to slender pointed bodies at high Mach Numbers. Briefly, the hypersonic similarity law states that the local pressure ratios,

$$\frac{p - p_\infty}{p_\infty},$$

at corresponding points for two bodies of similar geometries, but differing in fineness ratios, shall be equal if the Mach Numbers for the two bodies are so chosen that the above defined similarity parameter,  $K$ , remains unchanged. The correspondance of the local points is, in general, defined by a nondimensional affine transformation of the respective spatial field coordinates<sup>(14)</sup>.

When applied to investigations of pressure drag on cones,

$$C_{DOPCONE} = C_{PCONE} = \left(\frac{p - p_\infty}{p_\infty}\right) \left(\frac{p_\infty}{q_\infty}\right) = \frac{p - p_\infty}{p_\infty} \left[ (\gamma/2) M_\infty^2 \right]^{-1}, \quad (2.5-3)$$

with the cone base-area as reference, the parametric product,

$$M_\infty^2 \times C_{DOPCONE}, \quad (2.5-4)$$

is a function of the hypersonic similarity parameter,  $K$ , as the Mach Number,  $M_\infty$ , and the fineness ratio,  $L/D$ , are independently varied. One condition must be satisfied: the cone vertex angle should be below its critical value, when the oblique shock detaches. Using the hypersonic similarity law, the basic data from Fig (2.5-1) can be more conveniently expressed as the more general curves on Fig (2.5-2).

The pressure drag on cones can be in general computed accurately by a

somewhat lengthy "method of characteristics", or otherwise estimated directly from the ready-made tables<sup>(16)</sup>. Several shorter methods have been advanced by applying the hypersonic similarity laws to cones.<sup>(20)</sup> A graphical comparison of the results from various shorter theories, as well as their limitations and respective accuracies, is summarized in Fig (2.5-3). For the hypersonic similarity parameter ( $0 \leq K \leq 2$ ) range, which roughly corresponds to low-fineness ratio missile noses, the following may be concluded:

(a) The method of characteristics of Ehret<sup>(20)</sup> gives the best accuracy. It is very time-consuming for engineering use.

(b) The von Karman's and Moore's methods<sup>(7)</sup> use a linearized theory step-by-step procedure. It yields acceptable results for  $K$  values well below unity only.

(c) Newtonian impact theory<sup>(14)</sup> is eventually applicable only for  $K$  of the order of 2.

(d) Van Dykes's second order theory<sup>(12)</sup> yields a good accuracy for  $K$  up to 1.6.

(e) The "tangent cone" method is good only for  $K > 1.2$ .

(f) The "conical shock-expansion" theory by Eggers and Savin<sup>(25)</sup> is applicable only for values of  $K$  greater than 1.

### (3) Cone-Cylinder Combinations at $M = 1$

Spreiter and Alksne<sup>(19)</sup> derived pressure drag on a slender cone-cylinder at a free stream Mach Number of 1 by using the slender body theory based on approximate solution of the transonic flow equations.

The resulting expression is:

$$\begin{aligned} (C_{DOPN})_{M=1} &= \frac{\text{DRAG}}{\frac{\rho_\infty V_\infty^2}{2} \frac{\pi D^2}{4}} = \\ &= -\left(\frac{D}{L_N}\right)^2 \left[ 1.08965 + 4 \log_e \left(\frac{D}{L_N}\right) \right]. \end{aligned} \quad (2.5-5)$$

Miles<sup>(24)</sup> and Yoshihara<sup>(26,27)</sup> obtained similar expressions:

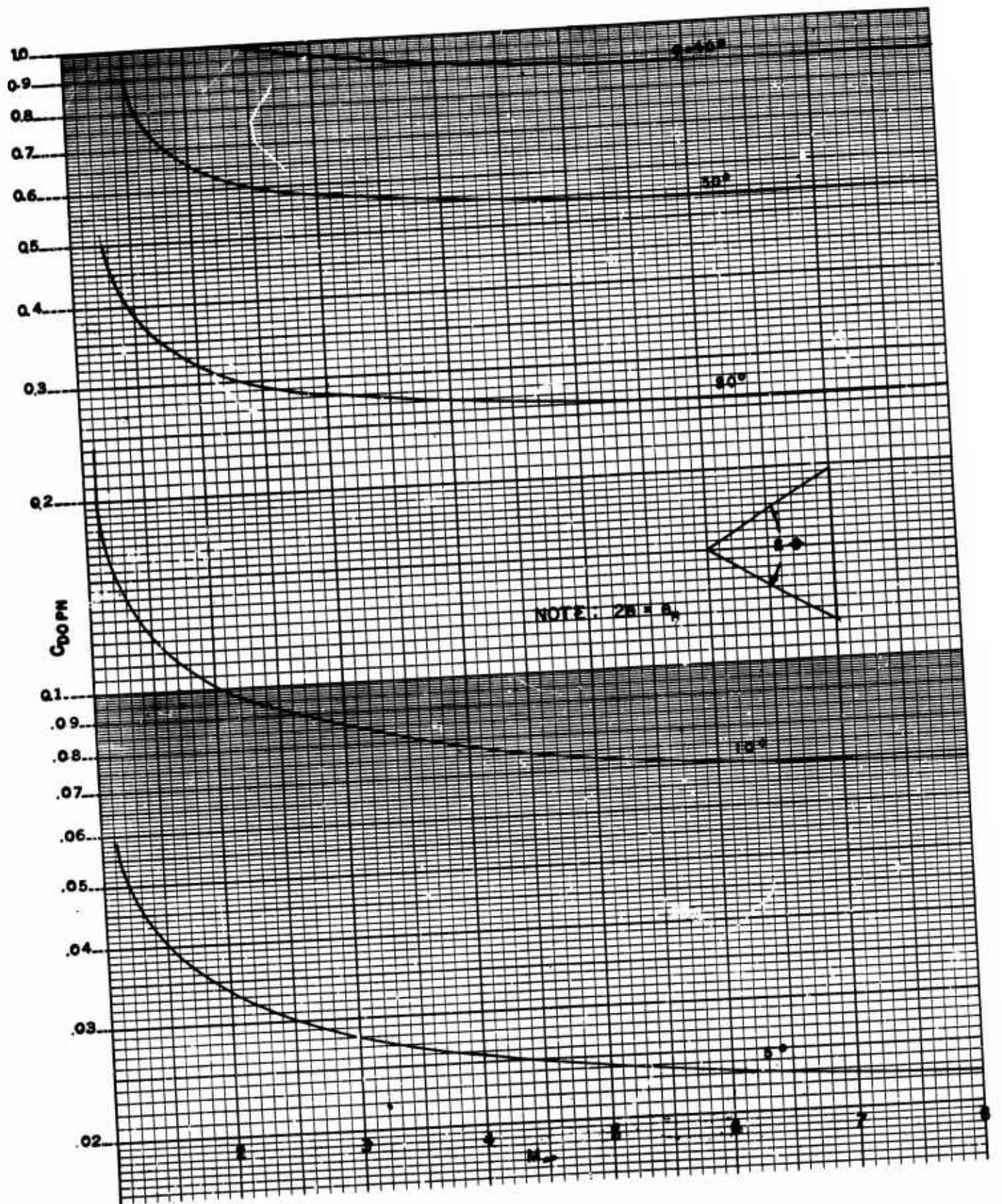


Fig (2.5-1) Drag coefficients of cones at supersonic speeds. Ref (2.5-18)

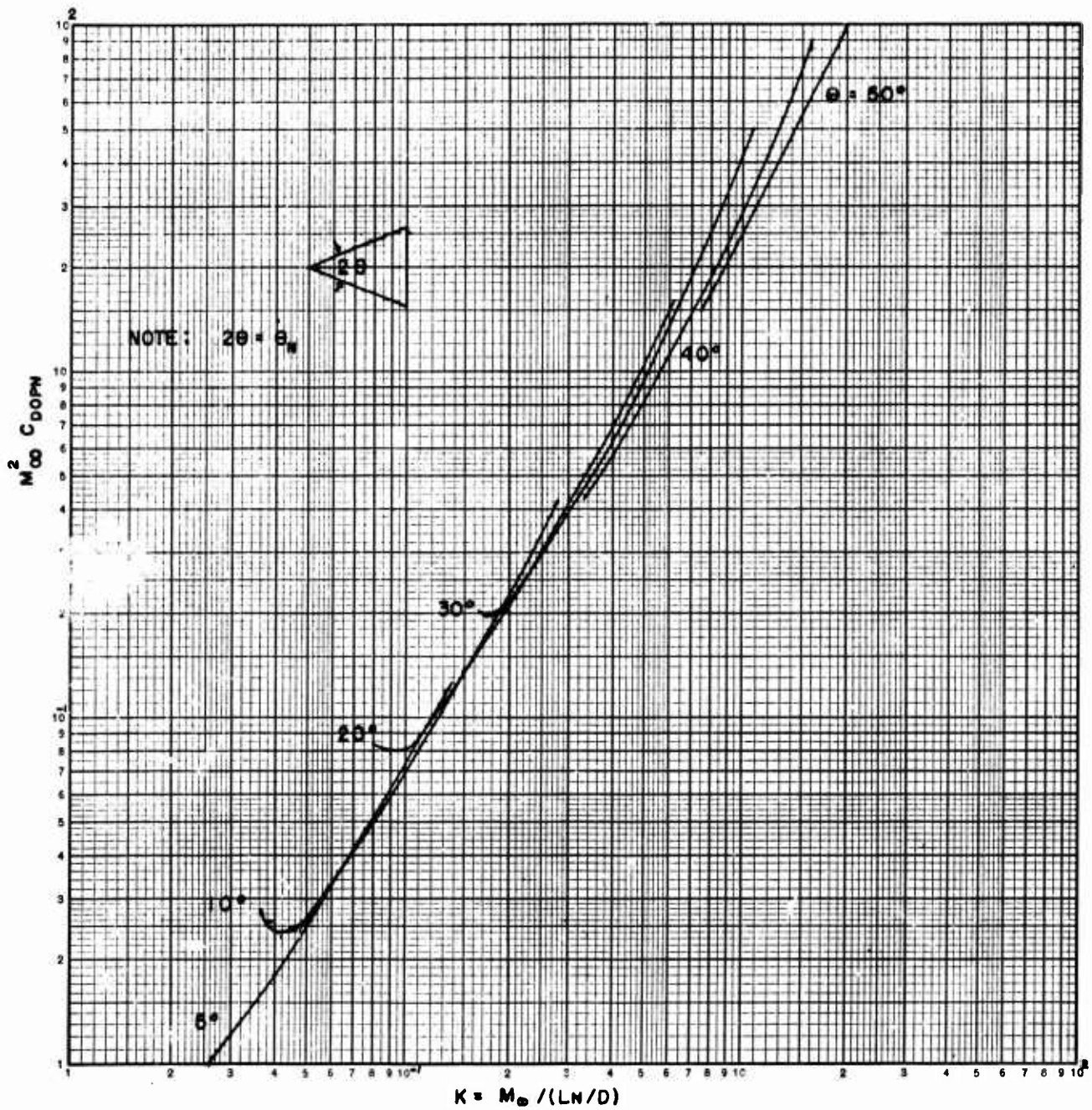


FIG (2.5-2) CORRELATION OF DRAG COEFFICIENTS OF CONES AT SUPERSONIC SPEEDS BY HYPERSONIC SIMILARITY PARAMETER. (REF 2.5-18)

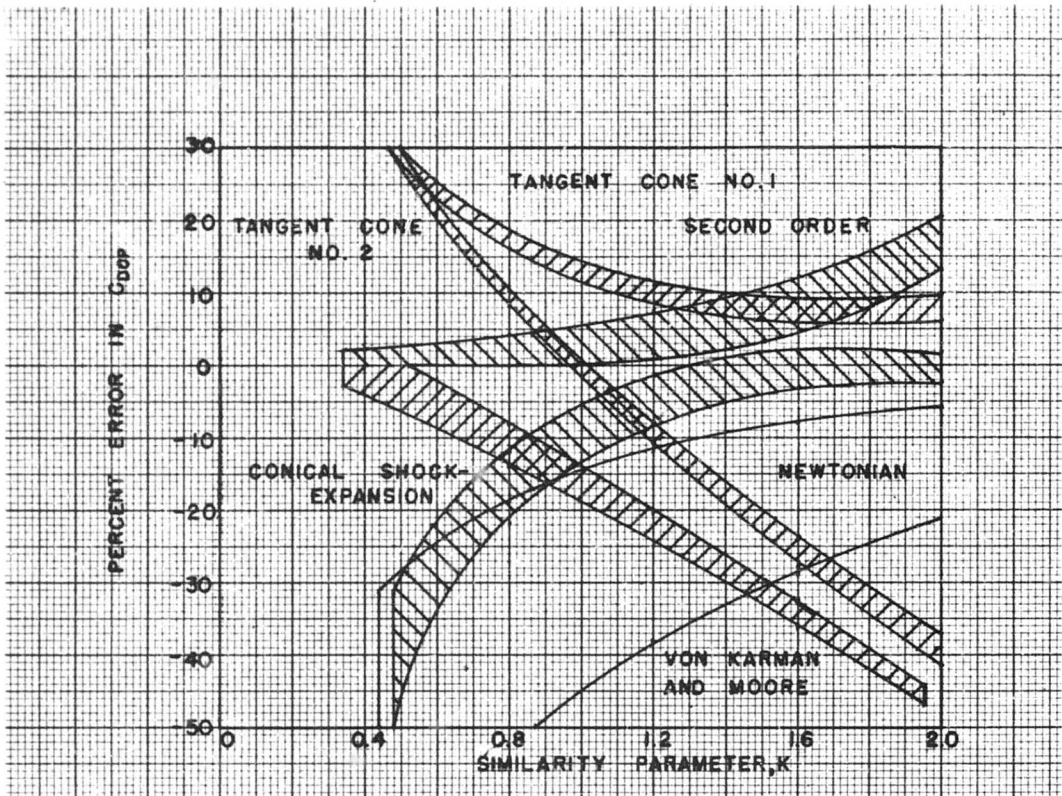


Fig (2.5-3) Accuracy of various methods for estimating pressure drag of nonslender missile noses at zero angle-of-attack. (Ref 2.5-20)

$$(C_{DOPN})_{M=1} = -\left(\frac{D}{L_N}\right)^2 \left[ .55 + 4 \log_e \left(\frac{D}{L_N}\right) \right], \text{ (Yoshihara)} \quad (2.5-6)$$

$$(C_{DOPN})_{M=1} = -\left(\frac{D}{L_N}\right)^2 \left[ .091 + 4 \log_e \left(\frac{D}{L_N}\right) \right], \text{ (Miles)} \quad (2.5-7)$$

All three solutions are plotted in Fig (2.5-4) for the cone reference base area.

For parabolic-arc bodies, the respective expressions are, Miles(24),

$$(C_{DOPN})_{M=1} = .0735 \left(\frac{D}{L_N}\right)^2, \quad (2.5-8)$$

or by Oswatitsch and Keune(21),

$$(C_{DOPN})_{M=1} = \left(\frac{7}{3}\right) \left(\frac{D}{L_N}\right)^2. \quad (2.5-9)$$

The results, together with some experimental evidence from Ref. (2.5-22), (2.5-23) and (2.5-29), are presented in Fig (2.5-4).

#### (4) Ogives at a Zero Angle of Attack

Ehret, Rossow and Stevens(30) and Rossow(31) extended the hypersonic similarity rule to ogives:

For fineness ratios of two or greater and Mach Numbers of 1.5 or greater, a correlation of the ogive results to those of cones was achieved within an accuracy of  $\pm 5\%$ . Based on the computations done by Rossow(31) the theoretical correlation curves for drag ( $M_\infty^2 C_{DOPN}$ ) of cones and tangent ogives are plotted in Fig (2.5-6) as a function of the hypersonic similarity parameter,  $K$ . Physically, the increased drag of ogives is due to an entropy gradient existing along the nose wave, since the wave pattern is not straight as with cones, but curved backward through expansion wavelets created by the ogive curvature. For cones having a straight nose wave pattern, there are no entropy changes along the wave, and the drag term is consequently less.

The actual pressure distribution on ogives is presented in Fig (2.5-7). The computations were done in the following way(1): the similarity law from the linearized theory was reformulated by van Dykes(32) into a combined supersonic-hypersonic similarity rule, which later was transformed into a hypersonic

similarity law by Tsien(17). The Van Dyke's formulation applies to bodies of geometrically similar profiles having different maximum thickness ratios,  $(L/D)$ . Then the pressure coefficient term,

$$4 C_p (L/D)^2, \quad (2.5-10)$$

is a function only of the similarity parameter,

$$\frac{(1/2)(M_\infty^2 - 1)^{1/2}}{(L/D)}, \quad (2.5-11)$$

where  $D$  is the maximum body diameter,  $M_\infty$  the free stream Mach Number, and  $L$  the body length. The main assumption, restricting applicability of the method, is that of small profile slopes. Respective checks of the law with exact numerical results from Ref. (2.5-4), (2.5-20) and (2.5-33), indicate a maximum error of  $\pm 5\%$ , if the maximum profile slope ( $dy/dx$ ) is kept below 0.4. With this restriction, the van Dykes' similarity law was used to obtain pressure distribution data on ogives, computed by the method of characteristics(13) (Isenberg), which takes into account vorticity behind the nose shock wave. Within the accuracy of the theory itself, the results are equally applicable to:

(a) Circular-arc tangent-ogive forebodies,

(b) Pointed parabolic-arc tangent-ogive forebodies,

(c) Secant-ogive forebodies, provided the values of forebody length ( $L_N$ ) and the maximum diameter ( $D$ ) are fictitiously determined by transforming the secant-ogive shape into a tangent-ogive profile generated by extension of the arc of the original circle (or parabola) of the secant-ogive shape up to the point where it becomes tangent to the fictitious new maximum diameter (see Fig 2.5-7).

#### (5) Bodies of Revolution for Least Pressure Foredrag at Zero Angle of Attack

The problem of configurations with the least pressure foredrag has been studied and solved by a number of authors within specifically prescribed common constraints, such as a fixed length, a fixed volume, a fixed base area, etc. The common hypothesis in all the various theories is that the base pressure be equal to the free

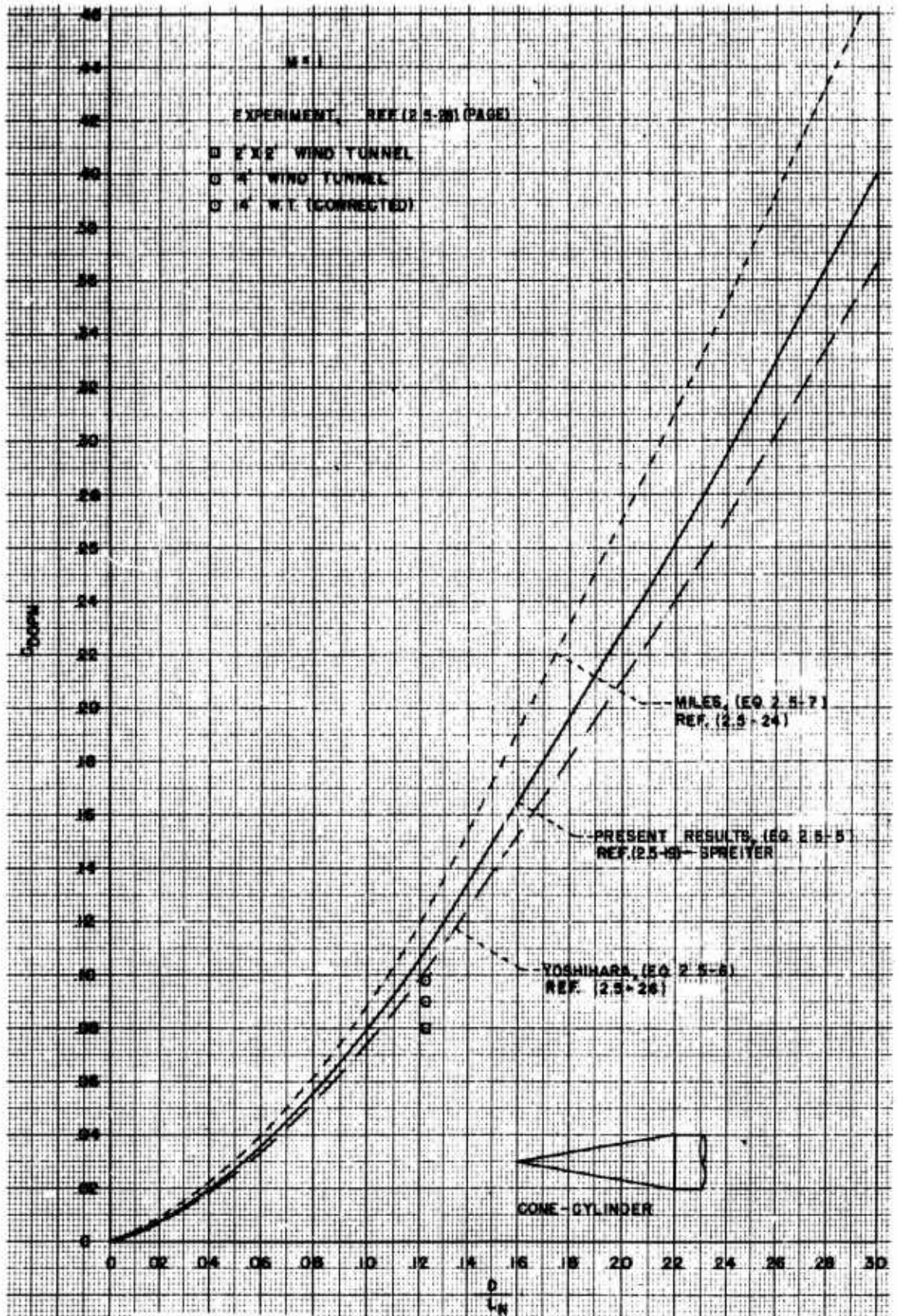


Fig (2.5-4) Variation of pressure - drag coefficient with thickness ratio for a cone-cylinder at Mach Number 1, as indicated by present 2.5-8 theory, by other theoretical results, and by experiment.

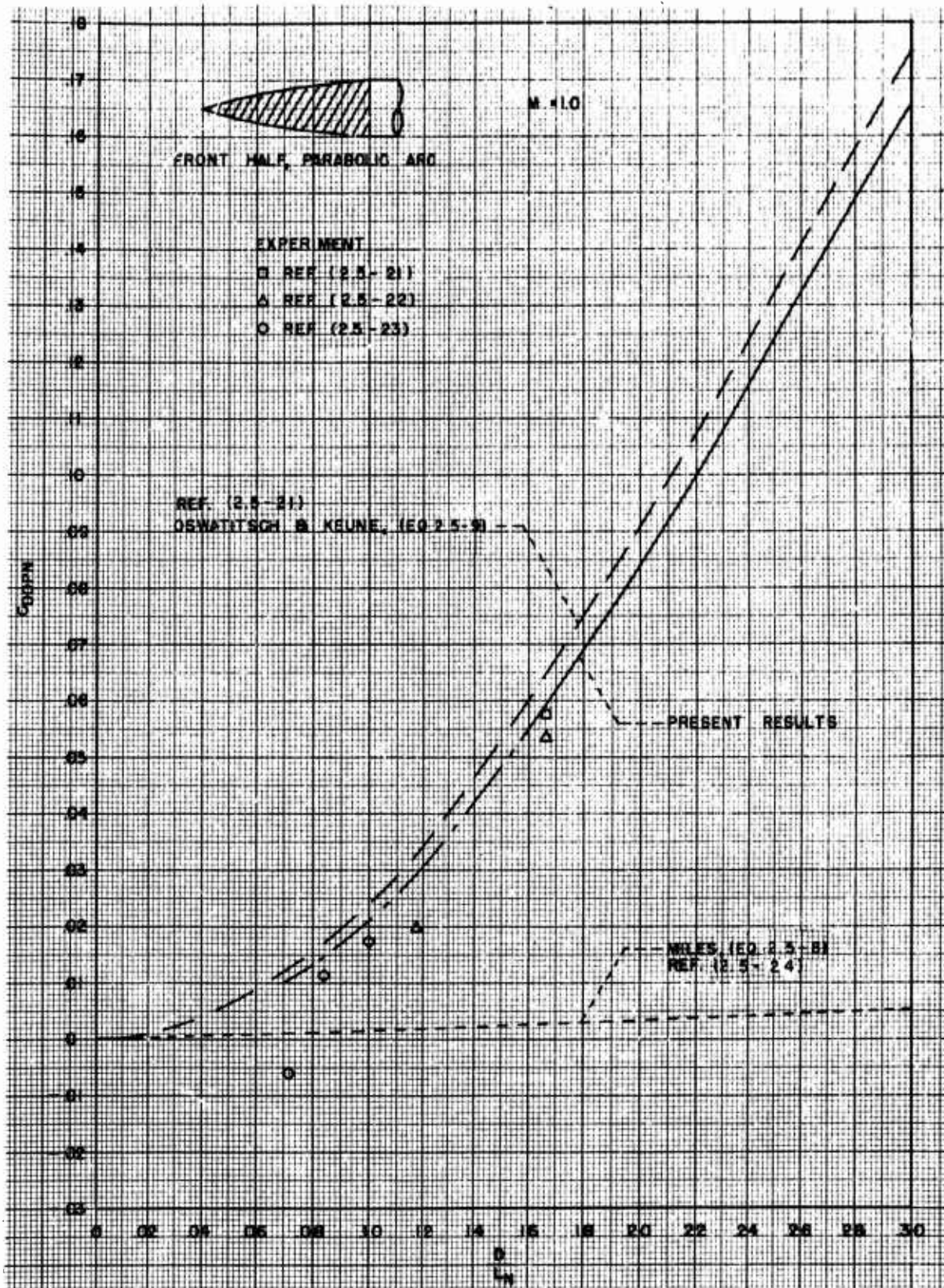


Fig (2.5-5) Variation of pressure-drag coefficient with thickness ratio for the front half of a parabolic-arc body at Mach Number 1, as indicated by present theory, by other theoretical results, and by experiment. Ref (2.5-20)

2.5-9

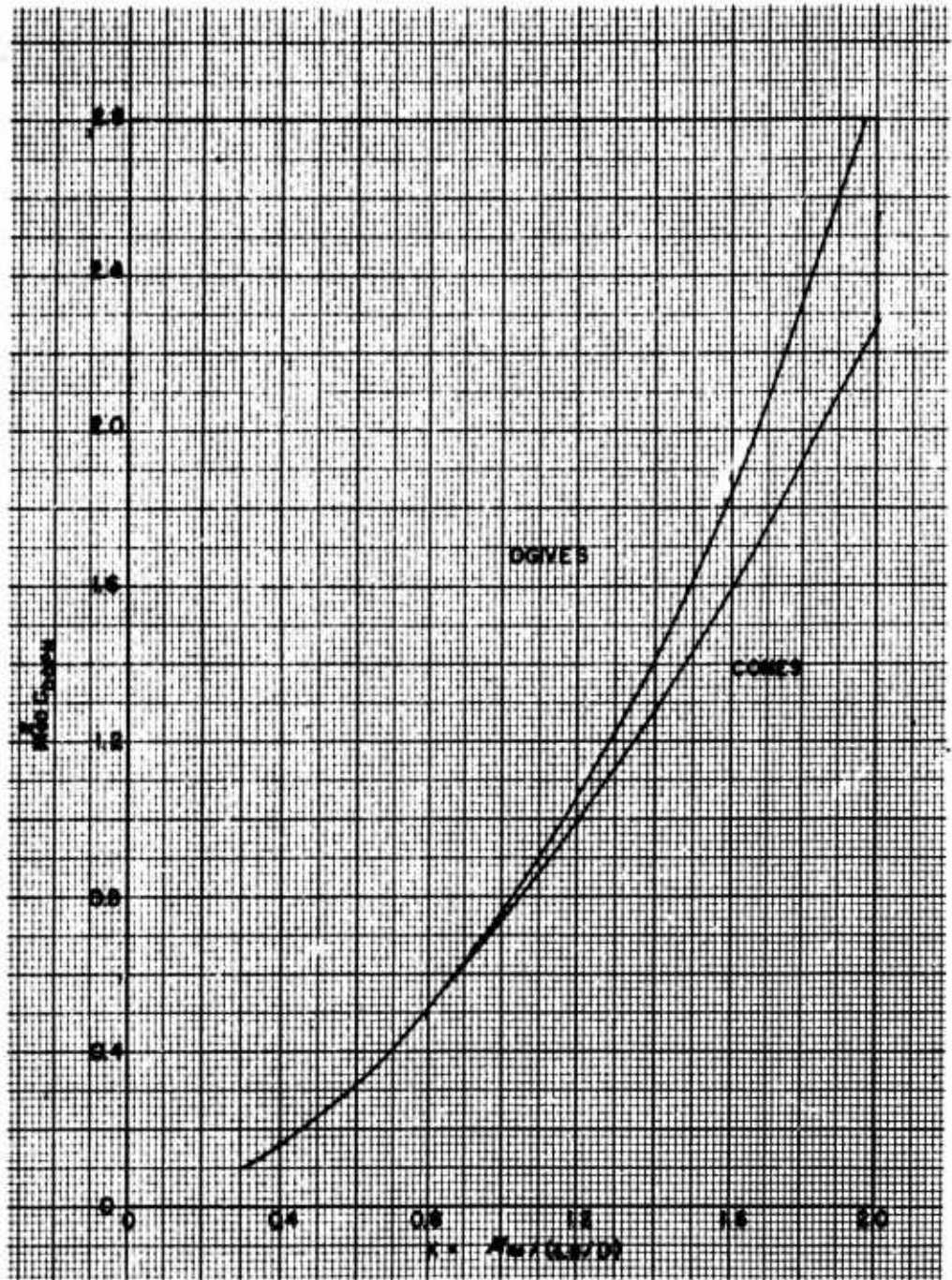


Fig (2.5-6) Correlation curves for drag of cones and tangent ogives on basis of hypersonic similarity parameter. Ref (2.5-31)

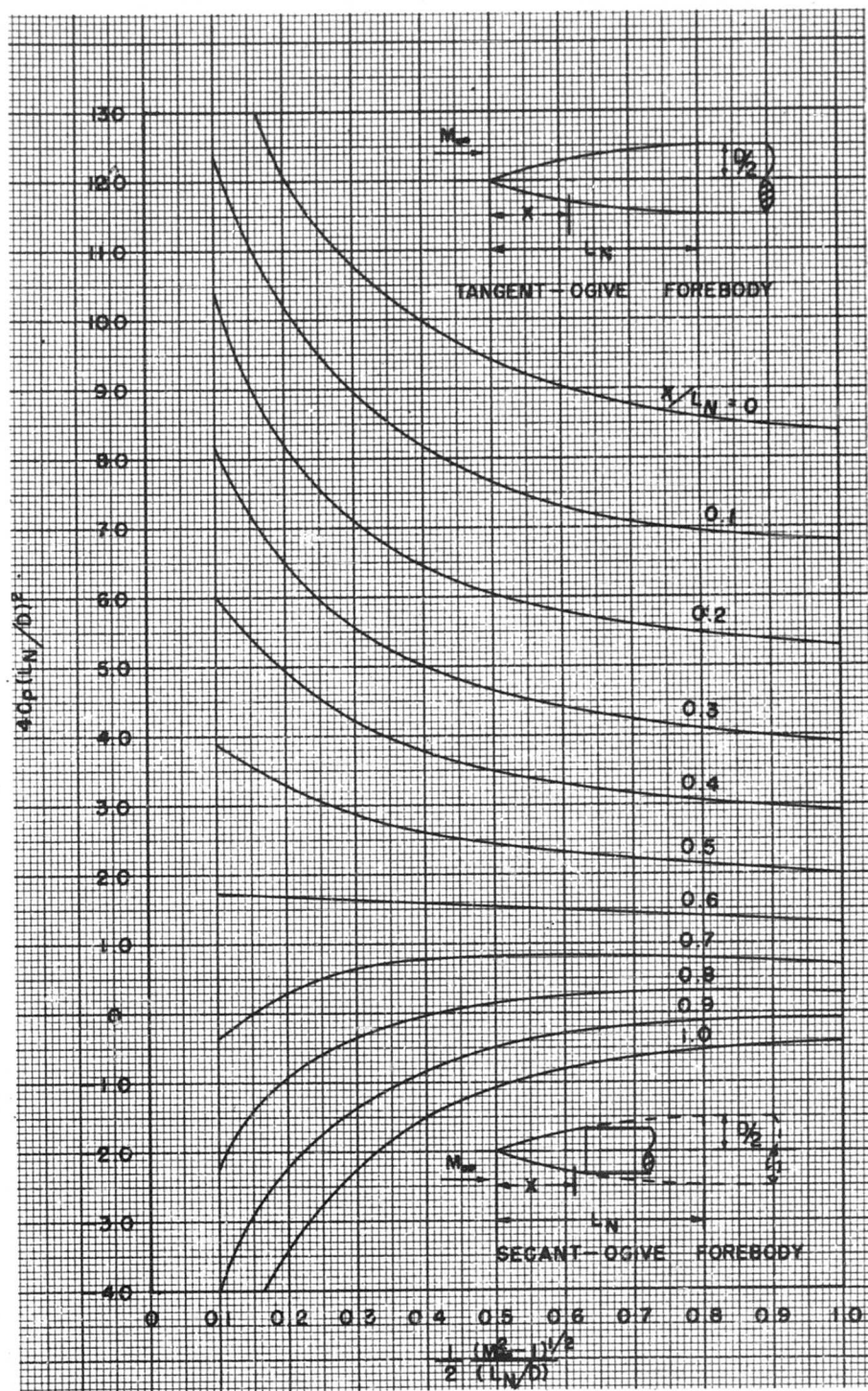


Fig (2.5-7) Pressure distribution on ogival forebodies at zero angle of attack. Ref (2.5-1) R.A.S. data sheets, aerodynamics, vol. 1, bodies S. 05.03.01

stream pressure in an inviscid fluid, i.e., the wave drag is equal to the pressure foredrag, with no base-drag taken into account.

The few well known minimum foredrag shapes are:

(a) Von Karman's ogive body, derived on the basis of slender body theory<sup>(34)</sup>. It has a least pressure foredrag for a given length and a cylindrical base of a given area:

$$\frac{D_{op}}{q_{\infty}} = \frac{16(\text{VOLUME})^2}{\pi L^3},$$

$$\therefore C_{Dop} = \frac{8(\text{VOL})}{\pi L^3}. \quad (2.5-12)$$

(b) The Sears-Haack body<sup>(35,36)</sup>, symmetrical about the midpoint of its axis, pointed at both ends. It represents a minimum pressure foredrag body for a zero base area and a given length and volume. Its shape was derived on the basis of slender body theory:

$$\frac{D_{op}}{q_{\infty}} = \frac{128(\text{VOLUME})^2}{\pi L^4},$$

$$\therefore C_{Dop} = \frac{24(\text{VOL})}{L^3}. \quad (2.5-13)$$

(c) Eggers, Dennis and Resnikoff<sup>(37)</sup> studied bodies of least pressure drag with various restraints by calculus of variation on the basis of the Newtonian impact theory. With a prescribed body length and base area, these Newtonian bodies are flat-nosed to some degree, depending upon the fineness ratio, but otherwise are by shape very similar to von Karman's ogive. The local pressure coefficient for Newtonian bodies is given by

$$C_p = \frac{p - p_{\infty}}{q_{\infty}} = 2 \sin^2 \delta, \quad (2.5-14)$$

where  $\delta^\circ$  is the angle between the local tangent to the body and the streamwise direction. The Newtonian foredrag values are a bit lower than von Karman's.

The actual shape of the Newtonian bodies can be closely approximated by a three-quarter power law:

$$\frac{d}{D} = \left(\frac{x}{L_N}\right)^n, \quad n = \frac{3}{4}, \quad (2.5-15)$$

where (d) and (D) are local and base diameters respectively, and ( $L_N$ ) is body (or nose) length.

A comparison of the cross-sectional area distributions for the bodies (a), (b) and (c) of minimum pressure foredrag is given in Table 2.5-1 and Figs (2.5-8) and (2.5-9).

### (iii) Inviscid Pressure Drag on Wings and Fins

#### (1) Two-Dimensional Theories

There are three main theoretical methods for calculation of the inviscid pressure distribution past two-dimensional airfoils at supersonic speeds. These methods are listed below in the respective order of accuracy:

(a) "Shock-expansion method", or nearly exact method.

(b) "Simple-wave flow method", approximating the isentropic conditions for small flow deflections (i.e., for thin airfoils).

(c) "Second and first order theory methods", using power series expansions for pressure distributions.

All these methods are restricted to inviscid flows with attached shock waves. Suitable charts and numerical data for computations can be found in Ref (2.5-1) (RAS Data sheets) for all the three methods. As an illustration of the respective accuracies, the computations for two symmetric double wedge sections of 3% and 10% thickness/chord ratios are presented in table (2.5-2). The difference proved to be small, the greatest being of the order of 10%.

#### (2) Three Dimensional Supersonic Wing Theories

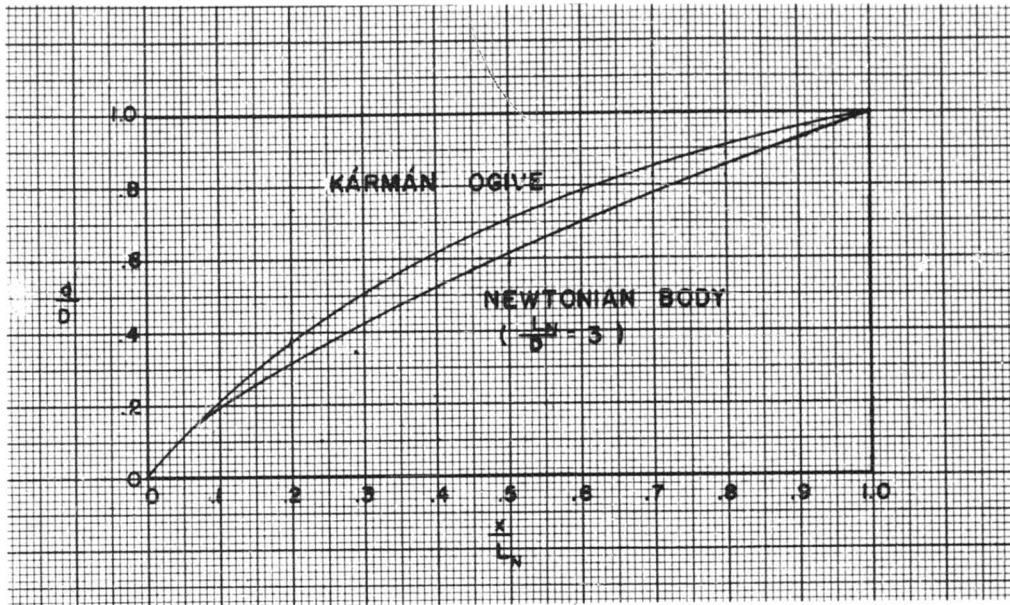
The linearized supersonic wing theory<sup>(18,39,40)</sup>, proves to be an acceptable basis for the evaluation of the wing pressure drag in a first approximation. The pressure distributions can be considered as resulting from:

(a) A thickness-drag component at a zero angle of attack,

(b) A camber-drag component at a zero angle of attack,

(c) Drag due to lift.

At a zero angle of attack, the respective (a) and (b) two-dimensional values for cambered double-wedge, un-



Fig(2.5-8) Comparison of shape of Kármán Ogive with that of Newtonian body of least pressure foredrag. Ref (2.5-18)

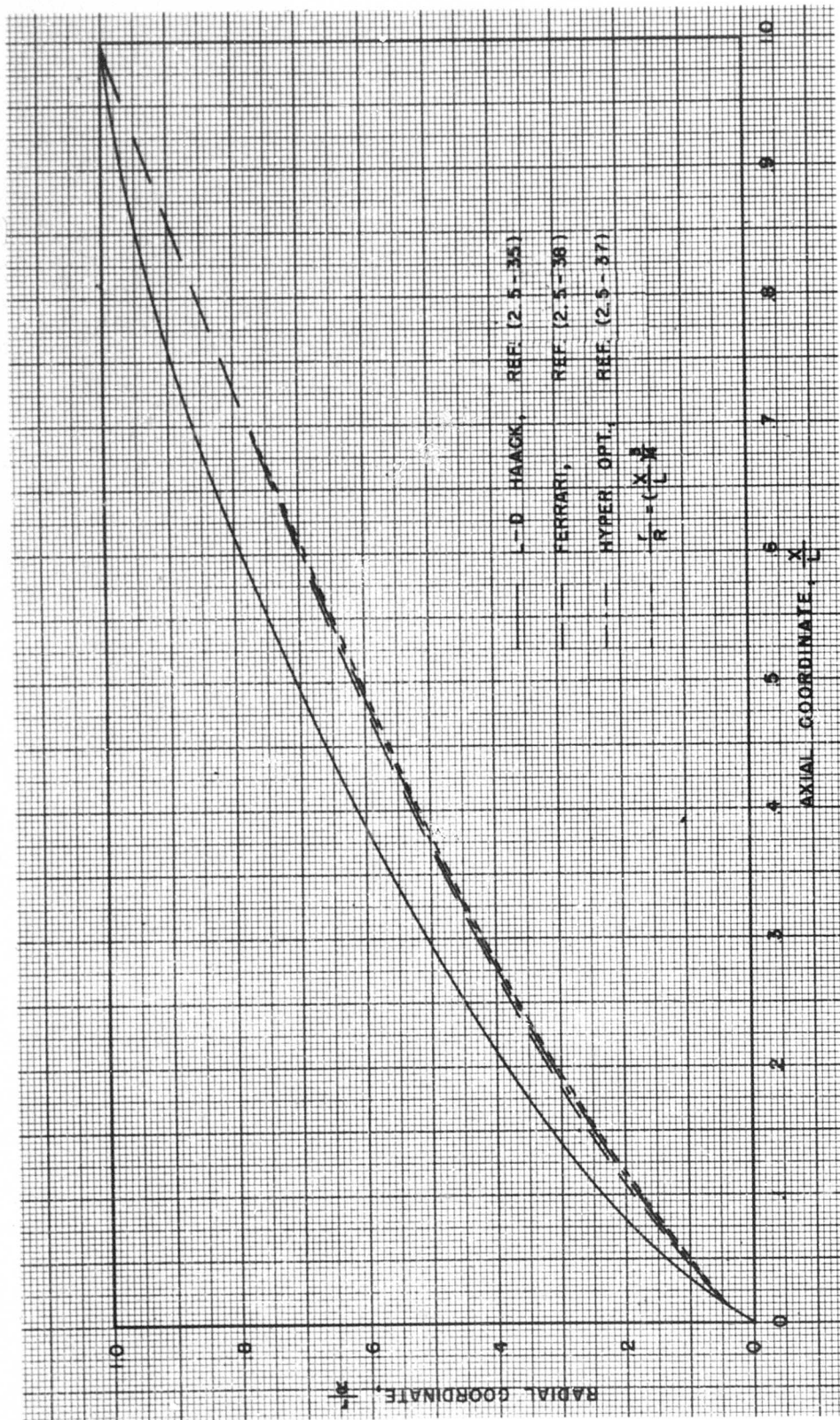


Fig (2.5-9) Comparison of profiles of minimum drag noses for given length and base diameter.

TABLE (2.5-1) COORDINATES OF BODIES OF LEAST WAVE DRAG

See Figs. (2.5-8) and (2.5-9)

d/D					
x/L <sub>N</sub>	Sears-Haack*	Karman ogive	Three quarter-power body	Newtonian bodies	
				L <sub>N</sub> /D = 3	L <sub>N</sub> /D = 5
0	0	0	0	0.0073	0.0015
0.02	0.089	0.069	0.053	0.060	0.055
0.04	0.148	0.116	0.089	0.099	0.091
0.06	0.199	0.156	0.121	0.129	0.123
0.08	0.245	0.194	0.150	0.159	0.153
0.10	0.288	0.228	0.178	0.186	0.181
0.20	0.465	0.377	0.299	0.305	0.300
0.30	0.609	0.502	0.405	0.412	0.407
0.40	0.715	0.611	0.503	0.509	0.505
0.50	0.806	0.707	0.595	0.599	0.596
0.60	0.877	0.791	0.682	0.685	0.682
0.70	0.932	0.865	0.765	0.767	0.765
0.80	0.970	0.926	0.846	0.847	0.846
0.90	0.922	0.974	0.924	0.925	0.924
1.00	1.000	1.000	1.000	1.000	1.000

\*Given volume and length  $2L_N$ ; maximum radius  $D/2$ .

Given base radius  $D/2$  and length  $L_N$ ; tangent-cylindrical base.

Given base radius  $D/2$  and length  $L_N$ .

REF (2.5-18)

TABLE (2.5-2)

Thickness / chord ratio = 3 per cent.

Mach number	1.5		3.0	
	$C_{LW}$	$C_{D0pW}$	$C_{LW}$	$C_{D0pW}$
Shock-expansion	0.3073	0.0302	0.1292	0.0126
Simple - wave	0.3206	0.0316	0.1249	0.0122
Second order	0.3122	0.0305	0.1234	0.0120

Thickness / chord ratio = 10 per cent.

Mach number	1.5		3.0	
	$C_{LW}$	$C_{D0pW}$	$C_{LW}$	$C_{D0pW}$
Shock-expansion	0.3296	0.0679	0.1274	0.0259
Simple - wave	0.3412	0.0691	0.1315	0.0260
Second order	0.3122	0.0630	0.1234	0.0249

ILLUSTRATION OF RESPECTIVE ACCURACIES OF VARIOUS THEORETICAL METHODS OF CALCULATING INVISCID PRESSURE DRAG ON TWO-DIMENSIONAL AIRFOILS. REF (2.5-1)

cambered double-wedge and bi-convex airfoils are:

$$(C_{DOP})_{DUE\ TO\ CAMBER} = \frac{4}{(M_{\infty}^2 - 1)\sqrt{2}} \left(\frac{t}{c}\right)^2, \quad (2.5-16)$$

$$(C_{DOP})_{DUE\ TO\ THICKNESS} = \frac{4}{(M_{\infty}^2 - 1)\sqrt{2}} \left(\frac{t}{c}\right)^2, \quad (2.5-17)$$

$$\therefore (C_{DOP})_{DUE\ TO\ CAMBER} = (C_{DOP})_{DUE\ TO\ THICKNESS}.$$

Since the wings of interest in missile designs are usually of symmetrical cross-section, in evaluating the three dimensional effects the camber influence will not be considered. For such zero-camber wings, the three-dimensional drag coefficient at a zero-lift depends on:

- (a) Wing planform and aspect ratio,
- (b) Wing section,
- (c) Mach Number.

The respective results for a wide range of wing planforms are given in the form of "ready-to-use" charts or tables in Refs. (2.5-1), (2.5-3), (2.5-39), (2.5-41), (2.5-42), (2.5-43), (2.5-44), (2.5-45), (2.5-46).

According to the supersonic wing theory, the pressure drag of a symmetrical wing section at a zero angle of attack is all wave drag, and is usually referred to as the "minimum wave drag".

Katzen and Kaattari<sup>(47)</sup> have conducted systematic comparisons between the measured and the theoretical drag coefficients at a zero-lift condition for a series of triangular wings with double-wedge sections of 8% thickness. From their investigations, two important conclusions may be drawn:

(a) The theoretical estimates seem to be higher than the experimental for fully developed supersonic flows,

(b) For the transonic range of speeds, i.e., as the leading edge, the line of maximum thickness and the trailing edge, are successively passing through locally sonic speeds, the supersonic theory is not valid, and experimentally "rounded" data are necessary.

(iv) Wing-Body Interference Drag,

$$\Delta C_{DOPW(B)} + \Delta C_{DOPM(W)}$$

The pressure drag of wing-body combinations can be suitably broken into

the following parts, see Section 1.7.4.

$$C_{DOP(W+B)} = C_{DOPWEXP} + C_{DOPFORE} + \Delta C_{DOPW(B)} + \Delta C_{DOPM(W)} \quad (2.5-18)$$

where:

$C_{DOPFORE}$  - is the foredrag of the body alone,

$C_{DOPWEXP}$  - is the pressure drag of the exposed wing area alone,

$\Delta C_{DOPW(B)}$  - is the pressure drag of the exposed wing due to presence of body,

$\Delta C_{DOPM(W)}$  - is the pressure drag of the body due to presence of wing (mainly the pressure drag on the "central part" of the body at the wing location for  $C_L = 0$ ).

There are several theories applicable to various wing-body combinations and shapes. Thus, for slender wing-body combinations of various shapes, the drag formula of Ward<sup>(18)</sup> can be used. For special cases of symmetrical cross-section wings, mounted on body sections of circular or nearly circular cylindrical shape, the drag of the wing-body combinations can be computed by Nielsen's special "W-function" linear theory<sup>(48)</sup>.

Katzen and Kaattari<sup>(47)</sup> computed by the method of Nielsen and Matteson<sup>(49)</sup>, the drag of triangular planforms of various sizes and aspect ratios mounted on a circular cross-section body, and concluded that the  $\Delta C_{DOPW(B)}$  term is a negligible percentage of the combination total pressure drag,  $C_{DOP(W+B)}$ . However, for wing planforms small compared to the body, it can constitute a substantial percentage, if referred to the isolated wing-drag alone,  $C_{DOPWEXP}$ .

When wings are mounted on body sections that are expanding or contracting, a correction should be added for existing longitudinal pressure gradients.

The  $\Delta C_{DOPM(W)}$  term is theoretically zero, if the body cross-section is circular. For other, more general shapes, the "W-function" method<sup>(48)</sup> can be used.

It should be emphasized that in the transonic speed range the problem of the wing-body-combination pressure drag,  $C_{DOP(W+B)}$ , (then called the thick-

ness pressure drag), could be approached without resorting to the drag decomposition shown by Eq (2.5-18), by using the Whitcomb's(50) area rule. According to it, the pressure "thickness drag" of a slender wing-body combination,  $C_{Dop(w+s)}$ , is equal to that of an "equivalent body of revolution", ( $C_{Dop}$ )<sub>EQUIVALENT BODY</sub>. The equivalent body of revolution has the same area distribution as the wing-body combination to suit the minimum pressure drag body concepts of Sears and Haack, von Karman, etc. The area rule has its upper Mach Number limit of applicability which is dependent on the sweep-back angle and the wing position with respect to the body. Beyond these Mach Numbers, the "supersonic area rules" of Jones(51), Lomax and Heaslet(52), Lomax(53) and Nielsen(54) can be used.

Nevertheless, in the present investigation, due to limitations of the possible missile configurations to slender, cylindrical, circular cross-section bodies, and relatively small planform symmetrical airfoil wings, the pressure drag breakdown as indicated by the Eq (2.5-18), has been adopted as suitable, since in a first approximation:

$$C_{DopB(w)} = C_{DopM(w)} \approx 0,$$

$$\text{and } C_{DopW(B)} = 0. \quad (2.5-19)$$

A summary of theoretical values of  $C_{DopWEXP}$  for supersonic speeds is given in Table (2.5-5). The three-dimensional wing effects spread inwardly from wing tips along the Mach lines, creating a suction (low pressure) region on the upper surfaces, and subsequently inducing a curled tip vortex from lower to upper surface, in the same way as at subsonic speeds. The interrelationship between the Mach lines and the leading-edge sweep back is of importance as can be seen from three delta configurations tabulated in the Table (2.5-5).

(v) Viscous Form Drag,  $C_{Dopwvis}$  and  $C_{Dopfv}$

A progressive boundary layer thickening between the leading and the trailing edges modifies the effective shape of the airfoil sections with respect to the inviscid outer flow. A subsequent change in the inviscid flow pressure distribution is thus created, resulting in an additional increase in pressure drag, which is called the viscous form drag. It can be computed (Ref. 2.5-1,

RAS Data Sheets), provided no trailing-edge flow separation is assumed.

The existing evidence indicates that the viscous form drag is generally small, and consequently, can be neglected in a first approximation. The more so, if the skin-friction drag is conservatively evaluated for an assumed fully turbulent boundary layer.

(vi) Boundary Layer-Shock Wave Interaction

From the summarized evidence in Ref. 2.5-1 (RAS Data Sheets), it appears that the boundary layer-shock wave interaction at a relatively sharp leading edge has but little effect on the inviscid pressure distribution, except for the immediate region up to approximately 0.02c from the leading edge.

At the trailing edge, the boundary layer-shock wave interference becomes more pronounced, causing a rapid thickening and an eventual separation of the boundary layer. The abrupt thickening of the boundary layer, caused by an adverse pressure gradient in the subsonic portion of the boundary layer affects, in its turn, the shock-wave pattern. This leads to a generally complex interplay of the two phenomena. There is little generalized evidence on how much quantitatively it affects the inviscid pressure drag term. Some restricted data on the changed upstream pressure distributions may be found in Ref. (2.5-55) by Zienkiewicz and in Refs. (2.5-56) and (2.5-57) by Holder. The downstream effects of the phenomena are partially covered by taking the trailing-edge "bluntness" base drag into account, as it is done later.

(vii) Leading Edge "Bluntness" Effects,  $C_{DopwLE}$  and  $C_{Dopfle}$

Due to usual manufacturing and structural restrictions, the actual leading edge of supersonic airfoils is never ideally sharp, as tacitly assumed in the idealized inviscid fluid theories. Therefore, the leading edge shock wave is not attached and straight, but rather has a small curved, detached shape immediately in front of the leading edge. The static pressure behind such a locally almost "normal" shock wave is appreciably increased as compared with the conditions existing behind an attached oblique shock.

No simple analytical methods are available for calculation of the blunt-ness effects. An approximate semi-empirical method is presented in Ref. (2.5-1) (RAS Data Sheets) in the form of "ready-to-use" graphs for engineering estimates. As an illustration of the magnitude of this drag increase:  $C_{DOPWLE} = .075 C_{DOPWEXP}$  for a double-wedge airfoil with a thickness/chord ratio of 6% at a Mach Number of 1.6 and a leading-edge bluntness of 0.005 in. on a 1 foot chord section.

A conservative assumption of an effective leading-edge "bluntness" radius of the order of 0.05 in. could be used as an average mean value for the actual leading edge bluntness under ordinary full scale manufacturing conditions.

Another possibility for calculation of the  $(C_{DOPWLE})$  term is by using the simple Newtonian impact theory, assuming a semi-cylindrical leading-edge shape of the bluntness radius  $R_{BL}$ , see Fig (2.5-10). Then:

$$\begin{aligned} D_{OPWLE} &= C_D \left( \frac{\rho V_N^2}{2} \right) 2R_{BL} \frac{b_{WEXP}}{\cos \Lambda_{WLE}} = \\ &= C_D \left( \frac{V_N}{V_\infty} \right)^2 q_\infty 2R_{BL} b_{WEXP} \end{aligned}$$

$$\therefore D_{OPWLE} = 2R_{BL} b_{WEXP} q_\infty C_D \cos^2 \Lambda_{WLE} =$$

$$= C_{DOPWLE} q_\infty \frac{\pi D^2}{4}$$

$$C_{DOPWLE} = 2.55 C_D \left( \frac{R_{BL}}{D} \right) \left( \frac{b_{WEXP}}{D} \right) \cos^2 \Lambda_{WLE} \quad (2.5-19a)$$

The Newtonian impact theory<sup>(14)</sup>, without accounting for centrifugal force effects, yields a value

$$C_{D0} = \frac{4}{3} \quad (2.5-20)$$

for circular cylinders in two-dimensional non-viscous flows. Thus, finally, it follows that regardless of Mach Number:

$$C_{DOPWLE} = 3.4 \left( \frac{R_{BL}}{D} \right) \left( \frac{b_{WEXP}}{D} \right) \cos^2 \Lambda_{WLE} \quad (2.5-21)$$

for wings, and

$$C_{DOPFLE} = 3.4 N \left( \frac{R_{BL}}{D} \right) \left( \frac{h_{FEXP}}{D} \right) \cos^2 \Lambda_{FLE} \quad (2.5-22)$$

for fins,

where  $(N)$  is the number of individual fins and  $(h_{FEXP})$  is the fin height.

The results are actually strictly valid only for  $M \rightarrow \infty$ , but may serve as a quick estimate at supersonic speeds in general, since the bluntness drag is relatively small anyhow.

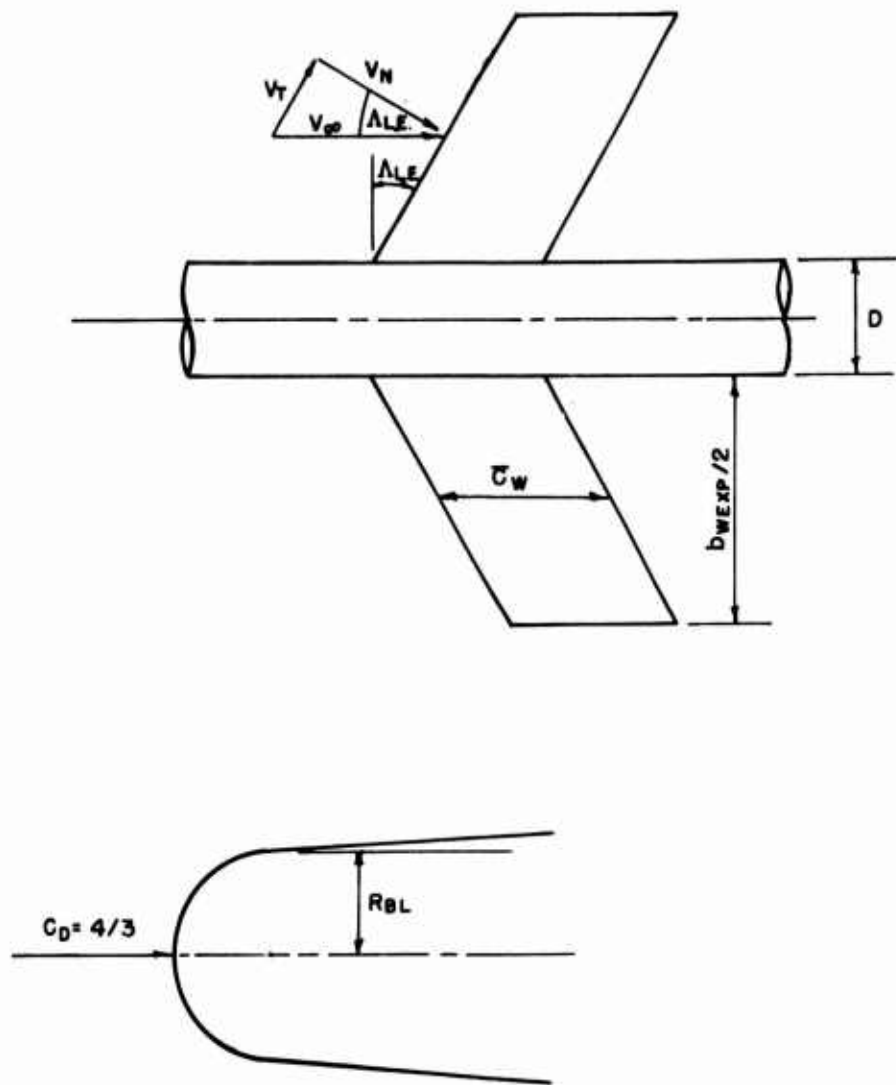


FIG (2 5-10) LEADING EDGE BLUNTNESS EFFECT, A SCHEME FOR APPROXIMATE ESTIMATES OF  $C_{DOPWLE}$  OR  $C_{DOPFLE}$

2.5.2 THE BASIC EXPRESSION FOR THE TOTAL ZERO LIFT PRESSURE DRAG COEFFICIENT (EXCLUSIVE OF BASE DRAG)

Note: The Figures (2.5-11) to (2.5-37) and the Tables (2.5-3) to (2.5-16) are compiled at the end of the Section 2.5.4.

$$\begin{aligned}
 C_{DOP} = & (C_{DOPFORE} + \Delta C_{DOPNTIP}) + (C_{DOPBT} + \\
 & + \Delta C_{DOPBT(F)} + \Delta C_{DOPBT(W)} + \Delta C_{DOPBT(FORE)}) + \\
 & + (C_{DOPWEXP} + \Delta C_{DOPW(B)} + \Delta C_{DOPM(W)}) + \\
 & + (C_{DOPFEXP} + \Delta C_{DOPF(W+B)} + \Delta C_{DOPF(BT)}) + \\
 & + (C_{DOPWLE} + C_{DOPFLE}) + (C_{DOPBTVIS} + \\
 & + C_{DOPWVIS} + C_{DOPFVIS}) \quad (2.5-23)
 \end{aligned}$$

The Eq (2.5-23) represents the total

pressure drag term (inviscid + viscous, exclusive of base drag).

Each of the terms in the Eq (2.5-23) is evaluated separately within the general classification of the main missile parts: nose section, cylinder + boattail, wings and fins, see Section 1.7.4.

A summary of the respective theoretical and experimental data, which are graphically presented in the corresponding Figures, is presented next, together with the main assumptions, approximations and limitations that are inherent to the data. The computational procedure is then presented in the following Section, 2.5.3, in a self-instructive stepwise manner, similar to that used for the skin-friction drag estimates.

2.5.3 THE EXPRESSIONS AND THE DATA FOR THE BODY PRESSURE DRAG COEFFICIENT ESTIMATES

$$(C_{DOPFORE} + \Delta C_{DOPNTIP}) + (C_{DOPBT} + \Delta C_{DOPBT(F)} + \Delta C_{DOPBT(W)} + \Delta C_{DOPBT(FORE)}) + C_{DOPBTVIS}$$

(2.5-24)

(i) Inviscid Forebody Pressure Drag,  
 $C_{DOPFORE} + \Delta C_{DOPNTIP}$

This represents a major portion of the pressure drag force. The contribution of the nose-section is all important, the cylindrical part of the body ahead of the wing having but negligible influence.

(1) Cones at supersonic speeds, zero angle of attack:  $C_{DOPFORE} \approx C_{DOPC}$

The exact solutions are available in Refs. (2.5-15) by Taylor and (2.5-16) (MIT Tables) with accompanying graphical presentations. A replot of the data in Fig (2.5-6) gives general curves in terms of the hypersonic similarity parameter,  $K = M_\infty / (L_N/D)$ .

Also, for direct engineering estimates, the concise graphs from Ref. (2.5-1) (RAS Data Sheets) can be used, see Fig (2.5-11). Applicability of the charts is restricted to purely supersonic conditions behind the attached front shock wave. The critical free stream Mach Number ( $M_{Cr}$ ), when the front shock detaches, is plotted in Fig (2.5-12) as a function of the cone vertex angle ( $\theta_N$ ). From the pressure coefficient readings in Figs (2.5-6) or (2.5-11), the corresponding values of the pressure drag coefficient are obtained:

$$C_{PCONE} = \frac{p_c - p_\infty}{q_\infty}$$

$$D_{OPCONE} = C_{DOPCONE} q_\infty \frac{\pi D^2}{4} =$$

$$= C_{PCONE} q_\infty \frac{\pi D}{2} L_N \sec\left(\frac{\theta_N}{2}\right) \sin\left(\frac{\theta_N}{2}\right),$$

$$C_{DOPFORE} \approx C_{DOPC} = 2 C_{PC} \left(\frac{L_N}{D}\right) \tan\left(\frac{\theta_N}{2}\right),$$

$$\left(\frac{L_N}{D}\right) = \frac{1}{2} \cot\left(\frac{\theta_N}{2}\right),$$

$$\therefore C_{DOPFORE} \approx C_{DOPC} = C_{PC} \quad (2.5-25)$$

(2) Ogives at supersonic speeds, zero angle of attack:  $C_{DOP0} = C_{DOPC} + \Delta C_{DOP0}$

The increased drag of ogives,  $\Delta C_{DOP0}$ , due to the entropy gradient along the curved nose wave, can be obtained from Fig (2.5-13). For fineness ratios of 2 or greater and Mach Numbers of 1.5 or greater, the accuracy in ( $C_{DOP0}$ ) is of the order of  $\pm 5\%$  of the respective cone value ( $C_{DOPC}$ ). The curve in Fig (2.5-13) could be used on all types of ogive forebodies in a first approximation. In the case of secant-ogive forebodies, a fictitious forebody length ( $L_N$ ) and a maximum diameter ( $D$ ) should be introduced as clearly shown in Fig (2.5-7). Then,

$$C_{DOPFORE} \approx C_{DOP0} = C_{DOPC} + \Delta C_{DOP0} \quad (2.5-26)$$

For  $1 < M < 1.5$ , the cone results should be used due to lack of data and the inherent uncertainty of drag estimates at transonic speeds.

(3) Minimum drag forebodies at supersonic speeds, zero angle-of-attack:  $C_{DOPFORE}$ , see Section 2.5.1 paragraph (ii) (5), and Fig (2.5-14)

(4) Cone-cylinder and parabolic tangent ogive pressure drag at  $M_\infty = 1$  zero angle-of-attack:

In Ref. (2.5-19) by Spreiter, an approximate solution of the nonlinear equations of the small disturbance theory for transonic flows was used for determining the inviscid pressure drag on cone-cylinders and parabolic tangent-ogives for free stream Mach Number,  $M_H = 1$ . The results are in good agreement with other theories: Page(28), Taylor(23), Drougge(22), Oswatitsch(21), Miles(24), Yoshikara(26), and can be used for engineering purposes at a zero angle-of-attack. The respective working charts are given in Figs (2.5-4) and (2.5-5). The corresponding analytical expressions are:

$$(C_{DOPN})_{M=1} = -\left(\frac{D}{L_N}\right)^2 \left[ 1.08965 + 4 \log_8\left(\frac{D}{L_N}\right) \right] \quad (Spreiter) \quad (2.5-27)$$

for cylinder-cone combinations, and

$$(C_{DOP0})_{M=1} = \left(\frac{7}{3}\right) \left(\frac{D}{L_N}\right)^2 \quad (Oswatitsch) \quad (2.5-28)$$

for parabolic tangent-ogives.

In the Figs (2.5-4) and (2.5-5) the solid line curves should be used. Applicability of the results from the slender body theory is restricted to  $(L_N/D) > 3.0$ .

(5) Forebody bluntness effects,  $\Delta C_{DOPNTIP}$ .

The theoretical assumption of an ideally sharp forebody is not met exactly in practice. Due to some tip-bluntness, an additional drag increment from the high pressure region behind a curved detached shock wave shall exist. No exact theoretical generalized treatment of the problem in this form is available. Experimental evidence, Ref. (2.5-59), with blunted cones indicates, however, that no appreciable drag rise has been found for Mach Numbers ( $1 < M < 7$ ), provided the bluntness does not exceed 15%, i.e.,

$$\frac{R_{BL}}{(D/2)} < 0.15 \quad (2.5-29)$$

Therefore, under the above conditions, no additional corrections of the pressure drag values of cones (or ogives) should be performed. For higher bluntness ratios, the semi-empirical curves in Fig (2.5-15) should be used. They are computed by the "normal shock" method and compared with experimental evidence. The curve corresponding to  $(L_F/R_{BL}) = 1$  (hemispherical bluntness) is recommended, with  $(R_{BL})$  determined as the actual case may require. The associated drag coefficient values,  $C_{DOBL}$  in Fig (2.5-15), are based on cross-sectional blunt area ( $\pi R_{BL}^2$ ) and should be subsequently reduced to the common reference area ( $\pi D^2/4$ ) before adding to the other pressure drag terms, i.e.,

$$\Delta C_{DOPNTIP} = 4 C_{DOBL} \left(\frac{R_{BL}}{D}\right)^2 \quad (2.5-30)$$

Alternatively, the simple Newtonian impact theory may be used, as specified in Section 2.5.2, paragraph (vii).

(ii) Inviscid Afterbody Pressure Drag,  $C_{DOPBT}$

This is the drag component that the afterbody would have due to boattailing, if it were theoretically situated behind an infinitely long midbody in an inviscid fluid flow, i.e., without any interference effects.

(1) Truncated conical afterbodies of circular cross-section

A working graph is presented in Fig (2.5-16). The curves were computed in Ref. (2.5-1) (RAS Data Sheets) by application of the similarity laws to the respective second order theories, assuming that the flow conditions upstream of the afterbody are uniform, and that the flow is parallel to the axis of the afterbody, (no base pressure, i.e., atmospheric conditions at the base, no trailing shock wave).

(2) Truncated parabolic afterbodies of circular cross-section

A working graph is presented in Fig (2.5-17). It is assumed that the parabolic arcs are tangential to the midbody. To the order of accuracy of the theory, the curves may be applied to circular arc afterbodies also. The curves were obtained by application of the similarity laws to the "method of characteristics" and "quasi-cylinder" results by van Dyke (12) and Fraenkel (33).

(3) A semiempirical method for inviscid afterbody pressure drag estimates

Alternatively, the following semi-empirical expressions from Stoney (60) can be used:

$$C_{DOPBT} = \frac{.001 \theta_p^2 + .00071 \theta_p^3}{M_H} \left[ 1 - \left(\frac{D_B}{D}\right)^n \right] \quad (2.5-30a)$$

where

$$n = 4 \text{ for } 1 < M_H < 3.5,$$

$$n = 3 \text{ for } M > 3.5,$$

and  $(\theta_p)$  is the slope of a parabolic afterbody in degrees at the base, used as positive and not exceeding  $15^\circ$ , see Fig (2.5-18).

In a first approximation, the Eq (2.5-30) can be used for conical afterbodies also, with  $(\theta_p)$  not exceeding  $7.5^\circ$ , since for any inscribed cone in a parabolic afterbody,

$$\theta_p = \frac{\theta_c}{2} \quad , \text{ see Fig (2.5-18)}. \quad (2.5-31)$$

A graphical presentation of the Eq (2.5-30) for direct computational use is given in Fig (2.5-19) as  $C_{DOPBT} = f(M_H, \theta_p)$ . Corresponding numerical values are tabulated in Tables (2.5-3) and (2.5-4) for  $\theta_p = 2^\circ, 4^\circ, 6^\circ, 8^\circ, 10^\circ, 12^\circ$ .

In the Fig (2.5-19), the geometric ratios  $(L_{BT}/D)$  and  $(D_B/D)$  for constant

( $\theta_p$ ) values are also presented for convenience as computed by the approximate expression,

$$\left(\frac{L_{BT}}{D}\right) \approx \frac{1 - (D_B/D)}{2 \tan(\theta_p/2)} \quad (2.5-32)$$

(4) Fin interference effects on afterbody pressure drag,  $\Delta C_{DOPBT(F)}$ .

Data not available.

(5) Forebody-afterbody inviscid interference drag,  $\Delta C_{DOPBT(FORE)}$ .

The interference drag can be calculated by the "slender-body" and the "quasi-cylinder" theories. Generally, it is a fairly small proportion of the total inviscid pressure drag, see Ref. (2.5-1)(R.A.S. Data Sheets) and Ref.(2.5-61)(Fraenkel). It should be taken into account only for small total fineness ratio bodies, with relatively short midbodies (cylindrical parts):

$$\left(\frac{L_{CYL}}{L_{BT}}\right) < 1.50, \quad \left(\frac{L}{L_{BT}}\right) < 350, \quad L = L_N + L_{CYL} + L_{BT} \quad (2.5-33)$$

In case of such "short" configurations, the working graphs on Fig (2.5-20) and Fig (2.5-21) can be used for conical and parabolic fore-afterbody configurations respectively. A modified equivalent afterbody length ( $L_{BT}$ ) should be determined as indicated in the figures. Then, with the first approximation, from the geometry:

$$\Delta D'_{OPBT(FORE)} = \Delta C'_{DOPBT(FORE)} S r q = \Delta C'_p S'_{WET} q \sin(\theta_B/2),$$

$$\Delta C'_{DOPBT(FORE)} = 2 \Delta C'_p \left[ \pi D L'_{BT} \sec(\theta_B/2) \sin(\theta_B/2) \right] / \pi D^2,$$

and since

$$\sec(\theta_B/2) \sin(\theta_B/2) = \tan(\theta_B/2) = \frac{1}{2} \left(\frac{D}{L_{BT}}\right),$$

$$\Delta C'_{DOPBT(FORE)} = \Delta C'_p \quad (2.5-34)$$

Furthermore:

$$\Delta D'_{OPBT(FORE)} = \Delta C'_p S'_{WET} q \sin(\theta_B/2)$$

$$\text{and } \Delta D_{OPBT(FORE)} = \Delta C'_p S_{WET} q \sin(\theta_B/2),$$

$$\text{i.e., } \Delta D_{OPBT(FORE)} = \Delta D'_{OPBT(FORE)} \frac{S_{WET}}{S'_{WET}}$$

$$\text{and } \Delta C_{DOPBT(FORE)} = \Delta C'_{DOPBT(FORE)} \frac{S_{WET}}{S'_{WET}},$$

where:

$$S'_{WET} = \frac{1}{2} \pi D L'_{BT} \sec(\theta_B/2),$$

$$S_{WET} = \frac{1}{2} \pi D L'_{BT} \sec(\theta_B/2) - \frac{1}{2} \pi D_B (L'_{BT} - L_{BT}) \sec(\theta_B/2),$$

$$\therefore S_{WET} = \left[ \frac{1}{2} \pi D L'_{BT} \sec(\theta_B/2) \right] \left[ 1 - (D_B/D) (1 - L_{BT}/L'_{BT}) \right] \quad (2.5-36)$$

and

$$\frac{S_{WET}}{S'_{WET}} = \left[ 1 - (D_B/D) (1 - L_{BT}/L'_{BT}) \right] \quad (2.5-37)$$

Finally:

$$\begin{aligned} \Delta C_{DOPBT(FORE)} &= \\ &= \Delta C'_{DOPBT(FORE)} \left[ 1 - (D_B/D) (1 - L_{BT}/L'_{BT}) \right] \end{aligned} \quad (2.5-38)$$

where  $\Delta C'_{DOPBT(FORE)}$  should be taken from Figs (2.5-20) and (2.5-21) for conical and parabolic afterbodies respectively. In both cases, ( $\theta_B$ ) is the slope angle of an inscribed cone, see Fig. (2.5-18).

(iii) Viscous Form Drag,  $C_{DOPBVIS}$

Due to lack of generalized data, the viscous form drag on bodies is not evaluated. It is believed that the error is negligible with the adopted methods of total drag estimates since:

(1) The afterbody viscous form drag is usually negative and to a greater or lesser extent, counterbalances the forebody viscous form drag, see Ref. (2.5-1) (RAS Data Sheets).

(2) The adopted fully turbulent boundary layer skin-friction coefficient estimates are sufficiently conservative to compensate for the other minor viscous effects.

(iv) The Final Expression for the Body Zero-lift Pressure Drag Coefficient at Supersonic Speeds, see Tables (2.5-14) and (2.5-15)

$$\begin{aligned} (C_{DOPC} + \Delta C_{DOPD} + \Delta C_{DOPNTIP}) \\ + (C_{DOPBT} + \Delta C_{DOPBT(FORE)}) \end{aligned} \quad (2.5-39)$$

The Eq (2.5-39) represents a working approximation of the initial Eq (2.5-24).

The second term is zero for no boat-tailing, i.e., for ( $\Theta_B = 0$ ).

At subsonic speeds, with the above approximations, the theoretical zero-lift pressure drag is zero. Instead, semi-empirical and experimental data should be used from the related

technical literature.

At transonic speeds, ( $M_{cr} < M < 1.2$ ), the experimental data are required for "rounding" off the theoretical drag curves.

At higher hypersonic speeds, ( $M_\infty > 15$ ), the simple Newtonian impact theory data can be used, see Ref. (2.5-14).

## 2.5.4 THE EXPRESSIONS AND THE DATA FOR THE PRESSURE DRAG COEFFICIENT ESTIMATES ON WINGS AND FINS

$$\begin{aligned}
 & (C_{DOPWEXP} + \Delta C_{DOPW(B)} + \Delta C_{DOPM(W)}) + \\
 & \quad (C_{DOPFEXP} + \Delta C_{DOPF(W+B)} + \\
 & \quad + \Delta C_{DOPF(ET)}) + (C_{DOPWLE} + C_{DOPFLE}) \\
 & \quad + (C_{DOPWVIS} + C_{DOPFVIS})
 \end{aligned}
 \tag{2.5-40}$$

The proposed working graphs for wings and fins and the respective analytical expressions are chosen on the basis of the "linearized" and the "second order" inviscid flow theory data.

The respective experimental inviscid pressure drag measurements, Ref. (2.5-1) (RAS Data Sheets), indicate a decisive limitation of the theoretical estimates to supersonic speeds ( $M_\infty > 1.2$ ). In the transonic region ( $M_{crw} < M < 1.2$ ) an experimentally biased "rounding off" of the excessive theoretical drag-peaks is necessary.

The theoretical curves resulting from Ackert's linearized supersonic wing theory, see Ref. (2.5-3), exhibit sharp "kinks" in the transonic region, indicating that the leading edges, the trailing edges, or the maximum thickness ridge lines have become sonic. Since the theory does not hold for ( $M \approx 1.0$ ), the engineering restriction, ( $M_\infty > 1.2$ ), is imposed to the theoretical results.

The supersonic ( $M_\infty > 1.2$ ) theoretical values of the inviscid pressure drag coefficient are believed to be slightly higher when compared with respective experimental pressure drag measurements, see Ref. (2.5-1) (RAS Data Sheets), the excess being of the order of + 5%. Since the wing pressure drag contributes but a small fraction, no corrections for the slightly higher theoretical results are considered necessary.

Interpretation of the related experimental pressure drag data requires some caution. In general, the tests are run at very low Reynolds Numbers, under ideal surface conditions, and with skin-temperatures largely different from those encountered under actual flight situations. Besides, the base-drag component at the trailing edge, the pressure changes along the wing surface due to boundary layer growth and the accompanying rear-end

wake formation, are difficult to separate from the experimentally measured total pressure data in order to obtain the pure "inviscid" pressure drag fraction. These effects are relatively significant with thin airfoils, where the viscous wake thickness at the trailing edge may be comparable to the airfoil thickness itself. Furthermore, the fully laminar boundary layer existence with some highly controlled experiments, associated with low test Reynolds Numbers and an idealized surface-finish, requires that the application of the wind tunnel inviscid pressure drag data to actual full scale flight conditions be done with due reservations, even if the wind tunnel data are tentatively "cleaned" from the viscous effects (which is rarely the case).

Use of the proposed theoretical charts and the related analytical expressions is thus based on the following main assumptions:

(a) The theoretical inviscid pressure drag data are valid only for ( $M > 1.2$ ). An attached oblique shock wave pattern at the leading edge is assumed, and the wake effects are neglected at the trailing edge. Therefore, before proceeding with use of the data, the "profile-angle limitation" curve in Fig (2.5-22) should be consulted, in order to ascertain that no shock-wave detachment occurs.

(b) The leading-edge bluntness effects, promoting a slight bow wave detachment and a consequent pressure increase, are taken into account separately. The pressure drag distribution on the rest of wing surface is not affected by this phenomena, except for the immediate neighborhood around the stagnation point, ( $\sim .02C$ ).

(c) Corrections for the boundary layer thickening and the viscous wake formation effects on the inviscid pressure distribution around the thin airfoils are additionally performed. Note that the trailing edge base-drag (or trailing edge-bluntness pressure drag) is considered separately in the next Section, 2.6.

(d) Effects of the actual skin-temperatures are considered restricted

to the boundary layer and therefore neglected in the inviscid flow analysis.

The associated theoretical and experimental evidence applied in evaluating the various terms in the Eq (2.5-40) is summarized as follows:

(i) Inviscid Pressure Drag,  $C_{DOPWEXP}$  and  $C_{DOPFEXP}$ .

At a zero angle-of-attack, the three dimensional, inviscid pressure drag coefficient at supersonic speeds is a function of the following main parameters:

- (a) airfoil thickness,
- (b) airfoil shape,
- (c) airfoil camber,
- (d) location of the maximum thickness line,
- (e) wing planform and aspect ratio,
- (f) sweep-back angles of the leading edge, the trailing edge, and the maximum thickness line,
- (g) wing taper ratio,
- (h) free stream Mach Number.

Following the usual missile design trends, only wing planforms with symmetric airfoil sections are considered. For cambered airfoil data see Refs. (2.5-1), (2.5-3), and (2.5-62).

In developing the working charts and the related analytical expressions, the "linearized" and the "second-order" supersonic theories were used. For other theoretical data, especially at hypersonic speeds, see Ref. (2.5-14). The subsonic speed regime and the related theoretical airfoil data can be found in the extensively elaborated forms in Ref. (2.5-62) and (2.5-1).

At supersonic speeds, the two-dimensional, double wedge, double symmetry airfoil, having the minimum theoretical inviscid pressure drag value, has been chosen as a basic reference in estimating the influence of various other airfoil shapes and the maximum thickness line positions. The viscous form drag contribution through the wake-formation on the inviscid pressure drag value is included directly here for the sake of convenience (but excluding trailing edge base

pressure effects).

(ii) Two-Dimensional Inviscid Plus Viscous Zero-Lift Pressure Drag of Double Wedge, Double Symmetry Airfoil Sections.

This represents the theoretical minimum pressure drag. According to the linearized theory by Ackeret(3):

$$C'_{DOPW} = 4 \frac{(t/c)^2}{\beta} = 2C_1(t/c)^2 \quad (2.5-41)$$

where

$$C_1 = \frac{2}{\beta} = \frac{2}{(M_\infty^2 - 1)^{1/2}} \quad (2.5-42)$$

is Busemann's coefficient, see Table (2.5-4) and Fig (2.5-22).

This basic minimum two-dimensional value should be corrected for viscous effects as follows(3):

A frictional wake is developed at the wing trailing edge, even at supersonic speeds. The width of the wake depends on the boundary layer type and the Reynolds Number value. It changes the effective profile shape and the inviscid pressure distribution at the rear of the airfoil, since the trailing edge region is immersed in a stagnant air of the wake. Consequently, the actual geometric shape of the trailing edge loses its relative importance, the profile shape being effectively not closed at the rear end. Considering the boundary layer thickness as a supplementary part of the solid body contour (as far as the external inviscid flow is concerned), the tail-wave losses shall be decreased through a lesser angle of the rear-flow deflection. As a consequence, the total inviscid pressure (wave) drag will be less than theoretically predicted (base drag effects are considered separately).

This wake-formation effect may be conveniently handled by assuming that the chord (and the exposed area) of the wing is shortened to an effective length up to the point where the wake starts. Subsequently, this decreases the pressure coefficient value as referred to the actual geometric wing planform.

By using the Fig (2.5-23), the decreased  $C'_{DOPW}$  value of any symmetrical airfoil section may be thus computed from the expression,

$$C'_{DOPW} \approx 2C_1 \left( \frac{t}{\bar{c}_{WEXP}} \right) \left( \frac{\bar{c}_e}{\bar{c}_{WEXP}} \right), \quad (2.5-43)$$

where  $(\bar{c}_e)$  is the effective mean geometric chord as referred to the shortened airfoil, see Fig (2.5-23) and Table (2.5-5) at the end of this Section:

$$\bar{c}_e = \bar{c}_{WEXP} \left[ 1 - \frac{2\delta_{TE} + t_{TE}}{t} r \right] \quad (2.5-44)$$

where

$\delta_{TE}$  - is the turbulent or laminar boundary layer thickness at the trailing edge, see (Table 2.5-6),

$t_{TE}$  - is the trailing edge bluntness due to manufacture,  $\sim .01$  ft,

$(1-r) = (x/\bar{c}_{WEXP})(t/\bar{c})_{max}$  - is the position of maximum thickness,  $(t/\bar{c})_{max}$ , in fractions of the mean geometric chord,  $\bar{c}_{WEXP}$ ,

$(\prime)$  - denotes the two-dimensional value.

Thus, a corresponding two-dimensional corrective factor, representing the viscous effects on the basic inviscid pressure drag distribution, can be formulated as

$$\zeta_1 = \frac{\bar{c}_e}{\bar{c}_{WEXP}} = \left[ 1 - \frac{2\delta_{TE} + t_{TE}}{t} r \right]. \quad (2.5-45)$$

For double-symmetry airfoils,  $r = .5$ .

Actually, there are no exact theoretical methods for an accurate treatment of this phenomena, and the above correction should be regarded only as approximate. The thinner the airfoil, the relatively more pronounced the viscous effect becomes, but the width of friction wake does not usually exceed 4% of the geometric airfoil chord, according to existing photographic observations, see Ref. (2.5-3).

The trailing edge bluntness,  $t_{TE}$ , in the Eq (2.5-45) depends upon the actual manufacturing procedure. An average value of 0.01 ft. may be assumed.

The compressible turbulent boundary layer thickness at the trailing edge,  $\delta_{TE}$ , can be determined from Fig (2.5-24) as

$$(\delta/\delta_i)_{TE} = f(M_\infty), \quad (\text{van Driest}) \quad (2.5-46)$$

where

$$\delta_i = \frac{.37L}{(Re_L)^{1/2}} \quad (\text{Blasius, T.B.L.}), \quad (2.5-46)$$

$$\text{or} \quad \delta_i = \frac{5.2L}{(Re_L)^{1/2}} \quad (\text{Blasius, L.B.L.}) \quad (2.5-47)$$

for incompressible turbulent boundary layers.

In a first approximation, the same  $(\delta/\delta_i) = f(M_\infty)$  law from Fig (2.5-24) may be used for laminar boundary layers, since the trailing edge bluntness analysis, as presented here, is very approximate in itself.

### (iii) Three-Dimensional Inviscid Plus Viscous Pressure Drag on Wings and Fins

The three-dimensional values of the pressure drag coefficient for various planforms, airfoil sections, taper ratios, maximum thickness line positions and sweep back angles are specified below. The respective working charts are presented in Figs (2.5-22) to (2.5-50). The corresponding analytical expressions are tabulated in Table (2.5-5).

In all cases, the drag coefficient,  $C'_{DOPW}$ , is reduced to the common reference area, for instance,

$$S_r = (\pi D^2/4); \quad C_{DOPWEXP} = \frac{S_{WEXP}}{(\pi D^2/4)} C'_{DOPW} \quad (2.5-48)$$

where  $C'_{DOPW}$  is referred to the wing exposed area, and is corrected for all viscous and three dimensional flow effects according to the self-explanatory Tables (2.5-5) and (2.5-6). The corrections are derived as follows:

#### (I) STRAIGHT RECTANGULAR PLANFORM WINGS, $C_{DOPWEXP}$ , see Tables (2.5-5), (2.5-6) and (2.5-7).

##### (I.1) STRAIGHT RECTANGULAR PLANFORM WINGS WITH DOUBLE WEDGE, DOUBLE SYMMETRY AIRFOIL, NO TAPER, ZERO ANGLE-OF-ATTACK

From the Busemann's finite wing theory, applied to this case (I.1), if the  $(t/\bar{c}_{WEXP})$  is small and the binomial expansion is used:

$$C_{DOPWEXP} = \zeta_7 \left\{ 2C_1 \left( \frac{t}{\bar{c}_{WEXP}} \right)^2 \times \zeta_1 \left[ 1 - \frac{1}{2AR\beta} \left( 1 - \frac{C_2}{C_1} \frac{t}{\bar{c}_{WEXP}} \right) \right] \right\}, \quad (2.5-49)$$

$\therefore C_{DOPWEXP} = \zeta_1 \zeta_7 \textcircled{A} \textcircled{B}$ , see T-(2.5-5) and (2.5-6) at the end of this section.

where: (2.5-50)

$(t/\bar{c}_{WEXP})$  - is the maximum airfoil thickness at mean geometric chord,

AR - is the exposed wing aspect ratio,

$C_1$  and  $C_2$  - are the Busemann's coefficients, see Table (2.5-4) or Fig. (2.5-22) for appropriate values as functions of Mach Number.

The Equation (2.5-50) is in good agreement with experimental evidence. The meaning of the terms is as follows:

$$\zeta_7 = 1.275 \left( \frac{D_{WEXP}}{D} \right) \left( \frac{\bar{c}_{WEXP}}{D} \right) = \frac{S_{WEXP}}{(\pi D^2)/4} \quad (2.5-51)$$

$\textcircled{A} = 2C_1 \left( \frac{t}{\bar{c}_{WEXP}} \right)^2$  - is the two-dimensional pressure coefficient value at a zero-angle of attack for a double-wedge, double-symmetry airfoil (Ackeret linear theory term), Eq (2.5-52),

$\zeta_1$  - is the corrective factor for viscous effects, Eq (2.5-45),

$\left[ 1 - \frac{1}{2AR\beta} \right]$  - is the correction factor for finite aspect ratio effects at wing-tips,

$\left[ 1 - \frac{C_2}{C_1} \left( \frac{t}{\bar{c}_{WEXP}} \right) \right]$  - is the second order corrective factor for finite thickness wings (Busemann),

$$\textcircled{B} = \left\{ \left[ 1 - \frac{1}{2AR\beta} \right] \left[ 1 - \frac{C_2}{C_1} \left( \frac{t}{\bar{c}_{WEXP}} \right) \right] \right\}, \quad (2.5-53)$$

$$\beta = (M_\infty^2 - 1)^{1/2} \quad (2.5-54)$$

In the following text, the additional corrections for variations in the airfoil sections are introduced. Since the corrective factors are taken from the Ackeret linear two-dimensional theory, they apply only to the two-dimensional term,  $\textcircled{A}$ , in Eq (2.5-50), and not to the last second order corrective factor  $\textcircled{B}$ .

(I.2) STRAIGHT RECTANGULAR PLANFORM WINGS WITH ARBITRARY AIRFOIL SECTION, NO TAPER, ZERO ANGLE-OF-ATTACK.

Correction for the profile shape should be introduced as follows:

(a) For a symmetrical biconvex airfoil section with the  $(t/c)_{max}$  at 50% of the chord, the value of the two-dimensional term,

$$\textcircled{A} = 2C_1 \left( \frac{t}{\bar{c}_{WEXP}} \right)^2,$$

in the Eq (2.5-50) should be multiplied by the factor  $\zeta_2 = 4/3$ , (Ackeret linear theory), i.e.,

$$C_{DOPWEXP} = \zeta_7 \left\{ \textcircled{A} \times \textcircled{B} \times \zeta_1 \times \zeta_2 \right\}, \quad (2.5-55)$$

where:

$$\textcircled{B} = \left\{ \left[ 1 - \frac{1}{2AR\beta} \right] \left[ 1 - \left( \frac{C_2}{C_1} \right) \left( \frac{t}{\bar{c}_{WEXP}} \right) \right] \right\},$$

$$\textcircled{A} = 2C_1 \left( \frac{t}{\bar{c}_{WEXP}} \right)^2, \quad (2.5-56)$$

$$\beta = (M_\infty^2 - 1)^{1/2} \quad (2.5-53)$$

and  $\zeta_1$ ,  $\zeta_2$  and  $\zeta_7$  are the corrective factors, defined earlier.

The relative increase in the zero-lift pressure drag is due physically to changes of the bow and trailing edge oblique shock patterns, caused by profile curvatures.

(b) For a symmetrical single-wedge airfoil with completely bluff base at its  $(t/c)_{max}$  section, assuming the inviscid theory pressure drag at the front part of the single wedge, excluding the bluff base. An expansion wave instead of a trailing-edge shock wave exists, which decreases the two-dimensional drag coefficient value to one-fourth as compared with a double-wedge, i.e., from  $2C_1 (t/\bar{c}_{WEXP})$  to  $1/2 C_1 (t/\bar{c}_{WEXP})$ . But, the existing experimental evidence, Ref (2.5-3), indicates that an average value of  $(p_b/p_H) = 1/3$  prevails for Mach Number values greater than 1.5 at the base, where  $p_b$  is the base pressure. So, according to the Ackeret linear theory, the corrective two-dimensional term should read:

$$\zeta_5 = \frac{2 \left[ 1 - (p_b/p_H) \right] (t/\bar{c}_{WEXP})}{8 M_\infty^2} + \frac{1}{2} C_1 (t/\bar{c}_{WEXP})^2, \quad (2.5-58)$$

$$\therefore \zeta_5 = \frac{.95 (t/\bar{c}_{WEXP})}{M_\infty^2} + \frac{1}{2} C_1 (t/\bar{c}_{WEXP})^2, \quad (2.5-59)$$

where the first term is an additional correction for the change in the expansion intensity at the trailing edge due to the empirical base pressure

ratio,  $(p_b / p_H) = 1/3$ .

The drag coefficient of the wing reads then:

$$C_{DOPWEXP} = \zeta_7 \times \zeta_5 \times \textcircled{B}, \quad (2.5-60)$$

where

$$\zeta_7 = 1.275 \left( \frac{b_{WEXP}}{D} \right) \left( \frac{\bar{C}_{WEXP}}{D} \right), \text{Eq}(2.5-51),$$

$$\zeta_5 = \text{Eq}(2.5-59),$$

$$B = \left\{ \left[ 1 - \frac{1}{2AR(M_\infty^2 - 1)^{1/2}} \right] \left[ 1 - \left( \frac{C_2}{C_1} \right) \left( \frac{t}{\bar{C}_{WEXP}} \right) \right] \right\} \cdot \text{Eq}(2.5-53)$$

(c) For a symmetrical biconvex half-airfoil with completely bluff base at its  $(t/c)_{MAX}$  section, following the statements presented in (b), the zero-lift pressure drag coefficient of the wing, reads:

$$C_{DOPWEXP} = \zeta_2 \times \left[ \zeta_7 \times \zeta_5 \times \textcircled{B} \right], \quad (2.5-61)$$

where  $\zeta_2 = 4/3$ , and  $\zeta_5$ ,  $\zeta_7$  and  $\textcircled{B}$  are as earlier.

(d) For a symmetrical double-wedge airfoil with the maximum thickness  $(t/c)_{MAX}$  position shifted either forward or backward, the pressure drag coefficient, Eq (2.5-49), should be multiplied by the corrective factor,  $\zeta_3$ , as presented in Fig (2.5-26), where

$$\zeta_3 = \frac{1}{4 \left( \frac{X}{C} \right) \left( 1 - \frac{X}{C} \right)}, \quad \text{Ref}(2.5-3) \text{ (Hilton)}, \quad (2.5-62)$$

where  $X$  is the chordwise position of the maximum thickness from the leading edge,

$$\text{i.e., } C_{DOPWEXP} = \zeta_7 \times \zeta_1 \times \zeta_3 \times \textcircled{A} \times \textcircled{B}, \quad (2.5-63)$$

where factors  $\zeta_1$ ,  $\zeta_3$ ,  $\zeta_7$ ,  $\textcircled{A}$  and  $\textcircled{B}$  are as defined earlier. The same corrective factor,  $\zeta_3$ , should be applied to the Eq (2.5-55) in the case of a biconvex airfoil with a shifted maximum thickness, i.e.:

$$C_{DOPWEXP} = \zeta_7 \left[ \textcircled{A} \times \textcircled{B} \times \zeta_1 \times \zeta_2 \right] \zeta_3. \quad (2.5-64)$$

(e) For a double-symmetry modified double-wedge airfoil section, the two-dimensional pressure drag coefficient term,  $2C_1(t/\bar{C}_{WEXP})$ , should be multiplied by  $(a_1 + a_2) / 4a_1a_2$ , if the three-dimensional wing pressure drag coefficient is based on the wing (exposed) total planform, see Table (2.5-5):

$$C_{DOPWEXP} = \left[ \zeta_7 \times \textcircled{A} \times \textcircled{B} \times \zeta_1 \right] \zeta_4, \quad (2.5-65)$$

where

$$\zeta_4 = \frac{a_1 + a_2}{4a_1a_2}, \quad (2.5-66)$$

and  $\textcircled{A}$ ,  $\textcircled{B}$ ,  $\zeta_1$ , and  $\zeta_7$  are as earlier.

All the corrections for various airfoil shapes are presented in the Table (2.5-5). The computation procedure for straight rectangular planforms is illustrated in Tables (2.5-6) and (2.5-7) at the end of this Section.

(II) DELTA WING PLANFORMS, see Tables (2.5-5), (2.5-6) and (2.5-9).

(II.1) SUPERSONIC DELTA WING WITH DOUBLE WEDGE SYMMETRIC AIRFOIL(69)

Linear theory data:

Case I: See the respective figure on Table (2.5-5).

Surfaces A, B, C, all supersonic, i.e., supersonic leading edge and supersonic maximum thickness line:

$$\beta > \tan \Lambda_0 > \tan \Lambda_1, \quad (2.5-67)$$

where

$$\beta = (M_\infty^2 - 1)^{1/2} = \cot m = \tan(90^\circ - m) = \tan \mu$$

and

$$m = \sin^{-1} \left( \frac{1}{M_\infty} \right).$$

The leading edge and the maximum thickness line sweep back angles are  $\Lambda_0$  and  $\Lambda_1$ , respectively.

The location of maximum thickness is defined as  $(1-r)$  chords from the tip, i.e.,

$$r = \frac{\tan \Lambda_1}{\tan \Lambda_0}. \quad (2.5-68)$$

The corresponding three-dimensional zero-lift pressure drag coefficient due to thickness, reduced to the reference area,  $S_r = (\pi D^2) / 4$  is:

$$C_{DOPWEXP} = \zeta_7 \times \zeta_1 \times C'_{DOPW},$$

$$\therefore C_{DOPWEXP} = \left[ 1.275 \left( \frac{b_{WEXP}}{D} \right) \left( \frac{\bar{C}_{WEXP}}{D} \right) \right] \times \left[ 1 - \frac{2\delta_{TE} + t_{TE}}{t} r \right] \times \quad (2.5-69)$$

$$\times \left\{ \frac{2}{\pi} \frac{(t/\bar{C}_{WEXP})^2}{\beta(1-r^2)} \left[ \frac{1}{(1-n^2)^{1/2}} \cos^{-1}(n) + \frac{1}{r(1-r^2 n^2)^{1/2}} \times \left( \frac{\pi}{2} + \sin^{-1}(rn) \right) \right] \right\} \quad (2.5-70)$$

for ( $n < 1$ ), and ( $0 < r < 1$ ), where

$$n = \frac{\tan \Lambda_0}{\beta}, \quad \beta = (M_\infty^2 - 1)^{1/2} = \cot m \quad (2.5-71)$$

Curves ( $C_{DOPW\beta}' / (t/\bar{c})^2$ ) versus ( $1-r$ ) are plotted in Fig (2.5-30).

**Case II:** See respective figures in Table (2.5-5).

Surfaces A and B are subsonic, surface C is supersonic, i.e., subsonic leading edge and supersonic maximum thickness line:

$$\tan \Lambda_1 > \beta > \tan \Lambda_0.$$

The three-dimensional zero-lift pressure drag coefficient due to thickness, reduced to the reference area,  $S_r = (\pi D^2/4)$ , takes the form:

$$C_{DOPWEXP} = \zeta_7 \times \zeta_1 \times C_{DOPW}' \quad (2.5-72)$$

$$C_{DOPWEXP} = \left[ 1.275 \left( \frac{b_{WEXP}}{D} \right) \left( \frac{\bar{C}_{WEXP}}{D} \right) \right] \times \left[ 1 - \frac{2\delta_{TE} + t_{TE}}{t} r \right] \times \left\{ \frac{2}{\pi} \frac{(t/\bar{C}_{WEXP})^2}{\beta} \left[ \frac{G_2(n,r)}{r(1-r)^2} + \frac{1}{r(1-r)} \left( \frac{\pi}{2} - \frac{\log_e n}{(n^2-1)^{1/2}} - \sin^{-1}\left(\frac{1}{n}\right) \right) \right] \right\}, \quad (2.5-73)$$

where:

$$G_2(n,r) = \frac{1-r}{1+r} \left[ \frac{\log_e n}{(n^2-1)^{1/2}} + \frac{r \cosh^{-1} n}{(n^2-1)^{1/2}} + \frac{2}{(1-r^2 n^2)} \tan^{-1} \left( \frac{(1-r^2 n^2)^{1/2}}{n + (n^2-1)^{1/2} - rn} \right) \right] \quad (2.5-74)$$

and

$$n = \frac{\tan \Lambda_0}{\beta} = \frac{\tan \Lambda_0}{\cot \mu},$$

valid for: ( $n > 1$ ) and ( $rn < 1$ ).

A crossplot of ( $C_{DOPW\beta}' / (t/\bar{c})^2$ ) versus ( $1-r$ ) is given in Fig (2.5-31) for ( $n > 1$ ).

**Case III:** See respective figure in Tables (2.5-5), (2.5-6) and (2.5-7).

Surfaces A, B, and C are all sub-

sonic, i.e., both the leading edge and the maximum thickness are subsonic:

$$\tan \Lambda_0 > \tan \Lambda_1 > \beta = (M_\infty^2 - 1)^{1/2}. \quad (2.5-75)$$

The three-dimensional zero-lift pressure drag coefficient due to thickness, reduced to the reference area,  $S_r = (\pi D^2/4)$ , is in this case:

$$C_{DOPWEXP} = \zeta_7 \times \zeta_1 \times C_{DOPW}'$$

$$C_{DOPWEXP} = \left[ 1.275 \left( \frac{b_{WEXP}}{D} \right) \left( \frac{\bar{C}_{WEXP}}{D} \right) \right] \times \quad (2.5-76)$$

$$\times \left[ 1 - \frac{2\delta_{TE} + t_{TE}}{t} r \right] \times \left\{ \frac{2}{\pi} \frac{(t/\bar{C}_{WEXP})^2}{\beta} \times \left[ \frac{G_2'(n,r)}{r(1-r)^2} - \frac{F'(n,r)}{(1-r)^2} + \frac{1}{r(1-r)} \left( \frac{\log_e nr}{(r^2 n^2 - 1)^{1/2}} - \frac{\log_e n}{(n^2 - 1)^{1/2}} + \sin^{-1}\left(\frac{1}{rn}\right) - \sin^{-1}\left(\frac{1}{n}\right) \right) \right] \right\}, \quad (2.5-77)$$

where:

$$G_2'(n,r) = \frac{1-r}{1+r} \left\{ \frac{\log_e n}{(n^2-1)^{1/2}} + \frac{r \cosh^{-1} n}{(n^2-1)^{1/2}} + \frac{1}{(r^2 n^2 - 1)^{1/2}} \log_e \left[ 1 + \frac{2(r^2 n^2 - 1)^{1/2}}{n(1-r) + (n^2-1)^{1/2} - (r^2 n^2 - 1)^{1/2}} \right] \right\}, \quad (2.5-78)$$

$$F'(r,n) = \frac{1-r}{1+r} \left\{ \frac{\log_e rn}{(r^2 n^2 - 1)^{1/2}} + \frac{1}{(n^2-1)^{1/2}} \times \log_e \left[ \frac{(rn^2-1) + (r^2 n^2 - 1)^{1/2} (n^2-1)^{1/2}}{n(1-r)} \right] \right\} \quad (2.5-79)$$

and

$$n = \frac{\tan \Lambda_0}{\beta}, \quad \beta = (M_\infty^2 - 1)^{1/2} = \cot \mu,$$

valid for ( $n > 1$ ), and ( $rn > 1$ ).

A crossplot of ( $C_{DOPW\beta}' / (t/\bar{c})^2$ ) versus ( $1-r$ ) is presented on Fig (2.5-31).

## (II.2) SUPERSONIC DELTA WING WITH ARBITRARY AIRFOIL SECTION

Corrections for airfoils different than the double wedge are performed in the same manner as for straight rectangular wing. The results are tabu-

lated in Table (2.5-5).

A detailed computation procedure is presented in Table (2.5-9)

(III) STRAIGHT TAPERED WING PLANFORMS, See Tables (2.5-5), (2.5-6) and (2.5-10)

(III.1) STRAIGHT TAPERED WINGS WITH DOUBLE WEDGE DOUBLE SYMMETRY AIRFOIL SECTION(69), See respective Figure in Table (2.5-5)

Here,  $(t/c)$  is constant along the span, or if not, an average  $(t/\bar{c}_{WEXP})$  should be used.

A crossplot of  $C_{DOPW} \beta / 4(t/\bar{c}_{WEXP})^2$  versus

$$n = \frac{\tan \Delta_0}{\tan \mu} = \frac{\tan \Delta_0}{\beta}$$

is presented in Fig (2.5-32) for three taper ratios:

$$\lambda = \frac{C_t}{C_r} = 0, .25, .50 \quad (2.5-80)$$

Note that the value  $4(t/\bar{c}_{WEXP})^2 / \beta = 2 C_t (t/\bar{c}_{WEXP})^2$  represents the two-dimensional pressure drag coefficient for double-wedge, double-symmetry airfoils of equal thickness ratio.

With the corrective factors  $(\zeta_1)$  and  $(\zeta_7)$  taken into account the final three-dimensional  $(C_{DOPWEXP})$  value, based on the reference area,  $S_r = (\pi D^2/4)$  takes the form:

$$C_{DOPWEXP} = \zeta_1 \times \zeta_7 \times C_{DOPW} \quad (2.5-81)$$

where  $C_{DOPW}$  should be read off from Fig (2.5-32).

(III.2) STRAIGHT TAPERED WINGS WITH ARBITRARY AIRFOIL SECTIONS.

Following the procedure indicated earlier for the straight rectangular wing planforms, the corrective factors for various airfoil shapes other than the double-wedge, double-symmetry basic airfoil, are tabulated in Table (2.5-5). A detailed computational procedure, is presented in the same table.

(IV) CLIPPED DELTA WING PLANFORMS

(IV.1) CLIPPED DELTA WING WITH DOUBLE WEDGE, DOUBLE SYMMETRY AIRFOIL SECTION(69)

Here,  $(t/c)$  is constant along the span, or if not, the average  $(t/\bar{c}_{WEXP})$  value should be used.

A comparative crossplot of the pressure drag parameter

$$(C_{DOPW} \beta) / 4(t/c)^2$$

versus

$$n = \frac{\tan \Delta_0}{\tan \mu} = \frac{\tan \Delta_0}{\beta}$$

is presented in Fig (2.5-33) for taper ratios,  $\lambda = 0$  and 0.50.

In comparison with the delta wing ( $\lambda = 0$ ) the relative drag reduction of a clipped delta wing is confined between  $.6 \leq n \leq 1.0$ . The absolute value of the drag reduction is small. For ( $n > 1$ ) the leading edge becomes subsonic.

The zero lift drag coefficient, reduced to the reference area and including the viscous corrective term, becomes:

$$C_{DOPWEXP} = \zeta_1 \times \zeta_7 \times C_{DOPW}$$

$$\therefore C_{DOPWEXP} = \left[ 1.275 \left( \frac{b_{WEXP}}{D} \right) \left( \frac{\bar{c}_{WEXP}}{D} \right) \right] \times \left[ 1 - \frac{2\delta_{TE} + t_{TE}}{t} r \right] \times C_{DOPW} \quad (2.5-82)$$

$$(2.5-83)$$

NOTE: Since the data in Fig (2.5-33) are based on linearized theory, it appears that, in a first approximation, the second-order pressure drag coefficient for delta wings (Table (2.5-9) and Figs (2.5-30) and (2.5-31)) can be used as valid for clipped delta wings also, the results being only slightly conservative. Thus, no additional computation table is necessary: the Table (2.5-9) can serve the purpose for both delta and clipped delta wings in a first approximation.

(IV.2) CLIPPED DELTA WING WITH ARBITRARY AIRFOIL SECTION.

Corrections for the airfoil shape and maximum thickness line position are presented in Table (2.5-5).

(V) STRAIGHT SWEEP-BACK NO TAPER WINGS, See Tables (2.5-5), (2.5-6) and (2.5-11)

Working graphs for swept-back wings with straight leading and trailing edges, streamwise tips, constant spanwise thickness/chord ratios with no

taper ( $\lambda = (C_f/C_r) = 1$ ), are presented in Figs (2.5-34), (2.5-35) and (2.5-36) in a generalized parametric form for zero-lift conditions. The airfoils are of double-wedge and parabolic arc sections with variable maximum thickness locations. The final expression for zero-lift pressure drag coefficient, reduces to the reference area,  $S_r = (\pi D^2)/4$ , with viscous form drag effects included, reads:

$$C_{DOPWEXP} = \zeta_1 \times \zeta_7 \times C'_{DOPW} \quad (2.5-84)$$

$$\therefore C_{DOPWEXP} = \left[ 1.275 \left( \frac{b_{WEXP}}{D} \right) \left( \frac{\bar{c}_{WEXP}}{D} \right) \right] \times \left[ 1 - \frac{2\delta_{TE} + t_{TE}}{t} r \right] \times C'_{DOPW} \quad (2.5-85)$$

Note: For variable spanwise thickness ratio ( $t/c$ ), an average value ( $t/\bar{c}_{WEXP}$ ) can be used as the reference in the first approximation.

The detailed computational procedure is presented in the Table (2.5-11).

(iv) Wing-Body Interference Drag:  $\Delta C_{DOPW(B)}$  and  $\Delta C_{DOPM(W)}$ .

Both the pressure drag increment of the exposed wing due to the presence of the body,  $\Delta C_{DOPW(B)}$ , and the pressure drag increment on the "central part" of the body at the wing location,  $\Delta C_{DOPM(W)}$ , are negligible for zero angle-of-attack of slender cylindrical bodies with relatively small planform symmetrical airfoil wings, i.e., in a first approximation (78):

$$\Delta C_{DOPW(B)} \approx 0 \quad ,$$

$$\Delta C_{DOPM(W)} \approx 0 \quad .$$

The same holds for fins:

$$\Delta C_{DOPF(W+B)} = 0 \quad .$$

$$\Delta C_{DOPF(BT)} = 0 \quad .$$

In Ref (2.5-79) by Coletti, it has been experimentally shown that the wing-body interference effects are mainly manifested as a slight increase of the skin-friction drag term, while the pressure drag stays almost unaffected. Since a sufficient margin is already allowed if a completely turbulent boundary layer on all missile parts is assumed, it is considered that no additional drag increment due to wing-body interference should be added. As a summary of technical data, respective to the problem, see Ref. (2.5-79) and other related References.

(v) Viscous Form Drag,  $C_{DOPWVIS}$  and  $C_{DOPFVIS}$ .

Effects of the viscous form drag with relatively thin airfoil sections are important, since the viscous wake and the respective boundary layer thicknesses are of the order of magnitude of the airfoil thickness itself. Changes in inviscid pressure drag due to effective change in airfoil shape are already included in the calculations of the inviscid pressure drag terms, see paragraph (i).

(vi) Leading Edge "Bluntness" Effects,  $C_{DOPWLE}$  and  $C_{DOPFLE}$ .

The manufacturing inevitable "bluntness" of the leading edge promotes a detached shock wave pattern, whose portion immediately ahead of the leading edge may be interpreted as a normal shock. The increased pressure behind a detached shock creates an additional drag term.

As an average engineering estimate, the bluntness effect may be approximated by a semi-cylindrical leading edge of radius,  $R_{BL} \approx .01t$ .

Two methods for  $C_{DOPWLE}$  or  $C_{DOPFLE}$  estimates are proposed:

(1) A quick approximate evaluation by the simple Newtonian impact theory, yielding independently of the Mach Number:

$$C_{DOPWLE} = 3.4 \left( \frac{R_{BL}}{D} \right) \left( \frac{b_{WEXP}}{D} \right) \cos^2 \Delta_{WLE} \quad (2.5-86)$$

and

$$C_{DOPFLE} = 3.4 N \left( \frac{R_{BL}}{D} \right) \left( \frac{h_{FEXP}}{D} \right) \cos^2 \Delta_{FLE} \quad (2.5-87)$$

where  $N$  is the number of individual fins,  $h_{FEXP}$  is the fin height, and  $\Delta_{LE}$  the leading edge sweep-back angle.

(2) A semi-empirical method from Ref. (2.5-1) (RAS Data Sheets), with ready to use working charts presented in the Fig (2.5-37). For semi-elliptical and semi-circular to completely blunt leading edges of two-dimensional airfoils, a stagnation pressure behind a normal shock is assumed, numerically the same at any point of the profile leading edge. The semi-circular curve in the Fig (2.5-37) is experimentally verified within  $\pm 10\%$  of accuracy and is recommended for use. The values of  $C_{DLE}$  from the figure are based on the leading edge projected area,  $(b_{WEXP}/\cos \Delta_{LE}) \times 2 R_{BL}$ , and there-

fore should be additionally reduced to the common reference area,  $S_r = \pi D^2/4$  :

$$C_{DOPWLE} = 2.55 C_{DLE} \frac{R_{BL}}{D} \frac{b_{WEXP}}{D} \cos^2 \Delta_{WLE} \quad (2.5-88)$$

and

$$C_{DOPFLE} = 2.55 C_{DLE} \frac{R_{BL}}{D} \frac{h_{FEXP}}{D} N \cos^2 \Delta_{FLE} \quad (2.5-89)$$

A detailed computational procedure is clearly indicated in the Table (2.5-12).

This second method is obviously more accurate. The order of magnitude of the  $(C_{DOPWLE})$  term is about 7% - 10% of the total wing pressure drag.

It is assumed that the slight bluntness does not affect the inviscid pressure distribution on the rest of the wing surface, except in the region near the leading edge, approximately up to  $.02c$ .

(vii) The Final Expression for the Wing and Fin Zero-Lift Pressure Drag

at Supersonic Speeds:

$$\begin{aligned} & [(C_{DOPWEXP} + C_{DOPWVIS}) + C_{DOPWLE}] + \\ & + [(C_{DOPFEXP} + C_{DOPFVIS}) + C_{DOPFLE}] \end{aligned} \quad (2.5-90)$$

The Equation (2.5-90) represents the final working form of the original Eq (2.5-40).

At subsonic speeds, the pressure drag is zero. At transonic speeds ( $M_{crw} < M < 1.2$ ), the curves must be "rounded", using experimental evidence.

In the Table (2.5-13), a comparative summary layout of results for various wing-planforms and airfoil shapes is schematically presented. It can be used for comparing variations in wing and profile shapes. For a chosen wing geometry, only one column in the Table in the final pressure drag analysis is necessary.

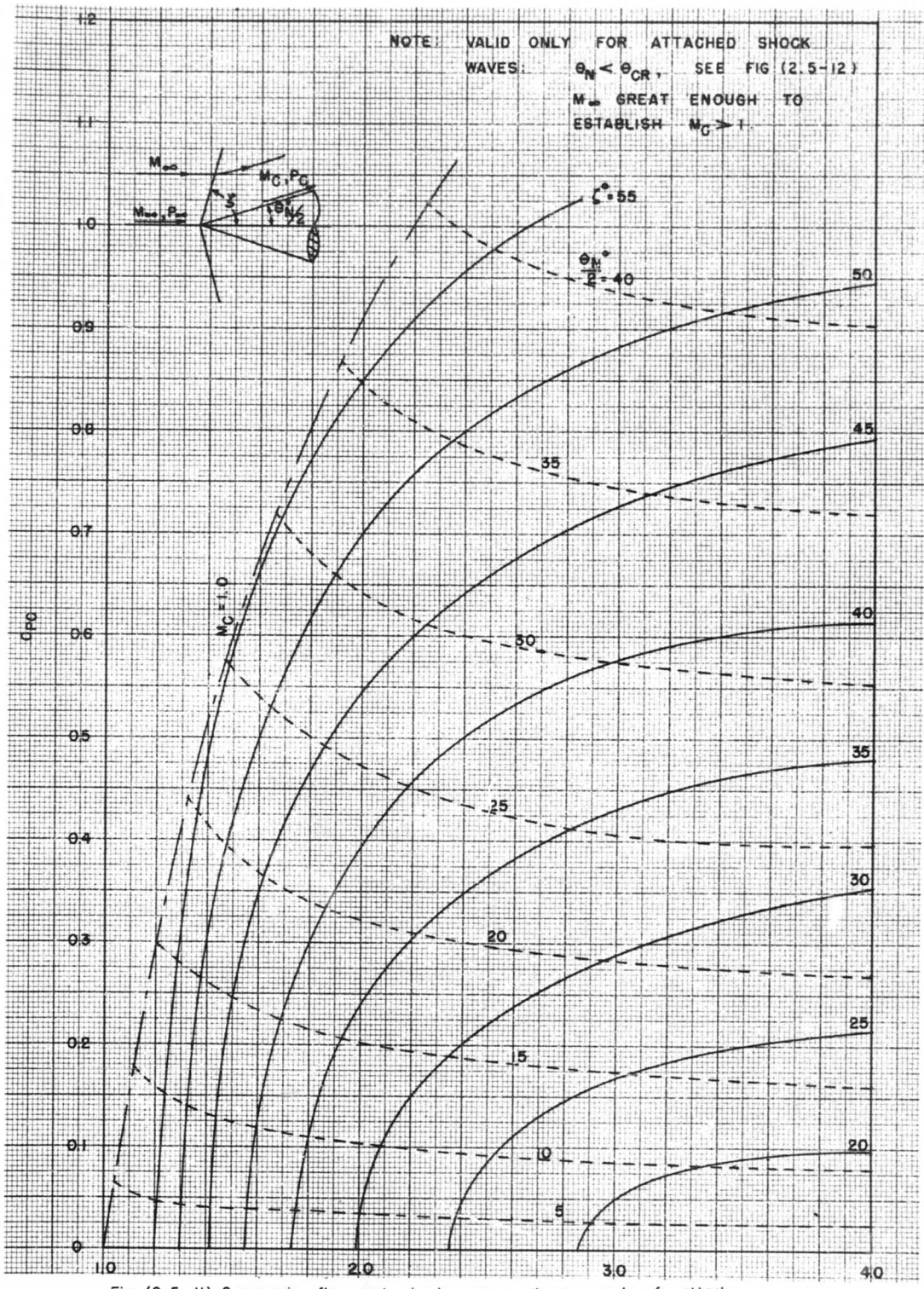


Fig (2.5-11) Supersonic flow past circular cones at zero angle-of-attack.  
 Ref (2.5-1), R.A.S. data sheets, aerodynamics, vol.1, S. 00.03.13 2.5-35

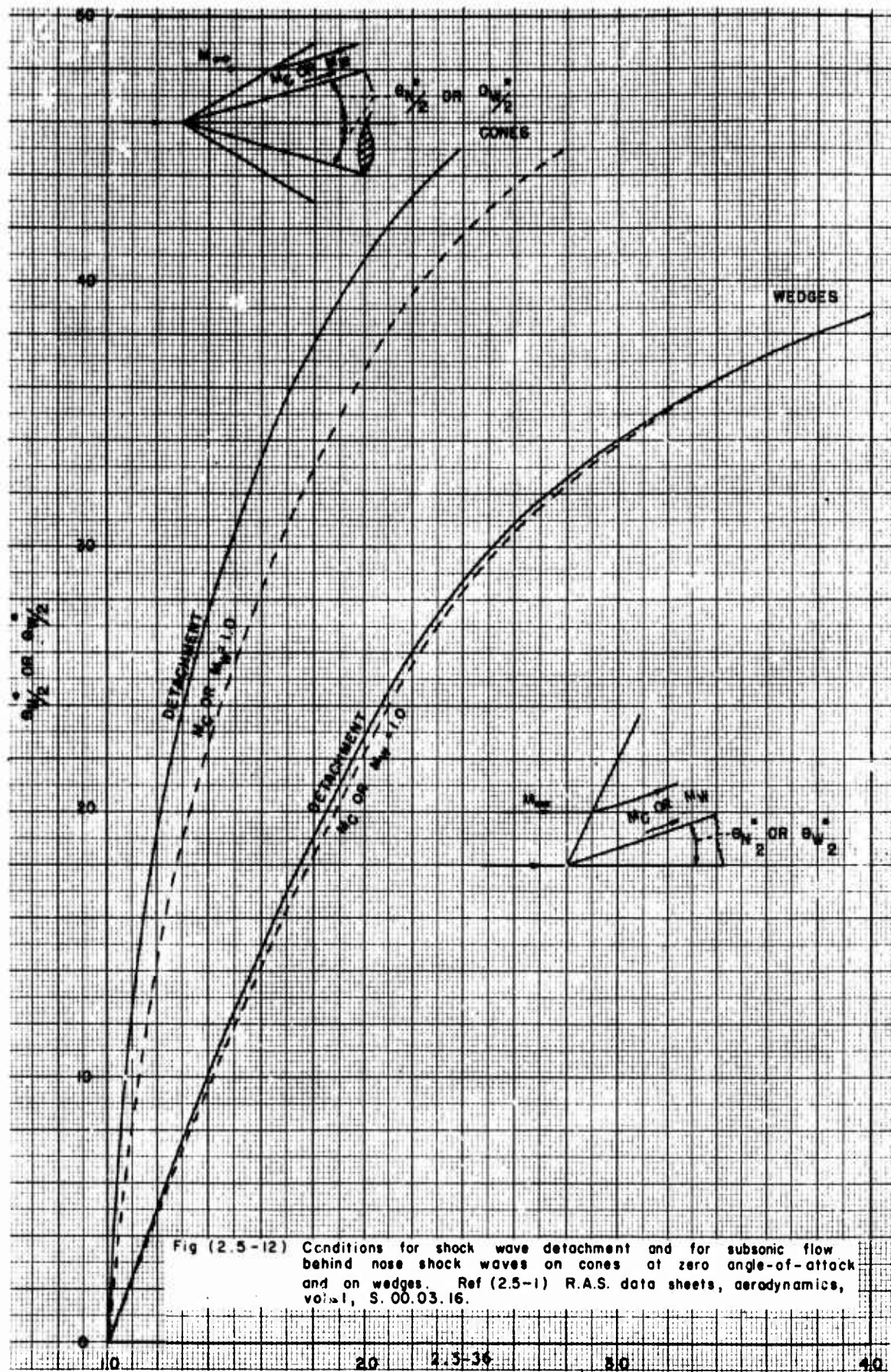


Fig (2.5-12) Conditions for shock wave detachment and for subsonic flow behind nose shock waves on cones at zero angle-of-attack and on wedges. Ref (2.5-1) R.A.S. data sheets, aerodynamics, vol.1, S. 00.03.16.

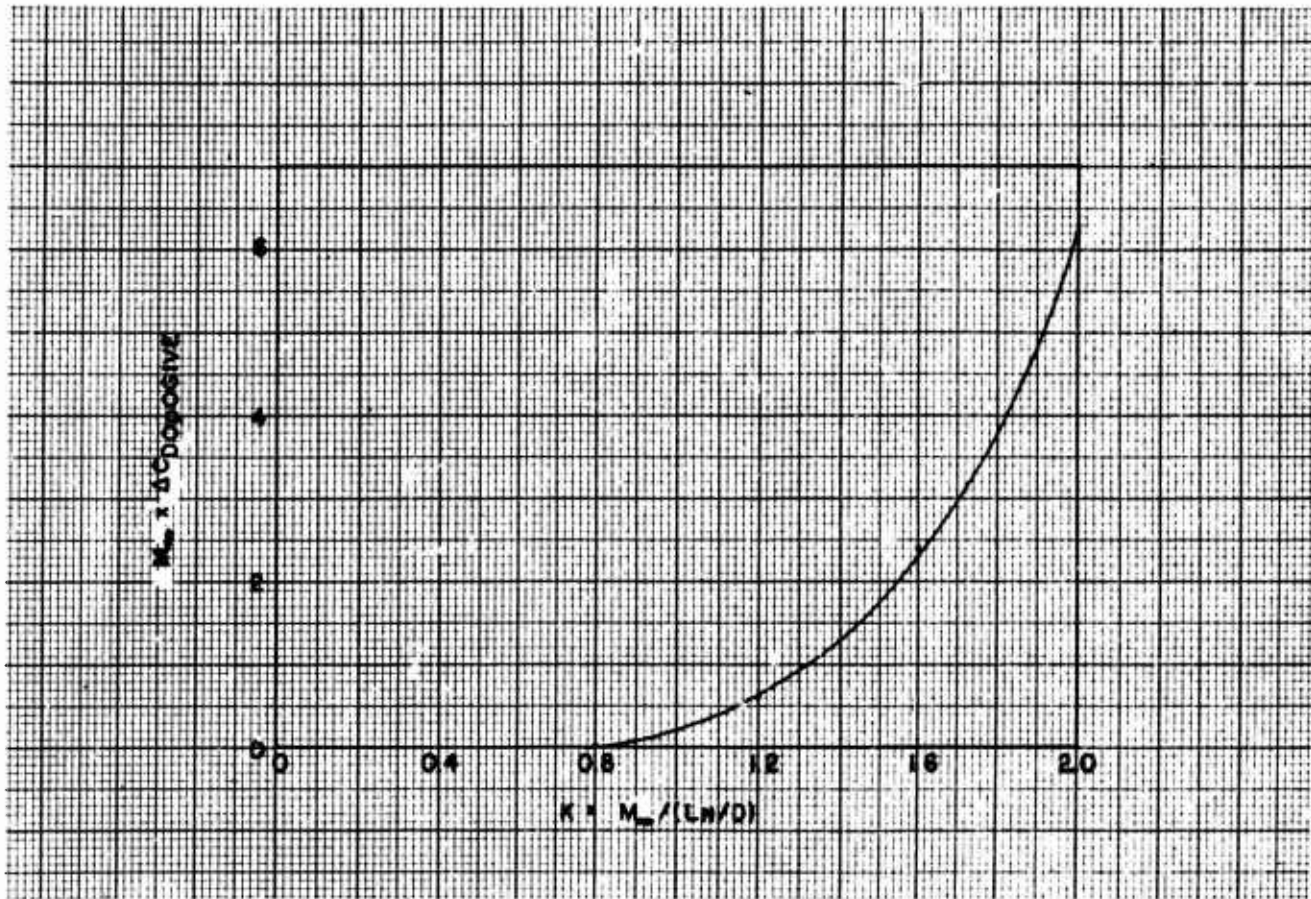


Fig (2.5-13) Drag increase of ogives as a function of similarity parameter, K.  
 Ref. (2.5-31)

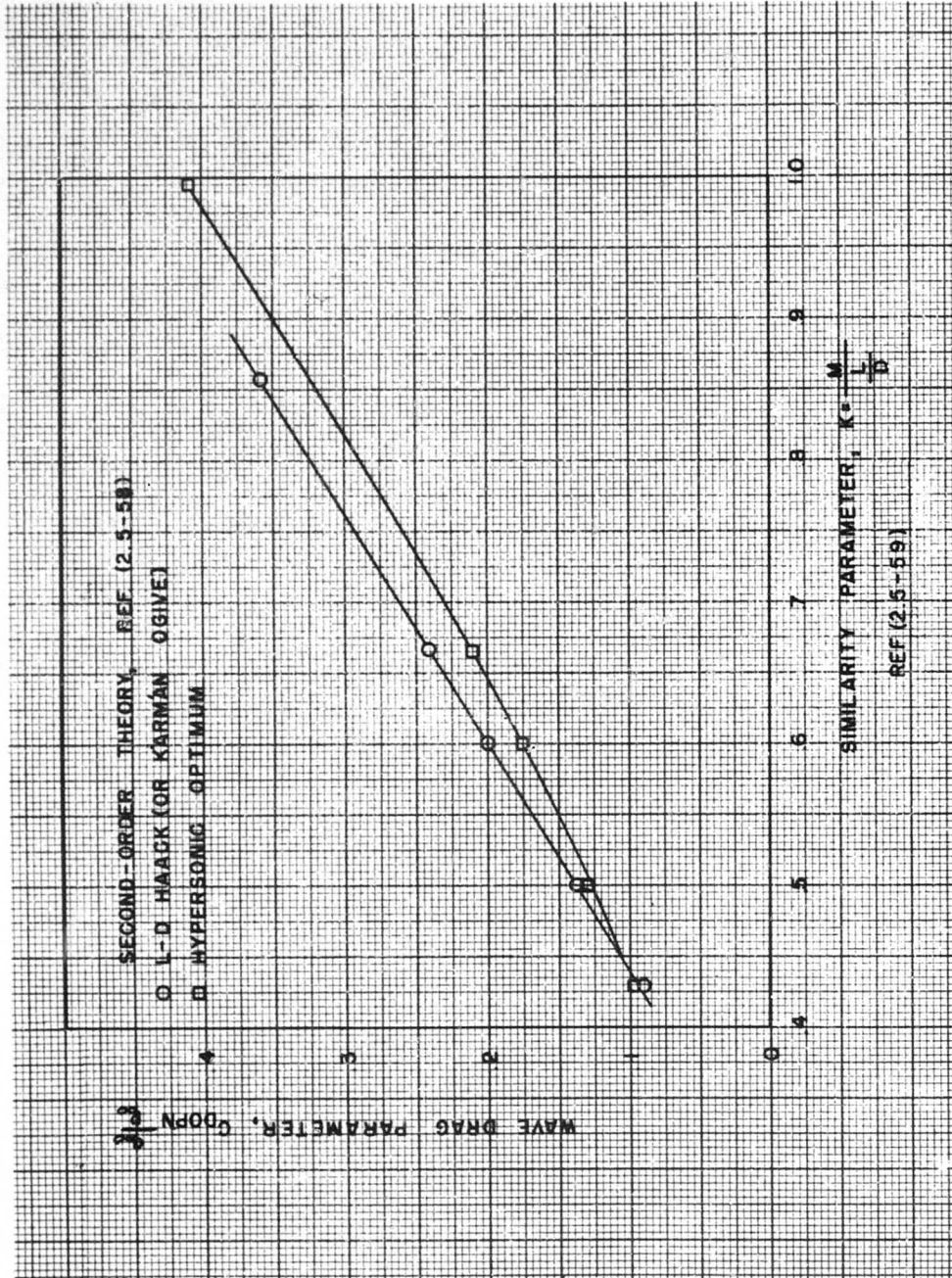


Fig (2.5-14) Variation of wave drag parameter,  $C_{DPN}$ , with the similarity parameter  $K = \frac{M^2}{D}$ , for the theoretical minimum drag nose shapes of specified length and diameter.

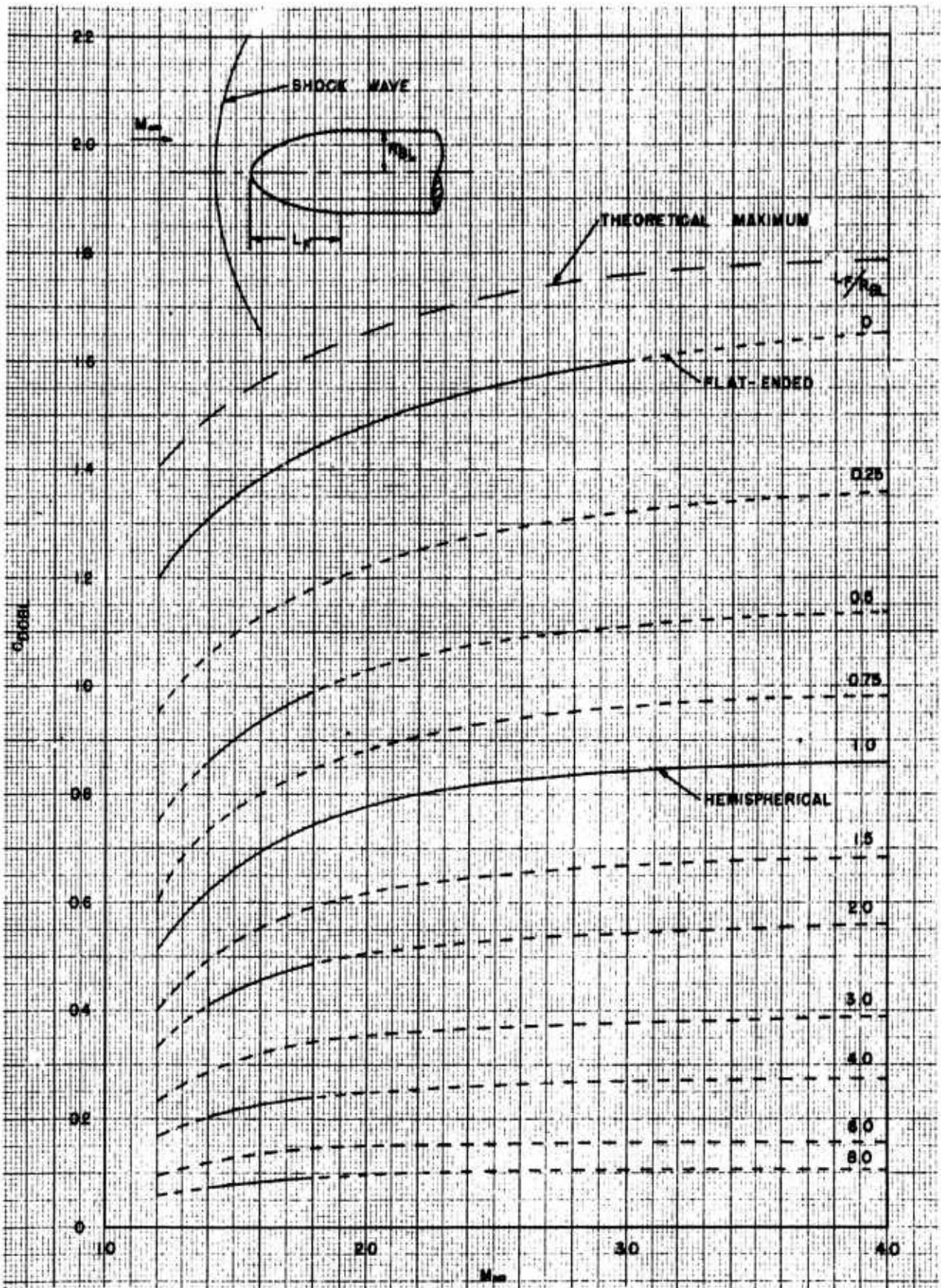


Fig (2.5-15) Pressure drag increase due to forebody tip-bluntness effects, zero angle-of-attack. Ref (2.5-1), R. A.S. data sheets, vol. 1, bodies S.02.03.06

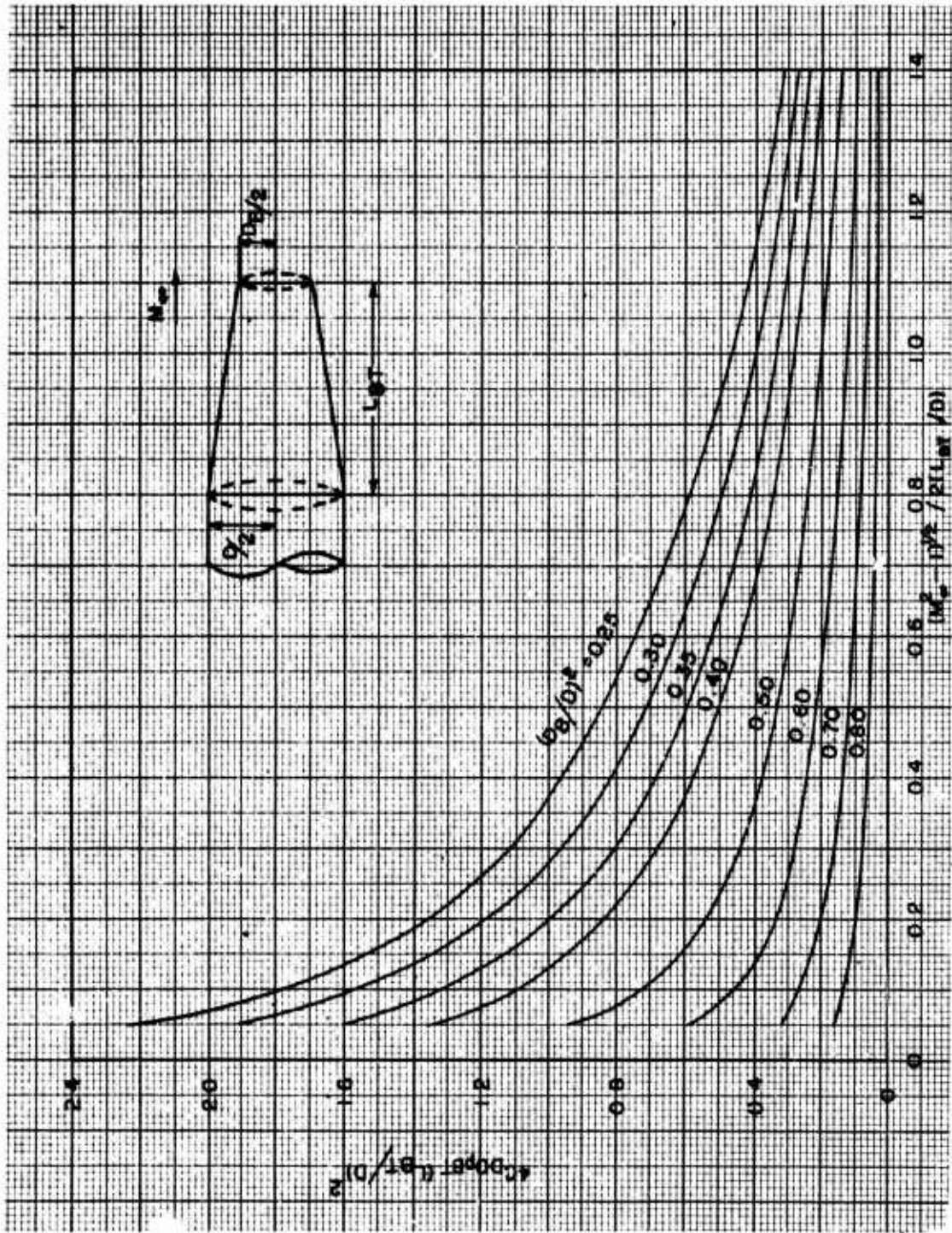


Fig (2.5-16) Inviscid pressure drag on truncated conical afterbodies of circular section at zero angle of attack. Ref (2.5-1) R.A.S. data sheets, aerodynamics, vol. 1, bodies S.02.03.04

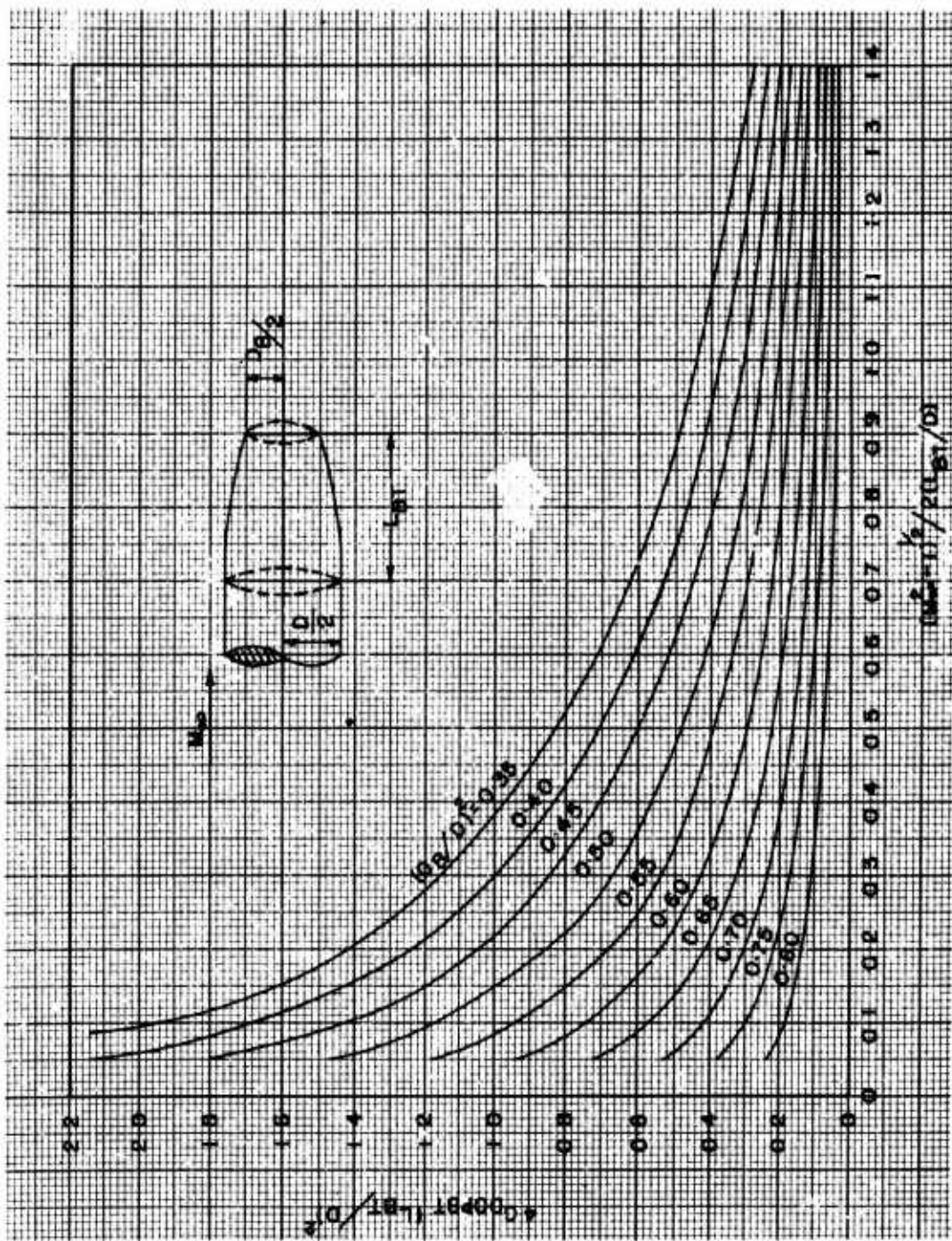
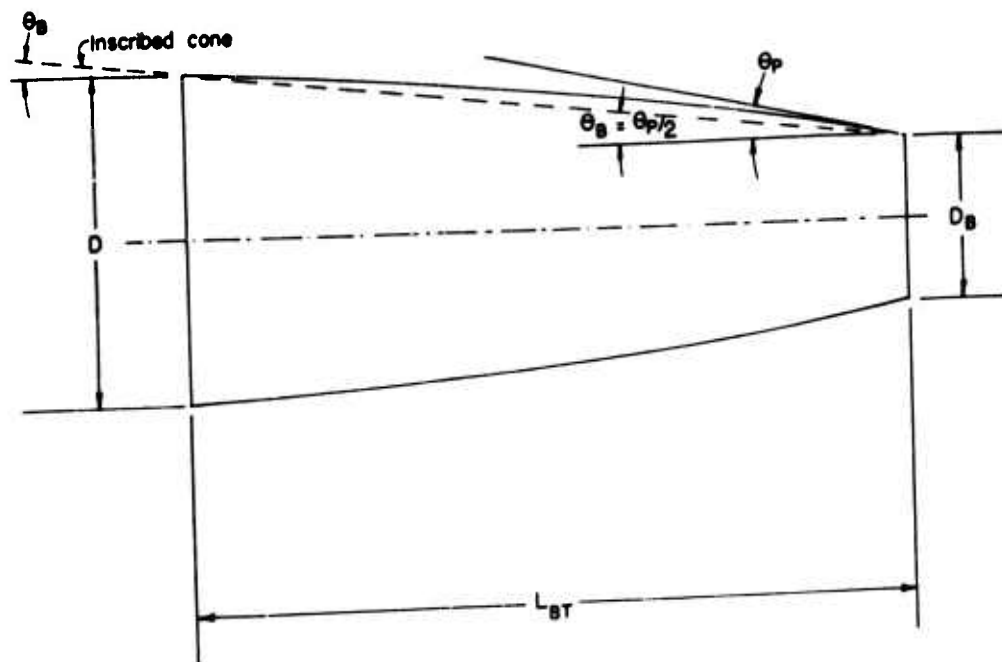


Fig (2.5-17) Inviscid pressure drag on truncated parabolic (or circular arc) after-bodies of circular section at zero angle-of-attack. Ref (2.5-1) R.A.S. data sheets, aerodynamics, vol. 1, bodies S.02.03.05.

PARABOLIC AFTERBODIES



$$\frac{D - D_B}{2L_{BT}} \approx \tan \frac{\theta_P}{2} ,$$

$$\frac{1 - \frac{D_B}{D}}{2 \frac{L_{BT}}{D}} \approx \tan \frac{\theta_P}{2} , \quad \frac{L_{BT}}{D} = \frac{1 - \frac{D_B}{D}}{2 \tan \frac{\theta_P}{2}} ,$$

$$0 < \theta_P = 2\theta_B < 15^\circ$$

FIG (2.5-i8) DETERMINATION OF THE FUNCTIONAL RELATIONSHIP

$$\frac{D_B}{D} = f\left(\frac{L_{BT}}{D}\right) \text{ FOR GIVEN VALUE } \theta_P^\circ$$

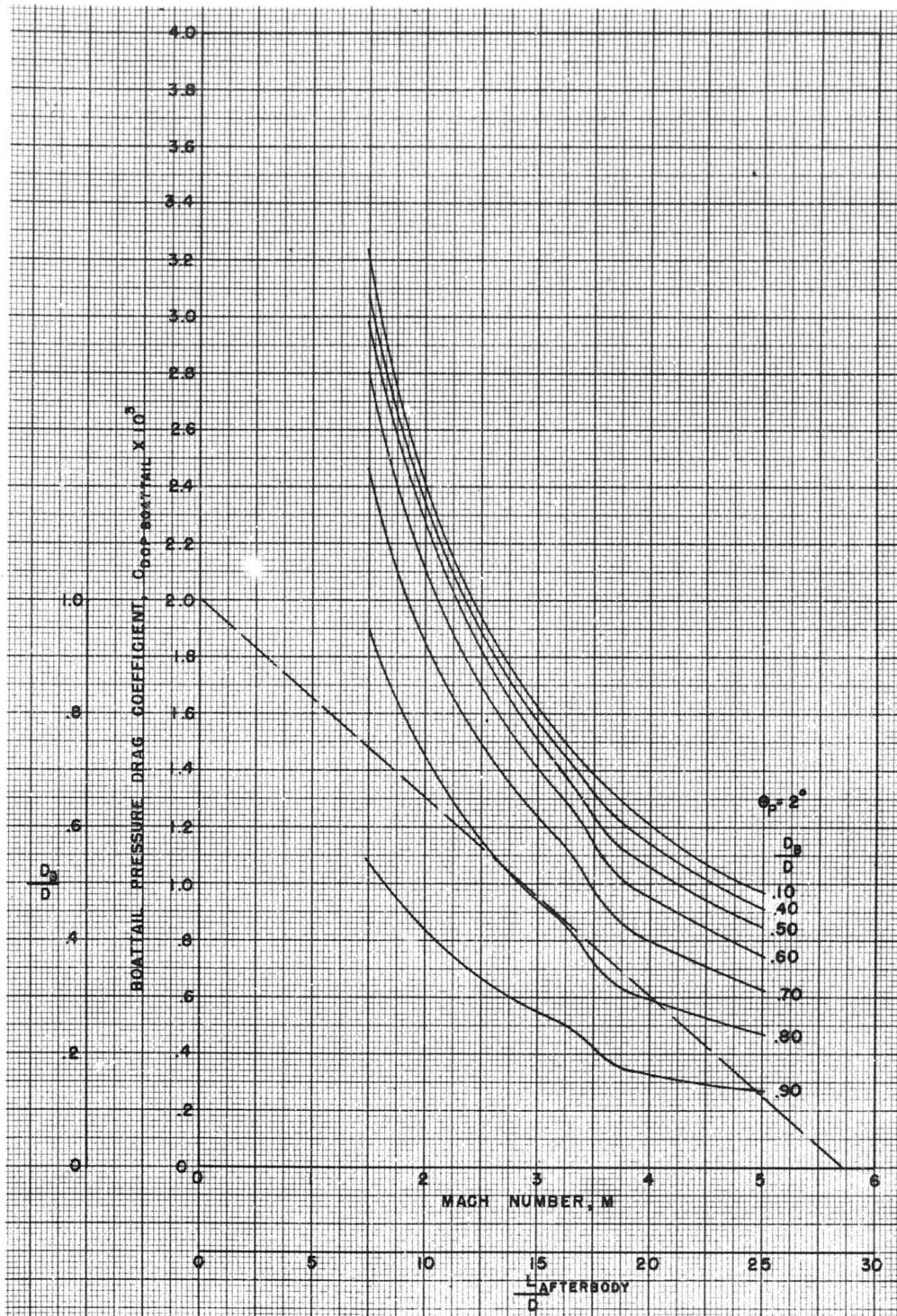


Fig (2.5-19) Pressure drag coefficient for boattails as a function of boattail base angle,  $\theta_p$ ,  $\frac{D_B}{D}$  and Mach Number. (Average values, Ref (2.5-60))  
 See tables (2.5-3) and (2.5-4)

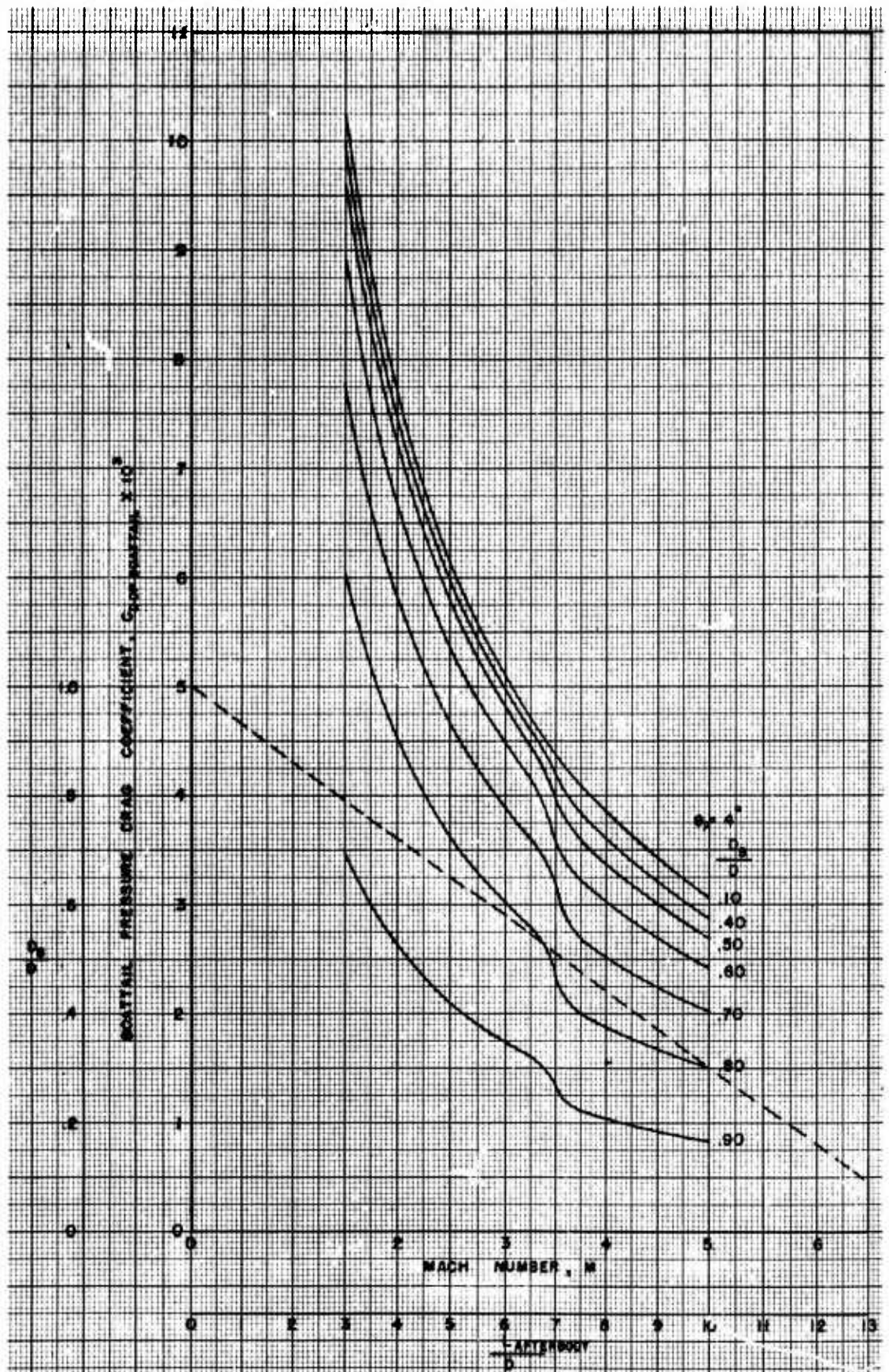


Fig (2.5-19) Continued (1)

2.5-44

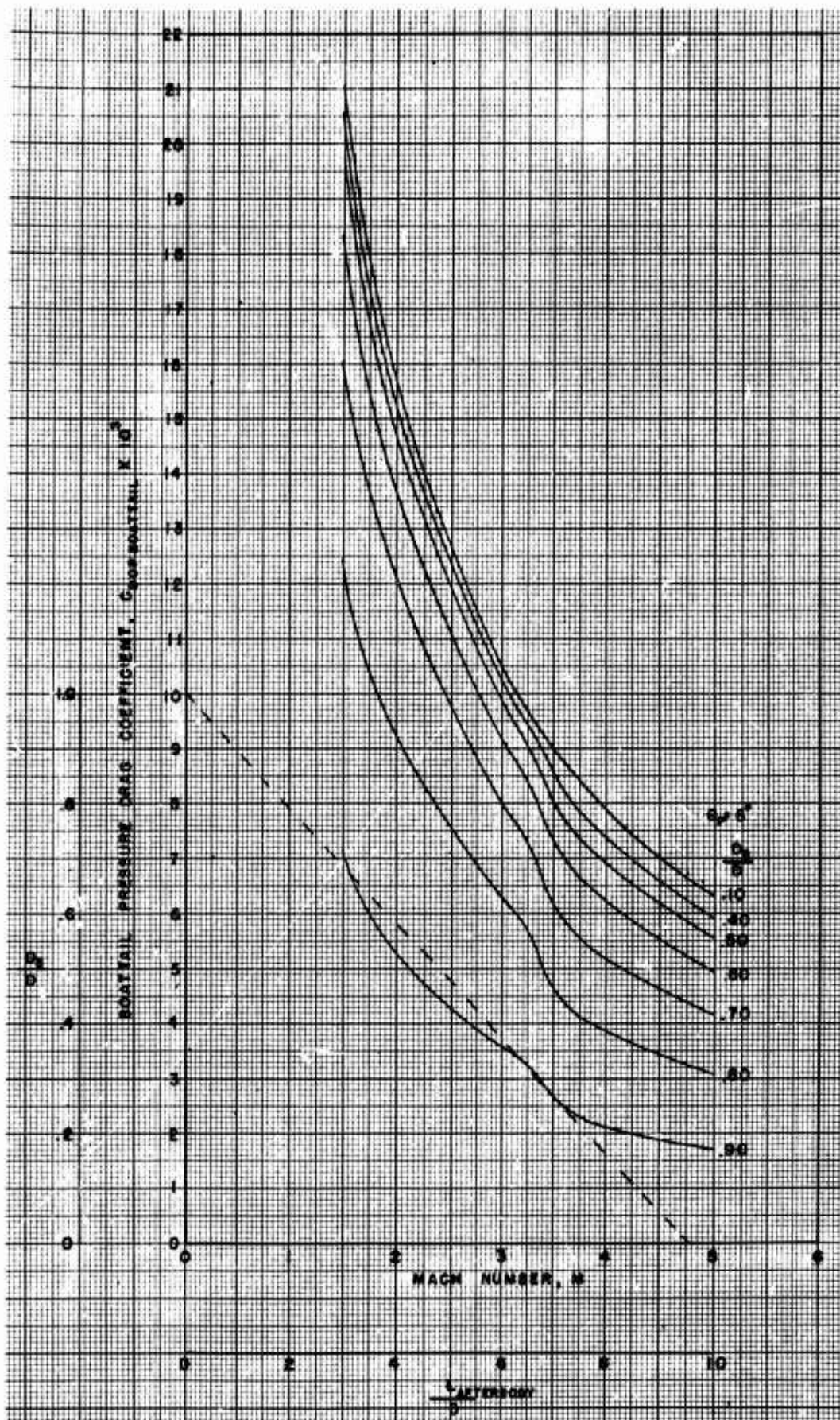


Fig (2.5-19) Continued (2)

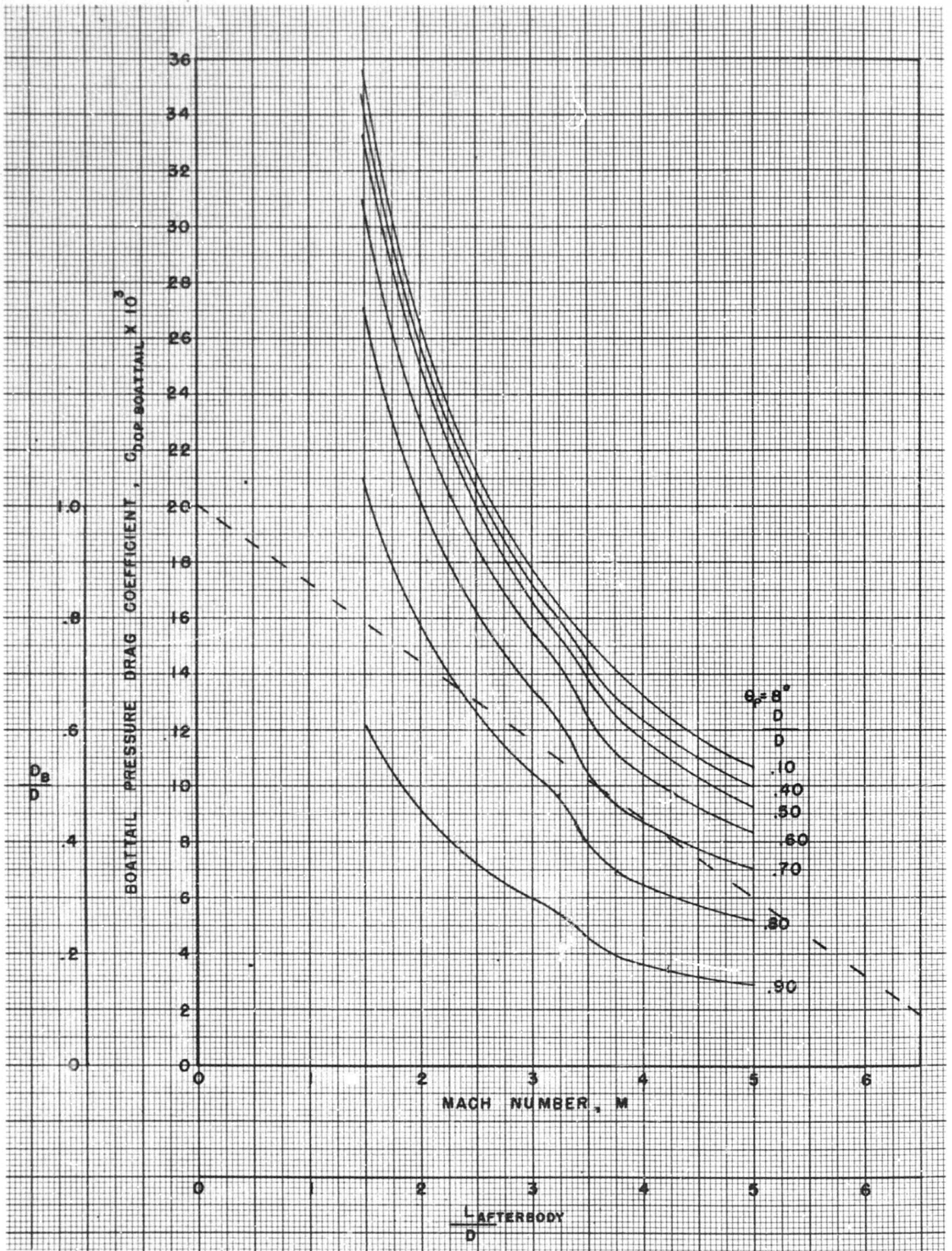


Fig (2.5-19) Continued (3)

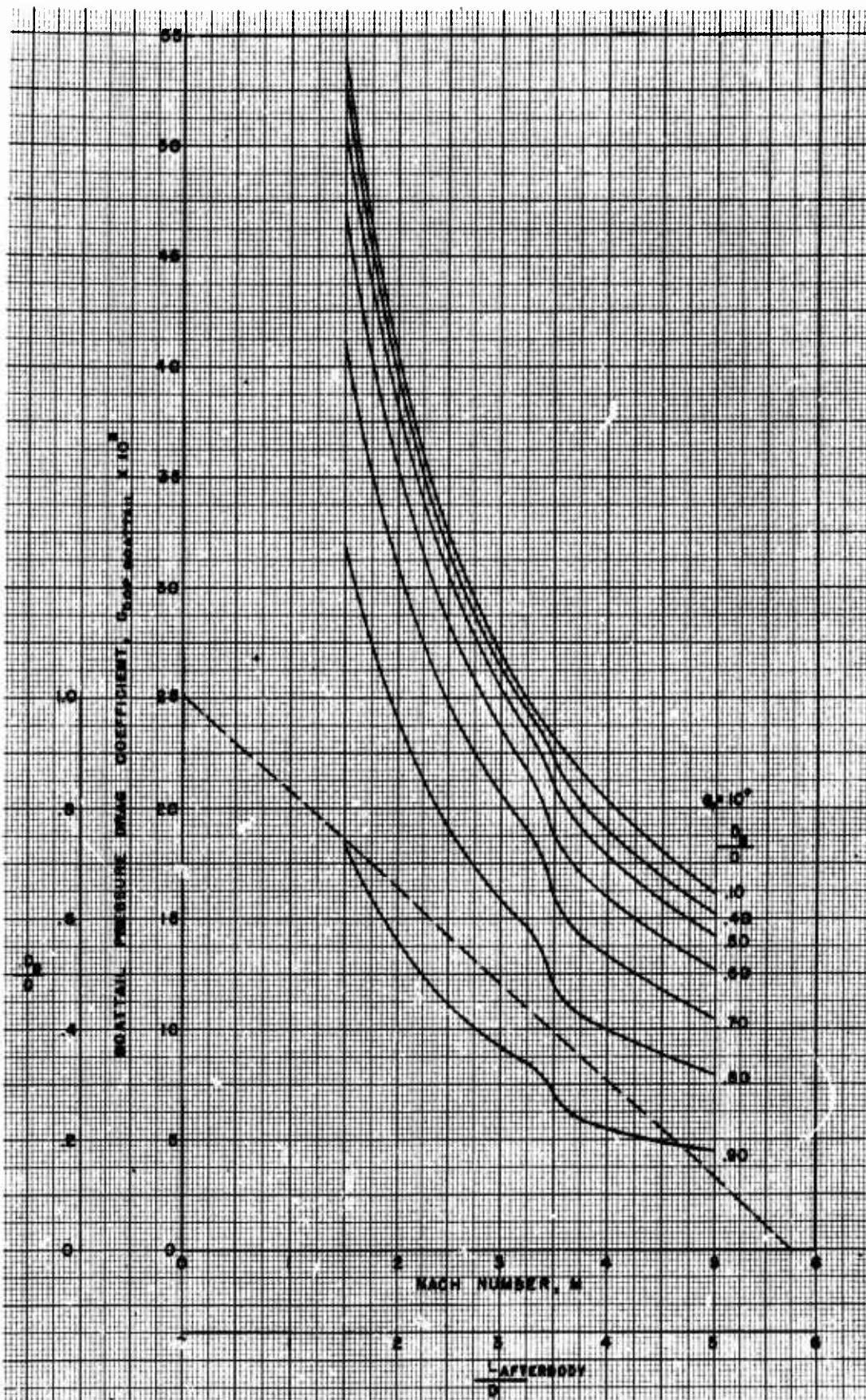


Fig (2.5-19) Continued (4)

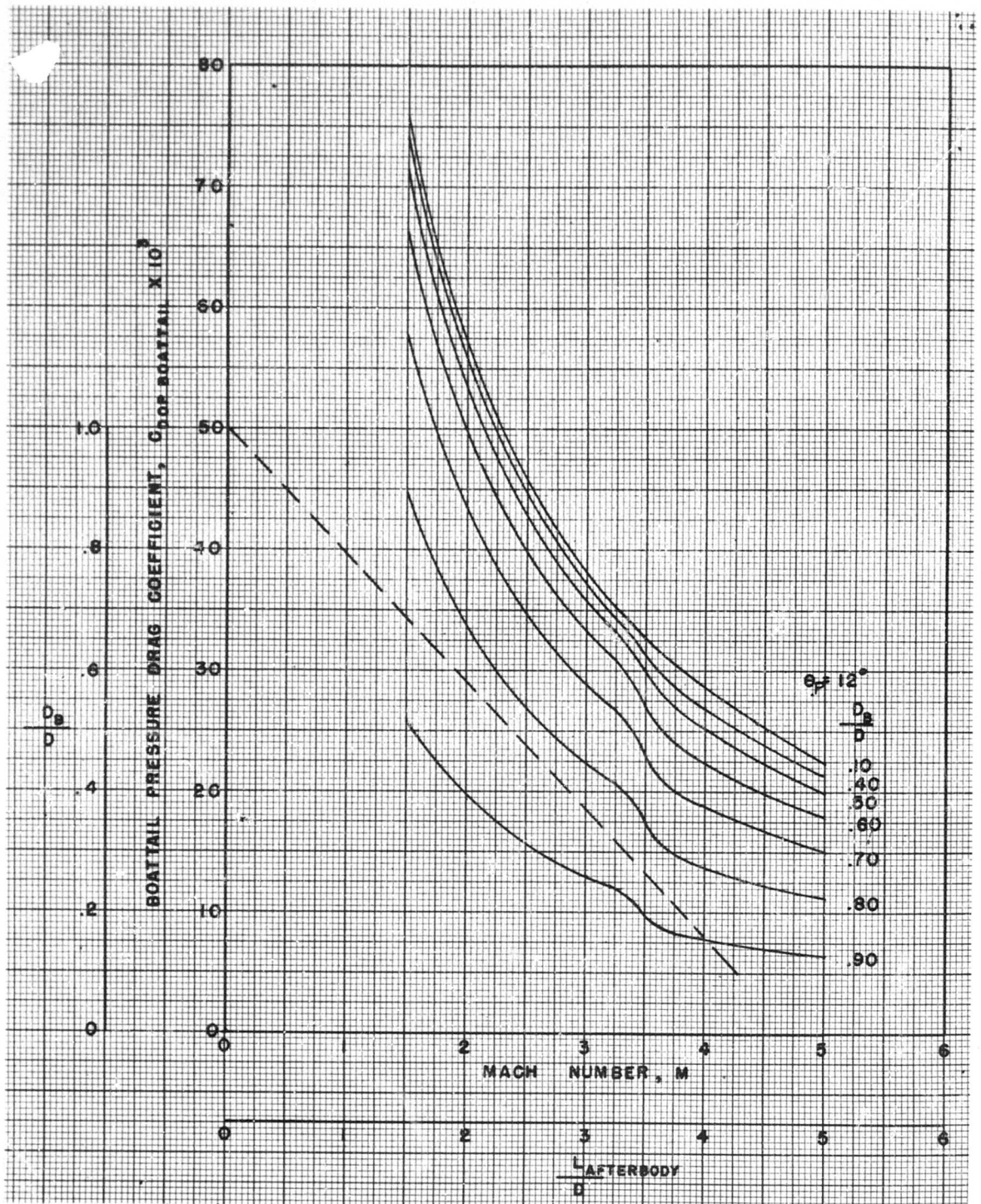


Fig (2.5-19) Continued (5)

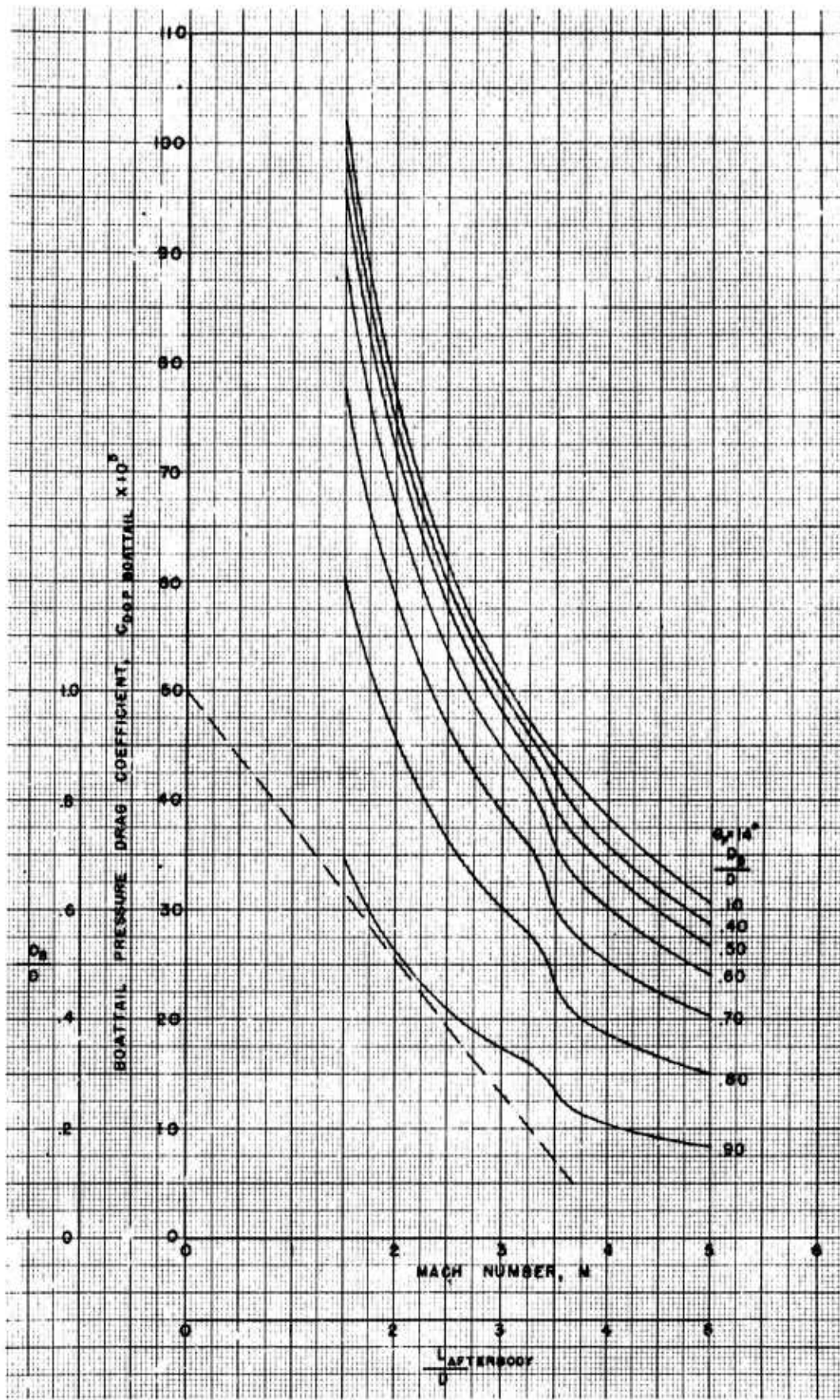


Fig (2.5-19) Continued (6)

2.5-49

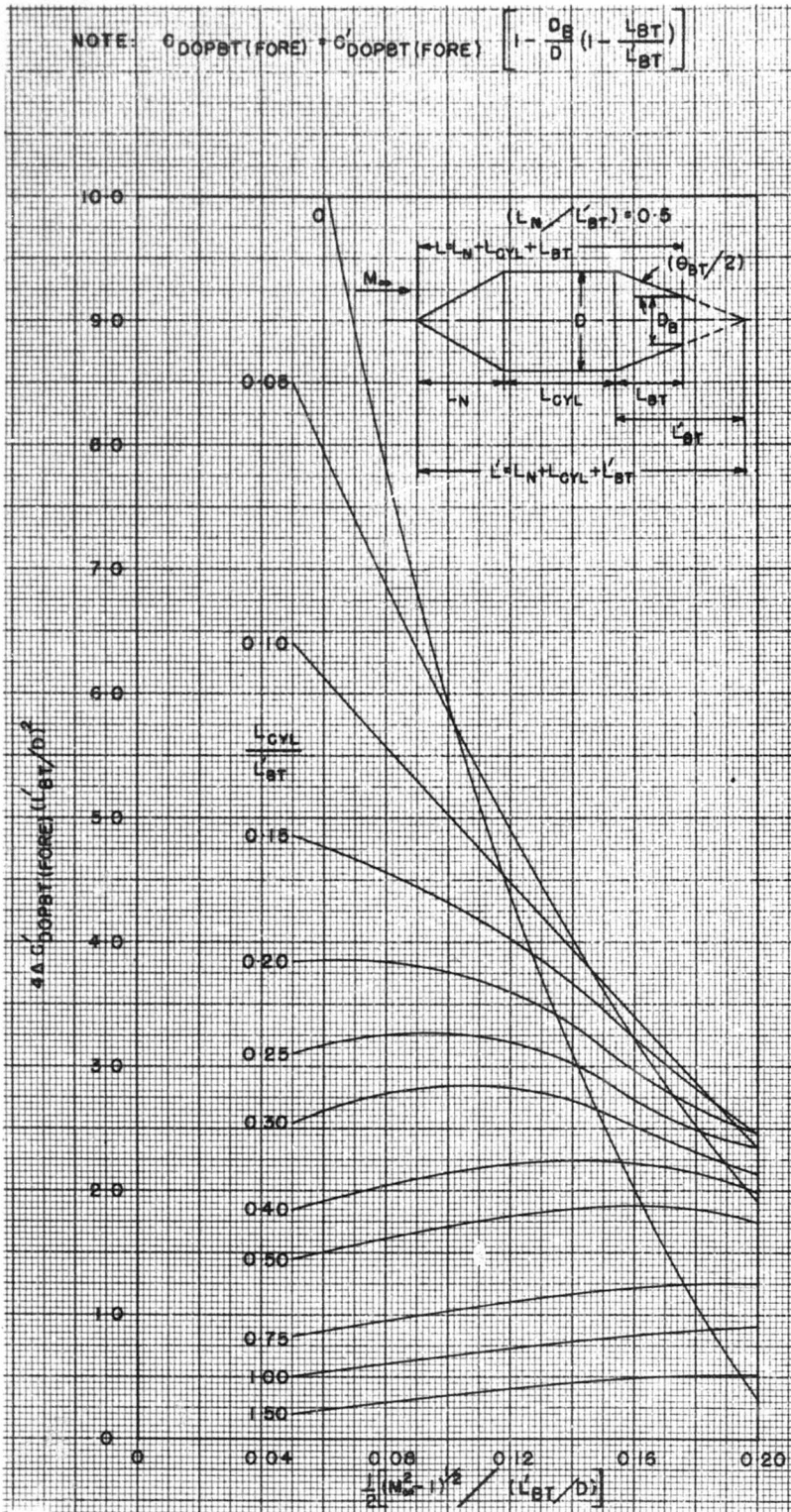


Fig (2.5-20) Forebody - afterbody inviscid interference pressure drag for pointed conical forebodies and afterbodies with midbodies, zero angle-of-attack. Ref. (2.5-1) R.A.S. data sheets, aerodynamics, vol. I, S.02.03.08

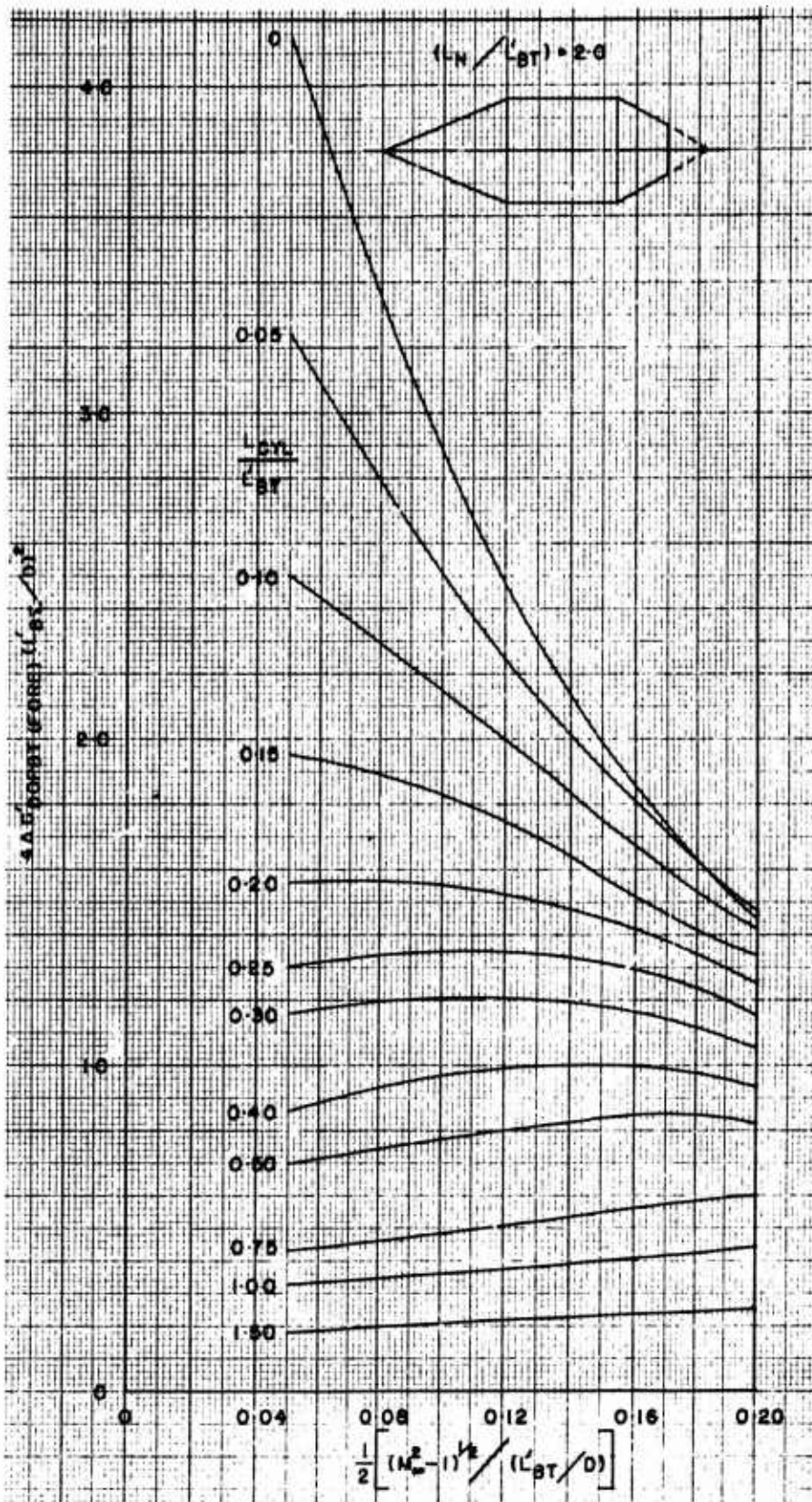


Fig (2.5-20) Continued (1)

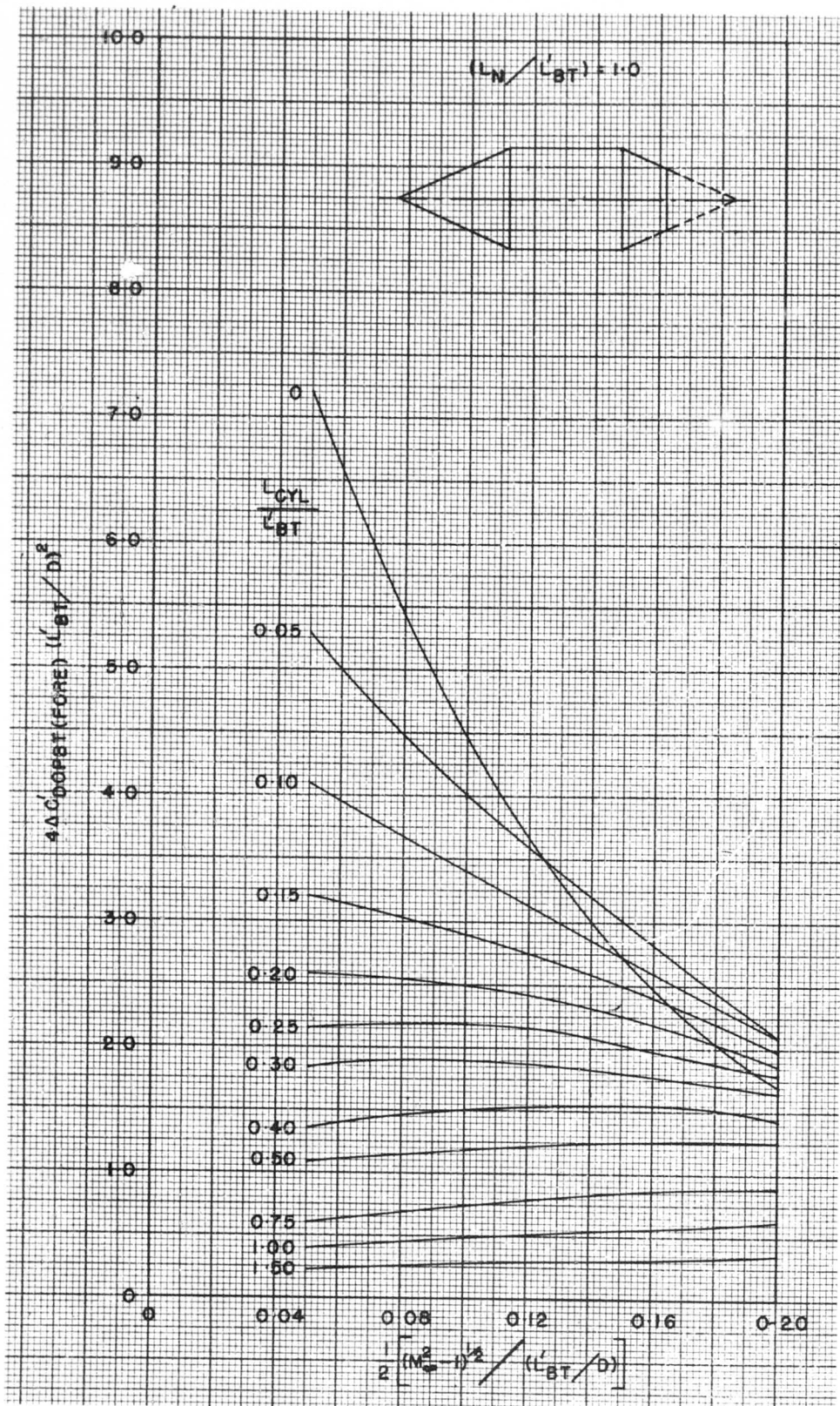


Fig (2.5-20) Continued (2)

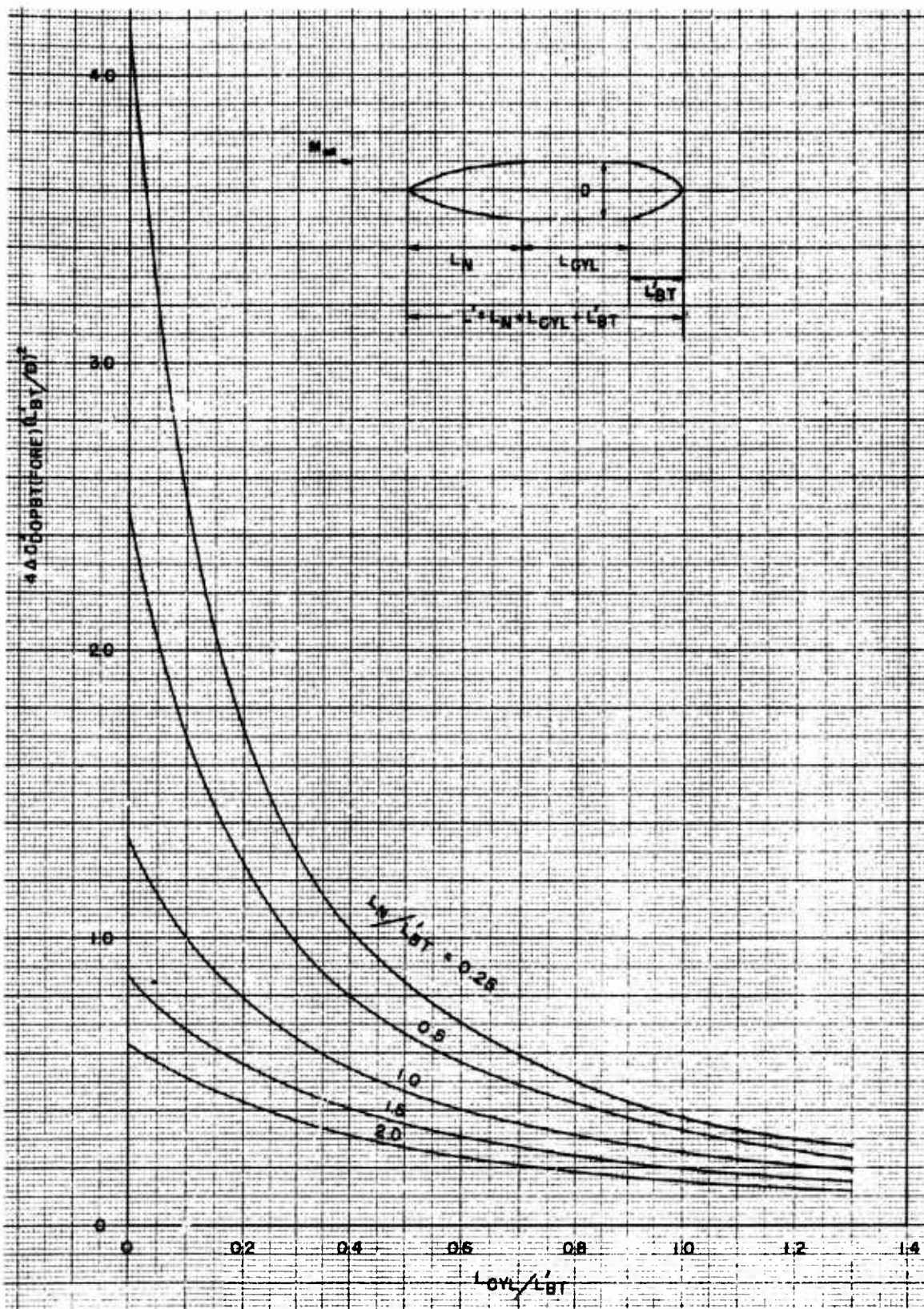


Fig (2.5-21) Forebody-afterbody inviscid interference pressure drag for pointed parabolic forebodies and afterbodies with midbodies, zero angle-of-attack. Ref R.A.S. data sheets, aerodynamics, vol. 1, bodies S.02.03.10. (2.5-1)

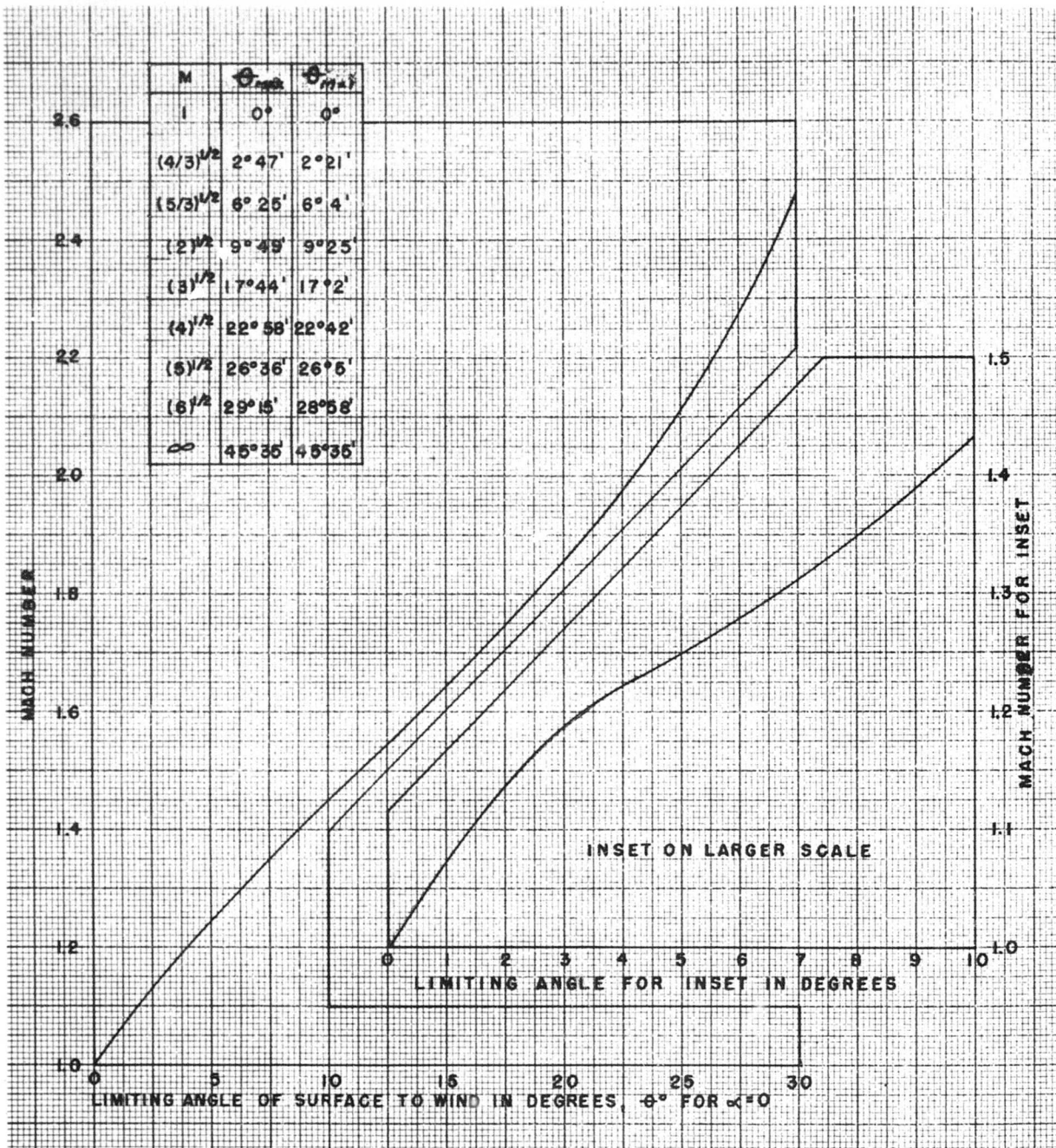


Fig (2.5-22) Graphs and table of limiting value of inclination of an element of surface to the wind, at various Mach Numbers. The front shock wave will be attached to the leading edge only if no part of the wing surface facing forward exceeds this limiting value.  
Ref. (2.5-3)

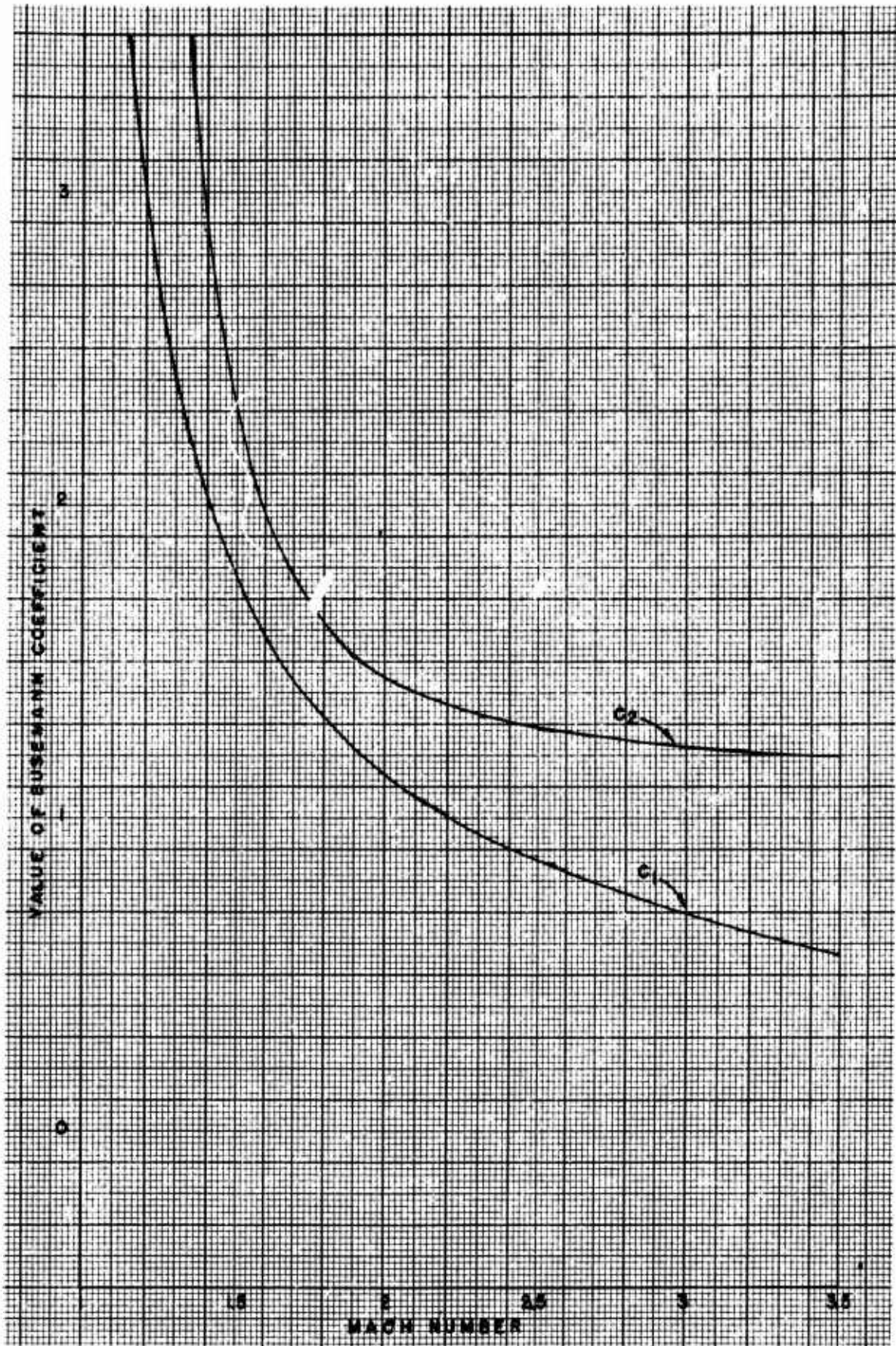
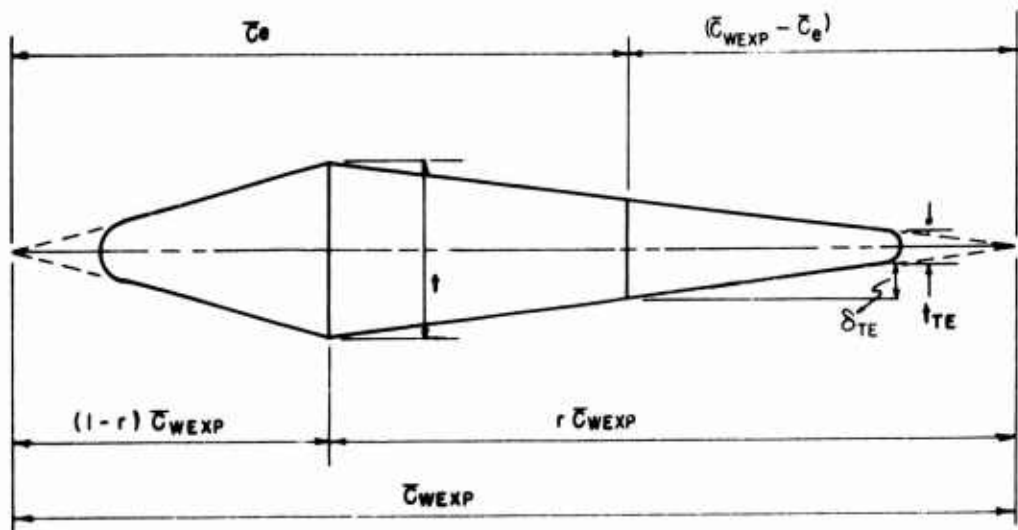


Fig (2.5-22a) Variation of Busemann coefficients with Mach Number.  
Ref (2.5-3)



$$y_1 = \left[ 1 - \frac{(2\delta_{TE} + t_{TE})r}{\bar{C}_{WEXP}} \right] = \frac{C_0}{\bar{C}_{WEXP}}$$

$r = 1/2$  FOR DOUBLE SYMMETRY

$t_{TE} \approx .01$  ft.

$\delta_{TE} =$  FROM TABLE T-1.22

$$\delta_i = (.37L)/(ReL)^2 \quad (\text{BLASIUS, T.B.L.})$$

FIG (2.5-23) CORRECTIVE FACTOR FOR VISCOUS FORM DRAG EFFECTS, TURBULENT, B.L.,  $C_{DOPVIS}$

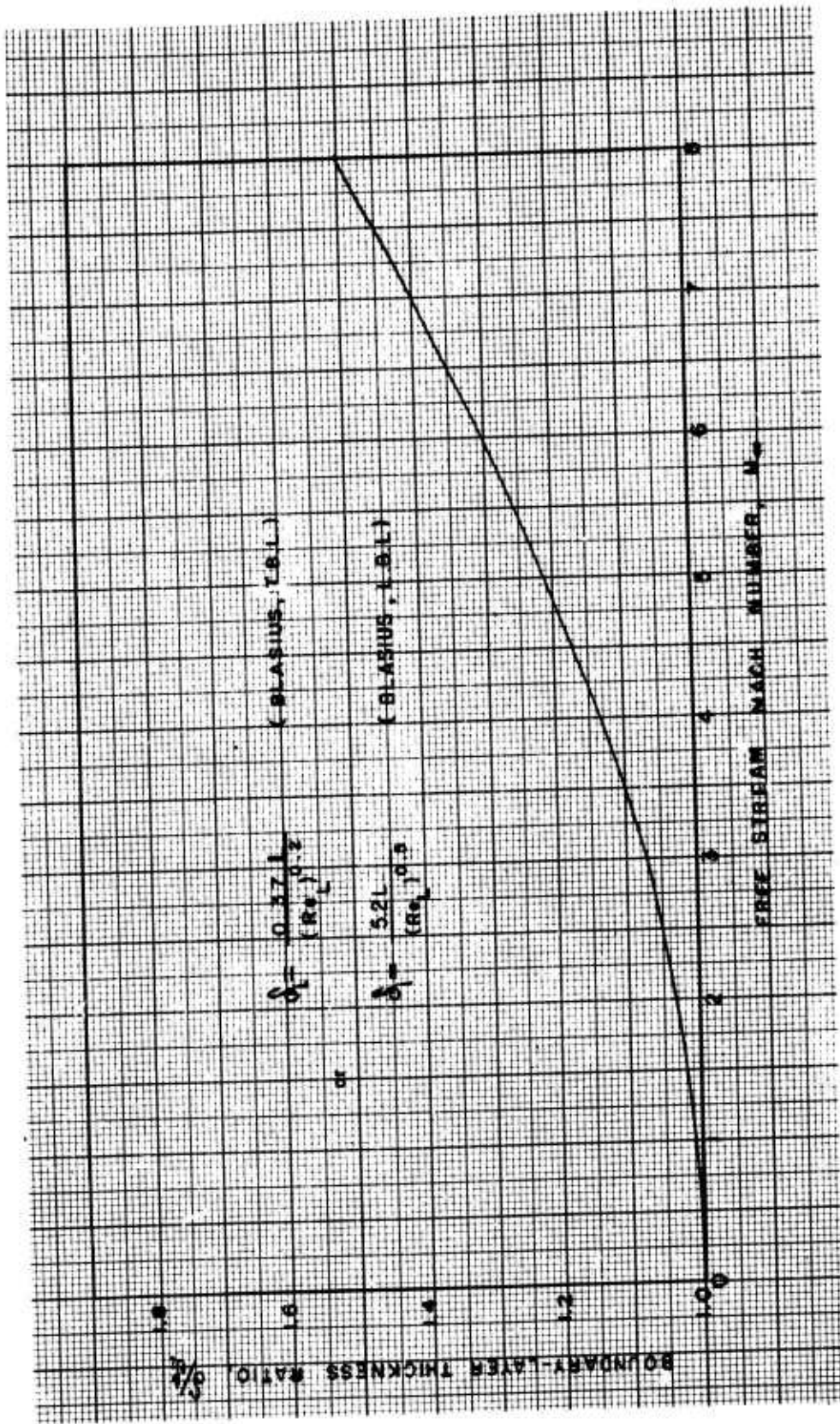


Fig (2.5-24) Van Driest's Law for turbulent boundary layer thickness ratio ( $\delta^*/\delta_t$ ) versus Mach Number,  $M_\infty$ . Use the same law for L.B.L. in evaluating  $\delta_{TE}$  in first approximation. Ref (2.5-63)

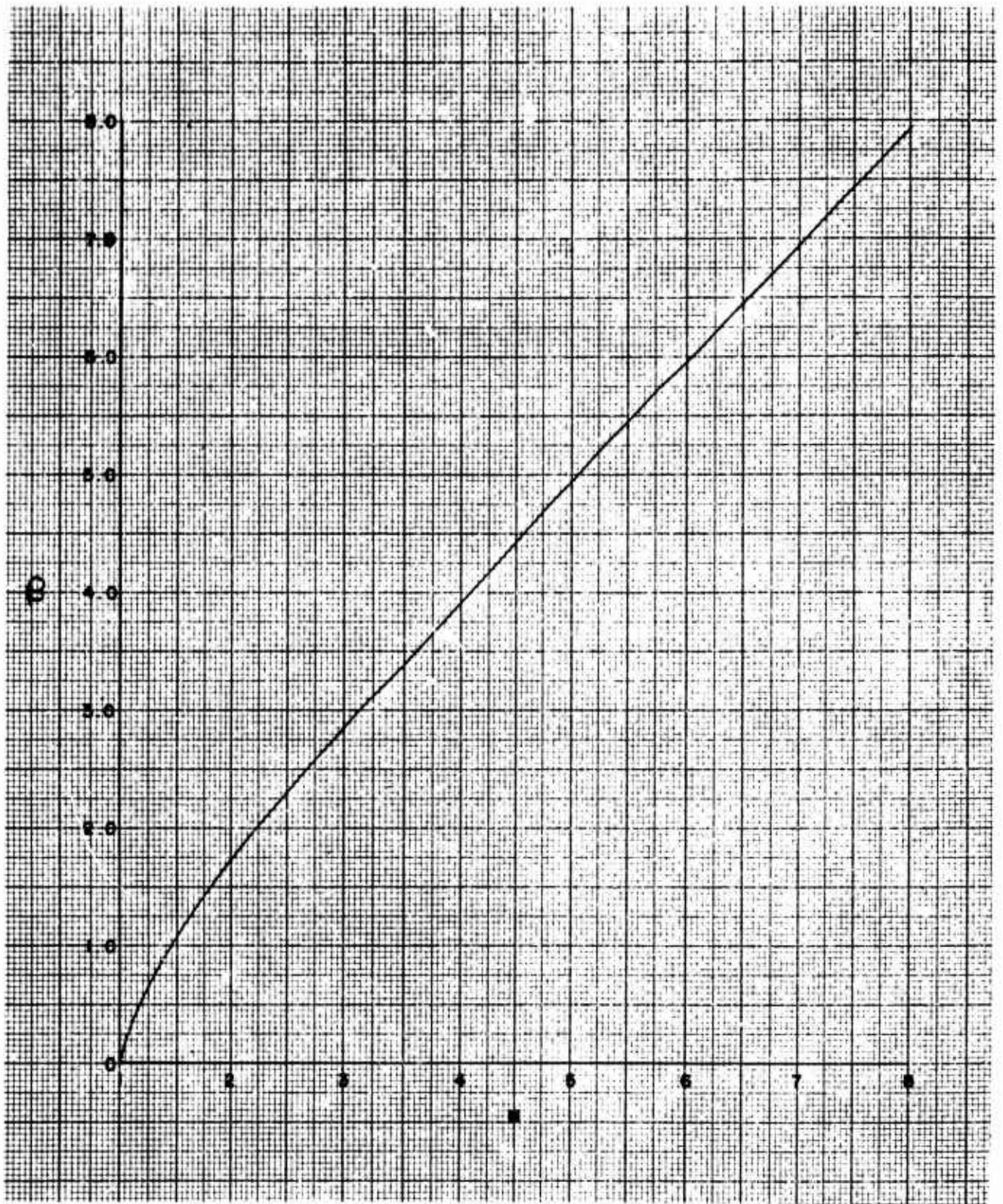
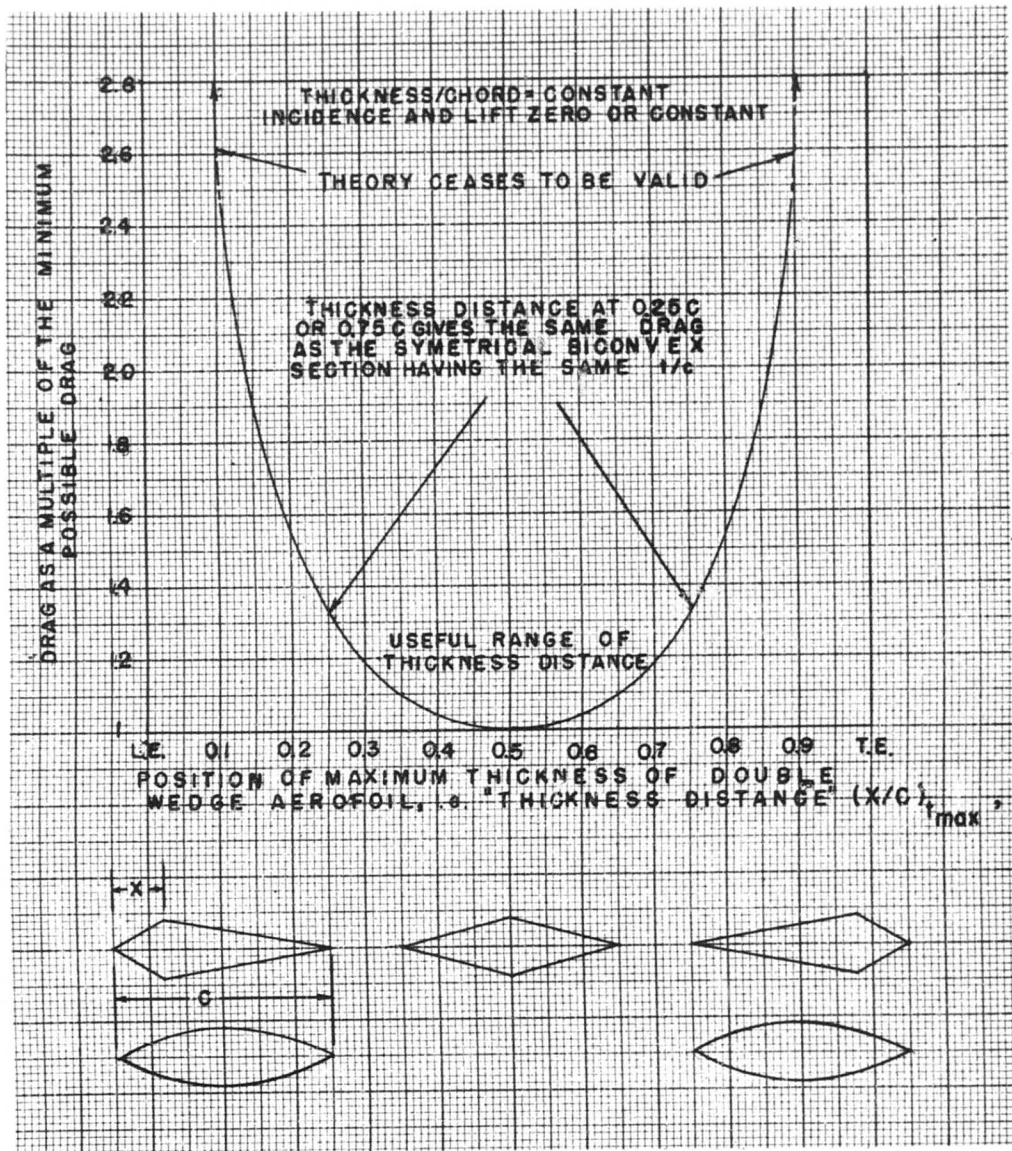


Fig (2.5-25)  $\beta = (M_\infty^2 - 1)^{1/2}$  versus  $M_\infty$



Fig(2.5-26) Effect on drag of chordwise shift of position of maximum thickness of double-wedge wing (thickness distance has no effect on moment or lift if shock wave remains attached), Ref (2.5-3)

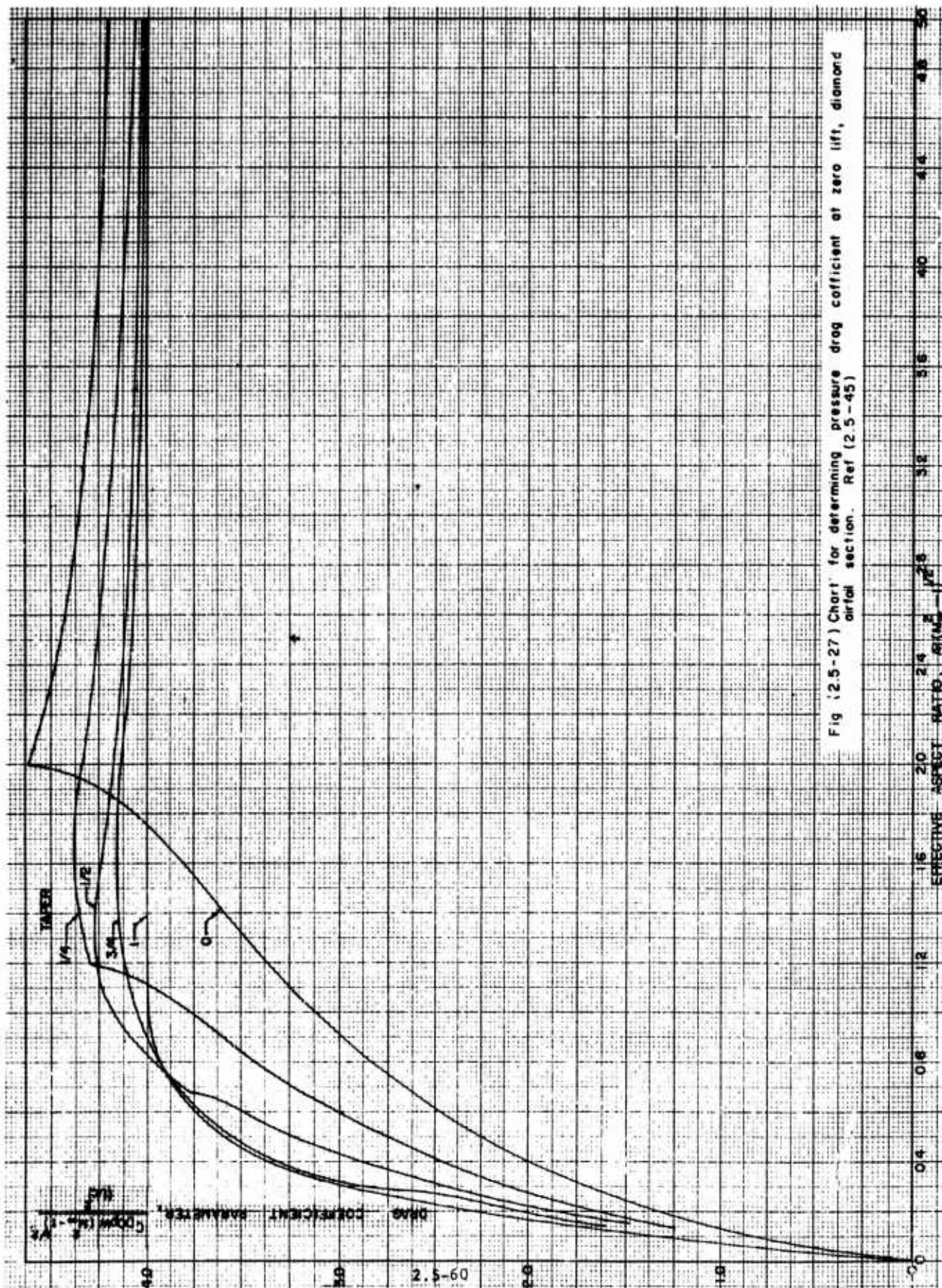


Fig (2.5-27) Chart for determining pressure drag coefficient at zero lift, diamond airfoil section. Ref (2.5-45)

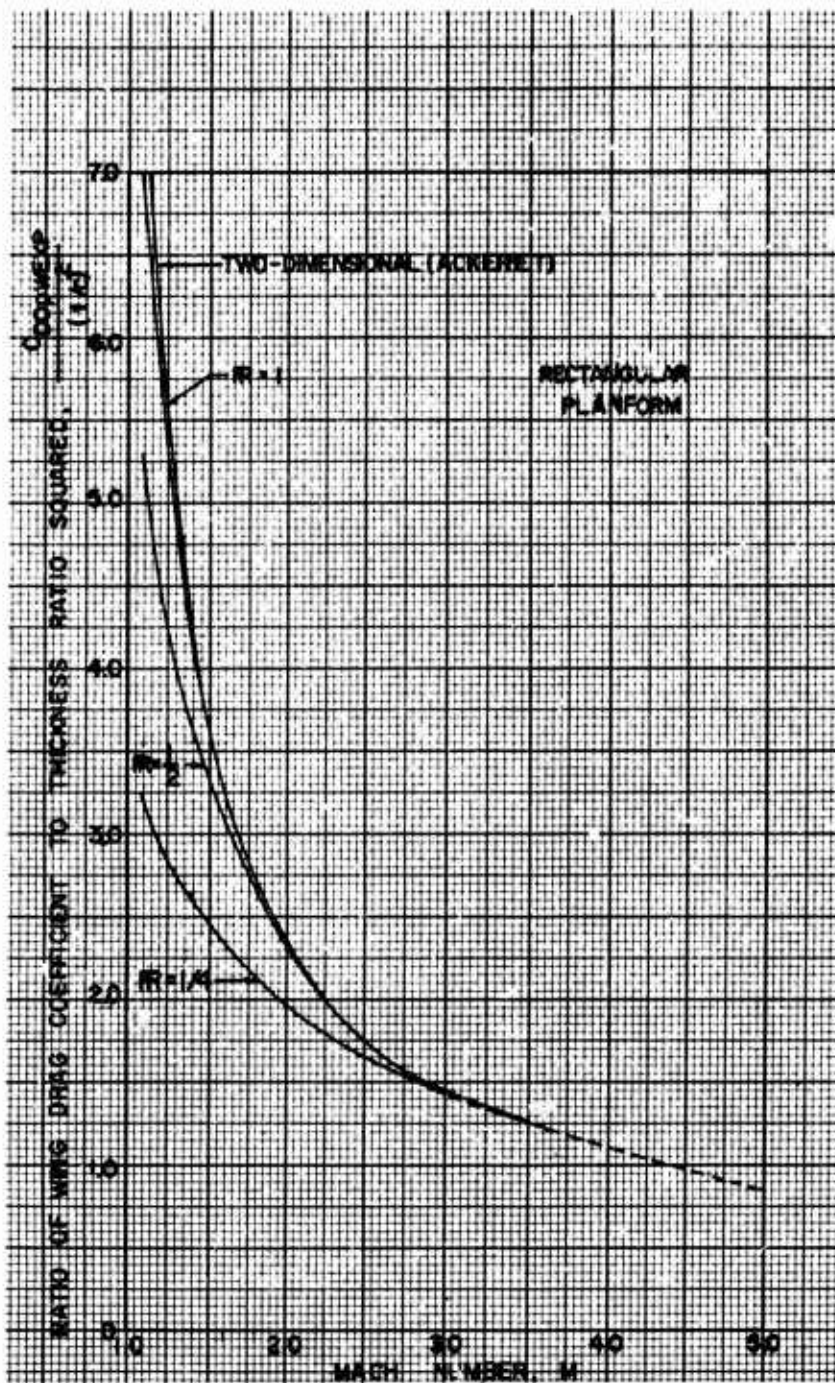


Fig (2.5-28) Ratio of wing drag coefficients to thickness ratio squared for several aspect ratios as a function of Mach Number. Ref (2.5-45)

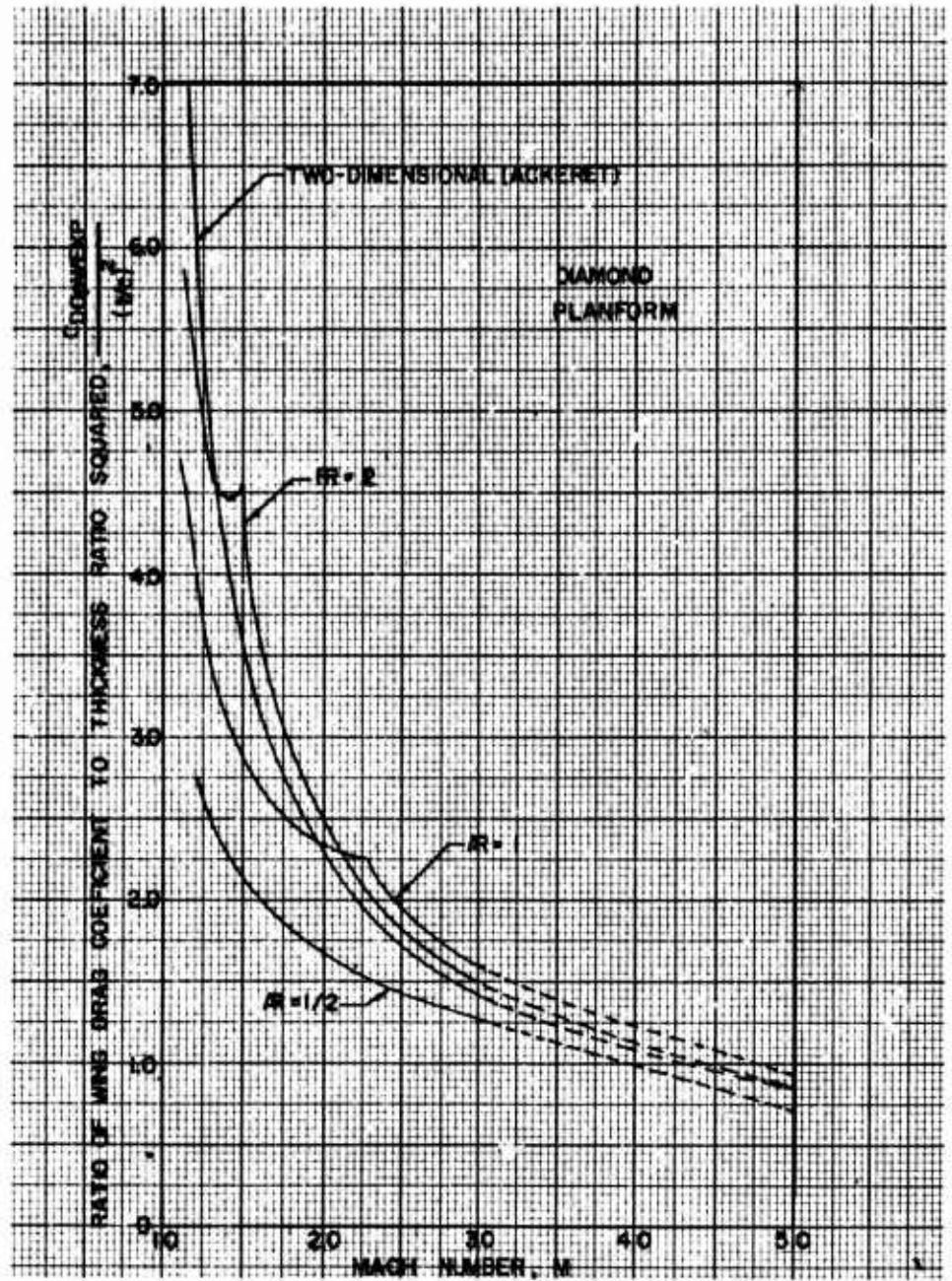


Fig (2.5-29) Ratio of wing drag coefficients to thickness ratio squared for several aspect ratio as a function of Mach Number. Ref (2.5-45)

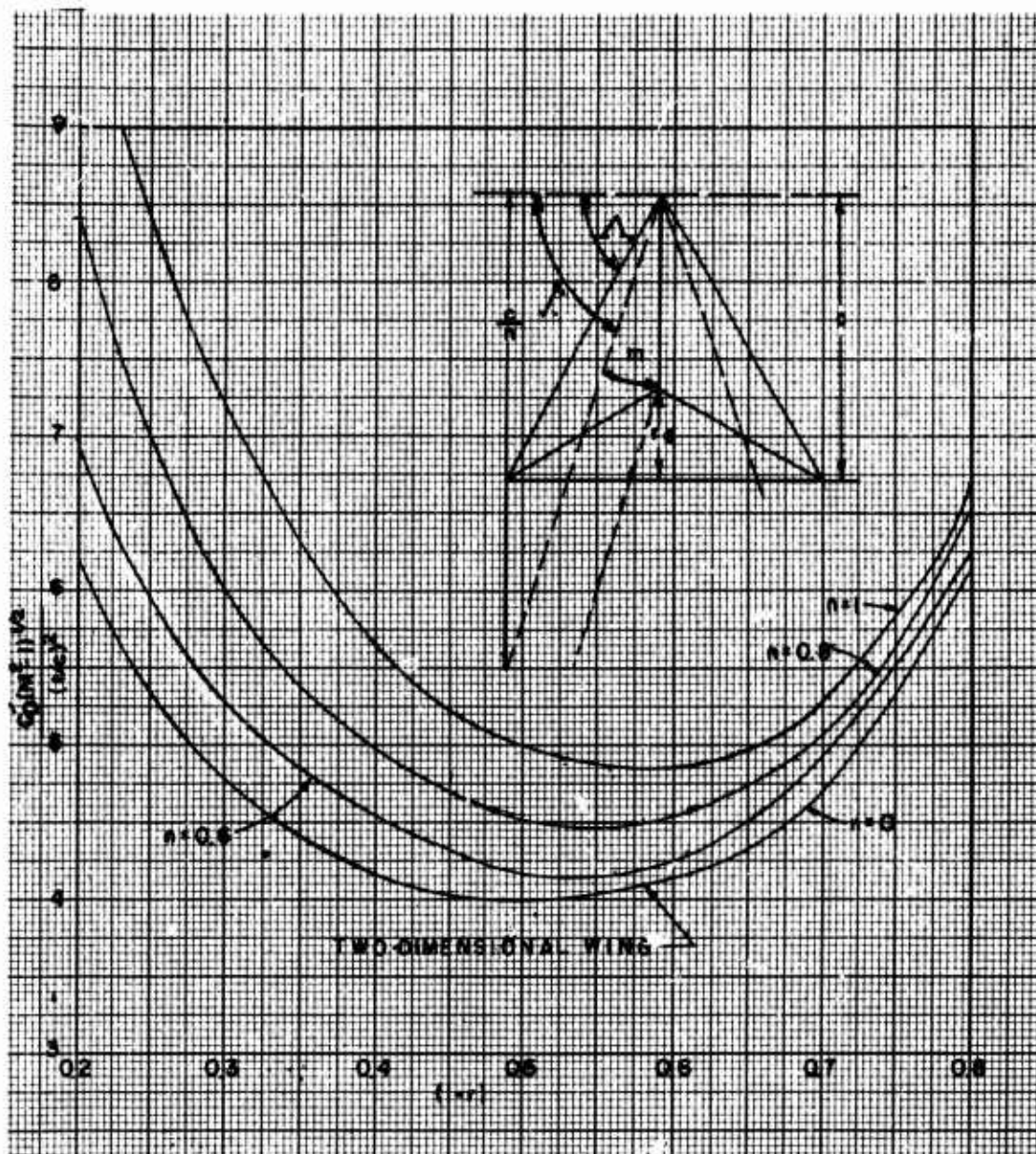


Fig (2.5-30) Drag of delta wing with supersonic leading edge. Parameter  $n$  measures the shape of the wing, and the Mach Number; parameter  $r$  measures the position of maximum thickness. Ref. (2.5-43)

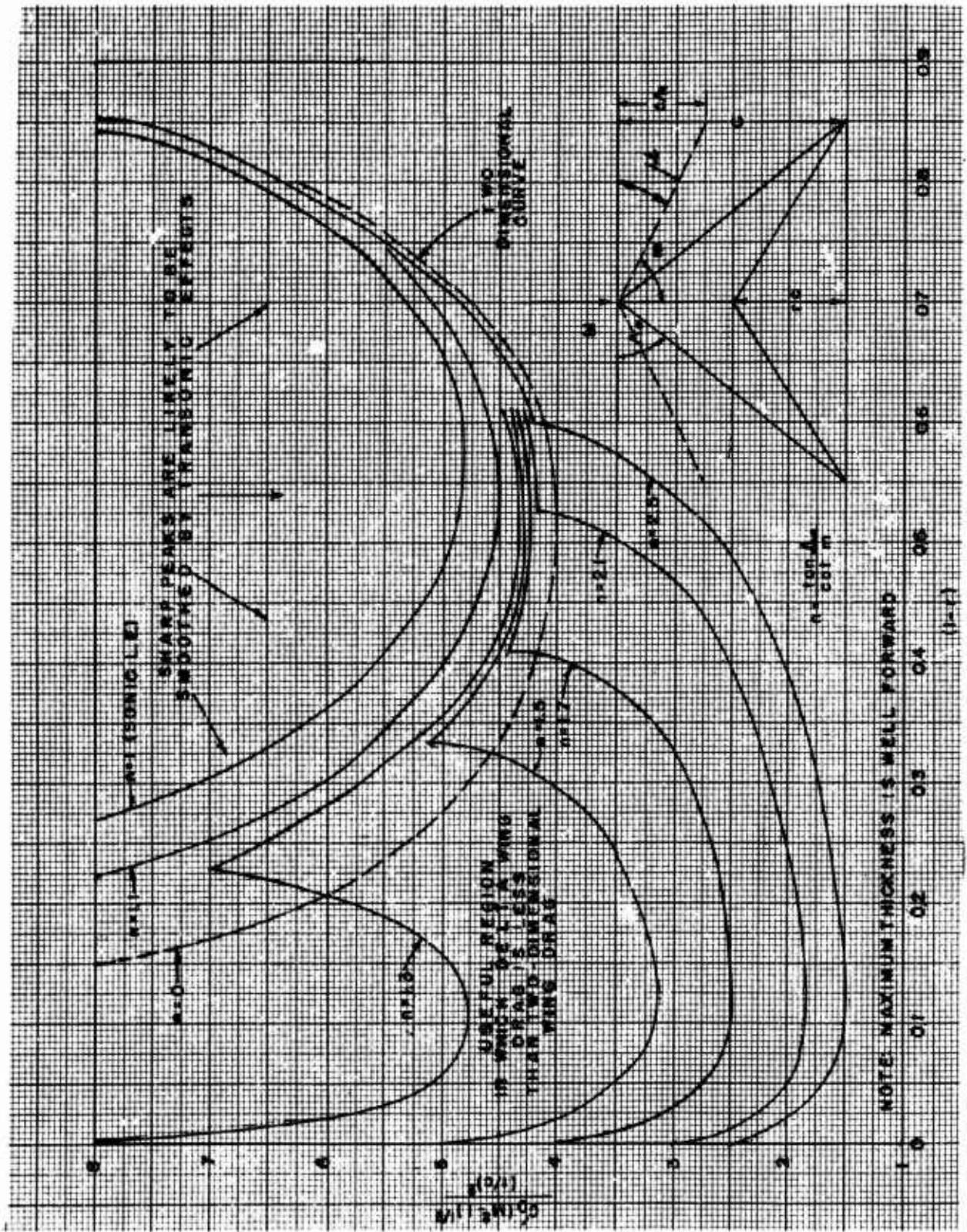


Fig (2.5-31) Drag of delta wing at zero lift, showing useful working range. Ref (2.5-69)

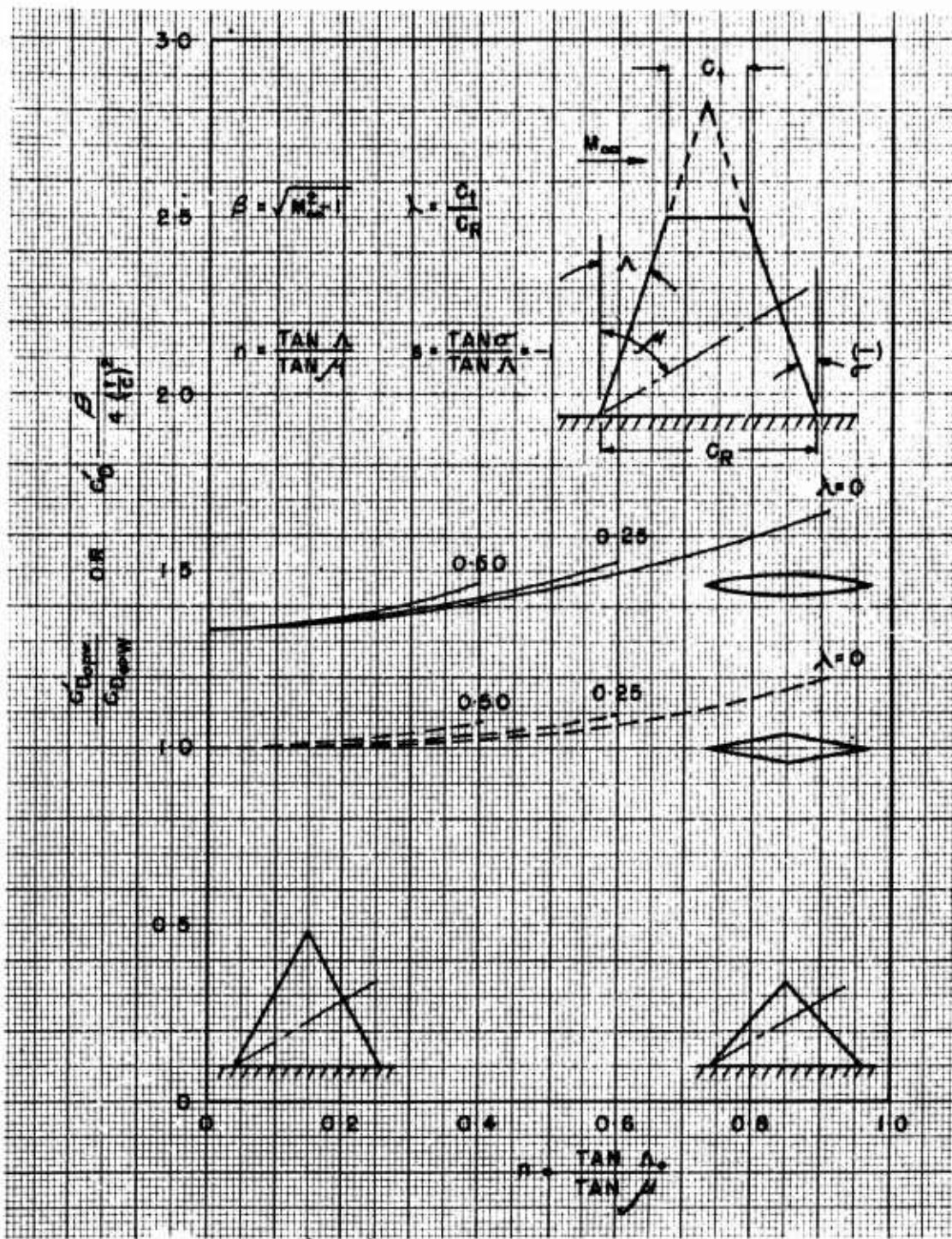


Fig (2.5- 32) Ratio of three dimensional pressure drag to its two-dimensional value for straight tapered wings. Ref (2.5-69)

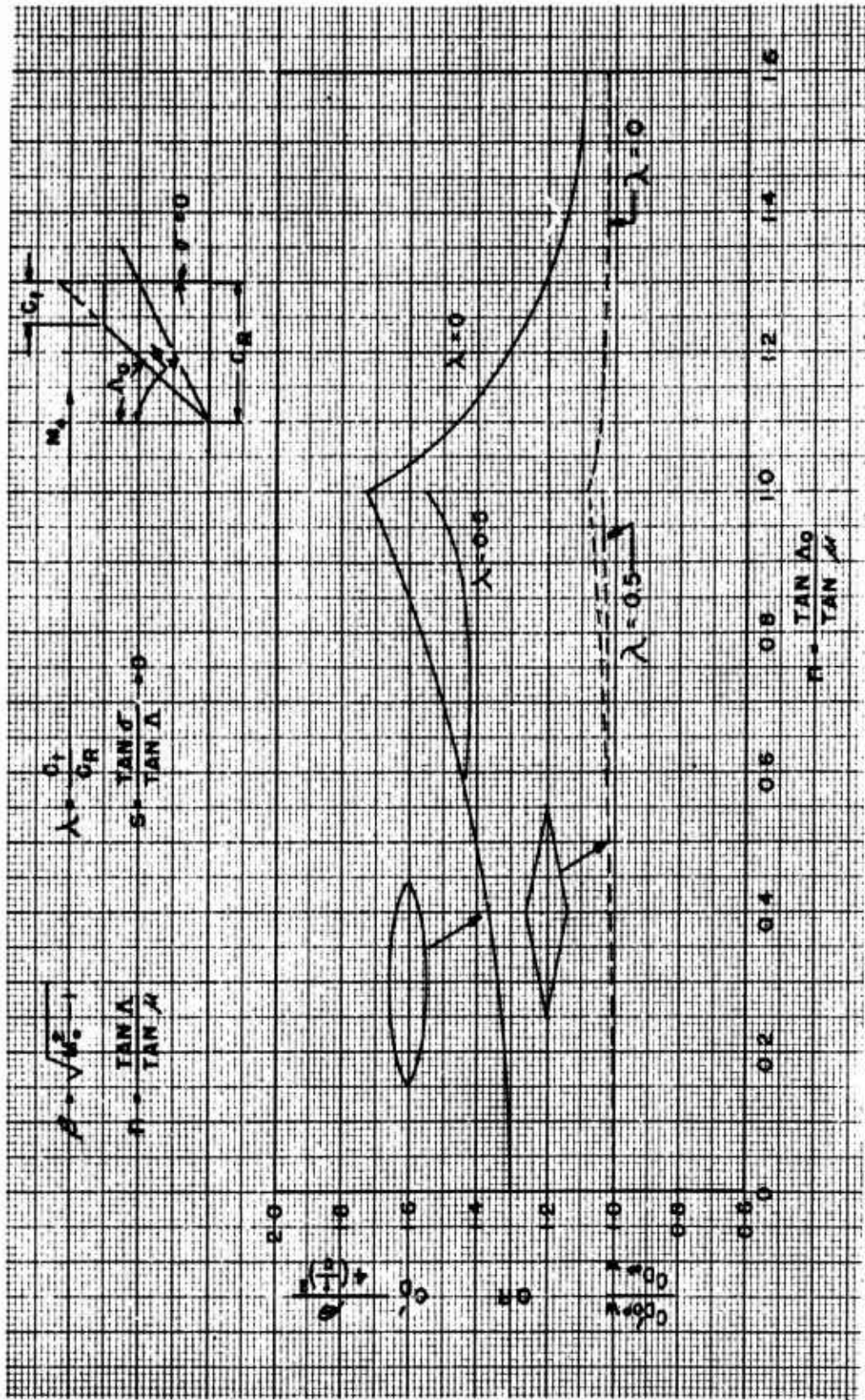


Fig (2.5-33) Ratio of three dimensional pressure drag coefficient to its two-dimensional value for clipped delta wings, linearized theory. Ref (2.5-69).

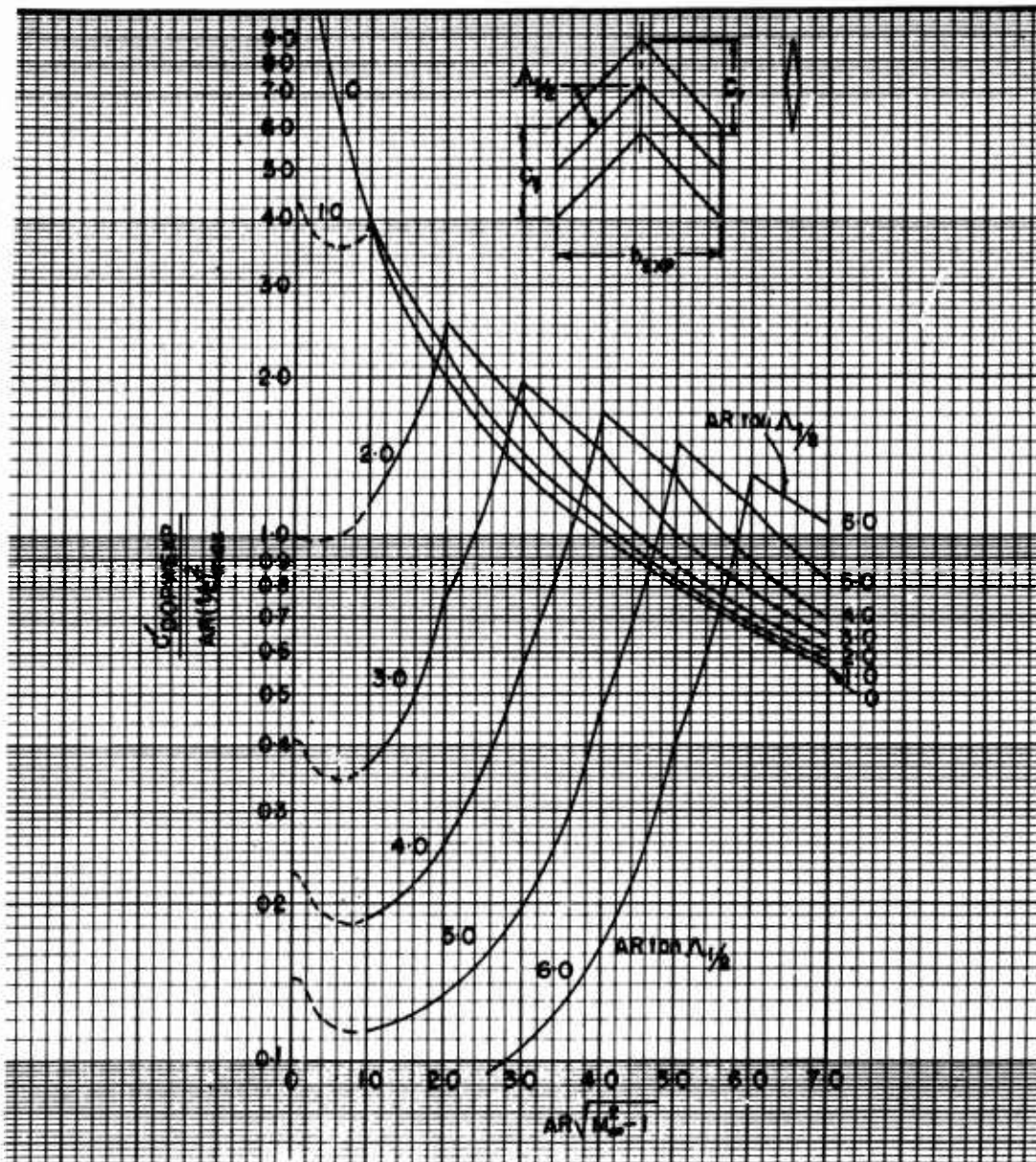


Fig (2.5-34) Inviscid pressure drag of wings with constant chord, constant spanwise thickness-chord ratio, double wedge sections, no taper, maximum thickness at  $0.5 \bar{c}$ . Ref (2.5-1) R.A.S. data sheets, aerodynamics, vol 2, wings S.02.03.01

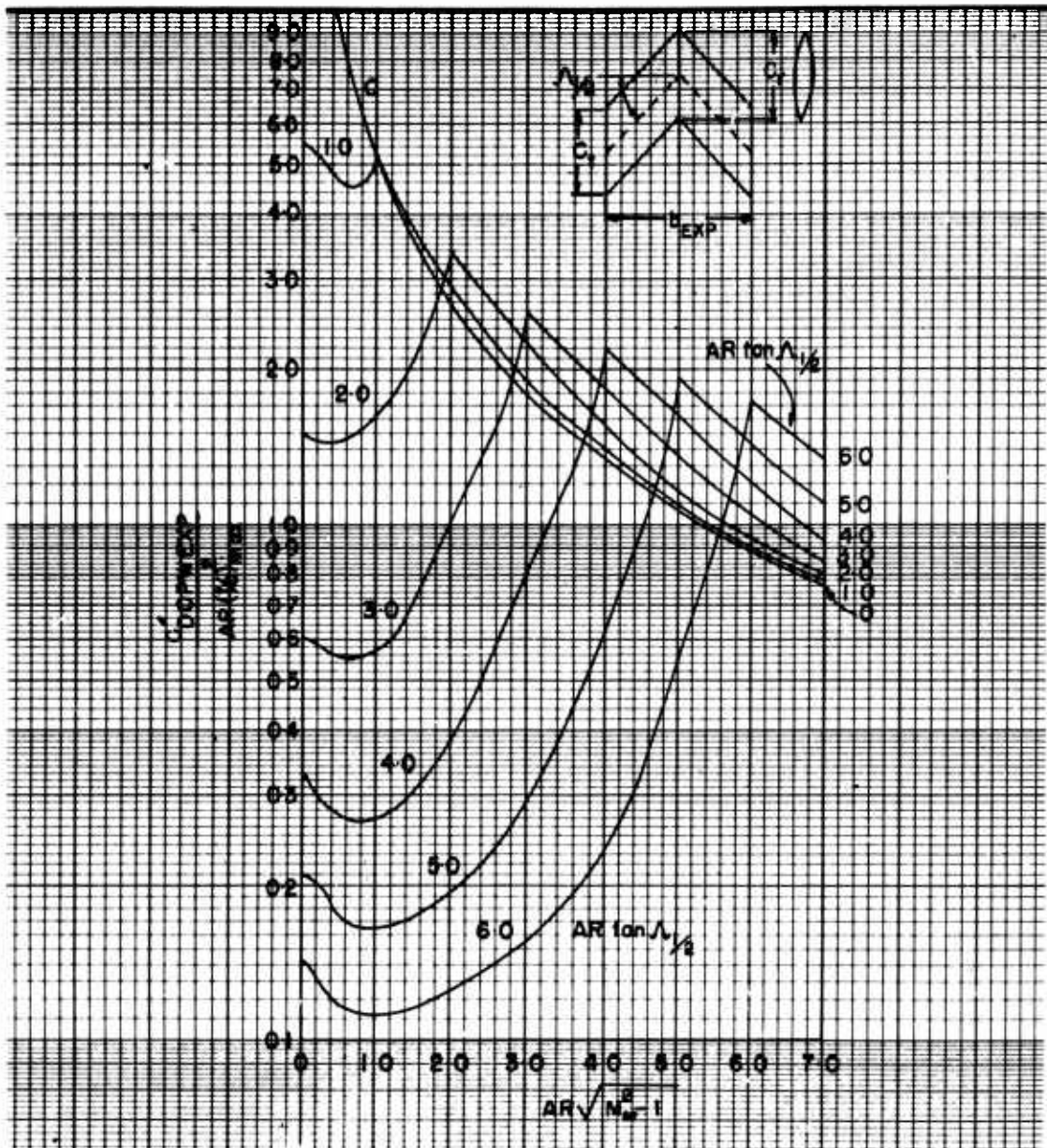


Fig (2.5-35) Inviscid pressure drag of wings with constant chord ratio, parabolic arc sections, no taper. Ref (2.5-1) R.A.S. data sheets, aerodynamics, vol. 2, wings S.02.03.01

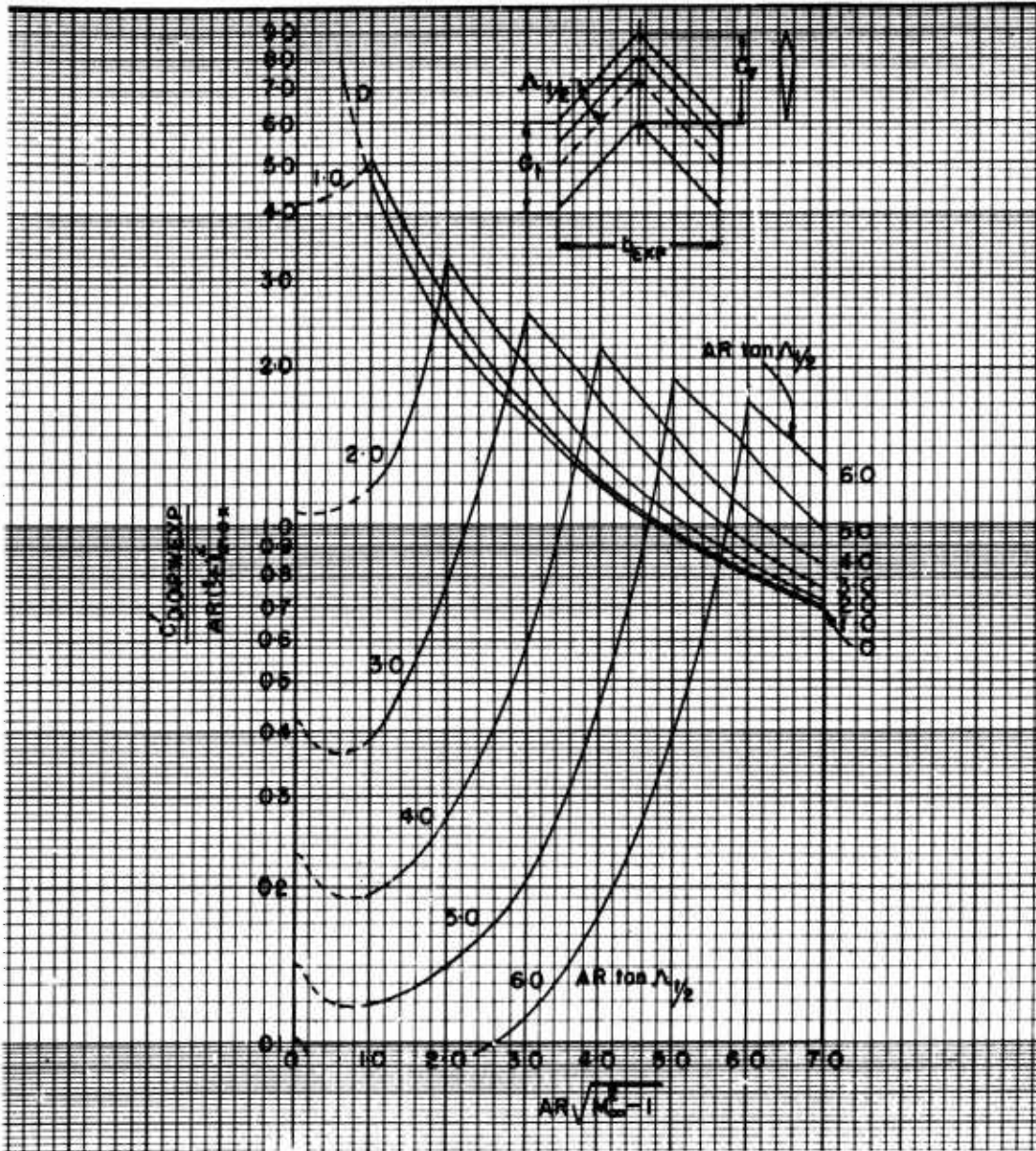


Fig (2.5-36) Inviscid pressure drag of wings with constant chord, constant spanwise thickness-chord ratio, double-wedge sections, no taper, maximum thickness at 0.3  $\bar{C}$ . Ref (2.5-1) R.A.S. data sheets, aerodynamics, vol. 2, wings S.02.03.0:

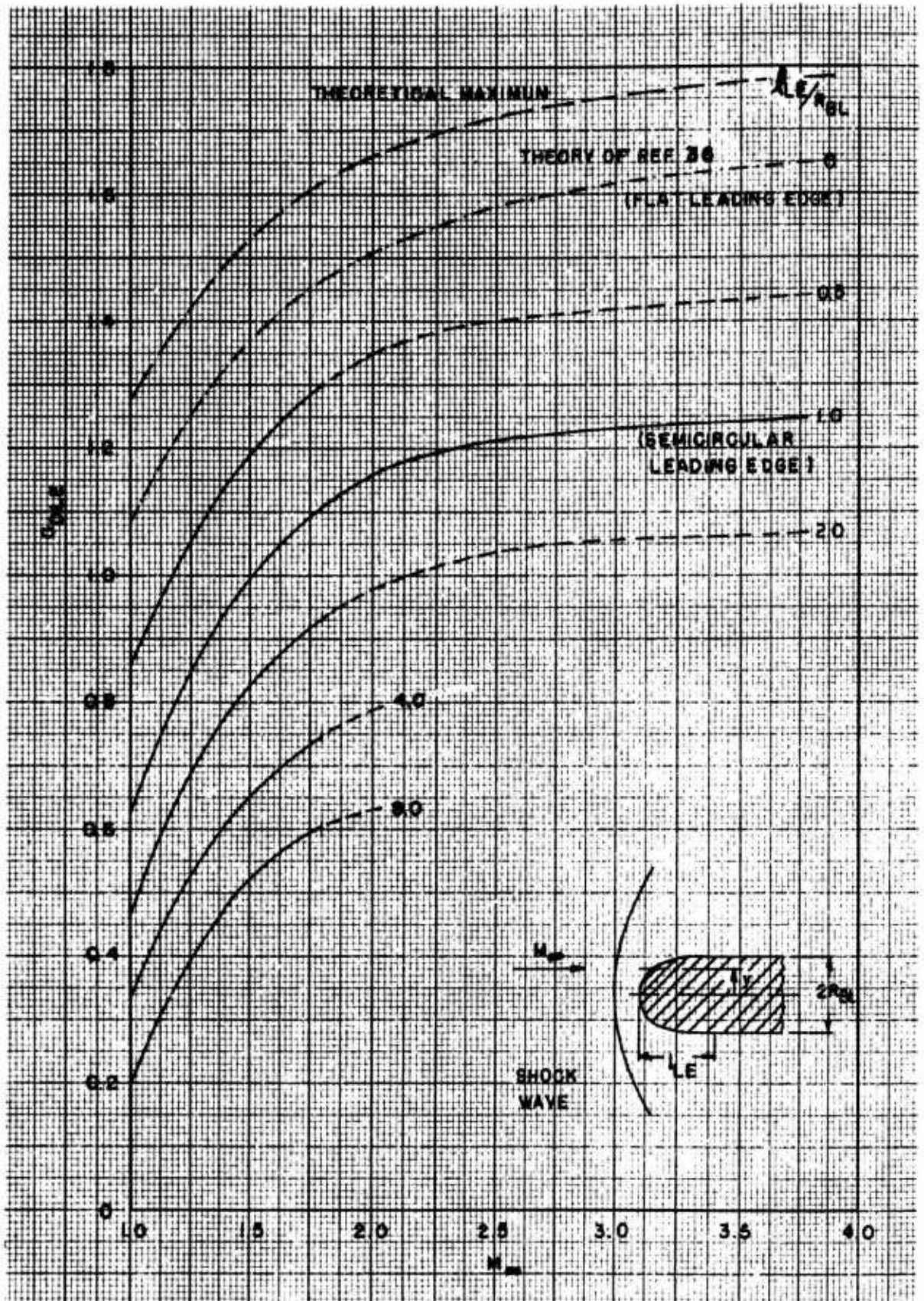


Fig (2.5-37) Leading edge pressure drag due to leading edge bluntness, two dimensional sections at zero angle-of-attack.  
 Ref (2.5-1) R.A.S. data sheets, aerodynamics, vol 2, wing  
 S.02.03.05

TABLE (2.5-3)

$$\frac{L_{\text{AFTERBODY}}}{D} = \frac{L_{\text{BT}}}{D} \approx \frac{1 - \frac{D_g}{D}}{2 \tan \frac{\theta_P}{2}}, \quad \theta = \frac{\theta_P}{2}$$

SEE FIG (2.5-19)

$D_B/D$	BOATTAIL BASE ANGLE,						
	2	4	6	8	10	12	14
.10	25.70	12.90	8.600	6.440	5.150	4.275	3.67
.20	23.85	11.45	7.640	5.725	4.570	3.80	3.26
.30	20.00	10.00	6.690	5.010	4.00	3.33	2.86
.40	17.15	8.600	5.740	4.300	3.43	2.86	2.445
.50	14.30	7.160	4.770	3.580	2.86	2.38	2.04
.60	11.41	5.730	3.820	2.865	2.285	1.905	1.63
.70	8.575	4.300	2.865	2.150	1.715	1.425	1.223
.80	5.720	2.865	1.910	1.431	1.142	0.953	0.815
.90	2.860	1.432	0.956	0.717	0.571	0.476	.4075
1.00	0	0	0	0	0	0	0
$L_{\text{AFTERBODY}}/D$							

TABLE (2.5-4)

Higher Order Busemann Coefficients

Calculated from equations 10.38 to 10.40, taking  $\gamma = 1.4$

M	C <sub>1</sub>	C <sub>2</sub>	C <sub>3</sub> (Isentropic)	b <sub>3</sub> (One Shock)	b <sub>4</sub> (One Shock)
1.1	4.364	30.32	568.98	544.4	12735.
1.2	3.015	8.307	54.034	53.22	480.51
1.3	2.408	4.300	14.247	14.53	77.41
1.4	2.041	2.919	5.801	6.128	22.51
1.5	1.789	2.288	3.059	3.331	8.964
1.6	1.601	1.950	1.937	2.153	4.302
1.7	1.455	1.748	1.4109	1.583	2.315
1.8	1.336	1.618	1.1444	1.280	1.334
1.9	1.240	1.529	1.0050	1.111	.7939
2.0	1.155	1.467	.9341	1.0161	.4711
2.2	1.021	1.386	.8946	.9394	.1272
2.4	.9167	1.337	.91921	.9356	- .0395
2.5	.8728	1.320	.94322	.9476	- .0918
2.6	.8333	1.306	.97189	.9654	- .1319
2.8	.7647	1.284	1.0382	1.013	- .1881
3.0	.7071	1.269	1.1116	1.069	- .2248
3.5	.5963	1.245	1.3090	1.231	- .2756
4.0	.5164	1.232	1.5132	1.405	- .3005
4.5	.4559	1.224	1.7191	1.584	- .3146
5.0	.4082	1.219	1.9250	1.764	- .3235
	0	1.2			- .3520

SEE FIG (2.5-22)

TABLE (2.5-4)

SEE FIG (2.5-19)

$$C_{DOPBT} = \frac{.001\theta_p - .00071\theta_p^2}{M} \left[ 1 - \left(\frac{D_B}{D}\right)^n \right]$$

WHERE  $n = 4$  FOR  $1 < M < 3.5$   
 $n = 3$  FOR  $M < 3.5$

$\theta_p$  IN DEGREES, SEE FIG (2.5-18)

$\theta_p = 2^\circ$	MACH NUMBER, M								
	1.50	2.00	2.50	3.00	3.25	3.75	4.00	4.50	5.00
$D_B/D$									
0.10	3.23	2.42	1.94	1.61	1.49	1.29	1.21	1.08	0.97
0.20	3.22	2.42	1.93	1.61	1.48	1.28	1.20	1.06	0.96
0.30	3.20	2.40	1.92	1.60	1.48	1.26	1.18	1.04	0.94
0.40	3.14	2.35	1.89	1.57	1.45	1.21	1.13	1.01	0.91
0.50	3.02	2.27	1.82	1.51	1.40	1.13	1.06	0.94	0.85
0.60	2.81	2.10	1.68	1.40	1.30	1.01	0.95	0.84	0.76
0.70	2.45	1.84	1.47	1.23	1.13	0.85	0.79	0.71	0.64
0.80	1.90	1.43	1.14	0.95	0.88	0.63	0.59	0.53	0.47
0.90	1.10	0.82	0.66	0.55	0.51	0.35	0.33	0.29	0.26

BOATTAIL PRESSURE DRAG COEFFICIENT,  $C_{DOP}$  BOATTAIL  $\times 10^3$

$\alpha_p = 4^\circ$		MACH NUMBER, M								
$D_B/D$	1.50	2.00	2.50	3.00	3.25	3.75	4.00	4.50	5.00	
0.10	10.23	7.67	6.13	5.11	4.72	4.09	3.84	3.41	3.07	
0.20	10.22	7.67	6.13	5.11	4.71	4.06	3.81	3.89	3.05	
0.30	10.16	7.62	6.09	5.08	4.68	3.98	3.73	3.32	2.99	
0.40	9.98	7.48	5.98	4.99	4.70	3.83	3.59	3.20	2.88	
0.50	9.60	7.20	5.76	4.80	4.42	3.58	3.36	2.99	2.69	
0.60	8.91	6.68	5.34	4.45	4.11	3.21	3.01	2.68	2.41	
0.70	7.78	5.83	4.66	3.89	3.59	2.69	2.52	2.24	2.02	
0.80	6.04	4.53	3.62	3.02	2.78	2.00	1.87	1.67	1.50	
0.90	3.48	2.61	2.09	1.74	1.60	1.11	1.04	0.92	0.83	

BOATTAIL PRESSURE DRAG COEFFICIENT,  $C_{DOP}$  BOATTAIL  $\times 10^3$

$\alpha_p = 6^\circ$		MACH NUMBER, M								
$D_B/D$	1.50	2.00	2.50	3.00	3.25	3.75	4.00	4.50	5.00	
0.10	21.05	15.78	12.63	10.52	9.71	8.42	7.89	7.02	6.31	
0.20	21.04	15.77	12.62	10.51	9.70	8.36	7.84	6.97	6.27	
0.30	20.90	15.67	12.54	10.44	9.64	8.19	7.68	6.83	6.14	
0.40	20.53	15.40	12.32	10.26	9.47	7.89	7.39	6.57	5.92	
0.50	19.75	14.81	11.85	9.87	9.11	7.38	6.91	6.14	5.53	
0.60	18.33	13.75	11.00	9.16	8.46	6.61	6.19	5.51	4.95	
0.70	16.01	12.01	9.61	8.00	7.39	5.53	5.18	4.61	4.15	
0.80	12.43	9.32	7.46	6.21	5.73	4.11	3.86	3.43	3.08	
0.90	7.16	5.37	4.30	3.58	3.30	2.28	2.14	1.90	1.71	

BOATTAIL PRESSURE DRAG COEFFICIENT,  $C_{DOP}$  BOATTAIL  $\times 10^3$

TABLE (2.5-4) CONT'D (1)

$\theta_p = 8^\circ$		MACH NUMBER, M								
$D_B/D$	1.50	2.00	2.50	3.00	3.25	3.75	4.00	4.50	5.00	
0.10	35.56	26.67	21.34	17.78	16.41	14.23	13.34	11.86	10.67	
0.20	35.54	26.66	21.33	17.77	16.40	14.13	13.24	11.77	10.59	
0.30	35.31	26.48	21.18	17.65	16.30	13.84	12.98	11.54	10.38	
0.40	34.69	26.02	20.81	17.34	16.01	13.33	12.50	11.11	10.00	
0.50	33.38	25.03	20.03	16.69	15.40	12.46	11.68	10.39	9.34	
0.60	30.97	23.23	18.58	15.49	14.29	11.16	10.47	9.31	8.37	
0.70	27.06	20.29	16.23	13.53	12.42	9.34	8.76	7.79	7.01	
0.80	21.00	15.75	12.60	10.50	9.69	6.95	6.51	5.79	5.21	
0.90	12.10	9.08	7.26	6.05	5.59	3.86	3.62	3.22	2.89	

BOATTAIL PRESSURE DRAG COEFFICIENT,  $C_{DOP}$  BOATTAIL  $\times 10^3$

$\theta_p = 10^\circ$		MACH NUMBER, M								
$D_B/D$	1.50	2.00	2.50	3.00	3.25	3.75	4.00	4.50	5.00	
0.10	53.9	40.46	32.37	27.97	24.90	21.58	20.23	17.98	16.18	
0.20	53.91	40.44	32.35	26.96	24.88	21.43	20.09	17.86	16.07	
0.30	53.56	40.17	32.13	26.78	24.72	21.00	19.68	17.50	15.75	
0.40	52.62	39.46	31.57	27.31	24.28	20.22	18.95	16.84	15.16	
0.50	50.62	37.97	30.38	25.31	23.36	18.90	17.72	15.75	14.18	
0.60	46.98	35.24	28.19	23.49	21.68	16.93	15.88	14.11	12.70	
0.70	41.04	30.78	24.62	20.52	18.94	14.17	13.28	11.81	10.63	
0.80	31.86	23.90	19.12	15.93	14.70	10.54	9.88	8.78	7.51	
0.90	18.36	13.77	11.02	9.18	8.47	5.85	5.49	4.88	4.39	

BOATTAIL PRESSURE DRAG COEFFICIENT,  $C_{DOP}$  BOATTAIL  $\times 10^3$

TABLE (2.5-4) CONT'D (2)

$\theta_p = 12^\circ$		MACH NUMBER, M								
$D_B/D$	1.50	2.00	2.50	3.00	3.25	3.75	4.00	4.50	5.00	
0.10	76.08	57.06	45.65	38.04	35.12	30.43	28.53	25.36	22.83	
0.20	76.04	57.03	45.63	38.02	35.09	30.22	28.33	25.19	22.67	
0.30	75.54	56.65	45.33	37.77	34.86	29.61	27.76	24.68	22.21	
0.40	74.21	55.66	44.53	37.11	34.25	28.51	26.73	23.77	21.39	
0.50	71.40	53.55	42.84	35.70	32.95	26.65	24.99	22.22	19.99	
0.60	66.26	49.69	39.76	33.13	30.58	23.88	22.39	19.91	17.91	
0.70	57.88	43.41	34.73	28.94	26.71	19.98	18.74	16.66	14.99	
0.80	44.93	33.70	26.96	22.47	20.74	14.86	13.94	12.39	11.15	
0.90	25.89	19.42	15.54	12.95	11.95	8.25	7.74	6.88	6.19	

BOATTAIL PRESSURE DRAG COEFFICIENT,  $C_{DOP}$  BOATTAIL  $\times 10^3$

$\theta_p = 14^\circ$		MACH NUMBER								
$D_B/D$	1.50	2.00	2.50	3.00	3.25	3.75	4.00	4.50	5.00	
0.10	102.03	76.52	61.22	51.02	47.09	40.81	38.26	34.01	30.61	
0.20	101.97	76.48	61.18	50.99	47.06	40.52	37.99	33.77	30.39	
0.30	101.29	75.97	60.78	50.65	46.75	39.71	37.23	33.09	29.78	
0.40	99.52	74.64	59.71	49.76	45.93	38.24	35.85	31.86	28.68	
0.50	95.75	71.81	57.45	47.88	44.19	35.74	33.51	29.78	26.81	
0.60	88.85	66.64	53.31	44.41	41.01	32.03	30.03	26.64	24.02	
0.70	77.62	58.22	46.57	38.81	35.83	27.80	24.12	22.33	20.10	
0.80	60.26	45.19	36.16	30.13	27.81	19.93	18.69	16.61	14.95	
0.90	34.72	26.04	20.84	17.36	16.03	11.07	10.38	9.22	8.30	

BOATTAIL PRESSURE DRAG COEFFICIENT,  $C_{DOP}$  BOATTAIL  $\times 10^3$

TABLE (2.5-4) CONT'D (3)

2.5.5 INSTRUCTIONS FOR USE OF THE PROPOSED METHODS FOR THE TOTAL ZERO LIFT PRESSURE DRAG COEFFICIENT ESTIMATES (EXCLUSIVE OF BASE DRAG)

(i) Basic Data Preparation

The basic geometric parameters of a given missile configuration, pertinent to the zero-lift pressure drag evaluation, should be numerically specified and tabulated as indicated in the respective Table (2.3-5).

(1) List of Working Graphs For Body Pressure Drag

(a) Supersonic speeds ( $1.2 \leq M \leq 5$ ).

Nose Cones,  $C_{DOPC}$  :

Figs (2.5-11) and (2.5-12) (set "A") or Figs (2.5-1) and (2.5-2) (set "B")

Nose Ogives,  $\Delta C_{DOP0}$  :

Fig (2.5-13)  
(Auxiliary: Fig (2.4-43))

Minimum Pressure Drag Nose Shapes,  $C_{DOPFORE}$  :

Fig (2.5-14)  
(Auxiliary: Figs (2.5-8) and (2.5-9))  
 $\Delta C_{DOPNTIP}$

Nose Tip Bluntness Effects,

Fig (2.5-15)

Conical Boattails,  $C_{DOPBTC}$  :

Fig (2.5-16) (set "A")  
Figs (2.4-44) and (2.5-19) (set "B")

Parabolic Boattails,  $C_{DOPBTO}$  :

Fig (2.5-17) (set "A")  
Fig (2.4-44) and (2.5-19) (set "B")

Forebody Interference,  $\Delta C_{DOPBT(FORE)}$  :

Fig (2.5-20) (Conical Afterbody-Forebody Combinations)  
Fig (2.5-21) (Parabolic Fore-Afterbody Combinations)

(b) Mach Number  $M = 1$ .

Nose Cones,  $C_{DOPC}$  :

Fig (2.5-4)

Nose Ogives,  $C_{DOP}$  :

Fig (2.5-5)

The accuracy of the charts is stated in the respective text, i.e., it is within the general accuracy of theories used in each case.

A self-explaining computation procedure is illustrated on the related Tables, using both sets "A" and "B" of the listed figures, see Tables (2.5-14) and (2.5-15).

Basic data for respective missile part geometries are presented in the Table (2.4-8) of the preceding Section 2.4.

(2) List of Working Graphs for Wing (or Fin) Pressure Drag

(a) Inviscid pressure drag,  $C_{DOPWEXP}$  or  $C_{DOPFEXP}$  :

Figs (2.5-22), (2.5-22a) and (2.5-25) (auxiliary data)

Profile shape corrections:

Fig (2.5-26)

Straight, no taper wings:

Figs (2.5-27), (2.5-28) and (2.5-29)

Delta wings:

Figs (2.5-30) and (2.5-31)

Straight tapered wings:

Fig (2.5-32)

Clipped delta wings:

Fig (2.5-33)

Swept back, no taper wings:

Figs (2.5-34), (2.5-35) and (2.5-36)

(b) Viscous pressure drag,  $C_{DOPWVIS}$  or  $C_{DOPFVIS}$  :

Figs (2.5-23) and (2.5-24)

(c) Leading edge bluntness drag,  $C_{DOPWLE}$  or  $C_{DOPFLE}$ :

Fig (2.5-37)

The accuracy of the charts is stated in the respective text, i.e., it is within the general accuracy of

theories used in each case.

A self-explaining computation procedure is illustrated in the related Tables (2.5-5) to (2.5-13).

Basic data for respective wing geometry are presented in Table (2.4-8) of the preceding Section 2.4.

(3) The Proposed Method for the Total Zero-lift Pressure Drag Coefficient Estimates (Exclusive of Base Drag)

The proposed computation procedure for the total zero-lift pressure drag coefficient evaluation is presented in the adopted stepwise self-instructive way in Tables (2.5-5) to (2.5-16).

Therefore, no specific additional instructions are required.

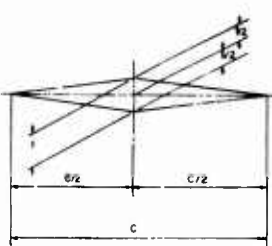
Within the reasonings and the approximations stated in this Section the final expression for the pressure drag coefficient takes the form:

$$\begin{aligned} C_{DOP} = & \left[ (C_{DOPC} + \Delta C_{DOPD} + \Delta C_{DOPNTIP}) + \right. \\ & \left. + (C_{DOPBT} + \Delta C_{DOPBT(FORE)}) \right] + \\ & + [C_{DOPWEXP} + C_{DOPWVIS} + C_{DOPWLE}] \\ & + [C_{DOPFEXP} + C_{DOPFVIS} + C_{DOPFLE}] \end{aligned}$$

(2.5-91)

TABLE (2.5-5)  
ANALYTICAL EXPRESSIONS AND RELATED GRAPHS FOR PRESSURE DRAG COEFFICIENT ESTIMATES  
AND LEADING EDGE BLUNTNESS EXCLUDED) [(M=1.2), ZERO ANGLE OF ATTACK. REFERENCE

BASIC DEFINITIONS

TYPE OF WING PLANFORM (1)	ZERO-LIFT INVISCID PRESSURE DRAG COEFFICIENT, $C_{D_{PR}}$ , REFERENCE AREA, $S_{REF}$ , $C_{D_{PR}} = C_{D_{PR}} \cdot S_{REF}$ (2)
BASIC TWO-DIMENSIONAL THEORETICAL MINIMUM DRAG DOUBLE WEDGE DOUBLE SYMMETRY AIRFOIL 	ACKERET LINEARIZED THEORY, REF (2.5-3) $C_{D_{PR}} = 4 \frac{11(C)^2}{\beta} + 2 C_1 (11/C)^2 \cdot (A)$ (see Table 2.5-4) $\beta = (M^2 - 1)^{-1/2}$ , (see FIG 2.5-25) $C_1 = \text{BUSEMANN'S COEFFICIENT} = \frac{2}{\beta}$ (see 2.5-4) or FIG (2.5-22a)

ON WINGS (FINS) AT SUPERSONIC SPEEDS, INCLUDING VISCOUS FORM DRAG (BASE DRAG AREA  $S_b = \pi D^2/4$ ). (CONSULT FIG-24 FOR CRITICAL PROFILE ANGLE RESTRICTIONS)

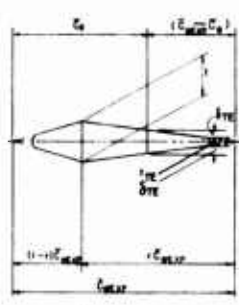
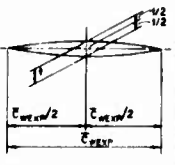
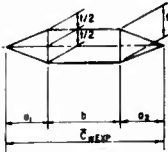
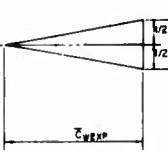
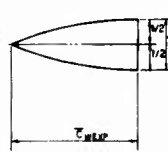
CORRECTIVE FACTOR FOR VISCOUS FORM DRAG EFFECTS, TURBULENT B.L., $C_{D_{VP}}$ (3)	CORRECTIVE FACTOR FOR VARIOUS AIRFOIL SHAPES DOUBLE SYMMETRICAL BICONVEX AIRFOILS (4)	MAXIMUM THICKNESS SPANWISE SHIFT (5)
 $\xi = \left[ 1 - \frac{(2B_{TE} + 1) r}{c} \right] \cdot \frac{C_0}{C_{D_{PR}}}$ $r = 1/2$ FOR DOUBLE SYMMETRY $r_{TE} = .0019$ $(B/B_0) = f(A)$ , (SEE FIG 2.5-24) $b_1 = (.37L)/W_0$ (BLADIUS)	 $\xi = 4.3$ , REF (2.5-3)	$\xi_0 = \frac{1}{4(1/C_{D_{PR}}) - 1/2}$ or $\xi_0$ - FROM FIG. (2.5-26) (THEORY, REF 2.5-3)

TABLE (2.5-5) CONTINUED

CORRECTIVE FACTOR FOR VARIOUS AIRFOIL SHAPES MODIFIED DOUBLE WEDGE SYMMETRIC AIRFOILS (6)	SINGLE WEDGE SYMMETRIC AIRFOILS (7)	BLUFF SYMMETRIC BICONVEX AIRFOILS (8)
 $\xi_0 = \frac{q_1 + q_2}{4q_1 q_2}$ , REF (2.5-11)	 SEMI-EMPIRICAL CORRECTION, REF. (2.5-3) $\xi_0 = \frac{95(11/C)^2}{2} + \frac{1}{2} C_1 (11/C)^2$ [ $\theta=1$ , $\xi_0=1$ ]	 SEMI-EMPIRICAL CORRECTION, REF. (2.5-3) $\xi_0 = \xi_0^* \cdot \xi_0^*$

NOTE: ALL CORRECTIVE FACTORS FOR AIRFOIL SHAPE VARIATIONS,  $\xi_1$  TO  $\xi_5$ , ARE SECOND ORDER CORRECTIONS (BUSEMANN) ARE NEGLECTED IN THIS CASE.

CORRECTIVE FACTOR FOR REFERENCE AREA $S_r = \pi D^2/4$ (9)	( $C_{D_{PR}} + C_{D_{VP}}$ ) FINAL EXPRESSION AND REFERENCE FIGURE (see Table 2.5-5) (10)
$\xi_7 = 1 - \xi_7 \left( \frac{b_{WEXP}}{D} \times \frac{C_{WEXP}}{D} \right)$	

BASED ON THE LINEAR (ACKERET) THEORY.

TABLE (2.5-5)  
STRAIGHT RECTANGULAR

(1)	(2)
<p>STRAIGHT RECTANGULAR PLANFORM WING WITH DOUBLE WEDGE DOUBLE SYMMETRY AIRFOIL</p> <p>NOTE: FOR SPANWISE VARIABLE <math>b(x)</math>, WITH FIRST APPROXIMATION USE AS REFERENCE <math>[1/(C)_{\text{average}} = \frac{1}{2} \{1/(C)_{\text{tip}} + 1/(C)_{\text{root}}\}]</math></p>	<p>BUSEMANN'S SECOND ORDER THEORY, REF 8</p> <p><math>C_{D_{\text{DOW}}} = \frac{2}{\pi} \left[ \frac{1}{2\pi R(M-1)} \left( 1 - \frac{C_2}{C_1^2} \right) \right] \cdot \text{A} \cdot \text{B}</math></p> <p>BUSEMANN'S COEFFICIENTS: <math>C_1</math> and <math>C_2</math> - see TABLE (2.5-4) and FIG. (2.5-22)</p>
STRAIGHT RECTANGULAR PLANFORM WITH DOUBLE SYMMETRY BICONVEX AIRFOIL	A, B
STRAIGHT RECTANGULAR PLANFORM WITH DOUBLE WEDGE SYMMETRIC AIRFOIL, WITH MAXIMUM THICKNESS $t/c$ SHIFTED FORWARD OR BACKWARD	A, B
STRAIGHT RECTANGULAR PLANFORM, BICONVEX SYMMETRIC AIRFOIL, WITH MAXIMUM THICKNESS $t/c$ SHIFTED FORWARD OR BACKWARD	A, B
STRAIGHT RECTANGULAR PLANFORM WITH MODIFIED DOUBLE WEDGE DOUBLE SYMMETRY AIRFOIL	A, B
STRAIGHT RECTANGULAR PLANFORM WITH SINGLE WEDGE SYMMETRIC AIRFOIL, BLUFF BASE AT $t/c$ MAX	$\left[ -\frac{1}{2\pi R(M-1)^2} \left( 1 - \frac{C_2}{C_1^2} \right) \right] \cdot \text{B}$
STRAIGHT RECTANGULAR PLANFORM WITH SYMMETRIC BICONVEX AIRFOIL WITH BLUFF BASE AT $t/c$ MAX	B

CONT (1)  
PLANFORMS

(3)	(4)	(5)	(6)	(7)	(8)	(10)
$J_1$	1	1	1	1	$J_2$	$(C_{D_{\text{DOW}}} + \Delta C_{D_{\text{DOW}}}) = \text{A} \cdot \text{B} \cdot \text{C} \cdot \text{D}$ $\text{C} = (1.275) \left( \frac{b_{\text{WEXP}}}{D} \right) \left( \frac{c_{\text{WEXP}}}{D} \right) \left[ \frac{1}{2} \left( 1 - \frac{t}{c} \right) \right]$ $\text{D} = \left[ -\frac{1}{2\pi R(M-1)^2} \left( 1 - \frac{C_2}{C_1^2} \right) \right]$
$J_1$	$J_2$	1	1	1	$J_2$	$(C_{D_{\text{DOW}}} + \Delta C_{D_{\text{DOW}}}) = \text{A} \cdot \text{B} \cdot \text{C} \cdot \text{D} \cdot \text{E}$
$J_1$	$J_2$	1	1	1	$J_2$	$(C_{D_{\text{DOW}}} + \Delta C_{D_{\text{DOW}}}) = \text{A} \cdot \text{B} \cdot \text{C} \cdot \text{D} \cdot \text{E} \cdot \text{F}$
$J_1$	$J_2$	$J_3$	1	1	$J_2$	$(C_{D_{\text{DOW}}} + \Delta C_{D_{\text{DOW}}}) = \text{A} \cdot \text{B} \cdot \text{C} \cdot \text{D} \cdot \text{E} \cdot \text{F} \cdot \text{G}$
$J_1$	1	$J_3$	1	1	$J_2$	$(C_{D_{\text{DOW}}} + \Delta C_{D_{\text{DOW}}}) = \text{A} \cdot \text{B} \cdot \text{C} \cdot \text{D} \cdot \text{E} \cdot \text{F} \cdot \text{G} \cdot \text{H}$
1	1	1	1	$J_2$	$J_2$	$(C_{D_{\text{DOW}}} + \Delta C_{D_{\text{DOW}}}) = \text{A} \cdot \text{B} \cdot \text{C} \cdot \text{D} \cdot \text{E} \cdot \text{F}$
1	$J_2$	1	1	$J_2$	$J_2$	$(C_{D_{\text{DOW}}} + \Delta C_{D_{\text{DOW}}}) = \text{A} \cdot \text{B} \cdot \text{C} \cdot \text{D} \cdot \text{E} \cdot \text{F}$

TABLE (2.5-5)  
STRAIGHT TAPERED

(1)	(2)
<p>STRAIGHT SYMMETRICALLY TAPERED WINGS WITH DOUBLE WEDGE, DOUBLE SYMMETRY AIRFOIL SECTION OF CONSTANT <math>t/c</math>.</p> <p><math>\lambda = C_1/C_2, \mu = \frac{2}{b_{\text{WEXP}}} \cdot \frac{b_{\text{WEXP}}}{c_{\text{WEXP}}} \cdot \frac{1}{c} \cdot \text{CROSS}</math></p> <p><math>\sigma = (M-1)^2, \mu = \frac{100 \Delta}{100 \Delta}</math></p>	<p>LINEARIZED THEORY, REF (2.5-3)</p> <p>CROSSPLOT OF <math>C_{D_{\text{DOW}}} \frac{b^2}{4(c)^2}</math> VERSUS <math>\lambda = \frac{b_{\text{WEXP}}}{c}</math> IS PRESENTED ON FIG (2.5-32)</p> <p>FOR THREE TAPER RATIOS: <math>\lambda = C_1/C_2 = 0, 25</math> and <math>50</math></p> <p><math>C_{D_{\text{DOW}}} = \text{B}</math></p>
STRAIGHT SYMMETRICALLY TAPERED WINGS WITH DOUBLE SYMMETRY BICONVEX AIRFOIL	B
STRAIGHT SYMMETRICALLY TAPERED WINGS WITH SYMMETRICAL DOUBLE WEDGE AIRFOIL, MAXIMUM THICKNESS LINE SHIFTED FORWARD OR BACKWARD FOR A CONSTANT PERCENTAGE OF CHORD ALONG THE SPAN.	B
STRAIGHT SYMMETRICALLY TAPERED WINGS WITH SYMMETRICAL BICONVEX AIRFOIL, MAXIMUM THICKNESS LINE SHIFTED FORWARD OR BACKWARD FOR A CONSTANT PERCENTAGE OF CHORD ALONG THE SPAN.	B
STRAIGHT SYMMETRICALLY TAPERED WINGS WITH A MODIFIED DOUBLE WEDGE, DOUBLE SYMMETRY AIRFOIL, $t/c$ CONSTANT ALONG THE SPAN	B

CONT'D (2)

(3)	(4)	(5)	(6)	(7)	(8)	(9)	(10)
$J_1$	1	1	1	1	$J_2$		$(C_{D_{\text{DOW}}} + \Delta C_{D_{\text{DOW}}}) = \text{A} \cdot \text{B} \cdot \text{C} \cdot \text{D}$ $\text{C} = (1.275) \left( \frac{b_{\text{WEXP}}}{D} \right) \left( \frac{c_{\text{WEXP}}}{D} \right) \left[ 1 - \frac{2 \Delta t E + t E}{c} \right] C_{D_{\text{DOW}}}$
$J_1$	$J_2$	1	1	1	$J_2$		$(C_{D_{\text{DOW}}} + \Delta C_{D_{\text{DOW}}}) = \text{A} \cdot \text{B} \cdot \text{C} \cdot \text{D} \cdot \text{E}$
$J_1$	$J_2$	1	1	1	$J_2$		$(C_{D_{\text{DOW}}} + \Delta C_{D_{\text{DOW}}}) = \text{A} \cdot \text{B} \cdot \text{C} \cdot \text{D} \cdot \text{E} \cdot \text{F}$
$J_1$	$J_2$	$J_3$	1	1	$J_2$		$(C_{D_{\text{DOW}}} + \Delta C_{D_{\text{DOW}}}) = \text{A} \cdot \text{B} \cdot \text{C} \cdot \text{D} \cdot \text{E} \cdot \text{F} \cdot \text{G}$
$J_1$	1	$J_3$	1	1	$J_2$		$(C_{D_{\text{DOW}}} + \Delta C_{D_{\text{DOW}}}) = \text{A} \cdot \text{B} \cdot \text{C} \cdot \text{D} \cdot \text{E} \cdot \text{F} \cdot \text{G} \cdot \text{H}$



TABLE (2.5-6)

(1)	(2)
<p>CLIPPED DELTA WING WITH DOUBLE WEDGE DOUBLE SYMMETRY AIRFOIL</p> <p><math>\lambda = G/G_c, \lambda_c = 1.000</math></p> <p><math>C_{D_{exp}} = \frac{G + G_c}{2} \cdot \lambda_c \cdot (1.275 - 1)^2</math></p> <p><math>\lambda_c = \frac{G_c}{G} \cdot \frac{1.275 - 1}{1.275 - 1}</math></p> <p><math>\lambda_c = \frac{G_c}{G}</math></p>	<p>LINEARIZED THEORY, REF (2.5-69)</p> <p>CROSSPLOT <math>C_{D_{exp}} = \frac{G + G_c}{2} \lambda_c</math> VERSUS <math>\lambda_c</math></p> <p>IS PRESENTED ON FIG (2.5-33)</p> <p>FOR TAPER RATIOS <math>\lambda = 0</math> AND 50</p> <p><math>C_{D_{exp}} = \textcircled{4}</math></p>
<p>CLIPPED DELTA WING WITH DOUBLE SYMMETRY BICONVEX AIRFOIL, <math>\lambda/c</math> CONSTANT ALONG SPAN</p>	<p><math>\textcircled{5}</math></p>
<p>CLIPPED DELTA WING WITH SYMMETRICAL DOUBLE WEDGE AIRFOIL, MAXIMUM THICKNESS LINE SHIFTED FORWARD OR BACKWARD FOR A CONSTANT PERCENTAGE OF CHORD ALONG SPAN</p>	<p><math>\textcircled{6}</math></p>
<p>CLIPPED DELTA WING WITH SYMMETRICAL BICONVEX AIRFOIL, MAXIMUM THICKNESS LINE SHIFTED FORWARD OR BACKWARD FOR A CONSTANT PERCENTAGE OF CHORD ALONG SPAN</p>	<p><math>\textcircled{7}</math></p>
<p>CLIPPED DELTA WING WITH A MODIFIED DOUBLE WEDGE DOUBLE SYMMETRY AIRFOIL, <math>\lambda/c</math> CONSTANT ALONG SPAN</p>	<p><math>\textcircled{8}</math></p>
<p>CLIPPED DELTA WING WITH SYMMETRICAL DOUBLE WEDGE AIRFOIL, MAXIMUM THICKNESS LINE SHIFTED FORWARD OR BACKWARD FOR A CONSTANT PERCENTAGE OF CHORD ALONG SPAN</p> <p><math>\lambda = G/G_c, \lambda_c = 1.000</math></p> <p><math>C_{D_{exp}} = \frac{G + G_c}{2} \cdot \lambda_c \cdot (1.275 - 1)^2</math></p> <p><math>\lambda_c = \frac{G_c}{G} \cdot \frac{1.275 - 1}{1.275 - 1}</math></p> <p><math>\lambda_c = \frac{G_c}{G}</math></p>	<p>LINEARIZED THEORY, REF (2.5-11)</p> <p><math>C_{D_{exp}}</math> FROM FIG (2.5-36) (DOUBLE WEDGE)</p> <p>FROM FIG (2.5-38) (BICONVEX)</p> <p><math>C_{D_{exp}} = \textcircled{1}</math></p>

NOTE FOR SPANWISE VARIABLE  $\lambda/c$ , WITH FIRST APPROXIMATION USE AS REFERENCE  $(\lambda/c)_{exp} = \lambda/c \cdot (1.275 - 1)$

(CONTINUED) (4)

(3)	(4)	(5)	(6)	(7)	(8)	(9)	(10)
$\zeta_1$	1	1	1	1	1	$\zeta_2$	$(C_{D_{exp}} + C_{D_{convex}}) \cdot \textcircled{1} \cdot \zeta_1 + \zeta_2 \cdot \textcircled{2}$ $\textcircled{3} = 1.275 \left( \frac{C_{D_{exp}}}{G} \lambda_c \frac{E_{TSEP}}{D} \right) \left( 1 - \frac{0.6 \delta_{TE} + 1.7 \tau}{1} \right) = C_{D_{exp}}$
$\zeta_1$	$\zeta_2$	1	1	1	1	$\zeta_3$	$(C_{D_{exp}} + C_{D_{convex}}) \cdot \textcircled{1} \cdot \zeta_1 + \zeta_2 \cdot \zeta_3 \cdot \textcircled{2} = \zeta_3$
$\zeta_1$	1	$\zeta_2$	1	1	1	$\zeta_4$	$(C_{D_{exp}} + C_{D_{convex}}) \cdot \textcircled{1} \cdot \zeta_1 + \zeta_2 \cdot \zeta_3 \cdot \textcircled{2} = \zeta_4$
$\zeta_1$	$\zeta_2$	$\zeta_3$	1	1	1	$\zeta_5$	$(C_{D_{exp}} + C_{D_{convex}}) \cdot \textcircled{1} \cdot \zeta_1 + \zeta_2 \cdot \zeta_3 \cdot \zeta_4 \cdot \textcircled{2} = \zeta_5$
$\zeta_1$	1	1	$\zeta_2$	1	1	$\zeta_6$	$(C_{D_{exp}} + C_{D_{convex}}) \cdot \textcircled{1} \cdot \zeta_1 + \zeta_2 \cdot \zeta_3 \cdot \zeta_4 \cdot \textcircled{2} = \zeta_6$
$\zeta_1$	1	1	1	1	1	$\zeta_7$	$(C_{D_{exp}} + C_{D_{convex}}) \cdot \textcircled{1} \cdot \zeta_1 + \zeta_2 \cdot \zeta_3 = \zeta_7$ $\textcircled{3} = 1.275 \left( \frac{C_{D_{exp}}}{G} \lambda_c \frac{E_{TSEP}}{D} \right) \left( 1 - \frac{0.6 \delta_{TE} + 1.7 \tau}{1} \right) = C_{D_{exp}}$

TABLE (2.5-6), SEE TABLE (2.5-5)  
TOTAL PRESSURE DRAG COEFFICIENT, EVALUATION OF TWO-DIMENSIONAL CORRECTIVE (WINGS OR FINS)

VISCOUS FORM DRAG CORRECTIVE FACTOR (TURBULENT S L)

$$\zeta_1 = \left[ 1 - \frac{2\delta_{TE} + 1.7\tau}{1} \right] \cdot \frac{C_{D_{exp}}}{C_{D_{exp}}} \cdot \frac{1}{1} \cdot \frac{1}{1} \cdot \frac{1}{1} \cdot \frac{1}{1}$$

MACH NO	REYNOLDS NUMBER	ALTIMITUDE H	$\delta_{TE}$	$\tau$	$\zeta_1$	$\zeta_2$	$\zeta_3$	$\zeta_4$	$\zeta_5$
(3)	(4)	(5)	(6)	(7)	(8)	(9)	(10)	(11)	(12)
T	T	T				FIG (2.5-24)	(13)	(14)	(15)
0.3-0.7	0.3-5	0.3-5							
1.2									
1.5									
2.0									
2.5									
3.0									
3.5									
4.0									
4.5									
5.0									

NOTE FOR LAMINAR S L, THE RESPECTIVE COLUMNS SHOULD READ: (37) (38)  $\frac{S L}{(R_{0.1})^{1/4}}$  (39)  $(R_{0.1})^{1/4}$

GENERAL NOTE: NUMBERING SYSTEM FOR PRESSURE DRAG IS INDEPENDENT OF THE NUMBERING SYSTEM USED FOR SKIN-FRICTION DRAG

(2.5-5) FACTOR FOR VARIOUS PROFILE SHAPES

$\frac{2\delta_{TE} + 1.7\tau}{1}$	$\zeta_1$	DOUBLE SYMMETRY BICONVEX AIRFOIL	NOTE FOR $\zeta_2$ AND $\zeta_3$ CORRECTIVE FACTORS A SPECIAL TABLE SHOULD BE ARRANGED FOLLOWING DATA IN T (2.5-5)
$\zeta_1 = 4/3$	$\textcircled{40}$		
$\zeta_1 = 1 - \textcircled{41}$	$\textcircled{42}$	MAXIMUM THICKNESS SPANNWISE SHIFT (BICONVEX OR DOUBLE WEDGE)	$\textcircled{43}$
$\zeta_1 = \frac{1}{4\tau(1-\tau)}$	$\textcircled{44}$		$\textcircled{45}$
$\zeta_1 = \frac{q_1 + q_2}{4 q_1 q_2}$	$\textcircled{46}$	MODIFIED DOUBLE WEDGE SYMMETRIC AIRFOIL	$\zeta_4$
	$\textcircled{47}$		$\textcircled{48}$
	$\textcircled{49}$		$\textcircled{50}$
	$\textcircled{51}$		$\textcircled{52}$
	$\textcircled{53}$		$\textcircled{54}$
	$\textcircled{55}$		
		CORRECTIVE FACTOR FOR REFERENCE AREA $S_c$	$\zeta_7$
	$\textcircled{56}$		$\textcircled{57}$
	$\textcircled{58}$		$\textcircled{59}$
	$\textcircled{60}$		$\textcircled{61}$
	$\textcircled{62}$		$\textcircled{63}$
	$\textcircled{64}$		$\textcircled{65}$
	$\textcircled{66}$		$\textcircled{67}$
	$\textcircled{68}$		$\textcircled{69}$
	$\textcircled{70}$		$\textcircled{71}$
	$\textcircled{72}$		$\textcircled{73}$
	$\textcircled{74}$		$\textcircled{75}$
	$\textcircled{76}$		$\textcircled{77}$
	$\textcircled{78}$		$\textcircled{79}$
	$\textcircled{80}$		$\textcircled{81}$
	$\textcircled{82}$		$\textcircled{83}$
	$\textcircled{84}$		$\textcircled{85}$
	$\textcircled{86}$		$\textcircled{87}$
	$\textcircled{88}$		$\textcircled{89}$
	$\textcircled{90}$		$\textcircled{91}$
	$\textcircled{92}$		$\textcircled{93}$
	$\textcircled{94}$		$\textcircled{95}$
	$\textcircled{96}$		$\textcircled{97}$
	$\textcircled{98}$		$\textcircled{99}$
	$\textcircled{100}$		$\textcircled{101}$



TABLE (2.5-8)  
SEE T (2.5-5) AND T (2.5-6)

ALTERNATIVE METHOD OF COMPUTING FACTOR  
 $(A) \times (B) = (70)$  FROM DIRECT READINGS OF  
 FIGS (2.5-27) (TAPER = 1) (FOR REST OF  
 CORRECTIONS FOLLOW T(2.5-7) ON)

MACH NO M	ALTITUDE H ft.	$(M_{\infty}^2 - 1)^{1/2}$	$AR(M_{\infty}^2 - 1)^{1/2}$	$\frac{(M_{\infty}^2 - 1)^{1/2}}{(t/c)^2}$	$C_{DOPW}$ (77)	(A) x (B)
(13)	(14)	(64)	(76)	(77)	(78)	(70)
T (2.3-5)	T (2.3-5)	FIG (2.5-25)	AR x (64)	(64)/(t/c) <sup>2</sup>	FIG (2.5-27)	(78)/(77)
1						
1.2						
1.5						
2.0						
2.5						
3.0						
3.5						
4.0						
4.5						
5.0	ETC.					

$(t/c)^2 =$

AR =

TABLE (2-5-9)

TOTAL PRESSURE DRAG COEFFICIENT.

CASE I  $\mu > \tan \Lambda_0 > \tan \Lambda_1$ ,  $n > 1$ ,  $0 < \epsilon < 1$ , CASE II

MACH NUMBER M	ALTITUDE H, ft	$M^2 \cdot 10^{-2} \cdot \mu$	$M^2 \cdot 10^{-2} \cdot \epsilon$	$n \cdot \tan \Lambda_0$	$\epsilon n$	TOTAL PRESSURE DRAG COEFFICIENT		
						CASE I $C_{Dp}^{(I)}$	CASE II $C_{Dp}^{(II)}$	CASE III $C_{Dp}^{(III)}$
1.0	1.0	1.0	1.0	1.0	1.0	1.0	1.0	1.0
1.2	1.2	1.44	1.44	1.44	1.44	1.44	1.44	1.44
1.5	1.5	2.25	2.25	2.25	2.25	2.25	2.25	2.25
2.0	2.0	4.0	4.0	4.0	4.0	4.0	4.0	4.0
2.5	2.5	6.25	6.25	6.25	6.25	6.25	6.25	6.25
3.0	3.0	9.0	9.0	9.0	9.0	9.0	9.0	9.0
3.5	3.5	12.25	12.25	12.25	12.25	12.25	12.25	12.25
4.0	4.0	16.0	16.0	16.0	16.0	16.0	16.0	16.0
4.5	4.5	20.25	20.25	20.25	20.25	20.25	20.25	20.25
5.0	5.0	25.0	25.0	25.0	25.0	25.0	25.0	25.0
ETC	ETC	ETC	ETC	ETC	ETC	ETC	ETC	ETC

$\mu = (M^2 - 1)^{-1/2} \cdot \cos \mu$

(SEE T (2-5-5) AND T (2-5-6))

(C<sub>Dp</sub>WEXP + C<sub>Dp</sub>WVIS), DELTA WING PLANFORMS.

CASE I  $\tan \Lambda_1 > \mu > \tan \Lambda_0$ ,  $n > 1$ ,  $\epsilon n < 1$ , CASE II  $\tan \Lambda_0 > \tan \Lambda_1$ ,  $n > 1$ ,  $\epsilon n > 1$

MACH NUMBER M	ALTITUDE H, ft	$M^2 \cdot 10^{-2} \cdot \mu$	$M^2 \cdot 10^{-2} \cdot \epsilon$	$n \cdot \tan \Lambda_0$	$\epsilon n$	CORRECTION FOR BICONVEX AIRFOILS, IF ANY, $\zeta_p = 4/3$		
						CASE I $C_{Dp}^{(I)}$	CASE II $C_{Dp}^{(II)}$	CASE III $C_{Dp}^{(III)}$
1.0	1.0	1.0	1.0	1.0	1.0	1.0	1.0	
1.2	1.2	1.44	1.44	1.44	1.44	1.44	1.44	
1.5	1.5	2.25	2.25	2.25	2.25	2.25	2.25	
2.0	2.0	4.0	4.0	4.0	4.0	4.0	4.0	
2.5	2.5	6.25	6.25	6.25	6.25	6.25	6.25	
3.0	3.0	9.0	9.0	9.0	9.0	9.0	9.0	
3.5	3.5	12.25	12.25	12.25	12.25	12.25	12.25	
4.0	4.0	16.0	16.0	16.0	16.0	16.0	16.0	
4.5	4.5	20.25	20.25	20.25	20.25	20.25	20.25	
5.0	5.0	25.0	25.0	25.0	25.0	25.0	25.0	
ETC	ETC	ETC	ETC	ETC	ETC	ETC	ETC	

$\mu = \frac{1}{\sqrt{M^2 - 1}}$        $\epsilon = \frac{1}{M^2 - 1}$   
 $(1/\sqrt{C_{Dp}WEXP})^2$        $(1/\sqrt{C_{Dp}WEXP})^2$   
 $\tan \Lambda_0$        $\tan \Lambda_1$

TABLE (2-5-10)

TOTAL PRESSURE DRAG COEFFICIENT, (C<sub>Dp</sub>WVIS + C<sub>Dp</sub>WEXP).

(LINEARIZED THEORY FOR DOUBLE WEDGE OR BICONVEX)

MACH NUMBER M	ALTITUDE H, ft	$2C_1(1/C)^2$	C <sub>Dp</sub> WEXP	C <sub>Dp</sub> WVIS	$\zeta_p$	$\zeta_p$	$\zeta_p \cdot \zeta_p$
1.0	1.0	1.0	1.0	1.0	1.0	1.0	1.0
1.2	1.2	1.44	1.44	1.44	1.44	1.44	1.44
1.5	1.5	2.25	2.25	2.25	2.25	2.25	2.25
2.0	2.0	4.0	4.0	4.0	4.0	4.0	4.0
2.5	2.5	6.25	6.25	6.25	6.25	6.25	6.25
3.0	3.0	9.0	9.0	9.0	9.0	9.0	9.0
3.5	3.5	12.25	12.25	12.25	12.25	12.25	12.25
4.0	4.0	16.0	16.0	16.0	16.0	16.0	16.0
4.5	4.5	20.25	20.25	20.25	20.25	20.25	20.25
5.0	5.0	25.0	25.0	25.0	25.0	25.0	25.0
ETC	ETC	ETC	ETC	ETC	ETC	ETC	ETC

$(1/\sqrt{C_{Dp}WEXP})^2$

STRAIGHT TAPERED WING PLANFORMS

DOUBLE SYMMETRY AIRFOILS

MACH NUMBER M	ALTITUDE H, ft	C <sub>Dp</sub> WEXP + C <sub>Dp</sub> WVIS	DOUBLE WEDGE OR BICONVEX AIRFOIL, SHOT OF MAXIMUM THICKNESS LINE		MODIFIED DOUBLE WEDGE AIRFOIL	
			$\zeta_p$	C <sub>Dp</sub> WEXP + C <sub>Dp</sub> WVIS	$\zeta_p$	C <sub>Dp</sub> WEXP + C <sub>Dp</sub> WVIS
1.0	1.0	1.0	1.0	1.0	1.0	1.0
1.2	1.2	1.44	1.44	1.44	1.44	1.44
1.5	1.5	2.25	2.25	2.25	2.25	2.25
2.0	2.0	4.0	4.0	4.0	4.0	4.0
2.5	2.5	6.25	6.25	6.25	6.25	6.25
3.0	3.0	9.0	9.0	9.0	9.0	9.0
3.5	3.5	12.25	12.25	12.25	12.25	12.25
4.0	4.0	16.0	16.0	16.0	16.0	16.0
4.5	4.5	20.25	20.25	20.25	20.25	20.25
5.0	5.0	25.0	25.0	25.0	25.0	25.0
ETC	ETC	ETC	ETC	ETC	ETC	ETC

$(1/\sqrt{C_{Dp}WEXP})^2$



TABLE (2.5-12)  
 PRESSURE DRAG COEFFICIENT DUE TO LEADING-EDGE BLUNTNES,  $C_{DOPWLE}$  OR  $C_{DOPFLE}$   
 (SEMICIRCULAR LEADING EDGE)

MACH NO M	ALTITUDE H ft	NEWTONIAN IMPACT THEORY (INDEPENDENT OF M)	SEMI-EMPIRICAL METHOD, $\lambda_{LE} = R_{BL}$	
		$C_{DOPWLE}$ or $C_{DOPFLE}$	$C_{DLE}$	$C_{DOPWLE}$ or $C_{DOPFLE}$
(13)	(14)	(97)	(98)	(97)
T (2.3-5)	T (2.3-5)	$\frac{3}{4} \left( \frac{R_{BL}}{D} \right) \left( \frac{b_{WEXP}}{D} \right) \cos^2 \Lambda_{LEW}$ or $\frac{3}{4} \left( \frac{R_{BL}}{D} \right) (N) \left( \frac{\eta_{FEXP}}{D} \right) \cos^2 \Lambda_{LEF}$	FIG (2.5-37)	$2.55 \left( \frac{R_{BL}}{D} \right) \left( \frac{b_{WEXP}}{D} \right) \cos^2 \Lambda_{LEW} \times (98)$ or $2.55N \left( \frac{R_{BL}}{D} \right) \left( \frac{\eta_{FEXP}}{D} \right) \cos^2 \Lambda_{LEF} \times (98)$
1.0				
1.2				
1.5				
2.0				
2.5				
3.0				
3.5				
4.0				
4.5				
5.0	ETC.			

NOTE:  $R_{BL} = .001$  ft                       $b_{WEXP} =$                        $\eta_{FEXP} =$

$\lambda_{LE} = R_{BL}$                                    $\Lambda_{LE} =$                                    $\cos^2 \Lambda_{LE} =$

$R_{BL}/D =$                                        $N =$

TABLE  
SUMMARY OF WING (OR FIN) TOTAL PRESSURE DRAG  
( $C_{DpWEXP} + C_{DpWVIS} + C_{DpWLE}$ )

MACH NO	ALTITUDE H FT	STRAIGHT RECTANGULAR WING PLANFORM, $C_{DpWEXP} + C_{DpWVIS}$				
		DOUBLE WEDGE SYMMETRY AIRFOIL	DOUBLE SYMMETRY BICONVEX AIRFOIL	MINIMUM THICKNESS SHIFT FOR X/C, DOUBLE WEDGE	MINIMUM THICKNESS SHIFT FOR X/C, BICONVEX	MODIFIED DOUBLE WEDGE
10		(71)	(72)	(73)	(74)	(75)
12		T(2.5-7)	T(2.5-7)	T(2.5-7)	T(2.5-7)	T(2.5-7)
15		(1)	(2)	(3)	(4)	(5)
20						
25						
30						
35						
40						
45						
50	ETC.					

(2.5-13)  
RESULTS AS COMPUTED IN TABLES (2.5-7) TO (2.5-12)  
OF ( $C_{DpWEXP} + C_{DpWVIS} + C_{DpWLE}$ )

DELTA WING PLANFORMS, $C_{DpWEXP} + C_{DpWVIS}$						STRAIGHT TAPERED WING PLANFORMS, $C_{DpWEXP} + C_{DpWVIS}$		
DOUBLE WEDGE AIRFOILS			BICONVEX AIRFOILS			DOUBLE WEDGE OR BICONVEX, DOUBLE SYMMETRY AIRFOILS	DOUBLE WEDGE OR BICONVEX, AIRFOILS SHIFT OF MAX THICKNESS, X/C	MODIFIED DOUBLE WEDGE AIRFOILS
CASE I	CASE II	CASE III	CASE I	CASE II	CASE III	(87)	(88)	(89)
(81)	(82)	(83)	(84)	(84)	(84)	(87)	(88)	(89)
T(2.5-9)	T(2.5-9)	T(2.5-9)	T(2.5-9)	T(2.5-9)	T(2.5-9)	T(2.5-10)	T(2.5-10)	T(2.5-10)
(91)	(92)	(93)	(94)	(94)	(94)	(97)	(98)	(99)

TABLE (2.5-13) CONTINUED

STRAIGHT, SWEEP-BACK NO TAPER WING PLANFORMS, $C_{DpWEXP} + C_{DpWVIS}$			LEADING EDGE BLUNTNESS $C_{DpWLE}$		TOTAL PRESSURE $C_{DpWLE} +$			
DOUBLE WEDGE OR BICONVEX, DOUBLE SYMMETRY AIRFOILS	DOUBLE WEDGE OR BICONVEX, AIRFOILS SHIFT OF MAX THICKNESS, X/C	MODIFIED DOUBLE WEDGE AIRFOILS	NEWTONIAN IMPACT THEORY	SEMI-EMPIRICAL METHOD	STRAIGHT RECTANGULAR WING PLANFORMS			
(90)	(90)	(90)	(97)	(97)	(98)	(98)	(98)	(98)
T(2.5-11)	T(2.5-11)	T(2.5-11)	T(2.5-12)	T(2.5-12)	(1 = 97)	(2 = 97)	(3 = 97)	(4 = 97)
(10)	(10)	(10)						

DRAG COEFFICIENT, WINGS OR FINS  
 $C_{DpWEXP} + C_{DpWVIS}$

	DELTA WING PLANFORMS			STRAIGHT TAPERED WING PLANFORMS			STRAIGHT, SWEEP BACK, NO TAPER		
	(90)	(90)	(90)	(98)	(98)	(98)	(98)	(98)	(98)
(2 = 97)	(3 = 97)	(4 = 97)	(5 = 97)	(6 = 97)	(7 = 97)	(8 = 97)	(9 = 97)	(10 = 97)	(11 = 97)

TABLE  
TOTAL PRESSURE DRAG COEFFICIENT ON BODIES OF REVOLUTION,  
( $C_{DopC} + \Delta C_{Dopo} + \Delta C_{DopTip}$ )  
WORKING CHARTS SET "A" FIGS (2.5-11), (2.5-12), (2.5-13), (2.5-17)

MACH NO M	ALTITUDE H ft	$R_{BL} = 4(R_{BL}/D)^2 + R$ FOREBODY (NOSE SECTION)					OF MINIMUM $M^2$
		CONE $C_{DopC}$	OGIVE				
		$K = M^2 A N/D$	$M^2 \Delta C_{Dopo}$	$\Delta C_{Dopo}$	$C_{DopC} + \Delta C_{Dopo}$		
(1)	(4)	(37)	(38)	(39)	(40)	(41)	(42)
T (2.5-5)	T (2.5-5)	FIG (2.5-11)	FIG (2.5-13)	(39)/(13)	(37) + (40)	(13)	(13)
1.0							
1.2							
1.5							
2.0							
2.5							
3.0							
3.5							
4.0							
4.5							
5.0	ETC.						

NOTE - First check from Fig (2.5-12) that no bow shock detachment occurs  
Nose-tip bluntness effect should be estimated only if  $R_{BL}/(D/2) > .15$   
using  $(L_N/R_{BL})^{.1}$  curve from Fig (2.5-15)  
No boattail term for cylindrical afterbodies

(2.5-14)  
CIRCULAR CROSS-SECTION - ESTIMATES USING FIGURE SET "A"  
 $+ (C_{DopBT} + \Delta C_{DopBTFORE})$

$L_N = (L_N/D) \cdot D$ ,  $\theta_N = (D/L_N)$

PRESSURE NOSE SHAPES	CONES $M=1$	OGIVES $M=1$	NOSE TIP BLUNTNESSES	
			$C_{DOBL}$	$\Delta C_{DopTip}$ $4(R_{BL}/D)^2 C_{DopBL}$
7M <sup>2</sup>	7M <sup>2</sup> C <sub>DopFORE</sub>	C <sub>DopFORE</sub>	C <sub>DopFORE</sub>	C <sub>DopFORE</sub>
(43)	(44)	(45)	(46)	(47)
7.8 (43)	FIG (2.5-14)	(44)/(45)	FIG (2.5-4)	FIG (2.5-5)
			FIG (2.5-15)	(43) + (44)

Consult T (2.5-5) for basic data  
 $L_N, (L_N/D), \theta_N, D/L_N, D,$   
 $L_{BT}, D_B, (D_B/L_{BT}), D_B/L_B, \theta_B = (\theta_N/2)$

TABLE (2.5-14) CONTINUED

FIGURES

TOTAL FOREBODY	BOATTAIL (IF ANY) $L_{BT} = D_B = (D_B/L_{BT}) \cdot D$				
	$M^2 = 1$	$(M^2 - 1)^{1/2}$	$\frac{(M^2 - 1)^{1/2}}{2(L_{BT}/D)}$	$\Delta C_{DopBT}(L_{BT}/D)^2$	$C_{DopBT}$
$C_{DopFORETOTAL}$	(48) + (49) + (50)	(51) + (52)	(53)	(54)	(55)
(43) + (44) + (45) + (46) + (47) for $M=1$			(53)/(5)	FIG (2.5-16)	(55)/(7)

Evaluate forebody-interference term  $\Delta C_{DopBTFORE}$  only if  $(L_{BT}/L_{BT}) > 0.1$  or  $(L_{BT}/L_{BT}) > 0.1$  or  $(L_{BT}/L_{BT}) > 0.1$   
If the case, consult Figure (2.5-17) for  $\Delta C_{DopBTFORE}$  where  $L_{BT}$  should be replaced by  $L_{BT}$  or (2.5-21)

COMMON TO BOTH SETS "A" AND "B" FIGS (2.5-4), (2.5-5), (2.5-13), (2.5-15), (2.5-20), (2.5-21)

$(D_B/L_{BT})^2$ ;  $\theta_B = \frac{\theta_N}{2} = \frac{D}{2(L_{BT}/D)}$ ;  $\Delta C_{DopBTFORE} = \frac{1}{2} \cdot \frac{4(L_{BT}/D)^2 \cdot T}{(L_{BT}/D)^2}$ ;  $2(L_{BT}/D) \cdot S$

PARABOLIC	FOREBODY INTERFERENCE	BOATTAIL TOTAL	TOTAL BODY PRESSURE DRAG
$\Delta C_{DopBT}(L_{BT}/D)^2$	$C_{DopBT}$	$\Delta C_{DopBTFORE} + C_{DopBT}$	$C_{DopBODYTOTAL}$
(56)	(57)	(58)	(59) + (60) + (61)
FIG (2.5-17)	(56)/(7)	FIG (2.5-20) or (2.5-21)	(59)/(7) + (60) + (61)

$\Delta C_{DopBT}(L_{BT}/D)^2 = (56)$ ,  $(L_{BT}/L_{BT}) = (57)$ , and  $[(M^2 - 1)^{1/2} / 2(L_{BT}/D)] = (53)$

TABLE (2.5-15)  
TOTAL PRESSURE DRAG COEFFICIENT ON BODIES REVOLUTION, CIRCULAR  
( $C_{D_{Dop}} + \Delta C_{D_{Dop}} + \Delta C_{D_{DopTIP}}$ )

WORKING CHARTS: SET 'A' FIGS. (2.5-1), (2.5-2), (2.5-10)

MACH NUMBER	ALTITUDE H, FT.	FOREBODY (NOSE SECTION), $L_N$ , $(L_N/D)^2$ , $\theta_N$ , $R_{BL}$					OSBIVE
		$C_{D_{Dop}}$	$K^2 (M^2/L_N/D)$	$M^2$	$M^2 C_{D_{Dop}}$	$C_{D_{Dop}}$	
0							
10							
15							
20							
25							
30							
35							
40							
45							
50	ETC						

NOTE: - FIRST CHECK FROM FIG. (2.5-10) THAT NO BOW-SHOCK DETACHMENT OCCURS - NOSE-TIP BLUNTNESSE EFFECTS SHOULD BE ESTIMATED ONLY IF  $(R_{BL}/D) > 1$  USING  $(L_T/R_{BL}) = 1$  CURVE FROM FIG. (2.5-15).  
- NO BOATTAIL TERM FOR CYLINDRICAL AFTERBODIES.

CROSS-SECTION - ESTIMATES USING FIGURE SET 'B'  
( $C_{D_{DopBT}} + \Delta C_{D_{DopBT(FORE)}}$ )

$4(R_{BL}/D)^2 \theta_N$

$\Delta C_{D_{Dop}}$	$C_{D_{Dop}} + \Delta C_{D_{Dop}}$	MINIMUM PRESSURE SHAPES		NOSE $C_{D_{Dop(FORE)}}$	CONES M=1 $C_{D_{Dop(FORE)}}$	OGIVES M=1 $C_{D_{Dop(FORE)}}$
		0.7 M <sup>2</sup>	0.7 M <sup>2</sup> C <sub>Dop</sub> FORM			
(10)	(10)	(10)	(10)	(10)	(10)	(10)
(10)/(10)	(10)/(10)	0.7(10)	FIG (2.5-14)	(10)/(10)	FIG (2.5-4)	FIG (2.5-5)

CONSULT (2.5-5) FOR BASIC DATA:  
 $L_N, (L_N/D), \theta_N, (D/L_N), D,$   
 $L_{BT}, D_B, (D_B/L_{BT}), (D_B/L_B),$   
 $C_B, (C_B/2)$

$> 0.15,$

TABLE (2.5-15) CONTINUED

NOSE TIP BLUNTNESSE $C_{D_{DopTIP}} = 4(R_{BL}/D) \theta_N$	TOTAL FOREBODY $C_{D_{Dop(FORE)}}$	BOATTAIL (IF ANY), $L_{BT}$	
		CONICAL ( $C_B \cdot C_B/2$ ) OR PARABOLIC ( $C_B$ )	$C_{D_{DopBT}}$
(10)	(10)	(10) + (10) + (10) OR (10) + (10) OR (10) + (10)	(10)
(10)	(10)	FIG (2.5-19) OR T (2.5-3)	

EVALUATE FOREBODY-AFTERBODY ( $L_{CYL}/L_{BT}) < 1.50$  AND IF THE CASE, CALCULATE  $4(L_{BT}/D)^2 \theta_N$ ,  $(L_{CYL}/D)$  AND  $(M^2-1)^2/2(L_{BT}/D)$  FROM FIGS. (2.5-20) OR

FIGURES COMMON TO BOTH SETS 'A' AND 'B': FIGS. (2.5-4), (2.5-5), (2.5-13), (2.5-14), (2.5-15), (2.5-20), (2.5-21)

$D_B, (D_B/L_{BT}), (D_B/L_B), C_B, C_B/2$

FOREBODY INTERFERENCE $\Delta C_{D_{DopBT(FORE)}}$	BOATTAIL TOTAL $C_{D_{DopBT}} + \Delta C_{D_{DopBT(FORE)}}$	TOTAL BODY $C_{D_{Dop(TOTAL)}}$
(10)	(10)	(10) + (10)
FIG (2.5-20) OR (2.5-21)	(10)/(10)	(10) + (10)

INTERFERENCE TERM,  $C_{D_{DopBT(FORE)}}$ , ONLY IF  $(L/L_{BT}) < 3.50$ ,  $L = L_N + L_{CYL} + L_{BT}$ .  
CORRECTIVE TERM  $[(1 - (D_B/D)(1 - L_{BT}/L_{BT}))^2]$  (2).  
= (10), WHERE  $L_{BT}$  SHOULD BE EVALUATED (2.5-21).

TABLE (2.5-16)

TOTAL PRESSURE DRAG FORCE OF A MISSILE CONFIGURATION

$$\begin{aligned}
 & [ ( C_{DopC} + \Delta C_{DopO} + \Delta C_{DopNTIP} ) + ( C_{DopBT} + \Delta C_{DopBT(FORE)} ) ] + \\
 & + [ ( C_{DopWEXP} + C_{DopWVIS} + C_{DopWLE} ) + ( C_{DopFEXP} + C_{DopFVIS} + C_{DopFLE} ) ] = (B_p) + (M_p) + (F_p)
 \end{aligned}$$

MACH NUMBER	ALTITUDE H, FT.	TOTAL BODY DRAG		TOTAL WING	TOTAL FIN	TOTAL MISSILE	
		METHOD 'A'	METHOD 'B'			(A)	(B)
(13)	(14)	(61)	(65)	(99W)	(99F)	(100)	(100)
T (2.3-5)	T (2.3-5)	T (2.5-14)	T (2.5-15)	T (2.5-13)	T (2.5-13)	(61) + (99W) + (99F)	(61) + (99W) + (99F)
1.0							
1.2							
1.5							
2.0							
2.5							
3.0							
3.5							
4.0							
4.5							
5.0	ETC.						

## 2.5.6 REFERENCES

- 2.5-1 Royal Aeronautical Society Data Sheets, Aerodynamics, Vol. 1, Eleventh Issue, October, 1960.
- 2.5-2 Hoerner, S. F. "Fluid Dynamics Drag", Author's Publication.
- 2.5-3 Hilton, W. F. High Speed Aerodynamics. Longman's, Green and Company, New York, 1951.
- 2.5-4 Fraenkel, L. E. "Calculations of the Pressure Distribution and Boundary Layer Development on a Body of Revolution With Various Parabolic Afterbodies at Supersonic Speeds" R.A.C. Report Aero. 2482, (1953).
- 2.5-5 Young, A. D. "The Calculation of the Profile Drag of Aerofoils and Bodies of Revolution at Supersonic Speeds" College of Aeronautics, Cranfield, Report No. 73 (1953).
- 2.5-6 Young, A. D. and Kirkby, S. "The Profile Drag of Biconvex and Double Wedge Sections at Supersonic Speeds" Proceedings of the N.P.L. Symposium on Boundary Layer Effects in Aerodynamics. H.M.S.O. 1955.
- 2.5-7 von Karman, T. and Moore, N. B. "Resistance of Slender Bodies Moving with Supersonic Velocities, with Special Reference to Projectiles" Transactions of the American Society of Mechanical Engineers, Vol. 54, No. 23, (1942).
- 2.5-8 Brown, C. E. and Parker, H. M. "A Method for the Calculation of External Lift, Moment and Pressure Drag of Slender Open-Nose Bodies of Revolution at Supersonic Speeds" N.A.C.A. Report 808 (1945).
- 2.5-9 Lighthill, M. J. "Supersonic Flow Past Slender Bodies of Revolution the Slope of Whose Meridian Section is Discontinuous" Quarterly Journal of Mechanics and Applied Mathematics, Vol. I, Part 2 (1948).
- 2.5-10 Ward, G. N. "The Approximate External and Internal Flow Past a Quasi-Cylindrical Tube Moving at Supersonic Speeds" Quarterly Journal of Mechanics and Applied Mathematics, Vol. I, Part 1, (1948).
- 2.5-11 van Dyke, M. D. "A Study of Second-Order Supersonic Flow Theory" N.A.C.A. T.N. 2200 (1951).
- 2.5-12 van Dyke, M. D. "Practical Calculations of Second-Order Supersonic Flow Past Non-Lifting Bodies in Revolution" N.A.C.A. T.N. 2744 (1952).
- 2.5-13 Isenbert, J. S. "The Method of Characteristics in Compressible Flow, Part I" H. Q. Air Material Command, Wright Field, Technical Report F-Tr-1173A-ND (1947).
- 2.5-14 Truitt, R. W. Hypersonic Aerodynamics. New York: The Ronald Press Company, 1959.
- 2.5-15 Taylor, G. I. and Maccoll, J. W. "The Air Pressure on a Cone Moving at High Speeds" Proc. Roy. Soc. A, Vol. 139 (1953).
- 2.5-16 Massachusetts Institute of Technology, Department of Electrical Engineering: "Tables of Supersonic Flow Around Cones" by the Staff of the Computing Section, Center of Analysis, Under Direction of Zdenek Kopal, M.I.T. Tech. Report 1, Cambridge, 1947.

- 2.5-17 Tsien, H. S. "Similarity Laws of Hypersonic Flows" *Journal of Mathematics and Physics*, Vol. 25, No. 3, (1946).
- 2.5-18 Nielson, Y. N. "Missile Aerodynamics" McGraw-Hill Series in Missile and Space Technology, McGraw-Hill Book Company, Inc., New York, 1960.
- 2.5-19 Spreiter, J. R. and Alksne, A. Y. "Slender-Body Theory Based on Approximate Solution of the Transonic Flow Equation" N.A.S.A. Tech. Report R-2, (1959).
- 2.5-20 Ehret, D. M. "Accuracy of Approximate Methods for Predicting Pressures on Pointed Non-Lifting Bodies of Revolution in Supersonic Flow" N.A.C.A. T.N. 276A (1952).
- 2.5-21 Oswatitsch, K. and Keune, F. "The Flow Around Bodies of Revolution at Mach Number 1" Proc. Conf. on High-Speed Aerodynamics Polytechnic Institute of Brooklyn, Brooklyn, N. Y. pp. 113-131, (1955).
- 2.5-22 Drouge, G. "Some Measurements on Bodies of Revolution at Transonic Speeds." Ninth International Congress of Applied Mechanics, Univ. of Brussels, p. 70-77, (1957).
- 2.5-23 Taylor, R. A. and McDevitt, J. B. "Pressure Distributions at Transonic Speeds for Parabolic-Arc Bodies of Revolution Having Finess Ratios of 10, 12, and 14" N.A.C.A. T.N. 4234, (1958).
- 2.5-24 Miles, J. W. "On the Sonic Drag of a Slender Body" *J. Aero. Sci.*, Vol. 23, No. 2, pp. 146-154, (1956).
- 2.5-25 Eggers, A. J. Jr. and Savin R. C. "Approximate Methods for Calculating the Flow About Non-Lifting Bodies of Revolution at High Supersonic Airspeeds" NACA TN 2579 (1951).
- 2.5-26 Gunderley, G. and Yoshihara, H. "An Axial-Symmetric Transonic Flow Pattern" *Quart. Appl. Math.*, Vol. 4, No. 4, pp. 333-339, (1951).
- 2.5-27 Gunderley, G. and Yoshihara, H. "Axial-Symmetric Transonic Flow Patterns" A. F. Tech. Rep. 5797, U.S.A.F. A.M.C., Dayton, Ohio, (1949).
- 2.5-28 Page, W. A. "Experimental Study of the Equivalence of Transonic Flow About Slender Cone-Cylinders of Circular and Elliptic Cross Section" N.A.C.A. T.N. 4233, (1958).
- 2.5-29 Chapman, D. R. "An Analysis of Base Pressure at Supersonic Velocities and Comparison With Experiment" N.A.C.A. Tech. Report 1051, (1951).
- 2.5-30 Ehret, D. M., Rossow, V. J. and Stevens, V. I. "An Analysis of the Applicability of the Hypersonic Similarity Law to the Study of Flow About Bodies of Revolution at Zero Angle of Attack" N.A.C.A. TN. 2250 (1950).
- 2.5-31 Rossow, V. J. "Applicability of the Hypersonic Similarity Rule to Pressure Distributions which Include the Effects of Rotation for Bodies of Revolution at Zero Angle of Attack" N.A.C.A. T.N. 2399 (1951).
- 2.5-32 van Dyke, M. D. "The Combined Supersonic-Hypersonic Similarity Rule" *Journal of the Aeronautical Sciences*, Vol. 18, No. 7, (1951).

- 2.5-33 Fraenkel, L. E. "Curves for Estimating the Wave Drag of Some Bodies of Revolution, Based on Exact and Approximate Theories" A.R.C. Current Paper 136 (1952).
- 2.5-34 von Karman, T. "The Problem of Resistance in Compressible Fluids" Atti V Convegno Fondazione Alessandro Volta, Rome, (1935).
- 2.5-35 Haack, W. "Geschossenformen Kleinsten Wellenwiderstandes" Ber. Lilienthal Ges. Luftfahrt, Vol. 139.
- 2.5-36 Sears, W. R. "On Projectiles of Minimum Wave Drag" Quart. Appl. Math., Vol. 14, No. 4, (1947).
- 2.5-37 Eggers, A. J., Jr., Resnikoff, M. M. and Dennis, D. H. "Bodies of Revolution for Minimum Drag at High Supersonic Airspeeds" N.A.C.A. Tech. Report 1306, (1958).
- 2.5-38 Ferrari, C. "The Body and Ogival Contour Giving Minimum Wave Drag" Atti Dell Accademia Delle Scienze Di Torino, Vol. 84, No. 1, pp. 3-18, (1949-50) (Translated by R. H. Cramer, Cornell Aero. Lab., Inc., Buffalo, N.Y., Presented at Session of Reale Accademia Delle Scienze Di Torino, Nov. 23, 1949)
- 2.5-39 Kueth, A. M. and Schetzer, J. D. "Foundations of Aerodynamics" Second Edition. John Wiley and Sons, Inc., New York, 1959.
- 2.5-40 Sears, W. R. (Editor). "General Theory of High Speed Aerodynamics" Vol. VI, High Speed Aerodynamics and Jet Propulsion, Princeton University Press, Princeton, New Jersey, 1954.
- 2.5-41 Bishop, R. A. and Cane, E. G. "Charts of the Theoretical Wave Drag of Wings at Zero Lift" R.A.E. Tech. Note Aero 2421, (1956).
- 2.5-42 Grant, F. C. and Morton, C. "Tables for the Computation of Wave Drag of Arrow Wings of Arbitrary Airfoil Section" N.A.C.A. T.N. 3185 (1954).
- 2.5-43 Puckett, A. E. "Supersonic Wave Drag of Thin Airfoils" J. Aero. Sci., Vol. 13, No. 9, pp. 475-484, (1946).
- 2.5-44 Laurence, T. "Charts of the Wave Drag of Wings at Zero Lift" R.A.E. Tech. Note Aero. 2139, Revised, (1952).
- 2.5-45 Nielsen, J. N. "Effects of Aspect Ratio and Taper on the Pressure Drag at Supersonic Speeds of Upswept Wings at Zero Lift" N.A.C.A. T.N. 1487 (1947).
- 2.5-46 Puckett, A. E. and Stewart, H. T. "Aerodynamic Performance of Delta Wings at Supersonic Speeds" J. Aero. Sci. Vol. 14, No. 10, pp. 567-578, (1947).
- 2.5-47 Katzen, E. and Kaattari, G. E. "Drag Interference Between a Pointed Cylindrical Body and Triangular Wings of Various Aspect Ratios at Mach Numbers of 1.50 and 2.02" N.A.C.A. T.N. 3794 (1956).
- 2.5-48 Nielsen, J. N. "Quasi-Cylindrical Theory of Wing-Body Interference at Supersonic Speeds and Comparison with Experiment" N.A.C.A. Tech Report 1252 (1955).
- 2.5-49 Nielsen, J. N. and Matteson, F. H. "Calculative Method for Estimating the Interference Pressure Field at Zero Lift on a Symmetrical Swept-Back Wing Mounted on a Circular Cylindrical Body" N.A.C.A. R.M. A9E19 (1949).

- 2.5-50 Whitcomb, R. T. "A Study of the Zero-lift Drag Rise Characteristics of Wing-Body Combinations Near the Speed of Sound" N.A.C.A. Tech. Ref. 1273 (1956).
- 2.5-51 Jones, R. T. "Theory of Wing-Body Drag at Supersonic Speeds" N.A.C.A. Tech. Report 1284 (1956).
- 2.5-52 Lomax, H. and Heaslet, M. A. "Recent Developments in the Theory of Wing-Body Wave Drag" J. Aero. Sci., Vol. 23, No. 12, pp. 1061-1074 (1956).
- 2.5-53 Lomax, H. "Nonlifting Wing-Body Combinations with Certain Geometric Restraints Having Minimum Wave Drag at Low Supersonic Speeds" N.A.C.A. Tech. Rep. 1297 (1957).
- 2.5-54 Nielsen, J. N. "General Theory of Wave-Drag Reduction for Combinations Employing Quasi-Cylindrical Bodies with an Application to Swept Wing and Body Combinations" N.A.C.A. T.N. 3722 (1956).
- 2.5-55 Ziekiewicz, H. K. "An Investigation of Boundary Layer Effects on Two-Dimensional Supersonic Airfoils" Cranfield Report 49, (1951)
- 2.5-56 Holder, D. W., Pearcy, H. H., and Gadd, G. E. "The Interaction Between Shock Waves and Boundary Layers" A.R.C. Report 16,077 (1953).
- 2.5-57 Holder, D. W. and Gadd, G. E. "The Interaction Between Shock Waves and Boundary Layers and its Relation to Base Pressure in Supersonic Flow". Proceedings of N.P.L. Symposium on Boundary Layer Effects in Aerodynamics, H. M. S. O. (1955).
- 2.5-58 van Dyke, M. D. "Second-Order Slender-Body Theory -- Axisymmetric Flow" N.A.C.A. T.N. 4281 (1958).
- 2.5-59 Perkins, E. W., Jorgensen, L. H. and Sommer, S. C. "Investigation of the Drag of Various Axially Symmetric Nose Shapes of Fineness Ratio 3 for Mach Numbers from 1.24 to 7.4" N.A.C.A. Report 1386, (1958).
- 2.5-60 Stoney, W. E., Jr. "Collection of Zero-lift Drag Data on Bodies of Revolution from Free-Flight Investigations" N.A.C.A. T.N. 4201, (1958).
- 2.5-61 Fraenkel, L. E. "The Theoretical Wave Drag of Some Bodies of Revolution" R.A.E. Report Aero. 2420 (1951).
- 2.5-62 Abbott, H. I. and Doenhoff, E. A. Theory of Wing Sections. New York: Dover Publications, Inc., 1959.
- 2.5-63 van Driest, E. R. "Turbulent Boundary Layer in Compressible Fluids" J. Aero. Sci., Vol. 18, no. 3, March, 1951, p. 145.
- 2.5-64 Jones, R. T. "Theoretical Determination of the Minimum Drag of Airfoils at Supersonic Speeds" J. Aero. Sci., Vol. 19, No. 12, pp. 813-822, (1952).
- 2.5-65 Jones, R. T. "Minimum Wave Drag for Arbitrary Arrangements of Wings and Bodies" N.A.C.A. Tech. Reports 1335, (1957).
- 2.5-66 Tsien, S. H. "The Supersonic Conical Wing of Minimum Drag" J. Aero. Sci., Vol. 22, No. 12, pp. 805-817, (1955).
- 2.5-67 Levy, L. L. Jr. "Supersonic and Moment-of Area Rules Combined for Rapid Zero-Lift Wave Drag Calculations" N.A.S.A. Memo 4-19-59A, (1959).

- 2.5-68 Levy, L. L. Jr. and Yoshikawa, K. K. "A Numerical Method for Calculating the Wave Drag of a Configuration from the Second Derivative of the Area Distribution of a Series of Equivalent Bodies of Revolution" N.A.S.A. Memo 1-16-59A, (1959).
- 2.5-69 Beane, Beverly. "The Characteristics of Supersonic Wings Having Biconvex Sections". J. Aero. Sci., Vol. 18, No. 1, (1951), pp. 7-20.
- 2.5-70 Spreiter, J. R. "Aerodynamics of Wings and Bodies at Transonic Speeds" J. Aero. Sci., Vol. 26, No. 8, pp. 465-486, (1959).
- 2.5-71 Cahn, M.S. and Oltstad, W.B. "A Numerical Method for Evaluating Wave Drag" N.A.C.A. T.N. 4258, (1958).
- 2.5-72 Holdaway, G. H. "Comparison of Theoretical and Experimental Zero-Lift Drag Rise Characteristics of Wing-Body-Tail Combinations Near the Speed of Sound" N.A.C.A. R.M. A53H17, (1953).
- 2.5-73 Bonney, E. A. "Aerodynamic Characteristics of Rectangular Wings at Supersonic Speeds" J. Aero. Sci., Vol. 14, No. 2, pp. 110-116 (1947).
- 2.5-74 Puckett, A. E. "Supersonic Wave Drag of Thin Airfoils" J. Aero. Sci., Vol. 13, No. 9, pp. 475-484, (1946).
- 2.5-75 Vincenti, W. G. "Comparison Between Theory and Experiment for Wings at Supersonic Speeds" N.A.C.A. Report 1033, (1951).
- 2.5-76 Cohen, Doris: "Formulas for the Supersonic Loading, Lift, and Drag of Flat Swept-Back Wings with Leading Edges Behind the Mach Lines" N.A.C.A. Report 1051, (1951).
- 2.5-77 Carter, W. J. "Optimum Nose Shapes for Missiles in the Super-aerodynamic Region" J. Aero. Sci., Vol. 24, No. 7, p. 527-532, (1957).
- 2.5-78 Nielsen, J. N. and Matteson, F. H. "Calculative Method for Estimating the Interference Pressure Field at Zero-Lift on a Symmetrical Swept-Back Wing Mounted on a Circular Cylindrical Body" N.A.C.A. R.M. A9E19, (1949).
- 2.5-79 Coletti, D. E. "Investigation of Interference Lift, Drag and Pitching Moment of a Series of Triangular Wing and Body Combinations at a Mach Number of 1.62", N.A.C.A. R.M. L55B25, (1955).
- 2.5-80 Kavanau, L. L. "Base Pressure Studies in Rarefied Supersonic Flows" J. Aero. Sci., Vol. 23, No. 3, pp. 193-208 (1956).
- 2.5-81 Harris, T. "Description and Discussion of the Air Disturbance Round Bullets in Free Flight" R. D. Ref. No. 63, Ordnance Research Department, Woolwich, England, (1925).
- 2.5-82 Gabeaud, M. "Sur la Resistance de L'Air Aux Vitesses Balistiques" Comptes Rendus de L'Academie de Sciences, Vol. 192, No. 11, pp. 1630 and 1790, (1931).
- 2.5-83 Depreux, M. "Sur la Resistance de L'Air a L'Arriere Des Projectiles" Comptes Rendus de L'Academie de Sciences, Vol. 193, No. 11, p. 439, (1931).
- 2.5-84 von Karman, T. and Moore, N. B. "The Resistance of Slender Bodies Moving at Supersonic Velocities" Trans. A.S.M.E., Vol. 54, p. 303, (1932).

2.5-85 Ames Research Staff. "Equations, Tables, and Charts for Compressible Flow" N.A.C.A. Tech. Reports 1135, (1953).

**BLANK PAGE**

TABLE OF CONTENTS

Section 2.6 Base Drag

SUBSECTION	PAGE
LIST OF FIGURES	2.6-ii
LIST OF TABLES	2.6-iv
LIST OF SYMBOLS	2.6-v
2.6.1 Introduction	2.6-1
2.6.2 A Brief Survey of the Base Pressure References	2.6-2
(i) Chapman's Solution of the Base Pressure	2.6-3
(ii) Love's Solution of the Base Pressure	2.6-6
2.6.3 A Summary Analysis of the Main Influential Parameters	2.6-10
(i) Reynolds Number Effects	2.6-10
(ii) Mach Number Effects	2.6-10
(iii) Combined Mach Number and Reynolds Number Effects	2.6-10
(iv) Boattail Effects	2.6-10
(v) Tail Fins Interference Effects	2.6-18
(vi) Jet Effects on Afterbody Drag Component	2.6-20
(vii) Trailing Edge Base Pressure	2.6-29
2.6.4 The Proposed Methods for the Base Drag Coefficient Evaluation	2.6-30
(i) Basic Assumptions	2.6-30
(ii) Cone (Ogive) Plus Cylindrical Body Without Boattailing	2.6-30
(iii) Boattail Effects on Base Pressure Drag	2.6-31
(iv) Fins Interference Effects	2.6-31
(v) Jet Interference Effects on the Base Pressure and the Boattail Drag	2.6-32
(1) Base Drag Coefficient Changes Due to Jet Effects	2.6-32
(2) Boattail Pressure Drag Coefficient Changes Due to Jet Effects	2.6-34
(3) Combined Afterbody (Base Plus Boattail) Drag Coefficient Decrement.	2.6-34
(vi) Trailing Edge Base Pressure Drag	2.6-36
(vii) Final Expressions for the Total Base Drag Coefficient	2.6-36
2.6.5 Computational Instructions for the Total Base Pressure Drag Coefficient Estimates	2.6-38
(i) Basic Data Preparation	2.6-38
(ii) List of Working Graphs for the Base Pressure Drag Estimates	2.6-38
(iii) Computational Procedure	2.6-38
2.6.6 References	2.6-53

LIST OF FIGURES

Section 2.6 Base Drag

FIGURE	TITLE	PAGE
2.6-1	Method of evaluating $P'$ together with some specific values, Ref. (2.6-5)	2.6-4
2.6-2	Effect of Reynolds Number on base pressure of bodies of revolution with turbulent boundary layers, Ref. (2.6-5)	2.6-5
2.6-3	Base-pressure correlation for bodies of revolution with relatively thin turbulent boundary layer, Ref. (2.6-5)	2.6-5
2.6-4	Base-pressure correlation for airfoils with relatively thin turbulent boundary layers, Ref. (2.6-5)	2.6-7
2.6-5	Effect of Reynolds Number on base pressure of airfoils with turbulent boundary layers, Ref. (2.6-5)	2.6-7
2.6-6	Base pressure on bodies of revolution having cylindrical afterbodies (no fins), Ref. (2.6-33)	2.6-8
2.6-7	Sketch of wake flow at low Reynolds Number, Ref. (2.6-11)	2.6-9
2.6-8	Average base pressure drag coefficient for cylindrical bodies with conical noses from various tests, Ref. (2.6-13) fig. 1, J.A.S. Vol. 18, no. 1, 1951, see table (2.6-1)	2.6-11
2.6-9	Base pressure on bodies of revolution having cylindrical afterbodies - collection of data	2.6-12
2.6-10	Geometry of models tested in Ref. (2.6-26)	2.6-15
2.6-11	Configurations for minimum afterbody drag at $M = 1.2$ , Ref. (2.6-36)	2.6-16
2.6-12	Sketch of typical afterbody and several nozzle configurations	2.6-21
2.6-13	Jet effects on boattail pressures. Typical case; free-stream Mach Number, 1.9; boattail angle, $5.6^\circ$ , Ref. (2.6-37)	2.6-23
2.6-14	Jet effect on boattail pressure drag at free-stream Mach Numbers of 1.9 to 2.0, Ref. (2.6-37)	2.6-25
2.6-15	Base pressure increment for parabolic afterbodies at zero angle-of-attack, transonic speeds. Rearranged from Ref. (2.6-16)	2.6-26
2.6-16	Fin effects upon base pressure with varying Mach Number for the basic reference configuration	2.6-42
2.6-17	Base drag coefficient decrement due to fin thickness decrease, Ref. (2.6-11) and (2.6-30)	2.6-43

2.6-18	Measurements and estimates of the effects of fin location upon base pressure at several Mach Numbers	2.6-44
2.6-19	Base pressure on bodies having cylindrical afterbodies (no fins)	2.6-45
2.6-20	Effect of free-stream Mach Numbers on base pressures for various jet-static pressure ratios. Reference configuration	2.6-46
2.6-21	The effects of Mach Number on base pressure for two-dimensional wings in turbulent flow, Ref. (2.6-7)	2.6-52

LIST OF TABLES  
Section 2.6 Base Drag

TABLE	TITLE	PAGE
2.6-1	Calculation of base drag coefficient using data on base pressure of cylindrical bodies from Ref. (2.6-13)	2.6-13
2.6-2	Geometrical data for models tested in Ref. (2.6-26), see Fig. (2.6-10)	2.6-17
2.6-3	Accuracy of measurements in Ref. (2.6-26), see Fig. (2.6-10)	2.6-17
2.6-4	Basic data for base drag evaluation	2.6-39
2.6-5	Total base drag coefficient estimates	2.6-40

## LIST OF SYMBOLS

### Section 2.6 Base Drag

#### I. GEOMETRY

- D - Cylinder diameter, ft.
- $D_B$  - Base diameter, ft.
- $D_N$  - Nozzle diameter, ft.
- N - Number of fins.
- $b_F$  - The fin total span.
- $h_{FEXP}$  - The individual fin height, ft.
- $(t/c)_F$  - The airfoil thickness ratio.
- $C_r$  - The fin root chord, ft.
- $(X/C_r)_F$  - The fin trailing edge root chord relative position with respect to body base, positive forward.
- $\Lambda_F$  - The fin sweep-back angle.
- $\theta_B$  - The conical boattail angle; for parabolic bodies, boattail angle of an inscribed cone, degrees,  $\theta_p = 2\theta_B$ .
- $\epsilon_N$  - The nozzle exit angle, positive for diverging exit profile, degrees.
- $b_{WEXN}$  - Exposed wing span, ft.
- $t$  - The bluntness of the wing or fin edge, approximately .01 ft.
- $\theta_B$  - Boattail angle.
- $S_r$  - Reference area.
- C - Airfoil chord.
- h - Airfoil base thickness.

#### II. PHYSICAL

- $T_j$  - The jet static temperature,  $^{\circ}R$ , absolute.
- $T_H$  - The ambient static temperature  $^{\circ}R$  absolute.
- P - The altitude static pressure,  $P_H = P_{\infty}$ , #/sq.ft.
- $M_H$  - The free-stream Mach Number,  $M_H = M_{\infty}$ .
- $P_b$  - The static pressure, #/sq.ft.
- $Re_E$  - The Reynolds Number, referred to exposed wing (or fin) mean geometric chord.

- K - Maximum diameter (location coefficient).
- $\psi$  - Stream function.
- $\delta$  - Boundary layer thickness.
- $C_{D0}$  - Zero-lift drag force coefficient, nondimensional, referred to the common reference area,  $S_r$ , and the flow conditions at "infinity", Standard Atmosphere at each flight altitude, H:

$$C_{D0} = \frac{\text{Zero-Lift Drag Force}}{q_H S_r}$$

- $C_{D0b}$  - Zero-lift base pressure drag force coefficient, nondimensional, referred to the common reference area,  $S_r$ , and the flow conditions at "infinity", Standard Atmosphere at each flight altitude, H:

$$C_{D0b} = (-C_{pb}) \left( \frac{S_{BASE}}{S_r} \right)$$

### III. SUBSCRIPTS

- B - Refers to the body in general.
- BT - Refers to the boattail section of body.
- BT(F) - Refers to the boattail in presence of fins.
- BT(FORE) - Refers to the boattail in presence of forebody.
- BT(W) - Refers to the boattail in presence of wings.
- CYL - Refers to the cylindrical section of body.
- F - Refers to fins.
- F(BT) - Refers to the fins in presence of boattail.
- FORE - Refers to the forebody, i.e., to the body section ahead of the wings.
- F(W+B) - Refers to fins in presence of the body and the wings.
- LE - Refers to wing or fin leading edge.
- T(JET) - Refers to tail in presence of the jet.
- TE - Refers to wing or fin trailing edge.
- W(B) - Refers to the wing in presence of body.
- WET - Refers to the wetted area of a missile part.
- $\infty$  - Refers to the local free stream conditions just outside the boundary layer.

### IV. SUPERSSCRIPTS

- ' - Mean value of quantity.

## 2.6 BASE DRAG

### 2.6.1 INTRODUCTION

For blunt-base bodies, the base drag component,  $C_{D0b}$ , (including the smaller contribution from trailing-edge bluntness effects) constitutes an appreciable fraction of the total drag force at supersonic speeds.

The base drag arises from the static pressure that is created in the viscous dead-air region at the rear of the body. It is largely influenced by the pattern in which the free stream flow closes in behind the body (usually through a slip-off expansion-compression wave combination) and by the manner in which the boundary layer at the base mixes with both the dead-air region and the outside free-stream flow. The phenomena is of a predominantly viscous nature and, consequently, cannot be treated within the concepts of potential fluid theory. Instead, semi-empirical correlations of various experimental data are required.

The fundamental assumptions, stated in Section 1.2, are applied to the present analysis of the base drag phenomena, i.e., only symmetric, steady (or eventually "quasi-steady") flow (or flight) in a Standard Atmosphere (void of any turbulence) are investigated.

The main parameters controlling the base drag phenomena within the steady flow concept are:

- (1) Type of flow: two-dimensional, axially symmetric, general three dimensional,
- (2) Type of boundary layer at the base: laminar, transitional, turbulent,
- (3) Base configuration: boattailing and general body shape ahead of base,
- (4) Mach Number,
- (5) Reynolds Number,
- (6) The shift of the transition point from laminar to turbulent boundary layer flows,
- (7) Thermal conditions at the base,
- (8) The angle-of-attack,
- (9) The fin-interference effects,

(10) The "jet-pump" effects,

(11) The flight altitude (rarefied gas effects).

In the proposed method of engineering analysis, only some of the influential parameters are taken into account. Thus, it is further assumed that:

(a) For the restrictive no-lift conditions, ( $C_L \sim 0$ ), it is assumed that the flow around the body near the base is not separated.

(b) The boundary layer is fully turbulent before slipping off the rear of the body.

(c) Thermal conditions at the base are not fully taken into account, since no extensive data on the heat effects are available. Partial corrections, when included, are from rather scarce experimental evidence.

Other effects, listed above under (1) to (11), are taken into consideration in preparing the working charts for the base drag coefficient estimates as follows:

For bodies of revolution, the external flow is taken as axially symmetric. Wings and fins are assumed two-dimensional when theoretical data are used, i.e., the tip effects and the spanwise flow streaming with swept-back configurations are not explicitly represented; they are automatically included in an implicit form in the respective experimental measurements. Base configurations consist of relatively restricted boattailing ( $\theta_B < 15^\circ$ ). The influence of fin size, shape and position on the base pressure is tentatively expressed as a separate interference effect and estimated on the basis of the few available empirical data. "Jet pump" effects are taken into account, mostly from data obtained from direct free-flight measurements.

In the following Sections, 2.6.2 and 2.6.3, a general survey of the technical literature used in the preparation of data and a qualitative summary analysis of various influence parameters on the base pressure values are presented

The explicit expressions for the base pressure evaluation and the proposed

method for direct computations are worked out in detail in Section 2.6.4.

### 2.6.2 A BRIEF SURVEY OF THE BASE PRESSURE REFERENCES

In the early Refs (2.6-1) to (2.6-4), (Harris, Gabeaud, Depreux, von Karman), the base pressure has been studied considering the inviscid influence of Mach Number only. The neglect of viscous effects, constituting actually the very basis of the phenomena, proved to be a serious shortcoming of the theories.

Studies of the viscous effects on base pressure were notably undertaken by Cope(6) and Chapman(5). They investigated simultaneously the Mach Number, the Reynolds Number, and the general viscous flow pattern effects at the base. Cope derived a semi-empirical method for the base drag estimates in terms of Mach Number, Reynolds Number and the boundary layer flow type. Chapman used "inviscid" supersonic wake solutions in combination with existing experimental evidence, and derived a general semi-empirical method which is described later.

The first pure theoretical treatment of the "viscous" problem in its simplest form (i.e., without any side-effects such as jet interference, temperature, etc.), has been presented by Crocco and Lees(9) by applying their "mixing theory" to the base pressure analysis on blunt trailing edge airfoils. Their conclusions agreed fairly well with the semi-empirical derivations of Chapman(7) and with the experimental data of Bogdanoff(8).

Thus, regarding cylindrical bodies of revolution with or without boattailing, as well as two-dimensional airfoil sections, useful engineering data may be found in Refs by Crocco and Lees(9), Chapman(5,7), Cortright and Schroeder(12), Cope(6), Gabeaud(2), Kurzweg(13) and Love(11). Assuming a turbulent boundary layer, semi-theoretical data in good agreement with the existing experimental evidence of base pressure estimates for bodies of revolution with or without boattailing, and for two-dimensional airfoils, may be found in Refs by Chapman(5,7) Cortright and Schroeder(12) and Love(11). Unfortunately, a direct application of their methods for engineering purposes

is recommendable only in cases of no boattailing, due to relative complexity of the methods in the case of boattailed bodies. For the latter, empirical data based on accumulated experimental evidence are easier to use.

As the importance of reliable predictions of the missile base pressure values has become more and more important, other experimental and semi-empirical data and methods, including many new variables (jet-effects, temperature conditions, rarefied gas effects, etc.), are constantly being accumulated, see respective Refs. (2.6-7), (2.6-8), (2.6-11), (2.6-14) to (2.6-31).

Thus, in the Refs. (2.6-5), (2.6-20), (2.6-21), (2.6-22), (2.6-27), (Chapman, Love Perkins, Hart, Reller), support interference effects on base pressure are investigated. Explicit effects of the Reynolds Number at a constant Mach Number are studied in Refs. (2.6-5), (2.6-13), (2.6-15), (2.6-19), (2.6-20), (2.6-27), (Chapman, Kurzweg, Perkins, Love, Reller). Fin interference and jet-pump effects are also partially covered in some of the references. Two-dimensional base pressures are well presented in Refs. (2.6-4) by von Karman and (2.6-31) by Morrow and Katz.

Regarding the relative magnitude of the base drag term at supersonic speeds, some wind-tunnel experiments indicate that the base drag component is small with respect to the total body drag when the body is plump with a blunt nose. However, the base drag is of the same order of magnitude as the skin friction drag when the bodies are sharp pointed and slender (supersonic long range missiles and projectiles).

Unfortunately, a unified theoretical or a semi-empirical treatment of all the variables which influence the base drag under the actual flight conditions has not been yet developed. Therefore, in proposing the working charts for design purposes, a gradual

build-up procedure from simple cylinder-cone to more complicated cases has been adopted. The number of variables is thus increased in an additive way as indicated by the proposed analytical expression for the base-pressure, see Section 1.7.4.

As an illustration of the semi-empirical methods used in the present base pressure analysis, the Chapman's and the Love's approaches to the problem are outlined below.

#### (i) Chapman's Solution of the Base Pressure

In the Ref (2.6-5), an interesting semi-theoretical approach to the base pressure evaluation (without jet-pump effects) has been defined by Chapman. Since the general Body configuration has effects on both the potential free-stream flow and the viscous boundary layer, Chapman split the problem into two parts. First, he defined a "mean static pressure of the outer, inviscid flow",  $p'$ , which accounts for the body configuration effects on the free-stream, including the boattail angle, the nose shape, and the cylindrical mid-section. This reference mean pressure,  $p'$ , represents a hypothetical average static pressure obtained by the method of characteristics which would exist if the body were prolonged for one diameter distance behind the base, see Fig (2.6-1). In this way, Chapman actually eliminated the body shape parameter as an explicit independent variable by taking its influence on the free stream implicitly through the above defined hypothetical reference pressure,  $p' = f(M')$ , where  $M'$  corresponds to  $p'$ . In the second step, the available experimental data were correlated through the pressure ratio ( $p_b/p'$ ) by a single correlation curve as the function of the Mach Number and the body geometry. This second term thus expresses the body shape influence on the boundary layer, i.e., the viscous effects. Analytically:

$$\left(\frac{p_b}{p_\infty}\right) = \left(\frac{p'}{p_\infty}\right) \left(\frac{p_b}{p'}\right), \quad (2.6-1)$$

where  $(p'/p_\infty)$  is the calculated average inviscid free stream static pressure ratio, and  $(p_b/p')$  the correlated experimental evidence.

Regarding applicability of data to design purposes, some useful approximations, based on observations, can be introduced for supersonic regimes:

(1) The nose shape influences the base pressure only if the total body fineness ratio ( $L/D$ ) is less than 5. It means that, in general, only the body shape up to some five diameters from the base affects appreciably the base pressure. Consequently, for slender, relatively high fineness ratio bodies without boattailing, the  $p'$  reference pressure can be approximately taken as equal to the  $p_\infty$  value. The experimental verifications of the above assumption can be found in Refs. by Love<sup>(11)</sup>, Reller<sup>(27)</sup>, Charters and Turetsky<sup>(23)</sup>.

(2) At supersonic speeds, the static pressure behind an airfoil in two-dimensional inviscid flow is equal to its free stream value,  $p_\infty$ . Therefore, in a first approximation, the pressure drag due to trailing edge bluntness can be taken as  $p' = p_\infty$ .

(3) Boattailing of bodies of revolutions increases the "afterbody pressure drag" in front of the base,  $p_b$ , but at the same time raises the reference,  $p'$ , value above that of the free-stream static pressure,  $p_\infty$ , i.e., decreases the base drag. By boattailing, the total pressure drag is eventually decreased. But "boattailing" of two-dimensional blunt-base airfoils has only little numerical effect on trailing-edge base pressure value, see Figs (2.6-2) and (2.6-3), i.e., far less than in the case of bodies of revolution.

(4) As stated later, there are three primary Mach Number effects on the base pressure. In applying the Chapman's method, a reference Mach Number,  $M'$ , corresponding to the reference pressure,  $p'$ , should be used. Such a choice of a reference Mach Number would presumably account for the various Mach Number effects as related to body shape, type of mixing process and the boundary layer characteristics.

(5) Assuming a fully turbulent flow on all wetted surfaces, the Reynolds Number effects, as related to the body geometry, can be represented by the ratio  $(\delta/D)$ . For small boattail angles ( $\theta_b < 15^\circ$ ), it can be assumed that the pressure-gradient variation does not affect the boundary layer thickness ( $\delta$ ) appreciably. Consequently, for the given value of  $M'$ , the boundary layer thickness can be considered as solely a function of the Reynolds Number at the base, i.e., for a turbulent boundary layer:

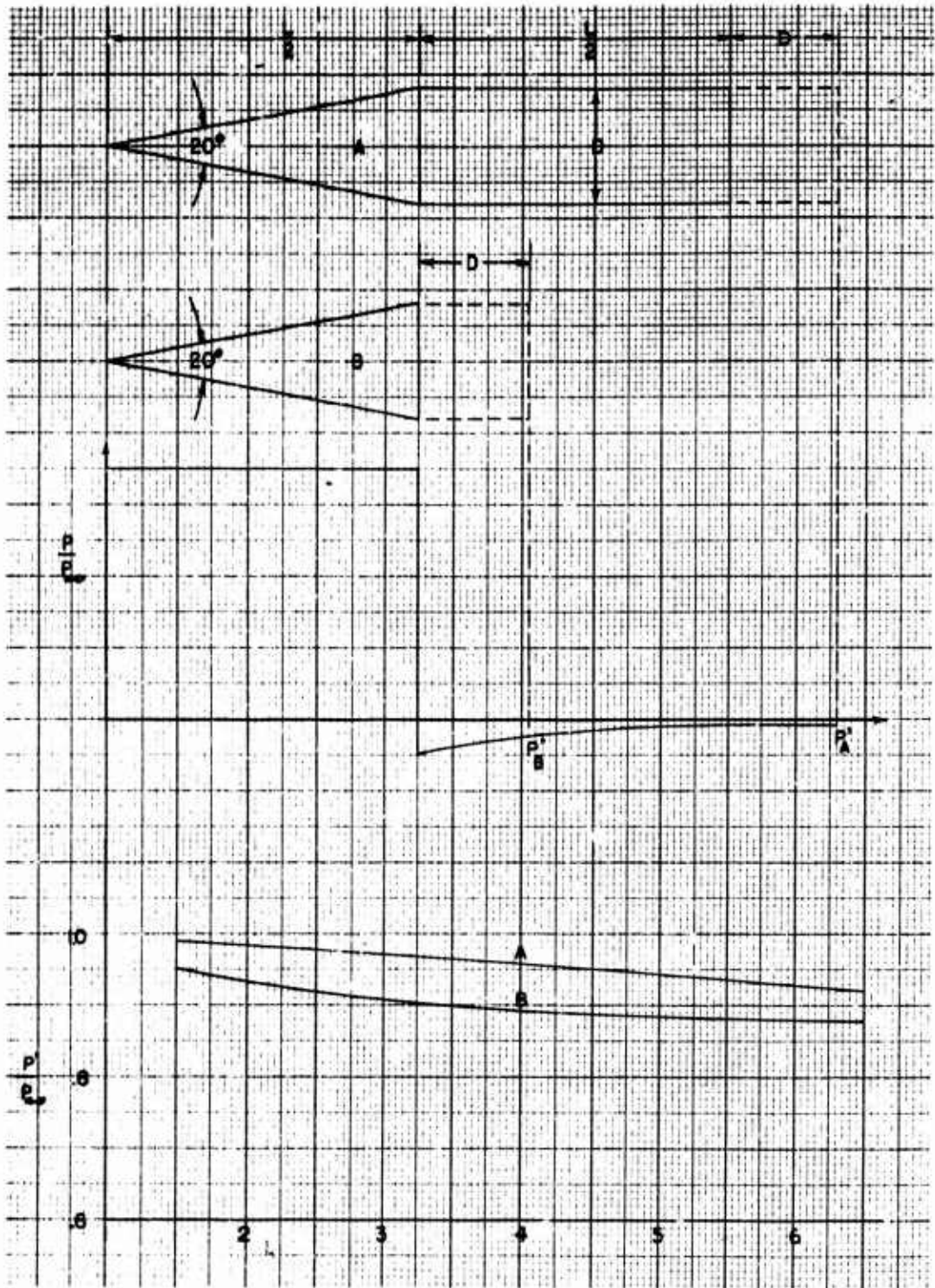


Fig (2.6-1) Method of evaluating  $P'$  together with some specific values. Ref (2.6-5)

$p'$  - reference mean pressure of outer flow  
 $M'$  - reference mean free-stream Mach Number

} as defined by Chapman,  
 Ref (2.6-5)

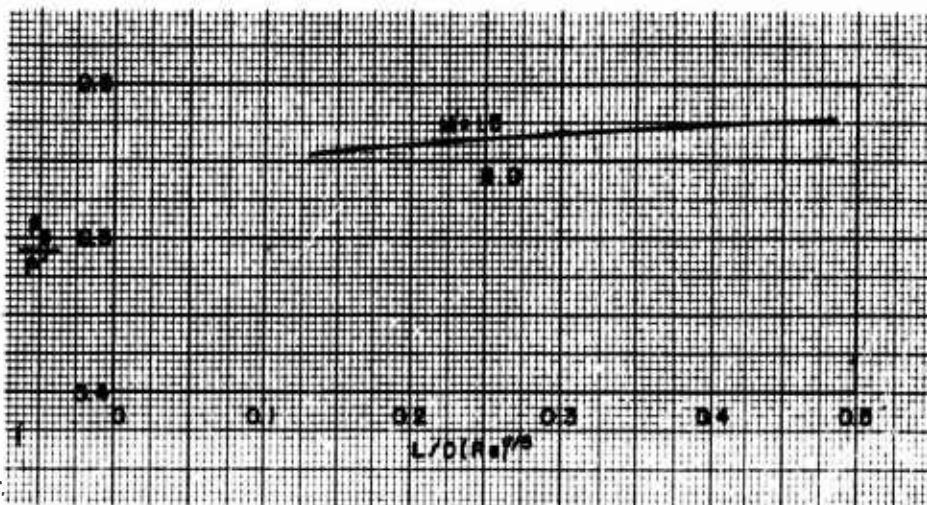


Fig (2.6-2) Effect of Reynolds Number on base pressure of bodies of revolution with turbulent boundary layers. Ref (2.6-5)

$p'$  - reference mean pressure of outer flow  
 $M'$  - reference mean free-stream Mach Number

} as defined by Chapman  
 Ref (2.6-5)

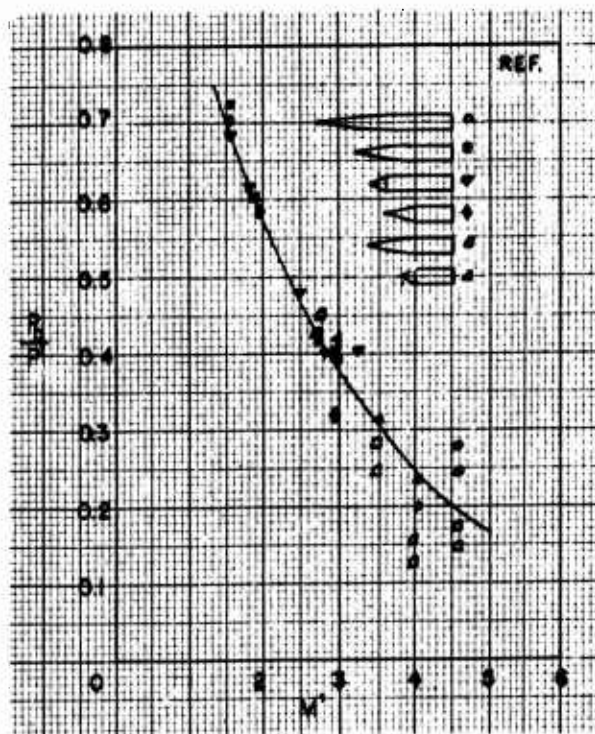


Fig (2.6-3) Base-pressure correlation for bodies of revolution with relatively thin turbulent boundary layer. Ref (2.6-5)

$$(\delta/L) \propto (Re_L)^{-1/5} \quad (2.6-2)$$

or, since the above interpretation represents the second term in Chapman's expression, Eq (2.6-1), it follows that:

$$\left(\frac{P_b}{P'}\right) = f(M', \delta/D) = \phi\left[M', \frac{(L/D)}{Re_L^2}\right] \quad (2.6-3)$$

With these simplifications for the  $(P'/P_\infty)$  and the  $(P_b/P')$  ratios, both the Mach Number and the Reynolds Number effects can be computed by Chapman's method. The results are in good agreement with experimental evidence, see Figs (2.6-2) and (2.6-3). The Reynolds Number effects prove to have but negligible effect for bodies of revolution with relatively thin boundary layers ( $\delta/D$  small); while, for two-dimensional airfoils the effect is appreciable, ( $\delta/t_b \approx 1$ ), see Fig (2.6-5). In both cases a turbulent boundary layer is assumed.

(ii) Love's Solution of the Base Pressure

In the Ref (2.6-33), Love presented

an alternative semi-empirical method for estimating base pressures for two-dimensional airfoil bases and the bases of bodies of revolution, assuming turbulent boundary layers. This method represents an extension of the Cortright's and Schroeder's analysis(12), and is verified by many direct experimental measurements. The results are in a very good agreement with Chapman's (5), see Fig (2.6-6). Additionally, boattailing effects and fin-interference effects are treated by using available experimental data.

Combining the Chapman's and the Love's results, the respective final working charts have been prepared for cylindrical bodies of revolution.

When comparing these semi-empirical curves with the respective experimental data, a cautious selection should be made. In some free-flight and wind-tunnel measurements, the pick-up orifices for base pressure readings have been located at the body outer envelope "near" the base, mostly because of structural reasons. Such "base pressure" readings, taken outside the dead wake region, are hardly representative for a proper base drag evaluation.

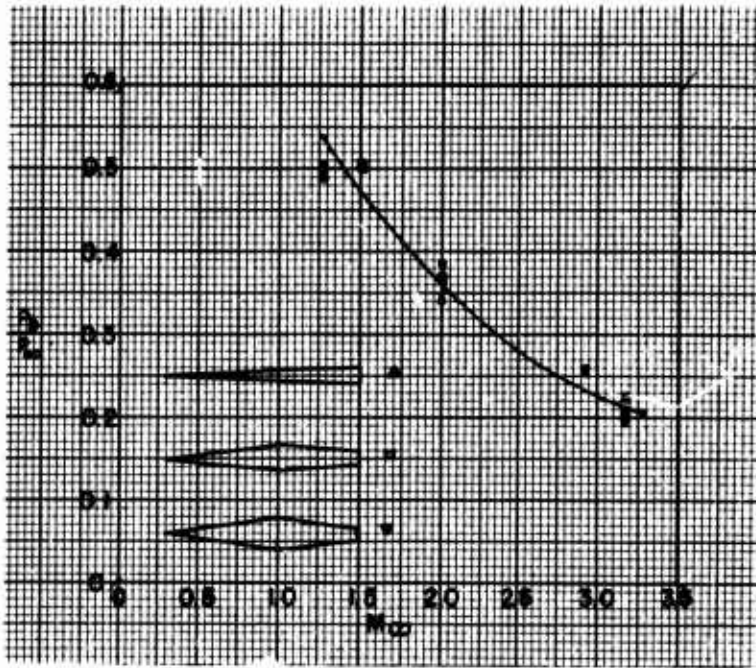


Fig (2.6-4) Base-pressure correlation for airfoils with relatively thin turbulent boundary layers. Ref(2.6-5)

c - airfoil chord  
 h - airfoil base thickness

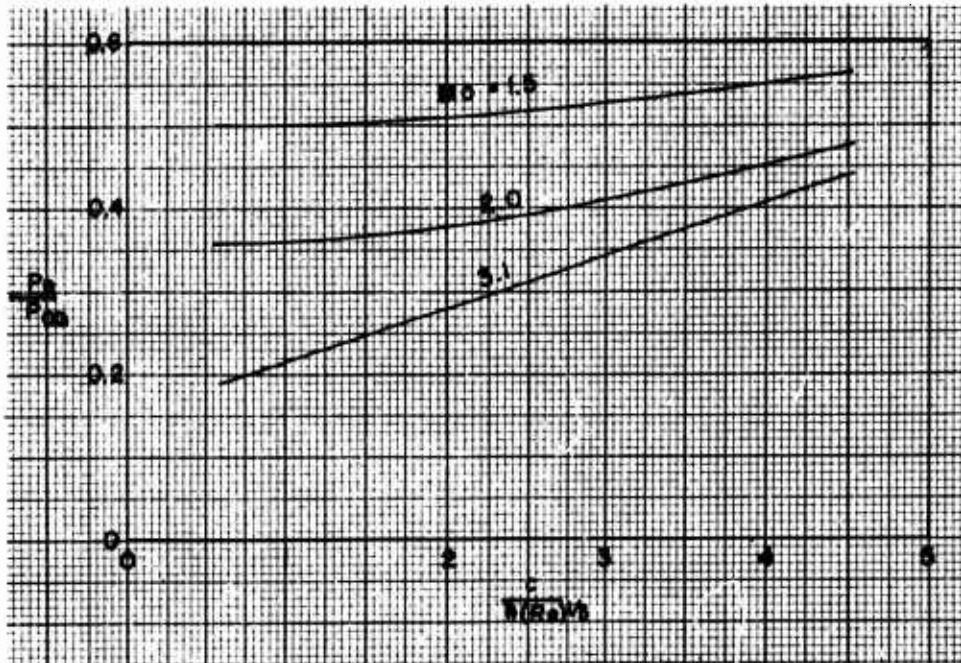


Fig (2.6-5) Effect of Reynolds Number on base pressure of airfoils with turbulent boundary layers. Ref(2.6-5)

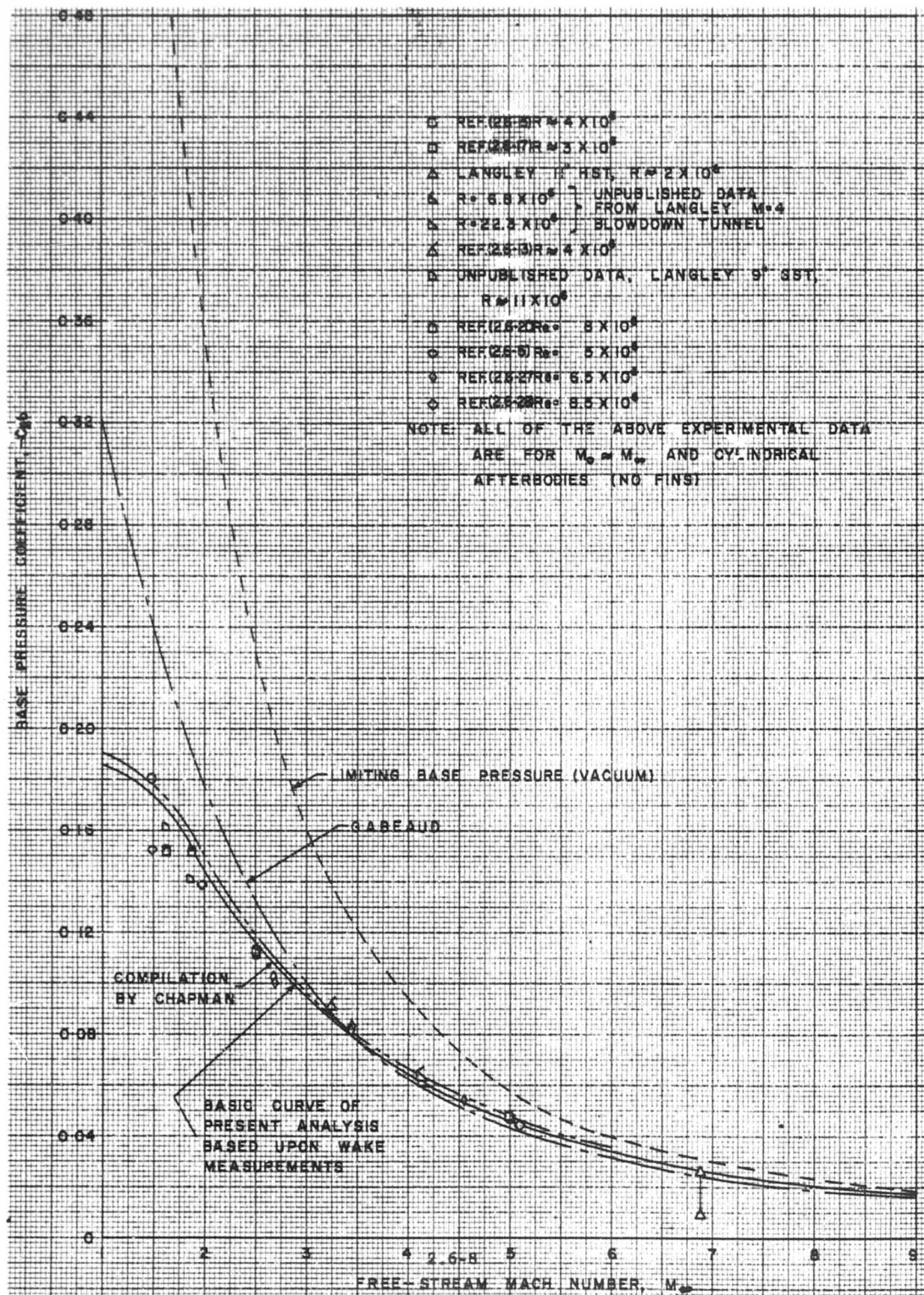


Fig (2.6-6) Base pressure on bodies of revolution having cylindrical afterbodies (No fins)  
 Ref (2.6-33)

$\psi$  - STREAM FUNCTION

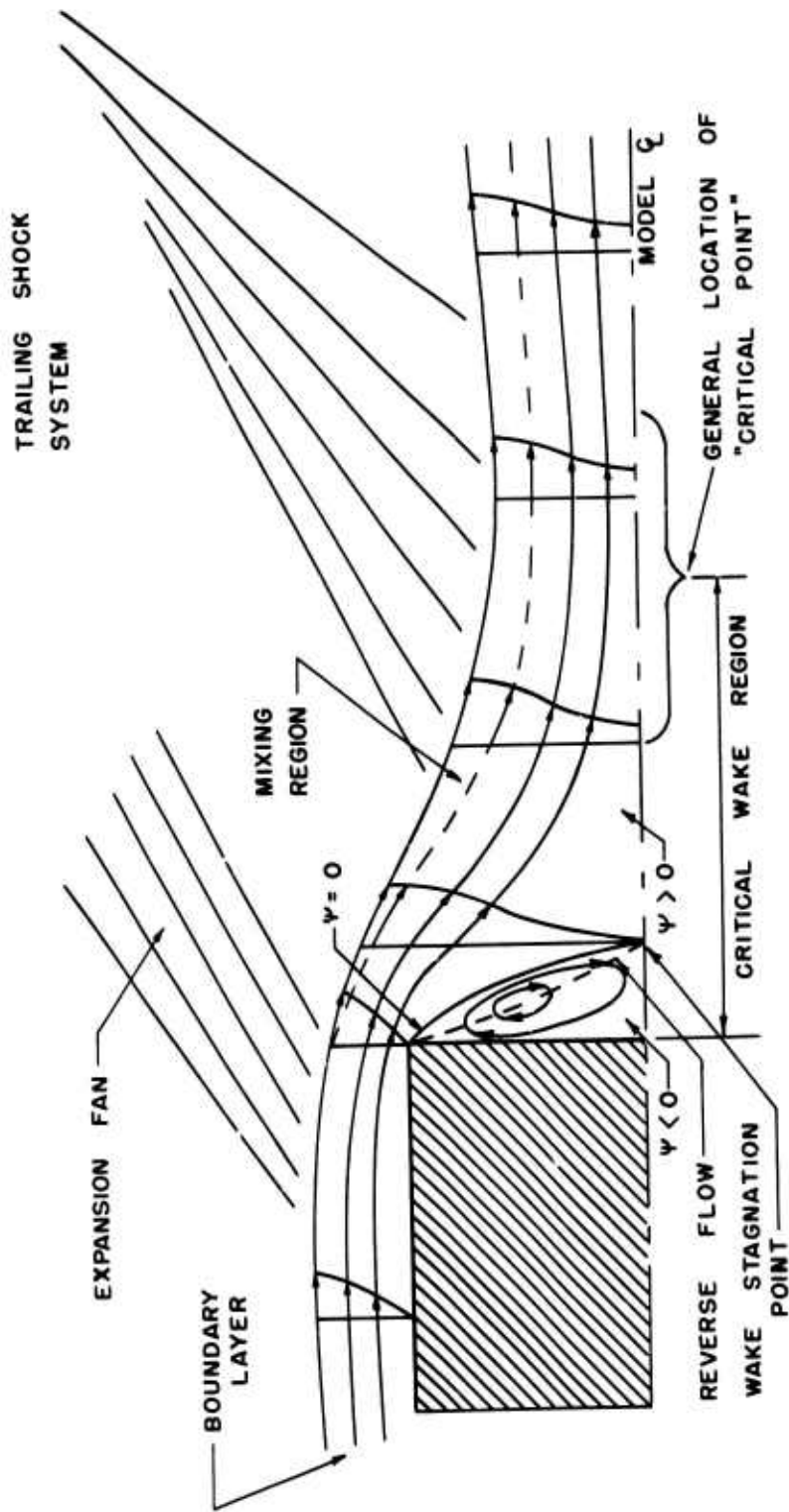


FIG. (2.6-7) SKETCH OF WAKE FLOW AT LOW REYNOLDS NUMBER

REF (2.6-II)

### 2.6.3 A SUMMARY ANALYSIS OF THE MAIN INFLUENTIAL PARAMETERS

A simplified schematic illustration of the base flow pattern is presented in Fig (2.6-7). Excluding rarefied gas effects and assuming a fully turbulent boundary layer over the rear portion of the missile configuration, the following brief conclusions regarding the main influential parameters may be derived from the existing theoretical and experimental evidence:

#### (i) Reynolds Number Effects

Being primarily a viscous phenomena, the base pressure is necessarily a strong function of the boundary layer type and its development history along the body. A shift of the transition point from laminar to turbulent boundary layers along the body length additionally affects the viscous flow conditions at the base (34) (Kavanau). Since a predominantly turbulent boundary layer has been assumed on the cylindrical part of the missile body, this effect can be neglected, see Chapman<sup>(5,7)</sup>, and Faro<sup>(17)</sup>. Thus, in a first approximation, it can be stated that the Reynolds Number affects the base pressure values through the conditions of the turbulent boundary layer as estimated at the base. Even with this simplification, experimental evidence indicates that the boundary layer state at the base may be in some cases additionally influenced by the geometry of the body configuration ahead of the base. Notably, if the nose configurations are not faired smoothly with the cylindrical portion of the body, and for low fineness-ratio values  $(L_N + L_{CYL})/D$ , the base drag may be adversely affected, i.e., increased.

From experimental evidence, Ref (2.6-8), by Bogdanoff, it can be concluded that the Reynolds Number effects on base pressure values with cone-cylinder configurations are in a more general case as follows:

- If a laminar boundary layer is maintained at the base, a rapid decrease in base pressure occurs with increased Reynolds Number. When the boundary layer transition occurs at the base, a further increase in Reynolds Number increases the base pressure. This is followed by a slow steady decrease in the base pressure values as the transition moves forward on the body. Thus, assuming a fully turbulent boundary layer along the body, only slightly conservative estimates of the base pressure may be anticipated,

since in most cases the transition point under free flight conditions should be well forward on the main body.

#### (ii) Mach Number Effects

The manifold effects caused by the Mach Number variation influences:

(1) The average pressure of the outer free stream flow,

(2) The average density and velocity profiles of the boundary layer at the base,

(3) The type of mixing process (expansion-compression wave pattern between the boundary layer and the air on each side of it, i.e., both in the free stream and in the dead air regions).

For the simplest body configuration of a cone plus cylinder, with the assumed turbulent boundary layer prevalence, an increase in the Mach Number promotes a strong decrease in the base pressure coefficient, see Figs (2.6-3), (2.6-6), (2.6-8) and (2.6-9).

#### (iii) Combined Mach Number and Reynolds Number Effects

The Mach Number and the Reynolds Number effects are coupled in a greater or lesser degree, depending upon the type of boundary layer and the shift of the transition point. A good general summary of the combined effects in various cases can be found in Ref (2.6-9) by Crocco and Lees. With the restriction to turbulent boundary layers, the Reynolds Number effects at supersonic speeds become of a second order of importance, see Fig (2.6-2) and Refs. (2.6-14) and (2.6-17).

#### (iv) Boattail Effects

As stated already, the boattail effects are also covered by the methods of Chapman and Love, but unlike the cylindrical body solutions, their methods of evaluating the boattail base pressures are too complicated for a practical use. Instead, a simpler empirical expression, based on experimental data for conical after-bodies from Ref (2.6-36) by Stoney, can be used:

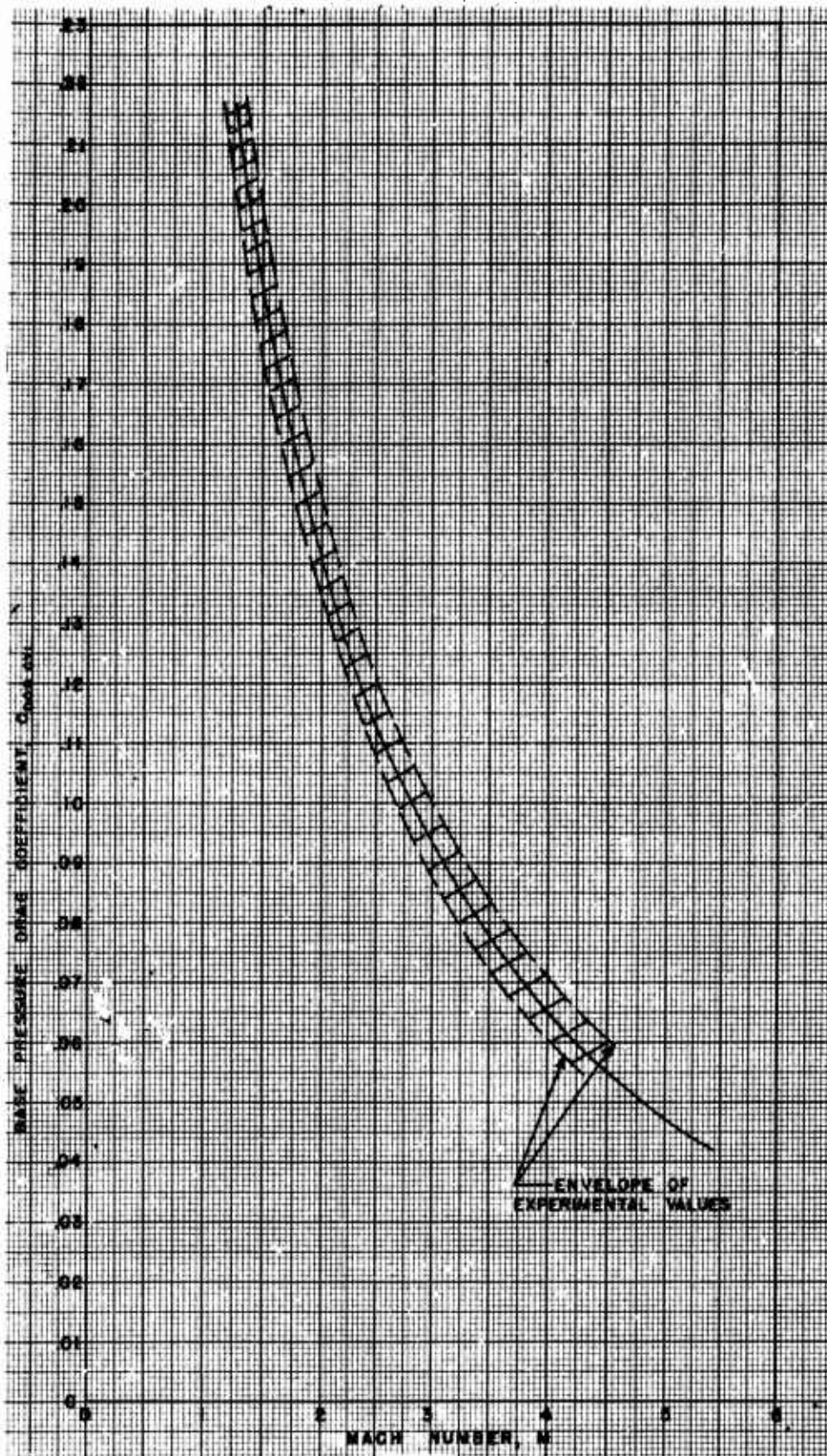


Fig (2.6-8) Average base pressure drag coefficient for cylindrical bodies with conical noses from various tests. Ref (2.6-13) fig. 1, J.A.S. vol. 16, no. 1, 1951 See table (2.6-1)

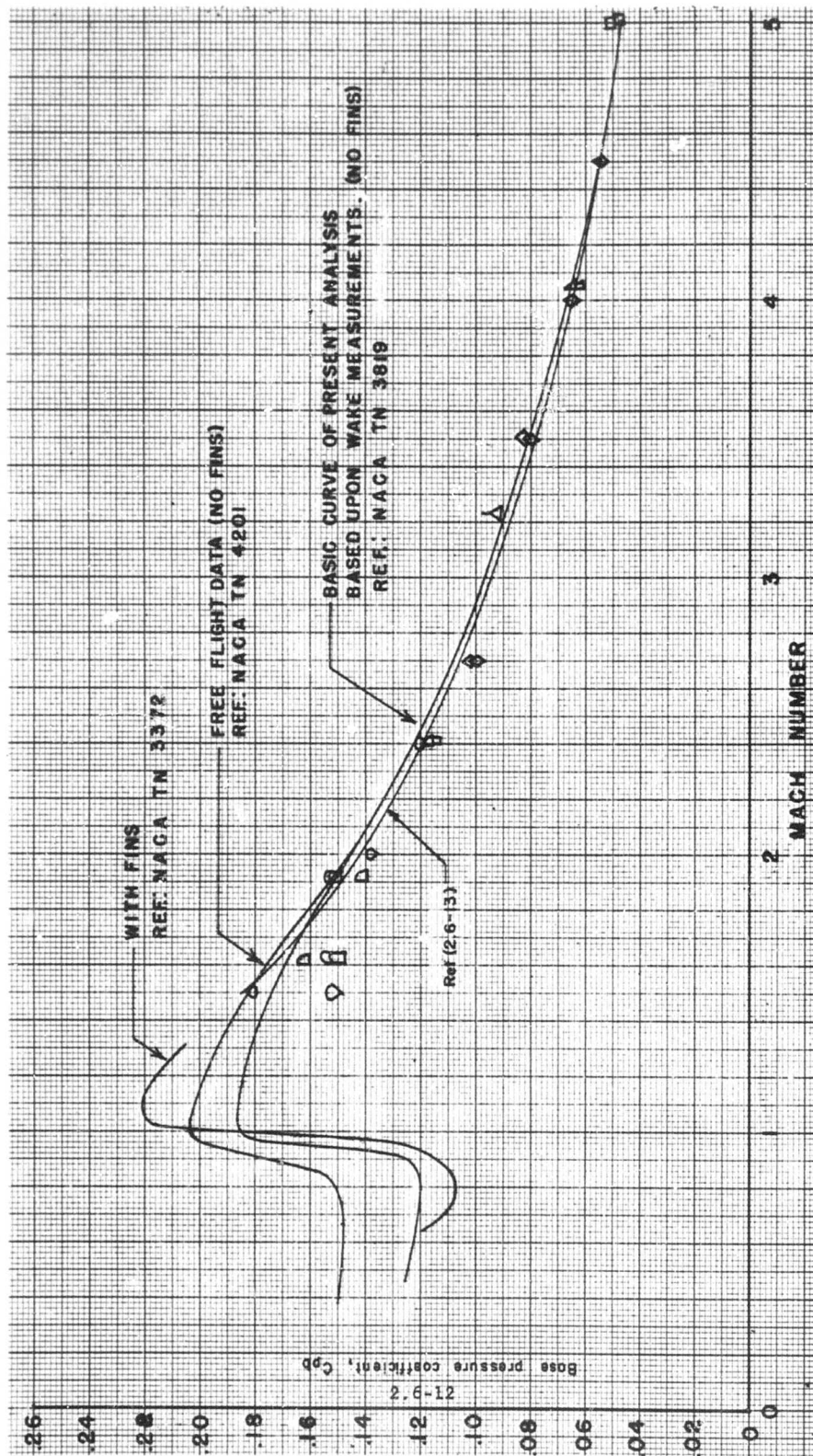


Fig (2.6-9) Base pressure on bodies of revolution having cylindrical afterbodies.  
— Collection of data —

TABLE (2.6-1)

MACH NUMBER, M	$\alpha$	$C_{DDB}$ CYL.
1.5	.730	.1715
1.5	.700	.1905
1.5	.680	.2030
2.0	.620	.1360
2.0	.600	.1430
2.0	.570	.1535
2.5	.520	.1100
2.5	.500	.1142
2.5	.470	.1210
3.0	.430	.0905
3.0	.400	.0953
3.0	.360	.1016
3.5	.380	.0723
3.5	.325	.0786
3.5	.280	.0840
4.0	.310	.0616
4.0	.260	.0660
4.0	.205	.0710
4.5	.210	.0558
5.0	.170	.0475

$$\alpha = \frac{P_B}{P} = f(M), \text{ READ FROM FIG. 1 REF. (2.6-13)}$$

$$C_{DDB} = \frac{1 - \alpha}{.7 M^2} \quad \text{SEE FIG. (2.6-8)}$$

CALCULATION OF BASE DRAG COEFFICIENT USING DATA ON BASE PRESSURE OF CYLINDRICAL BODIES FROM REF. (2.6-13)

$$\Delta C_{DobBT} = C_{DobCYL} \left[ \left( \frac{D_B}{D} \right)^3 - 1 \right], \quad (2.6-4)$$

where ( $D_B$ ) and ( $D$ ) are the base and the cylindrical body diameters respectively. Note that the reference area is  $S_r = (\pi D^2/4)$ .

It follows that the boattailing exerts a definite favorable effect, reducing the base drag. This expression can be used only for ( $\theta_B < 15^\circ$ ) with an acceptable accuracy. Optimum values of  $\theta_B$  are discussed later.

The Eq (2.6-4) holds both for subsonic and supersonic speeds, but care must be taken when applying it to pronounced boattail angles ( $\theta_B > 15^\circ$ ) at subsonic speeds, since a negative base drag can exist, see Ref (2.6-26) by Katz and Stoney.

The same expression (2.6-4), although derived for conical afterbodies, can be used, in a first approximation, for parabolic after-bodies also.

For the transonic range of speeds, ( $0.8 < M < 1.2$ ), the experimental data by Katz and Stoney(26) can be applied. They measured base pressures on several fin-stabilized bodies of parabolic arc profiles in free flight and at Reynolds Numbers ranging from  $20 \times 10^6$  to  $130 \times 10^6$ . The body length was varied from 6 to 25 diameters. The geometric data for the test models are presented in Figs (2.6-10) and (2.6-15) and in the related Table (2.6-2). The respective accuracy of the measurements is given in Table (2.6-3). Although in all these cases fins were present, they were located one chord length ahead of the base so that their effect on the base pressure proved to be negligible, see Ref(26-30) by Spahr and Dickey. The forebody configuration effects have also been found to be found to be negligible for the total fineness ratios investigated ( $L/D > 5$ ). Thus, the data from the Ref (2.6-26) suitably replotted in the form,

$$\Delta C_{pbBT} = f\left(\frac{L_B}{D}, M_\infty\right),$$

in the Fig (2.6-15), are recommended for use as the base pressure increments due to parabolic afterbody shapes as measured under actual flight conditions for Mach Numbers ranging from 0.8 to 1.4 and for afterbody fineness ratios up to 10. This does not include the actual fin-effects,

if they are mounted nearer to the base (closer than one fin-chord).

In the present paper, the inviscid pressure drag change around the body due to boattail (base drag excluded), has been taken care of in the "pressure drag term", see Section 2.5. In some literature, however, this boattail inviscid pressure drag can be found combined with the boattail base drag term, the two together called the "after-body drag". This is the case in many experimental treatments of the base pressures at large. For a quick separation of the two terms, the following semi-empirical expression can be used:

$$\begin{aligned} C_{DOPAF} &= \Delta C_{DOPBT} + \Delta C_{DobBT}, \\ C_{DOPAF} &= \frac{.001\theta_B + .00071\theta_B^2}{M_\infty} \left[ 1 - \left( \frac{D_B}{D} \right)^n \right] + \\ &+ C_{DobCYL} \left( \frac{D_B}{D} \right)^3, \quad (2.6-5) \end{aligned}$$

where

$$n = 4 \quad \text{for } M < 3.5,$$

$$n = 3 \quad \text{for } M > 3.5,$$

$$S_r = \pi D^2/4, \quad \text{reference area,}$$

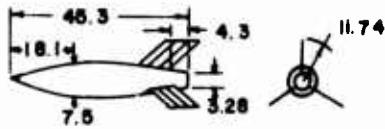
$\theta_B$  - is the angle of slope of a conical afterbody in degrees, used as positive, or angle of slope of an inscribed cone in the case of parabolic afterbodies (approximation), see Fig (2.5-18), Section 2.5.

The first term in Eq (2.6-5) approximates the second order theoretical values, as calculated by Jack<sup>(33)</sup>, while the second term is the empirical expression (2.6-3) taken in the form  $C_{DobCYL} + \Delta C_{DobBT}$ .

The applicability of Eq (2.6-5) is restricted to ( $\theta_B < 15^\circ$ ) if a reasonable accuracy is expected.

An eventual selection of minimum drag afterbodies, based on both theoretical and empirical evidence, can be easily done by following the simple rule:

- For a given ( $L_B/D$ ) ratio, the minimum afterbody drag is obtained when  $\theta_B^0 = 4.5^\circ$  for conical afterbodies, or when meridians have a base slope angle of  $\theta_p^0 = 9^\circ$  for parabolic afterbodies. Note that the tangent to the parabolic base angle is always exactly twice that of an inscribed conical body, see Fig.



Model 1;  $L/D=6.04$ ;  $K=L_N/L=0.40$   
 $L_N=18.1$ ,  $L=45.3$   
 $K$  = Max. Dia. Location Coefficient

FOR ALL MODELS:

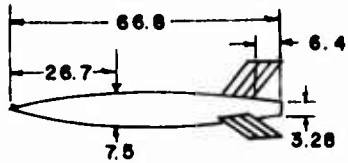
$$\pi D_0^2/4 = S = .307 \text{ ft}^2$$

$$\pi D_0^2/4 = S_b = .0586 \text{ ft}^2$$

$$\lambda_{L.E.} = 45^\circ$$

$$S_{FIN EXP. TOT.} = 1.69 \text{ ft}^2$$

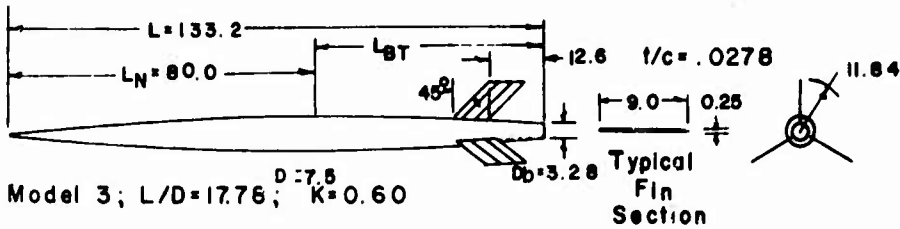
PARABOLIC BODY SHAPES



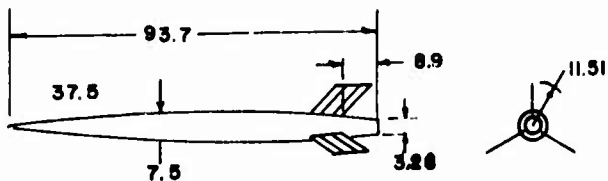
Model 2;  $L/D=8.91$ ;  $K=0.40$

$$\frac{2r}{D} = 1 - \frac{1}{K^2} \left( K - \frac{X}{L} \right)^2 \text{ WHEN } 0 \leq \frac{X}{L} \leq K$$

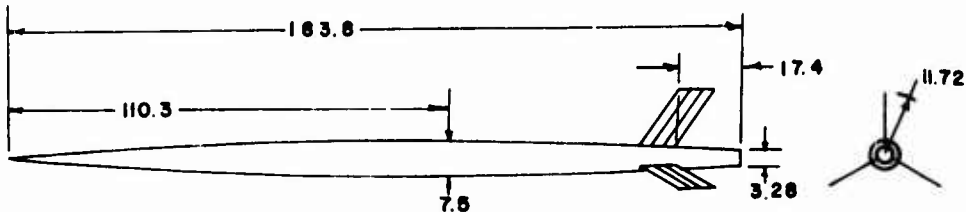
$$\frac{2r}{D} = 1 - \frac{.5627}{(1-K)^2} \left( \frac{X}{L} - K \right)^2 \text{ WHEN } K \leq \frac{X}{L} \leq 1$$



Model 3;  $L/D=17.76$ ;  $K=0.60$



Model 4;  $L/D=12.50$ ;  $K=0.40$



Model 5;  $L/D=24.50$ ;  $K=0.60$

FIG (2.6-10) GEOMETRY OF MODELS TESTED IN REF. (2.6-26)  
 ALL DIMENSIONS IN INCHES, IF NOT STATED OTHERWISE.

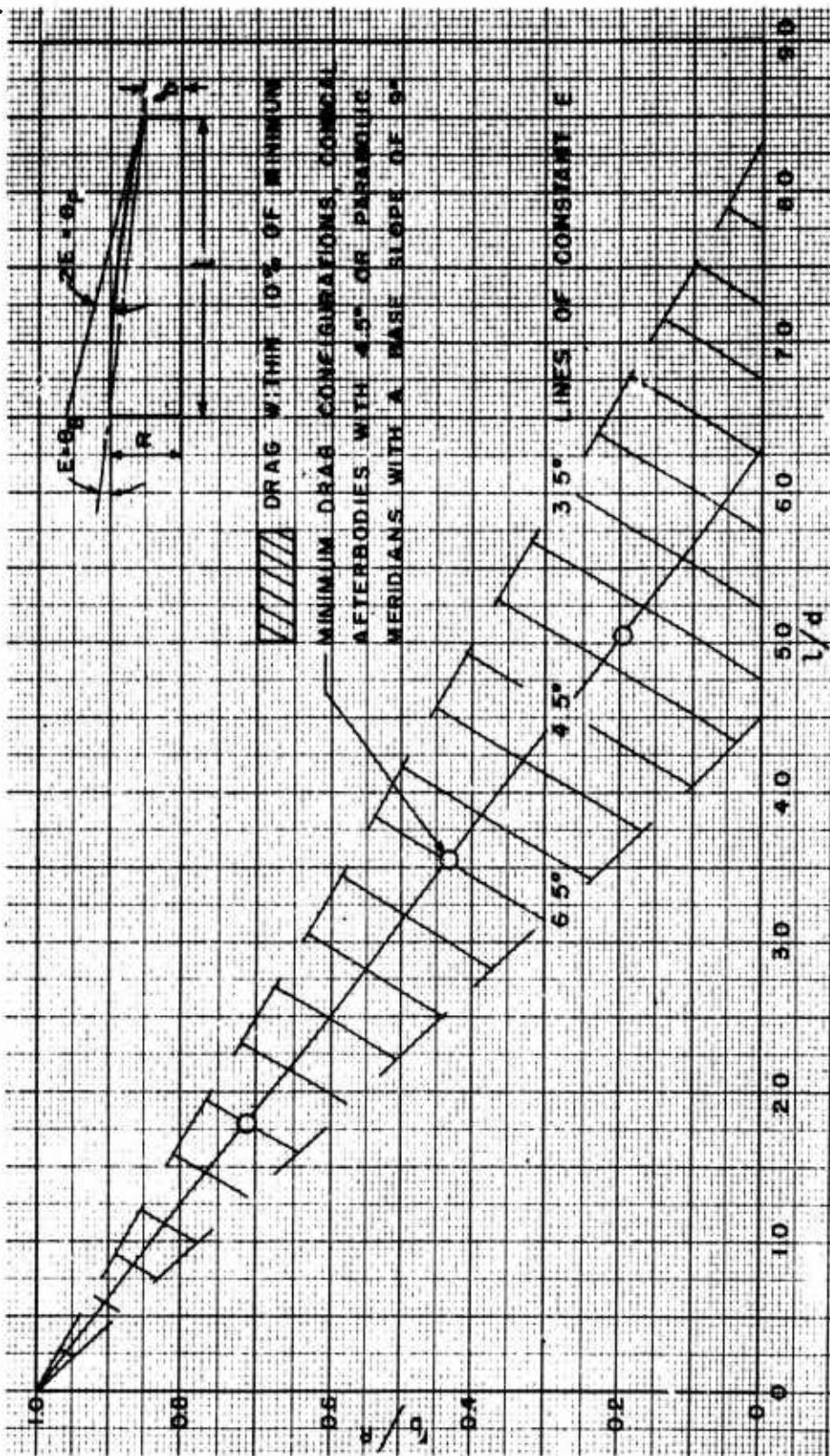


Fig (2.6-11) Configurations for minimum afterbody drag at  $M = 1.2$   
 Ref (2.6-36)

TABLE (2.6-2)

Model	$K=LN/L$	Total L/D length (diam.)	Afterbody length $L_T/D$ (diam.)	Forebody length $L_N/D$ (diam.)
1	0.40	6.04	5.62	2.42
2	0.40	8.91	5.35	3.56
3	0.60	17.78	7.11	10.67
4	0.40	12.50	7.50	5.00
5	0.60	24.50	9.80	14.70

Geometrical data for models tested in ref (2.6-26)  
See fig (2.6-10)

TABLE (2.6-3)

M	Errors of Measurement		
	M	$C_{Dob}$	$C_{pb}$
1.4	.005	.005	.008
1.1	.005	.007	.015
0.8	.005	.010	.030

Accuracy of measurements in Ref (2.6-26)  
See fig (2.6-10)

(2.6-11).

(v) Tail Fins Interference Effects,  
 $\Delta C_{Dob(F)}$

The presence of fins at the rear end of a body of revolution may or may not have an appreciable effect on the base pressure, depending upon the simultaneous interplay of the following primary influential variables:

- (1) Free stream Mach Number,  $M_\infty$ ,
- (2) Number of fins,  $N$ ,
- (3) Fin airfoil section,
- (4) Fins location,  $(x/c)_F$ ,
- (5) Fin thickness ratio,  $(t/c)_F$ ,
- (6) Fin height-body diameter ratio,  $(h_{FEXP}/D)$ ,
- (7) Finsweep-back,  $\Delta_{LE}$  and  $\Delta_{TE}$ ,
- (8) Body shape at fin's location (boattailing).

Relatively few experimental investigations of the fin interference effects, separated explicitly from the bulk-base drag measurements, are available, see Refs. (2.6-17) (Faro), (2.6-20) (Love), (2.6-22) (Hill), (2.6-24) (Hart), (2.6-30) (Spahr and Dickey), (2.6-36) (Stoney). The data are not systematized regarding the various influential factors mentioned previously, and in most cases only qualitative general conclusions may be derived for direct design purposes.

Expressed in terms of the total base pressure drag, the relative increase or decrease due to fin interference effects does not exceed  $\pm 10\%$  in the worst case, see Ref (2.6-11) (Love). Besides, since "jet-pump" effects may have a far bigger influence (up to 75%), and since they may be estimated only very roughly (as shall be seen later), it can be argued that the approximate method for fin-interference effects as proposed in Ref (2.6-11) is sufficiently accurate for engineering estimates. The experimental evidence supports fairly well the data for  $M > 1.5$ , and the overall sacrifice of accuracy is but a negligible percentage of the total base drag, as compared with a more sophisticated approach in fin-effect estimates.

For a more detailed explanation of

the proposed procedure for fin-interference predictions as specified below, the Ref. (2.6-11) by Love should be consulted.

In order to generalize and unify the effects of the various influential factors as related to fin effects, a basic reference configuration, which predominates in most experimental investigations, Refs. (2.6-17), (2.6-22), (2.6-30), have been chosen.

- A cylindrical body with an ogival nose and four ( $N=4$ ) equally spaced 10% thick fins of circular-arc sections and rectangular planforms. The ratio of fin span to body diameter is

$$(b_F/D) = (2 h_{FEXP} + D)/D = 3.5, \quad (2.6-6)$$

where  $h_{FEXP}$  is the individual fin height. The ratio of fin thickness to body diameter is

$$\left(\frac{t_F}{D}\right) = .15. \quad (2.6-7)$$

The trailing edges of the fins are flush with the cylindrical base. The boundary layer is turbulent.

For this basic configuration, the effect of the four ( $N=4$ ) fins, flush with the body base, are presented in Fig (2.6-16), as  $\Delta C_{Dob(F)REF} = (\Delta C_{Dob(FINTER)})_{REF}$  versus Mach Number. The plotted curve is a mean average from the theoretical results of Ref(2.6-11) by Love and the experimental results of Ref (2.6-30) by Spahr and Dickey, and free flight tests of Ref (2.6-17) by Faro.

Any other combination of the influential parameters, differing from the "reference" configuration, would then have the following changed effects:

- (1) A variation in number of fins ( $N$ ), all other data constant, shall proportionally change the fin interference effects, i.e., in a first approximation, based on data from Ref. (2.6-30):

$$\left[\Delta C_{Dob(F)}\right]_N = .2 \left[\Delta C_{Dob(F)}\right]_{REF} \times (N+1), \quad (2.6-8)$$

for  $N \geq 1$ ,

$$\therefore \left[\Delta C_{Dob(F)}\right]_N = .2 \left[\Delta C_{Dob(F)}\right]_{REF} \times (N+1) \left(\frac{D_B}{D}\right)^2 \quad (2.6-9)$$

with  $S_r = \pi D^2/4$ .

- (2) A variation in fin span-body

diameter ratio ( $b_F/D$ ) shall, in a first approximation, proportionally change the fin interference effects (all other data constant) as:

$$[\Delta C'_{Dob(F)}]_{(b_F/D)} = \frac{b_F}{3.5D} [\Delta C'_{Dob(F)}]_{REF} \quad (2.6-10)$$

$$\therefore [\Delta C_{Dob(F)}]_{(b_F/D)} = \frac{b_F}{3.5D} [\Delta C'_{Dob(F)}]_{REF} \times \left(\frac{D_B}{D}\right)^2 \quad (2.6-11)$$

with  $S_r = \pi D^2/4$ .

(3) A decrease in fin airfoil thickness ratio,  $(t/c)_{FIN}$ , all other data constant, decreases the base pressure coefficient value, but the effect is of a diminishing trend with increase of Mach Number. A semi-empirical variational law is presented in Fig (2.6-17) from Refs. (2.6-11) and (2.6-30) as:

$$[\Delta C'_{Dob(F)}]_{(t/c)_F, \Lambda_{FLE}=0} = f \left[ (t/c)_F, M_\infty \right] \quad (2.6-12)$$

Note that it has a negative value.

(4) The effect of sweep-back,  $\Lambda_{FLE}$ , is to decrease the fin interference effects upon the base pressure, since the thickness ratio of the fin parallel to the cylindrical body surface is effectively reduced through the relative increase of the fin's chord. Within a first approximation then, assuming a given absolute fin airfoil thickness,  $t_F$ , the reduction of the fin effects of a swept-back planform compared to the basic reference configuration may be estimated from:

$$[\Delta C'_{Dob(F)}]_{(t/c)_F, \Lambda_{FLE}} = [\Delta C'_{Dob(F)}]_{(t/c)_F, \Lambda_{FLE}=0} \times \cos \Lambda_{FLE} \quad (2.6-13)$$

$$[\Delta C_{Dob(F)}]_{(t/c)_F, \Lambda_{FLE}} = [\Delta C'_{Dob(F)}]_{(t/c)_F, \Lambda_{FLE}=0} \times \cos \Lambda_{FLE} \times \left(\frac{D_B}{D}\right)^2 \quad (2.6-14)$$

with  $S_r = \pi D^2/4$ .

(5) The effect of the position along the cylindrical body of the trailing edge of the fin root is very pronounced. In Ref (2.6-11) by Love, the empirical results from Ref (2.6-30) (Spahr) and the semi-empirical calculations based on three different methods are summarized for the earlier defined "reference"

missile configuration. Using these data, a convenient replot of the mean average values is presented in Fig (2.6-18) in the form of an incremental base drag coefficient:

$$[\Delta C'_{Dob(F)}]_{(x/\bar{c})_F} = f \left[ \left(\frac{x}{\bar{c}}\right)_F, M \right] \quad (2.6-15)$$

$$\therefore [\Delta C_{Dob(F)}]_{(x/\bar{c})_F} = [\Delta C'_{Dob(F)}]_{(x/\bar{c})_F} \left(\frac{D_B}{D}\right)^2 \quad (2.6-16)$$

where  $(x/\bar{c})_F$  is the relative actual fin position in fractions of the fin root chord along the body axis, measured from the reference "flushed" configuration ( $x=0$ ), with  $x$  positive for fin shifts forward, and negative for fin shifts backward into the dead-air region. From the results in Fig (2.6-18), it can be seen that the effect of the fin position becomes increasingly negligible for  $M > 2.5$ .

(6) Using a simple linear superposition law, the approximate expression for the total fin interference base drag increments, as produced by variations specified from (1) to (5), takes the form:

$$\Delta C_{Dob(F)} = [\Delta C_{Dob(F)}]_{(t/c)_F, \Lambda_{FLE}, N, (b_F/D), (x/\bar{c})_F}$$

$$\therefore \Delta C_{Dob(F)} = \left\{ [\Delta C'_{Dob(F)}]_{REF} + [\Delta C'_{Dob(F)}]_{(t/c)_F, \Lambda_{FLE}=0} \times \cos \Lambda_0 + [\Delta C'_{Dob(F)}]_{(x/\bar{c})_F} \right\} \times .2(1+N) \times \left(\frac{b}{3.5D}\right) \left(\frac{D_B}{D}\right)^2 \quad (2.6-17)$$

where  $(t/c)_F$ ,  $(\Lambda_{FLE})$ ,  $(N)$ ,  $(b_F/D)$  and  $(x/\bar{c})_F$  are the actual values of the fin airfoil thickness, the angle of fin leading edge sweep back, the number of fins, the fin span-body diameter ratio and the fin position with respect to the body base in terms of the fin mean geometric chord, respectively. The related value of  $(\Delta C'_{Dob(F)})_{REF}$ ,  $(\Delta C_{Dob(F)})_{(t/c)_F, \Lambda_{FLE}=0}$ , and  $(\Delta C_{Dob(F)})_{(x/\bar{c})_F}$  should be obtained from Figs (2.6-16), (2.6-17) and (2.6-18).

In the above expression (2.6-17), the effects of airfoil shape and body shape at the fin position (boattailing) are assumed negligible. This approximate expression is applicable for ( $M > 1.5$ ). For lower Mach Number values, ( $M < 1.5$ ), the results of the fin-interference on base pressure for  $(x/\bar{c})_F = 0$

tend to level off, since the leading edge shock wave nears detachment, and interferences from the shock waves on opposite fins occur.

Note that Eqs (2.6-8) to (2.6-17) are necessarily reduced to the common reference area,  $S_r = \pi D^2/4$ .

(vi) Jet Effects on Afterbody Drag Component,  $\Delta C_{DobJET}$ .

There are no generalized theoretical methods for predicting jet effects on the afterbody drag component as encountered in all its complex missile configurations and varying flight regimes. The experimental data are still limited and insufficient for a reliable unification of all of the influential factors in the form of generalized charts for direct design application. The quantitative method proposed herein is, therefore, very approximate and based mostly on the empirical evidence presented in Ref. (2.6-37) by Cortright and Kochendorfer.

Since in preparing the "working" graphs, a broad extrapolation and an averaging of the few reliable data are performed, the accuracy of the proposed predictions regarding jet effects is uncertain. It is hoped, nevertheless, that the general qualitative trend is preserved in accordance with experimental evidence.

The jet effects, influencing both the base drag proper and the pressures on the rear portions of the body, change completely the rear flow pattern. Therefore, it is considered convenient to investigate the two effects combined, i.e., as a total "afterbody" drag coefficient change due to jet effects, with the term ( $\Delta C_{DobJET}$ ) nominally included in the "base drag" equations, see Section 2.6.4.

For the engine-in-fuselage configuration, the main flow and geometric parameters influencing the afterbody drag through the jet-stream pressures are denoted in the illustrative Fig (2.6-12):

- The boattail angle,  $\theta_B$ , or afterbody contour,
- The diameters of the body,  $D$ , of the base,  $D_B$ , and of the nozzle exit,  $D_N$ ,
- The free stream static pressure,  $p_\infty$ , the boattail static pressure,  $p$ , the pressure just ahead of the base,  $p_o$ ,

the base pressure,  $p_b$ , the jet static pressure,  $p_j$ , the jet total pressure,  $P_j$ , and the jet total temperature,  $T_j$ ,

- The nozzle exit angle,  $\epsilon_N^\circ$ , positive as in Fig (2.6-12),

- The basic representative nozzle configurations: convergent nozzle, convergent-divergent nozzle, ejector nozzle and nozzle with annular base bleed.

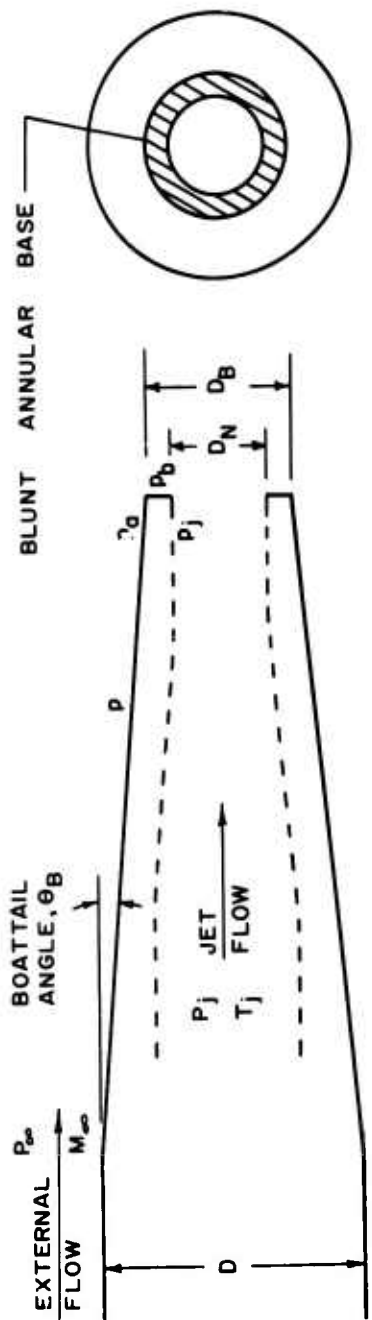
The convergent nozzle is the simplest to investigate, and therefore is taken as a basic reference in the jet-drag analysis. Effects of other, more complicated cases are then expressed as incremental terms in a way similar to that used for the fin interference investigations.

The convergent-divergent or ejector nozzles are used mostly for higher Mach Numbers, in order to yield a maximum thrust potential. As the engine design pressure ratio increases, the ratio of exit diameter,  $D_N$ , to throat diameter,  $D_T$ , of a convergent-divergent nozzle must be increased respectively. Secondary air flow in an ejector nozzle is introduced to cushion the expansion of the primary stream. With blunt annular bases, the air is sometimes discharged into the low pressure region through an air-bleed in order to reduce the base drag.

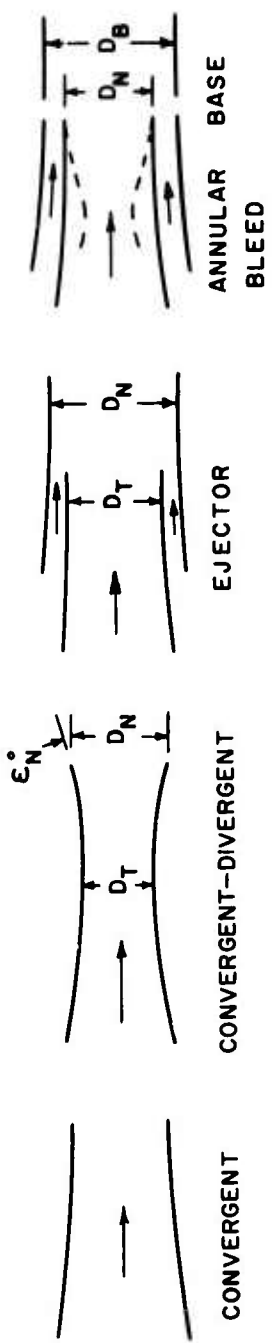
Jet effects on boattail pressure drag,  $\Delta C_{DobBT(JET)}$ .

A qualitative illustration of expanding jet effects on flow deflection for a conical afterbody with a convergent nozzle is presented in Fig (2.6-13). The boundary layer-shock wave interaction results in the boundary layer thickening with an accompanying pressure rise and a subsequent formation of compressible waves ahead of the trailing shock wave.(37) For higher jet to static pressure ratios, ( $p_j/p_\infty > 1$ ), the increased jet stream expansion may cause flow separation from the boattail. Thus, the pattern of the pressure changes at the boattail surface depend on many factors. Some of them are illustrated in Fig (2.6-13). Qualitatively, the following conclusions may be summarized, (Cortright and Kochendorfer(37) and Cabbage(38):

- (1) In case of no jet, for conical afterbodies of a fixed base-to-body diameter ratio, an increase in boattail angle increases considerably the boattail pressure at supersonic speeds.



(a) TYPICAL AFTERBODY.



(b) NOZZLE CONFIGURATIONS.

FIG.(2.6-12) SKETCH OF TYPICAL AFTERBODY AND SEVERAL NOZZLE CONFIGURATIONS.

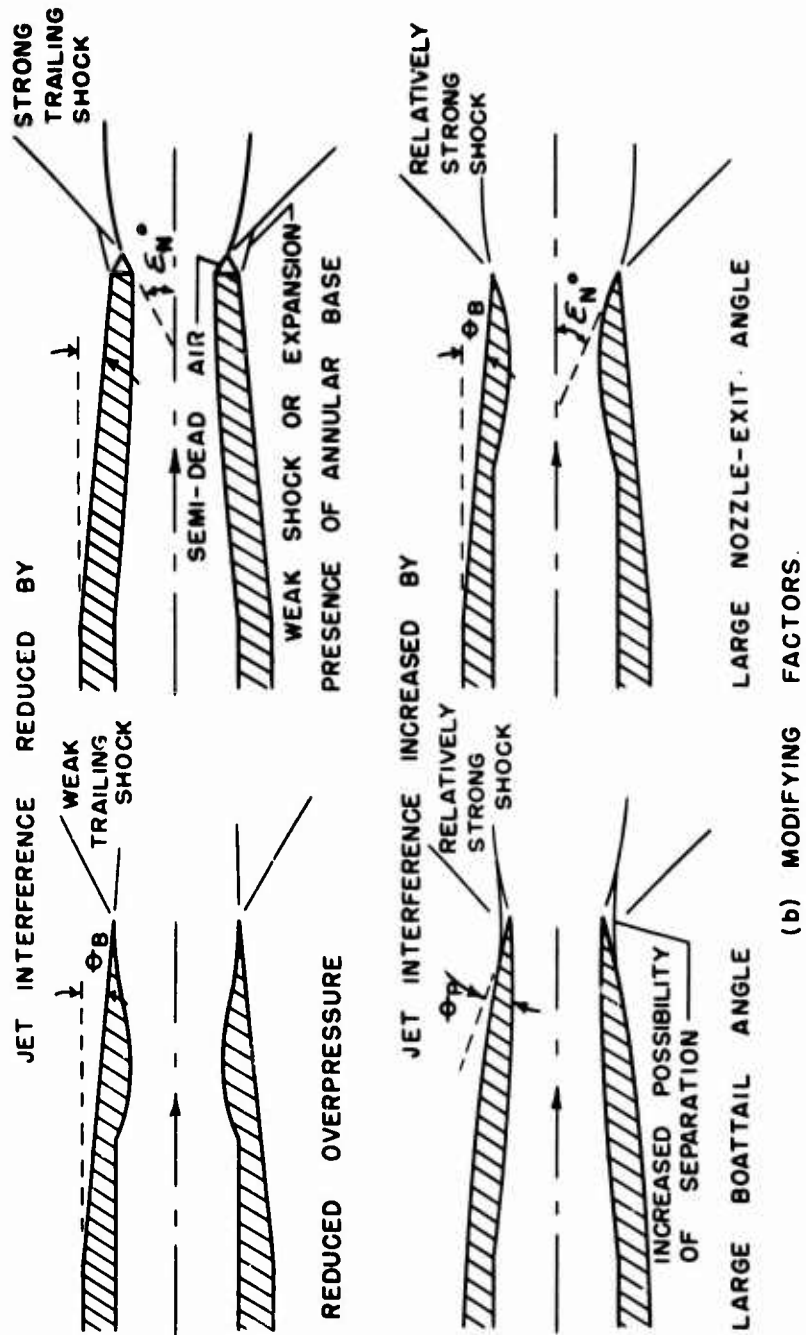


FIG. (2.6-12) CONCLUDED. JET EFFECTS ON BOATTAIL PRESSURES.

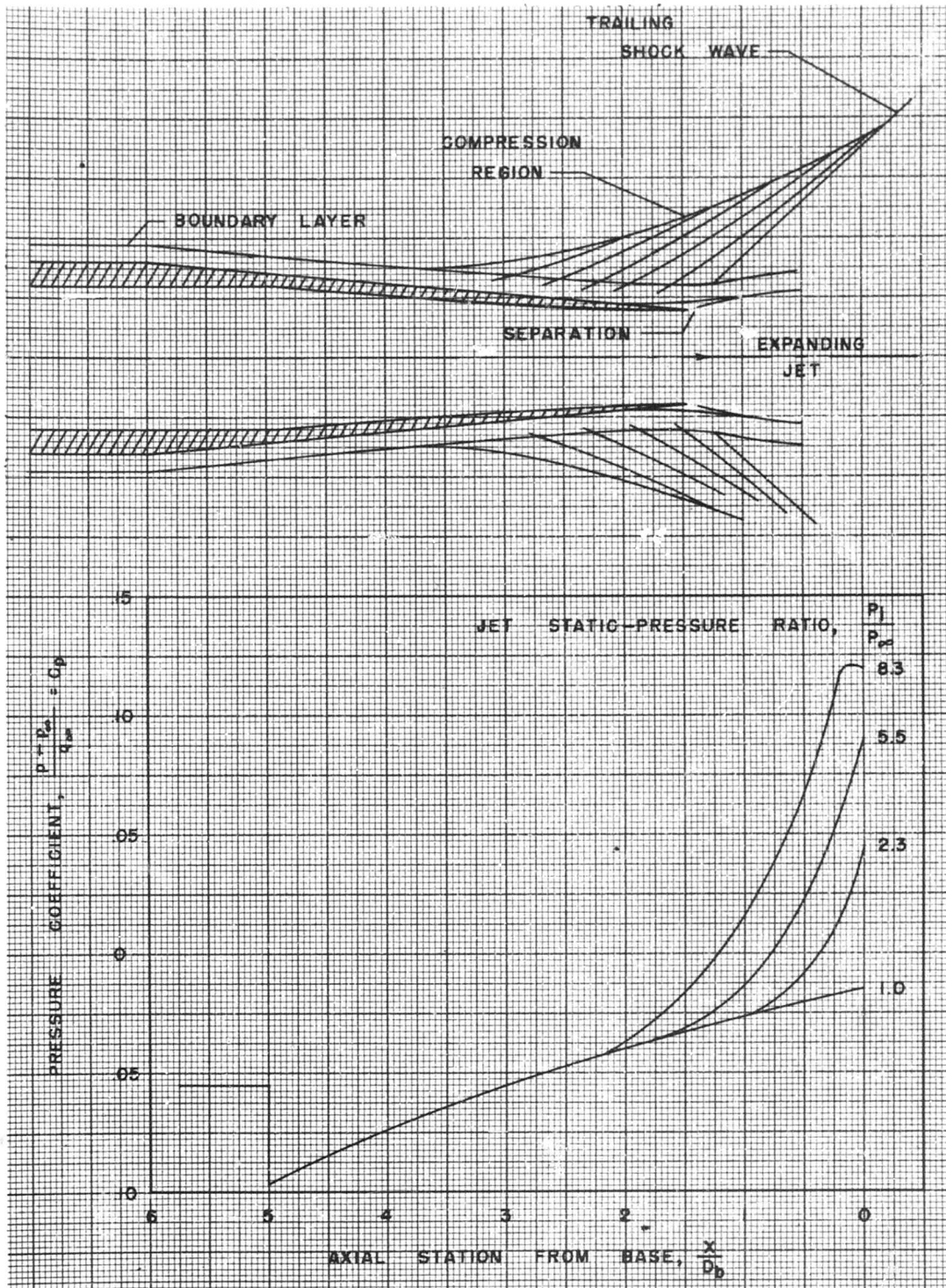


Fig (2.6-13) Jet effects on boattail pressures Typical case; free-stream Mach Number: 1.9; boattail angle, 5.6°. Ref (2.6-37)

(2) In case of a jet stream, issuing from a convergent nozzle having a zero exit angle, there is a beneficial jet interference that reduces the boattail pressure drag. This favorable effect increases with increase in boattail angle and jet-free stream pressure ratio. As a result, the boattail pressure drag, in general, decreases with jet interference. For parabolic afterbodies with higher sloping angles, this boattail pressure drag reduction due to jet interference is appreciably greater than for conical after-bodies under the same conditions, see Fig (2.6-15).

(3) The favorable jet interference effect in reducing the boattail pressure drag becomes greater with an increase of nozzle exit angle,  $\epsilon_N^0$ , for both the convergent and the convergent-divergent nozzles.

Combined jet effects on afterbody drag,

$$[\Delta C_{DOPBT(JET)} + \Delta C_{DOPD(JET)}] = \Delta C_{DOPJET}$$

From the experimental and the semi-empirical data presented in Refs. (2.6-37) (Cortright), (2.6-38) (Cubbage), (2.6-39) (Judd), (2.6-40) (Henry), (2.6-12) (Cortright) and (2.6-25) (Peck), the important conclusions regarding the base and the afterbody (base + boattail) drag can be summarized as follows, keeping in mind that here an increase in base pressure means a corresponding decrease of the base drag, and noting that for boattail pressure drag the opposite is true:

(1) At high subsonic speeds the boattail angle of conical afterbodies for minimum afterbody drag coefficient is in the range between  $50^\circ$  to  $80^\circ$ . At supersonic speeds the optimum boattail angle is in the range from  $2.50^\circ$  to  $50^\circ$ . The optimum values are not affected significantly with pressure variations.

(2) There is a marked difference in jet effects on base pressures at subsonic and supersonic speeds:

At subsonic speeds, for small base annuli,  $(D_B/D_N) < 1.5$ , a relatively strong increase in base pressure occurs with an increase in the jet-free stream pressure ratio, while for larger base annuli,  $(D_B/D_N) > 2.0$ , a strong decrease in base pressures accompanies the jet-free stream pressure ratio increase.

At relatively low supersonic speeds, ( $M \approx 2.0$ ), there is a pronounced increase in base pressures with increase

of the jet-free stream pressure ratio, the lower  $(D_B/D_N)$  value annuli experiencing a sharper trend of the pressure increase.

At higher supersonic speeds, ( $M > 3$ ), the jet effects on base pressures are appreciably reduced for all jet-free stream pressure ratios and annuli thicknesses.

(3) There are no essential differences in the above trends between the convergent and the convergent-divergent nozzles designed for a jet-free stream pressure ratio from 10.5 to 50. The absolute base pressure values are slightly higher for the convergent-divergent nozzles.

(4) A change in the afterbody geometry does not alter the above basic trends, provided the flow remains un-separated over the boattail, but the absolute values of the base pressure are changed.

(5) An increase in the nozzle exit angle,  $\epsilon_N^0$ , increases both the annular base pressure and the boattail pressure through an increased strength of the trailing shock.

(6) An increase in the jet temperature increases the base pressure value. Therefore, the use of experimental data with an unheated air jet is somewhat conservative regarding base drag estimates. An analysis of the temperature effects is complex, since the jet shape and its mixing with free stream are influenced by variations of the jet total temperature,  $T_j$ , the specific heat ratio,  $\gamma_j$ , and the gas constant,  $R_j$ .

(7) The Reynolds Number variation has but small effect on the base pressure and the jet interference effects, provided the boundary layer at the base is turbulent.

(8) The base drag can be appreciably reduced by use of an annular base bleed, see Refs. (2.6-41), by Cortright and Schroeder, and (2.6-42) by Hebrank, especially with convergent-divergent nozzles, which otherwise exhibit the highest blunt-base drag.

With an annular base bleed, the base drag coefficient, as referred to the annular base area, is a sum of three terms:

- the base drag due to base pressure,

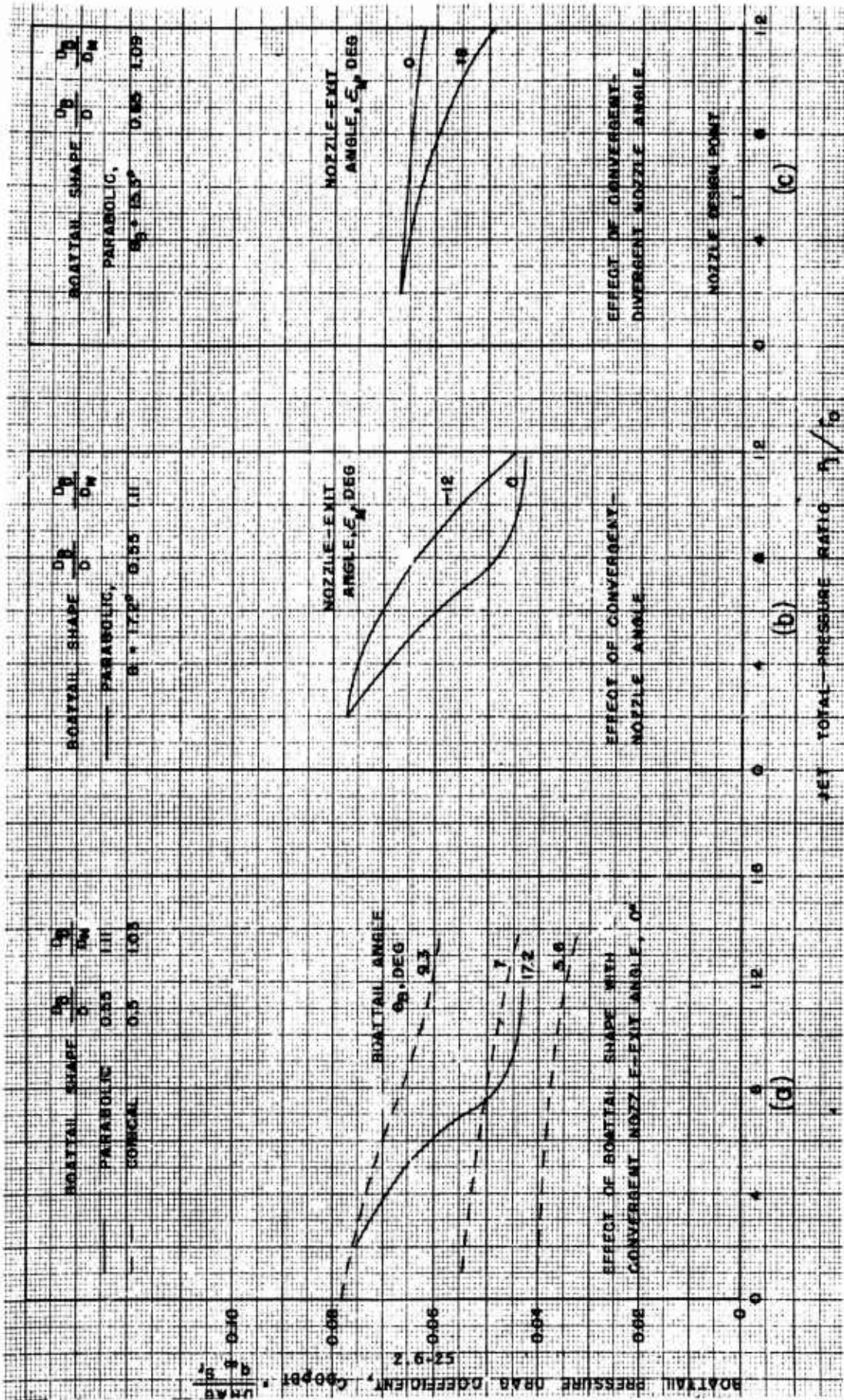


Fig (2.6-14) Jet effect on boattail pressure drag at free-stream Mach Numbers of 1.9 to 2.0  
 Ref (2.6-37)

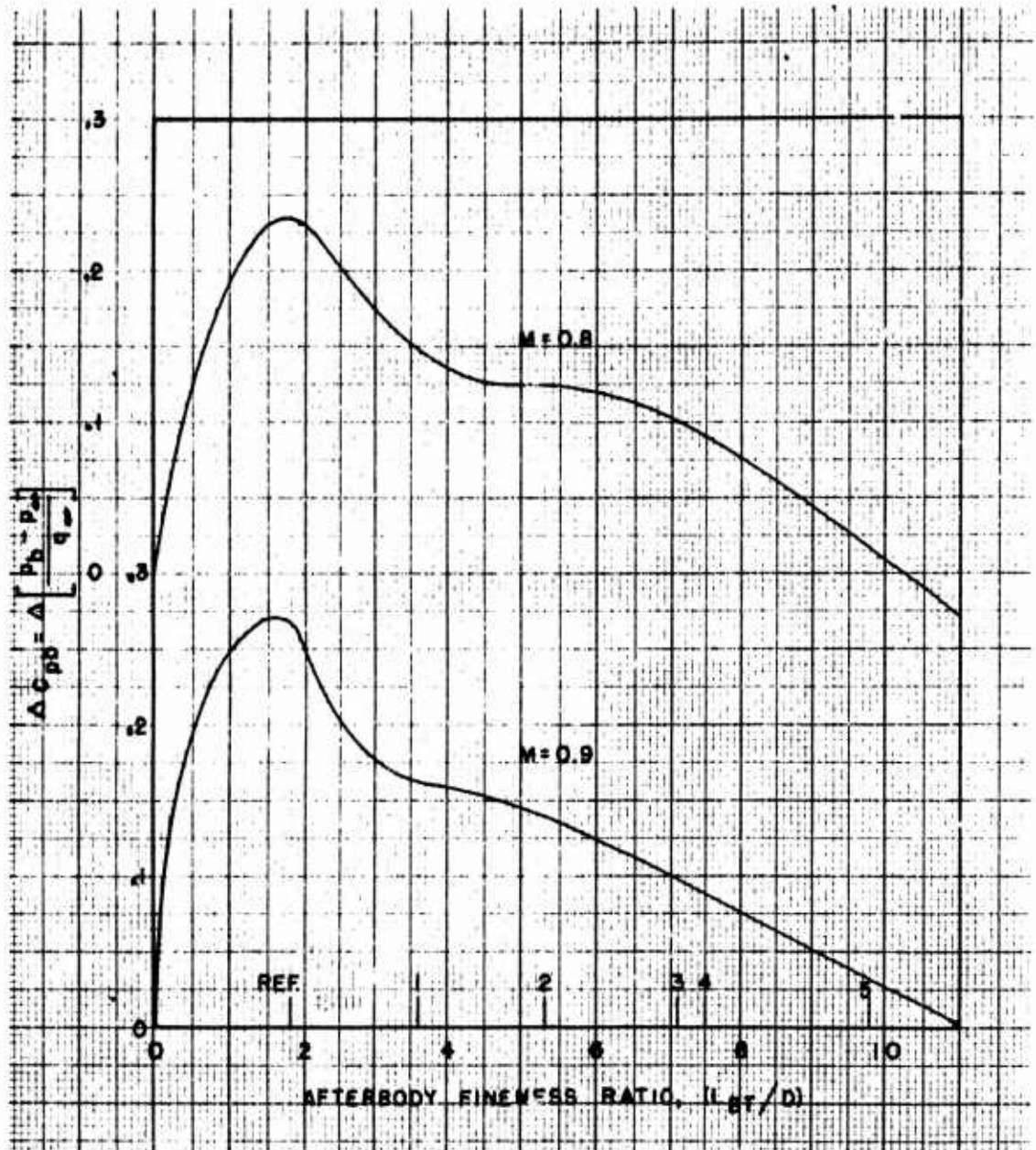


Fig (2.6-15) Base pressure increment for parabolic afterbodies at zero angle-of-attack transonic speeds. Rearranged from Ref (2.6-26)

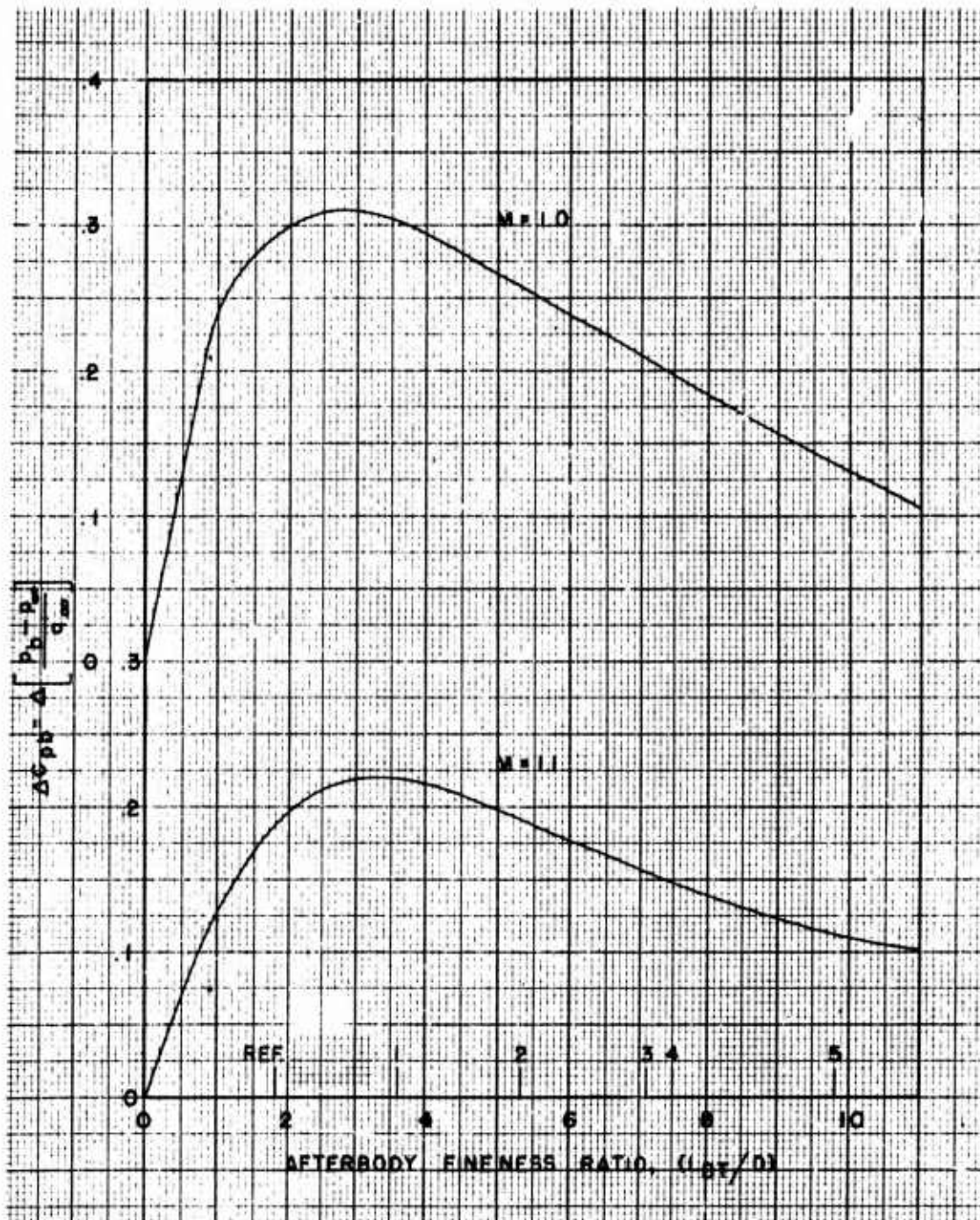


Fig (2.6-15) Continued (1)

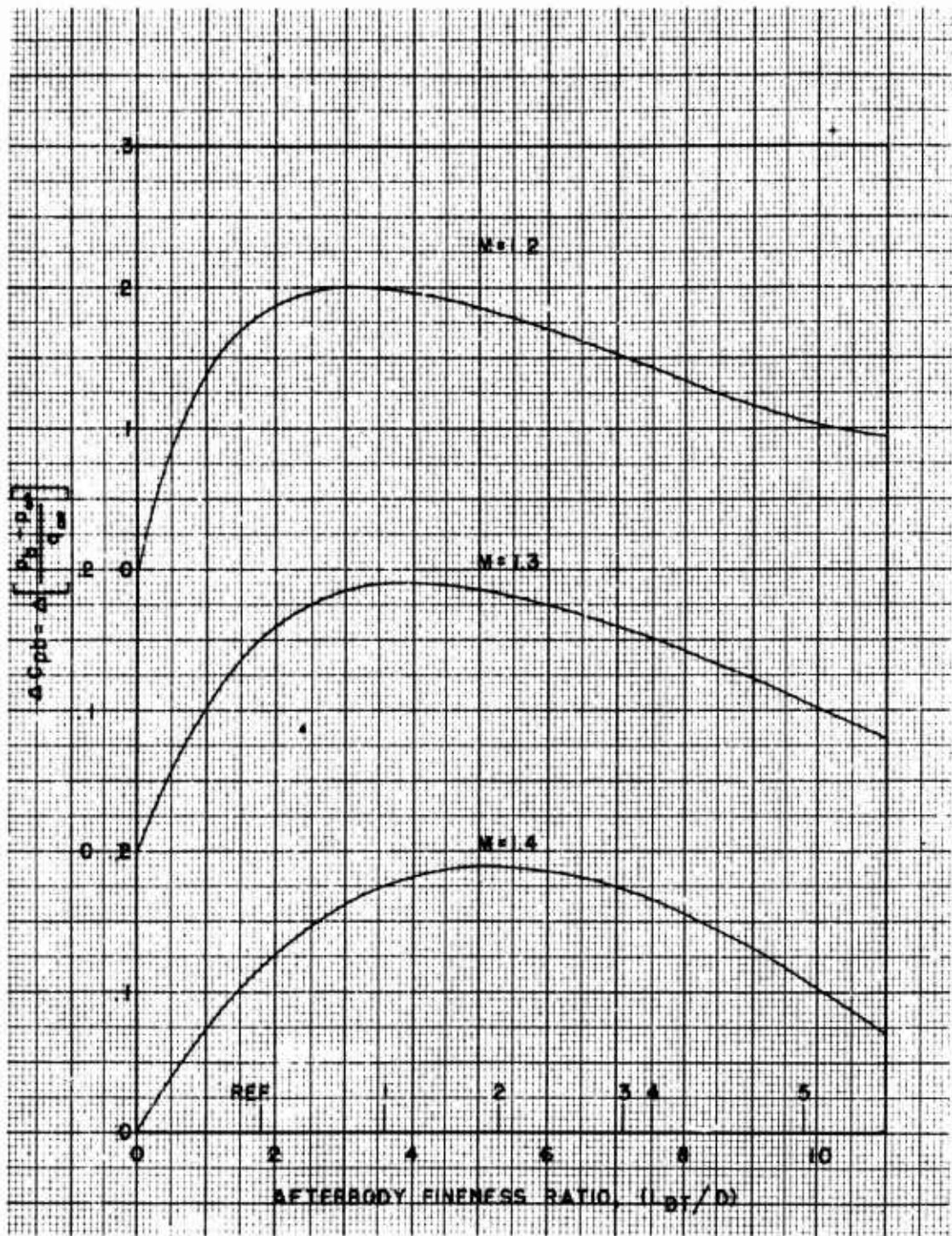


Fig (2.6-15) Continued (2)

- the base drag (reduction) due to exit momentum,

- the base drag (increment) due to free-stream inlet momentum.

With all the three terms present, there will be only a small initial reduction in drag for lower mass-flow values, followed by an increase (that later tends to level out) for larger mass flows. Thus, only if the bleed air is taken from some low energy source, and not by free-stream inlet, can the beneficial effect of the annular base bleed concept be realized.

Quantitative estimates of the various influential factors, described briefly above, are presented in the next Section, 2.6.4, for the respective experimental data that have been found available in the unclassified literature.

(vii) Trailing Edge Base Pressure,  
 $C_{DDBWTE}$  and  $C_{DDBFTE}$  .

The blunt trailing-edge airfoil data by Chapman, Windrow and Kester<sup>(7)</sup> for Mach Numbers up to 3.0, and the data by Syvertson and Gloria<sup>(32)</sup> for Mach Numbers between 2 and 5, can be used as a basis in evaluating the trailing-edge bluntness pressure drag increment for engineering purposes. When expres-

sing the base-pressure for airfoils, the reference pressure is ( $p' = p_\infty$ ) as stated later. A summary of the experimental data, including Reynolds Number effects, are presented in Figs (2.6-4), (2.6-5) and (2.6-21).

By comparing data from Fig (2.6-5) for airfoil base pressures and Fig (2.6-3) for base pressures of cylindrical bodies without boattailing, the following conclusions may be deduced:

(1) An increase in Mach Number causes a very sharp decrease in base pressure values for both cylindrical bodies and airfoils.

(2) The relative boundary layer-thickness ratio,  $(\delta/t_B)$ , where  $(t_B)$  is the trailing edge thickness, expressed conveniently through the boundary layer thickness parameter,  $c/(t_B Re^{.2})$ , for turbulent boundary layers shows no appreciable effect on base pressures for  $(M < 2)$ , but the influence becomes pronounced for  $(M > 2)$ .

For cylindrical bodies, this effect is negligible.

It is of interest to note that for turbulent boundary layers the angle of attack influence on the base pressure is negligible up to  $\alpha = 5^\circ$ , see Ref (2.6-7).

## 2.6.4 THE PROPOSED METHODS FOR THE BASE DRAG COEFFICIENT EVALUATION

The governing equation is:

$$C_{Dob} = \left[ (C_{DobCYL} + \Delta C_{DobBT} + \Delta C_{Dob(FORE)} + \Delta C_{Dob(F)} + \Delta C_{DobJET}) + (C_{DobWTE} + C_{DobFTE}) \right] \quad (2.6-18)$$

As stated earlier, due to lack of a unified method of analysis of the base pressure problem in its general form (i.e., with all influential factors under actual flight conditions present simultaneously), a stepwise additive treatment of the base pressure estimates is proposed, according to the above analytical expression, (2.6-18), and the following scheme:

(1) Cone (ogive) + cylindrical body configuration, fully bluff base, no boattailing, no jet-pump or fin effects,  $C_{DobCYL}$ ,

(2) Additive boattailing effect for small or moderate boattail angles, ( $\theta_B < 15^\circ$ ),  $\Delta C_{DobBT}$ ,

(3) Additive jet-pump effect on the whole afterbody (boattail + base): underexpanded and overexpanded jets. Thermal effects on the base pressure value eventually accounted for,  $\Delta C_{DobJET}$ ,

(4) Additive fin-interference effects on base pressure,  $\Delta C_{Dob(F)}$ ,

(5) Wing and fin trailing edge bluntness effects,  $C_{DobWTE} + C_{DobFTE}$ .

Note: The Figures and Tables, mentioned in the text, are compiled at the end of this Section, 2.6.4.

### (i) Basic assumptions:

In addition to the general assumptions of the "quasi-steady" flow conditions for symmetrical flight cases, pertinent to the whole drag

analysis in this paper, the following specific assumptions in computing the base drag term are introduced:

(1) For wing (fin) trailing edge base pressure estimates, the two-dimensional airfoil data are used. Three-dimensional tip-effects are thus neglected, since the error is negligibly small for engineering applications.

(2) The semi-empirical axially symmetric flow data are used for bodies with or without boattailing. The accuracy of the data is within limitations of the respective theories, as discussed in Section 2.6.5.

(3) The "jet-pump" and the fin-interference effects are estimated on a rather scarce empirical evidence. The accuracy of the proposed charts could not be established; nevertheless, it is expected that the presented data fit fairly well within the limited range of Mach and Reynolds Numbers.

(4) A turbulent boundary layer at the rear portions of all wetted areas is presumed. The boundary layer transition effects on base pressure are considered negligible. The estimates are thus but slightly conservative, since the transition point is well forward for the actual average missile atmospheric flight conditions and the usual manufacturing tolerances.

(5) The body fineness ratios greater than 5 are presumed, rendering nose-cone interference effects on base pressure values negligibly small.

(6) The angle-of-attack and the rarefied (higher altitude) gas effects are not considered. Their effects may be evaluated according to the methods presented in Section 2.4.

(7) Mach Number effects are fully accounted for. Relatively insignificant Reynolds Number effects are neglected for bodies with relatively thin boundary layers,  $(\delta/D) \ll 1$ , but they are fully taken into account for thin airfoils,  $(\delta/t) \sim 1$ .

### (ii) Cone (ogive) Plus Cylindrical Body Without Boattailing, $C_{DobCYL}$ .

Love's<sup>(11)</sup> and Chapman's<sup>(5)</sup> semi-empirical data for cylindrical bodies

of revolution with turbulent boundary layers are used. The working graph, Fig. (2.6-19), represents the average values from the two references for ( $M > 2$ ) and a mean value of experimental data for ( $0 \leq M < 2$ ). The wind tunnel and the free-flight base pressure measurements on models of fineness ratios greater than 5 with fully developed turbulent boundary layers show an agreement with the proposed base drag curves within  $\pm 5\%$  for ( $M > 1.2$ ).

The applicability of the graphs is restricted to bodies of revolution with nose cones (ogives) of a fineness ratio ( $L/D$ ) greater than 5. Under these conditions, nose cone interference effects on base pressure values are negligibly small.

The base drag coefficient, reduced to the reference area,  $S_r = (\pi D^2)/4$ , is then readily obtained from:

$$C_{D0bCYL} = -\left(\frac{P_b - P_\infty}{q_\infty}\right) = -C_{pb} \quad (2.6-19)$$

(iii) Boattail Effects on Base Pressure Drag,  $\Delta C_{D0bBT}$

Both for conical and for parabolic boattails, the respective decrease in base pressure drag can be obtained with an acceptable accuracy from the simple empirical expression, Ref. (2.6-36) (Stoney) and (2.6-18) (Hoerner):

$$\Delta C_{D0bBT} = C_{D0bCYL} \left[ \left(\frac{D_B}{D}\right)^3 - 1 \right] \quad (2.6-20)$$

$$\therefore C_{D0bCYL} + \Delta C_{D0bBT} = C_{D0bCYL} \left(\frac{D_B}{D}\right)^3 \quad (2.6-21)$$

where  $\Delta C_{D0bBT}$  represents a decrease in base pressure drag value, and ( $D_B$ ) and ( $D$ ) are the base and the cylinder diameters respectively.

The applicability of Eq (2.6-21) is restricted to afterbody cone angles ( $\theta_B < 7.5^\circ$ ) i.e., to parabolic afterbody base tangent slopes of ( $\theta_B < 15^\circ$ ). Within the restriction the agreement with experimental evidence is good both for supersonic and subsonic speeds.

For transonic speeds, ( $.8 < M < 1.4$ ), the experimental data from Ref (2.6-26) (Katz) can be used, see Fig (2.6-15) for both parabolic and conical afterbodies in a first approximation:

$$\Delta C_{D0bBT} = -\Delta C_{pb} \left(\frac{D_B}{D}\right)^2 \quad (2.6-22)$$

reduced to the reference area  $S_r = (\pi D^2)/4$ .

(iv) Fins Interference effects,  $\Delta C_{D0b(F)}$

The interference effects due to the fin location, the number of fins, the fin airfoil thickness ratio, fin height-body diameter ratio, the fin leading edge sweepback angle and the free stream Mach Number on the base drag coefficient value are estimated by a generalization of the empirical and semi-empirical data from Refs. (2.6-11) (Love), (2.6-17) (Faro), (2.6-22) (Hill), (2.6-30) (Spahr and Dickey), (2.6-24) (Hart). A reference configuration for which most of the data are available was necessarily chosen to serve as a common basis in presenting the generalized data. This reference configuration is:

- A cylindrical body with an ogival nose and four equally spaced 10% thick fins of circular-arc sections and of a rectangular planform. The ratio of the fin span-to-body diameter is 3.5. The fin trailing edges are flush with cylindrical base. The boundary layer is turbulent.

The fin interference effects for this reference configuration are presented graphically in Fig (2.6-16) in the form of a base drag coefficient increment,

$$\left[ \Delta C'_{D0b(F)} \right]_{REF} = - \left[ \Delta C_{pb(F)} \right]_{REF} = f(M_\infty) \quad (2.6-23)$$

$$\therefore \left[ \Delta C_{D0b(F)} \right]_{REF} = \left[ -\Delta C_{pb(F)} \right]_{REF} \left(\frac{D_B}{D}\right)^2 \quad (2.6-24)$$

which is properly reduced to the common reference area,

$$S_r = \pi D^2/4 .$$

Then, by specifying the influential parameters for any other design configuration, i.e., by defining:

( $t/c$ )<sub>F</sub> - the actual fin airfoil thickness ratio,

( $b_f/D$ ) - the actual total fin span-body diameter ratio, where  $h_{FEXP}$  is the height of one fin, i.e., ( $b_f/D$ ) = ( $2h_{FEXP} + D$ )/ $D$ ,

$N$  - the actual number of individual fins,

$\Lambda_{FLE}$  - the fin leading edge sweep-back

angle,

$(x/c)_f$  - the fin root trailing edge position along the cylindrical body, where  $(C_{r_f})$  is the fin root chord, and  $(x_f)$  is measured from the cylindrical base to the fin root chord trailing edge point, positive forward and negative for fin's shift backward into the dead air region of the wake. The above reference configuration value  $(\Delta C_{pb(f)})_{REF}$  from Fig (2.6-16) is subsequently corrected as follows, see Eq (2.6-17):

$$\Delta C_{Dob(f)} = -(\Delta C_{pb(f)})_{(t/c)_f, \Lambda_{FLE}, N, (b_f/D), (x/c)_f}, \quad (2.6-25)$$

$$\begin{aligned} \therefore \Delta C_{Dob(f)} = & .057(1+N)(b_f/D) [(-\Delta C_{pb(f)})_{REF} + \\ & + (\Delta C_{pb(f)})_{(t/c)_f, \Lambda_{FLE}=0} \times \cos \Lambda_{FLE} + \\ & + (\Delta C'_{Dob(f)})_{(x/c)_f} ] \left(\frac{D_B}{D}\right)^2, \quad (2.6-26) \end{aligned}$$

where

$$b_f = b_{FEXP} + D = 2h_{FEXP} + D,$$

$$[-\Delta C_{pb(f)}]_{REF} \text{ - from Fig.(2.6-16), a positive number,}$$

$$[\Delta C_{pb(f)}]_{(t/c)_f, \Lambda_{FLE}=0} \text{ - from Fig.(2.6-17), a negative number,}$$

$$[\Delta C'_{Dob(f)}]_{(x/c)_f} = [\Delta C_{Dob(f)}]_{(x/c)_f} \text{ - from Fig.(2.6-18), either positive, or negative.}$$

$$(2.6-27)$$

A more detailed interpretation of all the terms and corrective factors is given in Section 2.6.3. The airfoil shape and the boattailing effects on fin contributions to the base drag are neglected.

The proposed expression (2.6-26) is necessarily an approximate one, representing the mean average values replotted from the stated references. But, since absolute fin contribution is only a small percentage of the total base drag, the procedure is regarded as acceptable for Mach Numbers greater than 1.5. At lower speeds, ( $M < 1.5$ ), a leveling-off of the basic curves on Fig (2.6-16) occurs due to the leading edge shock detachment and the shock interferences from opposite fins.

#### (v) Jet Interference Effects on the Base and the Boattail Drag, $\Delta C_{DobJET}$

As stated earlier, the jet interference effects on the base and afterbody (base + boattail) drag coefficients depends on the following air flow and geometric parameters (see Fig 2.6-12):

(1) The boattail angle,  $\theta_B$ , and the afterbody contour (conical or parabolic).

(2) The diameters: of the body,  $D$ , of the base,  $D_B$ , and of the nozzle exit,  $D_N$ .

(3) The pressures: free stream ( $p_\infty = p_H$ ), boattail ( $p$ ), base ( $p_b$ ), jet static pressure ( $p_j$ ), jet total pressure ( $P_j$ ).

(4) The jet total temperature,  $T_j$ , the coefficient of specific heat ratio,  $\gamma_j$ , and the gas constant,  $R_j$ .

(5) The nozzle configurations: convergent, convergent-divergent, annular base bleed ejector nozzle, etc.

(6) The nozzle exit angle,  $\epsilon_N^\circ$ .

A quantitative analysis of the various factors is performed, based on the experimental evidence available, see Refs. (2.6-37), (2.6-38), (2.6-39). Due to scarcity of data, the accuracy of the proposed working charts are limited in value and only as good as the data themselves.

The jet effects influence considerably both the base drag proper and the pressures on the rear of the body, i.e., the boattail drag. It is therefore convenient to investigate the two effects combined. Thus, the total incremental drag term,

$$\Delta C_{DobJET} = [\Delta C_{DobBT(JET)} + \Delta C_{Dobp(JET)}], \quad (2.6-28)$$

in the Eq (2.6-18) represents the total "afterbody" (base + boattail) pressure drag coefficient change due to jet effects, computed as follows:

#### (1) Base Drag Coefficient Changes Due to Jet Effects, $\Delta C_{Dobp(JET)}$

The most consistent experimental data have been found for a convergent nozzle, which is the simplest to analyze. Therefore, in preparing the working graphs, the convergent nozzle

of an engine built-in in a conical afterbody of a relatively small (near optimum) boattail angle has been chosen as a basic reference configuration, assuming a cold jet. Effects of other flow and geometric parameters, different from the basic, are then expressed as additional corrective factors in a way similar to that used in the fin interference analysis.

In preparing the respective working graphs on Fig (2.6-20), many interpolations and extrapolations were involved due to the scarcity of actually measured data. Due care was taken to follow closely the existing qualitative trends in each case.

The basic reference configuration of a conical afterbody with a built-in convergent nozzle is specified by the following, see Figs (2.6-12) and (2.6-20):

$$\begin{aligned} \theta_B &= 5.6^\circ, \\ \left(\frac{D_N}{D}\right) &= .37, \\ \epsilon_N^\circ &= 0^\circ, \\ (D_B/D_N) &\text{ from 1.1 to 2.7,} \\ (p_j/p_H) &\text{ from 1 to 9} \end{aligned} \quad (2.6-29)$$

(a) The reference base pressure coefficient:

$$[(C'_{pb})_{JET}]_{REF} = \frac{p_b - p_\infty}{q_\infty}, \quad (2.6-30)$$

acting on the base annulus versus jet static pressure ratios ( $p_j/p_\infty$  from 1 to 9) is presented in Fig (2.6-20) for various base-to-nozzle diameter ratios ( $D_B/D_N$  from 1.1 to 2.7) and Mach Numbers of .9, 1.5, 2.0, 2.5, 3.0, and 4.0. The basic reference base drag coefficient, referred to the reference area,  $S_r = \pi D^2/4$ , is then:

$$\begin{aligned} [C_{DOPb(JET)}]_{REF} &= [(-C'_{pb})_{JET}]_{REF} \left[ \frac{D_B^2 - D_N^2}{D^2} \right] \\ &= f\left(\frac{D_B}{D_N}, M, \frac{p_j}{p_H}\right). \end{aligned} \quad (2.6-31)$$

For other intermediate Mach Number values, the interpolation should be used.

(b) Corrections for variations in the actual flow and geometry parameters in each individual case are performed

as follows:

- For different boattail angles,  $\theta_B \neq 5.6^\circ$ , of conical afterbodies, irrespective of the Mach Number, the  $p_j/p_H$  and the  $D_B/D_N$  ratios, an approximate correction by using the experimental data from Ref (2.6-37) (Cortright), gives:

$$[(C'_{pb})_{JET}]_{\theta_B} = \left\{ [(C'_{pb})_{JET}]_{REF} + .009 \theta_B^\circ - .05 \right\}. \quad (2.6-32)$$

- For both convergent and convergent-divergent nozzles an increase in the nozzle exit angle (from its zero-value) increases the base pressure coefficient, i.e., decreases the base drag. A mean corrective value is introduced on the basis of the experimental data presented in Ref. (2.6-37):

$$[(C'_{pb})_{JET}]_{\epsilon_N} = \left\{ [(C'_{pb})_{JET}]_{REF} + .0025 \epsilon_N^\circ \right\}. \quad (2.6-33)$$

- Effect of variation in the base-to-body diameter ratio, ( $D_B/D$ ), is automatically included in the basic curves, Fig (2.6-20), since for the given reference boattail angle, ( $\theta_B = 5.6^\circ$ ), and a constant ( $D_N/D$ ) ratio of .37, it follows that:

$$\frac{D_B}{D} = \frac{D_B}{D_N} \frac{D_N}{D} = .37 \frac{D_B}{D_N}. \quad (2.6-34)$$

No correction is thus needed.

- Effects of parabolic afterbodies, as compared with conical, should be confined to the boattail surface pressure drag changes. Regarding the base drag estimates, effects of parabolic afterbodies could be accounted for approximately by using for the boattail angle in the corrective expression (2.6-32), twice the value of ( $\theta_B$ ) for an inscribed conical afterbody, i.e.,

$$(\theta_P^\circ)_{PARABOLIC} = 2(\theta_B^\circ)_{CONICAL} \quad (2.6-35)$$

This relationship stems from the geometry of the afterbodies at the base.

- The corrections for convergent-divergent nozzles, as compared with the reference convergent nozzle, may be approximated by (37):

$$[(C'_{pb})_{JET}]_{CON-DIV} = \left\{ [(C'_{pb})_{JET}]_{REF} + .035 \right\}. \quad (2.6-36)$$

- The jet temperature effects are functions of the jet temperature,  $T_j$ , the specific heat coefficient,  $\gamma_j$ , the jet total pressure ratio,  $P_j/P_\infty$ , and the free stream Mach Number,  $M_H = M_\infty$ , for any given base-nozzle configuration. By using approximate mean values, an order of magnitude corrective factor may be formulated as:

$$[(C'_{pb})_{JET}]_{T_j} = \{[(C'_{pb})_{JET}]_{REF} + .2 \times 10^{-4} (T_j - T_H)\}, \quad (2.6-37)$$

where  $T_j$  and  $T_H$  are the jet and the ambient temperatures in  $^{\circ}F$  absolute, respectively.

- The Reynolds Number effects are negligible, see Ref (2.6-37).

Thus, taking all corrections into account the final expression for the base drag coefficient increment due to the jet effects becomes:

$$\begin{aligned} \Delta C_{Dopb(JET)} &= C_{Dopb(JET)} - [C_{DobCYL} + \Delta C_{Dob(BT)}], \\ \Delta C_{Dopb(JET)} &= C_{Dopb(JET)} - \{C_{DobCYL} + C_{DobCYL} \left[ \left( \frac{D_B}{D} \right)^3 - 1 \right]\}, \\ \therefore \Delta C_{Dopb(JET)} &= C_{Dopb(JET)} - C_{DobCYL} \left( \frac{D_B}{D} \right)^3, \end{aligned} \quad (2.6-38)$$

where:

$$\begin{aligned} [C_{Dopb(JET)}]_{CONV-DIV} &= - \left( \frac{D_B^2 - D_N^2}{D^2} \right) \{ [(C'_{pb})_{JET}]_{REF} + \\ &+ .009 \theta_B^{\circ} - .05 + .0025 \epsilon_N^{\circ} + \\ &+ .2 \times 10^{-4} (T_j - T_H) + .035 \}, \end{aligned} \quad (2.6-39)$$

Explicitly, for convergent nozzles,

$$\begin{aligned} [\Delta C_{Dopb(JET)}]_{CONV} &= - \left[ \frac{D_B^2 - D_N^2}{D^2} \right] \{ [(C'_{pb})_{JET}]_{REF} + \\ &+ 10^{-4} [90 \theta_B^{\circ} + 25 \epsilon_N^{\circ} + .2 (T_j - T_H) - \\ &- 500] \} - C_{DobCYL} \left[ \frac{D_B}{D} \right]^3, \end{aligned} \quad (2.6-40)$$

and for convergent-divergent nozzles,

$$\begin{aligned} [\Delta C_{Dopb(JET)}]_{CONV-DIV} &= [\Delta C_{Dopb(JET)}]_{CONV} - \\ &- \left[ \frac{D_B^2 - D_N^2}{D^2} \right] 350 \times 10^{-4}. \end{aligned} \quad (2.6-41)$$

NOTE: The algebraic value of  $[(C'_{pb})_{JET}]_{REF}$  should be taken from Fig (2.6-20).

For parabolic afterbodies instead of  $(\theta_B)$ , the corresponding  $(\theta_p = 2\theta_B)$  value should be substituted in the Eq (2.6-41).

### (2) Boattail Pressure Drag Coefficient Changes Due to Jet Effects,

$\Delta C_{DopbT(JET)}$ .

- The evaluation of jet-effects on the boattail pressure drag change is done on the basis of the sporadic data from Ref (2.6-37), (2.6-38) and (2.6-39), (Cortright, Cabbage, Judd). The tentative expressions, derived and proposed below, actually approximate the jet effects on boattail pressure drag for supersonic Mach Numbers of the order of 2, applicable to both convergent and convergent-divergent nozzles. The effects of the boattail angle,  $\theta_B$ , the nozzle exit angle,  $\theta_N$ , and the jet pressure ratio,  $p_j/p_H$ , are included. Using again the concept of the reference conical configuration, having  $(\theta_B^{\circ} = 5.6^{\circ})$  and  $(\epsilon_N^{\circ} = 0^{\circ})$ , the pressure drag coefficient decrement on boattail surfaces due to any other conical boattail angle  $(\theta_B^{\circ} \neq 5.6)$  and a nozzle angle  $(\epsilon_N^{\circ} \neq 0)$  can be approximated in the presence of a jet stream by:

$$\begin{aligned} \Delta C_{DopbT(JET)} &= -5 \times 10^{-4} \left( \frac{p_j}{p_H} \right) \frac{\theta_B^2}{31.4} - 5 \times 10^{-5} \epsilon_N^{\circ} \left( \frac{p_j}{p_H} \right), \\ \therefore \Delta C_{DopbT(JET)} &= -5 \times 10^{-4} \left( \frac{p_j}{p_H} \right) \left[ \frac{\theta_B^2}{31.4} + 10^{-1} \epsilon_N^{\circ} \right], \end{aligned} \quad (2.6-42)$$

where  $\theta_B$  and  $\epsilon_N^{\circ}$  are in degrees, and the reference area is  $S_r = \pi D^2/4$ .

For parabolic afterbodies, with an inscribed cone angle of  $(\theta_B^{\circ} = \theta_p^{\circ}/2)$ :

$$\Delta C_{DopbT(JET)} = -5 \times 10^{-4} \left( \frac{p_j}{p_H} \right) \left[ \frac{3\theta_B^2}{31.4} + 10^{-1} \epsilon_N^{\circ} \right]. \quad (2.6-43)$$

Expressions (2.6-42) and (2.6-43) are very approximate, and should be used cautiously for both convergent and convergent-divergent nozzles.

(3) Combined Afterbody (Base Plus Boattail) Drag Coefficient Decrement,  $\Delta C_{Dob(JET)}$ , referred to the reference area,  $S_r = \pi D^2/4$ , due to total jet effects thus becomes:

$$\Delta C_{DobJET} = \Delta C_{Dopb(JET)} + \Delta C_{DopbT(JET)}, \quad (2.6-44)$$

or explicitly for various boattail and nozzle configurations, differing from the arbitrarily chosen "reference"

case:

For conical afterbodies, convergent nozzles:

$$(\Delta C_{DobJET})_{CONV}^{CONE} = - \left[ \frac{D_B^2 - D_N^2}{D^2} \right] \left\{ [(C'_{pb})_{JET}]_{REF} + 10^{-4} [90\theta_B^0 + 25\epsilon_N^0 + .2(T_J - T_H) - 500] \right\} - 5 \times 10^{-4} \left( \frac{P_J}{P_H} \right) \left[ \frac{\theta_B^2}{31.4} + 10^{-1} \epsilon_N^0 \right] - C_{DobCYL} \left( \frac{D_B}{D} \right)^3. \quad (2.6-45)$$

For conical afterbodies, convergent-divergent nozzles:

$$(\Delta C_{DobJET})_{CONV-DIV}^{CONE} = - \left[ \frac{D_B^2 - D_N^2}{D^2} \right] \left\{ [(C'_{pb})_{JET}]_{REF} + 10^{-4} [90\theta_B^0 + 25\epsilon_N^0 + .2(T_J - T_H) - 150] \right\} - 5 \times 10^{-4} \left( \frac{P_J}{P_H} \right) \left[ \frac{\theta_B^2}{31.4} + 10^{-1} \epsilon_N^0 \right] - C_{DobCYL} \left( \frac{D_B}{D} \right)^3. \quad (2.6-46)$$

For parabolic afterbodies, convergent nozzles:

$$(\Delta C_{DobJET})_{CONV}^{PARA} = - \left[ \frac{D_B^2 - D_N^2}{D^2} \right] \left\{ [(C'_{pb})_{JET}]_{REF} + 10^{-4} [180\theta_B^0 + 25\epsilon_N^0 + .2(T_J - T_H) - 500] \right\} - 5 \times 10^{-4} \left( \frac{P_J}{P_H} \right) \left[ \frac{3\theta_B^2}{31.4} + 10^{-1} \epsilon_N^0 \right] - C_{DobCYL} \left( \frac{D_B}{D} \right)^3. \quad (2.6-47)$$

For parabolic afterbodies, convergent-divergent nozzle:

$$(\Delta C_{DobJET})_{CONV-DIV}^{PARA} = - \left[ \frac{D_B^2 - D_N^2}{D^2} \right] \left\{ [(C'_{pb})_{JET}]_{REF} + 10^{-4} [180\theta_B^0 + 25\epsilon_N^0 + .2(T_J - T_H) - 150] \right\} - 5 \times 10^{-4} \left( \frac{P_J}{P_H} \right) \left[ \frac{3\theta_B^2}{31.4} + 10^{-1} \epsilon_N^0 \right] - C_{DobCYL} \left( \frac{D_B}{D} \right)^3. \quad (2.6-48)$$

Alternatively, the Eq (2.6-46), (2.6-47) and (2.6-48), can be conveniently written as:

$$(\Delta C_{DobJET})_{CONV-DIV}^{CONE} = (\Delta C_{DobJET})_{CONV}^{CONE} - .035 \left[ \frac{D_B^2 - D_N^2}{D^2} \right], \quad (2.6-49)$$

$$(\Delta C_{DobJET})_{CONV}^{PARA} = (\Delta C_{DobJET})_{CONV}^{CONE} - 10^{-3} \left( \frac{P_J}{P_H} \right) \left( \frac{\theta_B^2}{31.4} \right),$$

$$(\Delta C_{DobJET})_{CONV-DIV}^{PARA} = (\Delta C_{DobJET})_{CONV}^{CONE} - 10^{-3} \left[ 35 \left( \frac{D_B^2 - D_N^2}{D^2} \right) + \left( \frac{P_J}{P_H} \right) \left( \frac{\theta_B^2}{31.4} \right) \right]. \quad (2.6-51)$$

In the above expressions:

$C_{DobCYL} \left( \frac{D_B}{D} \right)^3$  - from Fig. (2.6-19),

$[(C'_{pb})_{JET}]_{REF}$  - from Fig. (2.6-20), by its algebraic value,

$\left( \frac{P_J}{P_H} \right)$  - is the jet static pressure ratio,

$\theta_B = (\theta_p/2)$  and  $\epsilon_N$  in degrees.

$T_J$  and  $T_H$  - are the static jet and the atmospheric temperatures in °F absolute.

(vi) Trailing edge base pressure drag,  $C_{DobWTE}$  and  $C_{DobFTE}$ .

The wing and the fin trailing edge base-to-free stream pressure ratio,  $(p_b/p_H = p_b/p_\infty)$ , can be evaluated from Fig (2.6-4), irrespective of the airfoil shape. Since the data are for base pressures for airfoils with relatively thin turbulent boundary layers, the Reynolds Number effects for eventually relatively thick boundary layers may be additionally taken into account by using Fig (2.6-5). Instead, in this paper, it is deemed more convenient to express the  $p_b/p_H$  ratio directly through a scale effect parameter  $\xi/(t_B Re_\xi^2)$  as a function of Mach Number  $(M_H)$ ,

where  $\xi = \xi_{WEXP}$ , or  $\xi = \xi_{FEXP}$

and  $t_B = t_{TE} \approx .01ft$ , (2.6-52)

in accordance with Fig (2.6-21). Thus, the corrections for variations in boundary layer thickness with Reynolds Number are automatically taken into account through the variable effective trailing edge thickness parameter  $(t_B Re_\xi^2)$ .

The wing trailing-edge base drag coefficient is then given by

$$C_{DOPWTE} = 4 \left( \frac{p_H}{q_H} \right) \left( 1 - \frac{p_b}{p_H} \right) \frac{b_{WEXP}}{\cos \Lambda_{WTE}} \frac{t_{WTE}}{\pi D^2},$$

$$\therefore C_{DOPWTE} = 1.825 \left( \frac{b_{WEXP}}{D} \right) \left( \frac{t_{WTE}}{D} \right) \times \frac{\left[ 1 - \left( \frac{p_b}{p_H} \right)_W \right]}{\left[ M_H^2 \cos \Lambda_{WTE} \right]},$$

(2.6-53)

and the total fin trailing-edge base drag coefficient by

$$C_{DOPFTE} = 1.825 N \left( \frac{h_{FEXP}}{D} \right) \left( \frac{t_{FTE}}{D} \right) \times \frac{\left[ 1 - \left( \frac{p_b}{p_H} \right)_F \right]}{\left[ M_H^2 \cos \Lambda_{FTE} \right]},$$

(2.6-54)

as referred to the references area,  $S_r = \pi D^2 / 4$ , where:

$(p_b/p_H)$ - should be taken from Fig (2.6-21) as a function of the Mach Number,  $M_H$ , and the effective trailing edge thickness parameter,  $(\bar{c}/t_B Re \bar{c}^2)$ ,

$$\frac{4}{\pi} \frac{p_H}{q_H} = \frac{4}{\pi} \frac{2 p_H}{\gamma M_H^2 p_H} = \frac{1.825}{M_H^2} \quad \gamma = 1.40,$$

$b_{WEXP}$  - is the exposed wing span, ft.,

$h_{FEXP}$  - is the exposed fin height (one) ft.,

$Re \bar{c}$  - is the Reynolds Number, referred to exposed wing (or fin) mean geometric chord,  $\bar{c}_{EXP}$ ,

$t_B = t_{TE}$  - is the manufacturing trailing edge thickness, of the order of 0.01 to 0.02 (in ft),

$\Lambda_{TE}$  - is the absolute value of the trailing-edge sweep back (or forward) angle, degrees.

With the number of fins equal to (N), the final combined expression for the wing and the fins takes the form:

$$C_{DOPWTE} + C_{DOPFTE} = \frac{1.825}{D^2 M_H^2} \left[ \left( 1 - \frac{p_b}{p_H} \right)_W \left( \frac{b_{WEXP}}{\cos \Lambda_{WTE}} \right) t_{WTE} + N \left( 1 - \frac{p_b}{p_H} \right)_F \left( \frac{h_{FEXP}}{\cos \Lambda_{FTE}} \right) t_{FTE} \right].$$

(2.6-55)

(vii) Final expressions for the total base drag coefficient, (see Tables (2.6-4) and (2.6-5))

$$C_{Dob} = (C_{DobCYL} + \Delta C_{DobBT} + \Delta C_{Dob(F)} + \Delta C_{DobJET}) + (C_{DobWTE} + C_{DobFTE}) \quad (2.6-56)$$

or explicitly:

For conical afterbodies, convergent nozzles: (Case I):

$$C_{Dob} = C_{DobCYL} \left( \frac{D_B}{D} \right)^3 + \left\{ .057 (N+1) \left( \frac{b_F}{D} \right) \left( \frac{D_B}{D} \right)^2 \times \left[ (-\Delta C_{pb(F)})_{REF} + \cos \Lambda_{FLE} (\Delta C_{pb(F)})_{(1/C)_F, \Lambda_{FLE}=0} + (\Delta C'_{Dob(F)})_{(X/C)_F} \right] \right\} + \left\{ \frac{1.825}{D^2 M_H^2} \left[ \left( 1 - \frac{p_b}{p_H} \right)_W \left( \frac{b_{WEXP}}{\cos \Lambda_{WTE}} \right) t_{WTE} + N \left( 1 - \frac{p_b}{p_H} \right)_F \left( \frac{h_{FEXP}}{\cos \Lambda_{FTE}} \right) t_{FTE} \right] \right\} + \left\{ - \left( \frac{D_B^2 - D_N^2}{D^2} \right) \left[ (C'_{pb(JET)})_{REF} + 10^{-4} (90 \theta_B^2 + 25 \epsilon_N^2 + 2(T_j - T_H) - 500) \right] - 5 \times 10^{-4} \left( \frac{p_j}{p_H} \right) \times \left[ \frac{\theta_B^2}{31.4} + 10^{-1} \epsilon_N^2 \right] - C_{DobCYL} \left( \frac{D_B}{D} \right)^3 \right\}.$$

(2.6-57)

The last term,  $(\Delta C_{DobJET})_{CONE-CONV}$ , separated by vertical dash line "/" from the rest, represents the jet interference effects and should be taken equal to zero for the no-jet case. It is the only term that undergoes changes with various other nozzle designs, as follows:

For conical afterbodies, convergent-divergent nozzles: (Case II):

$$(\Delta C_{DobJET})_{CONV-DIV}^{CONE} = (\Delta C_{DobJET})_{CONV}^{CONE} - .035 \left[ \frac{D_B^2 - D_N^2}{D^2} \right].$$

(2.6-58)

For parabolic afterbodies, convergent nozzles: (Case III):

$$(\Delta C_{DobJET})_{CONV}^{PARA} = (\Delta C_{DobJET})_{CONV}^{CONE} - 10^{-3} \left( \frac{p_j}{p_H} \right) \left( \frac{\theta_B^2}{31.4} \right).$$

(2.6-59)

For parabolic afterbodies, convergent-

divergent nozzles: (Case IV):

$$(\Delta C_{D\text{OBJET}})_{\text{CONV-DIV}}^{\text{PARA}} = (\Delta C_{D\text{OBJET}})_{\text{CONV}}^{\text{CONE}} - 10^{-3} \left[ 35 \left( \frac{D_B^2 - D_N^2}{D^2} \right) + \left( \frac{p_j}{p_H} \right) \left( \frac{\theta_B^2}{31.4} \right) \right] \quad (2.6-60)$$

In the above expressions, the meaning of the different terms is as follows:

- D - is the cylinder diameter, ft,
- D<sub>B</sub> - is the base diameter, ft,
- D<sub>N</sub> - is the nozzle diameter, ft,
- N - is the number of fins,
- b<sub>F</sub> - is the fin total span b<sub>F</sub> = (2h<sub>FEXP</sub> + D), ft.
- h<sub>FEXP</sub> - is the individual fin height, ft,
- (t/c)<sub>F</sub> - is the fin airfoil thickness ratio,
- C<sub>r</sub> - is the fin root chord, ft.
- (x/c)<sub>F</sub> - is the fin trailing edge root chord relative position with respect to body base, positive forward,
- Λ<sub>FLE</sub> - is the fin leading-edge sweep-back angle, degrees,
- θ<sub>B</sub> - is the conical boattail angle; for parabolic bodies, boattail angle of an inscribed cone, degrees, θ<sub>p</sub> = 2θ<sub>B</sub>,
- ε<sub>N</sub> - is the nozzle exit angle, positive for diverging exit profile, degrees,
- T<sub>j</sub> - is the jet static temperature, OR absolute,
- T<sub>H</sub> - is the ambient static temperature, OR absolute,
- (p<sub>j</sub>/p<sub>H</sub>) - is the jet static pressure ratio, (p<sub>j</sub>/p<sub>H</sub>) = (p<sub>j</sub>/p<sub>∞</sub>),
- p<sub>H</sub> - is the altitude static pressure, p<sub>H</sub> = p<sub>∞</sub>, lb/sq.ft,

- M<sub>H</sub> - is the free-stream Mach Number, M<sub>H</sub> = M<sub>∞</sub>,
- b<sub>WEXP</sub> - is the exposed wing span, ft,
- Λ<sub>WTE</sub> - is the wing trailing-edge sweep angle, taken by absolute value, degrees,
- t<sub>TE</sub> - is the wing or fin trailing edge bluntness, approximately .01 ft,
- p<sub>b</sub> - is the static pressure, lb./sq.ft,
- C<sub>D0bCYL</sub> - is the base drag coefficient of a cylindrical body, see Fig. (2.6-19),
- [-ΔC<sub>pb(F)</sub>]<sub>REF</sub> - is the reference fin interference pressure coefficient, see Fig (2.6-16) (a positive number),
- [ΔC<sub>pb(F)</sub>]<sub>(x/c)<sub>F</sub>, Λ<sub>FLE</sub>=0</sub> - is the increment in fin-interference drag coefficient due to fin airfoil thickness, see Fig (2.6-17) (a negative number),
- [ΔC'<sub>D0b(F)</sub>]<sub>(x/c)<sub>F</sub></sub> - is the increment in fin-interference drag coefficient due to fin relative position with respect to body base, see Fig (2.6-18) (either positive, or negative),
- (p<sub>b</sub> / p<sub>H</sub>) - is the base-free stream pressure ratio for fins and wings, see Fig (2.6-21),
- [C'<sub>pb(JET)</sub>]<sub>REF</sub> - is the reference base pressure coefficient due to jet effects, see Fig (2.6-20).

A detailed, self-instructive computational procedure for the base pressure drag is presented in Table (2.6-5).

## 2.6.5 COMPUTATION INSTRUCTIONS FOR THE TOTAL BASE PRESSURE DRAG COEFFICIENT ESTIMATES, $C_{D0b}$

### (i) Basic Data Preparation:

For a given missile configuration the respective geometric parameters, entering the governing Eq (2.6-57) for  $C_{D0b}$ , should be numerically specified and tabulated in Table (2.6-4).

### (ii) List of Working Graphs for the Base Pressure Drag Estimates

Fig. (2.6-19) - Base drag coefficient,  $C_{D0b_{CYL}}$ , for cylindrical bodies without boattailing, having fineness ratios (L/D) greater than 5.

Fig. (2.6-15) - Base pressure coefficient increment,  $\Delta C_{pb}$ , for parabolic afterbodies at zero angle-of-attack, transonic speeds.

Fig. (2.6-16) - Reference fin-interference base pressure coefficient increment,  $(-\Delta C_{pb(F)})_{REF}$ .

Fig. (2.6-17) - Base pressure coefficient variation with the fin thickness ratio,  $(\Delta C_{pb(F)})_{(t/C)_F}$ ,  $\Lambda_{FLE} = 0$ .

Fig. (2.6-18) - Base pressure coefficient variation with the fin location with respect to the base,  $(\Delta C'_{D0b})_{(x/C)}$ .

Fig. (2.6-21) - Wing and fin trailing edge base pressures for turbulent boundary layers,  $(p_b/p_H)$ .

Fig. (2.6-20) - Effect of free stream Mach Number on base pressure for various jet-static pressure ratios, reference

configuration.

### (iii) Computational Procedure

A self-instructive computational procedure for the total base pressure drag coefficient estimates is presented in Table (2.6-5). Four possible cases are explicitly defined for the "jet-on" condition:

Case I - Conical frustrum boattails with built-in convergent nozzles, governing Eq (2.6-57).

Case II - Conical frustrum boattails with built-in convergent-divergent nozzles. The governing Eq (2.6-57) should be corrected in accordance with the auxiliary Eq (2.6-58).

Case III - Parabolic frustrum boattails with built-in convergent nozzles. The governing Eq. (2.6-57) should be corrected in accordance with the auxiliary Eq (2.6-59).

Case IV - Parabolic frustrum boattails with built-in convergent-divergent nozzles. The governing Eq (2.6-57) should be corrected in accordance with the auxiliary Eq (2.6-60).

In the "no-jet" case, the last term in the governing Eq (2.6-57), clearly separated by the vertical line "/", is non-existing. All four cases, specified above, reduce to one single expression, represented by the remaining terms in Eq (2.6-57).

TABLE (2.6-4)

BASIC DATA FOR BASE DRAG EVALUATION

D	ft		$\cos \Lambda_{WTE}$	—		$(D_B/D)^3$	$K_1$
$D_B$	ft		$\cos \Lambda_{FTE}$	—		$.057(N+1)(b_F/D)$	$K_2$
$D_N$	ft		$\Theta_B^\circ$	—		$1.825/D^2$	$K_3$
$b_{WEXP}$	ft		$C_N^\circ$	—		$\frac{b_{WEXP}}{\cos \Lambda_{WTE}} \times t_{WTE}$	$K_4$
$b_F$	ft		$T_j$	$^\circ R$		$N \frac{h_{FEXP}}{\cos \Lambda_{FTE}} \times t_{FTE}$	$K_5$
$h_{FEXP}$	ft		$p_j$	lb/ft <sup>2</sup>		$(D_B^2 - D_N^2)/D^2$	$K_6$
$t_{WTE} = t_B$	ft		L	ft		$10^{-4}(90\Theta_B^\circ + 25C_N^\circ - 500)$	$K_7$
$t_{FTE} = t_B$	ft		(L/D)	—		$5 \times 10^{-4} \left( \frac{\Theta_B^\circ}{31.4} + 10C_N^\circ \right)$	$K_8$
$\Lambda_{WTE}^\circ$	—		$L_{BT}$	ft		$\cos \Lambda_{OF}$	$K_9$
$\Lambda_{FTE}^\circ$	—		$(L_{BT}/D)$	—		$.035(D_B^2 - D_N^2)/D^2$	$K_{10}$
N	—		$\bar{C}_{FEXP}$	ft		$10^{-3}(\Theta_B^\circ/31.4)$	$K_{10}$
			$(1/\bar{C}_{FEXP})$	—		$(\bar{C}_{WEXP}/t_B)$	$K_{11}$
			$(b_F/D)$	—		$(\bar{C}_{FEXP}/t_B)$	$K_{12}$
			$\Lambda_{OF}^\circ$	—		$(D_B/D)^2 \times K_2$	$K_{13}$
			$\bar{C}_{WEXP}$	ft			
			$C_{rF}$	ft			
			$X_F$	ft			
			$(X/C_r)_F$	—			
			$(D_B/D)$	—			
			$\sqrt{D_B/D_N}$	—			

$b = 2h_{FEXP} + D^2$   
 $L = L_N + L_{OVL} + L_{BT}$

TABLE (2 6-5)

TOTAL BASE DRAG COEFFICIENT,  $C_{Dob}$ , ESTIMATES

$$C_{Dob} = (C_{DobTL} + \Delta C_{DobT} + \Delta C_{DobF} + \Delta C_{DobM}) + (C_{DobTE} + C_{DobTE})$$

$$\Delta C_{Dob} = K_1 C_{DobTL} + K_2 \frac{\Delta C_{DobT}}{M_0} + K_3 \frac{\Delta C_{DobF}}{M_0} + K_4 \frac{\Delta C_{DobM}}{M_0} + K_5 \frac{\Delta C_{DobTE}}{M_0} + K_6 \frac{\Delta C_{DobTE}}{M_0}$$

$$+ (K_7/M_0^2) \{ (1 - \rho_1/\rho_0) + K_8 + (1 - \rho_2/\rho_0) + K_9 \} + \{ (1 - K_9) [C_{Dob}^2]_{M_0} + K_7 \}$$

$$+ 0.8 \times 10^{-4} (T_1 - T_0) - K_{10} (\rho_1/\rho_0) - C_{DobTL} K_1$$

MACH NO	M <sub>0</sub>	ALTITUDE H <sub>1</sub> ft	FREE STREAM STATIC PRESSURE P <sub>01</sub> lb/in <sup>2</sup>	FREE STREAM TEMPERATURE (ABSOLUTE) T <sub>01</sub> °R	$\rho_0/\rho_{0REF}$	WIND REYNOLDS NUMBER $R_{0W}$	$\rho_0/\rho_{0REF}$	FIN REYNOLDS NUMBER $R_{0F}$
0	0	0	STANDARD ATMOSPHERE	STANDARD ATMOSPHERE	T = (2.3-5)	$\rho_0/\rho_{0REF}$	T = (2.3-5)	$\rho_0/\rho_{0REF}$
0.5	0.5	Y = (2.3-8)						
0.8								
1.0								
1.2								
1.5								
2.0								
2.5								
3.0								
3.5								
4.0								
4.5								
5.0	etc							

$R_{0W}^{0.2}$	$1/(R_{0W}^{0.2})$	$(R_{0W}^{0.2})^2$	$1/(R_{0W}^{0.2})^2$	T <sub>1</sub> - T <sub>0</sub> °F ADD	$\rho_1/\rho_0$	C <sub>DobTL</sub>	$\Delta C_{DobT} + \Delta C_{DobF} + \Delta C_{DobM} + \Delta C_{DobTE}$
0.2	0.2	0.04	25			0	0
0.5	0.04	0.25	4			0	0
1.0	0.01	1.0	1			0	0
2.0	0.0025	4.0	0.25			0	0
5.0	0.0004	25.0	0.04			0	0
10.0	0.0001	100.0	0.01			0	0
20.0	0.000025	400.0	0.0025			0	0
50.0	0.000004	2500.0	0.0004			0	0
100.0	0.000001	10000.0	0.0001			0	0
200.0	0.00000025	40000.0	0.000025			0	0
500.0	0.00000004	250000.0	0.000004			0	0
1000.0	0.00000001	1000000.0	0.000001			0	0

TABLE (2 6-5) CONTINUED (1)

$\Delta C_{DobTL}$ FIG 26-16	$\Delta C_{DobT}$ FIG 26-17	$\Delta C_{DobF}$ FIG 26-18	$\Delta C_{DobM}$ FIG 26-19	$\Delta C_{DobTE}$ FIG 26-20	$K_1$ FIG 26-21	$K_2$ FIG 26-22	$K_3$ FIG 26-23	$K_4$ FIG 26-24
0	0	0	0	0	0	0	0	0
0.5	0.5	0.5	0.5	0.5	0.5	0.5	0.5	0.5
1.0	1.0	1.0	1.0	1.0	1.0	1.0	1.0	1.0
1.5	1.5	1.5	1.5	1.5	1.5	1.5	1.5	1.5
2.0	2.0	2.0	2.0	2.0	2.0	2.0	2.0	2.0
2.5	2.5	2.5	2.5	2.5	2.5	2.5	2.5	2.5
3.0	3.0	3.0	3.0	3.0	3.0	3.0	3.0	3.0
3.5	3.5	3.5	3.5	3.5	3.5	3.5	3.5	3.5
4.0	4.0	4.0	4.0	4.0	4.0	4.0	4.0	4.0
4.5	4.5	4.5	4.5	4.5	4.5	4.5	4.5	4.5
5.0	5.0	5.0	5.0	5.0	5.0	5.0	5.0	5.0

$\Delta C_{DobTE}$ FIG 26-25	$\Delta C_{DobTE}$ FIG 26-26	$\Delta C_{DobTE}$ FIG 26-27	$\Delta C_{DobTE}$ FIG 26-28	$\Delta C_{DobTE}$ FIG 26-29	$\Delta C_{DobTE}$ FIG 26-30	$\Delta C_{DobTE}$ FIG 26-31	$\Delta C_{DobTE}$ FIG 26-32
0	0	0	0	0	0	0	0
0.5	0.5	0.5	0.5	0.5	0.5	0.5	0.5
1.0	1.0	1.0	1.0	1.0	1.0	1.0	1.0
1.5	1.5	1.5	1.5	1.5	1.5	1.5	1.5
2.0	2.0	2.0	2.0	2.0	2.0	2.0	2.0
2.5	2.5	2.5	2.5	2.5	2.5	2.5	2.5
3.0	3.0	3.0	3.0	3.0	3.0	3.0	3.0
3.5	3.5	3.5	3.5	3.5	3.5	3.5	3.5
4.0	4.0	4.0	4.0	4.0	4.0	4.0	4.0
4.5	4.5	4.5	4.5	4.5	4.5	4.5	4.5
5.0	5.0	5.0	5.0	5.0	5.0	5.0	5.0



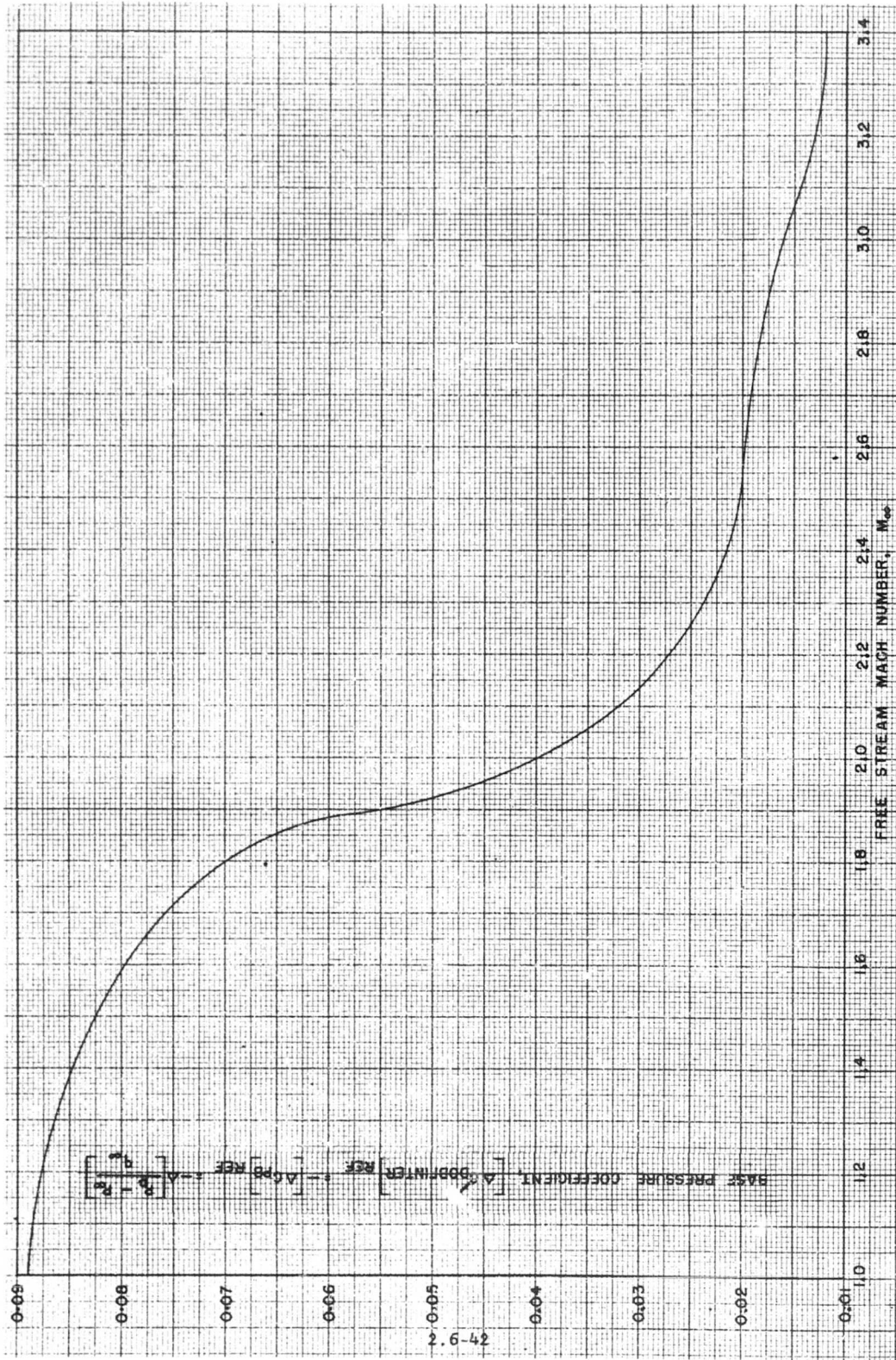


FIG. (2.6-16) IN EFFECTS UPON BASE PRESSURE WITH VARYING MACH NUMBER FOR THE BASIC REFERENCE CONFIGURATION,  $\frac{t}{c} = 0.10$ ,  $\frac{x}{c} = 0$ , ZERO SWEEPBACK,  $N = 4$ ,  $(h/D) = 0.15$ ,  $(2h/(N+D))/D = 1.5$ , NO BOATTAILING.

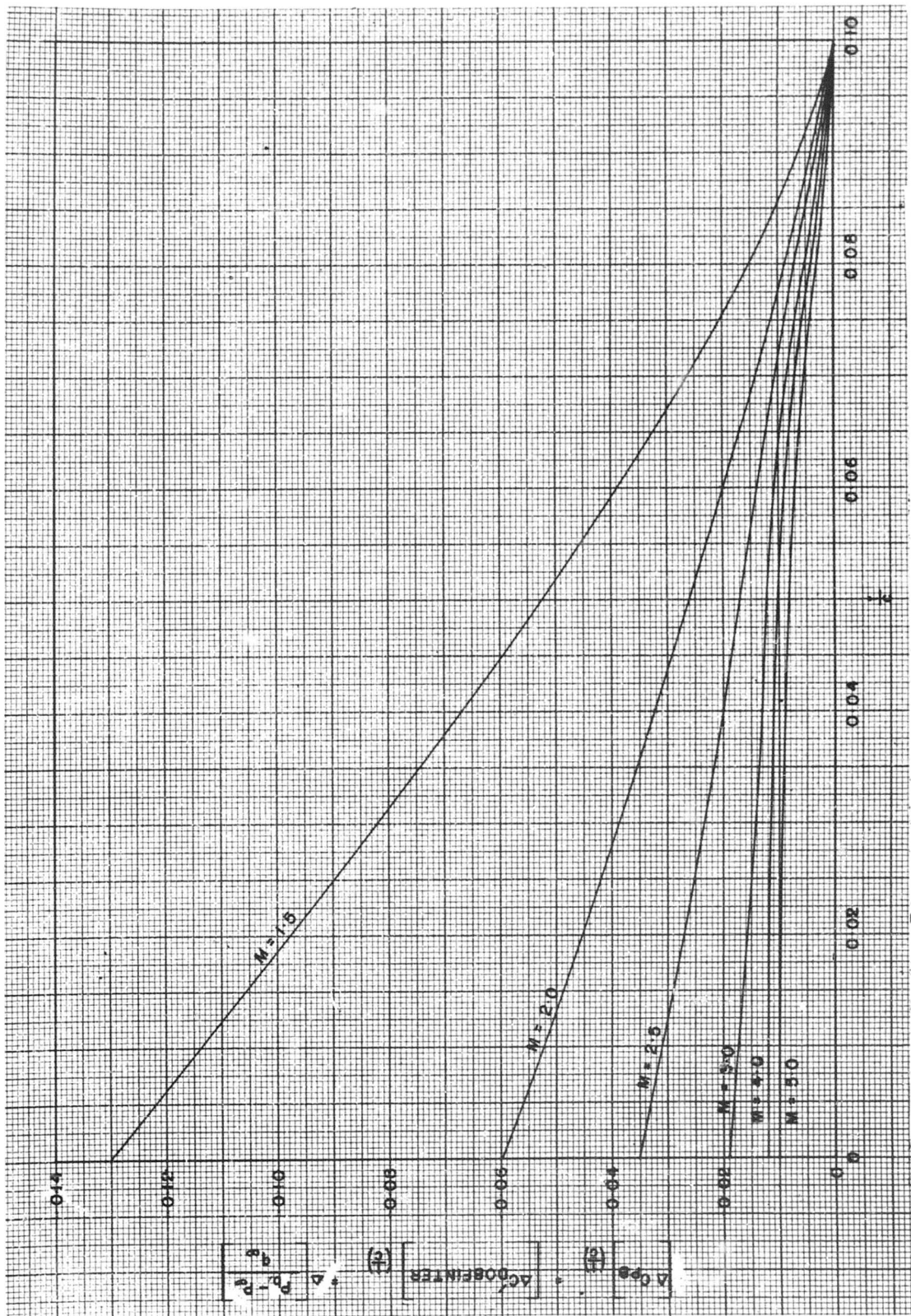


Fig (2.6-17) Base drag coefficient decrement due to fin thickness ratio decrease. Ref (2.6-11) § (2.6-30)

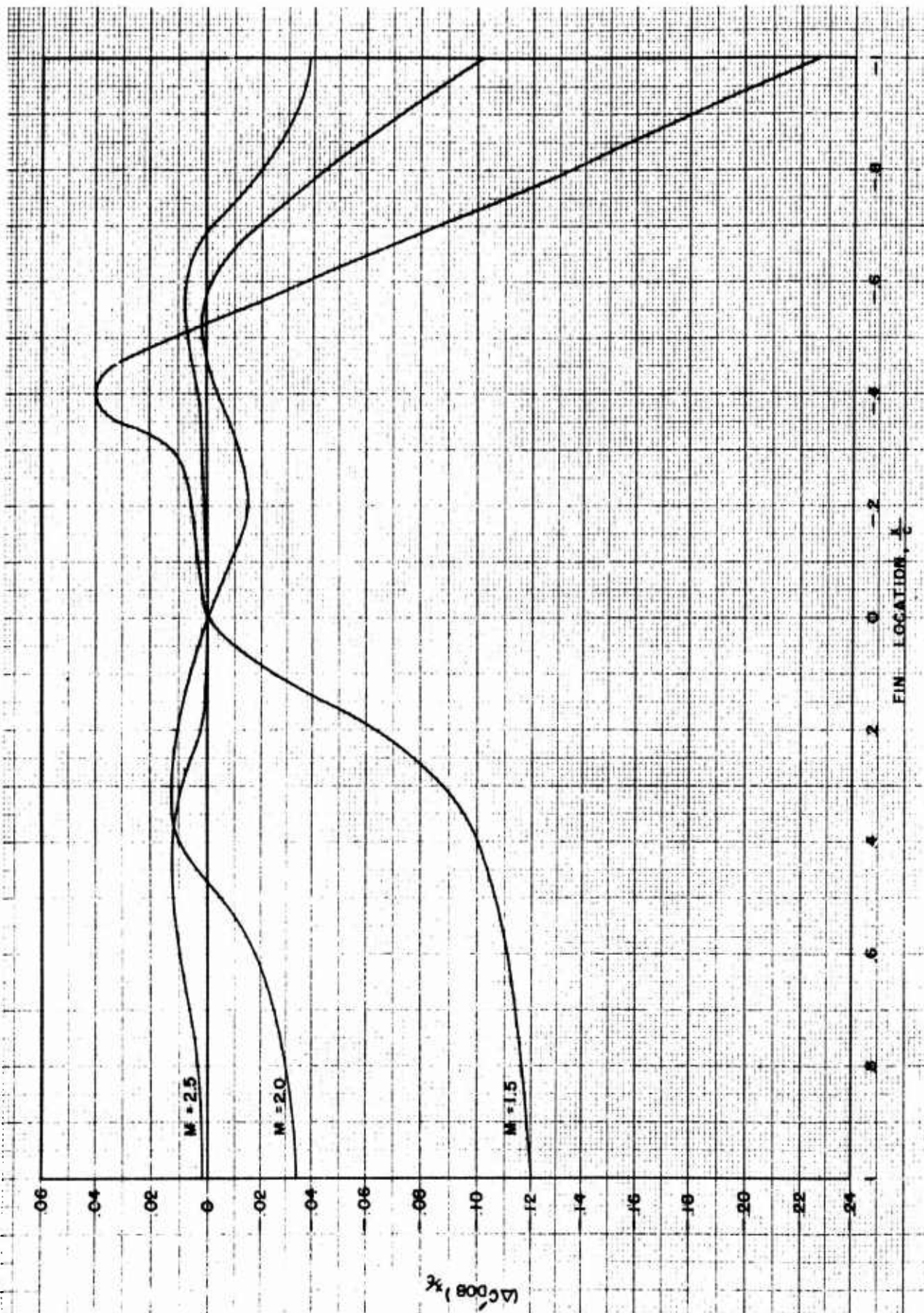


Fig (2.6-18) Measurements and estimations of the effects of fin location upon base pressure at several Mach Numbers.

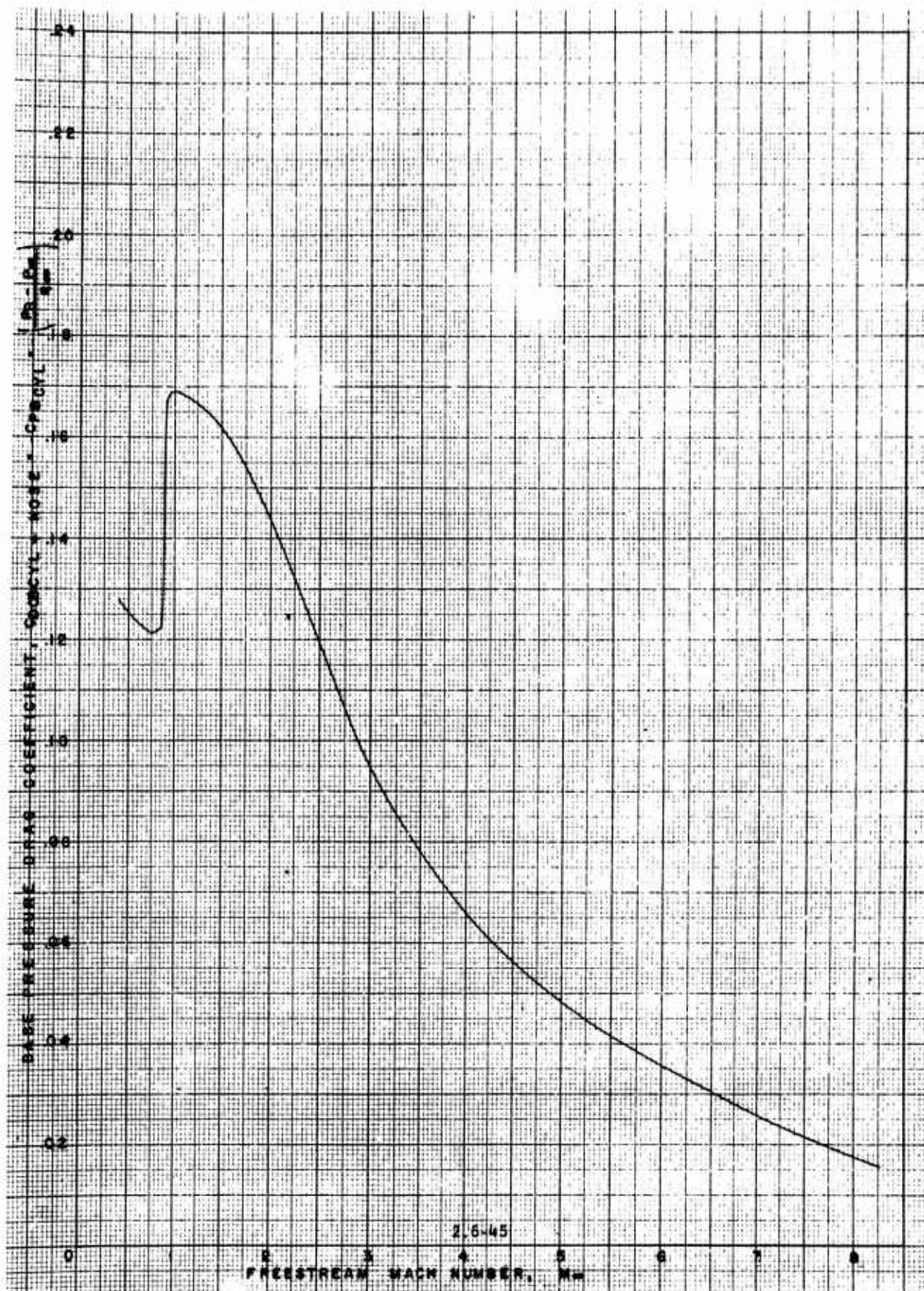


Fig (2.6-19) Base pressure on bodies having cylindrical afterbodies. (No fins)

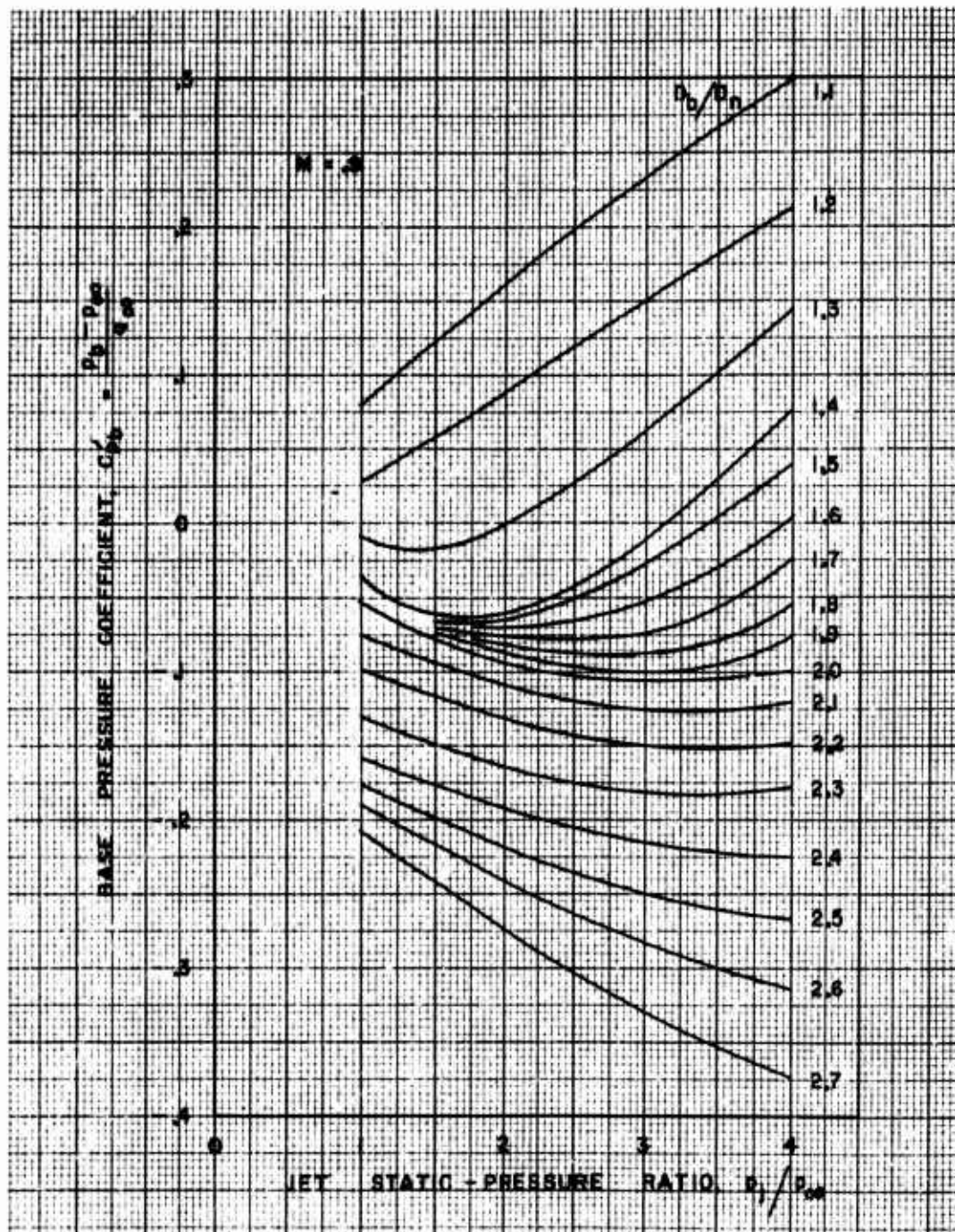


Fig (2.6-20) Effect of free-stream Mach Number. Boattail angle, 5.6°, nozzle-to-body diameter ratio, 0.37. Free-stream Mach Number, 0.9  
Ref (2.6-37)

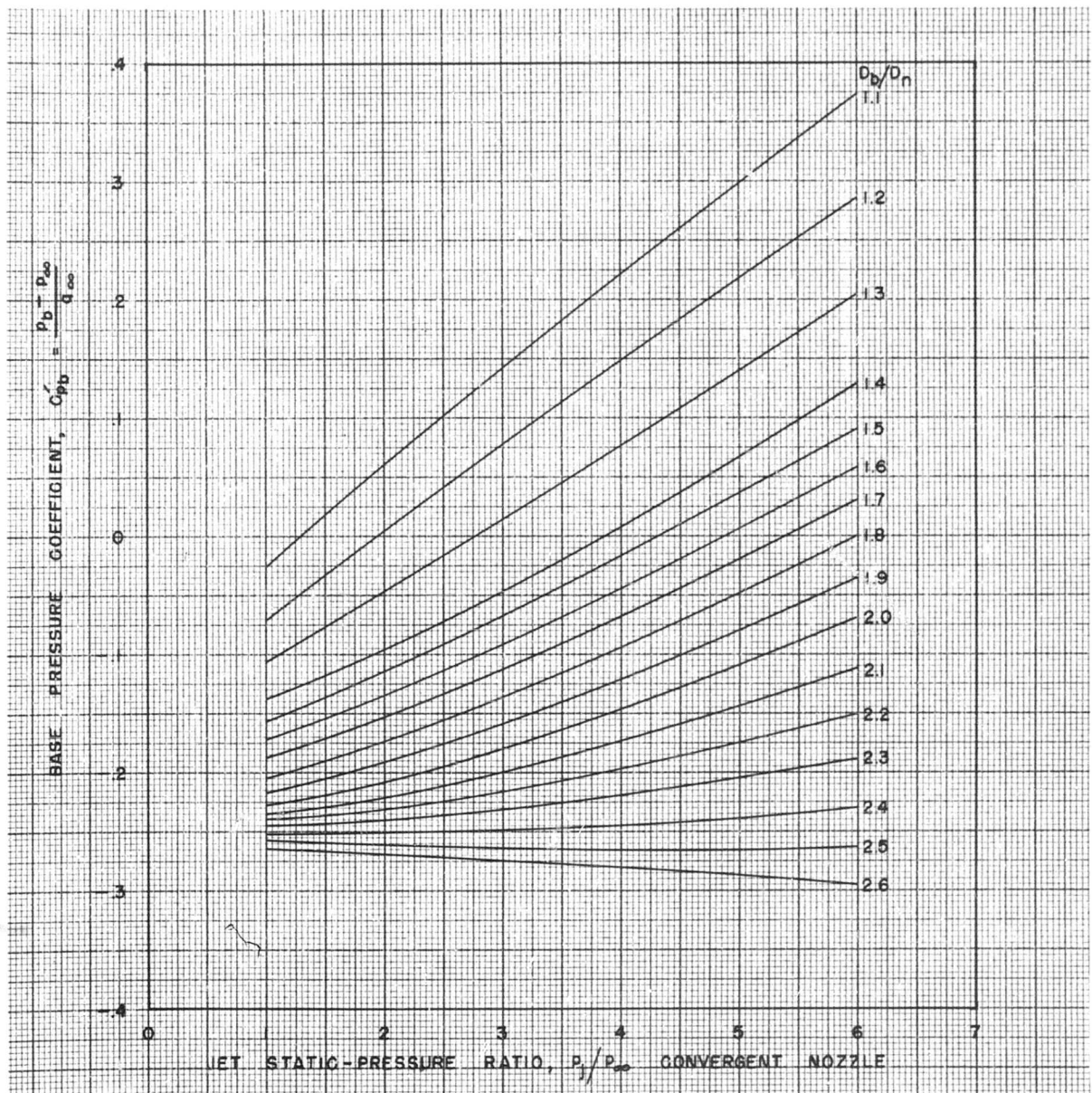


Fig (2.6-20) Continued (1) Free-stream Mach Number 1.5 Ref (2.6-37)

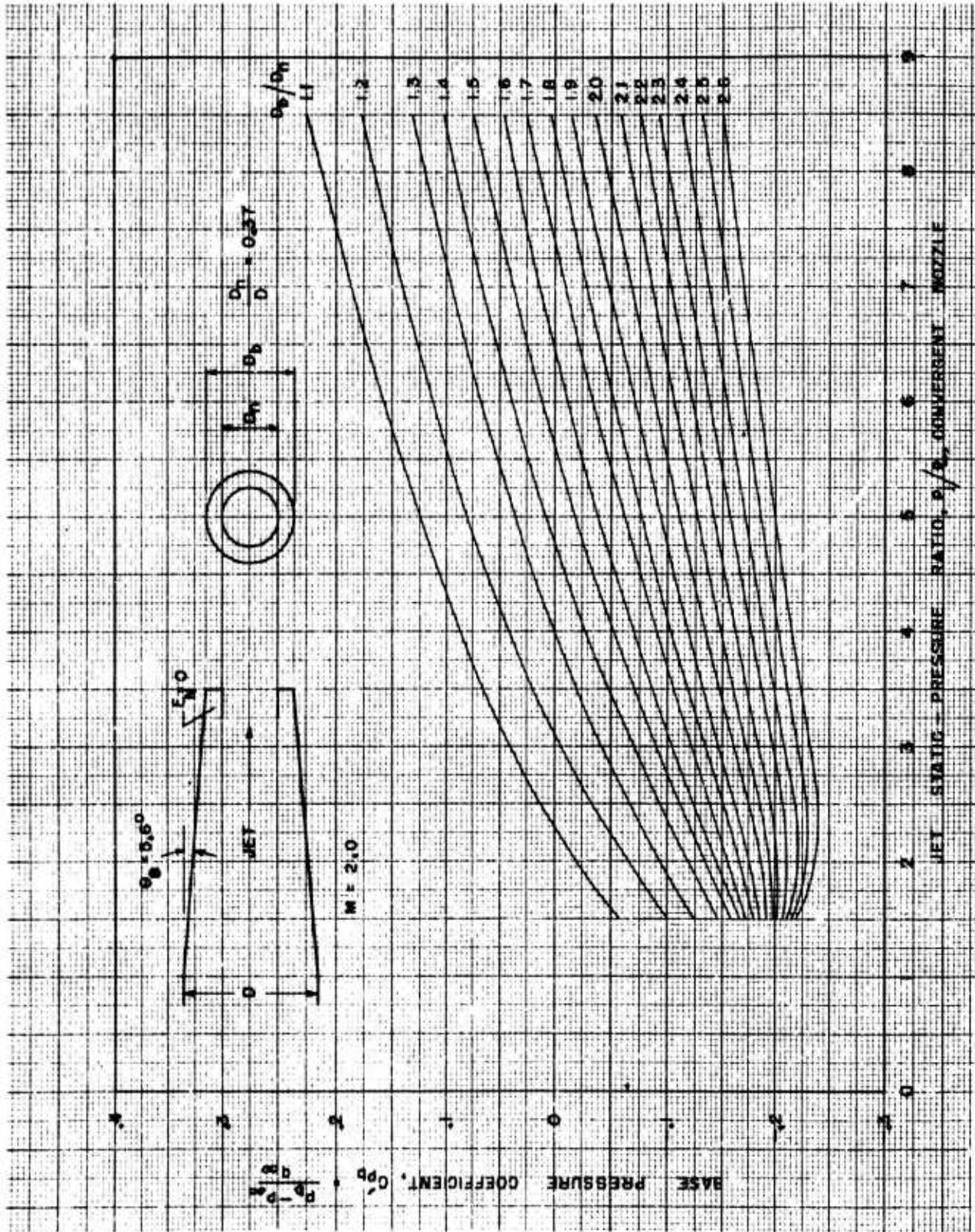


Fig (2.6-20) Continued (2) Free-stream Mach Number, 2.0 Ref (2.6-37)

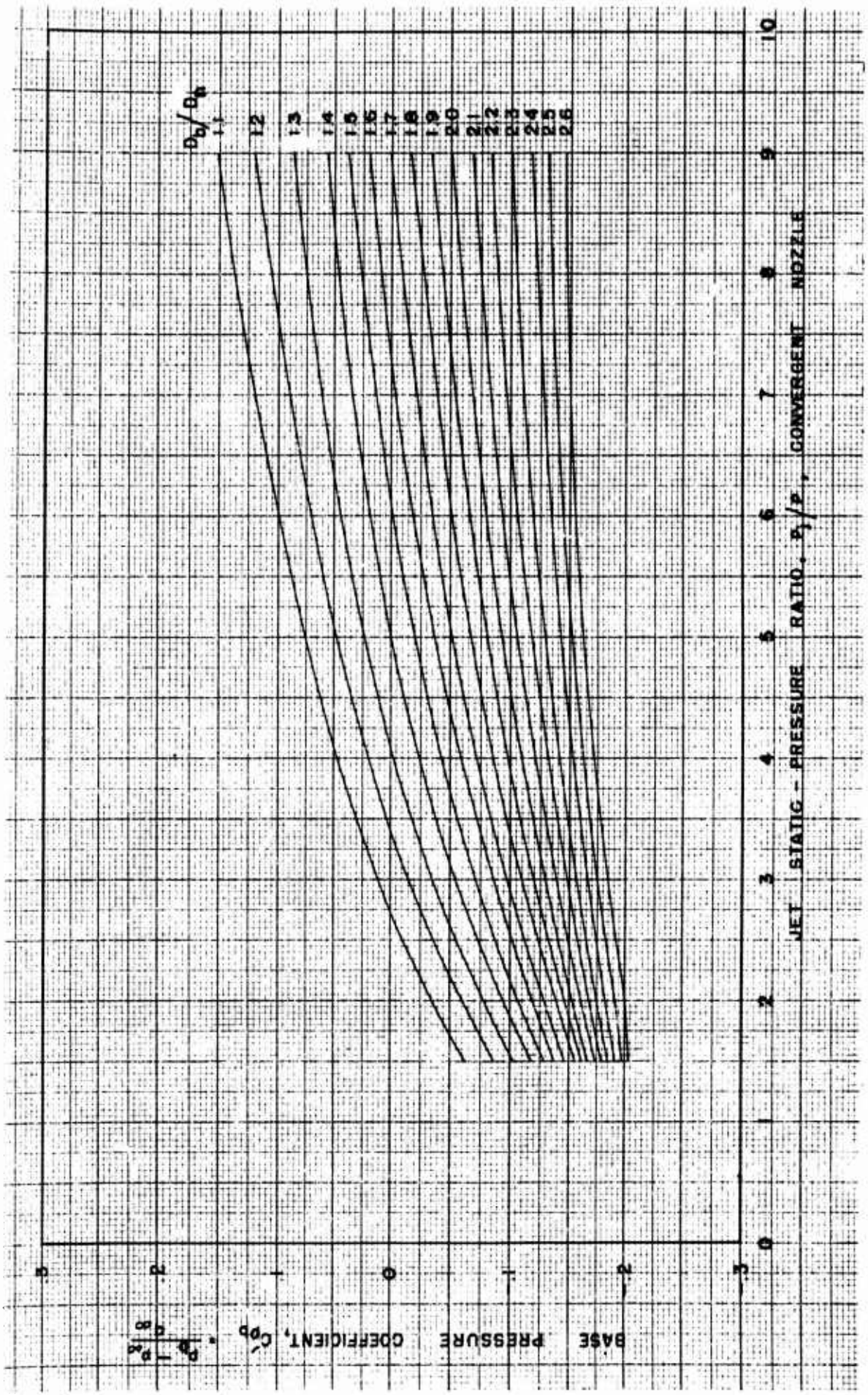


Fig (2.6-20) Continued (3) Free-stream Mach Number, 2.5 Ref (2.6-37)

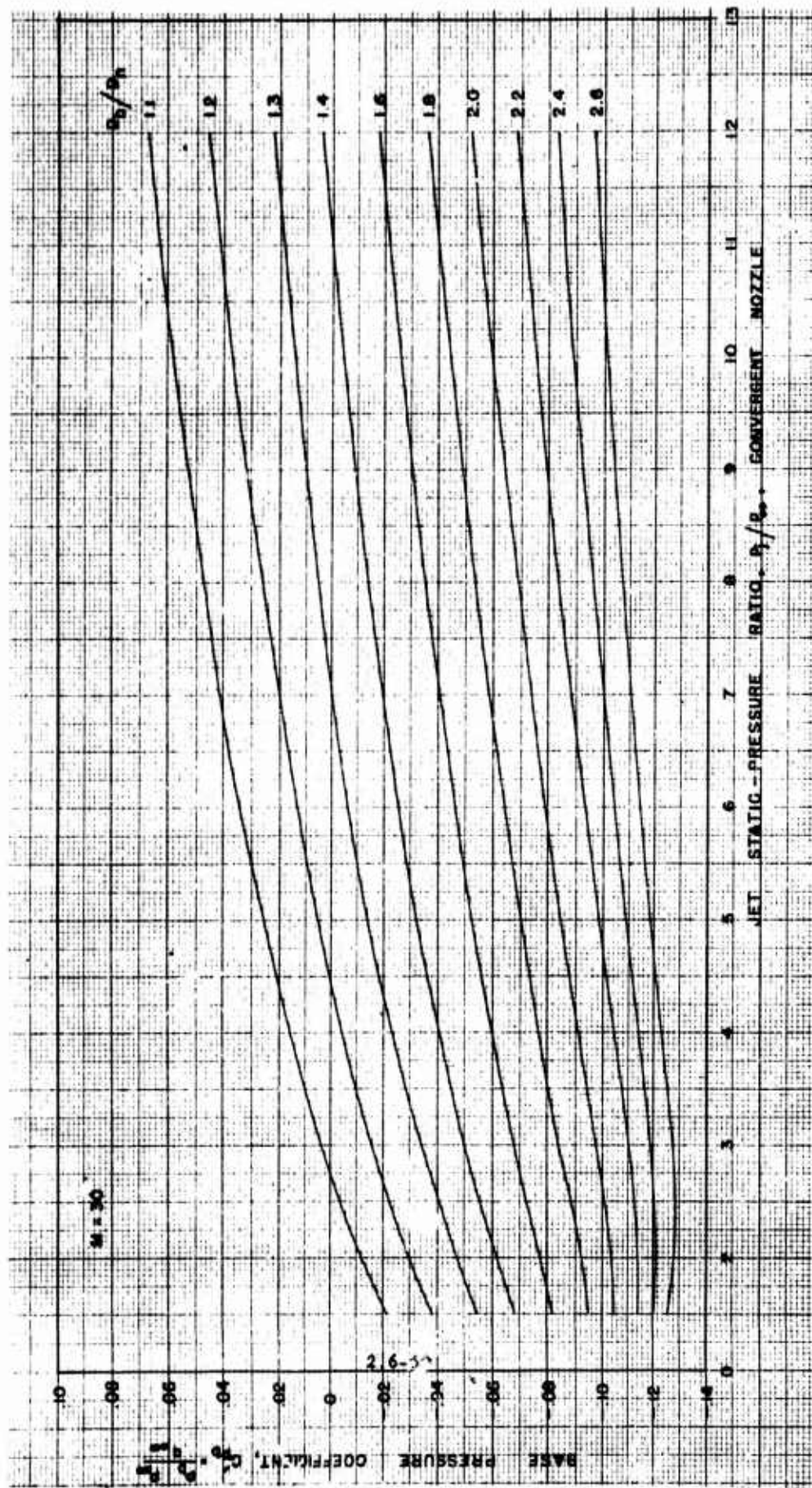


Fig (2.6-20) Continued (4) Free-stream Mach Number, 3.0 Ref (2.6-37)

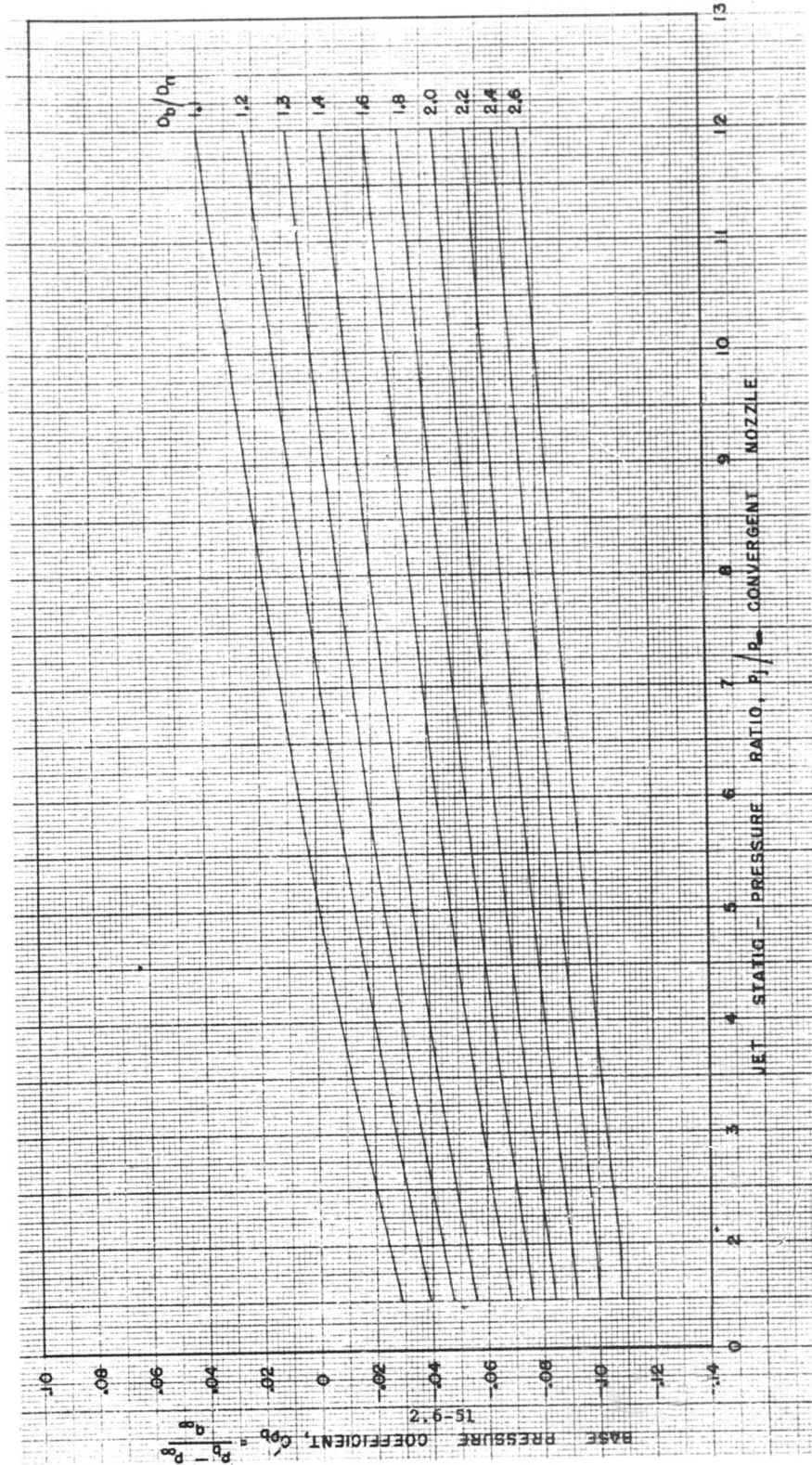


Fig (2.6-20) Continued (5) Free-stream Mach Number, 4.0 Ref (2.6-37)

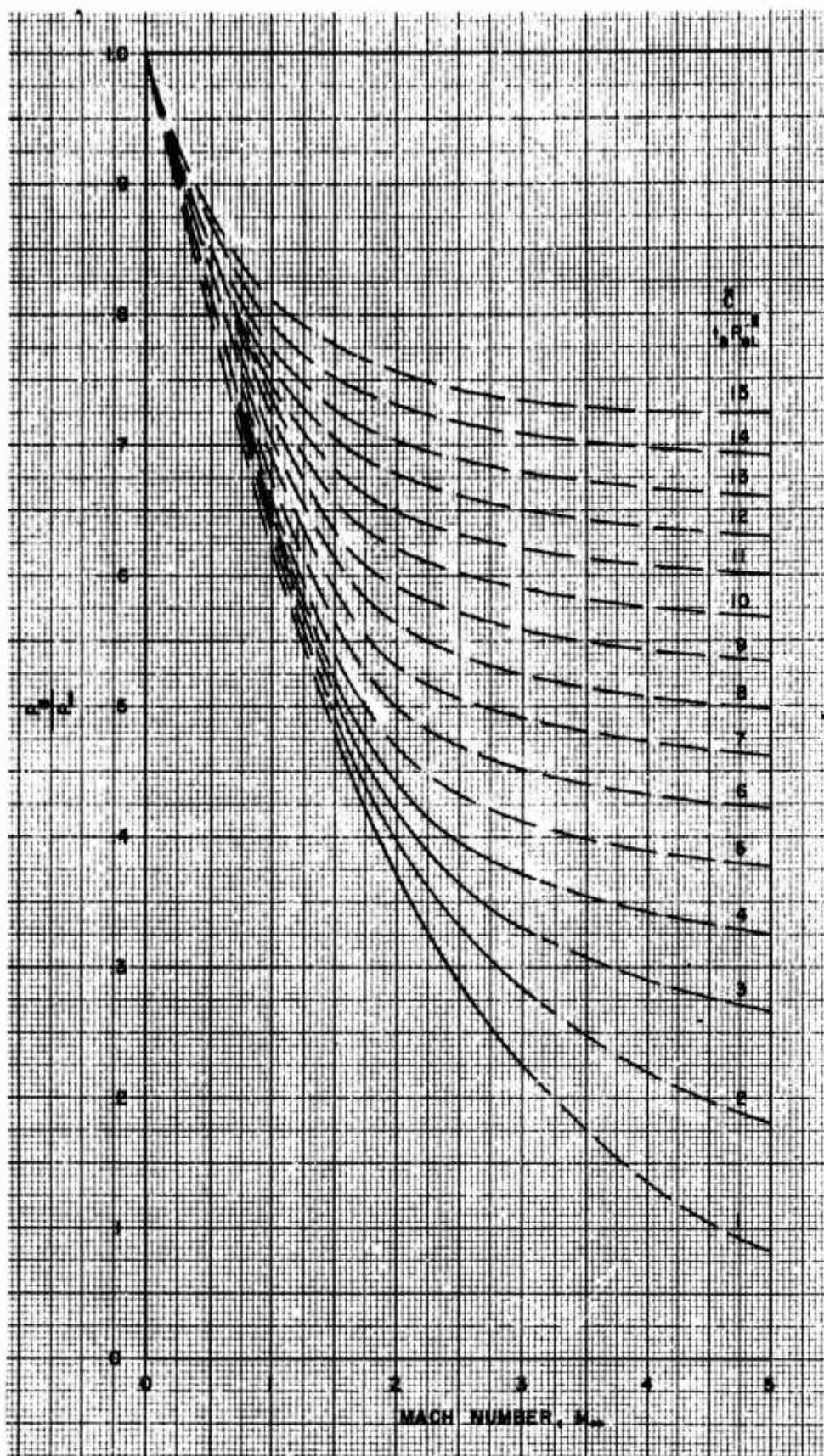


Fig (2.6-21) The effects of Mach Number on base pressure for two-dimensional wings in turbulent flow. Replot of data from Ref (2.6-7).

## 2.6.6 REFERENCES

- 2.6-1 Harris, T. "Description and Discussion of the Air Disturbance Around Bullets in Free Flight" R. D. Ref. No. 63, Ordnance Research Department, Woolwich England, (1925).
- 2.6-2 Gabeaud, M. "Sur la Resistance de L'Air Aux Vitesses Balistiques" Comptes Rendus de L'Academie de Sciences, Vol. 192, No. 11, pp 1630 and 1790, (1931).
- 2.6-3 Depreux, M. "Sur la Resistance de L'Air a L'Arriere Des Projectiles" Comptes Rendus de L'Academie de Sciences, Vol. 193, No. 11, p. 439, (1931).
- 2.6-4 von Karman, T. and Moore, N. B. "The Resistance of Slender Bodies Moving at Supersonic Velocities" Trans. A.S.M.E., Vol. 54, p. 303, (1932).
- 2.6-5 Chapman, D. R. "An Analysis of Base Pressure at Supersonic Velocities and Comparison with Experiment" N.A.C.A. Tech. Rep. 1051, (1951).
- 2.6-6 Cope, W. F. "The Effect of Reynolds Number on the Base Pressure of Projectiles" N.P.L. Rep. Eng. Div. 63/44, Jan. 1945.
- 2.6-7 Chapman, D. R., Winbrow, W. R., and Kester, R. H. "Experimental Investigation of Base Pressure on Blunt-trailing Edge Wings at Supersonic Velocities" N.A.C.A. Rep. 1109 (Superseded N.A.C.A. T.N. 2611, (1952).
- 2.6-8 Bogdanoff, S. M. "A Preliminary Study of Reynolds Number Effects on Base Pressure at  $M = 2.95$ " J. Aero. Sci., Vol. 19, No. 10, p. 649, (1952).
- 2.6-9 Crocco, L. and Lees, L. "A Mixing Theory for the Interaction Between Dissipative Flows and Nearly Isentropic Streams" J. Aero. Sci., Vol. 19, No. 10, p. 649, (1952).
- 2.6-10 Kavanau, L. L. "Some Base Pressure Results at Intermediate Reynolds Numbers with  $M = 2.84$ " J. Aero. Sci., Vol. 21, No. 4, p. 257, (1954).
- 2.6-11 Love, S. E. "The Base Pressure at Supersonic Speeds on Two-Dimensional Airfoils and Bodies of Revolution (With and Without Fins) Having Turbulent Boundary Layers" N.A.C.A. R.M. L53C02, (1953).
- 2.6-12 Cortright, E. M., Jr. and Schroeder, A. H. "Investigation at Mach Number 1.91 of Side and Base Pressure Distributions Over Conical Boattails Without and With Jet Flow Issuing From Base" N.A.C.A. R.M. E51F26, (1951).
- 2.6-13 Kurzweg, H. H. "Interrelationship Between Boundary Layer and Base Pressure" J. Aero. Sci., Vol. 18, No. 11, pp. 743-748, (1951).
- 2.6-14 Harris, T. "Description and Discussion of the Air Disturbance Round Bullets in Free Flight" R. D. Ref. No. 63, Ordnance Research Department, Woolwich, England, (1925).
- 2.6-15 Chapman, D. R. and Perkins, E. W. "Experimental Investigation of the Effects of Viscosity on the Drag and Base Pressure of Bodies of Revolution at a Mach Number of 1.5" N.A.C.A. Rep. 1036, (1951) (Supersedes N.A.C.A. R.M. A7A31a.)

- 2.6-16 Kurzweg, H. H. "The Base Pressure Measurements of Heated, Cooled, and Boattailed Models at Mach Numbers 1.5 to 5.0" N.A.V.O.R.D. Rep. 1651, Proc. of the Bur. of Ord. Symposium on Aeroballistics, (Defense Res. Lab. Rep. No. 267) Univ. Texas, pp. 119-142, (1950).
- 2.6-17 Faro, I. D. V. "Experimental Determination of Base Pressures at Supersonic Velocities" Bumblebee Rep. No. 106, The John Hopkins Univ. Appl. Physics Lab., (Nov. 1949).
- 2.6-18 Hoerner, S. F. "Base Drag, Thick Trailing Edges" J. Aero. Sci., Vol. 17, No. 10, pp. 622-628, (1950).
- 2.6-19 Love, E. S., Coletti, D. E. and Bromm, A. F., Jr. "Investigation of the Variation with Reynolds Number of the Base Wave, and Skin-Friction Drag of a Parabolic Body of Revolution (N.A.C.A. RM-10) at Mach Numbers of 1.62, 1.93, and 2.41 in the Langley 9-inch Supersonic Tunnel" N.A.C.A. R.M. - L52J21a, (1952).
- 2.6-20 Love, E. S. and O'Donnell, R. M. "Investigations at Supersonic Speeds of the Base Pressure on Bodies of Revolution With and Without Sweptback Stabilizing Fins" N.A.C.A. R.M. -L52J21a, (1952).
- 2.6-21 Perkins, E. W. "Experimental Investigation of the Effects of Support Interference on the Drag of Bodies of Revolution at Mach Number of 1.5" N.A.C.A. T.N. 2292, (1951).
- 2.6-22 Hill, F. K. and Alpher, R. A. "Base Pressures at Supersonic Velocities" J. Aero. Sci., Vol. 16, No. 3, pp. 153-160, (1949).
- 2.6-23 Charters, A. C. and Turetsky, R. A. "Determination of Base Pressure from Free-Flight Data" Rep. 653, Ballistic Res. Lab., Aberdeen Proving Ground, (1948).
- 2.6-24 Hart, R. G. "Effects of Stabilizing Fins and a Rear-Support Sting on the Base Pressures of a Body of Revolution in Free Flight at Mach Numbers from 0.7 to 1.3" N.A.C.A. R.M. -L52E06, (1952).
- 2.6-25 Peck, R. F. "Flight Measurements of Base Pressure on Bodies of Revolution with and without Simulated Rocket Chambers" N.A.C.A. R.M. - L50I28a, (1950).
- 2.6-26 Katz, E. R. and Stoney, W. E., Jr. "Base Pressures Measured on Several Parabolic-Arc Bodies of Revolution in Free Flight at Mach Numbers from 0.8 to 1.4 and at Large Reynolds Numbers" N.A.C.A. R.M. - L51F29, (1951).
- 2.6-27 Reller, J. O., Jr. and Hamaker, F. M. "An Experimental Investigation of the Base Pressure Characteristics of Nonlifting Bodies of Revolution at Mach Numbers from 2.73 to 4.98" N.A.C.A. R.M. A52E20, (1952).
- 2.6-28 Hill, F. K. "Base Pressures at a Mach Number of 5.1" APL/JHU/CF - 1306, Johns Hopkins Univ., Appl. Physics Lab., (July 11, 1949).
- 2.6-29 Goin, K. L. "Effects of Plan Form, Airfoil Section, and Angle of Attack on the Pressure Along the Base of Blunt-Trailing-Edge Wings at Mach Numbers of 1.41, 1.62, and 1.96" N.A.C.A. R.M.- L52D21, (1952).
- 2.6-30 Spahr, J. R. and Dickey, R. R. "Effect of Tail Surfaces on the Base Drag of a Body of Revolution at Mach Numbers of 1.5 and 2.0" N.A.C.A. T.N. 2360, (1951).

- 2.6-31 Morrow, J. D. and Katz, E. "Flight Investigation at Mach Numbers from 0.6 to 1.7 to Determine Drag and Base Pressures on a Blunt-Trailing-Edge Airfoil and Drag of Diamond and Circular-Arc Airfoils at Zero-lift" N.A.C.A. R.M. - L50E19a, (1950).
- 2.6-32 Syvertson, C. A. and Hermilo, R. G. "An Experimental Investigation of the Zero-Lift Drag Characteristics of Symmetrical Blunt-Trailing-Edge Airfoils at Mach Numbers from 2.7 to 5.0" N.A.C.A. Research Mem. A53B02, (1953).
- 2.6-33 Love, E. S. "Base Pressure at Supersonic Speeds on Two-Dimensional Airfoils and on Bodies of Revolution with and without Fins Having Turbulent Boundary Layers" N.A.C.A. T.N. 3819, (1957).
- 2.6-34 Kavanau, L. L. "Base Pressure Studies in Rarefied Supersonic Flows" J. Aero. Sci., Vol. 23, No. 3, pp. 193-208, (1956)
- 2.6-35 Jack, J. R. "Theoretical Pressure Distributions and Wave Drags for Conical Boattails" N.A.C.A. T.N. 2972, (1953).
- 2.6-36 Stoney, W. E., Jr. "Collection of Zero-Lift Drag Data on Bodies of Revolution from Free-Flight Investigations" N.A.C.A. T. N. 4201, (1958).
- 2.6-37 Cortright, E. M., Jr. and Kochendorfer, F. D. "Jet Effects on Flow Over Afterbodies in Supersonic Stream" N.A.C.A. R.M. - E53H25, (1953).
- 2.6-38 Cabbage, J. M., Jr. "Jet Effects on the Drag of Conical Afterbodies for Mach Numbers of 0.6 to 1.28" N.A.C.A. R.M. L57B21, (1957).
- 2.6-39 Judd, J. H. and Falanga, R. A. "Flight Investigation of the Effect of a Propulsive Jet Positioned According to the Transonic Area Rule on the Drag Coefficients of a Single-Engine Delta-Wing Configuration at Mach Numbers from 0.83 to 1.36" N.A.C.A. R.M. - L56A16, (1956).
- 2.6-40 Henry, B. Z., Jr. and Cahn, M. S. "Preliminary Results of an Investigation at Transonic Speeds to Determine the Effects of a Heated Propulsive Jet on the Drag Characteristics of a Related Series of Afterbodies" N.A.C.A. R.M.-L55A24a (1955).
- 2.6-41 Cortright, E. M., Jr. and Schroeder, A. H. "Preliminary Investigation of Effectiveness of Base Bleed in Reducing Drag of Blunt-Base Bodies in Supersonic Stream" N.A.C.A. R.M. E51A26, (1951).
- 2.6-42 Herbrank, W. H., Scanland, T. S., Platou, A. S., and Hicks, B. L. "The Effects on Base Pressure of Air Ejection from the Base Model Projectile at MA= 1.7 - Partial Evaluation of the External Ram Jet Principles" Memo. Rep. No. 539, Ballistic Res. Labs., Aberdeen Proving Ground (MD), Aug., 1951 (Proj. No. TB3-0110V, Res. and Dev. Div., Ord. Corps).
- 2.6-43 Deissler, R. G. and Loeffler, A. L., Jr. "Analysis of Turbulent Flow and Heat Transfer on a Flat Plate at High Mach Numbers with Variable Fluid Properties" NASA TR R - 17, 1959.
- 2.6-44 Truitt, R. W. Hypersonic Aerodynamics. New York: The Ronald Press Company, 1959.
- 2.6-45 Hoerner, S. F. Fluid Dynamics Drag: Author's Publication.

- 2.6-46 Royal Aeronautical Society Data Sheets, Aerodynamics, Vol. 1, Eleventh Issue, October, 1960.
- 2.6-47 Hilton, W. F. High Speed Aerodynamics. New York: Longman's Green and Company, 1951.
- 2.6-48 van Dyke, M. D. "Second-Order Slender-Body Theory -- Axisymmetric Flow" N.A.C.A. T.N. 4281, (1958).

TABLE OF CONTENTS

Section 2.7 Total Zero-Lift Drag Force Coefficient

PAGE

Table 2.7-1	Total zero-lift drag coefficient for the entire missile configuration	
-------------	---	--

## 2.7 TOTAL ZERO-LIFT DRAG FORCE COEFFICIENT

With all the approximations and limitations specified throughout the presented analysis, the final zero-lift drag coefficient expression in quasi-steady flight regimes (or tentatively in accelerated flight without the apparent mass effects accounted for) takes the form:

$$C_{DO} = [C_{DO_f} + (C_{DO_p} + C_{DO_{pv}}) + C_{DO_b}] \quad (2.7-1)$$

where the total frictional, pressure and base drag components are specified explicitly in the respective Sections, 2.3, 2.4, 2.5 and 2.6.

The final zero-lift drag coefficient values for the whole missile configuration are to be computed as indicated in

Table (2.7-1) for all the earlier specified flight and missile geometry conditions.

In conclusion, it is pointed out that the presented computational methods can be used for any other set of data. For instance, at hypersonic speeds, for the respective pressure and base drag coefficient computations the compiled data from Ref (2.6-44) can be used, while at subsonic speeds the additional, well elaborated data from Ref (2.6-46), are recommended. At lifting conditions, the induced drag term (see Sections 1.6, 1.7 and 1.8) is computed in the way closely similar to the one presented here, the respective pressure drag data being extensively assorted, for instance in Refs. (2.6-44), (2.6-45) (2.6-46), (2.6-47).



Unclassified

Security Classification

**DOCUMENT CONTROL DATA - R&D**

*(Security classification of title, body of abstract and indexing annotation must be entered when the overall report is classified)*

<b>1. ORIGINATING ACTIVITY (Corporate author)</b> Auburn Research Foundation, Auburn University Department of Aerospace Engineering		<b>2a. REPORT SECURITY CLASSIFICATION</b> Unclassified
		<b>2b. GROUP</b> N/A
<b>3. REPORT TITLE</b>  Aerodynamic Force Analysis		
<b>4. DESCRIPTIVE NOTES (Type of report and inclusive dates)</b>  Theoretical Technology Reference		
<b>5. AUTHOR(S) (Last name, first name, initial)</b>  Djordjevic, Branimir		
<b>6. REPORT DATE</b> 30 June 1966	<b>7a. TOTAL NO. OF PAGES</b> 858	<b>7b. NO. OF REFS</b>
<b>8a. CONTRACT OR GRANT NO.</b> DA-01-009-506-ORD-851(Z)	<b>9a. ORIGINATOR'S REPORT NUMBER(S)</b>  None	
<b>b. PROJECT NO.</b> 1S222901A206	<b>9b. OTHER REPORT NO(S) (Any other numbers that may be assigned this report)</b>  FR-851(Z)	
<b>c.</b>		
<b>d.</b>		
<b>10. AVAILABILITY/LIMITATION NOTICES</b> This document is subject to special export controls and each transmittal to foreign governments or foreign nationals may be made only with prior approval of this Command, Attn: AMSMI-RF.		
<b>11. SUPPLEMENTARY NOTES</b>	<b>12. SPONSORING MILITARY ACTIVITY</b> Future Missile Systems Division Directorate of Research & Development U. S. Army Missile Command	
<b>13. ABSTRACT</b>  Aerodynamic Force Analysis methods and technology from an extensive bibliography, originally prepared as an internal reference for the U. S. Army Missile Command, is presented in conjunction with definitive guidance for use and applicability. An altitude range from 0 to 400,000 feet and a Mach number range from low subsonic through orbital-re-entry level hypersonic is encompassed, with appropriate continuum, slip and free molecule flow treatments. The extensive coverage should prove useful as a reference for engineering analysis and for introductory educational purposes. The user is also directed to the extensive bibliography of source material for rigid proofs and intensive subject treatment.		

DD FORM 1473  
1 JAN 64

Unclassified

Security Classification

14. KEY WORDS	LINK A		LINK B		LINK C	
	ROLE	WT	ROLE	WT	ROLE	WT
Aerodynamics, force coefficients, lift, drag, side force, two dimensional flow, three dimensional flow, boundary layers, aerothermohypersonic flow.						

INSTRUCTIONS

1. **ORIGINATING ACTIVITY:** Enter the name and address of the contractor, subcontractor, grantee, Department of Defense activity or other organization (*corporate author*) issuing the report.

2a. **REPORT SECURITY CLASSIFICATION:** Enter the overall security classification of the report. Indicate whether "Restricted Data" is included. Marking is to be in accordance with appropriate security regulations.

2b. **GROUP:** Automatic downgrading is specified in DoD Directive 5200.10 and Armed Forces Industrial Manual. Enter the group number. Also, when applicable, show that optional markings have been used for Group 3 and Group 4 as authorized.

3. **REPORT TITLE:** Enter the complete report title in all capital letters. Titles in all cases should be unclassified. If a meaningful title cannot be selected without classification, show title classification in all capitals in parenthesis immediately following the title.

4. **DESCRIPTIVE NOTES:** If appropriate, enter the type of report, e.g., interim, progress, summary, annual, or final. Give the inclusive dates when a specific reporting period is covered.

5. **AUTHOR(S):** Enter the name(s) of author(s) as shown on or in the report. Enter last name, first name, middle initial. If military, show rank and branch of service. The name of the principal author is an absolute minimum requirement.

6. **REPORT DATE:** Enter the date of the report as day, month, year, or month, year. If more than one date appears on the report, use date of publication.

7a. **TOTAL NUMBER OF PAGES:** The total page count should follow normal pagination procedures, i.e., enter the number of pages containing information.

7b. **NUMBER OF REFERENCES:** Enter the total number of references cited in the report.

8a. **CONTRACT OR GRANT NUMBER:** If appropriate, enter the applicable number of the contract or grant under which the report was written.

8b, 8c, & 8d. **PROJECT NUMBER:** Enter the appropriate military department identification, such as project number, subproject number, system numbers, task number, etc.

9a. **ORIGINATOR'S REPORT NUMBER(S):** Enter the official report number by which the document will be identified and controlled by the originating activity. This number must be unique to this report.

9b. **OTHER REPORT NUMBER(S):** If the report has been assigned any other report numbers (*either by the originator or by the sponsor*), also enter this number(s).

10. **AVAILABILITY/LIMITATION NOTICES:** Enter any limitations on further dissemination of the report, other than those imposed by security classification, using standard statements such as:

- (1) "Qualified requesters may obtain copies of this report from DDC."
- (2) "Foreign announcement and dissemination of this report by DDC is not authorized."
- (3) "U. S. Government agencies may obtain copies of this report directly from DDC. Other qualified DDC users shall request through \_\_\_\_\_."
- (4) "U. S. military agencies may obtain copies of this report directly from DDC. Other qualified users shall request through \_\_\_\_\_."
- (5) "All distribution of this report is controlled. Qualified DDC users shall request through \_\_\_\_\_."

If the report has been furnished to the Office of Technical Services, Department of Commerce, for sale to the public, indicate this fact and enter the price, if known.

11. **SUPPLEMENTARY NOTES:** Use for additional explanatory notes.

12. **SPONSORING MILITARY ACTIVITY:** Enter the name of the departmental project office or laboratory sponsoring (*paying for*) the research and development. Include address.

13. **ABSTRACT:** Enter an abstract giving a brief and factual summary of the document indicative of the report, even though it may also appear elsewhere in the body of the technical report. If additional space is required, a continuation sheet shall be attached.

It is highly desirable that the abstract of classified reports be unclassified. Each paragraph of the abstract shall end with an indication of the military security classification of the information in the paragraph, represented as (TS), (S), (C), or (U).

There is no limitation on the length of the abstract. However, the suggested length is from 150 to 225 words.

14. **KEY WORDS:** Key words are technically meaningful terms or short phrases that characterize a report and may be used as index entries for cataloging the report. Key words must be selected so that no security classification is required. Identifiers, such as equipment model designation, trade name, military project code name, geographic location, may be used as key words but will be followed by an indication of technical context. The assignment of links, rules, and weights is optional.